ISSN 0021-9673

VOL. 659 NO. 2 JANUARY 28, 1994

JOURNAL OF CHROMATOGRAPHY A

INCLUDING ELECTROPHORESIS AND OTHER SEPARATION METHODS

ELSEVIER

JOURNAL OF CHROMATOGRAPHY A

INCLUDING ELECTROPHORESIS AND OTHER SEPARATION METHODS

Scope. The *Journal of Chromatography A* publishes papers on all aspects of **chromatography, electrophoresis** and related methods. Contributions consist mainly of research papers dealing with chromatographic theory instrumental developments and their applications. In the *Symposium volumes*, which are under separate editorship, proceedings of symposia on chromatography, electrophoresis and related methods are published. *Journal of Chromatography B: Biomedical Applications*—This journal, which is under separate editorship, deals with the following aspects: developments in and applications of chromatographic and electrophoretic techniques related to clinical diagnosis or alterations during medical treatment; screening and profiling of body fluids or tissues related to the analysis of active substances and to metabolic disorders; drug level monitoring and pharmacokinetic studies; clinical toxicology; forensic medicine; veterinary medicine; occupational medicine; results from basic medical research with direct consequences in clinical practice.

Submission of Papers. The preferred medium of submission is on disk with accompanying manuscript (see *Electronic manuscripts* in the Instructions to Authors, which can be obtained from the publisher, Elsevier Science B.V., P.O. Box 330, 1000 AH Amsterdam, Netherlands). Manuscripts (in English; *four* copies are required) should be submitted to: Editorial Office of *Journal of Chromatography A*, P.O. Box 681, 1000 AR Amsterdam, Netherlands, Telefax (+31-20) 5862 304, or to: The Editor of *Journal of Chromatography B: Biomedical Applications*, P.O. Box 681, 1000 AR Amsterdam, Netherlands. Review articles are invited or proposed in writing to the Editors who welcome suggestions for subjects. An outline of the proposed review should first be forwarded to the Editors for preliminary discussion prior to preparation. Submission of an article is understood to imply that the article is original and unpublished and is not being considered for publication elsewhere. For copyright regulations, see below.

Publication information. *Journal of Chromatography A* (ISSN 0021-9673): for 1994 Vols. 652–682 are scheduled for publication. *Journal of Chromatography B: Biomedical Applications* (ISSN 0378-4347): for 1994 Vols. 652–662 are scheduled for publication. Subscription prices for *Journal of Chromatography A*, *Journal of Chromatography B: Biomedical Applications* or a combined subscription are available upon request from the publisher. Subscriptions are accepted on a prepaid basis only and are entered on a calendar year basis. Issues are sent by surface mail except to the following countries where air delivery via SAL is ensured: Argentina, Australia, Brazil, Canada, China, Hong Kong, India, Israel, Japan, Malaysia, Mexico, New Zealand, Pakistan, Singapore, South Africa, South Korea, Taiwan, Thailand, USA. For all other countries airmail rates are available upon request. Claims for missing issues must be made within six months of our publication (mailing) date. Please address all your requests regarding orders and subscription queries to: Elsevier Science B.V., Journal Department, P.O. Box 211, 1000 AE Amsterdam, Netherlands. Tel.: (+31-20) 5803 642; Fax: (+31-20) 5803 598. Customers in the USA and Canada wishing information on this and other Elsevier journals, please contact Journal Information Center, Elsevier Science Inc., 655 Avenue of the Americas, New York, NY 10010, USA, Tel. (+1-212) 633 3750, Telefax (+1-212) 633 3764.

Abstracts/Contents Lists published in Analytical Abstracts, Biochemical Abstracts, Biological Abstracts, Chemical Abstracts, Chemical Titles, Chromatography Abstracts, Current Awareness in Biological Sciences (CABS), Current Contents/Life Sciences, Current Contents/Physical, Chemical & Earth Sciences, Deep-Sea Research Part B: Oceanographic Literature Review, Excerpta Medica, Index Medicus, Mass Spectrometry Bulletin, PASCAL-CNRS, Referativnyi Zhurnal, Research Alert and Science Citation Index.

US Mailing Notice. *Journal of Chromatography A* (ISSN 0021-9673) is published weekly (total 52 issues) by Elsevier Science B.V., (Sara Burgerhartstraat 25, P.O. Box 211, 1000 AE Amsterdam, Netherlands). Annual subscription price in the USA US$ 4994.00 (US$ price valid in North, Central and South America only) including air speed delivery. Second class postage paid at Jamaica, NY 11431. **USA POSTMASTERS**: Send address changes to *Journal of Chromatography A*, Publications Expediting, Inc., 200 Meacham Avenue, Elmont, NY 11003. Airfreight and mailing in the USA by Publications Expediting.

See inside back cover for Publication Schedule, Information for Authors and information on Advertisements.

0021-9673/94/$07.00

This issue is printed on acid-free paper.

Printed in the Netherlands

VOL. 659, NO. 2 JOURNAL OF CHROMATOGRAPHY A JANUARY 28, 1994

CONTENTS

(Abstracts/Contents Lists published in Analytical Abstracts, Biochemical Abstracts, Biological Abstracts, Chemical Abstracts, Chemical Titles, Chromatography Abstracts, Current Awareness in Biological Sciences (CABS), Current Contents/Life Sciences, Current Contents/Physical, Chemical & Earth Sciences, Deep-Sea Research/Part B: Oceanographic Literature Review, Excerpta Medica, Index Medicus, Mass Spectrometry Bulletin, PASCAL-CNRS, Referativnyi Zhurnal, Research Alert and Science Citation Index)

REVIEW

REGULAR PAPERS

Column Liquid Chromatography

(Continued overleaf)

SHORT COMMUNICATIONS

Column Liquid Chromatography

Gas Chromatography

Journal of Chromatography A, 659 (1994) 231–245
Elsevier Science B.V., Amsterdam

CHROM. 25 624

Review

Improved detection and derivatization in capillary electrophoresis

Michael E. Szulc and Ira S. Krull*

Northeastern University, Department of Chemistry, 102 Hurtig Building, Boston, MA 02115 (USA)

(First received August 11th, 1992; revised manuscript received October 5th, 1993)

ABSTRACT

Capillary electrophoresis is well known for its low mass detectabilities, but suffers from poor concentration detection limits. This review will discuss improvements in concentration detectability with an emphasis on derivatization methods. Sample concentration techniques and improved detector designs will also be discussed. Pre- and post-capillary derivatization methods for biofluid analytes such as amino acids, peptides, proteins, oligonucleotides, and oligosaccharides will be examined in detail.

CONTENTS

1. INTRODUCTION

Capillary electrophoresis (CE) is rapidly becoming an accepted routine analytical technique, characterized by short run times and high efficiencies. The method is applicable to small molecules, and most importantly, biopolymers such as peptides, proteins, and oligonucleotides. Because the separation mechanism (charge migration, isoelectric focusing, sieving) is orthogonal to chromatographic separation mechanisms, the techniques may be considered complementary in establishing purity, or identifying structural components or impurities in a sample. The major disadvantage to CE is its low concentration sensitivity. Because the entire system volume is only a few μl, detector flow cells require narrow, short path lengths that ultimate-

* Corresponding author.

0021-9673/94/$26.00
SSDI 0021-9673(93)E1066-9

ly limit absorbance or fluorescence sensitivities. The frequently reported mass detection limits in the pmol/fmol range for sample injections of low nanoliter volumes actually translate to only mg/l (ppm) or high μg/l (ppb) concentration detection limits, easily obtainable in high-performance liquid chromatography (HPLC). Thus, there is a great desire to improve sensitivities for analyte detection in CE. An example of the difference between reported mass and concentration detection limits is the work of Nickerson and Jorgenson [1]. By using laser-induced fluorescence (LIF) for improved detection of naphthalene dicarboxaldehyde (NDA) amino acid derivatives in CZE, they report detection of $2.5 \cdot 10^{-18}$ mol of arginine. These mass detection limits are impressive by any yardstick. However, because of only nl injection volumes, the concentration detection limits are on the order of 10^{-8} *M*. Many other reports of detection limits that offer low mass detection limits often have concentration limits of only 10^{-6} *M*. Thus, the resolving power and efficiency of CE, coupled with low concentration sensitivites of small sample volumes, is the goal of many analytical laboratories. Progress in the area of CE derivatizations using LIF detection has lowered mass detection limits to the zmol (10^{-21} mol) range, with concentration detection limits on the order of 10^{-12} *M*. For instance, Cheng and Dovichi [2] have used LIF detection for fluorescein isothiocyanate (FITC) derivatized amino acids for detectabilities of fewer than 6000 molecules, or 10^{-21} mol. These mass detection limits translate into 10^{-12} *M* concentration detection limits.

While several recent review articles have addressed the separation mechanisms and methods of detection [3–9] available in CE, less focus has been placed on the discussion of fundamental attempts to lower concentration detectabilities. This review will address the issue of improved detection of trace amounts of analytes in CE through derivatization for improved fluorescence (FL) determination of samples in a biological matrix. However, it should also be noted that there are alternative methods for improving concentration sensitivities. These include alternative detector designs for improved sensitivity, and sample concentration techniques, such as sample stacking or C_{18} or isotachophoretic preconcentration. Detectability of an analyte will ultimately hinge on careful choice of preconcentration conditions, detector design, and derivatization reagent.

2. SAMPLE CONCENTRATION TECHNIQUES

The major disadvantage of capillary electrophoresis is the limited amount of sample that can be loaded onto the capillary. By concentrating a large amount of a dilute sample at the beginning of the capillary, prior to separation, loadability is increased, and detectabilities can be lowered several orders of magnitude.

The most popular method of preconcentration in CE is sample stacking. Sample stacking has recently been reviewed [10], and several researchers have been investigating the fundamentals and applications [11,12]. Sample stacking depends on a matrix difference (pH, ionic strength) between the sample buffer and capillary buffer, so that the electric field across the sample zone is more than in the capillary region. In sample stacking, a large volume of sample in a low concentration buffer is introduced for preconcentration at the head of the capillary. The capillary is filled with a buffer of the same composition, but a higher concentration. When the sample ions reach the capillary buffer and the lower electric field, they stack into a concentrated zone. Sample stacking has increased detectabilities 1–3 orders of magnitude.

Another method of preconcentration is to apply isotachophoresis (ITP) prior to the free zone CE separation of analytes [13–15]. ITP is an electrophoretic technique which allows μl volumes of sample to be loaded onto the capillary, in contrast to the low nl injection volumes typically associated with CE. The technique relies on inserting the sample between two buffers (leading and trailing electrolytes) of higher and lower mobility, respectively, than the analyte. The technique is inherently a concentration technique, where the analytes concentrate into pure zones migrating with the same speed. The technique is less popular than stacking methods because of the need for several

choices of leading and trailing electrolytes, and the ability to separate only cationic or anionic species during a separation. Nevertheless, impressive increases in detectability have been demonstrated. Stegehuis *et al.* [13] used ITP coupled with capillary zone electrophoresis (CZE) for the determination of *o*-phthaldehyde (OPA) and FITC amino acid derivatives. ITP was performed prior to CZE separation in a capillary with a wider diameter than the CZE capillary. This allowed a 5000-fold increase in the loadability of the sample onto the CZE capillary, although the decrease in capillary diameter required a 1:100 split of the running buffer. Fig. 1 shows the remarkable effect of ITP preconcentration on the separation of FITC-derivatized amino acids.

Samples can also be concentrated at the head of the capillary using techniques typically associated with chromatography, notably concentration of hydrophobic analytes using a bonded C_{18} stationary phase, or specific isolation and concentration of an analyte using an affinity ligand [16]. Guzman *et al.* [16] employed an antibody covalently bound to a solid support to concentrate and determine urinary components such as uric acid, amphetamine, and methamphetamine. The antibodies were bound to controlled-pore aminopropyl glass beads and packed into a 100 μm I.D. capillary. The antibody sites were saturated with sample, then an elution buffer was applied to separate the retained analytes. Although recovery yield varied from 20–65%, because of irreproducibility of the preparation of the bound antibody concentrator, the concentrator is reusable, and up to 350 ng of analyte can be loaded onto the capillary.

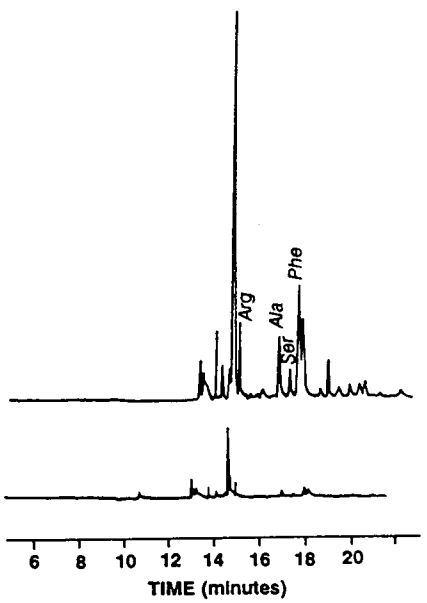

Fig. 1. Electropherograms of an FITC derivatization mixture of some amino acids. LIF detection 488/514 nm. Lower trace: single CE; electrokinetic injection (5 kV, 5 s) of 10 mmol FITC amino acid derivatives; 25 kV applied voltage. Upper trace: coupled ITP–CE; 25-μl ITP injection; followed by CE electrokinetic injection (5 kV, 5 s). Applied voltage, 10 kV ITP; 25 kV CE. From ref. 13.

3. FLUORESCENCE DETECTORS FOR CE

While several alternate modes of detection to UV absorbance have been applied, including electrochemical, mass spectrometric, and indirect detection techniques [4,17,18], the most promising area for lowering detectability of analytes is by LIF. However, there are not many biological samples of interest applicable to analysis by CE that naturally possess a high FL intensity. Also, analysis of natively fluorescent compounds is limited by their differing excitation maxima, and their compatability with available laser excitation wavelengths. Therefore, FL derivatization with a chromopore that fluoresces with an excitation maximum near the wavelength of the laser is an important technique for improved detection in CE. The most popular lasers for excitation in LIF are helium–cadmium lasers, emitting at 325 nm, and argon ion lasers, emitting at 488 nm. An excellent review of the components and optimal parameters for LIF detectors is given by Wu and Dovichi [19].

Sweedler *et al.* [20] developed an improved FL detector for CZE using a charge-coupled device (CCD). Normally with LIF, the laser is focused perpendicularly onto a narrow region of the capillary. With this detector, the output of the laser beam was focussed axially onto the end of the capillary illuminating a 2-cm channel, and the FL emission was collected. The detector operated in two modes, snapshot and time delay integration. Because CCDs have a slow readout

rate, several seconds are required to read a large array and transfer its information into digitalized form. This data transfer is normally performed in the snapshot mode, where, after exposure to the fluorescent signal, the shutter is closed and the array read. Because of the delay between exposures, it is possible to miss an analyte in a narrow observation zone. However, because the laser is focussed axially over 2 cm, it is usually possible to obtain 10–30 exposures per analyte. This process also entails a large amount of data processing from the exposures. Operating in the time delay integration mode eliminated the need for the shutter by synchronizing the transfer of data from the array to the digital processer with the migration of the analyte through the capillary. This technique allowed for less data processing than the snapshot mode, allowed the fluorescence to be integrated over the entire time in the observation zone, and resulted in a 2–5 times decrease in noise. Limits of detection with this detector for FITC-labelled amino acids for a 13-nl injection were in the range of 20–80 zmol.

Hernandez *et al.* [21] used a fluorescence microscope as a detector for CE. The authors report detection of 0.5 fmol of riboflavin, and improved detectabilities using larger diameter capillaries in tandem with either a high-powered UV lamp and photomultiplier tube (PMT), or an argon-ion laser, PMT and photon counter. However, the larger diameter capillaries allow detection of only 0.05 nl volumes, so that there is no real gain in concentration detectabilities.

Cheng *et al.* [22] used a sheath flow cuvette design to improve FL sensitivites. In a sheath flow cuvette, the sample stream is injected into the center of a flowing sheath stream, so that the sample flows as a narrow stream through the center of the capillary. The sheath stream was adjusted to a similar refractive index as the sample stream to minimize light scattering, and flat flow chambers for low FL background were used. Wu and Dovichi [19] used this detector design for a 10-fold improvement in detectability. Analysis of FITC-labeled amino acids yielded detectabilities ranging from arginine $1.3 \cdot 10^{-12}$ M (1.7 zmol) to cysteine $5.6 \cdot 10^{-12}$ M (6 zmol) with signal linearity extending over five orders of magnitude.

Yu and Dovichi [23] have used an argon-ion laser in association with thermoptical absorbance detection for attomole (10^{-8} M) detectability for dabsyl-labeled amino acids. Other applications of lasers in novel detection modes have been used to improve selectivity of detection, but not necessarily improved detectability. These include using a He–Cd laser for laser-based refractive index detection [24] and for FL photodiode array detection [25], and an argon-ion laser for FL circular dichroism detection [26].

4. DERIVATIZATION IN CE

Chemical derivatization of an analyte improves the sensitivity and detectability of an analyte by introduction of an FL chromophoric group, and increases the selectivity of an analyte if it can be shown that the derivatizing reagent reacts in the biological matrix solely with the analyte of interest. Derivatizations can be performed pre-, post- and on-column with respect to the electrophoretic separation.

Post-capillary techniques allow improved detection of analytes after separation in their native state, while pre-capillary derivatizations change both detection and electrophoretic properties. Post-capillary derivatizations require a rapid reaction time with a reagent that does not share the detection properties of the derivative, so that reagent blank interference is minimal. Detection limits with post-capillary methods are not usually as low as with pre-capillary methods, so that their major application is when derivatives are unstable, or when there are multiple derivatization sites that may yield a mixture of products. Since the reaction is being performed on the analyte electrophoretically resolved from its matrix, it is not necessary for the reaction to go to completion, or for only a single derivative to be formed; however, the percent derivatizations should be reproducible and should not change with concentration. These reactions are often easy to automate for on-line detection of the derivatives. Disadvantages of the technique are possible reagent instability, more complex hardware requirements, and lower sensitivities than pre-capillary derivatization reagents.

For pre-capillary derivatizations, rapid reac-

tion conditions are not necessary. However, percent derivatization of the analyte should be high, 100% if possible, since derivatization may be matrix dependent, and should yield only a single derivative. Pre-column derivatization reagents also often share the detection properties of the derivative, so that it is necessary to remove excess reagent before separation, or to resolve the excess reagent from the derivative. Both pre- and post-capillary methodologies have been developed for derivatization in CE, although the majority of the work has been in pre-capillary derivatizations.

4.1. Derivatization of amino acids, peptides and proteins

Both fluorescamine and OPA are reagents with no inherent FL properties, but offer enhanced detectability of primary amino acids with fluorescent detection. They are both common reagents for the pre- and post-capillary derivatization of amino acids and small peptides. Fluorescamine has the disadvantage of being unstable in aqueous eluents, while OPA has better FL yields and is stable in an aqueous environment. Other common derivatization reagents include FITC, 9-fluorenylmethyl chloroformate (FMOC-Cl), 5-dimethylaminonaphthalene-1-sulfonyl chloride (dansyl chloride), 4-(dimethylamino) azobenzene-4′-sulfonyl chloride (dabsyl chloride), and other acyl chlorides. Because excess reagent undergoes fluorescence and must be resolved from the analytes, these reagents can only be used for pre-capillary derivatizations.

Albin *et al.* [27] have compared FITC, fluorescamine, FMOC-Cl, and OPA for pre- and post-capillary derivatization in CE. For the pre-capillary derivatization and micellar electrokinetic chromatography (MEKC) separation of six amino acids, FMOC-Cl offered the lowest limit of detection, 10 ng/ml, or 0.5 fmol. FMOC-Cl has a rapid reaction time with primary and secondary amino acids, but also yields a FL hydrolysis product that can interfere with detection, unless it is resolved from the analytes or removed by extraction. OPA also has low detection limits (50 ng/ml) for primary amino acids, but the derivatives can be unstable.

While FITC shows good detectability for primary and secondary amino acids, it requires a long reaction time, so that it is impractical for routine use [27]. Excess reagent also interferes with detection. Fluorescamine has a rapid reaction time (milliseconds) with primary amino acids, and excess reagent is hydrolyzed to a non-FL product. Detectabilities are as low as 360 ng/ml. Fluorescamine has also been used for the determination of polyamines in brain, stomach and lung tissue using an internal standard [28]. Guzman *et al.* [29] have also used fluorescamine for the derivatization of proline and hydroxyproline. Although the products were non-FL, they were able to be determined with improved sensitivity (800 fold) at 214 nm, and resolution was also improved. Response was linear from 19–304 nmol/100 μl.

Nickerson and Jorgenson [30] compared FITC, NDA and OPA for pre-column labeling of amino acids, using phenylalanine as a model. A He–Cd laser operated at 326 nm for OPA and 442 nm for NDA and FITC was used for excitation. Detection limits were 20 n*M* for OPA, 1.6 n*M* for NDA, and 0.22 n*M* for FITC. The better detection limits for FITC and NDA arise from the greater intensity of the 442 nm laser line excitation source. NDA has the further advantage that the excess reagent does not fluoresce, while the FITC reagent must be extracted from the sample or resolved from the analyte.

Ueda *et al.* [31] used cyclodextrin-modified MEKC for the chiral resolution of NDA-labeled amino acids. The excitation maxima of these derivatives coincides with the output of a He–Cd laser. The cyclodextrin-modified running buffer allowed separation of the enantiomers based on differences in partitioning into the cavity of the chiral cyclodextrin to form diastereomeric complexes, while the ability for LIF detection allowed determination of amino acids as low as 0.9 amol/2.5 nl injected.

In CZE, Waldron *et al.* [32] demonstrated improved detectabilities of amino acids with fluorescein thiohydantoin (FTH) and dimethylaminoazobenzene thiohydantoin (DABTH) derivatives. Separation of DABTH derivatives was difficult because of elimination of the primary amine and the carboxylic acid. An

acidic pH was required to protonate the secondary amine, and acetonitrile was added to reduce electroosmotic flow and increase the separation time. The FTH amino acids were anions under basic conditions, and were able to be separated with higher efficiency in CZE than the DABTH derivatives. Although these reagents were applied only to standard solutions of amino acids, the authors point out the application that they would have application as substituted phenyl isothiocyanate derivatives, replacing the phenyl group with a superior chromophore for improved detection of amino acids in Edman degradation sequencing analysis for CZE.

Higashijima *et al.* [33] developed a new derivatization reagent compatible with a semi-conductor laser. Semi-conductor lasers have the advantages of being inexpensive and rugged, but lack chromophores at suitable wavelengths without frequency doubling. The authors developed a thiazine chromophore fluorescent in the deep-red region, compatible with a semi-conductor laser, and with a succinimidyl-activated ester to couple with an amino acid. Detection limits were reported to be only 10 pmol, but the work reported was preliminary, and shows the possible utility of semi-conductor lasers for excitation in CE.

A variety of FL derivatization techniques exist for improving sensitivity and selectivity of peptide fragments. Because peptides contain several functional groups, derivatization generally yields a mixture of products, so that derivatizations are usually carried out post-column, after the separation of the native peptides. Pre-capillary derivatizations must be limited to small peptides or peptides with only a single functional group. In addition, it is desirable for the derivative to fluoresce at wavelengths high enough so that the native fluorescence of Trp or Tyr does not interfere. Many of the derivatization reagents used for amino acids are not useful for peptide derivatizations. OPA does not react significantly with the N-terminal amino group of the peptide, except for dipeptides and other small peptides, and dansyl chloride does not react except at high concentrations of peptides. Fluorescamine has been shown to derivatize the amino group of peptides for sensitive detection in the low pmol range for peptides of less than 20 amino acids in length [34].

Swaile and Sepaniak [35] investigated the FL detection of proteins using native FL, pre-column labeling, and on-column labeling with arylaminonaphthelene-sulfonates. Detection of the protein's (conalbumin) native fluorescence was performed using a frequency doubled argon ion laser (514 nm excitation), for excitation at 257 nm of the aromatic amino acids. The detection limit was 14 n*M*. Precolumn labeling of the protein with FITC lowered the detectability to 0.1 n*M*, but produced a mixture of derivatives. The authors also used fluorescent hydrophobic probes such as 1-anilinenaphthalene-sulfonate (ANS) and 2-*p*-toluidinonaphthalene-6-sulfonate (TNS). These probes undergo non-covalent, hydrophobic interactions with the proteins and change their FL properties. FL properties of the complex are extremely solvent dependent. Quantum efficiencies in aqueous solvents are as low as 0.01, but can increase to 0.6 in viscous or non-polar solvents. Because of solvent requirements for the separation, detection limits with these on-column labeling agents was only 360 n*M* for TNS and 615 m*M* for ANS.

3-(4-Carboxybenzoyl)-2-quinolinecarboxaldehyde (CBQCA) [36] was used for the improved detection of primary amines, amino acids, and peptides. CBQCA-derivatized amino acids were detectable at masses as low as 10–70 amol. Detection limits for peptides containing a single amino functionality were also in the low amol range, with a dynamic range over 4 orders of magnitude. The reagent has the advantage of being transparent in the reagent blank, and induces an additional charge onto the derivative. Although the reagent was also reactive toward proteins, the formation of multiple peaks negated the reagent's utility for protein derivatization.

The previously described reagents for peptide derivatizations are non-specific and react with free amino groups on all peptides. The reagents yield improved sensitivities for *all* peptides in a peptide map. For more specificity, reagents can be chosen which react with particular amino acids to selectively detect particular peptides.

Cobb and Novotny [37] used benzoin and 4-methoxy-1,2-phenylenediamine for the derivatization of arginine and tyrosine containing peptides, respectively. FL detection employing a He–Cd laser (325 nm) is well suited to detect the derivatives from both reagents. A tryptic digest of chicken egg white lysozyme was reacted separately with each reagent. Cobb and Novotny [38] further characterized the benzoin derivatization of arginine containing peptides obtained from a tryptic digest of human serum albumin. Attomole mass detection limits were reported. Fig. 2 shows the UV trace for the tryptic digest, and the LIF trace for the benzoin derivatized tryptic digest. There is a 10^3 difference in the mass injected.

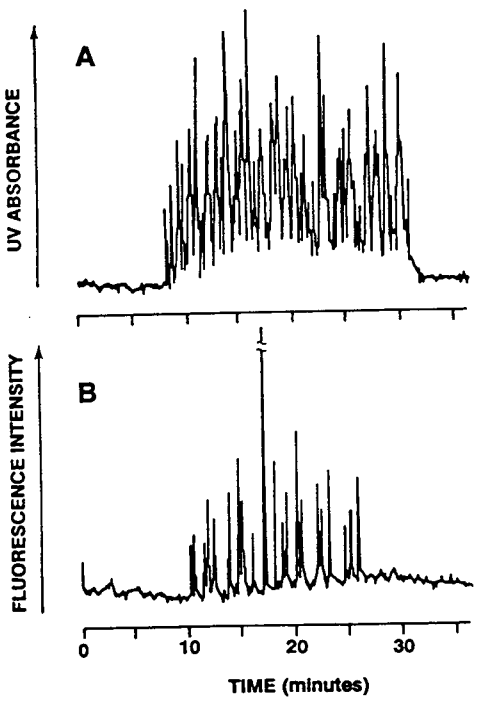

Fig. 2. Tryptic digest of reduced and alkylated human serum albumin (HSA). (A) UV detection 215 nm; 100 fmol of HSA digest; 0.05 *M* 2-(cyclohexylamino)ethanesulfonic acid (CHES) buffer pH 9.7; capillary 55 cm (40 cm to detector) × 50 μm, coated with linear polyacrylamide; 25 kV applied voltage; 12 μA. (B) LIF detection of benzoin-derivatized HSA digest. 360 amol of digest injected; off-scale peak due to derivatization reagent; 0.05 *M* 3-(cyclohexylamino)-1-propanesulfonic acid (CAPS), pH 9.1; 0.06 *M* SDS; 10% acetonitrile; capillary 70 cm × 50 μm (50 cm to detector), uncoated capillary; applied voltage 25 kV, 20 μA. From ref. 38 (© American Chemical Society).

Other derivatization reagents useful for FL derivatization of amines, amino acids, peptides, and proteins include dansyl-chloride for both achiral [39,40] and chiral [41] analysis, dabsyl chloride [28,42], N2-(5-fluoro-2,4-dinitrophenyl)-L-alanine amide (Marfey's reagent) [43], phenylisothiocyanate [44], 4-chloro-7-nitrobenzofurazan (NBD-chloride) [45] and NDA [1,46].

4.2. Post-capillary reaction detection

Post-capillary derivatization is most often applied to analytes whose derivatives may be unstable, or to analytes that possess multiple derivatization sites that may yield a mixture of products, such as free amino groups on peptides or proteins. The methods rely on either hydrostatic or hydrodynamic addition of the reagent, or to use differential electroosmotic flow to introduce the reagent. Albin *et al.* [27] used a 75-μm reaction capillary separated from a 50-μm separation capillary at a liquid junction containing the buffered reagent, resulting in a flow imbalance where the electroosmotic flow is greater in the larger I.D. capillary. This flow imbalance is made up by introduction of reagent. This system was applied to OPA and fluorescamine derivatization. After optimization of reagent concentrations and temperatures, limits of detection were reported, 60 ng/ml (3.3 fmol) for OPA, and 440 ng/ml (19.2 fmol) for fluorescamine. Fluorescamine was applied to the post-capillary derivatization of a tryptic digest of β-lactoglobulin, Resulting in an 8-fold increase in sensitivity over absorbance detection. The UV and FL traces for the fluorescamine derivatized tryptic digest are shown in Fig. 3. There is a 40-fold decrease in the concentration monitored by the FL trace.

Pentenoy *et al.* [47] designed an OPA post-column reactor fashioned by inserting two 75-μm capillaries into either side and perpendicular to a drilled 75 μm I.D. capillary. Reagent was delivered by hydrostatic pressure, by raising the reagent reservoirs above the buffer reservoirs for a determined amount of time. This was done by filling the separation capillary with running buffer, submersing the ends of the reagent capil-

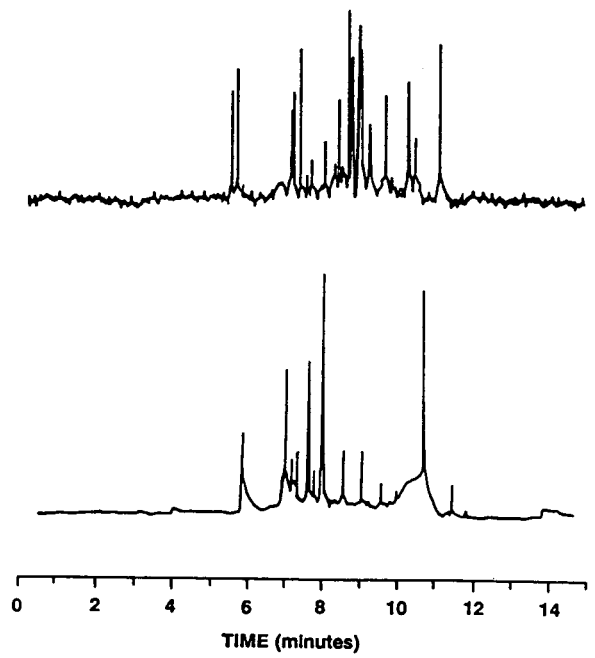

Fig. 3. Free solution electrophoresis of a tryptic digest of β-lactoglobulin. 20 m*M* sodium tetraborate buffer pH 9.5. Field strength 278 V/cm. 30°C. Upper trace: FL detection after post-capillary derivatization with fluorescamine. Xenon lamp 390/450 nm; 0.5 nmol/ml sample concentration; 7 s electrokinetic injection at 5 kV. Lower trace: absorbance detection 200 nm. Deuterium lamp; 20 nmol/ml sample concentration; 1 s vacuum injection. From ref. 27 (© American Chemical Society).

laries in the elevated OPA reagent reservoirs, and applying high voltage for 25 min (Fig. 4). The detection limit for histidine was $9 \cdot 10^{-7}$ *M*. This method is for applications where derivatives are unstable when formed pre-column, or when multiple products can form, since the detection limits are 10^3 higher than pre-column methods.

Rose and Jorgenson [48] describe a post-capillary reactor for OPA derivatization. The coaxial capillary reactor consists of a separation capillary with a smaller outer diameter, inserted into a reaction capillary of a larger inner diameter. The reagent capillary is perpendicular to these capillaries in a stainless-steel tee. Reagent is delivered by raising the reagent reservoir above the buffer reservoirs. The reactor was optimized for enhanced signal and zone broadening, and characterized using glycine and a mixture of proteins. The FL signal was linear over 3.5 orders of magnitude, with a detection limit of $7.5 \cdot 10^{-8}$ *M* glycine (83 amol) and 22.1 amol for whale skeletal muscle myoglobin. Derivatization resulted in a 100-fold improvement in signal to noise ratio *vs.* UV detection. Fig. 5 shows the UV and FL electropherograms for a mixture of whale skelatal muscle myoglobin, carbonic anhydrase, β-lactoglobulin B, and β-lactoglobulin A. Nickerson and Jorgenson [49] used a similar reactor design for OPA and NDA derivatization, with reagent pumped into the reaction capillary using helium pressure. LIF detection with a He–Cd excitation source was performed on the reaction capillary. The detection limit for horse heart myoglobin derivatized with OPA was $1.2 \cdot 10^{-8}$ *M*, and linear over 3 orders of magnitude.

Rose [50] described a post-column reactor for OPA derivatization in CZE. The electrophoresis capillary was terminated in a static solution of OPA, acting as both a cathodic reservoir and a free solution reactor. Zones from the separation capillary mix and react with the OPA reagent to produce the FL derivative. Only the utility of the reactor was described, emphasizing the importance of convective forces for mixing analyte and reagent. No detection parameters or other analytical figures of merit were reported with this work. Fig. 4 shows the post-column reaction

Fig. 4. Post-capillary reaction schemes. (A) A secondary buffer containing a FL reagent is mixed with the running buffer by virtue of the different electroosmotic flow in the different diameter capillaries; from ref. 27 (© American Chemical Society). (B) Experimental set-up of the CZE–LIF reaction detector: 1 = on-column connector; 2 = buffer reservoirs; 3 = derivatization reagent reservoirs; 4 = LIF detector housing; from ref. 47 (© American Chemical Society). (C) Cross-sectional view of post-column reactor; from ref. 48. (D) Cross-sectional schematic of reactor [(a) top and (b) side view]: RR = reagent reservoir; EC = electrophoresis capillary; SC = glass support capillary; CF = compression fitting; SW = silica window; FO = optical fiber; PA = PMT adapter; CL = collection lens; UF = UV cutoff filter; from ref. 50. (E) Schematic diagram of post-column detection system in CE: 1 = positive terminal; 2 = 4-way connector for earth terminal and mixing of column media and buffer; 3 = 3-way connector for mixing with FL reagent; 4 and 5 = PTFE tubes 0.5 mm I.D. of length 5 and 70 cm, respectively. Column medium, alkaline buffer solution and FL reagent supplied by pumps 1, 2, and 3, respectively; from ref. 51.

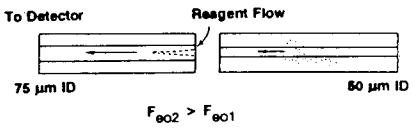
To Detector
Reagent Flow
75 μm ID
50 μm ID
$F_{eo2} > F_{eo1}$

A

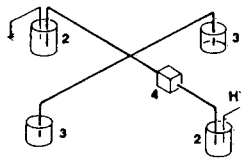
1
2
3
4
H
3
2

B

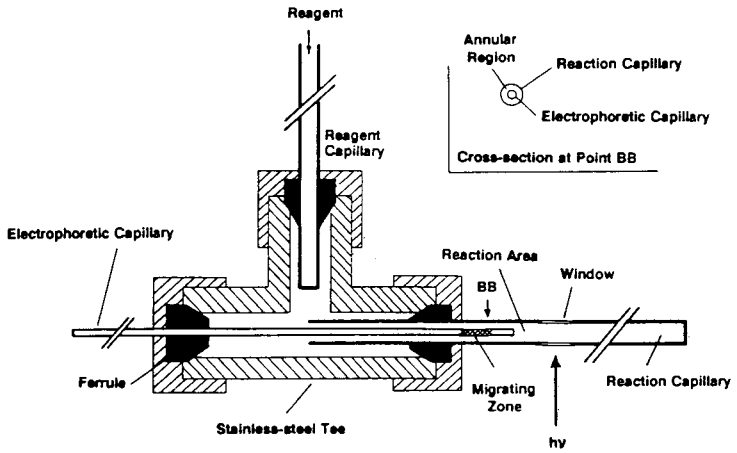
Reagent
Annular Region
Reaction Capillary
Electrophoretic Capillary
Cross-section at Point BB
Reagent Capillary
Electrophoretic Capillary
Reaction Area
BB
Window
Ferrule
Migrating Zone
Reaction Capillary
Stainless-steel Tee
hν

C

a b

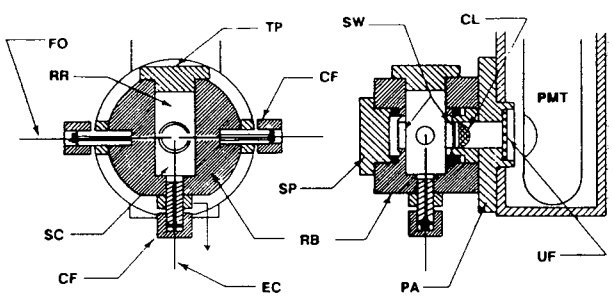
FO
TP
RR
CF
SW
CL
PMT
SP
SC
RB
UF
CF
EC
PA

D

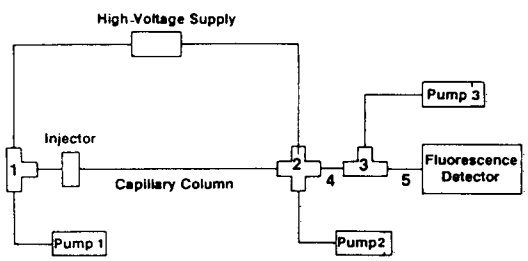
High-Voltage Supply
Pump 3
Injector
1
2
3
Fluorescence Detector
Capillary Column
4
5
Pump 1
Pump2

E

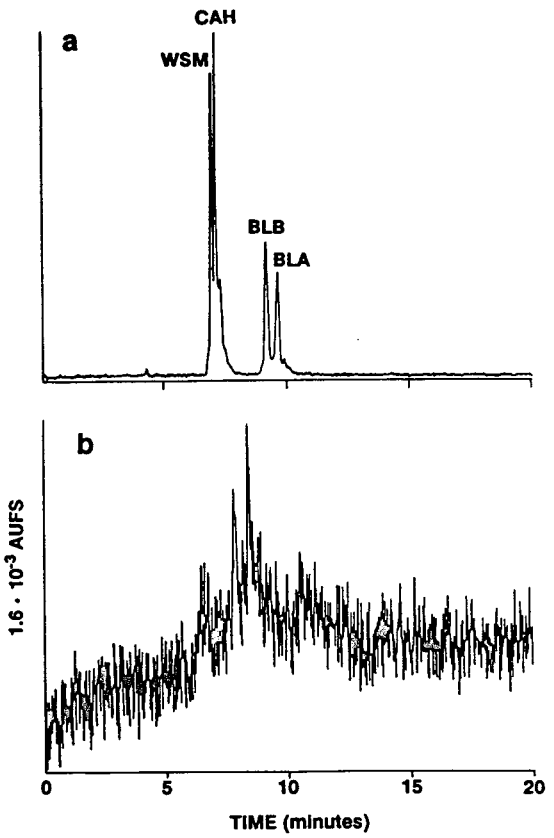

Fig. 5. Comparison of post-capillary FL and UV detection of 0.01% (w/v) whale skeletal muscle myoglobin (WSM), 0.01% carbonic anhydrase (CAH), 0.005% β-lactoglobulin B (BLB), and 0.005% β-lactoglobulin A (BLA). (a) Post-capillary FL detection; (b) UV (229 nm) detection; operating and OPA reagent buffer 50 m*M* borate–50 m*M* KCl, pH 9.5. Sample introduction, 2 s at 30 kV; operating voltage at 30 kV; $\Delta h = 16$ cm. From ref. 48.

schemes for each of the reactors described above.

Tsuda *et al.* [51] utilized three pumps and two mixing chambers for post-column detection with fluorescamine derivatization (Fig. 4). After the separation, pump 2 delivers alkaline buffer and pump 3 delivers the fluorescamine reagent. Pressure buildup at the outlet resulted in flow reversal, so that pump 1 was operated at a few μl/min to maintain forward flow. The method was applied to acetylpolyamines in urine.

4.3. DNA derivatization

Improved detection of oligonucleotides in nucleic acid sequence analysis is necessary for the low mass concentrations associated with micro-sequencing analysis. Chen *et al.* [52] used tetramethylrhodamine isothiocyanate (TRITC) for coupling to the dideoxynucleotide. The derivatized oligonucleotide was excited by a green helium–neon laser (543.5 nm) using a sheath flow detector design. Mass detection limits of 500 ymol (ymol = 10^{-24} mol), or $1.28 \cdot 10^{-10}$ *M*, were reported in the free solution mode.

Chen *et al.* [53] also used a single channel labeling technique, using a fluorescent dye in capillary gel electrophoresis (CGE) for Southern blotting. Drossman *et al.* [54] used fluorescein to label DNA fragments generated in enzymatic DNA sequencing reactions for separation via CGE. Detection limits in unfilled capillaries were 0.1 amol or 60 000 molecules. Swerdlow *et al.* [55] also used fluorescein to label DNA fragments for LIF detection in a sheath-flow cuvette, and reported mass detection limits as low 10^{-20} mol.

Swerdlow *et al.* [56] characterized three DNA sequencing methods, utilizing 4 channel, dual channel, and single channel detection. Four spectral channel sequencing is accomplished using four different fluorescent dyes, to be used with each dideoxynucleotide reaction. Two lines from an argon–ion laser (514.5 nm and 488 nm) are used to excite fluorescence, and emission at four wavelengths is achieved using interference filters (540, 560, 580 and 610 nm). Detection limits are on the order of 200 zmol for all four labeled primers.

The two spectral channel sequencing technique was achieved using succinylfluorescein dyes to label the four dideoxynucleotides. A single wavelength (488 nm) is used to excite fluorescence, and emission is monitored at 510 and 540 nm. The ratio of the FL intensities is monitored to distinguish the terminating dideoxynucleotide. The detection limit is 20 zmol for a labeled dideoxynucleotide triphosphate, and 5 zmol for a 100-mer oligonucleotide.

For single channel monitoring, a fluorescent dye was coupled to the nucleotide, and excited with a green helium–neon laser. Detection of 1200 molecules was achieved. Fig. 6 shows the 4-channel, dual-channel and single-channel

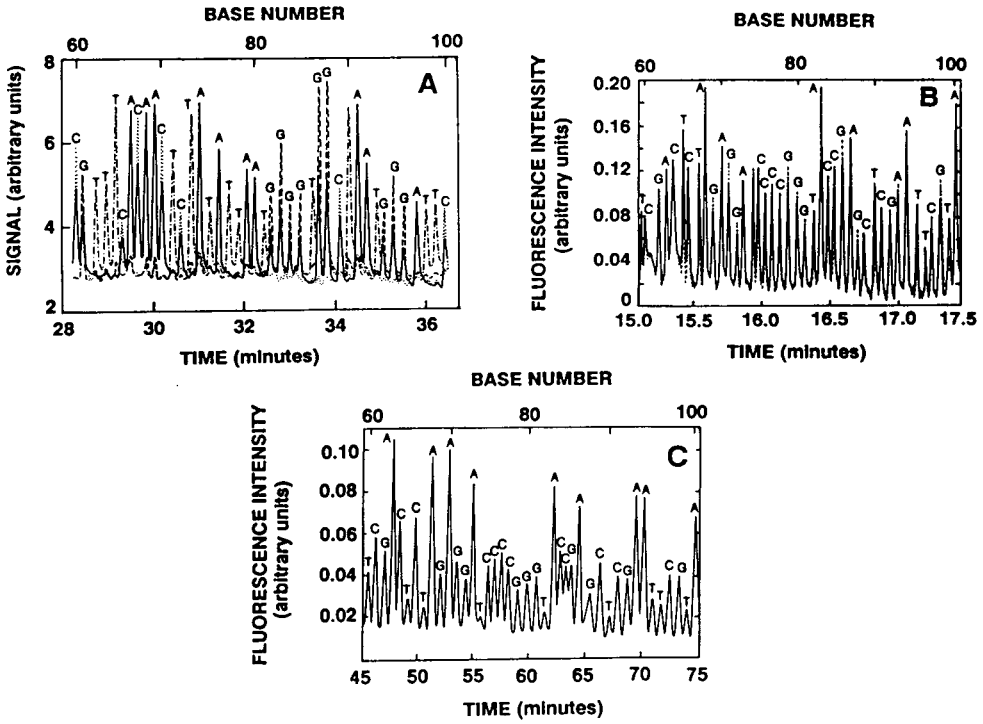

Fig. 6. CGE separation for the pooled reaction products for the DNA sequence of a M13mp18 histidine *t*RNA clone. (A) Four channel sequencing; capillary 41 cm × 50 μm; 27 cm to detector; Electrophoretic injection 30 s at 150 V/cm; traces for C, A, G, and T correspond to emission centered at 540, 560, 580, and 610 nm, respectively. (B) Two spectral channel sequencing; solid trace emission at wavelengths longer than 525 nm; dashed trace emission at wavelengths less than 525 nm. (C) One spectral channel sequencing. From ref. 56 (© American Chemical Society).

traces for the pooled reaction products of a DNA sequence analysis of an M13mp18 histidine *t*RNA clone. The data has not been treated to account for overlap in the spectral channels.

Kasper *et al.* [57] used FL detection (not LIF) for the determination of ethidium bromide stained DNA. Excitation at 232 and emission at 458 nm was used. The greatest sensitivity was obtained at low concentration of reagent, but linearity was lost with high concentration of analyte, necessitating higher concentration of reagent. Detectability was actually 5 times worse than using UV detection, but offered the advantage of elimination of absorbing interferents at 260 nm.

4.4. *Oligosaccharide derivatization*

Derivatization of carbohydrate molecules is necessary for spectrophotometric detection because of the lack of chromophoric groups. Derivatizations are most often performed on reducing carbohydrates. Non-reducing oligosaccharides are analyzed after acid hydrolysis to the component monosaccharides. Reagents for oligosaccharide derivatizations in HPLC have recently been reviewed by Honda [58]. Derivatization for CE of oligosaccharides and carbohydrates is somewhat complicated by the fact that the original analytes are uncharged at most pH values. This has been addressed by either inducing a charge onto the analyte with the derivative, or forming charged borate complexes with the derivative.

Liu *et al.* [59] derivatized aldose oligosaccharides into primary amines, followed by derivatization of the reducing end of an amino sugar with 3-(4-carboxybenzoyl)-2-quinoline carboxaldehyde (CBQCA) or 3-benzoyl-2-napthaldehyde (BNA). The reagents show no background fluorescence, and introduction of these FL chromo-

phores also introduce a charged moiety onto the carbohydrate molecule to form highly fluorescent isoindole derivatives. Detection was via LIF using an argon–ion laser operated at 457 nm. The reagents were applied to the derivatization of hydrolyzed maltooligosaccharides and enzymatically degraded samples separated on polyacrylamide gel-filled capillaries. Liu *et al.* [60] further characterized the CBQCA reagent for derivatization of monosaccharides, acid-hydrolyzed polysaccharides, and glycoprotein digested carbohydrates. In this report, the carbohydrate derivatives (maximum 442 nm) were detected with a helium–cadmium laser. This reagent was characterized to yield mass detection limits of 240 amol and concentration detection limits of $8.0 \cdot 10^{-7}$ *M*. Signal was linear over four orders of magnitude. A representative electropherogram for the separation of six CBQCA amino sugars is shown in Fig. 7. Unfavorable mass-to-charge ratios made separation of large oligosaccharides impractical in the free solution capillary format. Liu *et al.* [61] also applied the CBQCA reagent to the derivatization of larger oligosaccharides (degree of polymerization up to 67) for separation via CGE. Low attomole mass detection limits were reported.

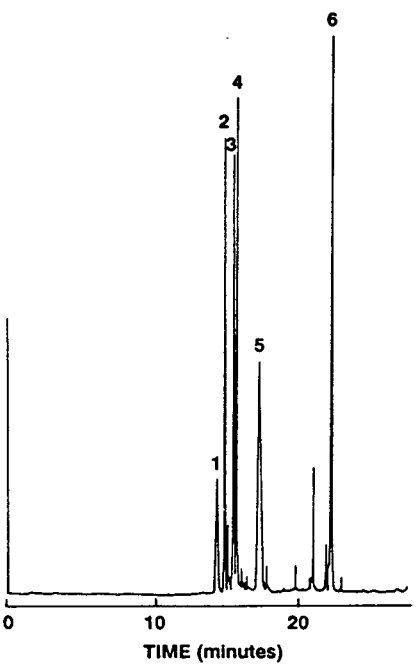

Fig. 7. Electrophoretic separation of six model amino sugars derivatized with CBQCA. 1 = 1-amino-1-deoxyglucose; 2 = 1-amino-2-deoxygalactose; 3 = 2-amino-2-deoxyglucose; 4 = 2-amino-2-deoxygalactose; 5 = 6-amino-6-deoxyglucose; 6 = D-galactosaminic acid. From ref. 60 (© American Chemical Society).

Other reagents for the derivatization of carbohydrates for detection by UV absorbance include 3-methyl-1-phenyl-2-pyrozolin-5-one [62] and 2-amino pyridine [63,64] for separation of borate complexes, and 2,4-dinitrophenylhydrazine [65] for the separation of coupled amino acid–aldehydic sugars.

4.5. Polymeric reagents for CE

One of the disadvantages of all previous pre-column derivatization reagents is dilution of the derivative concentration by the reagent. Post-capillary techniques may minimize the dilution problem, but the detection limits are higher than pre-capillary methods. This is due to the compromises that must be made between the optimum separation conditions and reaction conditions which limit complete formation of the derivative (solvent, time, temperature, pH, etc). We are investigating using a solid-phase reagent containing a fluorescent tag (FMOC) immobilized on a solid polystyrene support. This reagent has been used in HPLC for derivatization of amines [66], amino acids [67], and aminoalcohols [68] in biological fluids. The reagent is stable in an aqueous environment, so that it may be used for on-line derivatizations. By using SDS below its critical micelle concentration (CMC), proteins in biological samples are solubilized, and direct injection and derivatization of analytes in human serum is possible [69] (Fig. 8).

This reagent can be packed into a capillary, so that derivatizations can be performed on-line in free solution CE and MEKC. There are a number of advantages in using solid-phase reactors (SPRs) for CE, beyond eliminating dilution of the analyte with the reagent. The amount of immobilized reagent is in great excess to the analyte concentration, but only the amount that reacts with the analyte is released. The remainder is bound to the solid support, so that the reactor can be used for multiple derivatizations. Because the reagents cannot interact with other

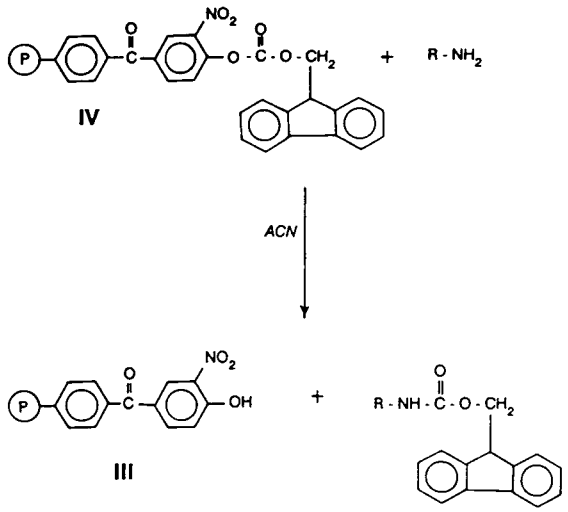

Fig. 8. Reaction of amine with polymeric FMOC reagent. ACN = Acetonitrile.

immobilized reagents, several polymeric reagents may be packed into the same reactor for quantitation using multiple derivatives [66]. Also, when the reagent is exhausted, the tagged reagent can be regenerated in a short, one hour reaction.

By using the CE instrument in the MEKC mode, samples in biological fluid (urine, serum) may be injected directly onto the instrument. This is a significant advantage of MEKC over other modes of capillary separations; however, if derivatization with solution phase reagents is required to lower detectability, analyte extraction and sample clean-up must still be performed prior to injection. SPRs will allow direct injection of analytes in biological fluids onto the capillary. The hydrophobic nature of the SPR will act to preconcentrate the analyte, or it can be used in tandem with an affinity concentrator [16]. By using SPRs, analytes in biological samples may be injected directly onto the capillary for derivatization, followed by separation and FL detection. SPRs contribute to a significant decrease in analysis time, sample clean-up, detectability, and expense for analyses in CE.

5. CONCLUSIONS

Capillary electrophoresis has emerged as a premier technique for the rapid, high-resolution separation of analytes of biological interest. It is especially valuable for biotechnology related samples, such as DNA sequencing products, and biotechnology synthesized peptides and proteins. By careful choice of detector design, derivatization reagent, laser excitation wavelength, and preconcentration steps, low concentration detection limits are possible. The method is complementary to HPLC in the information it provides, so that with low concentration detectability, CE becomes an attractive method for the routine analysis and characterization of samples with biological interest.

6. ACKNOWLEDGEMENTS

Our work in the field of polymeric reagents is supported, in part, by an unrestricted grant from Pfizer, Inc., Pfizer Central Research, Analytical Research Department, Groton, CT, USA, a research and development contract from Supelco, Inc., Division of Rohm and Haas Corporation, State College, PA, USA, and an NIH-Biomedical Research Support Grant to Northeastern University, No. RR07143, Department of Health and Human Resources (DHHS). We acknowledge Isco, Inc. (Lincoln, NE, USA) for their support and collaboration in the field of CE. Finally, we are most appreciative of a Fellowship from the United States Pharmacopeial Convention, Inc., Rockville, MD, USA, to M.E.S.

REFERENCES

1 B. Nickerson and J.W. Jorgenson, *J. High Resolut. Chromatogr. Chromatogr. Commun.*, 11 (1988) 533–534.
2 Y.-F. Cheng and N.J. Dovichi, *Science*, 242 (1988) 562–564.
3 M.J. Gordon, X. Huang, S.L. Pentoney and R.N. Zare, *Science*, 242 (1988) 224–228.
4 Z. Deyl and R. Struzinsky, *J. Chromatogr.*, 569 (1991) 63–122.
5 J.W. Jorgenson, *Anal. Chem.*, 58 (1986) 743A–760A.
6 H.H. Lauer and D. McManigill, *Trends Anal. Chem.*, 5 (1986) 11–15.
7 R.A. Wallingford and A.G. Ewing, *Adv. Chromatogr.*, 29 (1989) 1–76.
8 B.L. Karger, A.S. Cohen and A. Guttman, *J. Chromatogr.*, 492 (1989) 585–614.

9 A.G. Ewing, R.A. Wallingford and T.M. Olefirowicz, *Anal. Chem.*, 61 (1989) 292A–303A.
10 R.-L. Chien and D.S. Burgi, *Anal. Chem.*, 64 (1992) 489A–496A.
11 D.S. Burgi and R.-L. Chien, *Anal. Chem.*, 63 (1991) 2042–2047.
12 R.-L. Chien and J.C. Helmer, *Anal. Chem.* 63 (1991) 1354–1361.
13 D.S. Stegehuis, H. Irth, U.R. Tjaden and J. van der Greef, *J. Chromatogr.*, 538 (1991) 393–402.
14 F. Foret, V. Sustacek and P. Bocek, *J. Microcol. Sep.*, 2 (1990) 229–233.
15 P. Jandik and W.R. Jones, *J. Chromatogr.*, 546 (1991) 431–443.
16 N.A. Guzman, M.A. Trebilcock and J.P. Advis, *J. Liq. Chromatogr.*, 14 (1991) 997–1015.
17 J.D. Olechno, J.M.Y. Tso and J. Thayer, *Am. Lab.*, March (1991) 59–62.
18 R.A. Wallingford and A.G. Ewing, *Anal. Chem.*, 59 (1987) 1762–1766.
19 S. Wu and N.J. Dovichi, *J. Chromatogr.*, 480 (1989) 141–155.
20 J.V. Sweedler, J.B. Shear, H.A. Fishman, R.N. Zare and R.H. Scheller, *Anal. Chem.*, 63 (1991) 496–502.
21 L. Hernandez, L. R. Marquina, J. Escalona and N.A. Guzman, *J. Chromatogr.*, 502 (1990) 247–255.
22 Y.F. Cheng, S. Wu, D.Y. Chen and N.J. Dovichi, *Anal. Chem.*, 62 (1990) 496–503.
23 M. Yu and N.J. Dovichi, *Anal. Chem.*, 61 (1992) 37–40.
24 D.J. Bornhop and N.J. Dovichi, *Anal. Chem.*, 59 (1987) 1632–1636.
25 D.F. Swaile and M.J. Sepaniak, *J. Microcol. Sep.*, 1 (1989) 155–158.
26 P.L. Christensen and E.S. Yeung, *Anal. Chem.*, 61 (1989) 1344–1347.
27 M. Albin, R. Weinberger, E. Sapp and S. Moring, *Anal. Chem.*, 63 (1991) 417–422.
28 T. Tsuda, Y. Kobayashi, A. Hori, T. Matsumodo and O. Suzuki, *J. Microcol. Sep.*, 2(1) (1990) 21–25.
29 N.A. Guzman, J. Moschera, K. Iqbal and A.W. Malick, *J. Liq. Chromatogr.*, 15 (1992) 1163–1177.
30 B. Nickerson and J.W. Jorgenson, *J. High Resolut. Chromatogr. Chromatogr. Commun.*, 11 (1988) 878–881.
31 T. Ueda, F. Kitamura, R. Mitchell, T. Metcalf, T. Kuwana and A. Nakamoto, *Anal. Chem.*, 63 (1991) 2979–2981.
32 K.C. Waldron, S. Wu, C.W. Earle, H.R. Harke and N.J. Dovichi, *Electrophoresis*, 11 (1990) 777–780.
33 T. Higashijima, T. Fuchigami, T. Imasaka and N. Ishibashi, *Anal. Chem.*, 64 (1992) 711–714.
34 D.S. Brown and D.R. Jenke, *J. Chromatogr.*, 410 (1987) 157–162.
35 D.F. Swaile and M.J. Sepaniak, *J. Lig. Chromatogr.*, 14 (1991) 869–893.
36 J. Liu, H. You-Zoung, D. Wiesler and M. Novotny, *Anal. Chem.*, 63 (1991) 408–412.
37 K.A. Cobb and M.V. Novotny, *Anal. Biochem.*, 200 (1992) 149–155.
38 K.A. Cobb and M.V. Novotny, *Anal. Chem.*, 64 (1992) 879–886.
39 C.P. Ong, C.L. Ng, N.K. Lee and S.F.Y. Li, *J. Chromatogr.*, 559 (1991) 537–545.
40 B.W. Wright, G.R. Ross and R.D. Smith, *J. Microcol. Sep.*, 1 (1989) 85–89.
41 P. Gozel, E. Gasmann, H. Michelson and R.N. Zare, *Anal. Chem.*, 59 (1987) 44–49.
42 M. Heber, Chr. Liedke, H. Korte, E. Hoffmann-Posorske, A. Donella-Deana, L.A. Pinna, J. Perich, E. Kitas, R.B. Johns, and H.E. Meyer, *Chromatographia*, 34 (1992) 347–350.
43 H. Bruckner and C. Keller-Hoehl, *Chromatographia*, 30 (1990) 621–629.
44 H.E. Meyer, E. Hoffmann-Posorske, H. Korte, A. Donella-Dena, A.-M. Brunati, L.A. Pinna, J. Coull, J. Perich, R.M. Valerio and R.B. Johns, *Chromatographia*, 30 (1990) 691–695.
45 A.T. Balchunas and M.J. Sepaniak, *Anal. Chem.*, 59 (1987) 1466–1470.
46 T. Ueda, F. Kitamura, R. Mitchell, T. Metcalf, T. Kuwana and A. Nakamoto, *Anal. Chem.*, 63 (1991) 2979–2981.
47 S.L. Pentoney, X. Huang, D.S. Borgi and R.N. Zare, *Anal. Chem.*, 60 (1988) 2625–2629.
48 D.J. Rose and J.W. Jorgenson, *J. Chromatogr.*, 447 (1988) 117–131.
49 B. Nickerson and J.W. Jorgenson, *J. Chromatogr.*, 480 (1989) 157–168.
50 D.J. Rose, *J. Chromatogr.*, 540 (1991) 343–353.
51 T. Tsuda, Y. Kobayashi, A. Hori, T. Matsumoto and O. Suzuki, *J. Chromatogr.*, 456 (1988) 375–381.
52 D.Y. Chen, H.P. Swerdlow, H.R. Harke, J.Z. Zhang and N.J. Dovichi, *J. Chromatogr.*, 559 (1991) 237–246.
53 J.W. Chen, A. Cohen and B.L. Karger, *J. Chromatogr.*, 559 (1991) 295–305.
54 H. Drossman J.A. Luckey, A.J. Kostichka, J. D'Cunha and L.M. Smith, *Anal. Chem.*, 62 (1991) 900–903.
55 H. Swerdlow, H.R. Harke, S. Wu and N.J. Dovichi, *J. Chromatogr.*, 516 (1990) 61–67.
56 H. Swerdlow, J.Z. Zhang, D.Y. Chen, H.R. Harke, R. Grey, S. Wu, N.J. Dovichi and C. Fuller, *Anal. Chem.*, 63 (1991) 2835–2841.
57 Y.J. Kasper, M. Melera, P. Gozel and R.G. Brownlee, *J. Chromatogr.*, 458 (1988) 303–312.
58 S. Honda, *Anal. Biochem.*, 140 (1984) 1–45.
59 J. Liu, O. Shirota and M. Novotny, *J. Chromatogr.*, 559 (1991) 223–235.
60 J. Liu, O. Shirota and M.V. Novotny, *Anal. Chem.*, 63 (1991) 413–417.
61 J. Liu, O. Shirota and M.V. Novotny, *Anal. Chem.*, 64 (1992) 973–975.
62 W. Nashabeh and Z. El Rassi, *J. Chromatogr.*, 514 (1990) 57–64.
63 Z. Deyl, I. Miksik and R. Struzinsky, *J. Chromatogr.*, 516 (1990) 287–298.
64 S. Honda, S. Iwase , A. Makino and S. Fujiwara, *Anal. Biochem.*, 176 (1989) 72–77.

65 S. Honda, K. Yamamoto, S. Suzuki, M. Ueda and K. Kakehi, *J. Chromatogr.*, 588 (1991) 327–333.
66 M.E. Szulc and I.S. Krull, *Biomed. Chromatogr.*, (1992) in preparation.
67 A.J. Bourque and I.S. Krull, *J. Chromatogr.*, 537 (1991) 123–152.
68 F.-X. Zhou, B. Feibush and I.S. Krull, *J. Chromatogr.*, 648 (1993) 357–365.
69 F.-X. Zhou, I.S. Krull and B. Feibush, *J. Chromatogr.*, 609 (1992) 103–112.

Journal of Chromatography A, 659 (1994) 247–253
Elsevier Science B.V., Amsterdam

CHROM. 25 668

Ensemble averaging and digital filtering in chromatography and electrophoresis

Michael F. Regehr, Sandeep K. Paliwal and Fred E. Regnier*

Department of Chemistry, Purdue University, West Lafayette, IN 47907 (USA)

ABSTRACT

Ensemble averaging and digital filtering were implemented for signal-to-noise ratio improvement in the separation techniques of size-exclusion chromatography, immunoaffinity chromatography, capillary zone electrophoresis and capillary ion analysis. Results of ensemble averaging were always greater than statistically predicted. Techniques included five to nine replicate separations and yielded signal-to-noise improvement factors of 2.5 to 9.3. Running-average and time constant (RC)-convolution digital filters yielded increases in the signal-to-noise ratio ranging from zero to twelve. This paper will discuss and illustrate the usage of ensemble averaging and digital filtering in liquid-phase separation techniques.

INTRODUCTION

Efforts to lower detection limits are an ongoing trend in analytical chemistry. Sensitivity enhancement in liquid chromatography has been achieved by a variety of methods including the use of derivatizing agents, miniaturization, advances in electronics, optimization of absorbance detectors, and the introduction of laser fluorescence and electrochemical detection. Recent studies suggest that computational methods associated with data processing may be another method of increasing sensitivity.

Acquisition, storage and manipulation of digital data are becoming more accessible to the chromatography laboratory due to the increasing use of computers to automate chromatography systems. Recent trends in digital data handling can be found in the articles from "The Data File" column of Ouchi [1–5]. Digital data can be stored, displayed and analyzed regardless of the method used to perform a separation.

Data-handling software allows for easier display and reporting of chromatograms with the additional possibility of extensive computational analysis. The use of ensemble averaging and digital filtering to improve signal-to-noise (S/N) ratios in chromatographic and electrophoretic techniques will be examined here. Ensemble averaging is predicted to improve S/N ratios as the square root of the number of chromatograms summed [6]. The problem with ensemble averaging in chromatography had been that considerable time was required to carry out the multiple runs needed for averaging. Recent advances in liquid chromatography media allow separations of biological macromolecules to be achieved an order of magnitude faster [7]. Digital filtering improvements are dependent on the nature of the noise and the filter applied to the data.

Ensemble averaging was applied to four different separation techniques with the goal of lower-

* Corresponding author.

0021-9673/94/$07.00
SSDI 0021-9673(93)E1116-H

ing detection limits: size-exclusion chromatography for lysozyme, immunoaffinity chromatography for bovine IgG, capillary zone electrophoresis for α-amylase and capillary ion analysis for benzyltriethylammonium chloride.

EXPERIMENTAL

Materials

Potassium phosphate, magnesium chloride, sodium chloride and sodium sulfate were purchased from Mallinckrodt (Paris, KY, USA). Lysozyme, bovine IgG, α-amylase and Tris (TRIZMA) base were purchased from Sigma (St. Louis, MO, USA). Acetic acid was purchased from J.T. Baker (Phillipsburg, NJ, USA). Mesityl oxide and benzyltriethylammonium chloride were purchased from Aldrich (Milwaukee, WI, USA).

Size-exclusion chromatography (SEC)

Liquid chromatography was performed on the BioCAD HPLC system, a gift from PerSeptive Biosystems (Cambridge, MA, USA). SEC was achieved with an 300×8 mm column packed with TSK G3000SW packing material. Columns were packed according to manufacturers instructions on an HPLC column packer (Shandon Southern Instruments, Sewickley, PA, USA). The buffer contained 100 m*M* potassium phosphate and 100 m*M* sodium sulfate at pH 7.0. Flow-rate was 0.5 ml/min. The analyte was lysozyme (1 mg/ml). Absorbance was monitored at 254 nm. Chromatograms were transferred to Quattro Pro (Borland, Scotts Valley, CA, USA) and referenced by the point of injection.

Immunoaffinity chromatography (IAC)

IAC was performed on the BioCAD HPLC system with a 30×4.6 mm POROS A/M column (a gift from PerSeptive Biosystems). Loading buffer for the affinity column was the same as that for the SEC separation. Desorption buffer contained 0.3 *M* magnesium chloride and 2% acetic acid. Flow-rate was 3.0 ml/min. The bovine IgG analyte (1 mg/ml) was detected at 254 nm. Chromatograms were transferred to Quattro Pro and referenced by the point of injection.

Capillary zone electrophoresis (CZE)

CZE experiments were performed on the ISCO Model 3850 capillary electrophoresis system (ISCO, Lincoln, NE, USA). Data collection was achieved with a 486/33 personal computer (IBM compatible) running DAQWare to drive a PC-LPM-16 multifunction input/output board (National Instrument Corporation, Austin, TX, USA). The fused-silica capillary (Polymicro Technologies Inc, Phoenix, AZ, USA) was 45 cm total length (25 cm separation length) $\times$ 75 μm I.D. Applied voltage was 178 V/cm. Running buffer contained 50 m*M* TRIZMA base and 120 m*M* sodium chloride at pH 7.0. The analytes were mesityl oxide (1 mg/ml) and α-amylase (45 μg/ml) in TRIZMA–NaCl buffer. Detection was at 214 nm. Hydrostatic injections were made by 10 cm vertical displacement. Injection volumes were estimated hydrostatically. The instrument was set to 0.8 s rise times (10–90% response) and 0.005 AUFS output. Electropherograms were transferred to Quattro Pro and referenced on the mesityl oxide peak.

Capillary ion analysis (CIA)

CIA was performed on the ISCO Model 3850 capillary electrophoresis system utilizing the same data collection system and instrument settings noted above. The fused-silica capillary was 40 cm total length (20 cm separation length) $\times$ 103 μm I.D. The applied voltage was 300 V/cm. Running buffer contained 25 m*M* TRIZMA base at pH 7.0. The benzyltriethylammonium chloride analyte (30 n*M* in distilled water) was detected at 210 nm. Electrokinetic injections were performed at 12 kV for 20 s. Electropherograms were transferred to Quattro Pro and referenced to the benzyltriethylammonium migration peak.

RESULTS AND DISCUSSION

Ensemble averaging

Ensemble averaging has proven to be useful to increase S/N ratios in gas chromatography [6,8]. It involves repeated separations and the numerical addition of chromatograms. The advantage of this approach is that peak heights increase proportional to the number of chromatograms sum-

med (n), while amplitude of the baseline noise will only increase as the square-root of n [6]. Ensemble averaging four chromatograms should double the S/N ratio. Applications to liquid chromatography and electrophoresis have been hindered by the generally longer separation times required. The advent of perfusion chromatography and high-performance capillary electrophoresis have reduced separation times to a point where the time invested in ensemble averaging can be worth the effort.

Digital filtering

Digital filtering was performed within a spreadsheet by two algorithms: two-column and convolution. In the two-column method, mathematical equations indicating the desired derivation were placed alongside the column of data. The convolution algorithm required the establishment of a functional worksheet.

The running-average filter, the simplest application of the two-column algorithm, derives each filtered datapoint by averaging all values between a specified distance before and after the point being evaluated. The cells of the filtered-data column either contain an algebraic equation quoting each necessary cell of the original column, or utilize a spreadsheet function. Each datapoint is given equal weight in this evaluation. For example, a five-point running-average filter sums points $x-2$ through $x+2$ and normalizes with division by five.

A Savitsky–Golay filter [9] finds the filtered-data value from the least-squares fit to the portion of data under consideration. A weighted contribution scheme can be derived mathematically based on the dimensions of the data segment evaluated. For example, a five-point Savitsky–Golay filter is weighted (-3,12,17,12, -3) with a normalization constant of 35 [10].

The convolution algorithm utilizes spreadsheet functions or macros to approximate the convolution integration shown below.

$$h(x) = \int f(u)g(x-u)\,du$$

In the algorithm developed for our study, the Quattro Pro "sumproduct" function was used, multiplying each point of the convolving function (g) with the corresponding point of the data (f), and summing the products. The algorithm must be written for a specific length of data set and convolving function. Running-average and Savitsky–Golay filters can be run in a convolution algorithm by using a data set containing the appropriate weighing factors in place of the convolving function.

Ensemble averaging applications

Capillary electrophoresis has been widely applied to the separation of charged molecules. Narrow, fused-silica capillaries provide rapid heat dissipation and suppression of induced convection [11,12]. This allows application of larger axial field strengths. The result is a rapid, high-resolution separation. Application of ensemble averaging requires that migration times are reproducible over multiple runs [6]. Variation would broaden the ensemble-averaged peak and give S/N gains lower than expected. Two examples of compensation are illustrated in the electrophoretic applications.

CZE of α-amylase was performed using a marker to identify the position of the electropherogram in the collected data set. No further time scaling was done to compensate for variation of electroosmotic flow. Limits of detection were challenged by high current and a modest detector time constant. Ensemble averaging was performed with five electropherograms of 0.3-μl injections. A S/N enhancement of 2.5 was found when compared to a single injection (Fig. 1).

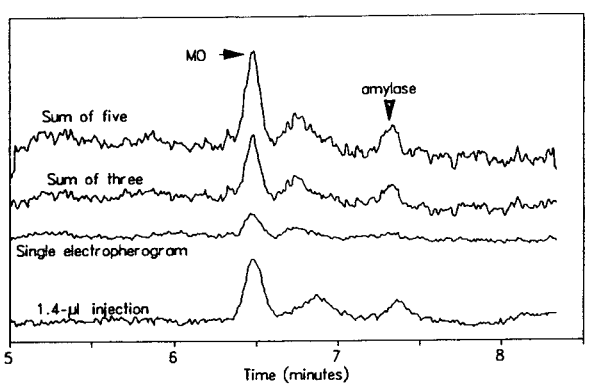

Fig. 1. Ensemble averaging of CZE electropherograms.

The ensemble average is now comparable to a single 1.4-μl injection.

CIA electropherograms showed a 7% R.S.D. variation in migration time of the analyte peak over nine sequential runs. This could be blamed on variations in interaction between the negatively charged silica surface and the positively charged analyte, the bane of bare silica in separations [13]. Ensemble averaging yielded meaningless peak heights until each data set was aligned such that analyte peaks coincided precisely. This was facilitated by a spreadsheet cut-and-paste option. A selected subset of the data (*i.e.* 20 s before and after the peak maximum) can be cut from the original data and pasted into a new area before averaging. A S/N enhancement of 3.3 compared to a single injection was achieved (Fig. 2).

SEC inherently leads to dilution of the sample component as it is being separated. This limits the use of this technique to moderately concentrated samples. Concentration has been known in a variety of cases [14] to induce dimer formation and skew the final results. Also, process stream samples can be run under overloaded condition, but resolution is lost. Therefore, there is a definite need to get better S/N ratios. Ensemble averaging nine chromatograms of 5-μl injections resulted in a S/N enhancement of 3.5 (Fig. 3). The result was baseline corrected by digital subtraction of a straight line approximating the baseline slope. The same correction would be possible with a median filter [15] if the peak were not so broad relative to the entire data set. Removal of pump noise will be addressed later in the digital filtering applications.

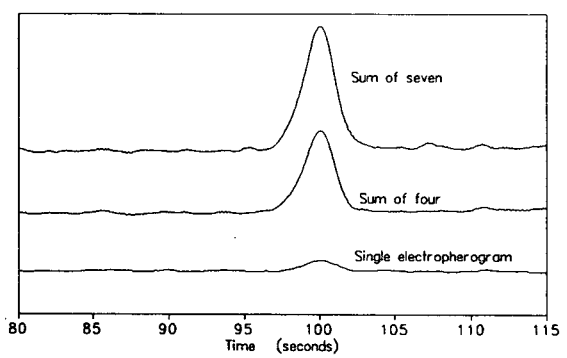

Fig. 2. Ensemble averaging of CIA electropherograms.

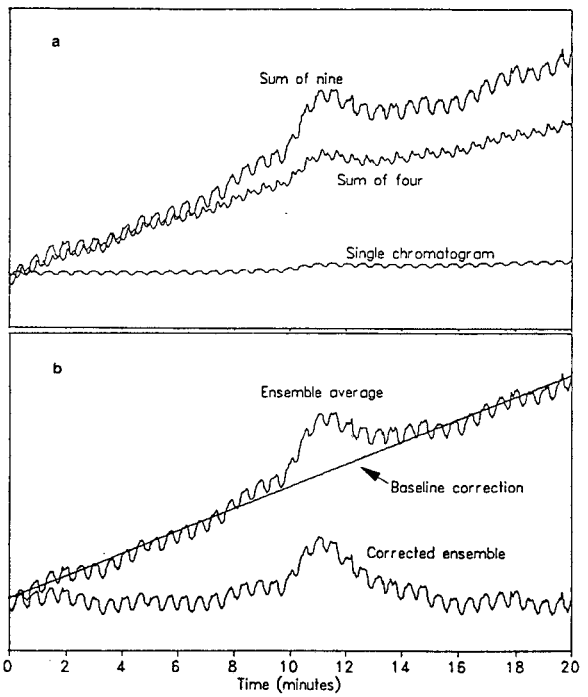

Fig. 3. (a) Ensemble averaging of SEC chromatograms. (b) Baseline subtraction of SEC ensemble average.

With the advent of perfusion chromatography [7,16,17], it is now routinely possible to do very-high-speed separations. This form of chromatography utilizes the throughpores of the particles, thus permitting the use of very high flow-rates and diminishing mass transfer. Column back pressure remains significantly low under these conditions. Perfusion chromatography has major implications in process monitoring. Recently, production and purity of anti-fibronectin antibody was analyzed on-line from CRL-1606 hybridomas [18]. A similar immunoaffinity procedure was performed here with low levels of bovine IgG. Elution peaks did not appear in chromatograms of 2-μl injections. For such an experiment, ensemble averaging would be the technique of choice to enhance peak height (Fig. 4a). Background subtraction compensated for baseline drift (Fig. 4b). Ensemble averaging seven chromatograms of 2-μl injections resulted

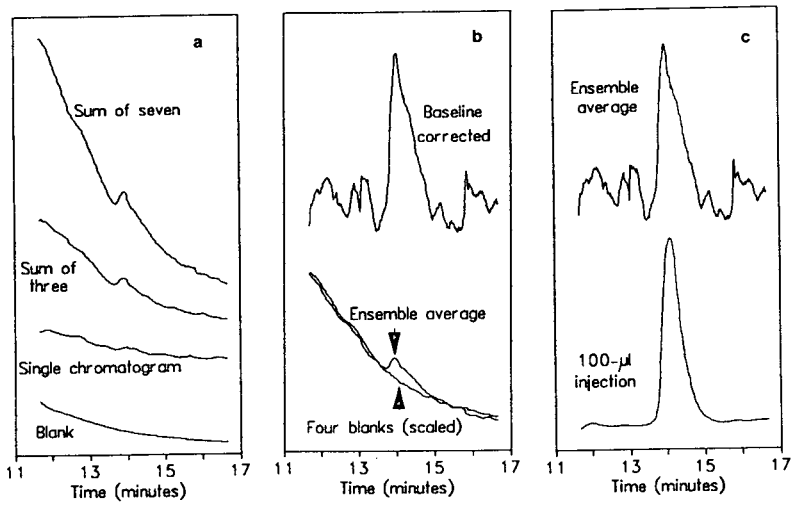

Fig. 4. (a) Ensemble averaging of IAC chromatograms. (b) Blank subtraction for baseline correction of IAC ensemble average. (c) Comparison of IAC ensemble averaging to larger injection.

in a S/N enhancement of 9.3. Comparison of the ensemble average to a 100-µl injection demonstrates the S/N enhancement and that the elution time is not distorted (Fig. 4c). In all four techniques, the experimental enhancement from ensemble averaging was greater than the $\sqrt{n}$ factor expected.

Digital filtering applications

Digital filtering of chromatograms and electropherograms is not to be considered a perversion of empirical data. Manipulation of the time constant (RC or τ) of absorbance detectors has been an acceptable method for smoothing baselines. This is an analog filtering technique which is often ignored. Use of an RC waveform in a convolution algorithm mimics the function of the time constant with a digital filter.

Electropherograms were taken with the same CZE capillary and buffer used previously, but analyte and voltage were not applied (Fig. 5). The result was white noise (noise of equal intensity at all frequencies) due to limitations of the apparatus. As Hieftje [19] has given the standard deviation of the samples to be equivalent to the noise, N, it was used to make comparisons. The standard deviation of each 2-min data sample (600 data points) was determined for various time constants.

Increased detector time constants resulted in decreased noise levels. The same noise reduction was possible by digital filtering. If the recording of $\tau = 0.05$ s was considered "unfiltered" data, we could mimic the effects of the detector settings. Reversed RC-decay waveforms were produced as exp (time/τ). Convolution of the "unfiltered" data set with the decay functions produced a pattern of noise reduction similar to the analog filter. Variations can be attributed to the assumptions that a 0.05-s time constant was non-filtering, time constants of the detector were accurately reported, and the white noise was

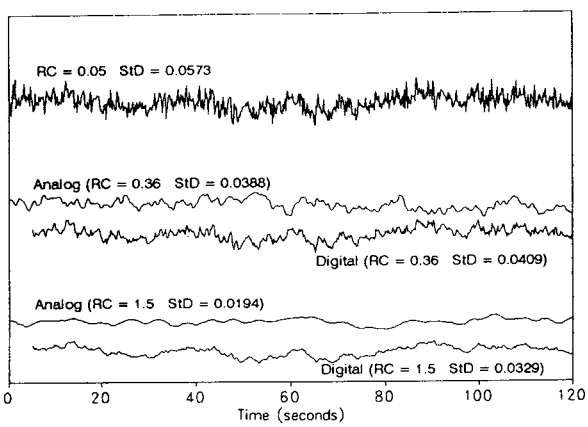

Fig. 5. Comparison of analog and digital baseline smoothing based on the time constant of the filters and the standard deviation of the data.

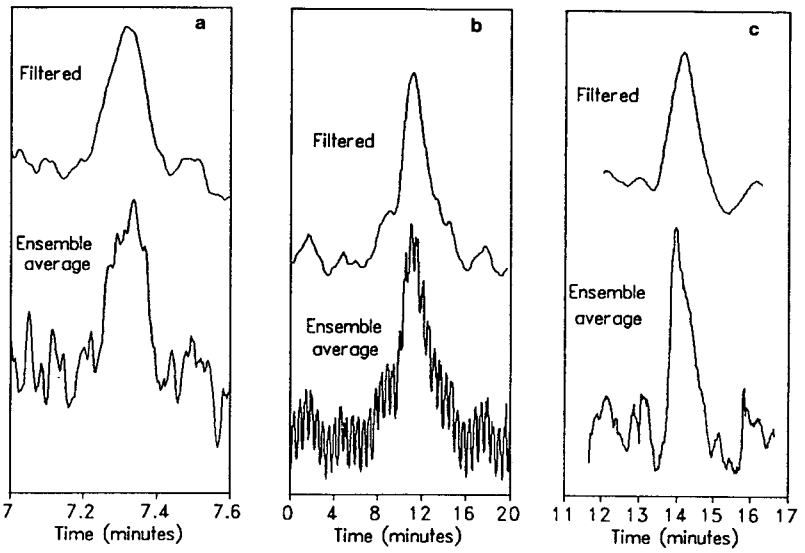

Fig. 6. (a) RC filtering of CZE ensemble average. (b) Running-average filtering of SEC ensemble average. (c) Running-average filtering of IAC ensemble average.

statistically invariant throughout the data collection process.

For electrophoretic experiments, the RC-convolution filter was applied because it mimicked the analog filtering normally conducted by the detector. This showed greater improvement than running-average or Savitsky–Golay filters, and the noise spectrum was assumed to be white. A 3-s τ was used to generate a 26-point (5.2-s) waveform resulting in a S/N increase of eight for the CZE ensemble average (Fig. 6a). The same filter gave no measurable S/N improvement when applied to the ensemble average of the CIA experiment.

For SEC and IAC, the major noise source was pressure variation throughout the cycle of the pump piston. This was proven by monitoring the column back pressure. The apparent frequency of the pump noise was found from either the absorbance or pressure recordings. Frequency may be aliased[a] dependent on rate of data acquisition. The running-average filter selectively removed the pump noise. The SEC ensemble average was filtered with a 33-s running-average, giving a S/N increase of twelve (Fig. 6b). The IAC ensemble average was filtered with a 45-s running average, giving a S/N increase of 4.5 (Fig. 6c).

The selectivity of this method can be explained in two ways. Most simply, the width of the running average was chosen so as to extend one wavelength [(noise frequency)$^{-1}$] and would reflect a net contribution of zero from the pump noise. The selectivity can also be explained by the frequency-domain behavior of the filter. In the time domain, the running-average filter is a square pulse with a maximum of one. The Fourier transform (conversion between the time and frequency domain) is the sinc function $\{=[\sin(\pi\nu)]/(\pi\nu)\}$ (Fig. 7). Since convolving two functions or data sets is the same as multiplying their Fourier transforms, the pulse will eliminate all frequencies $x\nu_0$ or x/τ_0 [10] where τ_0 is the pulse width. The first crossing was used for frequency cancellation because higher crossings require even greater pulse widths for the same noise frequency.

CONCLUSIONS

This paper demonstrates that techniques are now applicable for ensemble averaging and digital filtering chromatographic and electrophoretic data. In each experiment, the ensemble average

[a] The term aliasing is from the Nyquist Sampling Theorem and describes how frequencies greater than half the sampling frequency (f_N) will yield an erroneous frequency between 0 and f_N.

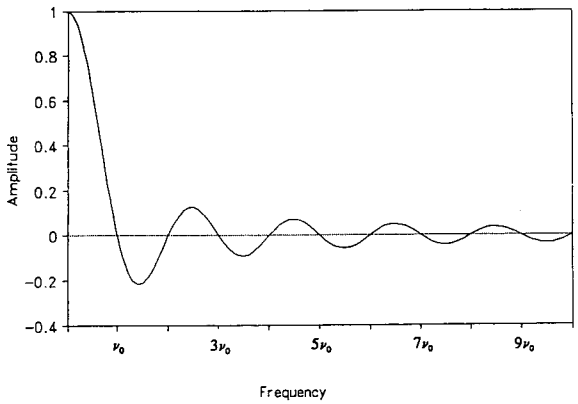

Fig. 7. A running-average filter is a sinc function in the frequency domain where the filter width is defined as τ_0 or $(\nu_0)^{-1}$.

increased the S/N ratio by a factor at least as large as the square root of the number of chromatograms summed. Digital filtering can take many forms, from baseline subtraction to filter convolution algorithms. S/N gains ranged from none to twelve, and were dependent on the type and degree of noise present.

ACKNOWLEDGEMENTS

This work was supported by NIH grant number GM-25431. M.F.R. acknowledges Fellowship support from the Department of Education and DuPont.

REFERENCES

1 G. Ouchi, *LC·GC*, 9 (1991) 474.
2 G. Ouchi, *LC·GC*, 9 (1991) 628.
3 G. Ouchi, *LC·GC*, 9 (1991) 767.
4 G. Ouchi, *LC·GC*, 10 (1992) 106.
5 G. Ouchi, *LC·GC*, 10 (1992) 436.
6 L. Ghaoui and L.D. Rothman, *J. High Resolut. Chromatogr.*, 15 (1992) 36.
7 N.B. Afeyan, N.F. Gordon, I. Mazsaroff, L. Varady, S.P. Fulton, Y.B. Yang and F.E. Regnier, *J. Chromatogr.*, 519 (1990) 1.
8 L.J. Lorenz, R. Culp and L.B. Rogers, *Anal. Chem.*, 42 (1970) 979.
9 H.H. Madden, *Anal. Chem.*, 50 (1978) 1383.
10 F.E. Lytle, *Signal-to-Noise Enhancement in Analytical Chemistry*, Purdue University, West Lafayette, IN, 1992, in preparation.
11 J.W. Jorgenson and K.D. Lukacs, *Anal. Chem.*, 53 (1981) 1298.
12 S. Hjertén, *J. Chromatogr.*, 270 (1983) 1.
13 J.K. Towns and F.E. Regnier, *Anal. Chem.*, 64 (1992) 2473.
14 T.K. Nadler, S.K. Paliwal and F.E. Regnier, *J. Chromatogr.*, submitted for publication.
15 A.W. Moore, Jr. and J.W. Jorgenson, *Anal. Chem.*, 65 (1993) 188.
16 F.E. Regnier, *Nature*, 350 (1991) 634.
17 S.P. Fulton, N.B. Afeyan, N.F. Gordon and F.E. Regnier, *J. Chromatogr.*, 547 (1991) 452.
18 S.K. Paliwal, T.K. Nadler and F.E. Regnier, *Anal. Chem.*, in press.
19 G.M. Hieftje, *Anal. Chem.*, 44 (1972) 81A.

Journal of Chromatography A, 659 (1994) 255–259
Elsevier Science B.V., Amsterdam

CHROM. 25 603

Comparison of two injection systems to be used with 5 μm I.D. open-tubular columns

Antonio L. Crego, Manuel V. Dabrio and José C. Díez-Masa*

Instituto de Química Orgánica General (CSIC), Juan de la Cierva 3, 28006 Madrid (Spain)

(First received June 25th, 1993; revised manuscript received September 29th, 1993)

ABSTRACT

The split injection system and the pressure pulse-driven stopped-flow injection system (PSI) were compared in terms of band broadening and sample injection volume reproducibility for 5 μm I.D. open-tubular columns. It was found that the PSI injector has a better injection profile factor than the split injector, maximum column efficiency being obtained with higher injection volumes (ten times) using the PSI injector. The repeatability of the injected volumes obtained with the PSI injector is twice as good as that with the split injector. The peak efficiency reproducibility is similar with both injectors (R.S.D. = 3–4%).

INTRODUCTION

The use of open-tubular columns (OTCs) in high-performance liquid chromatography (HPLC) is promising in microseparation techniques. Plate counts higher than $0.5 \cdot 10^6$ m^{-1} [1], plate generation velocities around 1000 s^{-1} [1,2] and enhanced mass sensitivity [3] have been obtained using such columns. Despite their advantages, OTCs are not as popular in HPLC as their counterparts in gas chromatography. This may be due to the demanding features of the injection and detection systems associated with these columns.

The maximum sample volume (V_{inj}) to be injected into an HPLC column for a relative loss in the plate number smaller than Θ^2 is given by [4]

$$V_{inj} = (\pi/4)\Theta^2 K\varepsilon(1 + k')(L/\sqrt{N})d_c^2 \quad (1)$$

where N is the column plate number, k' is the solute capacity factor, L is the column length, ε is the porosity of the packed bed ($\varepsilon = 1$ for OTCs), K is the injection profile factor and d_c is the inner diameter (I.D.) of the column. As OTCs should have very small d_c (<10 μm) to achieve a very high plate generation velocity [1], the injection volume should be as small as a few picolitres to achieve a very small efficiency loss ($\Theta^2 < 0.05$). The injection of such a small amount of sample in a reproducible way without excessive band broadening is a major challenge in OTC instrumentation design.

Several injection systems, including stopped-flow [5,6], sample tube technique [7], in-column injection [7,8], split injection [9], groove injection [10], heart-cut injection [11], moving injection technique (MIT) [12,13] and pressure pulse-driven stopped-flow injection (PSI) [14] have been used with OTCs. However, only a few of them (split injector, MIT and PSI) can introduce subnanolitre-range sample volumes accurately. It has been shown [15,16] that, for fairly large I.D. (>40 μm) columns, the MIT system shows poor reproducibility (R.S.D. > 24%) when the sample volume injected approaches the subnanolitre range.

In this work, we compared the simple and

* Corresponding author.

0021-9673/94/$07.00
SSDI 0021-9673(93)E1034-W

cost-effective split injection system with the more sophisticated and expensive PSI system in terms of band broadening and injection volume reproducibility when used with 5 μm I.D. OTCs.

EXPERIMENTAL

Samples and chemicals

The mobile phase [water–methanol (30:70, v/v)] was prepared by mixing water purified with a Milli-Q system (Millipore, Bedford, MA, USA) with HPLC-quality methanol (Scharlau, Barcelona, Spain). The mobile phase was degassed by sparging with helium for 30 s. In all experiments, the sample was phenanthrene (Fluka, Buchs, Switzerland) dissolved in methanol.

Instrumentation

The OTCs utilized were prepared following the method described elsewhere [1] using fused-silica capillary tubing of 5 μm I.D. × 365 μm O.D. (Polymicro Technologies, Phoenix, AZ, USA). In the determination of the injection profile factors, empty open-capillary tubing (without stationary phase) was employed instead of the column.

The chromatographic system was composed of a Model 590 pump (Waters, Milford, MA, USA) and a Waters Model 440 detector. This detector was modified in-house for on-column monitoring, featuring an illuminated volume of *ca.* 6 pl. The split injection system consisted of a VICI CI4W injection valve with an internal 60-nl sample loop (VICI, Valco Europe, Schenkon, Switzerland), a Swagelock SS-1FO-36C T-piece (Crowford Fitting, Solon, OH, USA) and fused-silica capillaries of several sizes (I.D. and length) (Polymicro Technologies) used as restrictors. The PSI system was similar to that described by Claessens *et al.* [16] and was kindly lent by Dr. Van Tilburg (Valco Europe). This injection system consisted of two VICI C6W valves, a VICI C3W valve (all from VICI, Valco Europe) and a digital valve sequence programmer (DVSP) from Valco. Each valve was rotated using a Valco A4C10WT helium actuator, two of which were equipped with Model 125A pilot valves (Humphrey Products, Kalamazoo, MI, USA) for fast valve switching. The actuation sequence of the valves was controlled by the DVSP and six three-way solenoid valves. The gas pressure [4 atm (1 atm = 101 325 Pa)] used to pulse the sample into the column, wash the system and move the actuators was obtained from a C55-quality helium cylinder (Carburos Metalicos, Madrid, Spain).

Procedures

The sample volume injected (V_{inj}) using the PSI system depends on the pressure applied (P_i) during the pulse, the pulse time (t_i), and the characteristics of the column used. It has been calculated that

$$V_{inj} = \frac{\pi}{4} \cdot \frac{d_c^4}{\eta L \phi} \cdot P_i t_i \quad (2)$$

where η is the viscosity of the mobile phase, ϕ is the column flow resistance (32 for an OTC) and the other parameters are as defined above. For a given P_i, the volume injected can be calculated using eqn. 2 if the injection time is known.

The volume injected with the split injector was estimated using data obtained from the PSI injector. A straight line ($r = 0.9996$) for the plot of the peak area *versus* the volume injected was obtained using the PSI injector. Using the same sample, the volume injected from the split injector was deduced by interpolating the peak area obtained in each instance. The area used in these calculations was an average of six injections for each point.

The area under the peak was calculated by multiplying the peak height by the peak width at half-height, which was measured using a magnifying glass. As, the peaks were symmetrical in this work, this was an easy and exact method for area measurement.

Peak efficiency was calculated from the peak width at half-height on the recorder trace obtained at increased paper speed. The peak width at half-height was also used to calculate the peak variance in those instances where the injection profile factor (K) of the injector was measured.

RESULTS AND DISCUSSION

Performance

The efficiency (N) obtained depends on the efficiency of the column itself (N_{col}) and the contribution of the extra-column effects to the band broadening. If it is accepted that here the contribution of the detector to the band broadening is very small ($\Theta^2 < 5\%$), the efficiency obtained is given by the equation

$$\frac{1}{N} = \frac{1}{N_{col}} + \frac{V_{inj}^2}{K} \cdot \frac{1}{V_R} \quad (3)$$

where V_{inj} is the sample volume, K is the injection profile factor and V_R is the retention volume of the sample. According to Eqn. 3, the contribution of the injector to the band broadening can be considered to be negligible when the efficiency obtained does not change with the volume injected. The variation of $1/N$ with the sample volume using the split and PSI systems is shown in Fig. 1. In both instances, as predicted by Eqn. 3, the efficiency decreases with increasing sample volume from a given V_{inj} value. Fig. 1 also shows that to avoid a significant efficiency loss (<5%) using the split injector, a sample volume smaller than 1 pl should be injected into the column, whereas the same efficiency loss is obtained when as much as 10 pl are injected with the PSI injector. As deduced from Eqn. 3, for a given sample retention, the maximum injected volume without considerable efficiency loss depends on the injection profile factor (K) of the injector used.

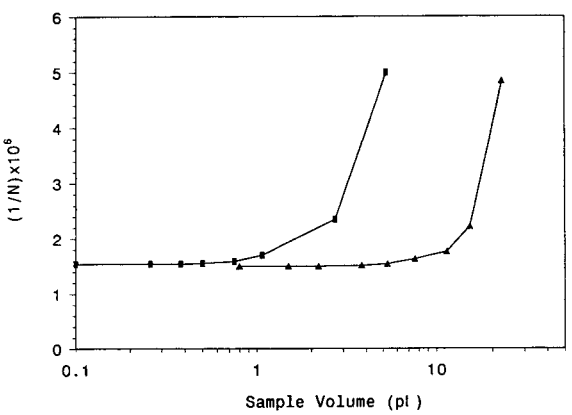

Fig. 1. Semi-logarithmic plot of the inverse of the column efficiency *versus* sample volumes injected for (□) the split injector and (▲) the PSI injector. Conditions, splitting ratio and pulse times correspond to Tables I and II.

We measured the K^2 value for both injection systems studied utilizing an empty capillary tube (100 cm × 5 μm I.D.) instead of the column. The plot of the phenanthrene peak variance *versus* the square of the injection volume gave a good straight line ($r = 0.999$) for a wide range of injection volume (2–35 pl) in both instances. From the slopes of these lines, values of $K^2 = 3.6$ and 7.0 were obtained for the split and the PSI injector, respectively. These values demonstrate that the PSI injector gives a better quality injection (more like ideal plug injection for which $K^2 = 12$) than the split injector. Consequently, larger sample volumes can be injected without any significant efficiency loss using the PSI injector. Data from Claessen *et al.* [16] suggest that the range of injection volumes to give $K^2 > 6$ with the PSI injector decreases with decreasing column I.D. This could justify why, when using 5 μm I.D. columns, sample volumes in the picolitre range should be injected to obtain a similar K^2 value. Further, Claessen *et al.* also observed that K^2 increases with increasing volume injected. This result was not observed in this work, probably because we studied a much smaller sample volume range.

Reproducibility

Another important feature of the injection system is its reproducibility, because of its effect on the precision in quantitative analysis. We compared the two injection systems in terms of sample injection volume and efficiency reproducibility. The results obtained for the split injector and the PSI injector are given in Tables I and II, respectively. Sample reproducibility was deduced from the peak area obtained for the sample peak. The sample injection volume estimated and calculated for the split injector and the PSI injector, respectively, are given in the second column in each table. In both experiments the area irreproducibility was not due to flow variations because the flow stability was better than 0.1%, as was deduced from the R.S.D. for sample retention. It can be concluded

TABLE I

SAMPLE AND EFFICIENCY REPRODUCIBILITY OBTAINED USING THE SPLIT INJECTOR

Open-tubular column, 120 cm × 5 μm I.D.; stationary phase, chemically bonded silica gel C_{18}; mobile phase, water–methanol (30:70, v/v); mobile phase linear velocity, 1.1 mm/s; sample, phenanthrene ($k' = 0.1$) in methanol (1 mg/ml); detection, on-column at 254 nm.

Estimated splitting ratio	V_{inj} [a] (pl)	R.S.D.$_{V_{inj}}$ [b] (%)	Efficiency (plates)	R.S.D.$_N$ [b] (%)
60 000	5.2	8.0	200 000	4.0
120 000	2.7	10.5	424 000	4.5
360 000	0.8	11.6	627 600	3.5
607 000	0.5	15.0	645 600	4.0
1 215 000	0.3	18.0	646 850	3.7

[a] The sample injected was estimated using the area under the phenanthrene peak (see Experimental).
[b] Relative standard deviation ($n = 6$).

from Tables I and II that the injection volume reproducibility decreases with increasing volume injected with both injectors. For the same volume injected (*ca.* 5 pl), the reproducibility of the PSI injector (R.S.D. ≈ 4%) is better than that obtained with the split injector (R.S.D. ≈ 8%). Further, the reproducibility of the PSI injector is roughly three times better than that of the split injector at maximum column efficiency with the highest volumes injected. These results show that the PSI injector is better than the split injector in terms of sample injection volume reproducibility, particularly when the maximum column efficiency has to be achieved with the maximum sample volume. This could be the case in trace analyses of complex samples. In terms of peak efficiency reproducibility, which could be of some interest in theoretical studies for OTCs, both injection systems give similar reproducibility (R.S.D. = 3–4%). This value is fairly good when compared with the reproducibility obtained for injections in packed columns using sample valves (R.S.D. ≈ 2.5%).

TABLE II

SAMPLE AND EFFICIENCY REPRODUCIBILITY OBTAINED USING THE PSI INJECTOR

Conditions as in Table I.

Pulse time (s) (at 4 atm)	V_{inj} [a] (pl)	R.S.D.$_{V_{inj}}$ [b] (%)	Efficiency (plates)	R.S.D.$_N$ [b] (%)
7.03	22.7	1.7	206 400	2.7
3.51	11.4	2.4	566 300	3.1
1.64	5.3	3.8	646 900	3.3
1.17	3.8	4.3	660 600	3.4
0.69	2.2	5.4	663 000	3.2

[a] Sample volume calculated using eqn. 2.
[b] Relative standard deviation ($n = 6$).

CONCLUSIONS

This study has demonstrated that the PSI injector presents a better injection profile factor than the split injector. Subsequently, although maximum efficiency of the 5 μm I.D. columns can be achieved using both injectors, larger injection volumes (ten times) can be injected with the PSI injector without a substantial efficiency loss. The sample injection volume reproducibility obtained using the PSI injector is twice as good as that obtained with the split injector using 5 μm I.D. columns. This PSI injector feature is important with regard to quantitative analysis using OTCs. Finally, in terms of cost effectiveness, the PSI injector is about five times more expensive than the less sophisticated split injector.

ACKNOWLEDGEMENTS

This work was supported by CICYT (grant No. PB91-0077-C03-02). Thanks are due to M. van Tilburg (VICI, Valco Europe) for the loan of the PSI injector and to M. Campos for technical assistance.

REFERENCES

1 A.L. Crego, J.C. Díez-Masa and M.V. Dabrio, *Anal. Chem.*, 65 (1993) 1615.
2 C.A. Moning, D.M. Dohmeier and J.W. Jorgenson, *Anal. Chem.*, 63 (1991) 807.
3 M. de Frutos, S.K. Paliwal and F. Regnier, *Anal. Chem.*, 65 (1993) 2159.
4 M. Martin, C. Eon and G. Guiochon, *J. Chromatogr.*, 108 (1975) 229.

5 Y. Hirata and M. Novotny, *J. Chromatogr.*, 186 (1979) 521.
6 D. Ishii and T. Takeuchi, *J. Chromatogr. Sci.*, 18 (1980) 462.
7 M.J. Capacci and M. Sepaniak, *J. Liq. Chromatogr.*, 9 (1986) 3365.
8 T. Tsuda, K. Tsuboi and K. Nakagawa, *J. Chromatogr.*, 214 (1981) 283.
9 T. Tsuda and M. Novotny, *Anal. Chem.*, 50 (1978) 271.
10 V. Berry and K. Lawson, *J. High Resolut. Chromatogr. Chromatogr. Commun.*, 11 (1988) 121.
11 V.L. McGuffin and M. Novotny, *Anal. Chem.*, 55 (1983) 580.
12 M. Harvey and S. Stearns, *J. Chromatogr. Sci.*, 21 (1983) 83.
13 M. Harvey and S. Stearns, *Anal. Chem.*, 56 (1984) 837.
14 A. Manz and W. Simon, *J. Chromatogr.*, 387 (1987) 187.
15 V. Berry and K. Lawson, *J. Liq. Chromatogr.*, 10 (1987) 3257.
16 H.A. Claessens, A. Burcinona and C.A. Cramers, *J. Microcol. Sep.*, 2 (1990) 132.

Journal of Chromatography A, 659 (1994) 261–265
Elsevier Science B.V., Amsterdam

CHROM. 25 634

Reordering/resolvation studies of alkylamide phases

P. Kasturi, B. Buszewski[☆], M. Jaroniec and R.K. Gilpin*

Department of Chemistry, Kent State University, Kent, OH 44242 (USA)

(First received August 7th, 1993; revised manuscript received October 5th, 1993)

ABSTRACT

A series of chemically bonded liquid chromatographic packings containing a specific interaction site localized in the interior region of the attached ligands has been prepared by a two-step synthetic route. In the first-step an amino phase is formed and then it is converted to an alkylamide group via reaction with an acid chloride. Using this procedure materials have been prepared with immobilized terminal alkyl groups with chain lengths ranging from C_5 to C_8. Subsequently, the conformation of these modified surfaces have been investigated as a function of temperature under totally aqueous mobile phase conditions. Plots of ln k' *vs.* $1/T$ curves have been found to be similar to those reported for alkyl phases. However, the onset of reordering/resolvation of the attached ligands is shifted to lower temperatures and the incremental change per methylene group is smaller.

INTRODUCTION

Separations in reversed-phase liquid chromatography are based on a combination of specific and non-specific interactions which arise between the solute, the eluent and the bound interfacial layer. The dominance of particular interactions over others is controlled by electronic and structural properties of the solute, composition and secondary additives in the mobile phase [1–3], and the structure and dynamics of the bonded layer [1,3–6] as well as experimental variables such as temperature. Although a large volume of experimental data have been collected using reversed-phase systems, many aspects of the mechanisms controlling separations still are not understood clearly, especially in terms of the microscopic properties of the surface and the complex interplay between the bonded ligands, intercalated solvent and underlying silanol groups.

The most often used reversed-phase systems are alkyl-modified silica (*i.e.*, which contain either C_8 or C_{18} ligands) in combination with aqueous binary eluents such as methanol–water and acetonitrile–water [1,2,7]. Thus, a considerable amount of effort has been directed towards characterizing the surface of these packings in terms of the degree of coverage, the influence of alkyl chain length, the effect of structure and heterogeneity of the underlying surface [1,4–6,8] as well as the importance of more complex features such as conformation, organization and dynamics of the interface [1–3,9,10]. Under certain conditions large differences in conformation and organization of the immobilized ligands may be observed [1–6,9–12].

Previously, systematic investigations have been carried out using high to totally aqueous eluents in order to examine the orientation of chemically immobilized alkyl chains [11,13–18]. In these studies various system parameters have been examined such as alkyl chain length [13–21], bonding density [13], attachment chemistry [19], heterogeneity of the silica [20], solute structure [21] as well as temperature and concentration of trace organic modifier present in hydro–organic mobile phases [13–17]. Under

* Corresponding author.
☆ Permanent address: Faculty of Chemistry, Maria Curie Sklodowska University, Pl-20 031 Lublin, Poland.

0021-9673/94/$07.00
SSDI 0021-9673(93)E1080-J

such conditions non-linear thermal behavior is observed which can be explained on the basis of a two-state model where the alkyl chains assume either a folded or extended configuration depending on the experimental conditions. The initial temperature at which there is a change in the conformation of the bound alkyl chain has been termed the reordering/resolving temperature (T_0). In the current work this same approach has been used to examine a new class of phases which contain an alkyl tail attached to the surface via an alkylamide group.

EXPERIMENTAL

Reagents and materials

The LiChrosorb Si-60 silica, which was used to prepare the chemically bonded phases, was from EM Science (Cherry Hill, NJ, USA) and the remaining reagents used for surface modification, γ-aminopropyltriethoxysilane, pentanoyl chloride, hexanoyl chloride, heptanoyl chloride, octanoyl chloride and morpholine were purchased from Aldrich (Milwaukee, WI, USA). Likewise, the solvents, methanol, acetonitrile, 2-propanol, toluene and *n*-hexane, were from Aldrich. The remaining chemicals which were used as test solutes, 4-hydroxybiphenol (HBP) and 4-ethylphenol (EP), were obtained from Sigma (St. Louis, MO, USA). The deionized water, was purified in-house using a Millipore (El Paso, TX, USA) Model Milli-Q reagent water system.

Column preparation

Chemically bonded phases were prepared via a two-step synthesis as previously described [4]. In the first step, the silica was placed in a glass reactor, dried under vacuum (10^{-2} Pa) for 12 h, and reacted with γ-aminopropyltriethoxysilane. In the second step, chain lengths ranging from C_5 to C_8 were attached to the initially modified aminopropyl surface by treating it with a given acid chloride [4,22,23]. Subsequently, about 1.0 g of the modified silica was made into a slurry with 30 ml of 2-propanol and placed in a dynamic packing apparatus [24]. The 60 mm × 2.1 mm I.D. stainless-steel columns were packed in upward fashion under a pressure of 50 MPa using a Haskel (Burbank, CA, USA) Model DSTV-52C air-driven fluid pump and methanol as the delivery solvent.

Equipment

The chromatographic system consisted of a Spectra-Physics (San Jose, CA, USA) Model SP-8810 precision isocratic pump, a Model Spectra 100 variable-wavelength UV detector, set at 254 nm, and a Model Chromjet integrator. Samples were injected using a Rheodyne (Berkeley, CA, USA) Model 7125 valve equipped with 20-μl loop. In all chromatographic experiments the flow-rate was monitored using a Phase Separation (Queensferry, UK) Model F108OA flow meter and the columns were maintained to within ± 0.1 K using a Fisher Scientific (Pittsburgh, PA, USA) Model 9500 Isotemp refrigerated circulator bath.

Thermal studies

All thermal investigations were carried out according to methods described previously [13–20]. In doing this, columns were initially conditioned with 100 ml of acetonitrile followed by an equal volume of water. Subsequently, solute retention (HBP and EP) was measured every 5 K from 278 K to 333 K at a flow-rate of 1 ml/min using water as the eluent (initial evaluation). Following this initial run the column was cooled to the starting temperature and a second set of data collected in a similar fashion (reevaluation).

RESULTS AND DISCUSSION

In the current study, four different alkylamide phases were prepared by a two-step reaction which has been discussed elsewhere [4,22,23]. In the first step, the silica was treated with γ-aminopropyltriethoxysilane in a sealed glass reactor in order to form aminopropyl modified silica which had a coverage of 4.66% carbon and 1.09% nitrogen. Based on the elemental nitrogen results, the bonding density of the attached aminoalkylsilyl groups was 0.88 mmol per gram of reacted silica [25,26]. Further by assuming that the elemental carbon data also should give the same bonding density on an average one residual ethoxy group remained per bonded amino-

alkylsilyl molecule. The presence of residual alkoxy groups following surface modification of silica with trialkoxysilanes have been observed by others [26,27]. Subsequently, materials with C_5, C_6, C_7 and C_8 terminal alkyl groups were prepared by treating the aminoalkyl phase with the corresponding acid chloride. Each of the final phases were examined by solid-state NMR spectrometry [8,12,22,23] as well as elemental analysis. The corresponding coverages for the four different phases are summarized in Table I. The results from the elemental carbon analysis are summarized in the second column and the corresponding calculated bonding densities, assuming no loss of the remaining ethoxy groups in the first-step of the reaction, appear in the third column. Based on these numbers the degree of amidization was statistically equivalent and was approximately 75% complete for the four different phases. However, the overall degree of amidization becomes better if some of the ethoxy groups were lost during the secondary modification (*i.e.*, the ethoxy groups were converted to hydroxyl groups). For example, a 50% loss in the ethoxy groups would result in a 93% reaction yield. Unfortunately, based only on the elemental analysis data it is not possible to determine the exact extent of the amidization reaction. As such, isotopic labelling work is in progress in order to further elucidate the chemical nature of the final alkylamide phases.

Shown in Fig. 1 is a representative plot of ln k' *vs.* $1/T$ for 4-ethylphenol on the octylamide phase. Similar plots were obtained for the other phases with C_5, C_6 and C_7 terminal alkyl chains.

TABLE I

SURFACE COVERAGE AND ON-SET TEMPERATURE FOR THE ALKYLAMIDE-MODIFIED MATERIALS

R = Length of the terminal alkyl chain; P_c = carbon loading (%); N_A = bonding density (mmol/g); T_0 = mean values determined from multiple injections of the two solutes (K).

R	P_c	N_A	T_0
$-C_5H_{11}$	8.38	0.66	284.0
$-C_6H_{13}$	9.01	0.66	293.7
$-C_7H_{15}$	9.47	0.64	300.2
$-C_8H_{17}$	10.29	0.68	306.8

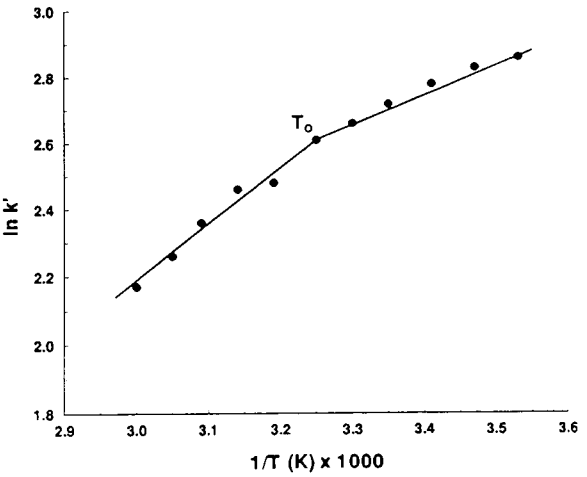

Fig. 1. Plot of ln k' *vs.* $1/T$ for 4-ethylphenol chromatographed on the octylamide phase using neat water as the eluent. Flow-rate: 1 ml/min. The onset temperature for reordering/resolvation is 306.8 K.

In all cases biphasic behavior was observed which is consistent with trends reported in other studies of silica modified with linear alkyl groups [13–20] and phases containing alkyl chains with terminal polar groups [18]. In these earlier studies the biphasic behavior was explained in terms of a major conformational change in the immobilized ligands between a folded aggregated state and an extended solvated state.

Listed in Table I are the mean onset temperatures (T_0) obtained from plots of ln k' *vs.* $1/T$ for the four different phases prepared in the current study. These values were obtained by fitting the lower and higher temperatures region of the Van 't Hoff plots by linear regression analysis and using the slope and intercept values of the fits to determine the onset temperature. In most cases the regression fits were 0.99 or better. Shown in Fig. 2 is a plot of T_0 *vs.* carbon number in the terminal alkyl portion of the immobilized ligand. Also shown in the same figure are the error bars for the mean T_0 values which reflect the precision of the measurements made using two different solutes. As has been reported for normal alkyl phases [28], an incremental increase in T_0 was observed per addition of a methylene unit. However, for the current phases the change was smaller (*i.e.*, 7.4 ± 0.7 K per methylene unit)

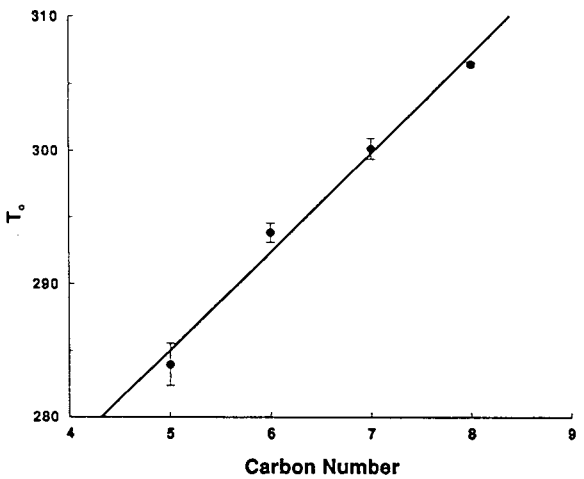

Fig. 2. Plot of T_0 (K) *vs.* number of carbon atoms in the terminal alkyl chain.

compared to normal hydrocarbon phases (*i.e.*, 9.5 ± 1.1 K per methylene unit). Based on a statistical analysis of the two data sets (*i.e.*, *t*-test) the values are significantly different at the 95% probability level and presumably arises from variations in structural features of the bonded phases and their influence on surface solvation.

Under totally aqueous conditions, the thermally induced reordering/resolvation of bonded hydrophobic ligands has been attributed to a combination of cohesive (chain–chain), hydrophobic (chain–solvent) and specific (solvent–surface) interactions. The non-linear biphasic behavior presented in Fig. 1 and the incremental change in T_0 are consistent with these same ideas except the degree and type of interactions are influenced by differences in bonding as well as the underlying amino groups and the amide groups within the chain.

CONCLUSIONS

The current study further demonstrates that totally aqueous non-linear chromatographic experiments are useful for characterizing the conformational aspects of hydrophobic phases including the new type of alkyl-modified materials based on immobilization via an amide linkage. Currently spectroscopic studies are in progress in order to characterize further the structural features of the surfaces in an effort to explain the differences in T_0.

ACKNOWLEDGEMENT

This work was supported by US Army Research Office Grant DAAL03-90-G-0061.

REFERENCES

1 K.K. Unger (Editor), *Packings and Stationary Phases in Chromatographic Techniques*, Marcel Dekker, New York, Basel, 1990.
2 M. Jaroniec, *J. Chromatogr.*, 656 (1993) 37.
3 J.G. Dorsey and K.A. Dill, *Chem. Rev.*, 89 (1989) 331.
4 B. Buszewski, *D.Sc. Thesis*, Slovak Technical University, Bratislava, 1992.
5 L.C. Sander and S.A. Wise, *CRC Crit. Rev. Anal. Chem.*, 18 (1987) 299.
6 R.K. Gilpin, *J. Chromatogr. Sci.*, 22 (1984) 371.
7 C.F. Poole and S.R. Poole, *Chromatography Today*, Elsevier, Amsterdam, 1991.
8 B. Buszewski, *Chromatographia*, 29 (1990) 233.
9 R.K. Gilpin, M. Jaroniec and S. Lin, *Anal. Chem.*, 62 (1990) 2092.
10 C.H. Lochmüller and D.R. Wilder, *J. Chromatogr. Sci.*, 17 (1979) 574.
11 R.K. Gilpin, *J. Chromatogr. Sci.*, 22 (1984) 371.
12 B. Buszewski, Z. Suprynowicz, P. Staszczuk, K. Albert, B. Pfleiderer and E. Bayer, *J. Chromatogr.*, 499 (1990) 305.
13 R.K. Gilpin and J.A. Squires, *J. Chromatogr.*, 19 (1981) 195.
14 R.K. Gilpin, M.E. Gangoda and A.E. Krishen, *J. Chromatogr. Sci.*, 20 (1982) 345.
15 R.K. Gilpin, *Anal. Chem.*, 57 (1985) 1465A.
16 P. Kasturi and R.K. Gilpin, presented at the *43th.Pittsburgh Conference, New Orleans, LA, March 1992*, abstract 722.
17 S.S. Yang and R.K. Gilpin, *J. Chromatogr.*, 394 (1987) 295.
18 S.S. Yang and R.K. Gilpin, *J. Chromatogr.*, 408 (1987) 93.
19 S.S. Yang and R.K. Gilpin, *J. Chromatogr.*, 449 (1988) 115.
20 R.K. Gilpin and L. Wu, *J. Chromatogr.*, 556 (1991) 415.
21 S.S. Yang and R.K. Gilpin, *Talanta*, 36 (1989) 327.
22 B. Buszewski, J. Schmid, K. Albert and E. Bayer, *J. Chromatogr.*, 552 (1991) 415.
23 B. Buszewski, A. Jurasek, J. Garaj, L. Nondek, I. Novak and D. Berek, *J. Liq. Chromatogr.*, 10 (1987) 2325.
24 R.K. Gilpin and W.R. Sisco, *J. Chromatogr.*, 194 (1980) 285.

25 B. Buszewski, M. Jaroniec and R.K. Gilpin, *J. Chromatogr.*, (1994) in press.
26 G.E. Berendsen and L. de Galan, *J. Liq. Chromatogr.*, 1 (1978) 561.
27 D.W. Sindorf and G.E. Maciel, *J. Am. Chem. Soc.*, 105 (1983) 12.
28 S.S. Yang, *Ph.D Thesis*, Kent State University, Kent, OH, 1987.

Journal of Chromatography A, 659 (1994) 267–273
Elsevier Science B.V., Amsterdam

CHROM. 25 694

Allowance for kinetics of solute partitioning in the determination of rate constants by affinity chromatography

Peter D. Munro and Donald J. Winzor*

Centre for Protein Structure, Function and Engineering, Department of Biochemistry, University of Queensland, Brisbane, Queensland 4072 (Australia)

John R. Cann

Department of Biochemistry/Biophysics/Genetics, and the University of Colorado Cancer Center, University of Colorado Health Sciences Center, Denver, CO 80262 (USA)

(Received September 1st, 1993)

ABSTRACT

An improved method is described for evaluation of the dissociation rate constant for the solute–matrix interaction from affinity chromatographic elution profiles in which the flow-rate dependence of the variance reflects the combined effects of chemical and partition kinetics. Results of a previous investigation of the interaction between saccharides and concanavalin A immobilized on CPG 3000 are reconsidered in terms of the new procedure, which takes advantage of an analytical expression to separate the two contributions. Although the revised analysis confirms the adequacy of the earlier empirical approach to this problem, it also renders redundant the necessity for the empiricism.

INTRODUCTION

Although affinity chromatography has been proposed as a means of measuring rate constants for over a decade [1–3], reasonable progress towards achievement of that goal is a relatively recent development [4,5]. Major contributing factors to this greatly improved outlook for the determination of rate constants by affinity chromatography have been (i) replacement of zonal by frontal affinity chromatography to avoid the necessity of creating two infinitely sharp boundaries an infinitesimal distance apart, and (ii) use of the flow-rate dependence of the boundary variance to evaluate the kinetic contribution to boundary spreading [6].

In the numerical simulations of affinity chromatographic migration designed to test the feasibility of the intended procedure [4,5] the problem of solute partition was avoided by considering the matrix sites to be immobilized on the surface of an impenetrable matrix. Experimentally, however, it transpires that the required flow-rates dictate the use of porous glass beads for an acceptable concentration of matrix sites to be achieved. Consequently, the contribution of partition kinetics between the mobile and stationary phases needs to be taken into account if the flow-rate dependence of boundary spreading is to be used to evaluate the rate constant for the chemical kinetics of solute dissociation from its complex with affinity-matrix sites.

In our previous attempt to determine the rate

* Corresponding author.

SSDI 0021-9673(93)E1148-S

constant for the dissociation of *p*-nitrophenylmannoside from concanavalin A immobilized on CPG 3000 [5], simple additivity of the partition- and chemical-kinetics contributions was assumed in order to take into account the small but significant dependence of variance upon flow-rate observed in chromatography of the saccharide on an otherwise identical column of underivatized CPG 3000 beads. However, we now show that this empirical assumption may be avoided by using an analytical expression [7] which describes the simultaneous operation of partition and chemical kinetics. In this communication we consider in greater detail the question of partition kinetics by additional numerical simulations of affinity chromatographic migration and by subjecting the earlier results [5] to the improved analytical procedure.

EXPERIMENTAL

Summary of previous protocol

Because the goal of the present investigation is to remove the element of empiricism from an earlier analysis, the affinity chromatography experiments and results to be considered have already been published [5]. However, it seems appropriate to reiterate the essential features of that experimental protocol as a prelude to description of the procedures used to effect the improved analysis.

Briefly, the interaction of *p*-nitrophenylmannoside with immobilized concanavalin A was quantified by subjecting solutions of the sugar (10–50 μM) to frontal chromatography on a standard HPLC column (25 × 0.46 cm) of concanavalin A–CPG 3000, equilibrated with phosphate–chloride buffer (pH 5.5; ionic strength, I 0.5) and operated at flow-rates in the range 2–10 ml/min. The absorbance at 305 nm was recorded continuously by transfer of the ISCO V^4 monitor response to a data acquisition system. Standard procedures were then used to obtain the first moment (mean elution volume, $\bar{V}_A$) and second moment (variance in elution volume, σ_A^2) of the boundaries.

For the corresponding characterization of the competing interaction between methylmannoside and immobilized lectin, the same procedure was followed except that the buffer and applied solutions were supplemented with competing saccharide (100 μM). In a third series of experiments the kinetics of partitioning of *p*-nitrophenylmannoside was examined by subjecting solutions of the saccharide to frontal chromatography on an identical HPLC column of underivatized CPG 3000, equilibrated with the same phosphate–chloride buffer and operated at a similar range of flow-rates. Equivalence of the two columns was gauged by identity of the elution volumes obtained on the underivatized column and on the affinity column in the presence of a saturating concentration of competing saccharide.

The chromatographic behaviour of *p*-nitrophenylmannoside (A) was considered in terms of its interaction with immobilized-lectin sites (X) via the reaction scheme

$$A + X \underset{k_{-1}}{\overset{k_{+1}}{\rightleftharpoons}} AX;\ K_{AX} = k_{+1}/k_{-1} \qquad (1a)$$

k_{+1} and k_{-1} being the respective association and dissociation rate constants, and K_{AX} the association equilibrium constant. Effects of methylmannoside (B) were considered in terms of the analogous scheme

$$B + X \underset{k_{-2}}{\overset{k_{+2}}{\rightleftharpoons}} BX;\ K_{BX} = k_{+2}/k_{-2} \qquad (1b)$$

for the additional reaction of matrix sites with the competing saccharide.

Evaluation of kinetic parameters for the solute–matrix interaction

For situations in which the elution profile reflects contributions from partition kinetics and the kinetics of the solute–matrix interaction, DeLisi and Hethcote [7] have provided the following analytical expression (their eqn. 222) for the dependence of σ_A^2 upon flow-rate, F.

$$\sigma_A^2 = 2(V_A^* - V_0)\{(1 + K_{AX}[X])^2/k_{-p} + K_{AX}[X]/k_{-1}\}F \qquad (2)$$

Effects of partition kinetics are reflected in eqn. 2 by the appearance of k_{-p}, the rate constant for efflux of partitioning solute from a stationary phase with volume $(V_A^* - V_0)$: V_0 is the volume of

mobile phase (column void volume) and V_A^* the column volume accessible to partitioning solute. Terms in [X], the concentration of uncomplexed matrix sites distributed in the volume $(V_A^* - V_0)$, are eliminated by introducing $\bar{V}_A$, the elution volume obtained from the first moment of the boundary, and taking advantage of the relationship

$$K_{AX}[X] = (\bar{V}_A - V_A^*)/(V_A^* - V_0) \quad (3)$$

which follows directly from eqn. 221 of ref. 7. The flow-rate dependence of the variance then becomes

$$d\sigma_A^2/dF = 2\{(\bar{V}_A - V_0)^2/[k_{-p}(V_A^* - V_0)] + (\bar{V}_A - V_A^*)/k_{-1}\} \quad (4)$$

k_{-p} may be evaluated independently, and hence the rate constant for dissociation of solute–matrix complex (k_{-1}) may be determined as the only parameter of unknown magnitude in eqn. 4. However, because linear kinetics is an inherent assumption in eqns. 2 and 4, the apparent rate constant so determined (k_{-1}^{obs}) must be extrapolated to zero solute concentration in order to meet that condition.

An assumption inherent in the above procedure is the presumed dominance of partition and chemical kinetics contributions to the flow-rate dependence of boundary spreading. Although such neglect of restricted diffusion in the stationary phase is a reasonable approximation for the present system involving partition of small solutes (monosaccharides) within the relatively large pores of CPG 3000, extension of the approach to systems with larger partitioning solutes could well require modification of the quantitative expressions to take into account the effects of the internal diffusional resistance encountered by a macromolecular solute within matrix pores [8]. Allowance for this diffusional phenomenon introduces an element of non-linearity into the variance variation with flow rate by virtue of a dependence on $\sqrt{F}$ [5].

Evaluation of the rate constants for partition kinetics

The rate constant for the kinetics of *p*-nitrophenylmannoside efflux from the stationary phase into the mobile phase (k_{-p}) has been obtained from the corresponding flow-rate dependence of σ_A^2 in experiments on the underivatized CPG 3000 column. Use is made of the relationship

$$k_{-p} = 2(V_A^* - V_0)/(d\sigma_A^2/dF) \quad (5)$$

the expression obtained by setting $\bar{V}_A = V_A^*$ in eqn. 4, which is equivalent to setting [X] = 0 in eqn. 2. On the grounds that the ratio k_{+p}/k_{-p} defines K_p, the equilibrium parameter describing partition of solute between the two phases, the rate constant for influx of solute into the stationary phase has been determined from the expression $k_{+p} = k_{-p}K_p$, where $K_p = (V_A^* - V_0)/V_0$.

Numerical simulation of elution profiles

The advancing elution profiles of saccharide A in the absence and presence of 100 μM competing saccharide B were simulated for a porous matrix by an adaptation of the theoretical plate model of chromatography [9] with the transfer volume set at 1.7% of the mobile phase volume in a plate (segment). In the absence of competing saccharide the chromatographic column initially contained only free matrix sites at the constituent concentration $\bar{C}_X$. In the presence of competing saccharide, the initial equilibrium concentration of B in the mobile phase (volume V_0) of the column, C_B, was assigned the value of 100 μM, whereupon the concentration of uncomplexed matrix sites follows from the conservation equation

$$\bar{C}_X = [X] + K_p K_{BX}[X]C_B \quad (6)$$

The concentrations of B and BX in the accessible volume within the stationary phase $(V_A^* - V_0)$ also follow from the appropriate mass action expressions. The elution profiles were then generated according to the procedure described previously [5], except that the set of differential equations was extended to include the kinetics of partitioning of solute(s) between the mobile phase and the accessible volume within the stationary phase. After each transfer of a volume increment, δV, which corresponds to a time interval (δt) via flow-rate, F, a subroutine for partition and chemical kinetics was called to

evaluate the new distribution of solute(s) between complexed and free states in each column segment. This kinetics subroutine entailed numerical solution of the set of differential equations by the 4th-order Runge–Kutta method.

RESULTS AND DISCUSSION

In the previous attempt to evaluate a dissociation rate constant for the solute–matrix interaction in affinity chromatography [5], we used an empirical approach to the separation of contributions of partitioning kinetics and chemical kinetics to the flow-rate dependence of boundary spreading in frontal chromatography. Subsequently we have become aware that DeLisi and Hethcote [7] had already provided an analytical solution (eqn. 2) to the problem. It is therefore of interest to test the adequacy of the earlier approach. However, a factor that requires consideration is the compatibility of results inferred from eqn. 2 with the earlier thermodynamic and kinetic characterization, which was based on the concept of matrix sites distributed throughout the volume accessible to partitioning solute (V_A^*). Because eqn. 2 is based on a reaction volume confined to the pores of the stationary phase, $(V_A^* - V_0)$, the validity of identifying parameters in eqn. 2 with those in eqn. 1 clearly needs to be checked.

The question is addressed by considering the expressions for mass conservation of partitioning solute that apply to the two thermodynamic descriptions of the system. If the matrix sites are considered to be confined to the volume of stationary phase accessible to partitioning solute, $(V_A^* - V_0)$, the expression for mass conservation of solute (A) within that volume is

$$(V_A^* - V_0)[\bar{A}] = (\bar{V}_A - V_0)[A] \quad (7)$$

where [A] and $[\bar{A}]$ denote the free and total concentrations of solute. By writing the consequent equation for $[\bar{A}]$, it readily follows that

$$([\bar{A}] - [A])/[A] = (\bar{V}_A - V_A^*)/(V_A^* - V_0) = K_3[X] \quad (8)$$

which is, in fact, eqn. 3 because the ratio on the left-hand side defines the product of the free concentration of matrix sites and the association constant for the solute–matrix interaction, designated here as K_3 [7] to distinguish it from the corresponding parameter (K_{AX}) in eqn. 1. Adoption of the convention wherein matrix sites are considered to be distributed throughout the same volume as partitioning solute (V_A^*) leads to the analogous relationship [4]

$$(\bar{C}_A - [A])/[A] = (\bar{V}_A - V_A^*)/V_A^* = K_{AX}C_X \quad (9)$$

where different terminology for the total solute concentration ($\bar{C}_A$) and the concentration of uncomplexed matrix sites (C_X) is used to signify differences in magnitude from their counterparts in eqn. 8. In order to compare the magnitudes of the two equilibrium constants defined by eqns. 8 and 9, we note that the relationship

$$[X](V_A^* - V_0) = C_X V_A^* \quad (10)$$

expresses the condition that the two conventions merely differ in the volume occupied by the same number of matrix sites. By substituting the consequent expression for [X] in eqn. 8 we obtain

$$K_3 C_X = (\bar{V}_A - V_A^*)/V_A^* \quad (11)$$

which essentially duplicates eqn. 9 and thereby establishes the identity of equilibrium constants emanating from either convention. We therefore proceed with the envisaged analysis of the earlier experimental results [5].

The effect of column flow-rate on the variance of the advancing elution profile in frontal chromatography of *p*-nitrophenylmannoside (40 μM) is shown (O) in Fig. 1a, together with the corresponding dependence (□) obtained on an identical column of underivatized CPG 3000. The latter yields a value of 0.011 ml min for $d\sigma_A^2/dF$, which needs to be combined with V_A^* and V_0 in eqn. 5 to obtain k_{-p}, a prerequisite for determining k_{-1}, the rate constant for dissociation of saccharide–matrix complex, via eqn. 4.

A value of 3.58 ml for V_A^* has been determined experimentally, but direct measurement of the void volume (V_0) was precluded by unavailability of a sufficiently large solute to guarantee its complete exclusion from the 300 nm pores of the

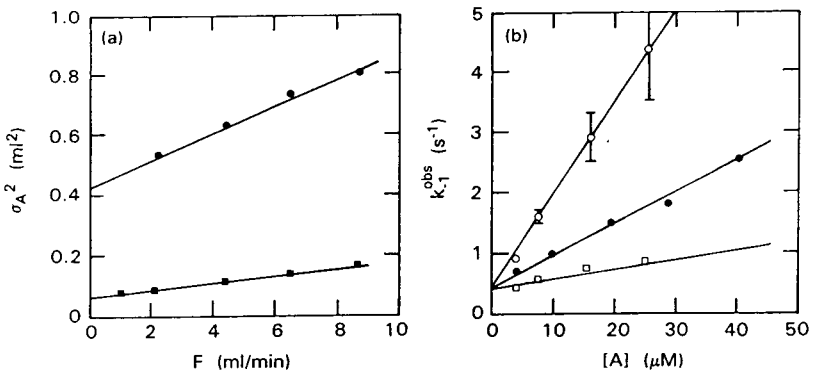

Fig. 1. Chromatographic evaluation of the rate constant for desorption of *p*-nitrophenylmannoside from concanavalin A immobilized on CPG 3000. (a) Published [5] effect of flow-rate on the variance of elution profiles of the saccharide (40 μM) on the affinity column (●) and identical CPG 3000 column devoid of matrix sites (■). (b) Effect of *p*-nitrophenylmannoside concentration on the apparent rate constant for saccharide desorption obtained (eqn. 4) from the flow-rate dependence of the variance of the advancing (○) and trailing (□) elution profiles: ● = corresponding dependence derived from the advancing elution profile in experiments where the applied solution and equilibrating buffer were supplemented with 100 μM methylmannoside.

glass matrix. For columns of CPG beads with similar mesh but smaller pore size, direct measurement of V_0 has yielded estimates of 0.485 [10] and 0.476 [11] for V_0/V_t, the ratio of the void and total column volumes. Indeed, a similar value, 0.480, emanates from the manufacturer's specification of pore volume (1.07 ml/g) for the present beads, the density of glass (2.6 g/ml) and consideration of the volume of glass to be $(V_t - V_A^*)$. For the present column with a total volume of 4.15 ml we shall therefore take V_0 as 2.00 ml, which corresponds to a value of 0.482 for V_0/V_t. On the basis of the above magnitudes for V_0, V_A^* and $d\sigma_A^2/dF$, the partition rate constant for efflux of *p*-nitrophenylmannoside from the stationary phase of CPG 3000 (k_{-p}) is 4.79 s^{-1}.

Consideration of the results for *p*-nitrophenylmannoside obtained from advancing (○) and trailing (□) elution profiles on the affinity column in terms of eqn. 4 leads to essentially linear dependences of k_{-1}^{obs} upon [A] (Fig. 1b), the ordinate intercepts of which signify a rate constant (k_{-1}) of 0.40 (±0.05) s^{-1} for dissociation of the saccharide from its complex with immobilized concanavalin A. Furthermore, the corresponding analysis of results obtained from the advancing profile in the presence of 100 μM methylmannoside (●, Fig. 1b) also extrapolates to the same intercept. Comparison of these findings with those from the previous empirical analysis (Fig. 7 of ref. 5) reveals general agreement. First, essentially the same dissociation rate constant (0.40 *cf.* 0.42 s^{-1}) is obtained by use of the analytical expression encompassing the combined effects of chemical and partition kinetics, thereby establishing the adequacy of the simple subtractive procedure adopted previously [5]. Secondly, an essentially identical ordinate intercept from results obtained in the presence of competing saccharide contrasts with the previous experimental finding, but confirms the inference drawn from simulations of affinity chromatographic migration (Fig. 4 of ref. 5) that the two ordinate intercepts should coincide. Thirdly, in keeping with previous findings, both experimental and simulated, the concentration dependence of k_{-1}^{obs} in the presence of competing saccharide is smaller. It is therefore of interest to ascertain whether the ratio of these two slopes can be used to deduce the magnitude of k_{-2} by comparison with the corresponding ratios from results of simulations of chromatographic behaviour for a range of k_{-2} values.

In numerical simulations of the affinity chromatography in the absence and presence of competing saccharide B (100 μM) k_{-1} has been taken as 0.42 s^{-1} (Fig. 1b), k_{-p} as 4.79 s^{-1} and k_{+p} as 3.49 s^{-1}; k_{-2} ranged between 0.2 and 2.0 s^{-1}. Parameters carried over from the previous

investigations included $K_{AX} = 24\,000\ M^{-1}$ [5,12] and $K_{AB} = 9\,000\ M^{-1}$ [5]. Whereas previously the volume increment could be set at 10% of the mobile-phase volume in a segment, a much smaller transfer volume had to be used to accommodate the 20-fold larger magnitudes of the partition rate constants without violating the validity of the substitution of $\delta c/\delta t$ for $\partial c/\partial t$ in the numerical integration of continuity equations [13–16].

As in the previous simulations [5] the dependences of k_{-1}^{obs} upon concentration of *p*-nitrophenylmannoside in the presence and absence of inhibitor exhibited a common ordinate intercept (as in Fig. 1b), and a ratio of slopes dependent upon the magnitude assigned to k_{-2}, the rate constant for dissociation of the methylmannoside–matrix complex (Fig. 2). On the basis of this calibration plot and the slope ratio of 0.36 (±0.03) inferred from the experimental results (Fig. 1b), the rate constant for the dissociation of methylmannoside from immobilized concanavalin A is 0.8 (±0.2) s^{-1}, which substantiates the value of 1 s^{-1} reported previously [5].

By confirming the findings of its predecessor [5], this revised analysis has served two useful roles. First, it certainly verifies the adequacy of the previous empirical approach to allowance for the contribution of partition kinetics to the flow-rate dependence of the variance of the eluted boundary of partitioning solute. More importantly, however, it draws attention to the availability of an analytical expression for making such allowance, and thereby eliminates the need for the earlier empiricism. Finally, this study has highlighted the existence of two different conventions for description of the solute–matrix interaction. From the thermodynamic viewpoint it is immaterial whether the solute–matrix interaction is considered to occur throughout the volume accessible to the partitioning solute or to be restricted to the accessible volume of the stationary phase. Consequently, awareness of the convention pertaining to a particular quantitative expression is important in any attempt to assign physical meaning to an experimental parameter derived therefrom.

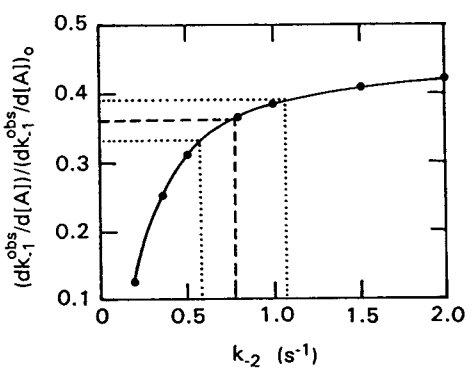

Fig. 2. Revised calibration plot (*cf.* Fig. 5 of ref. 5), based on results of numerical simulations, for evaluating k_{-2}, the rate constant for dissociation of methylmannoside from immobilized concanavalin A, from its effect on the affinity chromatographic behaviour of *p*-nitrophenylmannoside. Broken lines indicate the magnitude of the experimentally determined ratio of slopes (Fig. 2b) and the consequent estimate of k_{-2}: dotted lines define the error envelope associated with the extent of experimental uncertainty inherent in the experimentally evaluated slope.

ACKNOWLEDGEMENTS

The support of this investigation by the Australian Research Council (D.J.W.) and the University of Colorado Cancer Center (J.R.C.) is gratefully acknowledged, as is the excellent technical assistance of Robert O. Coombs in the numerical simulation aspects of this work.

REFERENCES

1 I.M. Chaiken, *Anal. Biochem.*, 97 (1979) 1.
2 V. Kasche, K. Bucholz and B. Galunsky, *J. Chromatogr.*, 216 (1981) 169.
3 K. Nilsson and P.-O. Larsson, *Anal. Biochem.*, 134 (1983) 72.
4 D.J. Winzor, P.D. Munro and J.R. Cann, *Anal. Biochem.*, 194 (1991) 54.
5 P.D. Munro, D.J. Winzor and J.R. Cann, *J. Chromatogr.*, 646 (1993) 3.
6 E.D. Katz, K.L. Ogan and R.P.W. Scott, *J. Chromatogr.*, 270 (1983) 51.
7 C. DeLisi and H.W. Hethcote, in I.M. Chaiken (Editor), *Analytical Affinity Chromatography*, CRC Press, Boca Raton, FL, 1987, p. 1.
8 R. Lortie and G. André, *Chem. Eng. Sci.*, 45 (1990) 1133.
9 E. Glueckauf, *Trans. Faraday Soc.*, 51 (1955) 34.
10 L.W. Nichol, R.J. Siezen and D.J. Winzor, *Biophys. Chem.*, 10 (1979) 17.

11 R.J. Siezen, L.W. Nichol and D.J. Winzor, *Biophys. Chem.*, 14 (1981) 221.
12 D.J. Winzor, P.D. Munro and C.M. Jackson, *J. Chromatogr.*, 597 (1992) 57.
13 W.B. Goad, in J.R. Cann (Editor), *Interacting Macromolecules: The Theory and Practice of Their Electrophoresis, Ultracentrifugation and Chromatography*, Academic Press, New York, 1970, Ch. 5.
14 J.R. Cann, *J. Theor. Biol.*, 127 (1987) 461.
15 J.R. Cann and D.J. Winzor, *Arch. Biochem. Biophys.*, 256 (1987) 78.
16 J.R. Cann, A.G. Appu Rao and D.J. Winzor, *Arch. Biochem. Biophys.*, 270 (1989) 173.

Journal of Chromatography A, 659 (1994) 275–287
Elsevier Science B.V., Amsterdam

CHROM. 25 641

Novel affinity separations based on perfluorocarbon emulsions

Use of a perfluorocarbon affinity emulsion for the direct extraction of glucose-6-phosphate dehydrogenase from homogenised bakers' yeast

Graham E. McCreath* and Howard A. Chase

Department of Chemical Engineering, University of Cambridge, Pembroke Street, Cambridge CB2 3RA (UK)

Christopher R. Lowe

Institute of Biotechnology, University of Cambridge, Tennis Court Road, Cambridge CB2 1QT (UK)

(First received July 22nd, 1993; revised manuscript received October 12th, 1993)

ABSTRACT

A perfluorocarbon affinity emulsion has been generated by homogenisation of perfluorodecalin with poly(vinylalcohol) and with subsequent cross-linking and derivatisation with Procion Red H-E7B. This affinity emulsion was tested for its applicability in direct extraction. The affinity emulsion exhibited limited fouling when contacted with a crude homogenate of bakers' yeast (*Saccharomyces cerevisiae*) and could be washed clear from cell debris using an aqueous buffer. Adsorption isotherm experiments showed that the capacity of the affinity emulsion for glucose-6-phosphate dehydrogenase (G6PDH) was not severely affected by the presence of whole yeast cell and cell debris. Two different contacting techniques were examined for G6PDH purification directly from a yeast homogenate. The first technique, expanded bed affinity chromatography (EBAC), which is an essentially batch operation, was carried out under conditions optimised through frontal analysis and was compared with a second technique, PERCAS (perfluorocarbon emulsion reactor for continuous affinity separations). G6PDH could be successfully purified using both techniques with an average purification factor of 18 directly from a crude homogenate. An analysis of system productivity showed that PERCAS had a productivity of some 2.25 times higher than expanded bed affinity chromatography under similar process conditions.

INTRODUCTION

While affinity chromatography is now well established as a popular unit operation for the purification of proteins, its position in the downstream processing flowsheet has frequently not been optimised. Classically, affinity chromatography has been reserved as one of the final stages of purification [1] even when it is obvious that the inclusion of a highly selective purification step early in the sequence of separation would generate more favourable process economics as greater step yields would be achieved with fewer steps necessary downstream [2–4]. Often, the implementation of affinity chromatography as one of the final steps used is due to the expense

* Corresponding author.

0021-9673/94/$07.00
SSDI 0021-9673(93)E1084-D

and lability of the affinity media [5] and the need for prior removal of particulates [3]. However, although the use of ultrastable matrices, linkage chemistries and affinity ligands may circumvent some of these problems [6,7]; even with ultrastable affinity media, it is not usually possible to use the technique early on in the process. The presence of particulate matter, be it whole cells or cell debris, totally prohibits the use of conventional packed bed techniques and hence early use of an affinity chromatography step requires practical innovations in the area of contactor design. For example, as an alternative to using a packed bed with prior clarification of the feed stock, affinity chromatography has recently been carried out using an expanded (liquid fluidised) bed of an adsorbent designed for conventional packed bed operation, Blue Sepharose Fast Flow [3]. Alternatively, affinity chromatography has been carried out in stirred tanks [8,9]. The physical nature of the adsorbent has also been changed and the use of affinity partitioning [10] and reversed micelles [11] is well documented.

We have recently described the development of a novel affinity support based on perfluorocarbon emulsions stabilised by an adsorbed layer of polymeric surfactant previously derivatised with affinity ligands and subsequently cross-linked *in situ* [12]. These emulsions were used successfully for the purification of human serum albumin from plasma in an expanded bed [13]. We later showed that continuous affinity chromatography is possible using perfluorocarbon emulsions and a four stage mixer-settler, a system we have named PERCAS (perfluorocarbon emulsion reactor for continuous affinity separations) [14]. In this paper we compare both techniques, expanded bed affinity chromatography (EBAC) and PERCAS in the direct extraction of glucose-6-phosphate dehydrogenase (G6PDH) from unclarified homogenised bakers' yeast using a perfluorocarbon affinity emulsion incorporating the reactive dye Procion Red H-E7B. Liquid perfluorocarbon emulsions have certain advantages over some of the techniques mentioned above for direct extraction in that they are inherently transportable by pumping due to their liquid nature and they have a high density resulting in rapid phase separation under gravity. They are also, chemically, very stable and hence are able to withstand cleaning and sterilisation. The purification of an enzyme from yeast cell homogenates was chosen as a model system showing the typical features of direct extraction. G6PDH was chosen as the target enzyme as it is used widely in clinical analysis for both glucose and hexokinase determinations [15] and purification protocols based on triazine dyes have been published previously [16–19].

EXPERIMENTAL

Materials

Poly(vinylalcohol) (PVA) (M_r 115 000, 100% hydrolysed) was purchased from Aldrich (Gillingham, UK) as was triethanolamine–HCl and magnesium chloride. Perfluorodecalin (Flutec PP6) was obtained from ISC Chemicals (Avonmouth, Bristol, UK). Non-ionic fluorosurfactant (Zonyl FSN) was obtained from E.I. du Pont de Nemours & Co. (DE, USA). Bakers' yeast was purchased in the form of pressed blocks from a local supplier. All other chemicals and reagents were purchased from Sigma (Poole, UK). Masterflex peristaltic pumps (Cole-Palmer, UK) were used for the fluidisation experiments and were also used, partly, as delivery pumps to PERCAS, the remaining delivery and extraction pumps were a Pharmacia P-1 (Pharmacia Biotechnology, Milton Keynes, UK) and a Minipuls II (Gilson, France).

Synthesis of Procion Red H-E7B perfluorocarbon affinity emulsion

A solution of PVA (M_r 115 000, 100% hydrolysed, 40 mg/ml, 200 ml) was added to perfluorodecalin (90 g) and homogenised (Ultra-Turrax T-25, half speed, 1 min) in a conical flask. The emulsion suspension was then made to a total volume of 900 ml by the addition of distilled water and heated to 40°C while stirring; HCl (5 *M*, 64 ml) was added and stirring continued for 20 min followed by the dropwise addition of glutaraldehyde [25% (w/v), 0.5 ml], the suspension was stirred for a further 2 h to allow cross-linking. Following cross-linking, the emulsion phase was allowed to settle and the supernatant decanted; the emulsion was washed

(5×) with distilled water (300 ml) and then transferred to a 500-ml conical flask containing a solution of PVA (M_r 115 000, 100% hydrolysed, 20 mg/ml, 40 ml) and HCl (5 *M*, 20 ml). Glutaraldehyde [25% (w/v), 0.2 ml] was then added and the emulsion suspension stirred for 20 min after which dilute HCl (0.17 *M*, 380 ml) was added and the suspension was stirred rapidly for a further 2 h. The emulsion was allowed to settle and the top phase decanted and replaced with distilled water to a final volume fraction of 50%. The emulsion suspension was transfered to a Buchner flask where it was vigorously degassed for 1 h after which the settled emulsion was washed (10×) with distilled water (200 ml) and finally suspended as a 50% emulsion phase volume fraction in distilled water.

Washed emulsion suspension (120 ml, 50% emulsion phase volume fraction) was added to a solution of Procion Red H-E7B (3.5 g, 80 ml) and heated to 65°C for 20 min with mixing after which NaOH (5 *M*, 10 ml) was added and mixing continued for 3 h. The emulsion was allowed to settle and washed with distilled water until washings were clear of free dye as determined spectrophotometrically. The emulsion was additionally washed (2 ×) with a solution of Zonyl FSN (100 ml, 0.01% in distilled water) to displace any remaining unattached dye and finally it was washed with distilled water (5 × 200 ml) before being suspended as a 50% emulsion phase volume fraction in distilled water.

Homogenisation of bakers' yeast

Glass ballotini (0.50–0.59 mm, 30 ml) were de-ashed by adding to a solution of concentrated nitric acid (100 ml) followed by stirring overnight. The beads were then vacuum washed with concentrated nitric acid (100 ml) followed by distilled water (1000 ml) and 0.1 *M* triethanolamine–HCl, pH 8.0 (200 ml). Bakers' yeast (4.5 g, net mass) was added to ice-cold 0.1 *M* triethanolamine–HCl, pH 8.0 (4.5 ml) and mixed; to this suspension was added phenylmethylsulphonyl fluoride (PMSF) to 1 m*M* and β-mercaptoethanol to 5 m*M*. Ice-cold de-ashed glass ballotini (9 ml) were then added and the whole suspension further cooled on melting ice (4°C) for 30 min. The suspension was vortex mixed (Vortex Genie 2, full speed) for a total vortexing time of 10 min carried out intermittently (1 min vortexing, 1 min cooling on melting ice). After this time the supernatant (8.0–8.5 ml) was removed and the ballotini washed with ice-cold extraction buffer (0.1 *M* triethanolamine–HCl, pH 8.0, 1 m*M* PMSF, 5 m*M* β-mercaptoethanol, 2 ml). The wash was then added to the previously collected supernatant to produce what will now be referred to as stock homogenate. In experiments involving the use of whole homogenates, the stock homogenate was used directly or after dilution with extraction buffer. In experiments involving cell free extracts, the stock homogenate was centrifuged (Eppendorf, 8800 *g*, 10 min) and filtered (0.22 μm) before use.

Protein determination and G6PDH assay

Protein determination was carried out with the Pierce Coomassie protein assay reagent using BSA as a standard. Calibrations were performed on stock solutions whose initial concentrations were determined at 280 nm assuming an extinction coefficient of 0.66 ml mg^{-1} cm^{-1} for BSA [20]. Spectrophotometry was carried out using a Shimadzu UV-160A spectrophotometer (VA Howe, Oxon, UK). Serial dilutions of stock solutions (20 μl) were incubated with assay reagent (1 ml) for 10 min at room temperature. The absorbance was then read at 595 nm against a buffer blank in order to prepare a standard curve. In order to determine the total protein concentration in homogenates, dilutions (1 in 50–1 in 100) of stock homogenate were taken and centrifuged (Eppendorf, 8800 *g*; 10 min) and the supernatant assayed. By carrying out dilutions on stock homogenates, the variation in apparent concentration between unclarified and clarified solutions caused by the presence of cells/cell debris could be determined.

G6PDH was assayed by adding enzyme solution (33 μl) to a 1-ml disposable polystyrene cuvette containing the following solutions: 0.1 *M* triethanolamine–HCl (pH 8.0) (870 μl), 0.2 *M* $MgCl_2$ (33 μl), 38.5 m*M* glucose-6-phosphate in ice-cold 5 m*M* potassium phosphate buffer (pH 7.4) (33 μl) and 13 m*M* $NADP^+$ in ice-cold 5 m*M* potassium phosphate buffer (pH 7.4) (33

μl). Enzyme activity was measured spectrophotometrically (20°C) at 340 nm by monitoring the reduction of $NADP^+$ to NADPH. Results are expressed in units of enzyme activity where 1 unit is defined as that amount of enzyme needed to convert 1 μmol of substrate to product in 1 min at 20°C.

Determination of the degree of fouling of the affinity emulsions

Aliquots (1 ml) of settled Procion Red H-E7B perfluorocarbon affinity emulsion and stock yeast cell homogenate were added to each of 3 test tubes. The tubes were mixed by rotary tumbling for 1 h, after which the emulsions were allowed to settle under gravity (1 min) before the supernatant was carefully removed. A sample of wash buffer (100 m*M* NaCl in 50 m*M* triethanolamine–HCl, pH 8.0) was then added to each tube to generate emulsion volume fractions of 50, 33 and 20%, respectively. The tubes were mixed for 10 min, the emulsion was then allowed to settle and the supernatant removed. Wash buffer was added to the settled emulsion to generate the original emulsion volume fraction and the emulsions were then re-washed. This procedure was carried out until the emulsions had been washed 6 times. After the last wash, 1 ml of a solution containing ethanol (60%), NaOH (0.5 *M*) and urea (4 *M*) was added to each tube. The tubes were again mixed for 30 min at room temperature, after which the emulsions were allowed to settle and the supernatant removed. The absorbance of samples of each of the collected supernatants was measured at 600 nm, and this was taken as an indication of the turbidity of the solution. Where necessary, dilutions were taken so that the absorbance was less than 1 AU.

Equilibrium adsorption isotherms

Aliquots (0.5 ml) of settled Procion Red H-E7B perfluorocarbon affinity emulsion were added to a series of 1.5-ml Eppendorf microtest tubes. The emulsions were washed (3×) with 50 m*M* triethanolamine–HCl, pH 8.0 after which the supernatant was removed. To each set of test tubes was added serial dilutions of unclarified or clarified bakers' yeast homogenate (0–6.5 U/ml, 1 ml). The test tubes were mixed in a rotary mixer for 1 h after which the emulsions were allowed to settle (1 min) and the supernatant assayed for both total protein and specifically for G6PDH activity.

Frontal analysis of G6PDH in an expanded emulsion bed

The experimental apparatus for expanded bed affinity chromatography is shown in Fig. 1. The system was arranged around a 2 cm I.D. column (BDH, UK) fitted with a hemi-spherical inlet and P160 sintered disc (average pore size 160 μm) which acted as a distributor. Two delivery pumps were used connected through a 2-way valve which allowed the pumps to be used simultaneously, one for delivery and one for priming with feed solution or eluent. When expanded bed experiments were carried out, the head space between the top of the bed and the outlet was kept to a minimum (2–3 cm) to minimise the dead volume of liquid within the column. A mesh at the top of the column before the outlet ensured no elutriation of smaller emulsion droplets took place if the bed were to over expand.

Procion Red H-E7B perfluorocarbon affinity emulsion was poured into the column to give a settled bed height of 3.4 cm (10.7 ml). The emulsion was fluidised with buffer (50 m*M* triethanolamine–HCl, pH 8.0) at a flow-rate of

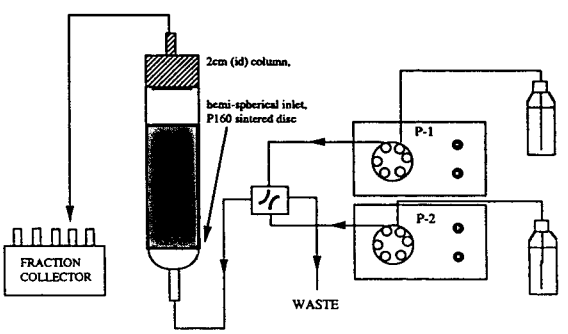

Fig. 1. Experimental apparatus used for expanded bed affinity chromatography of G6PDH using Procion Red H-E7B perfluorocarbon affinity emulsion. P-1 and P-2 are pumps.

5.75 ml/min (108 cm/h) to give a stable expanded bed height of 10.2 cm (31 ml). Stock yeast homogenate was diluted with buffer (50 m*M* triethanolamine–HCl, pH 8.0) to give 70 ml of a solution containing 9.4 mg/ml protein and 2.98 U/ml G6PDH. During the experiment, the flow-rate of solution to the column was progressively decreased to maintain a constant degree of bed expansion; the increased viscosity and density of the homogenate solutions decreases the terminal velocity of the emulsion droplets and hence to avoid elutriation of the emulsion, the superficial velocity must be decreased. The initial superficial velocity (108 cm/h) was decreased to 26 cm/h towards the end of the experiment. Fractions (2.2 ml), collected throughout the experiment, were immediately stored on ice and were subsequently assayed for turbidity, protein concentration and G6PDH concentration.

G6PDH purification in an expanded emulsion bed

Procion Red H-E7B perfluorocarbon affinity emulsion was poured into the column described above to give a settled bed height of 3.25 cm (10.2 ml). The emulsion was fluidised with buffer (50 m*M* triethanolamine–HCl, pH 8.0) at a flow-rate of 5.75 ml/min (108 cm/h) to give a stable expanded bed height of 9.8 cm (30.1 ml). Stock yeast homogenate (diluted with buffer, 50 m*M* triethanolamine–HCl, pH 8.0) (11.8 mg/ml protein, 2.71 U/ml G6PDH, 5 ml) was then pumped onto the expanded bed at the same flow-rate. Non-bound components were washed from the bed using 50 m*M* triethanolamine–HCl, pH 8.0. Elution of bound components was carried out firstly with 0.27 *M* NaCl in 50 m*M* triethanolamine–HCl, pH 8.0 and secondly with 0.88 *M* NaCl in 50 m*M* triethanolamine–HCl, pH 8.0. The eluent was washed from the bed using 50 m*M* triethanolamine–HCl, pH 8.0. Fractions (5 ml) collected throughout the experiment were assayed for turbidity, protein concentration and specific G6PDH activity. Fractions from the eluent washing stage were also measured for conductivity (Schott, Konduktometer CG 855).

Continuous G6PDH purification directly from a bakers' yeast homogenate using PERCAS

A description of PERCAS, and its use in the continuous purification of serum albumin from human plasma, has been reported in detail previously [14]. The basic operation is shown in Fig. 2, the system consists of four mixer-settlers arranged in series and in a loop. Perfluorocarbon affinity emulsion travels continuously through the system where it is contacted at different stages with different solutions, *i.e.* adsorption solution, wash buffer, eluent and re-equilibration buffer. In each stage, separation of emulsion from the bulk liquid phase is carried out by settling under gravity in the settler tanks. These tanks are separated from the mixing tanks by a weir, and the settled emulsion is transported by peristaltic pumps to the next stage.

PERCAS, containing Procion Red H-E7B perfluorocarbon affinity emulsion (35 ml, settled volume) was equilibrated at the flow-rates and stream compositions shown in Table I. After 1 h equilibration, the input to stage 1 (adsorption) was step changed from buffer to stock bakers' yeast homogenate (12.19 mg/ml protein, 2.29 U/ml G6PDH) at the same flow-rate. The experiment was carried out for 4 h with aliquots (1 ml) being removed from the top of each settler every 15 min. The collected fractions were stored on ice until analysis. Three sets of analysis were carried out; firstly, biomass profiles were determined by assaying the fractions spectrophotometrically (600 nm) diluting where necessary to obtain readings of less than 1 AU. Fractions collected from stage 1 (flow through) and stage 3

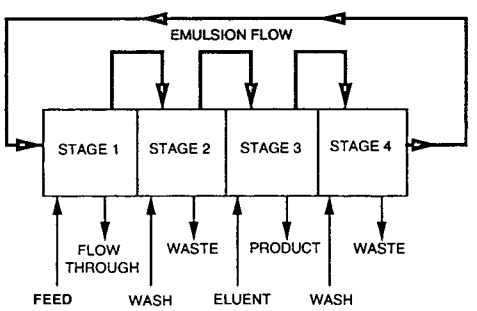

Fig. 2. Diagramatic representation of PERCAS operation as described in text.

TABLE I

PERCAS STREAM COMPOSITIONS

Operational set-up of PERCAS using Procion Red H-E7B perfluorocarbon affinity emulsion for the continuous direct extraction of G6PDH from homogenised bakers' yeast.

Stage	Buffer concentration (*M*)	NaCl concentration (*M*)	Flow-rate (ml/min)	Emulsion volume fraction (%)
Adsorption	0.1	0.1	1.21	46
Washing	0.1	0.35	3.41	23
Elution	0.1	2.0	0.84	55
Washing	0.1	0	3.86	21

(elution) were assayed for total protein and G6PDH activity, and appropriate dilutions were carried out where necessary.

RESULTS AND DISCUSSION

Generation of flocculated Procion Red H-E7B perfluorocarbon affinity emulsions

In our previous reports of the preparation of perfluorocarbon affinity emulsions incorporating C.I. Reactive Blue 4 [13] or C.I. Reactive Blue 2 as affinity ligands [14], the emulsions were prepared by first derivatising the polymeric surfactant with the ligand followed by homogenisation with perfluorodecalin. However, the presence of two equally reactive triazine rings on Procion Red H-E7B precluded the use of this technique as PVA was precipitated from solution during derivatisation. To overcome this problem, the emulsion floccule was prepared first and then derivatised with dye–ligand in much the same way as a solid support. After homogenising the PVA with perfluorodecalin the emulsion was cross-linked firstly at low emulsion volume fraction (5%) to ensure emulsion stability and secondly at high emulsion volume fraction (50%) to generate floccules. After this, the emulsion was stirred in dilute HCl at a low emulsion phase volume fraction (14%) to allow any more stabilising cross-links to form on the inside of the floccule. The ability to generate affinity emulsions in this way opens up possibilities for immobilising a range of ligands. For example, Protein A could be immobilised for the purification of IgG and enzymes could be immobilised in a similar fashion to generate new supports for use in biotransformations, which would be resistant to attrition.

Washing of the affinity emulsion was carried out first using water to remove bulk unreacted dye and secondly with a solution of non-ionic fluorosurfactant (Zonyl FSN, 0.01%) to displace any dye adsorbed to the surface of the perfluorocarbon oil though gaps in the PVA layer. The Zonyl FSN wash was successful in removing unreacted dye as subsequent storage of emulsions in distilled water, Zonyl FSN (0.2%) and NaOH (0.5 *M*) have revealed no further evidence of dye leakage. Under microscopic examination, the affinity emulsions appeared similar to those described previously [14] with the same range of floccule diameters (100–150 μm).

Homogenisation of bakers' yeast

Vortexing bakers' yeast with ballotini routinely produced soluble protein concentrations in stock homogenates of approximately 30 mg/ml (before washing or dilution) for a 50% (w/v) yeast suspension.

Emulsion fouling

In order that a selective adsorbent can be used for direct extraction, it must be shown that non-specific adsorption of contaminating substances is minimal. Non-specific adsorption may occur on both the ligand and the support matrix. Therefore, an assessment of the degree of fouling of adsorbents is a prerequisite to their

possible application in direct extraction. In this experiment perfluorocarbon affinity emulsion was contacted with a stock homogenate solution for 1 h, after which the samples of the emulsion were washed with a solution of aqueous buffer. Increasing volumes of buffer were added to generate progressively lower emulsion phase volume fractions. In the operation of the PERCAS unit, phase volume changes can be made by increasing or decreasing the appropriate input flow-rates to generate higher or lower emulsion phase volume fractions. The results from this experiment are shown in Fig. 3 where it can be seen that increasing the wash buffer volume fraction from 50 to 80% decreases the number of washes required to obtain a baseline absorbance from 6 to 2. It is evident therefore, that the most efficient washing in PERCAS will be carried out using a low emulsion phase volume fraction as this leads to maximum dilution of contaminants in the system.

When the emulsions were washed with a solution containing ethanol (60%), NaOH (0.5 *M*) and urea (4 *M*) there was little evidence of release of adsorbed components as assessed by measuring the absorbance of the supernatant at 600 nm, assuming that the release of adsorbed components would increase the absorbance of the solution at that wavelength. In each of the three test tubes the absorbance (at 600 nm) was 0.06–0.08 which does indicate that very little material had adsorbed and subsequently been released by this cocktail. More importantly, there was no evidence to suggest that dye leakage had occurred even after incubation in the cocktail for 72 h at room temperature.

Equilibrium adsorption isotherms

Adsorption isotherms were carried out to ascertain if the presence of suspended cellular material influenced the adsorption of G6PDH from a crude preparation. Hence, both unclarified and clarified homogenates were used. Fig. 4 presents the results from this experiment where it can be seen that the presence of cell debris has little effect at low concentration but has a slight effect at higher concentrations. The parameter q_m (maximum adsorption capacity) was determined for both systems by using a least-square fit analysis of a linearised form of the Langmuir equation [21]. In the case of the clarified homogenate q_m for G6PDH was equal

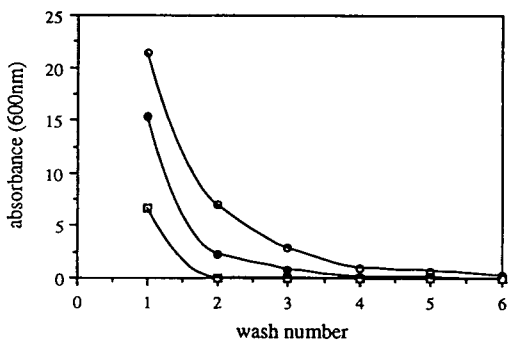

Fig. 3. Cell debris washout profiles for Procion Red H-E7B perfluorocarbon affinity emulsions. Samples of settled emulsion (1 ml) were incubated with yeast homogenate suspension (1 ml) by rotary tumbling for 1 h. After settling under gravity, the supernatant was removed and replaced with a solution of buffer (50 m*M* triethanolamine–HCl, pH 8.0) to generate final emulsion volume fractions of 50, 33 and 20%. The emulsions were washed with these solutions for a total of 6 washes. After each wash the supernatant was carefully removed and replaced with fresh solution. After each wash, the collected supernatant was assayed for turbidity by measuring the absorbance at 600 nm. Wash buffer volume fractions: ○ = 50%; ● = 67%; □ = 80%.

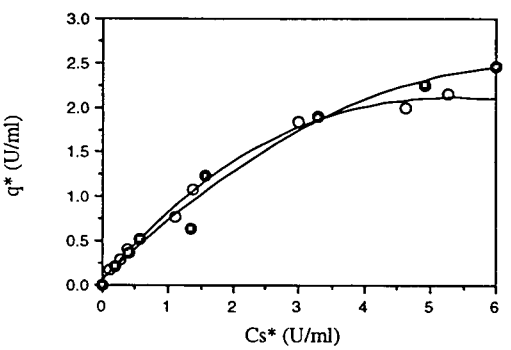

Fig. 4. Equilibrium adsorption isotherms for crude G6PDH on Procion Red H-E7B perfluorocarbon affinity emulsion. Aliquots (0.5 ml) of settled emulsion were washed (3×) with 50 m*M* triethanolamine–HCl, pH 8.0. Following this, serial dilutions of either clarified or unclarified bakers' yeast homogenate (0–6.5 U/ml, 1 ml) were added and the tubes rotary mixed for 1 h after which the supernatant was assayed for both total protein and specifically for G6PDH activity as described in Experimental. ○ = Homogenate, ● = clarified homogenate. q^* is the equilibrium capacity of the affinity emulsion of G6PDH (units of enzyme activity bound per ml of settled emulsion). Cs* is the equilibrium concentration of G6PDH in the non-emulsion phase.

to 2.6 U/ml which decreased to 2.1 U/ml in the presence of cell debris. This small drop in capacity is encouraging as it demonstrates that the capacity of the emulsion for G6PDH does not decrease significantly even in the presence of the high concentrations of cell debris.

Frontal analysis of G6PDH

An examination of the breakthrough curves presented in Fig. 5 shows that cell debris appeared first in the outlet followed by non-G6PDH protein and finally by G6PDH. This is a desirable situation as it demonstrates that G6PDH was being selectively removed from the feedstock by the emulsion. The capacity of the affinity emulsion for G6PDH was estimated by calculating the amount of enzyme contained in the difference of the volumes resulting between the breakthrough of non-G6PDH protein and the breakthrough of G6PDH. The capacity was found to be 1.8 U/ml and is similar to the equilibrium capacity obtained from the adsorption isotherm experiments in unclarified homogenates (2.1 U/ml) and shows that capacity was not compromised by the dynamic mode of operation.

Expanded bed affinity chromatography of G6PDH

The results from this experiment are shown graphically in Fig. 6. The volume of homogenate loaded onto the expanded bed column was such that the column would not be saturated with G6PDH and any loss of yield should not be due to breakthrough of unadsorbed G6PDH. Therefore, 13.55 U was loaded which corresponded to 74% of the maximum dynamic capacity of the column. As can be seen from Fig. 6, almost all the G6PDH was removed from the homogenate solution. Washing of the expanded bed was carried out with aqueous buffer and viscosity enhancers were not added to the wash solution [3] as the wash superficial velocity was sufficiently high to remove cell debris effectively in approximately 3–4 (expanded) bed volumes. The first elution step was carried out with 0.27 *M* NaCl in wash buffer (50 m*M* triethanolamine–HCl) as the results from a previous investigation [22] showed that irrigation with this concentration of NaCl does not elute G6PDH but does elute some other adsorbed protein. As can be seen from the trace of absorbance at 600 nm, there was some evidence of turbid material also being eluted and we attribute this to result from the desorption of some cell debris or cellular

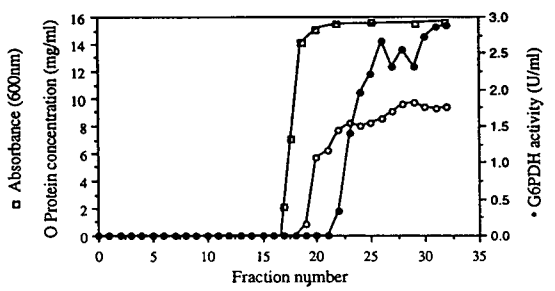

Fig. 5. Determination of dynamic binding capacity for G6PDH by frontal analysis on Procion Red H-E7B perfluorocarbon affinity emulsion. Settled bed height 3.4 cm (10.7 ml) expanded to 10.2 cm (31 ml) when fluidised with 50 m*M* triethanolamine–HCl, pH 8.0 at 5.75 ml/min (108 cm/h). Bakers' yeast homogenate (9.4 mg/ml protein, 2.98 U/ml G6PDH) was injected onto the expanded bed. Fractions (2.2 ml) collected throughout the course of the experiment were assayed for turbidity (absorbance at 600 nm), protein concentration and G6PDH activity as described under Experimental.

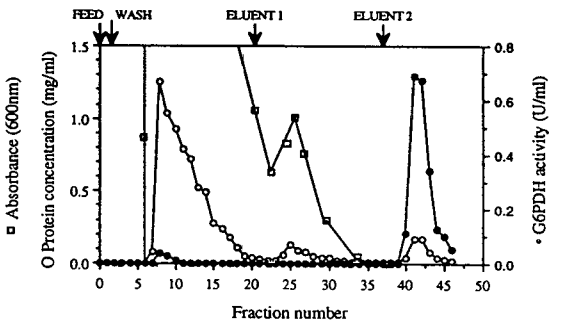

Fig. 6. Expanded bed affinity chromatography of G6PDH on Procion Red H-E7B perfluorocarbon affinity emulsion. Settled bed height 3.25 cm (10.2 ml) expanded to 9.8 cm (30.1 ml) when fluidised with 50 m*M* triethanolamine–HCl, pH 8.0 at 5.75 ml/min (108 cm/h). Bakers' yeast homogenate (5 ml, 11.8 mg/ml protein, 2.71 U/ml G6PDH) was injected onto the expanded bed. Non-bound fractions were washed from the bed using 50 m*M* triethanolamine–HCl, pH 8.0, followed by elution with 0.27 *M* NaCl in 50 m*M* triethanolamine–HCl, pH 8.0, followed by elution with 0.88 *M* NaCl in 50 m*M* triethanolamine–HCl, pH 8.0. The column was then re-equilibrated with 50 m*M* triethanolamine–HCl, pH 8.0, where the conductivity was monitored to establish when re-equilibration was complete. Fractions (5 ml) collected throughout the experiment were assayed for turbidity (absorbance at 600 nm), protein concentration and specific G6PDH activity as described under Experimental.

material. Further investigations are being carried out to identify this material, but it was present in very low concentration and was completely removed by this first elution step. G6PDH was eluted by irrigation of the column with 0.88 *M* NaCl. This step elution is not optimal for the achievement of high purification factors but as our investigations were more concerned with the contacting rather than the elution stage, at this time, we did not deem it necessary to use elaborate gradients or specific elution strategies. However, we are currently investigating the optimisation of the elution protocol to obtain G6PDH of the highest specific activity. In order to prepare the column for a possible further purification cycle, the eluent was washed from the bed using wash buffer (50 m*M* triethanolamine–HCl, pH 8.0). Washing was followed by monitoring the conductivity of effluent. Eluent was washed out, and the column re-equilibrated, after approximately 2 (expanded) bed volumes had been passed through. The purification details from this experiment are shown in Table II, and an overall purification factor of 16.8 for G6PDH was achieved in 77% yield with the eluted fraction being clear from particulate material as assessed by nephelometric analysis.

One possible disadvantage of the use of perfluorocarbon emulsions in expanded bed affinity chromatography is that, as a result of their compressible liquid nature they are deformable under pressure. This necessitates that elution is carried out in an expanded rather than packed bed mode which does lead to some dilution of the product. Another problem is encountered in the batch mode of operation, in that purified product is only being obtained in 1 out of 4 stages (adsorption, washing elution, re-equilibration). This being the case, direct extraction using perfluorocarbon affinity emulsions may be better carried out using some other contacting technique, and we therefore decided to investigate direct extraction using a continuous affinity separation system, PERCAS.

Continuous direct extraction of G6PDH from homogenised bakers' yeast using PERCAS

The stock yeast homogenate was diluted with buffer (100 m*M* triethanolamine–HCl, pH 8.0) to a total protein concentration of 12.2 mg/ml (2.3 U/ml G6PDH, 0.19 U/mg) before being pumped into PERCAS at a flow-rate of 1.21 ml/min (2.77 U/min). Fig. 7 shows both protein and enzyme profiles from stage 1 (adsorption) and stage 3 (elution). As can be seen from the graphs, steady state is achieved in stage 1 in about 2 h. By multiplying the average G6PDH concentration (U/ml), over the steady state region, by the flow-rate, the rate of non-adsorbed enzyme loss from this stage can be calculated at 0.53 U/min which corresponds to 19% of the amount of G6PDH in the input to the system.

The same characteristic profile is observed in the bottom graph showing the profile in the elution stage (stage 3). Steady state is achieved

TABLE II

EXPANDED BED AFFINITY CHROMATOGRAPHY OF G6PDH USING PROCION RED H-E7B PERFLUOROCARBON AFFINITY EMULSION

G6PDH was purified from bakers' yeast homogenate (5 ml, 11.8 mg/ml protein, 2.71 U/ml G6PDH) using an expanded bed of Procion Red H-E7B perfluorocarbon affinity emulsion. Column volume, 10.5 ml settled, 30.1 ml when fluidised at 5.75 ml/min (108 cm/h) with 50 m*M* triethanolamine–HCl, pH 8.0. Elution carried out firstly with 0.27 *M* NaCl, followed by elution with 0.88 *M* NaCl, both in running buffer (50 m*M* triethanolamine–HCl, pH 8.0). Fractions (5 ml) were collected and assayed for turbidity (A^{600nm}), protein concentration (Pierce Coomasie assay) and specific G6PDH activity.

Stage	Volume (ml)	Total protein (mg)	G6PDH (U)	G6PDH activity (U/mg)	Yield (%)	Purification (fold)
Homogenate	5	59	13.55	0.23	(100)	(1)
Elution 1	65	3.23	0	0	–	–
Elution 2	35	2.71	10.47	3.86	77	16.8

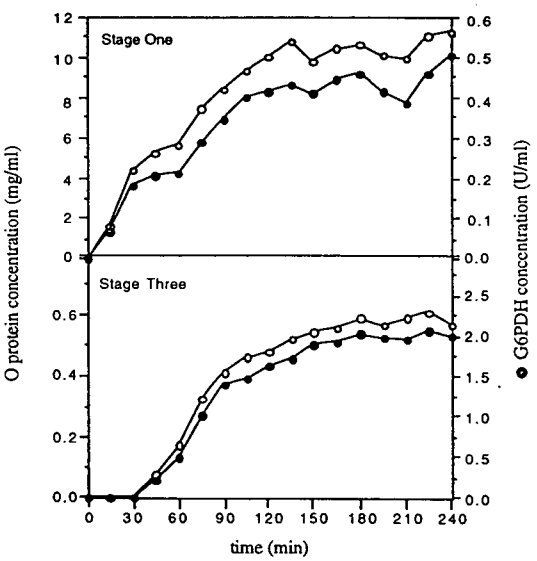

Fig. 7. Total protein and enzyme profiles appearing in PERCAS during the continuous purification of G6PDH from a bakers' yeast homogenate in the liquid leaving stage 1 (flow through) and the liquid leaving stage 3 (the eluted product). Bakers' yeast homogenate (12.19 mg/ml protein, 2.29 U/ml G6PDH) was pumped into PERCAS (stage 1) at a flow-rate of 1.21 ml/min. Purified G6PDH was collected from stage 3 after elution with 2.0 *M* NaCl in 50 m*M* triethanolamine–HCl, pH 8.0 at a flow-rate of 0.84 ml/min. Other experimental conditions described in text. Assays performed as described under Experimental.

in this stage after about 3 h. G6PDH is eluted from this stage at a concentration of 2.0 U/ml which corresponds to a rate of 1.68 U/min. By dividing the output rate of G6PDH from stage 3 by the input rate to stage 1, the yield of G6PDH in stage 3 can be calculated at 61%. At steady state, the specific activity of G6PDH leaving stage 3 is 3.42 U/mg which corresponds to a purification factor of 18.4. These results have been summarised in Table III, which compares steady state results from all 4 stages. The total recovery of G6PDH from PERCAS was calculated by addition of all individual stage yields at 93%. In terms of individual stages, 19% of G6PDH was lost in the flow through from stage 1, 8.3% at stage 2 and 4.7% at stage 4. The majority of the biomass flows over in stage 1 with each subsequent stage showing a progressively lower biomass concentration. Based on an initial biomass input to PERCAS of 37.5 (absorbance at 600 nm), 82% of the biomass was washed out in stage 1, 89% by stage 2, 93% by stage 3 and 98% by stage 4. This implies that the eluted stream (stage 3) contained 7% of the original biomass which demonstrates that clarification was reasonably effective although not complete.

TABLE III

CONTINUOUS PURIFICATION OF G6PDH FROM HOMOGENISED BAKERS' YEAST USING PROCION RED H-E7B PERFLUOROCARBON AFFINITY EMULSION AND PERCAS

G6PDH was purified on a continuous manner from homogenised bakers' yeast using Procion Red H-E7B perfluorocarbon affinity emulsion. Settled emulsion volume in PERCAS, 35 ml; running buffer (in stage 1), 100 m*M* NaCl in 50 m*M* triethanolamine–HCl, pH 8.0. Washing (primary elution) buffer (stage 2), 0.35 *M* NaCl in 50 m*M* triethanolamine–HCl, pH 8.0; elution buffer (stage 3), 2 *M* NaCl in 50 m*M* triethanolamine buffer–HCl, pH 8.0. Washing (re-equilibration) buffer (stage 4), 50 m*M* triethanolamine–HCl, pH 8.0. Flow-rate of applied homogenate stream, 1.21 ml/min; flow-rate of eluted stream, 0.84 ml/min. Affinity emulsion recycle flow-rate, 1.06 ml/min. Fractions were collected and assayed for turbidity (A^{600nm}), protein concentration (Pierce Coomasie assay) and specific G6PDH activity.

Stage	Flow-rate (ml/min)	Protein concentration (mg/ml)	G6PDH specific activity (U/mg)	G6PDH concentration (U/ml)	G6PDH flow-rate (U/min)	Yield (%)	Purification (fold)	Absorbance (600 nm)
5 —in broth	1.21	12.19	0.186	2.29	2.77	(100)	(1)	37.5
1 —out	1.21	10.47	0.033	0.44	0.53	19.1	–	30.75
2 —out	3.41	1.46	0.046	0.67	0.23	8.3	–	4.12
3 —out	0.84	0.586	3.42	2.00	1.68	61	18.4	2.62
4 —out	3.82	0.014	2.49	0.034	0.13	4.7	–	0.75

Therefore, using the PERCAS system, G6PDH has been purified 18.4-fold in a single step with 61% yield and with a 93% reduction in particulate content. Optimisation of this procedure could be carried out at all stages in the operation. In stage 1, the capture of G6PDH could be improved by increasing the volume fraction of emulsion, alternatively more than one adsorption stage could be used. This is also true for stage 2 where a reduction in the emulsion volume fraction or the inclusion of multiple washing stages would increase contaminant dilution and therefore decrease contamination of the eluted product. Similarly, elution could be optimised by operating a series of elution stages either of increasing ionic strength or containing different eluents.

G6PDH has been purified previously from bakers' yeast using triazine dyes as selective ligands in a variety of techniques. For example, a 7-fold purification (to 41% pure) from a partially purified extract [16] has been reported using a packed bed of Procion Red H-8BN Sepharose using $NADP^+$ as a selective eluent. These authors also pointed out that the success of the dye–ligand affinity chromatography step depends on the degree of substitution of the ligand. Separations using aqueous two-phase affinity partitioning have also been reported. Using Procion Yellow HE-3G liganded PEG an elaborate 4-step partitioning procedure resulted in a 43.6-fold purification of the enzyme (to 2.4% pure) in 74% yield after an initial PEG precipitation [17]. The same authors have successfully applied their techniques to counter-current distribution with similar results [18]. More recently, techniques have been described where G6PDH has been purified using Cibacron Blue F3GA immobilised onto readily available microporous membranes. A 26-fold purification of the enzyme (to 56% pure) was achieved using specific elution with $NADP^+$ and ethylene glycol from a partially purified extract [19].

Comparison of techniques

As both PERCAS and the expanded bed adsorption studies were carried out under similar conditions of adsorption, washing and elution, they can be compared directly. Firstly, in terms of product quality, both techniques delivered partially purified G6PDH with approximately the same specific activity and final yield. The somewhat lower yield associated with PERCAS was mainly attributed to un-adsorbed G6PDH appearing in the flow through. This un-adsorbed fraction could possibly be reduced by increasing the emulsion phase volume fraction in stage 1 or, alternatively, by including a second adsorption stage. The modular design of PERCAS readily allows for the incorporation of additional stages. Both techniques could be readily automated, for example we have previously described the semi-continuous purification of serum albumin from human plasma using automated fast protein liquid chromatography [13]. PERCAS is a continuous process and as such has certain advantages over conventional affinity chromatography which, although can operate repetitively, only produces product during one out of the four batch stages of operation (load, wash, elute, wash). In the experiment described here, the time taken for the expanded bed column to go through one cycle of operation (including washing) was 48 min. During this cycle, 10.5 U of G6PDH was recovered from 10.2 ml of emulsion; this gives rise to a productivity of 1.28 U/h per ml of emulsion. In the case of PERCAS, even with flow-rates approximately 5 times lower, the productivity at 2.88 U/h per ml of emulsion was some 2.25 times higher than the expanded bed adsorption experiment under similar conditions.

Although, the productivity of both techniques appears rather low, it should be remembered that the separations were not optimised. Our present work has shown that G6PDH purification factors of at least an order of magnitude higher are possible from a crude homogenate using more selective elution strategies. Translating this into productivity, the PERCAS unit described in this paper, if run continuously, would be able to produce partially purified G6PDH at a rate of 2400 U/day.

CONCLUSIONS

In this paper perfluorocarbon affinity emulsions have been assessed for their application in

direct extraction. Contacting experiments have showed that the affinity emulsions are very resistant to fouling and present a passive support. They have been shown to be stable to solvents commonly used in *in situ* cleaning and are readily autoclaved. Furthermore, they are reasonably inexpensive to manufacture as all the chemicals used in their synthesis are cheap. Their one disadvantage is their limited capacity which is due to their non-porous nature; for example, the capacity of the emulsion is some 10 times lower than an agarose support employing Procion Red H-8BN as a selective ligand [16]. Capacity comparisons are, however, difficult to make as in most other work capacity has been determined from partially pure G6PDH extracts in which possible adsorbing proteins may have been removed. In continuous operations, a smaller capacity may not be such a limiting problem as continuous recycle is employed. The lack of porosity may also be advantageous as it presents a smaller surface area for possible fouling agents and results in a support that is more easily washed clean. The purification of G6PDH from a crude homogenate was chosen as a model in which to assess the applicability of these novel supports in direct extraction and to compare modes of operation on the overall productivity. Both EBAC and PERCAS were successful in producing a partially purified and clarified preparation. PERCAS was perhaps the better system as it easily allows for changes in operating conditions, has a higher productivity per unit volume of adsorbent and could be easily integrated into a production system that is operated continuously. Although such continuous production processes are not in operation at present, chronic illnesses such as emphysema which require replacement therapy by α-1-antitrypsin at doses of up to 4 g/week per patient [23] may necessitate the use of such production strategies. Alternatively, the system could be thought of as providing trouble free continuous affinity chromatography from a batch fermentation.

However, although the purification factors obtained seem quite low in comparison to some of the techniques discussed above, our separations were not optimised and employed only step elution. One common aspect of all the above mentioned work on G6PDH purification from bakers' yeast is that the affinity chromatographic step has been reserved to the penultimate or final step following such techniques as centrifugation, precipitation and ion exchange which result in feed solutions with partial contaminant removal. To the best of our knowledge, this paper presents the first results for the direct extraction of G6PDH from a crude homogenate where no prior clarification/purification has taken place. The systems were successful in achieving partial purification and clarification in a single step with a high yield of eluted product. The affinity emulsion has proved to be re-usable showing no signs of deterioration over many months. An important aspect of continuous affinity separations is the maintenance of high yield over many cycles of purification and this is an aspect we are investigating. We believe that direct extraction procedures have great potential in industrial biotechnology where the rapid extraction of proteins from, sometimes, inhospitable environments, such as cell homogenates, is desirable. Our research into direct extraction is on-going, at present we are evaluating both liquid and solid perfluorocarbons for potential in direct extraction using both expanded bed techniques and novel continuous reactor formats.

ACKNOWLEDGEMENTS

G.E.McC. gratefully acknowledges the Biotechnology Directorate of the Science and Engineering Research Council (UK) for the provision of a research studentship.

H.A.C. and C.R.L. acknowledge support from the Separations Initiative of the Science and Engineering Research Council (UK).

REFERENCES

1 J. Bonnerjea, S. Oh, M. Hoare and P. Dunnill, *Bio/Technology*, 4 (1986) 954.
2 B.D. Kelley and T.A. Hatton, *Bioseparation*, 1 (1991) 333.
3 H.A. Chase and N.M. Draeger, *J. Chromatogr.*, 597 (1992) 129.
4 D. Sii and A. Sadona, *J. Biotechnol.*, 19 (1991) 83.

5 D.J. Stewart, D.R. Purvis, J.M. Pitts and C.R. Lowe, *J. Chromatogr.*, 623 (1992) 1.
6 C.R. Lowe, S.J. Burton, N. Burton, D.J. Stewart, D.R. Purvis, I. Pitfield and S. Eapen, *J. Mol. Recognit.*, 3 (1990) 117.
7 D.J. Stewart, D.R. Purvis and C.R. Lowe, *J. Chromatogr.*, 510 (1990) 177.
8 N.F. Gordon and C.L. Cooney, in M.R. Ladisch, R.C. Wilson, C.-D.C. Painton and S.E. Builder (Editors), *Protein Purification, From Molecular Mechanisms to Large-Scale Processes (ACS Symposium Series*, No. 427), American Chemical Society, Washington, DC, 1990, p. 118.
9 J.H.T. Luong and K.B. Male, *Bio/Technology*, 5 (1987) 514.
10 S.P. Foaden, *Ph.D. Thesis*, University of Cambridge, 1990.
11 J.M. Woll, T.A. Hatton and M.L. Yarmush, *Biotechnol. Prog.*, 5 (1989) 57.
12 G.E. McCreath, H.A. Chase, D.R. Purvis and C.R. Lowe, *Proceedings from I. Chem. E. Res. Event, Queens College, Cambridge, January 9 and 10, 1991*, p. 67.
13 G.E. McCreath, H.A. Chase, D.R. Purvis and C.R. Lowe, *J. Chromatogr.*, 597 (1992) 189.
14 G.E. McCreath, H.A. Chase, D.R. Purvis and C.R. Lowe, *J. Chromatogr.*, 629 (1993) 201.
15 H.U. Bergmeyer, *Methods of Enzymatic Analysis*, Vol. 2, Verlag Chemie, Weinheim, 1983.
16 E.E. Farmer and J.S. Easterday, *Anal. Biochem.*, 141 (1984) 79.
17 G. Johansson and M. Joelsson, *Enzyme Microb. Technol.*, 7 (1985) 629.
18 G. Johansson, M. Andersson and H.-A. Akerlund, *J. Chromatogr.*, 298 (1984) 483.
19 B. Champluvier and M.-R. Kula, *Biotechnol. Bioeng.*, 40 (1992) 33.
20 D.M. Kirschenbaum, *Handbook of Biochemistry and Molecular Biology*, Vol. 2, CRC Press, Cleveland, OH, 3rd ed., 1976, p. 54.
21 H.A. Chase, *J. Chromatogr.*, 159 (1984) 179.
22 G.E. McCreath, *Ph.D. Thesis*, University of Cambridge, Cambridge, 1993.
23 G. Wright, presented at the *Developments in the Isolation of Proteins, Society of Chemical Industry Meeting, London, May 24, 1993.*

Journal of Chromatography A, 659 (1994) 289–298
Elsevier Science B.V., Amsterdam

CHROM. 25 654

Application of temperature-induced phase partitioning at ambient temperature for enzyme purification

Patricia A. Alred

Department of Biochemistry, Chemical Center, University of Lund, P.O. Box 124, S-221 00 Lund (Sweden)

Antoni Kozlowski and J. Milton Harris

Department of Chemistry, University of Alabama in Huntsville, Huntsville, AL 35899 (USA)

Folke Tjerneld*

Department of Biochemistry, Chemical Center, University of Lund, P.O. Box 124, S-221 00 Lund (Sweden)

(First received July 7th, 1993; revised manuscript received October 18th, 1993)

ABSTRACT

Aqueous two-phase partition and temperature-induced phase separation using a non-ionic, random copolymer composed of 20% ethylene oxide, 80% propylene oxide (EO_{20} PO_{80}) has been used for purification of glucose-6-phosphate dehydrogenase, hexokinase and 3-phosphoglycerate kinase from bakers' yeast. This $EO_{20}PO_{80}$ copolymer has a cloud point of 18°C, at which temperature it phase separates from water. Enzymes were first partitioned at 4°C in an initial $EO_{20}PO_{80}$–dextran T500 aqueous two-phase system. This system had an upper copolymer-rich phase and a lower dextran-rich phase. After phase separation had occurred the upper $EO_{20}PO_{80}$-rich phase was removed and placed at 24°C. This resulted in formation of a new two-phase system with an upper water phase and a lower phase containing 98% copolymer and 2% water. Enzymes were recovered exclusively in upper water phase leaving a polymer-rich lower phase free of contamination. The phase diagram for the system $EO_{20}PO_{80}$ and dextran T500 at 4°C has been determined.

INTRODUCTION

Aqueous two-phase systems are widely used for separation and purification of biomolecules [1–3]. Use of these systems for purification of biological materials on a large scale has also been described [1,4–7]. In most instances these systems are composed of a poly(ethylene glycol) (PEG)-enriched upper phase and a dextran- or hydroxypropyl starch-enriched lower phase. Both phases contain 80–95% water. Phase separations can also be obtained by using PEG and a high concentration of salt. One problem encountered with these systems is difficulty separating target molecules from polymer solution. In other words, partitioning has the disadvantage that the process begins by adulteration of the target with two new polymers that must also be removed. These systems would also be more cost efficient if the polymer could be readily recycled without costly ultrafiltration or chromatography steps. Temperature-induced phase partitioning avoids these problems.

Many studies have been done on a group of non-ionic, linear polymers composed of poly(ethylene glycol) which are normally soluble in water, but which separate from solution when heated sufficiently [8–11]. The temperature at

* Corresponding author.

0021-9673/94/$07.00
SSDI 0021-9673(93)E1098-K

which this phenomenon occurs is known as the cloud point (CP) of the polymer. This phase separation results in a water-rich upper phase and a PEG-rich lower phase. It is possible to vary the temperature at which this separation occurs by changing the molecular mass of the polymer or by addition of various salts to the solution [11,12]. Studies have shown that incorporation of propylene oxide groups, to form a random copolymer of ethylene oxide and propylene oxide, also lowers the cloud point [13]. The degree to which the cloud point is lowered is dependent on the ratio of ethylene oxide to propylene oxide. Non-ionic surfactants containing ethylene oxide groups also exhibit a cloud point in aqueous solution. A surfactant of this type, Triton X-114, has been used for isolation of membrane proteins with temperature-induced phase separation [14].

Temperature-induced phase separation combined with aqueous two-phase partitioning or affinity partitioning offers a viable solution to problems of polymer removal and recycling. Recently, these systems have been introduced for enzyme purification [13,15]. Partition of steroids has also been studied in these systems [16]. Random, non-ionic copolymers of 50% ethylene oxide and 50% propylene oxide (UCON) when mixed with dextran or hydroxypropyl starch form aqueous two-phase systems very similar to a PEG–dextran system which can be used to purify biomolecules [13,15]. Target molecules are first partitioned at room temperature in a system composed of UCON and dextran or hydroxypropyl starch. UCON is enriched in upper phase and dextran or hydroxypropyl starch in lower phase. After separation has occurred, upper UCON-rich phase is removed and its temperature increased above the cloud point of UCON. This results in formation of a new two-phase system with an upper water phase and a lower UCON-rich phase. The cloud point of UCON (50°C) can be lowered to 37°C by addition of salt. In this new two-phase system biomolecules partition exclusively to the upper water phase, allowing the lower UCON-rich phase to be recovered and recycled for a second extraction. A simple purification scheme for biomolecules using temperature-induced phase partition combined with aqueous two-phase partition or affinity partition has been developed [13,15].

This study deals with application of a random, non-ionic copolymer composed of 20% ethylene oxide and 80% propylene oxide ($EO_{20}PO_{80}$) for aqueous two-phase partition and temperature-induced phase separation. Increasing propylene oxide concentration from 50% to 80% reduces the cloud point to 18°C which eliminates the need to add salt and lowers the polymer concentrations required to obtain two-phase separation. When $EO_{20}PO_{80}$ is mixed with dextran in water, it forms an aqueous two-phase system with a dextran-rich lower phase and a copolymer-rich upper phase. Enzyme partition and purification in an $EO_{20}PO_{80}$–dextran system could thus be performed at 4°C. Upper phase can be removed and placed at room temperature, 24°C, which is above the copolymer's cloud point. This results in formation of a new two-phase system with an upper water phase containing the biomolecules, and a lower copolymer-rich phase. We here present results of this study with glucose-6-phosphate dehydrogenase, hexokinase and 3-phosphoglycerate kinase. The phase diagram for the system $EO_{20}PO_{80}$, dextran T500 and water at 4°C has been determined. Partition and purification of glucose-6-phosphate dehydrogenase, hexokinase and 3-phosphoglycerate kinase from bakers' yeast have been performed using a combination of aqueous two-phase partition with $EO_{20}PO_{80}$–dextran T500 and temperature-induced phase separation at 24°C.

MATERIALS AND METHODS

Chemicals

Dextran T500 (M_r 500 000) was obtained from Pharmacia (Uppsala, Sweden) and PEG 4000 (M_r 4000) from Merck (Darmstadt, Germany). UCON 50-HB-5100 was a kind gift from Union Carbide (New York, USA). A random copolymer of 20% ethylene oxide and 80% propylene oxide ($EO_{20}PO_{80}$) was obtained from Berol Nobel (Stenungsund, Sweden). $EO_{20}PO_{80}$ was further purified by dissolving the polymer in water and adding dichloromethane. The polymer was extracted into the dichloromethane phase.

The solution of polymer in dichloromethane was dried with magnesium sulfate. Solvent was evaporated under vacuum at 65°C. After purification, copolymer purity, ratio of ethylene oxide to propylene oxide and molecular weight (M_r 2000) were determined by NMR in [$^2H_6$] dimethylsulphoxide (DMSO) solvent by comparing area of butyl groups (one butyl end group per copolymer molecule) to area of ethylene oxide and propylene oxide groups. All other chemicals were of analytical reagent grade.

Proteins

Glucose-6-phosphate dehydrogenase (G6PDH) from bakers' yeast (EC 1.1.1.49), hexokinase from bakers' yeast (EC 2.7.1.1) and 3-phosphoglycerate kinase (3-PGK) from bakers' yeast (EC 2.7.2.3) were purchased from Sigma (St. Louis, MO, USA).

Yeast extract

Yeast homogenate was prepared from commercial bakers' yeast by sonication after a 1:1 dilution in 50 m*M* triethanolamine–HCl buffer, pH 8.0, containing 2.0 m*M* EDTA. β-Mercaptoethanol was added to the solution to a concentration of $1.23 \cdot 10^{-3}$ *M*. Sonication was for 15 min in a Branson CP-30 sonifier. After testing for enzyme activity and protein concentration, yeast homogenate was centrifuged for 10 min at 12 000 *g* to remove cell debris. The pellet was discarded and supernatant was used for enzyme extraction experiments.

Two-phase systems and temperature-induced phase separation

All polymer concentrations were calculated as % (w/w). Aqueous two-phase systems were prepared from stock solutions of the polymers in water, 20% (w/w) $EO_{20}PO_{80}$, 30% (w/w) UCON, 30% (w/w) PEG 4000 and 20% (w/w) dextran T500. Dextran concentration was determined by polarimetry using an Optical Activity AA-5 automatic polarimeter (Optical Activity, UK) equipped with a sodium lamp set for 589 nm [2].

Polymer solutions were weighed out and mixed with water and buffer. The systems containing $EO_{20}PO_{80}$ were allowed to equilibrate 1 h at 4°C before addition of protein sample. Systems with either PEG or UCON for upper phase polymer were allowed to phase separate at room temperature. Addition of yeast extract was accomplished by adding 2 g extract to a phase system so that the total weight of the system was 10 g including extract. All partition experiments were performed in duplicate, with enzyme assays and protein determination being performed in triplicate. Systems without yeast extract were allowed to sit 30 min at 4°C to achieve phase separation. Systems containing yeast extract were centrifuged 5 min at 125 *g* to accelerate phase separation. The upper $EO_{20}PO_{80}$-rich phase was removed and isolated in a separate container. For systems with $EO_{20}PO_{80}$, separated upper phase was allowed to equilibrate 30 min at 24°C before centrifugation for 10 min at 125 *g*. This resulted in formation of a new two-phase system consisting of an upper water phase and a lower $EO_{20}PO_{80}$-rich phase [13,15,16]. Due to its high viscosity, this lower phase was diluted 5:1 before analysis, while the upper water-rich phase was analyzed without dilution.

Partition of enzymes between the phases was determined by removing appropriate amounts of each phase and assaying for enzyme activity. Partition of protein between the two phases is expressed by the partition coefficient, *K*, defined as

$$K = C_t / C_b$$

where C_t and C_b are concentrations of partitioned substance in moles per liter of top and bottom phases, respectively. For enzymes, *K* is measured as activity in units per ml in the top and bottom phases [2].

In many cases it is also advantageous to calculate the distribution ratio, *G*, defined as

$$G = K \cdot (V_t / V_b)$$

where V_t and V_b are volumes of upper and lower phases respectively. *G* gives the ratio between total amount of protein or enzyme in each phase [2].

Protein and enzyme assays

Protein was determined according to Bradford [17] using Coomassie Brilliant Blue G and mea-

sured at 595 nm with bovine serum albumin as standard.

Enzyme activity was determined photometrically at 340 nm using a Hewlett-Packard 8452A Diode Array Spectrophotometer (Hewlett-Packard, Palo Alto, CA, USA). Descriptions of the assays are found in the following references: glucose-6-phosphate dehydrogenase according to Noltmann *et al.* [18]; hexokinase according to Maitru [19]; 3-phosphoglycerate kinase according to Scopes [20].

Determination of binodal and tie lines

The binodal represents the borderline between one and two phases and the tie line describes composition of the two phases when in equilibrium. The binodal for the system $EO_{20}PO_{80}$ and dextran T500 was determined as described by Albertsson [2] (Fig. 1). Tie lines for this system were determined by removing samples from upper and lower phases after separation was complete and measuring dextran concentration. Since total phase composition was known from weight of polymers added, knowledge of dextran concentration in upper and lower phases allowed determination of tie lines.

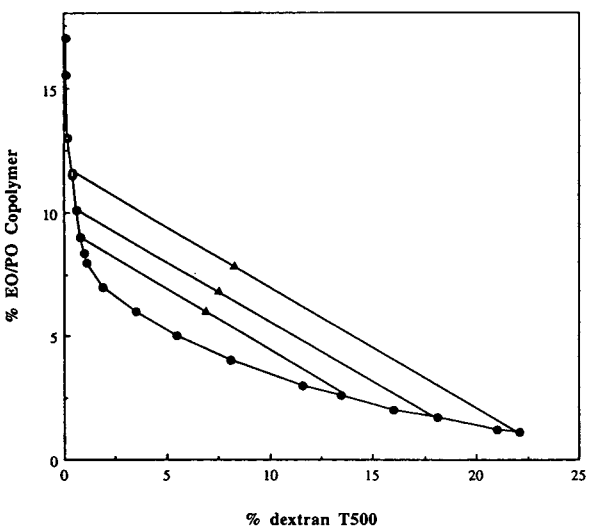

Fig. 1. Phase diagram for $EO_{20}PO_{80}$ (M_r 2000) and dextran T500 (M_r 500 000) and water at 4°C. (●) Points obtained by titration [2] or (▲) analysis of separated phases of the systems.

Cloud point determination and composition of copolymer phase at 24°C

The cloud point (CP) of $EO_{20}PO_{80}$ copolymer was determined visually by placing a 10% solution of polymer in water in a sealed glass tube and placing the tube into an ethanol bath. Temperature was increased in 1°C increments from 4°C, where the solution was clear, to 18°C, where the solution became cloudy.

Composition of lower copolymer phase at 24°C was determined by removing upper water phase and placing lower $EO_{20}PO_{80}$-enriched phase at 80°C under vacuum until a constant weight was reached. To remove any residual water, toluene was added to a concentration of 50% and solution was returned to 80°C and vacuum. After 3 hours constant weight was again obtained. Amount of water contained in this lower phase was calculated by subtracting final weight of sample from starting weight.

RESULTS AND DISCUSSION

Phase diagram

The phase diagram for $EO_{20}PO_{80}$, dextran T500 and water at 4°C is shown in Fig. 1. Ethylene oxide–propylene oxide copolymer was enriched in upper phase while dextran T500 was enriched in lower phase. Comparison of the phase diagram for this system with the phase diagram of PEG 4000–dextran T500 shows that the critical points of these systems are similar, even though the molecular mass of the $EO_{20}PO_{80}$ copolymer (2000) is half that of PEG 4000 [13]. This means that polymer concentrations required to achieve two-phase separations are lower with the $EO_{20}PO_{80}$ copolymer compared with PEG. For a PEG 2000–dextran T500 system the critical point must be higher than for $EO_{20}PO_{80}$–dextran T500, since lowering the polymer molecular mass increases the polymer concentrations required for phase separation [2]. Phase separation at lower polymer concentrations can be explained by increased hydrophobicity of $EO_{20}PO_{80}$ copolymer (20% ethylene oxide and 80% propylene oxide) when compared to PEG (100% ethylene oxide). This increase in hydrophobicity leads to an increase in net repulsive interaction between polymers, and thus to

phase separation at lower polymer concentrations [2,21]. Lower temperatures may result in a slightly lower binodal, but this effect is small [2,22]. Comparison of binodal lines at 8°C, 23°C, 38°C and 50°C for the system PEG 6000/dextran T70 shows that the temperature change has very little effect on the critical point [23].

Cloud point and composition of copolymer phase at 24°C

PEG (100% ethylene oxide) is a linear non-ionic polymer which is water soluble until heated above its cloud point (112°C for PEG M_r 20 000) [8–10]. Decreased solubility at higher temperatures can be explained by conformational changes in the ethylene oxide chain. At lower temperatures polar conformations of the polymer chain are dominating whereas at higher temperatures non-polar conformations are more abundant. The non-polar conformations are less hydrophilic than the polar conformations so that excess of non-polar conformations leads to decreased polymer solubility [11]. The increase in temperature results in polymer separating from water and forming a separate phase. It is possible to manipulate the cloud point of a polymer by addition of salt or by changing polymer molecular mass [11,12]. Changing the ratio of ethylene oxide to propylene oxide will also lower the cloud point [13]. A random, linear non-ionic copolymer (UCON 50-HB-5100, M_r 4000) which is composed of 50% ethylene oxide and 50% propylene oxide has a cloud point of 50°C [13,15,24]. As long as water solubility is retained these copolymers will form aqueous two-phase systems with dextran T500. The polymer used in this study is a linear, non-ionic random copolymer of 20% ethylene oxide and 80% propylene oxide with a relative molecular mass of 2000. The cloud point for a 10% solution of this copolymer was determined to be 18°C, which is below normal room temperature. In order to achieve an aqueous two-phase system with dextran, it was necessary to perform partition experiments below the cloud point of $EO_{20}PO_{80}$. This was accomplished by using a cold room at 4°C for initial partitioning steps. Removal of this initial upper phase from the cold room and placement at room temperature, 24°C, resulted in formation of a new aqueous two-phase system with an upper water-rich phase and a lower copolymer-rich phase. The composition of lower phase formed at 24°C, as determined by vacuum drying, is 98% $EO_{20}PO_{80}$ and 2% water.

Partition of pure glucose-6-phosphate dehydrogenase, hexokinase and 3-phosphoglycerate kinase

Commercially prepared G6PDH, hexokinase and 3-PGK from bakers' yeast were partitioned in two different $EO_{20}PO_{80}$–dextran T500 systems. The first system was 7% copolymer, 4% dextran and 0.01 M sodium phosphate buffer (Table I). The K values at 4°C for partition between the $EO_{20}PO_{80}$ and dextran phases were 0.75 for G6PDH, 1.01 for hexokinase and 0.71

TABLE I

PARTITION OF GLUCOSE-6-PHOSPHATE DEHYDROGENASE, HEXOKINASE AND 3-PHOSPHOGLYCERATE KINASE

Primary phase system: 7% $EO_{20}PO_{80}$, 4% dextran T500, 0.01 M sodium phosphate buffer, pH 7.0, 20 units glucose-6-phosphate dehydrogenase, 20 units hexokinase and 45 units 3-phosphoglycerate kinase. K and G values at 24°C are for partition between water and $EO_{20}PO_{80}$ phases formed by the increase in temperature. Y = % yield of enzymes recovered in water phase at 24°C.

Enzyme	K (4°C)	G (4°C)[a]	K (24°C)[b]	G (24°C)	Y
G6PDH	0.75	1.77	40	368	60
Hexokinase	1.01	2.38	141	>1000	61
3-PGK	0.71	1.67	29	272	62

[a] Volume ratio = $(V_t/V_b) = 2.36$.
[b] Volume ratio = $(V_t/V_b) = 9.17$.

for 3-PGK. At 24°C the partition values were much higher for all enzymes. K was 40 for G6PDH, 141 for hexokinase and 29 for 3-PGK. These very high partition values at 24°C reflect the reluctance of biomolecules to go into this hydrophobic phase which contains a high concentration of copolymer [13,15,16]. G values at 24°C were high due to large partition coefficients, small volumes of lower copolymer-rich phase and large volumes of upper water phase in this system. Amount of enzyme recovered in this upper water phase at 24°C was 60% for G6PDH, 61% for hexokinase and 62% for 3-PGK. The percentage of recovered enzyme activity is calculated from the original added enzyme activity at 4°C. No enzyme activity was lost in the initial aqueous two-phase system.

While partition coefficients for the above system were good, to achieve a higher yield it was desirable to find a system with a higher ratio of V_t/V_b at 4°C. For this reason the system 8.5% $EO_{20}PO_{80}$, 2.0% dextran T500 and 0.01 M sodium phosphate buffer was chosen (Table II). This system has a volume ratio of 4.28 for copolymer–dextran phases at 4°C, and 7.69 for water–copolymer phases at 24°C. However, moving further away from the critical point of the phase diagram resulted in lower partition coefficients [2]. At 4°C, K was 0.19 G6PDH, 0.58 for hexokinase and 0.54 for 3-PGK. At 24°C, increased concentration of copolymer served to drive enzymes completely into upper water phase, as no activity was detected in lower $EO_{20}PO_{80}$ phase. Increased G values at 4°C helped to increase enzyme recovery to 73% for G6PDH, 124% for hexokinase and 72% for 3-PGK. Hexokinase recovery was probably over 100% due to inactivation of this enzyme in concentrated, hydrophobic upper phase at 4°C. After partitioning to upper water phase which was virtually free of copolymer at 24°C, enzyme activity increased greatly resulting in a high yield.

Partition of enzymes in three systems with differing hydrophobicities has also been studied (Table III). Systems were chosen with equal tie line lengths so that enzyme partition in the phases could be compared [2]. All systems contained 0.01 M sodium phosphate buffer, pH 7.0. While partition in PEG–dextran and UCON–dextran was performed at 22°C, partition in the $EO_{20}PO_{80}$–dextran system was at 4°C. However, this temperature change should have little effect on enzyme partition [22]. The polymers which formed the upper phase were either PEG 4000 (M_r 4000), UCON 50-HB-5100 (M_r 4000) or $EO_{20}PO_{80}$ (M_r 2000), while bottom-phase polymer was dextran T500 in all systems. Since the amount of ethylene oxide groups was 100, 50 and 20%, respectively, this made it possible to study the effect of both hydrophobicity and molecular mass on enzyme partition. Decreasing the molecular mass of a polymer should increase enzyme partition into

TABLE II

PARTITION OF GLUCOSE-6-PHOSPHATE DEHYDROGENASE, HEXOKINASE AND 3-PHOSPHOGLYCERATE KINASE

Primary phase system: 8.5% $EO_{20}PO_{80}$, 2% dextran T500, 0.01 M sodium phosphate buffer, pH 7.0, 20 units glucose-6-phosphate dehydrogenase, 20 units hexokinase and 45 units 3-phosphoglycerate kinase. K and G values at 24°C are for partition between water and $EO_{20}PO_{80}$ phases formed by the increase in temperature. Y = % yield of enzymes recovered in water phase at 24°C.

Enzyme	K (4°C)	G (4°C)[a]	K (24°C)[b]	G (24°C)	Y
G6PDH	0.19	1.42	>100	>100	73
Hexokinase	0.58	4.41	>100	>100	124
3-PGK	0.54	4.11	>100	>100	72

[a] Volume ratio = $(V_t/V_b) = 4.28$.
[b] Volume ratio = $(V_t/V_b) = 7.69$.

TABLE III

PARTITION OF G6PDH, HEXOKINASE AND 3-PGK IN THREE-PHASE SYSTEMS WITH DIFFERENT HYDROPHOBICITY IN THE UPPER PHASE IN THE ORDER PEG 4000 < UCON < $EO_{20}PO_{80}$

Systems contained 0.01 *M* sodium phosphate buffer, pH 7.0. For systems with PEG 4000 and UCON *K* values are for partition between upper and lower phase at 22°C. For system with $EO_{20}PO_{80}$ *K* values are for partition between upper and lower phase at 4°C. All systems were chosen so that tie line lengths were equal.

System	*K* G6PDH	*K* hexokinase	*K* 3-PGK
7.0% PEG 4000–7.0% dextran T500	0.21	0.50	0.43
5.1% UCON 50-HB-5100–7.0% dextran T500	0.13	0.50	0.36
7.0% $EO_{20}PO_{80}$–4.0% dextran T500	0.19	0.58	0.54

the phase rich in that polymer [31,32]. Comparison of partition between the PEG 4000 and UCON systems shows that the increase in hydrophobicity lowered the *K* values for G6PDH (0.21 to 0.13) and 3-PGK (0.43 to 0.36), while hexokinase was unaffected (0.50 in both systems). However, in the $EO_{20}PO_{80}$ systems *K* values increased for hexokinase (0.58) and 3-PGK (0.54). *K* for G6PDH (0.19) was higher than in the UCON system, and only slightly lower than in the PEG system. These results are interesting in that they show that decreased molecular mass has more effect on enzyme partition than an increase in hydrophobicity.

Partition and purification of enzymes from yeast homogenate

Partition and purification of G6PDH, hexokinase and 3-PGK from yeast homogenate after centrifugation were performed in a system composed of 8.5% $EO_{20}PO_{80}$, 2% dextran T500, 0.02 *M* sodium phosphate buffer, pH 7.0, and 20% yeast extract (Tables IV and V). Partition was carried out as previously described except that primary phase system at 4°C was centrifuged 5 min at 125 *g* to accelerate phase separation when yeast extract was present. Most protein and cell debris partitioned to lower dextran-rich phase, resulting in increased volume and viscosity for this phase, while upper copolymer-rich phase remained clear. Total protein content and enzyme activity were measured in raw homogenate, homogenate after centrifugation, upper and lower phases at 4°C, and upper and lower phases at 24°C. Specific activity (units per mg protein) was calculated for each enzyme, with specific activity in raw homogenate (uncentrifuged) being set equal to a purification factor of 1. *K* values at 4°C were 0.05 for protein, 0.18 for G6PDH, 0.53 for hexokinase and 0.98 for 3-PGK, with G values of 0.2, 0.75, 2.21 and 4.07, respectively (Table IV).

In previous reports, after removing upper copolymer-rich phase formed during this primary partitioning step, it was necessary to add sodium sulfate to a concentration of 0.2 *M* to lower the cloud point of this phase, since many enzymes are denatured at 50°C [13,15]. However, since the cloud point of $EO_{20}PO_{80}$ is 18°C, no salt addition was necessary and phase separation could be achieved close to room temperature (24°C). The time required for phase separation

TABLE IV

PARTITION OF GLUCOSE-6-PHOSPHATE DEHYDROGENASE, HEXOKINASE AND 3-PHOSPHOGLYCERATE KINASE FROM YEAST EXTRACT

Primary phase system: 8.5% $EO_{20}PO_{80}$, 2.0% dextran T500, 0.02 *M* sodium phosphate buffer, pH 7.0, and 20% yeast extract. *K* and *G* values at 24°C are not given as there was no detectable enzyme activity or protein in the lower phase at this temperature.

Sample	*K* (4°C)	*G* (4°C)[a]
Protein	0.05	0.20
G6PDH	0.18	0.75
Hexokinase	0.53	2.21
3-PGK	0.98	4.07

[a] Volume ratio = $V_t/V_b = 4.0$.

TABLE V

PURIFICATION OF GLUCOSE-6-PHOSPHATE DEHYDROGENASE, HEXOKINASE AND 3-PHOSPHOGLYCERATE KINASE FROM YEAST HOMOGENATE

Primary phase system: 8.5% $EO_{20}PO_{80}$, 2.0% dextran T500, 0.02 *M* sodium phosphate buffer, pH 7.0, and 20% yeast extract. *Y* = % yield of enzymes. *PF* = purification factor at 24°C[a].

Sample	G6PDH		Hexokinase		3-PGK	
	PF	*Y*	*PF*	*Y*	*PF*	*Y*
Raw homogenate	1	–	1	–	1	–
After centrifugation	2.4	71	2.1	64	3.2	96
Upper phase 4°C	4.2	52	13.0	69	15.7	80
Upper phase 24°C	5.3	50	15.3	67	15.4	72

[a] The specific activity of an enzyme (units per mg protein) in the homogenate was equivalent to a purification factor of 1.

was reduced by centrifugation at 125 *g*. At 24°C, no enzyme activity or protein was detected in lower copolymer-rich phase. All of the enzyme activity and protein were contained in the upper water-rich phase free of copolymer. Recovery of enzyme in this upper water phase at 24°C was 50% for G6PDH, 67% for hexokinase and 72% for 3-PGK (Table V). Purification factors in this system were also good, with 5.3 for G6PDH, 15.3 for hexokinase and 15.4 for 3-PGK. These high purification factors are a result of the extremely low protein partition coefficient (0.05) at 4°C, which resulted in most of the protein and cell debris being found in lower dextran-rich phase.

Purification scheme using temperature-induced phase separation

Currently a popular method for large-scale separation of biomolecules is based on a two-phase system composed of PEG and high concentrations (7 to 10%) of a salt such as sodium phosphate or sodium sulfate [1,25–27]. These systems allow recovery and recycling of PEG polymer. Calculations have shown that a purification scheme using aqueous two-phase partitioning is economically competitive with other purification methods [4,5,28–30]. However, the high concentration of salt in PEG-salt systems is a drawback. Disposal of salts presents an ecological problem, and many biomolecules are denatured by these systems. In addition, it is impossible to use an affinity ligand in these systems when binding is based on electrostatic forces.

A scheme for enzyme purification using temperature-induced phase formation has been previously proposed [13,15]. A purification scheme which allows enzyme to be obtained in a water–buffer–salt phase free of cell debris and includes recycling of UCON polymer was presented [13]. After formation of the second phase system at increased temperature, the lower UCON-rich phase was recovered and recycled in a second extraction. In another example an affinity ligand was attached to UCON polymer and used to selectively purify G6PDH from yeast extract, with recovery of G6PDH in a water–buffer–salt solution and recovery of UCON-ligand in final UCON phase [15]. In contrast to these schemes which called for addition of salt to a concentration of 0.2 *M* and a substantial increase in temperature, when using the copolymer $EO_{20}PO_{80}$ formation of a second aqueous two-phase system requires no salt and this system forms readily at room temperature (Fig. 2). The low temperature (24°C) at which temperature-induced phase separation is performed eliminates any heat denaturation of sensitive biomolecules and simplifies use of affinity ligands as no salt is present in the system.

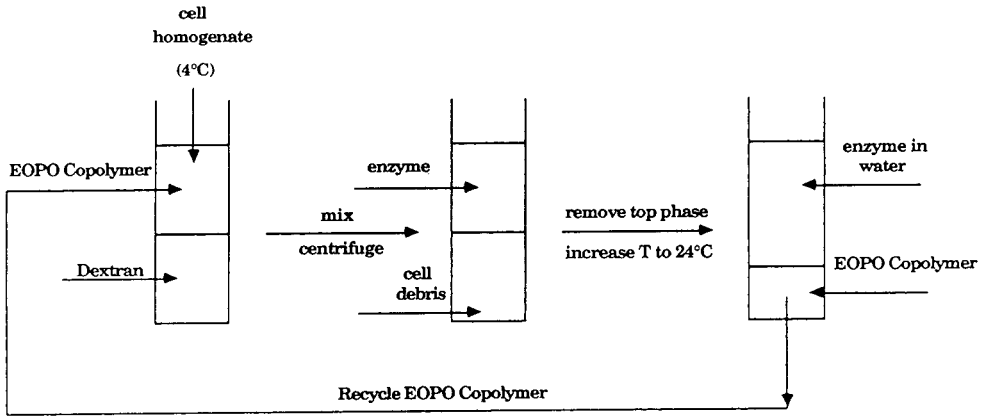

Fig. 2. Enzyme purification scheme using aqueous two-phase partitioning at 4°C and temperature-induced phase separation at 24°C, with recycling of the $EO_{20}PO_{80}$ copolymer.

CONCLUSIONS

A copolymer of 20% ethylene oxide and 80% propylene oxide with a cloud point at 18°C has been used in aqueous two-phase partitioning to purify enzymes from yeast homogenate. This copolymer forms an aqueous two-phase system at 4°C when mixed with dextran T500. The copolymer is enriched in the upper phase and dextran T500 in the lower phase. Proteins partition strongly to the lower dextran phase of this system. After phase separation occurs, the upper copolymer phase containing target enzymes is removed and placed at 24°C, which is above this polymer's cloud point. The temperature increase leads to formation of a new two-phase system composed of a water upper phase and a concentrated copolymer lower phase. Enzymes and proteins partition almost exclusively to the upper water phase of this system. Enzyme yield can be increased by manipulation of polymer concentrations. A simple purification scheme for biomolecules based on this extraction technique is proposed, in which target molecules are recovered in a water–buffer solution and copolymer can be easily recovered and recycled.

ACKNOWLEDGEMENTS

The authors gratefully acknowledge the generous financial support of The National Institute of Health, The National Aeronautics and Space Administration and The Swedish National Board for Industrial and Technical Development (NUTEK). Also, we thank Berol Nobel AB, Stenungsund, Sweden, for synthesis of the 20% ethylene oxide–80% propylene oxide random copolymer.

REFERENCES

1 H. Hustedt, K.H. Kroner and M.-R. Kula, in H. Walter, D.E. Brooks and D. Fisher (Editors), *Partitioning in Aqueous Two-Phase Systems: Theory, Methods, Uses and Applications to Biotechnology*, Academic Press, Orlando, FL, 1985, pp. 529–587.
2 P.-Å. Albertsson, *Partition of Cell Particles and Macromolecules*, Wiley, New York, 3rd ed., 1986.
3 G. Johansson, in J.-C. Janson and L. Rydén (Editors), *Protein Purification: Principles, High Resolution Methods and Applications* VCR Publishers, New York, 1989, pp. 330–345.
4 A. Cordes and M.-R. Kula, *J. Chromatogr.*, 376 (1986) 375–384.
5 G. Johansson and F. Tjerneld, *J. Biotechnol.*, 11 (1989) 135–142.
6 F. Tjerneld and G. Johansson, *Bioseparations*, 1 (1990) 255–263.
7 F. Tjerneld, in J.M. Harris (Editor), *Poly(EthyleneGlycol) Chemistry: Biotechnical and Biomedical Applications*, Plenum Press, New York, 1992, pp. 85–102.
8 F.E. Bailey, Jr and J.V. Kloeske, *Poly(ethylene oxide)*, Academic Press, New York, 1976.
9 S. Saeki, N. Kuwahara, M. Nakata and M. Kaneko, *Polymer*, 17 (1976) 685–689.

10 R. Kjellander and E. Florin, *J. Chem. Soc., Faraday Trans. 1*, 77 (1981) 2053–2077.
11 G. Karlström, *J. Phys. Chem.*, 89 (1985) 4962–4964.
12 E. Florin, R. Kjellander and J. Eriksson, *J. Chem. Soc. Faraday Trans 1*, 89 (1984) 2889–2919.
13 P.A. Harris, G. Karlström and F. Tjerneld, *Bioseparations*, 2 (1991) 237–246.
14 C. Bordier, *J. Biol. Chem.*, 25 (1981) 1604–1607.
15 P.A. Alred, F. Tjerneld, T. Kozlowski and J.M. Harris, *Bioseparations*, 2 (1992) 363–373.
16 P.A. Alred, F. Tjerneld and R. Modlin, *J. Chromatogr.*, 628 (1993) 205–214.
17 M.M. Bradford, *Anal Biochem.*, 72 (1976) 248–254.
18 E.A. Noltmann, C.J. Gubler and S.A. Ruby, *J. Biol. Chem.*, 236 (1961) 1225–1230.
19 P.K. Maitru, *Methods Enzymol.*, 42 (1975) 25–30.
20 R.K. Scopes, *Methods Enzymol.*, 42 (1975) 127–134.
21 Å. Gustafsson, H. Wennerström and F. Tjerneld, *Polymer*, 27 (1986) 1768–1770.
22 D. Forciniti, C.K. Hall and M.-R. Kula, *Fluid Phase Equilibria*, 61 (1991) 243–262.
23 B.Y. Zaslavsky, T.O. Bagirov, A.A. Borovskaya, N.D. Gulaeva, L.H. Miheeva, A.U. Mahmudov and M.N. Rodnikova, *Polymer*, 30 (1989) 2104–2111.
24 H.-O. Johansson, G. Karlström and F. Tjerneld, *Macromolecules*, 26 (1993) 4478–4483.
25 M.-R. Kula, K.H. Kroner and H. Hustedt, *Adv. Biochem. Eng.*, (1982) 73–118.
26 K.H. Kroner, H. Hustedt and M.-R. Kula, *Process. Biochem.*, 19 (1984) 170–179.
27 M.-R. Kula, *Bioseparations*, 1 (1990) 181–189.
28 K.H. Kroner, A. Cordes, A. Schelper, M. Morr, A.F. Buckmann and M.-R. Kula, in T.C.J. Gribnau, J. Visser and R.J.F. Nivard (Editors), *Affinity Chromatography and Related Techniques*, Elsevier, Amsterdam, 1982, pp. 491–501.
29 G. Johansson and M. Joelsson, *Biotechnol. Bioeng.*, 27 (1985) 621–625.
30 F. Tjerneld, G. Johansson and M. Joelsson, *Biotechnol. Bioeng.*, 30 (1987) 809–816.
31 P.-Å. Albertsson, A. Cajarville, D.E. Brooks and F. Tjerneld, *Biochim. Biophys. Acta*, 926 (1987) 87–93.
32 N.L. Abbot, D. Blankschtein and T.A. Hatton, *Macromolecules*, 24 (1991) 4334–4348.

Journal of Chromatography A, 659 (1994) 299–305
Elsevier Science B.V., Amsterdam

CHROM. 25 600

Salting effects in reversed mobile phases on chiral separation of benzonaphthazepine stereoisomers

Jian G. Ning

Schering-Plough Research Institute, Department of Chemical Development Control and Compliance, 1011 Morris Avenue, Union, NJ 07083 (USA)

(First received August 5th, 1993; revised manuscript received September 28th, 1993)

ABSTRACT

The salting-in effect of $NaClO_4$ in reversed mobile phases *versus* the salting-out effect of NaCl on the separation of benzonaphthazepine (BNA) stereoisomers was evaluated. The critical role of $NaClO_4$ in the mobile phase was examined. A hypothesis was proposed on the salting-in effect compared with the effect of ion-pair reagents. A mechanism of separation of BNA stereoisomers was suggested based on molecular modeling of BNA enantiomers and diastereomers.

INTRODUCTION

There is much research and development work reported on the salting effects on protein purification [1–3], ion-exchange chromatography [4–6], thin-layer chromatography [7–9], and headspace gas chromatography [10]. For instance, Roettger *et al.* [1] reported that aqueous mobile phases with high salt concentrations are often used to adsorb proteins onto mildly hydrophobic supports. Jandera *et al.* [5] described the separation of saccharides, aldehydes, ketones, ethers, and alcohols by salting-out and solubilization chromatography on ion-exchange columns. Cserhati *et al.* [8] studied salting-in and salting-out effects on reversed-phase thin-layer chromatography of 15 dansylated amino acid derivatives. Another interesting paper, by Nagai [10], reported the improved sensitivity of headspace gas chromatography by salting effects and its application to residual solvent analysis of medicines.

Recently Ishikawa and Shibata [11] reported that a reversed mobile phase system similar to the one described in this paper attained good chiral separation on propranolol, and $NaClO_4$ and other salts were added as anionic chaotropes in the mobile phase. The paper also reported that the use of conventional ion-pair reagents such as undecanesulfonate was not successful in an attempt to replace $NaClO_4$ salt. However, the authors explained the separation mechanism in terms of chaotropicity and tried to generalize the critical role of $NaClO_4$ as that of conventional ion-pair reagents.

This paper describes the use of $NaClO_4$ as salting-in agent to promote chiral selectivity of a oligocellulose tris(3,5-dimethylphenylcarbamate) stationary phase on benzonaphthazepine (BNA) stereoisomers. The behavior of analytes in terms of interactions with two different kinds of salts in the mobile phase and chiral stationary phase was examined. A hypothesis of the separation mechanism different from conventional ion-pair chromatography is proposed at the molecular level with the assistance of CAche a three-dimensional molecular modeling tool.

EXPERIMENTAL

Reagents

The following reagents were used: deionized water (MilliQ Reagent Water System, Milli-

0021-9673/94/$07.00
SSDI 0021-9673(93)E1027-W

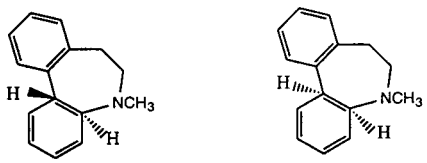

Fig. 1. Molecular structures of BNA stereoisomers.

pore), acetonitrile (ACN) (Optima, Fisher Chemical), sodium chloride (Certified ACS, Fisher Chemical), sodium perchlorate (HPLC grade, Fisher Chemical) and potassium dihydrogen phosphate (Certified ACS, Fisher Chemical).

HPLC system and chromatographic conditions

The chromatographic equipment consisted of a Waters Module I networked into a Waters 840 ExpertEase Station with a Chiralcel OD-R 25 cm × 4.6 mm I.D. column (10 μm particle size, manufactured by Daicel Chemical Industries) and a UV detector (210 nm). The flow-rate was 1.0 ml/min and temperature 40°C. The mobile phase was (0.25 to 0.75 *M* $NaClO_4$–0.02 *M* KH_2PO_4, pH 4.7)–acetonitrile (60:40). The samples were dissolved in acetonitrile–water (50:50).

RESULTS AND DISCUSSION

The molecular structures of the benzonaphthazepine (BNA) stereoisomers are shown in Fig. 1. BNA has two chiral centers, and therefore, two pairs of enantiomers and four stereoisomers, *i.e.*, (−)*trans*, (+)*trans*, (−)*cis*, and (+)*cis* isomers.

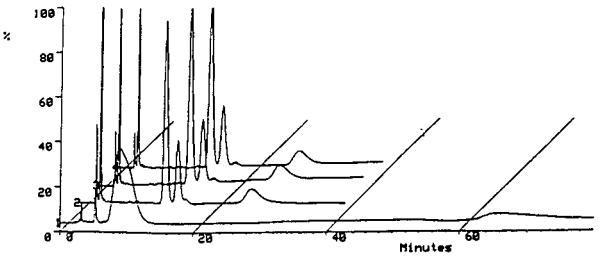

Fig. 2. The effect of the concentration of $NaClO_4$ on the separation of BNA. Chromatograms: 1 = 0 *M* $NaClO_4$; 2 = 0.25 *M* $NaClO_4$; 3 = 0.50 *M* $NaClO_4$; 4 = 0.75 *M* $NaClO_4$.

$NaClO_4$ salt effects on separation

The critical role of $NaClO_4$ on the separation of four stereoisomers of BNA is shown in Table I.

Fig. 2 shows the overlay of four chromatograms Nos. 1–4, corresponding to the concentrations of $NaClO_4$ in the mobile phase from 0 to 0.75 *M*. The amazing separating power of $NaClO_4$ was clearly demonstrated and it was shown that the separation was concentration dependent. Without $NaClO_4$, the last peak eluted at 65 min and the critical pair of (+)*trans* and (−)*cis* isomers of BNA coeluted. As the concentration of $NaClO_4$ increased from 0.25 to 0.50 and 0.75 *M* (in terms of aqueous constituent), the run time did not increase, while the resolution factor increased from 0.8 to 1.0 and 1.4 correspondingly, which was further optimized to 1.6 in later experiments.

TABLE I

THE $NaClO_4$ EFFECT ON SEPARATION

Mobile phase: 0–0.75 *M* $NaClO_4$, pH 4.7–ACN (60:40), 1 ml/min.

$NaClO_4$ (*M*)	t_R (min)				R_s (−)*cis* and (+)*trans*
	(−)*trans*	(−)*cis*	(+)*trans*	(+)*cis*	
(1) 0.00					no separation
(2) 0.25	10.9	13.0	14.4	24.4	0.8
(3) 0.50	12.0	13.5	15.0	25.0	1.0
(4) 0.75	12.7	14.1	16.0	25.2	1.4

TABLE II

SALTING-IN EFFECT OF $NaClO_4$ ON $CHCl_3$

	Into water	Into water–ACN (1:1)
Add $CHCl_3$	$CHCl_3$ lower phase	$CHCl_3$ rises to top
Add $NaClO_4$	$CHCl_3$ dissolves in water	$CHCl_3$ dissolves, one phase
Add NaCl	$CHCl_3$ lower phase	$CHCl_3$ mixed in ACN, upper phase, water lower phase

Research has indicated that addition of certain kinds of salt into a hydrocarbon solute–water solution increases the hydrophobic effect by electrostriction of water that decreases the solubility of hydrocarbons and thus promotes their association [12]. These kinds of salts are known as salting-out agents. On the other hand, addition of other salts in a hydrocarbon solute–water solution will decrease the hydrophobic effect, by breaking up the electrostriction of water that increases the solubility of hydrocarbons and thus demotes their association. The latter are referred to as salting-in agents. The salting effects on non-electrolytes can be measured by the salting coefficient [13]. In a diluted solution the linear term usually suffices:

$$\log S^0/S = K_s C_s \quad (1)$$

where S^0 is the solubility of solute in pure solvent, S the solubility of solute in salt–solvent system, K_s the salt–non-electrolyte interaction (or salting) parameter, and C_s the molar concentration of the solute.

The experiments given in Table II are designed to see salting-in effects of $NaClO_4$ salt on a hydrocarbon–water solution in a qualitative way at a higher concentration (compared to the diluted concentration of the salt in the mobile phase).

As we noticed, the addition of $NaClO_4$ in a $CHCl_3$–water or a water–ACN solution turns a heterogeneous solution into a homogenous one. This is an indication of the salting-in effect of $NaClO_4$ on a $CHCl_3$–water or a water–ACN system, promoting solubility of $CHCl_3$ in the system. However, NaCl does not have the same salting-in effect as $NaClO_4$, leaving $CHCl_3$ in the heterogeneous solution. Referring to eqn. 1, we would conclude that the salting parameter K_s of $NaClO_4$ in the system is negative since $S^0 < S$. To see if there is the same kind of salting effect of $NaClO_4$ in a BNA–water–ACN system, the experiment described in Table III was carried out.

The results show that although BNA does not dissolve in water alone in the presence of either of the salts (this is probably because of the limited solubility of BNA in water), $NaClO_4$ does help BNA get into the solution in a water–ACN system. It was further observed, that addition of NaCl to a BNA–water–ACN solution first will cause the organic layer to phase out from a homogeneous solution, and that sub-

TABLE III

SALTING-IN EFFECT OF $NaClO_4$ ON BNA

	Into water	Into water–ACN (1:1)
Add BNA	BNA is suspended	BNA dissolves
Add more BNA	–	Solution is turbid
Add $NaClO_4$	BNA is suspended	Solution is clear
Add NaCl	BNA is suspended	Solution separates into two phases

sequent addition of $NaClO_4$ will bring the two phases together again into a homogeneous solution. This is to say that it is the type of the salt, not the quantity of the salt, that makes BNA soluble in the system, and obviously $NaClO_4$ salts-in BNA into the solution, while NaCl salts-out BNA from the solution.

The different salting effects of $NaClO_4$ and NaCl on the separation of BNA in the chromatographic system were further investigated and the results are shown in Table IV.

Figs. 3–5 show the chromatograms generated from mobile phases with two different kinds of salts under identical chromatographic conditions

Under almost identical chromatographic conditions, $NaClO_4$ plays a distinctive role in the separation of the four isomers with satisfactory resolution, but NaCl can not resolve the (−)*trans* and (−)*cis* isomers. Further attempts were made to separate the (−)*trans* and (−)*cis* isomers in NaCl mobile phase: variables included concentration of the salt, percentage of ACN, flow-rate, etc. None of them produced acceptable results. In one of the attempts we decreased the percentage ACN in the mobile phase in order to separate the (−)*trans* from the (−)*cis* isomer through the increased retention of BNA in the stationary phase. The result is shown in Fig. 5.

The (−)*trans* isomer still coelutes with the (−)*cis* isomer and the resolution between other peaks is also lost because of the 10% decrease of ACN.

Obviously, the properties of different salts give significantly different chromatographic effects. The salting-in effect of $NaClO_4$ makes BNA stereoisomers more soluble in the mobile

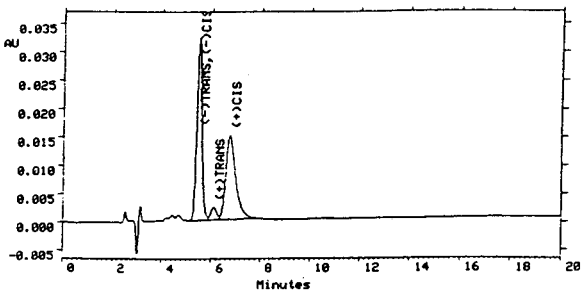

Fig. 3. The effect of the NaCl mobile phase on the separation of BNA isomers.

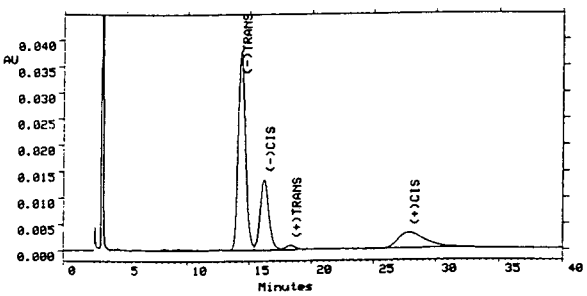

Fig. 4. The effect of $NaClO_4$ on the separation of BNA isomers.

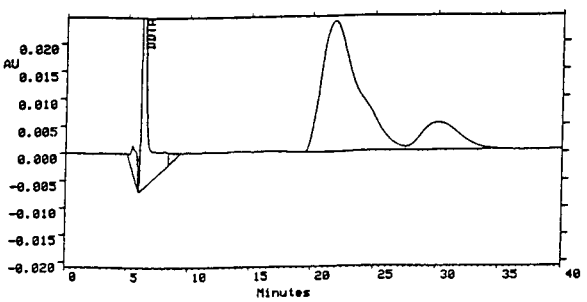

Fig. 5. Chromatogram after a decrease of %ACN in the NaCl mobile phase. Mobile phase: 0.75 *M* NaCl, pH 4.7–ACN (70:30), 0.5 ml/min.

TABLE IV

COMPARISON OF THE EFFECTS OF $NaClO_4$ AND NaCl IN MOBILE PHASE

Mobile phase: (0.75 *M* $NaClO_4$ or NaCl, pH 4.7)–ACN (60:40), 1 ml/min.

Salt	t_R (min)				R_s (−)*cis* and (+)*trans*
	(−)*trans*	(−)*cis*	(+)*trans*	(+)*cis*	
NaCl	5.6	5.6	6.1	6.8	no separation
$NaClO_4$	14.5	16.6	18.4	27.8	1.5

phase so that a chiral stationary phase can selectively retain four stereoisomers in an optimal condition. The salting-out effect of NaCl promotes hydrophobic association of stereoisomers themselves more than the retention of stereoisomers to the chiral stationary phase so that the chiral stationary phase cannot discriminate between the (−)*trans* and (−)*cis* isomers.

Based on this observation, it is proposed that the salting-in agent in this chiral system works in quite a different way from what a conventional ion-pair reagent does in a non-chiral reversed-phase system. In a non-chiral reversed-phase system, ionic solutes are paired with organic ion-pair reagents to increase the hydrophobic interaction in the mobile phase and, therefore, the retention of the solutes in the stationary phase (by increasing the affinity of solutes to the stationary phase). In this chiral system, an inorganic salt is introduced into the mobile phase to increase the hydrophilic interaction of the stereoisomers (by increasing the solubility of the solute in the mobile phase) and to provide optimal conditions for the chiral stationary phase to work with. In a sense, the salting-in agent works more with the mobile phase, while the ion-pair reagent works more with the stationary phase. However, the salting-in agent cannot be solely responsible for the separation. The synergy is only achieved by the combination of an appropriate eluting strength of composition of the organic and aqueous phases, a proper concentration of the salting-in agent, the "magic" pH effect, and the chiral recognition of the stationary phase.

The chemistry of the chiral stationary phase Chiralcel OD-R was first revealed as the oligomer cellulose tris(3,5-dimethylphenyl carbamate) on a 10-μm silica gel [14], however, there exist no exact data about its molecular mass. The mechanism of chiral recognition of Chiralcel OD-R was proposed as a stacking model [15] in general, since the column shows non-conventional sensitivity to non-planarity, and steric hindrance. From the chemistry of Chiralcel OD-R, it is not difficult to locate many spots in the stationary phase where stacking can easily take place between aromatic rings and between methyl groups and aromatic rings.

Proposed separation mechanism based on molecular modeling

Using computer and conventional molecular modeling tools, we are able to see something at the molecular level.

The computer software for molecular modeling used in this study is the three-dimensional CAChe version 3.0.4. It gives the lowest energy conformation of the molecule. Fig. 6 shows two pairs of enantiomers of BNA in the lowest energy conformations.

The upper pair are the *trans* enantiomers, and the lower pair are the *cis* enantiomers. Unfortunately, in two dimensions we can not appreciate the beauty of the magnificent stereoscopic effects on CAChe's "three-dimensional" CRT screen. The conformations of BNA shown above are in their calculated lowest energy according to the quantum mechanics; Fig. 7 illustrates the energy levels *versus* different conformations of the BNA *cis* isomer.

The position of the filled circle indicates the lowest energy point (8.07 kcal/mol) among many other conformations. The two pairs of BNA enantiomers in Fig. 6 are all at their lowest energy conformations.

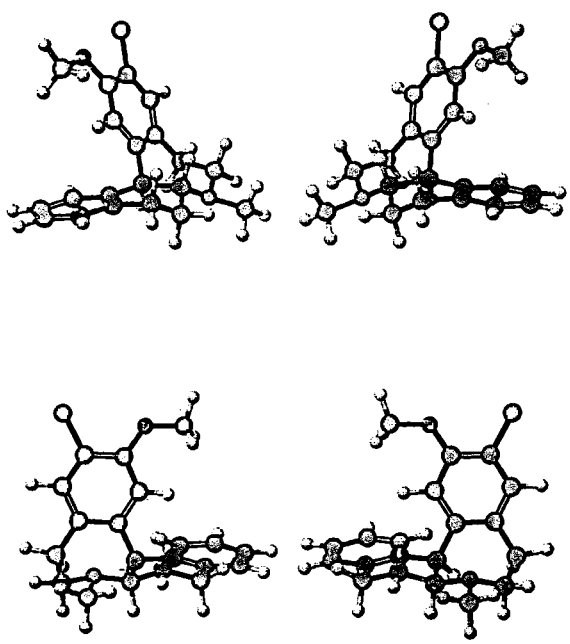

Fig. 6. BNA molecular structures.

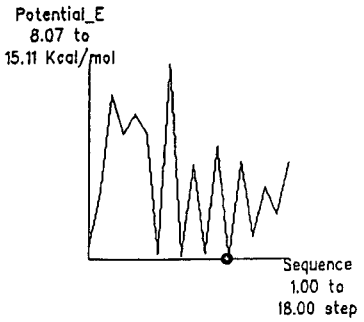

Fig. 7. The energy levels associated with the conformations of *cis*-BNA.

From Fig. 4, the elution order of the four BNA isomers is (−)*trans*, (−)*cis*, (+)*trans*, then (+)*cis*. Note that the enantiomers are segregated by their diastereomers. This seems inexplicable in that enantiomers having exactly the same chemical and physical properties do not follow each other in elution order.

By studying the molecules at the most stable conformation, it is found that because the two diastereomer molecules possess so-called "matching structures", the *cis* isomer can be stacked perfectly on the top of the *trans* isomer molecule without significant increase in physical space compared to a single molecule, just as placing one stackable chair on the top of another does not occupy a two-chair space. Two enantiomer molecules do not possess "matching structures" and cannot even be placed close with all efforts.

When a *trans* molecule encounters a *cis* molecule, they are attracted to each other by a hydrophobic force and matching conformations, and are then stabilized by sharing π electrons between two pairs of benzene rings. Their conformations fit each other so well that the increase in the size of the two stacked molecules is hardly noticeable, so they move in pairs freely in and out of the mobile phase until they get trapped by the stacking mechanism in a cavity of the proper size of the chiral stationary phase, where they get further discriminated by their subtle conformational differences.

In contrast, the enantiomer molecules do not possess the properties of matching conformations, and therefore they are moving around individually, get picked up at random by the chiral stationary phase, and are then separated widely. That gives the possible explanation why an enantiomer does not immediately follow its mirror image but a diastereomer does in this system.

Notice also from the chromatogram in Fig. 4 that the *trans* isomer elutes first, followed by the *cis* isomer. If we study their subtle conformational differences further, it is not difficult to see that the angle between two benzene rings in the *trans* isomer (60.659°) is about 6° less than that in the *cis* isomer (66.639°). So the *cis* isomer has more steric hindrance than does the *trans* isomer, and *cis* isomer's mobility in chiral stationary phase is more likely restricted and therefore more retained in the stationary phase.

CONCLUSIONS

Baseline resolution of BNA stereoisomers was achieved using a salting-in agent in a reversed mobile phase. The study of the molecular structures of BNA with computer molecular modeling tools suggests a chiral separation model for BNA at the molecular level. The proposed hypothesis of the separation mechanism based on the knowledge of the structures is in good agreement with the observed experimental results.

ACKNOWLEDGEMENTS

We would like to thank Mr. William Folley and Mr. Robert Strack for their kind encouragement, Mr. Peter Rausch for his excellent comments, and Dr. Junning Lee for sharing his knowledge of the CAche 3-D Molecular Modeling software.

REFERENCES

1 B.F. Roettger, J.A. Myers, M.R. Ladisch and F.E. Regnier, *Biotechnol. Prog.*, 5 (1989) 79–88.
2 C.J.O.R. Morris, *Trends Biochem. Sci.*, 1 (1976) N207–N208.
3 M.K. Gil'manov and T.K. Kozhanov, *Tr. Inst. Bot. Akad. Nauk Kaz. SSR*, 29 (1971) 216–226.
4 P. Jandera and J. Churáček, *J. Chromatogr.*, 98 (1974) 1–54.

5 P. Jandera and J. Churáček, *J. Chromatogr.*, 98 (1974) 55–104.
6 P. Jandera and J. Churáček, *J. Chromatogr.*, 86 (1973) 423–449.
7 R.L. Munier, *Qual. Plant. Mater. Veg.*, 16 (1968) 12–34.
8 T. Cserhat and Z. Illes, *J. Liq. Chromatogr.*, 14 (1991) 1495–1510.
9 G. Vučković, D. Miljević, T.J. Janjić and M.B. Ćelap, *J. Chromatogr.*, 609 (1992) 427–431.
10 Y. Nagai, *Bunseki Kagaku*, 41 (1992) 491–495.
11 A. Ishikawa and Shibata, *J. Liq. Chromatogr.*, 16 (1993) 859–878.
12 R. Breslow, *J. Am. Chem. Soc.*, 113 (1991) 4340.
13 J.E. Gordon, *The Organic Chemistry of Electrolyte Solutions*, Wiley, NY, 1975.
14 Y. Okamoto, M. Kawashima and K. Hatada, *J. Chromatogr.*, 363 (1986) 173.
15 K. Tachibana, *Theoretical Mechanism of Daicel Cellulose-Based Chiral Stationary Phase HPLC Columns, Chiral Technologies, Seminar at Schering-Plough, Bloomfield, NJ, July 1, 1992.*

Journal of Chromatography A, 659 (1994) 307–315
Elsevier Science B.V., Amsterdam

CHROM. 25 638

Structure–retention relationships of diastereomeric mixtures of lipidic amino acid conjugates on reversed-phase stationary phases

D. Korakas [☆], K. Valkó [*], I. Wood, W.A. Gibbons and I. Toth [☆☆]

Department of Pharmaceutical Chemistry, School of Pharmacy, University of London, 29–39 Brunswick Square, London WC1N 1AX (UK)

(First received September 22nd, 1993; revised manuscript received October 11th, 1993)

ABSTRACT

The retention parameters of diastereomeric mixtures of 19 lipidic amino acid conjugates have been determined on Spherisorb ODS and Supelcosil LC-ABZ stationary phases by changing the acetonitrile concentration in acetonitrile–0.1% trifluoroacetic acid–water mobile phases. In general, better resolution of the diastereomeric mixtures was obtained on the Supelcosil LC-ABZ stationary phase but in some cases the Spherisorb ODS column showed better separation. The presence of silanol groups improved the separation of the diastereomers in those cases. The log k' values were plotted against the acetonitrile concentrations. In the case of basic derivatives parabolic relationships could be observed on the Spherisorb ODS stationary phase which contains free silanol groups, while always straight lines were obtained on the Supelcosil LC-ABZ column. The slope and the intercept values were calculated for the straight lines obtained. The octanol–water partition coefficients (log P) and the dissociation constants (pK_a) of the compounds were also calculated and were related to the chromatographic parameters. It was found that the chromatographic parameters obtained on the Spherisorb ODS stationary phase showed slightly better correlations with the calculated hydrophobicity and pK_a parameters than those obtained on the Supelcosil LC-ABZ column, which shows that different retention mechanism can be expected on the two stationary phases.

INTRODUCTION

The lipidic amino acids are possible conjugates for biologically active molecules through their bifunctional nature as it was described by Gibbons *et al.* [1]. They have a membrane-like character and are able to facilitate drug absorption to the receptor site. The quantitative structure–activity correlation study [2] revealed the role of the lipidic side chain in the *in vivo* activity of the lipidic amino acid conjugates of β-lactam antibiotics. As the racemic forms of lipidic amino acids are used for conjugation the synthesis always results in diastereomeric mixtures. The separation of diastereomers does not require chiral separation conditions and therefore is easier and cheaper. However, the lipidic amino acid conjugates have amphophilic and surface-active character, so even their separation is not straightforward, and the structure–retention relationship study can reveal their retention mechanism. As the Supelcosil LC-ABZ column was designed specially for anionic, basic and zwitterionic compounds without silanophilic effects it seemed worth trying for the separation of the diastereomeric mixtures.

* Corresponding author. On leave from Central Research Institute for Chemistry, Hungarian Academy of Sciences, P.O. Box 17, H-1025 Budapest, Hungary.
☆ On leave from Department of Chemistry, Section of Organic Chemistry and Biochemistry, University of Ioannina, 451 10 Ioannina, Greece.
☆☆ On leave from Central Research Institute for Chemistry, Hungarian Academy of Sciences, P.O. Box 17, H-1025 Budapest, Hungary

0021-9673/94/$07.00
SSDI 0021-9673(93)E1075-B

In this study the retention parameters of 19 lipidic amino acid conjugate mixtures were measured and the structure–retention relationships were studied. The chemical structure of the compounds was characterized by calculated log P values (the logarithmic values of the octanol–water partition coefficients) and the dissociation constants (pK_a).

EXPERIMENTAL

The lipidic dipeptides **1–19** were synthesized by coupling the appropriately protected amino acids to methyl amino tetradecanoate employing the hydroxybenzotriazole assisted carbodiimide coupling method as described by Gibbons *et al.* [1]. Infrared spectra were recorded with a Perkin-Elmer 841 spectrophotometer. ^1H NMR spectra were obtained with Varian XL-300 and Bruker AM500 instruments operating at fields of 300 and 500 MHz, respectively; chemical shifts were checked in ppm downfield from internal tetramethylsilane. Mass spectra were run with a VG analytical ZAB-SE instrument, using the fast-atom bombardment (FAB) techniques; 20 kV Cs^+ ion bombardment, with 2 μl appropriate matrix either 3-nitrobenzyl alcohol or thioglycerol with NaI (MeOH solution) added when necessary to produce nitrated species where no protonated molecule ions were observed. The reaction process was monitored by thin-layer chromatography on Kieselgel PF_{254} using CH_2Cl_2–MeOH (10:1), (10:0.5) or (10:0.25) solvent as required. Purification was achieved by TLC using Kieselgel $PF_{254+366}$ (Merck) on 20 × 20 cm plates 1.5 mm thick with the beforementioned solvent systems. Solvents were evaporated under reduced pressure with a rotary evaporator. The chemical structure and their identification parameters can be seen in Table I.

The compounds were dissolved in 1 mg/ml concentration in acetonitrile–water–trifluoro-

TABLE I

CHEMICAL STRUCTURES OF THE INVESTIGATED DIASTEREOMERIC LIPIDIC AMINO ACIDS

$(CH_3)C–O–CO–N^*H–C(R)H–CO–NH–CH(C_{12}H_{25})–COOCH_3$

Compound	R	Yield (%)	MS (m/z)
1	H	78.6	438
2	$CH(CH_3)_2$	72.8	479
3	CH_3	76.8	453
4	$CH_2–CH(CH_3)_2$	72.8	494
5	$CH(CH_3)C_2H_5$	67.4	495
6	$–CH_2–CH_2–CH_2–N^*$ [a]	68.6	478
7	$CH_2–C_6H_5$	51.2	528
10	$CH_2–S–CH_2–NH–CO–CH_3$	65.5	555
11	$(CH_2)_2–S–CH_3$	65.6	512
12	$CH(CH_3)–O–CH_2–C_6H_5$	76.5	572
13	$CH_2–O–CH_2–C_6H_5$	80.1	558
14	$(CH_2)_4–NH–CO–O–CH_2–C_6H_5$–*o*-Cl	58.9	678
15	$(CH_2)_3–NH–C(NH)–NH–SO_2–C_6H_5$–*p*-$CH_3$	63.9	712
16	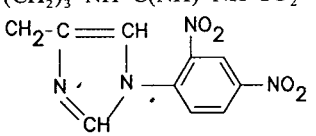	77.3	684
17	$CH_2–CO–O–CH_2–C_6H_5$	65.2	586
18	$(CH_2)_2–CO–O–CH_2–C_6H_5$	74.3	601
19	$CH_2–CO–NH_2$	64.1	495

[a] * denotes the position for forming a ring in compound **6**.

acetic acid (TFA) (95:5:0.1) and 20 μl of this solution were injected three times on the columns. The solvent peak was regarded as the dead time, and the log k' values were calculated from the average retention time obtained from the three injections.

A Gilson HPLC system (pump Model 303, variable-wavelength UV detector M 115, Rheodyne injector) was obtained from Anachem (Luton, UK). The flow-rate was always 1.00 ml/min. The detection was carried out at 210 nm with 1 AUFS. Spherisorb ODS 5 μm (50 × 4.6 mm) (Phase Sep, Deeside, UK) and Supelcosil LC-ABZ (150 × 4.6 mm) (Supelco, Bellefonte, PA, USA) columns were used for the separations. The mobile phases were various concentrations of acetonitrile ranging from 95 to 65% (v/v), water and 0.1% TFA.

The calculation of the log P and pK_a values were carried out by ELUEX 3.0 expert system developed by CompuDrug Chemistry (Budapest, Hungary) for predicting the optimum mobile phase composition for HPLC separations. The correlation study was carried out by Drugidea software developed by Chemicro (Budapest, Hungary).

RESULTS AND DISCUSSION

The log k' values were determined for each compound on both stationary phases using various concentrations of acetonitrile in the mobile phase. The log k' values were plotted against the acetonitrile concentration. In most cases straight lines were obtained with correlation coefficients higher than 0.99. Only for compounds **16a** and **16b** a parabolic relationship was found as can be seen in Fig. 1 for the data obtained on the Spherisorb ODS column.

As can be seen from Table I, compound **16** has basic nitrogens which can interact with the free silanol groups of the Spherisorb ODS stationary phase, and that causes the parabolic relationship between the log k' values and the acetonitrile concentrations. Fig. 2 shows the straight lines obtained for compounds **16a** and **16b** on the Supelcosil LC-ABZ column which does not have free silanol groups. The letters **a** and **b** denote the separated diastereomers. Three diastereomer pairs could not be separated on the two columns at all, compounds **11**, **18** and **19**; no satisfactory explanations can be given. Only their hydrophobicities do not differ sufficiently to be able to differentiate between them under the studied chromatographic conditions. Compound **1** is an enantiomeric mixture; therefore no separation can be expected in non-chiral chromatographic conditions.

In general, higher resolution of the diastereomers could be observed on Supelcosil LC-ABZ

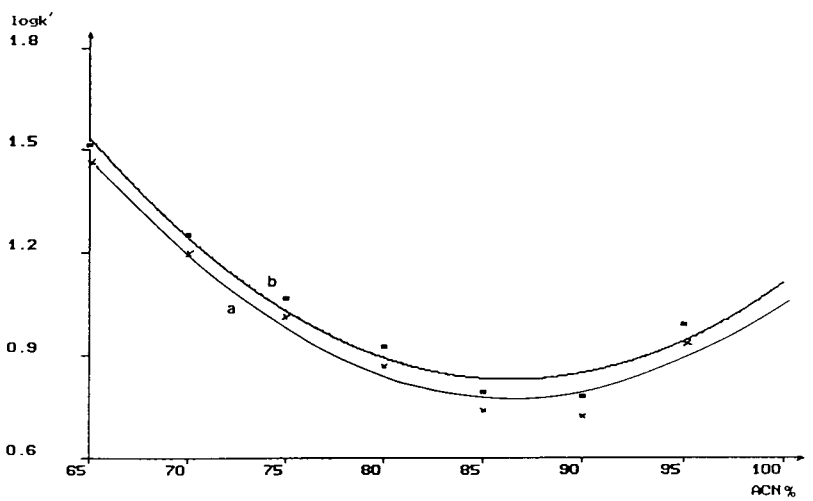

Fig. 1. The plot of log k' *vs.* acetonitrile concentration in the mobile phase for compounds **16a** and **16b** obtained on a Spherisorb ODS column.

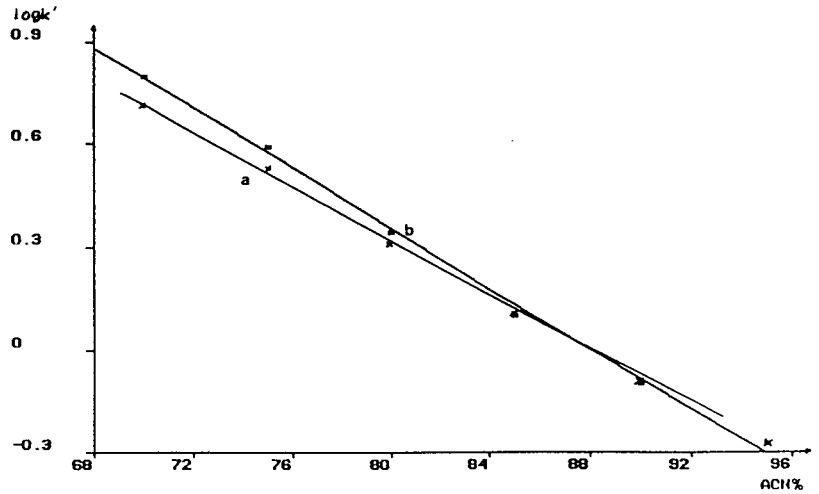

Fig. 2. The plot of log k' *vs.* acetonitrile concentration in the mobile phase for compounds **16a** and **16b** obtained on a Supelcosil LC-ABZ column.

column as can be seen in Figs. 3–5. For compounds **12** and **13** better separation was obtained on the Spherisorb ODS column. These two compounds were the only aromatic ether type in the series (see Figs. 6 and 7).

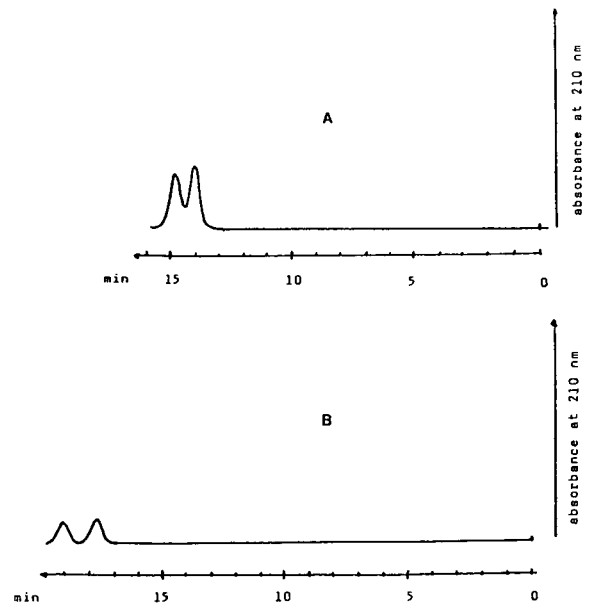

Fig. 3. Separation of the diastereomeric mixture of compound **2** by using acetonitrile–TFA–water (70:0.1:30, v/v/v) as the mobile phase. Flow-rate: 1.00 ml/min. Detection at 210 nm. (A) Spherisorb ODS 5 μm, 50 × 4.6 mm column; (B) Supelcosil LC-ABZ 150 × 4.6 mm column.

Tables II and III present the calculated slope (S) and intercepts (log k'_0) values of the straight lines obtained by plotting log k' values against the acetonitrile concentration (ϕ) for each compound on the Spherisorb ODS and Supelcosil LC-ABZ columns, respectively. When parabolic relationships were observed only the linear portion of the relationship was considered in the calculation of the values. Table III also shows the calculated hydrophobicity values (log P) and the dissociation constants (pK_a). In order to reveal the structure–retention relationships, correlation analysis was carried out on the data shown in Tables II and III. The correlation coefficients summarized in a correlation matrix can be seen in Table IV. On both columns the slope (S) and intercept (log k'_0) values showed high correlation coefficients (−0.95 and −0.98) which means that the set of compounds behaved as structurally related [3]. As expected the dissociation constants (pK_b) alone did not show good correlations to the chromatographic parameters on the reversed-phase columns where hydrophobicity governs the retention. The log P values showed better correlation to the chromatographic parameters obtained on the Spherisorb ODS column when the data obtained at higher organic concentrations, where the silanol effect could be observed, were not included in the calculations. This suggests that the

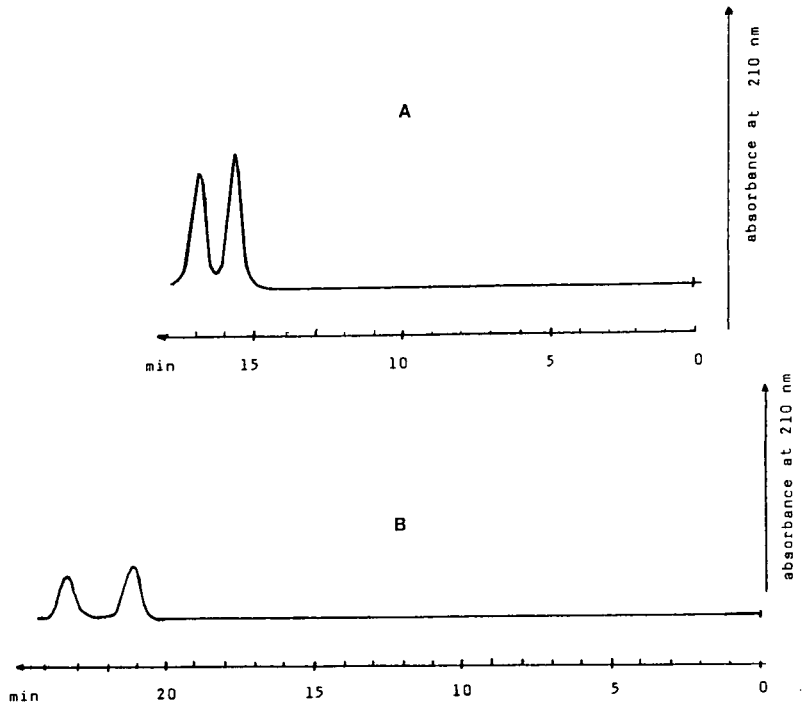

Fig. 4. Separation of the diastereomeric mixture of compound **4**. Conditions and columns as in Fig. 3.

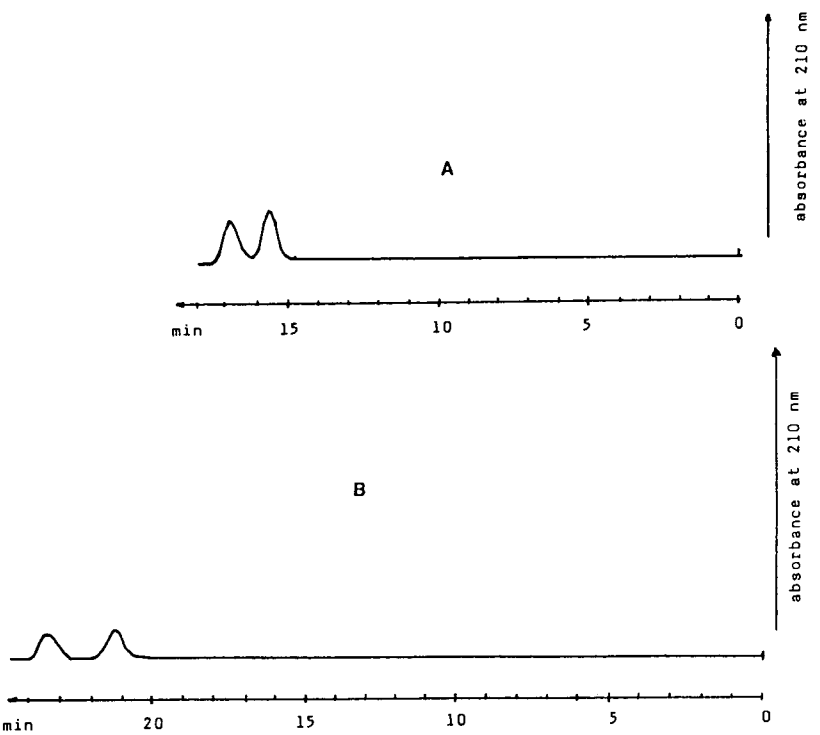

Fig. 5. Separation of the diastereomeric mixture of compound **5**. Conditions and columns as in Fig. 3.

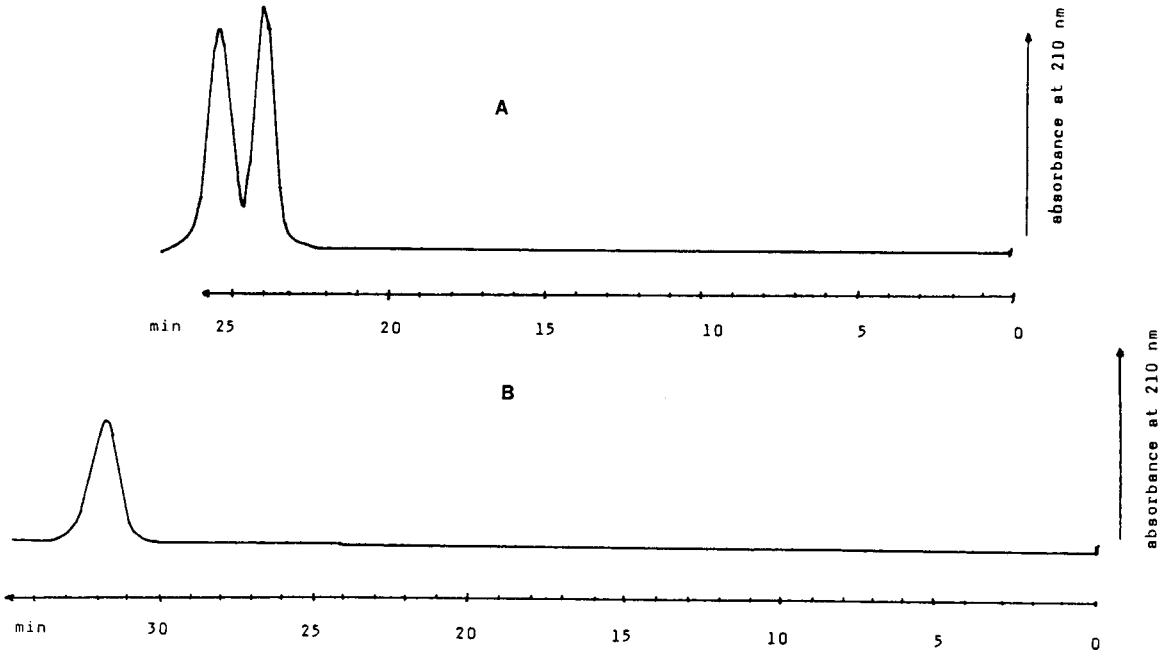

Fig. 6. Separation of the diastereomeric mixture of compound **12**. Conditions and columns as in Fig. 3.

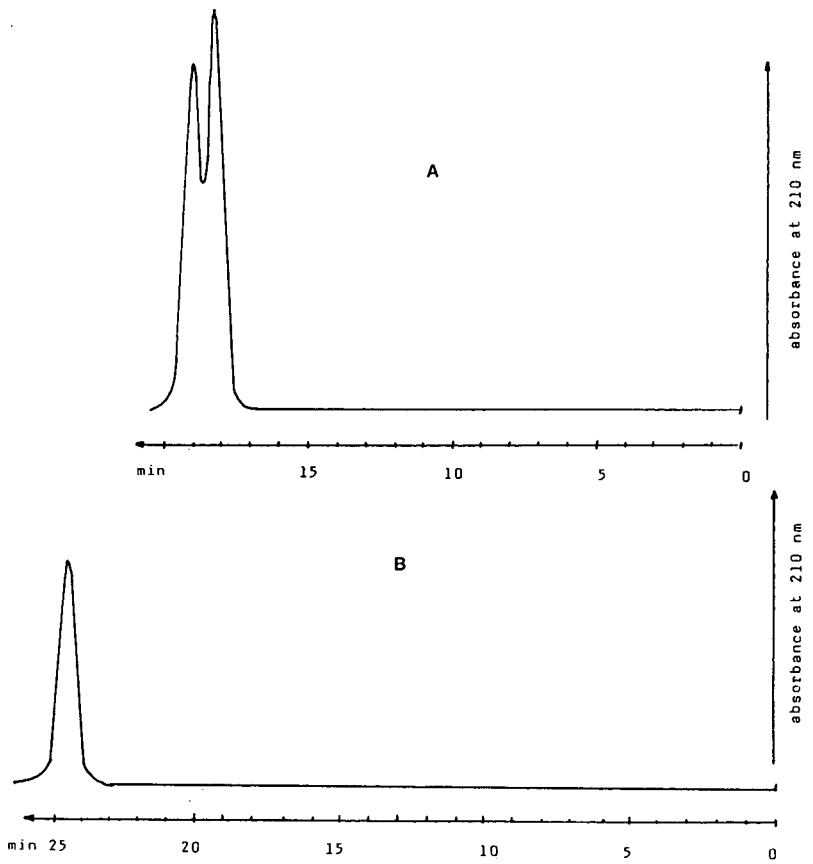

Fig. 7. Separation of the diastereomeric mixture of compound **13**. Conditions and columns as in Fig. 3.

TABLE II

SLOPE (S), INTERCEPT (LOG k'_0) AND CORRELATION COEFFICIENT (R) VALUES OF THE COMPOUNDS OBTAINED ON SPHERISORB ODS (Sph) COLUMN ACCORDING TO THE EQUATION LOG $k' = \text{LOG } k'_0 - S\phi$ (WHERE ϕ IS THE VOLUME FRACTION OF ACETONITRILE)

Compound	S_{Sph}	log k'_{0Sph}	R
1	36.3	3.366	0.999
2a	40.6	3.828	0.999
2b	40.3	3.830	0.999
3a	35.5	3.357	0.998
3b	35.5	3.357	0.998
4a	40.4	3.853	0.998
4b	41.8	4.011	0.998
5a	42.9	4.056	0.999
5b	42.4	4.059	0.999
6a	31.7	3.254	0.998
6b	31.7	3.254	0.998
7a	43.0	4.048	0.995
7b	43.2	4.089	0.998
10a	34.8	3.154	0.996
10b	32.9	3.062	0.994
11	41.1	3.829	0.998
12a	46.5	4.497	0.999
12b	47.0	5.565	0.999
13a	42.6	4.065	0.996
13b	42.8	4.134	0.997
14a	43.5	4.075	0.997
14b	44.4	4.158	0.996
15a	38.9	3.455	0.996
15b	40.5	3.610	0.998
16a	30.4	3.308	0.999[a]
16b	30.5	3.377	0.999[a]
17a	43.5	4.080	0.990
17b	44.4	4.158	0.993
18	43.1	4.051	0.993
19	28.5	2.570	0.998

[a] In these cases parabolic relationships were found by plotting the log k' values as a function of the organic phase concentration. For the calculation of the S, log k'_0 and R values, only the linear section of the curve was considered.

TABLE III

SLOPE (S), INTERCEPT (LOG k'_0) AND CORRELATION COEFFICIENT VALUES OF THE COMPOUNDS OBTAINED ON SUPELCOSIL LC-ABZ (Sup) COLUMN ACCORDING TO THE EQUATION LOG $k' = \text{LOG } k'_0 - S\phi$ AND THE CALCULATED HYDROPHOBICITY (LOG P) AND DISSOCIATION CONSTANTS (pK_b) OF THE COMPOUNDS INVESTIGATED

Compound	S_{Sup}	log k'_{0Sup}	R	log P	pK_b
1	40.4	3.459	0.999	7.25	3.3
2a	43.9	3.918	0.998	8.80	3.2
2b	45.0	4.042	0.995	8.80	3.2
3a	42.0	3.643	0.998	7.76	3.3
3b	42.9	3.723	0.998	7.76	3.3
4a	45.5	4.124	0.999	9.32	3.3
4b	44.8	4.117	0.999	9.32	3.3
5a	45.6	4.133	0.998	9.32	3.3
5b	43.6	4.032	0.999	9.32	3.3
6a	38.4	3.433	0.999	6.52	2.2
6b	38.8	3.484	0.999	6.52	2.2
7a	47.0	4.234	0.999	8.90	3.7
7b	47.4	4.288	0.998	8.90	3.7
10a	39.6	3.275	0.999	7.29	3.6
10b	38.5	3.252	0.999	7.29	3.6
11	44.4	3.946	0.999	8.29	3.4
12a	47.9	4.483	0.999	9.46	3.6
12b	47.9	4.483	0.999	9.46	3.6
13a	51.1	4.597	0.990	8.94	3.6
13b	51.1	4.597	0.990	8.94	3.6
14a	48.5	4.281	0.998	10.75	3.3
14b	49.2	4.343	0.998	10.75	3.3
15a	43.9	3.716	0.996	9.76	8.1
15b	45.4	3.856	0.997	9.76	8.1
16a	40.0	3.511	0.999	7.27	3.3
16b	43.8	3.855	0.997	7.27	3.3
17a	49.4	4.466	0.998	9.23	3.8
17b	49.4	4.466	0.998	9.23	3.8
18	51.7	4.607	0.998	9.17	3.5
19	33.1	2.662	0.998	6.19	3.6

hydrophobicity governed the retention. On the contrary in the retention data obtained on the Supelcosil LC-ABZ column other types of interactions are possibly involved as well, as the stationary phase contains charged moieties among the long hydrophobic alkyl chains.

When step-wise regression analyses were carried out on the data it was found that the calculated hydrophobicity values showed good correlations to the S and the pK_b values as described by eqns. 1 and 2 for the data obtained on the Spherisorb ODS and the Supelcosil LC-ABZ columns, respectively.

$$\log P = 1.936(\pm 0.186)S_{Sph} + 0.23(\pm 0.08)pK_b + 0.12$$
$$n = 30 \quad r = 0.910 \quad s = 0.517 \quad F = 64.7 \qquad (1)$$

$$\log P = 2.086(\pm 0.279)S_{Sup} + 0.26(\pm 0.10)pK_b - 1.86$$
$$n = 30 \quad r = 0.848 \quad s = 0.660 \quad F = 34.5 \qquad (2)$$

TABLE IV

CORRELATION COEFFICIENTS BETWEEN THE CHROMATOGRAPHIC AND PHYSICO-CHEMICAL PARAMETERS

	S_{Sph}	$\log k'_{Sph}$	S_{Sup}	$\log k'_{Sup}$	$\log P$	pK_b
S_{Sph}	1.00	−0.95	0.86	−0.88	−0.88	−0.15
$\log k'_{Sph}$	−0.95	1.00	−0.88	0.94	0.81	−0.02
S_{Sup}	0.86	−0.88	1.00	−0.98	−0.80	−0.13
$\log k'_{Sup}$	−0.88	0.94	−0.98	1.00	0.78	0.01
$\log P$	−0.88	0.81	−0.80	0.78	1.00	0.37
pK_b	−0.15	−0.02	−0.13	0.01	0.37	1.00

where n is the number of compounds, r is the multiple regression coefficient, s is the standard error of the estimate, F is the Fisher-test value (significant at 0.01% level). Usually the $\log k'_0$ values are expected to show good correlation with the partition coefficients of compounds. Similar, significant correlations can be found in our case as well (see eqns. 3 and 4), but the mathematical statistical parameters are slightly worse than those of eqns. 1 and 2.

$$\log P = 2.124(\pm 0.22) \log k'_{0Sph} + 0.368(\pm 0.082)pK_b - 0.738$$
$$n = 30 \quad r = 0.896 \quad s = 0.552 \qquad (3)$$

$$\log P = 1.940(\pm 0.249) \log k'_{0Sup} + 0.346(\pm 0.095)pK_b - 0.386$$
$$n = 30 \quad r = 0.857 \quad s = 0.642 \qquad (4)$$

As the S and the $\log k'_0$ values show high correlations with each other, they are interchangeable. As can be seen, slightly better correlation was obtained on the Spherisorb ODS column (again data, where the silanol effect could be observed were not included in the calculations), which proves that on the Supelcosil LC-ABZ other than only hydrophobic interactions took place. The plots of the $\log P$ *vs.* the

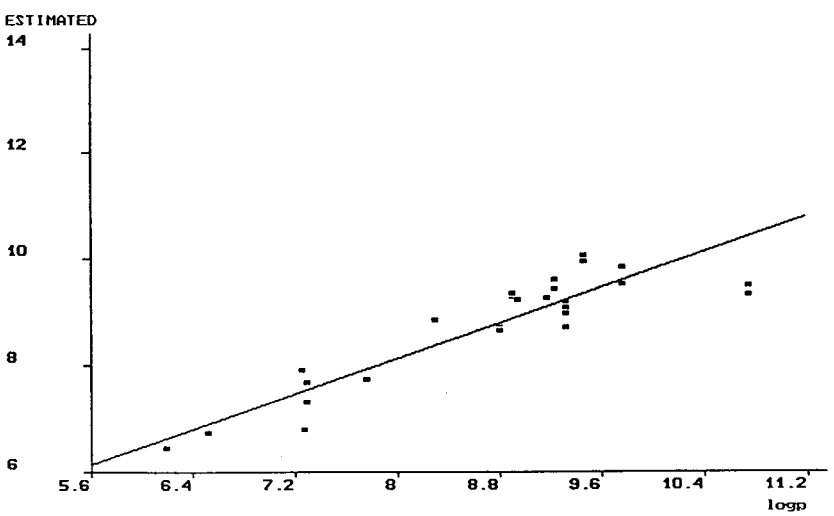

Fig. 8. Plot of the log P values *vs.* the estimated values obtained on the Spherisorb ODS column by eqn. 1.

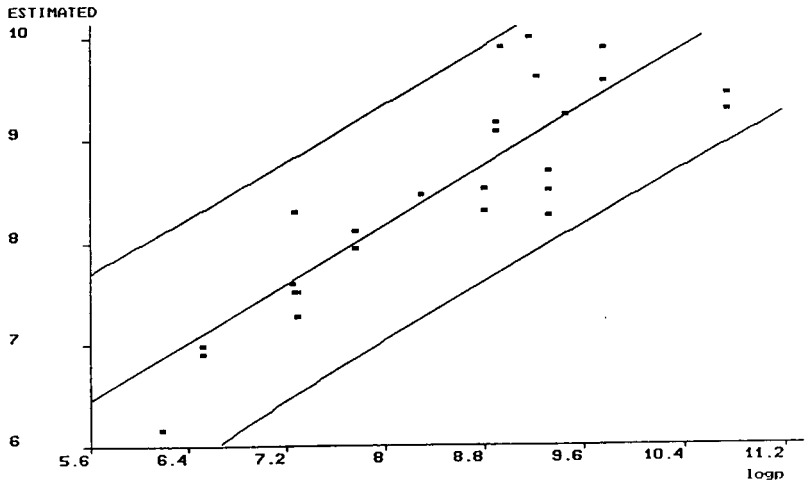

Fig. 9. Plot of the log P values *vs.* the estimated values obtained on the Supelcosil LC-ABZ column by eqn. 2.

estimated log P values by eqns. 1 and 2 are presented in Figs. 8 and 9, respectively.

In conclusion, most of the diastereomeric lipidic amino acid mixtures could be separated under reversed-phase conditions. The retention of the compounds was governed by hydrophobicity on the Spherisorb ODS column and the effect of the free silanol groups could be observed for basic derivatives. The Supelcosil LC-ABZ column did not show a silanophilic effect, in most cases better separation of the diastereomers could be observed and other than hydrophobic interactions governed the retention as well.

ACKNOWLEDGEMENT

The contribution of K.V. to the work was supported by a Maplethorpe Fellowship from the University of London, which is gratefully acknowledged.

REFERENCES

1 W.A. Gibbons, R. Hughes, M. Charalambous, M. Christodoulu, A. Szeto, A.E. Aulabaugh, P. Mascagni and I. Tóth, *Liebigs Ann. Chem.*, 1990 (1990) 1175.
2 K. Valkó, I. Toth, P. Ward, P. Slegel and W.A. Gibbons, *Int. J. Pharmaceutics*, 87 (1992) 123.
3 K. Valkó, *J. Liq. Chromatogr.*, 10 (1987) 1663.

Journal of Chromatography A, 659 (1994) 317–320
Elsevier Science B.V., Amsterdam

CHROM. 25 639

Process monitoring of the production of γ-interferon in recombinant Chinese hamster ovary cells

Timothy K. Nadler, Sandeep K. Paliwal and Fred E. Regnier*

Chemistry Department, Purdue University, West Lafayette, IN 47907 (USA)

Rahul Singhvi and Daniel I.C. Wang

Biotechnology Process Engineering Center, Massachusetts Institute of Technology, Cambridge, MA 02139 (USA)

(First received April 14th, 1993; revised manuscript received September 22nd, 1993)

ABSTRACT

The production of recombinant γ-interferon was monitored using high-performance liquid chromatographic methods. These methods were able to distinguish between glycosylated and non-glycosylated forms of γ-interferon by complexing the carbohydrate with borate. Sufficient quantities of standard glycosylated γ-interferon were not available for peak identification so immunological techniques were used to identify γ-interferon variants. These techniques were validated with the non-glycosylated form. The non-glycosylated form was then shown to be retained only on a cation-exchange column, while the glycosylated form, complexed with borate, was retained only on an anion-exchange column. Samples were drawn at 2-h intervals over a 60-h production cycle and analyzed by both anion- and cation-exchange chromatography. Results indicated that the production of each form was coincidental and that the glycosylated form of γ-interferon is produced in greater abundance than non-glycosylated.

INTRODUCTION

The production of recombinant proteins in mammalian cell culture is a process of growing importance. Unlike prokaryotic hosts (*e.g. E. coli*), eukaryotic production systems are more adept at producing recombinant proteins with the proper post translational modifications [1,2]. However, these modifications add complexity to the production system because the product recombinant protein may consist of additional classes of post translational variants. When analyzing unmodified proteins, only primary structural variants and folding variants were important. Post translational variants add another dimension of complexity which multiplies previous complications.

Previously, various researchers have demonstrated various methods for analyzing γ-interferon (IFN-γ) [3–5]. It was the aim of this research to develop rapid, automated, analytical methods for the purification of both glycosylated and non-glycosylated IFN-γ. Further, to test the ruggedness of the analytical methods, a 60-h experiment was performed to demonstrate the reliability of the techniques and to monitor the actual production process for recombinant IFN-γ.

EXPERIMENTAL

Instrumentation

The HPLC system used was a BioCAD Perfusion Chromatography Workstation (PerSeptive Biosystems, Cambridge, MA, USA) with a built-in variable wavelength UV–Vis detector, pH meter and conductivity probe. The HPLC columns used were a POROS S/H cation-exchange

* Corresponding author.

0021-9673/94/$07.00
SSDI 0021-9673(93)E1074-A

column (100 × 4.6 mm), a POROS Q/M anion-exchange column (100 × 4.6 mm), a POROS A/M protein A affinity column (30 × 2.1 mm), and a POROS G/M protein G affinity column (30 × 2.1 mm) (all columns from PerSeptive Biosystems, Cambridge, MA, USA).

Reagents

Tris(hydroxymethyl)aminomethane, boric acid, hydrochloric acid and sodium chloride were used for HPLC (Mallinckrodt, Paris, KY, USA). Schiff's reagent (Mallinckrodt), sodium periodate (Sigma, St. Louis, MO, USA), and sodium metabisulfite (Allied Chemical, Morristown, NJ, USA) were used for Fuchsin–Sulfite staining of glycoproteins. Anti-human γ-interferon polyclonal antibody was used for immuno-subtractive chromatography (Endogen, Boston, MA, USA) as was anti-human γ-interferon monoclonal antibody (ICN Biomedicals, Costa Mesa, CA, USA). The monoclonal antibody was directed against the C-terminal region of γ-interferon. Therefore, it is expected to cross-react with a variety of glycoforms of γ-interferon since the glycosylated region is located more closely to the N-terminal domain. Non-glycosylated γ-interferon standard was used in HPLC calibrations (a generous donation from Genentech, San Francisco, CA, USA). An ELISA kit (Endogen, Boston, MA, USA) was used to verify peak identities. A small amount of glycosylated γ-interferon standard was obtained (Sigma) which was used to show that the glycosylated form of γ-interferon was not retained on either the cation- or anion-exchange sorbent but could be retained on an anion-exchange sorbent in the presence of borate.

Cell culture

Recombinant Chinese hamster ovary cells (γ-CHO) engineered to produce γ-interferon were used in these studies. A 1:1 mixture of Dulbecco's Modified Eagle's (DME) medium and Ham's F12 medium (JRH Biosciences, Lenexa, KS, USA) was used to cultivate the cells. The medium was supplemented with 10% fetal bovine serum (FBS, Sigma), 4 m*M* L-glutamine, $2.4 \cdot 10^{-7}$ *M* methotrexate (Sigma), 10 units/l of penicillin and 10 mg/l of streptomycin. Cells were cultivated on Plastispex microcarriers (JHR Biosciences, 90–150 μm diameter) in 250-ml spinner flasks (Bellco). Microcarriers were washed 3 times with phosphate-buffered saline in siliconized spinner flasks (Sigmacote, Sigma) and sterilized by autoclaving for 30 min. After a final wash with culture medium, the microcarriers were seeded with cells at $2 \cdot 10^5$ cells/ml. The spinner flasks were then placed in an incubator (37°C, 10% CO_2, humidified) on a spinner plate (Bellco). The agitation was kept constant throughout the culture period at 50 rpm. Cell confluency on microcarriers was evaluated microscopically by taking culture samples daily. Upon confluency, the growth medium was replaced with medium without FBS. Samples from this serum-free cell culture were collected to monitor the production of IFN-γ.

RESULTS AND DISCUSSION

The aim of the research was to develop rapid automatable analytical methods that could be performed in real-time. This means that the methods can take no longer than 30 min if samples are taken hourly and the two forms of IFN-γ are to be analyzed separately. We chose perfusion chromatography because of its speed and reliability. Proteins may be separated in as little as 15 s with this technology [5]. Polystyrene-based columns were chosen for their durability and tolerance at extremes of pH. The advantage of the chromatographic based system is the ability to automate sample collection, product analysis, data management and feed back control.

The BioCAD workstation has recently been used to process monitor the production of monoclonal antibodies in hybridoma cultures [6]. However, the focus of the hybridoma study was automated sample handling of cell culture media and the integration of sampling, analysis, and data management. Unlike the hybridoma monitoring study, this set of experiments is complicated by the fact that more than one product needs to be determined and more than one method is required for these determinations.

The first objective was to develop HPLC methods for the determination of dilute quantities of IFN-γ in conditioned media. To enhance the response of the HPLC detector to poly-

peptides, the wavelength was set at 225 nm. The extinction coefficient of IFN-γ is higher at this wavelength than either 254 or 280 nm. Although IFN-γ absorbs even more at wavelengths below 225 nm, the mobile phase also begins to absorb significantly in this region. Therefore, 225 nm was chosen as an optimum for these conditions. Detection was also enhanced by using larger injection volumes; 1000-μl injections of conditioned IFN-γ media were used when dealing with dilute samples.

Sufficient quantities of glycosylated IFN-γ standard were not available for HPLC calibration. Antibodies to IFN-γ were obtained and immobilized on a protein G affinity column. The sample was then passed through this column, to remove any IFN-γ, before subsequent ion-exchange analysis. These chromatograms were then compared to chromatograms in which antibody was not used (Fig. 1). This subtractive technique was first described by Riggin *et al.* [7] for the analysis of human growth hormone. The technique was validated for non-glycosylated IFN-γ for which the standard was available. The missing peak in the conditioned media sample was then further confirmed by spiking the sample with non-glycosylated IFN-γ (Fig. 2). Once the subtractive technique was validated, it was applied to the glycosylated form of IFN-γ, for which standard was not available. To confirm the identity of the putative IFN-γ peaks, they were collected and shown to contain IFN-γ by enzyme-linked immunosorbent assays (ELISA) [data not shown]. They were also analyzed by sodium dodecyl sulphate-polyacrylamide gel electrophoresis (SDS-PAGE), and stained with Fuchsin–Sulfite reagent to show that they were glycosylated, and also exhibited an apparent molecular mass shift to higher molecular mass.

The results of mobile phase optimization show that the non-glycosylated form of IFN-γ will adsorb to a cation exchanger at pH 7.0 in 20 m*M* Tris. It may then be eluted with a 10-min gradient to 1.0 *M* NaCl in 20 m*M* Tris pH 7.0 at 4.0 ml/min. Most of the other proteins in the conditioned media have lower isoelectric points than IFN-γ and are not retained by the column. They elute in the void volume.

The glycosylated form of IFN-γ did not adsorb to the cation exchanger at pH 7.0. There may be shielding of the amino acid side chains by the carbohydrate portion of the molecule. It is not retained by the anion-exchange column either,

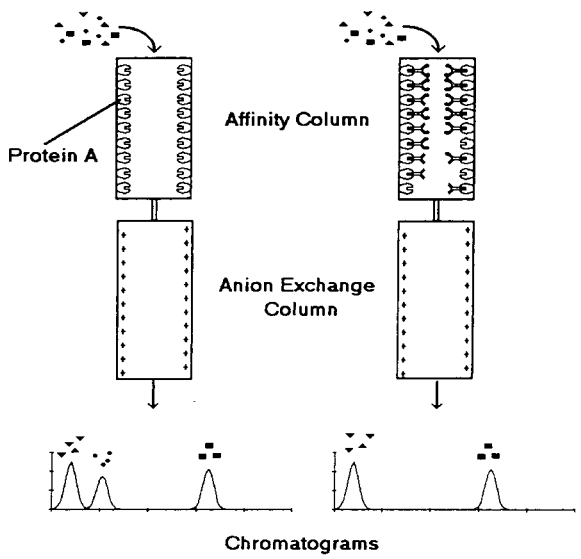

Fig. 1. Subtractive chromatography can be used to identify peaks. The sample is passed through a protein A column loaded with an antibody which will remove the protein of interest. A chromatogram of this sample is compared with a chromatogram of the same sample without antibody to determine the retention time of the protein.

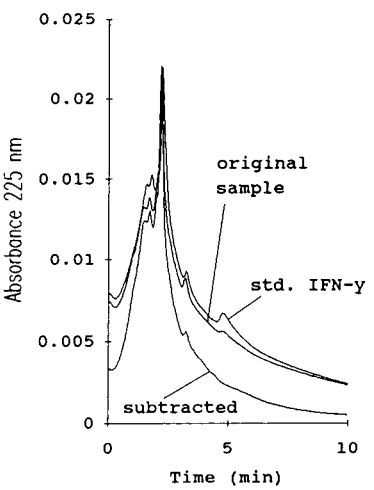

Fig. 2. Subtractive chromatography for γ-interferon. Conditioned γ-CHO medium was analyzed by cation-exchange chromatography (original sample). The subtracted sample was also analyzed, and the last small peak disappeared (subtracted). To further confirm the location, pure IFN-γ was added to the original sample (std. IFN-γ).

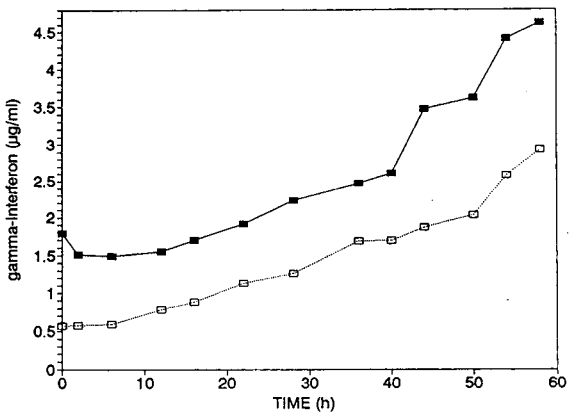

Fig. 3. Production of IFN-γ. □ = non-glycosylated and ■ = glycosylated IFN-γ.

unless the buffer contains borate (borate complexes with *cis* diols in the carbohydrate portion of the molecule, imparting negative charge [8,9]). This charge then causes retention of the glycosylated form of IFN-γ on the anion-exchange column. The pH of the mobile phase in this case was above 9. It is this alkaline pH which dictates the use of pH-stable packing material such as polystyrene. Silica-based media will dissolve at this alkaline pH.

Unfortunately, the antibiotics and methotrexate in the media co-eluted with the glycosylated IFN-γ. It is ironic that they also co-eluted with IFN-γ in capillary electrophoresis as well [10]. Since the antibiotics and methotrexate are small molecules, they were removed from the samples by size-exclusion cartridges (PD-10) prior to analysis. This precluded totally automated sample handling, but only added 5 min to the length of the assay. However, the added benefit of removing many other contaminating species, such as phenol red, was also acquired, making the chromatograms somewhat simpler to interpret.

The second objective was to demonstrate the ruggedness of the method and test its suitability for process monitoring. The production of both forms of IFN-γ were monitored with these HPLC methods over the course of a 60-h fermentation. Samples were removed from the bioreactor and analyzed immediately by the HPLC methods previously mentioned. Production curves show that both forms of IFN-γ are produced at roughly the same rate, although there is more glycosylated IFN-γ than non-glycosylated (Fig. 3).

CONCLUSIONS

Rapid HPLC methods for the determination of glycosylated and non-glycosylated IFN-γ were developed. These methods were then used to monitor IFN-γ production over a 60-h fermentation. These experiments demonstrate the efficacy of rapid, automated, chromatographic analyses for monitoring the production of recombinant proteins. Future work should be directed toward developing a direct interface between the HPLC and the bioreactor, to complete the on-line monitoring system.

ACKNOWLEDGEMENTS

The authors wish to thank Dr. Noubar Afeyan for valuable discussions. γ-Interferon for these studies was generously supplied by Dr. Jeffrey L. Cleland of Genentech. The BioCAD HPLC system was a gracious loan from PerSeptive Biosystems. This work was funded by a NSF grant under contract No. EEC 8803014.

REFERENCES

1 R.R. Burgess, in D.L. Oxender and C.F. Fox (Editors), *Protein Engineering*, Alan R. Liss, New York, 1987, p. 81.
2 C.F. Goochee, M.J. Gramer, D.C. Andersen, J.B. Bahr and J.R. Rasmussen, *Bio/Technology*, 9 (1991) 1347.
3 A.L. Smiley, W.-S. Wu and D.I.C. Wang, *Biotechnol. Bioeng.*, 33(9) (1989) 1182.
4 J. Notani, Y. Saitoh, M. Terada, H. Yamada, Y. Ishii, S. Satoh, M. Tomoi and M. Niwa, *Biotechnol. Prog.*, 5(1) (1989) 40.
5 N.B. Afeyan, S.P. Fulton and F.E. Regnier, *LC/GC*, 12(9) (1991) 824.
6 S.K. Paliwal, T.K. Nadler, D.I.C. Wang and F.E. Regnier, *Anal. Chem.*, in press.
7 A. Riggin, J.R. Sportsman and F.E. Regnier, *J. Chromatogr.*, 632 (1993) 37.
8 S. Chapelle and J.-F. Verchere, *Tetrahedron*, 44 (1988) 4469.
9 S. Hoffstetter-Huhn, A. Paulus, E. Gassmann and H.M. Widmer, *Anal. Chem.*, 63 (1991) 1541.
10 C. Lee, personal communication.

Journal of Chromatography A, 659 (1994) 321–328
Elsevier Science B.V., Amsterdam

CHROM. 25 689

Direct high-performance liquid chromatographic separation of an enantiomeric peptidoleukotriene antagonist and its homologues

Ted K. Chen*

Department of Analytical Sciences, SmithKline Beecham Pharmaceuticals, P.O. Box 1539 (UW2960), King of Prussia, PA 19406-0939 (USA)

Robert J. Mills

Department of Synthetic Chemistry, SmithKline Beecham Pharmaceuticals, P.O. Box 1539 (UW2820), King of Prussia, PA 19406-0939 (USA)

(First received July 6th, 1993; revised manuscript received October 26th, 1993)

ABSTRACT

Racemic SK&F 106203 and its homologues can be directly separated on Chiralcel OD, Chiralpak AD and AS columns. The corresponding dimethyl esters, however, can only be resolved on the Chiralcel OD column. Hydrogen bonding between the carboxylic acid proton of the analyte and the chiral stationary phase appears critical for chiral recognition on Chiralpak AS column for these carboxylic acid compounds. Substitution at the 2 position of the parent phenyl ring appeared to aid chiral separation on Chiralcel OD column. The elution order of SK&F 106203 obtained on a Chiral OD column can also be reversed on a Chiralpak AS column.

INTRODUCTION

Leukotriene D_4 (LTD_4), formed from the metabolism of arachidonic acid by 5′-lipoxygenase, is considered an important receptor–mediator of human bronchial asthma [1]. Considerable efforts are ongoing in the pharmaceutical industry in pursuing specific leukotriene LTD_4 receptor antagonists as potential therapeutics for the treatment of 'asthma. Among compounds of this class are ICI-204, 219, SK&F 104353, SK&F 106203 [2] and ONO-1078 [3].

With the current emphasis on enantiospecific pharmacological evaluations in drug development [4,5], chiral chromatography has become increasingly important. Where significant pharmacological differences exist between two enantiomers, the eutomer should be developed, and the other enantiomer may be regarded as an impurity. SK&F *S*-106203 {3(*S*)-[2-(carboxyethyl)thio]-3-[2-(phenyloctyl)phenyl]propanoic acid (**1**)} is a potent and selective LTD_4 receptor antagonist that is currently in clinical trials. The two enantiomers of this LTD_4 receptor antagonist showed markedly different pharmacological activities. We have described the direct enantiospecific separation of **1** and reported on the utility of this chiral HPLC method in assigning absolute stereochemistry to the disodium salt of **1**, a non-crystalline amorphous compound which

* Corresponding author.

0021-9673/94/$07.00
SSDI 0021-9673(93)E1155-S

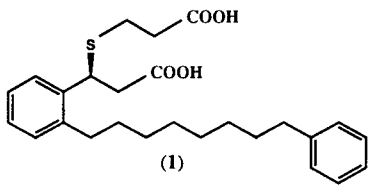

(1)

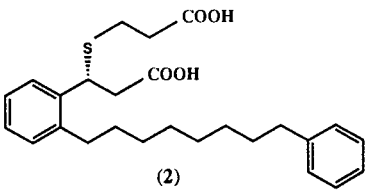

(2)

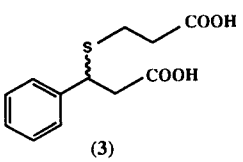

(3)

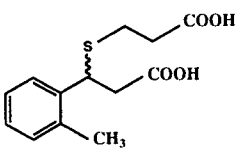

(4)

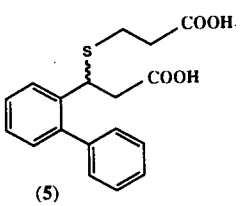

(5)

is not amenable to single crystal X-ray analysis [6]. In this communication, we report on the chiral HPLC of **1** and its homologues on cellulose Chiralcel OD, amylose Chiralpak AD and amylose Chiralpak AS columns.

EXPERIMENTAL

Apparatus

The liquid chromatograph system consisted of a Beckman System Gold HPLC pump connected to an HP 1050 series autosampler and variable-wavelength UV detector. Chiralcel OD, Chiralpak AD and Chiralpak AS column (all three 250 × 4.6 mm) were obtained from Chiral Technologies (Exton, PA, USA). Data were acquired and processed using a Waters 860 networking computer system.

Chemicals

Trifluoroacetic acid (Baker Analyzed HPLC reagent-grade ampoules) and HPLC-grade isopropanol and *n*-hexane were obtained from J.T. Baker (Phillipsburg, NJ, USA). All compounds used in this investigation were synthesized in our laboratory, and were fully characterized by NMR, IR, MS, elemental analysis and impurity profile by HPLC.

Chromatographic conditions

All experiments were performed at ambient temperature and with UV detection at 215 nm. Mobile phase compositions optimized for the separation of **1** and **2** were: for Chiralcel OD, *n*-hexane–isopropanol–trifluoroacetic acid (96.5:3.5:0.1), flow-rate, 2 ml/min; for Chiralpak AD, *n*-hexane–isopropanol–trifluoroacetic acid (94:6:0.1), flow-rate, 0.6 ml/min; for Chiralpak AS, *n*-hexane–isopropanol–trifluoroacetic acid (88:12:0.1), flow-rate, 0.6 ml/min.

RESULTS AND DISCUSSION

In order to evaluate the toxicological profile of the single SK&F *R*-106203 enantiomer (**2**), we required an enantiospecific HPLC method to measure its chiral purity. On cellulose Chiralcel OD column, the *R*-enantiomer, SK&F *R*-106203 eluted first, followed by the *S*-enantiomer, SK&F *S*-106203 (**1**) [6]. For low detection, it is advantageous to have the undesired enantiomer eluted first so that it will not be affected by the tailing of the major component. Since amylose-based Chiralpak AS column has a chiral center in the *S*-configuration at the phenylethyl group which can serve as an additional chiral selector [7] (Fig. 1), we attempted the chiral HPLC of racemic SK&F 106203 on a Chiralpak AS column. As shown in Fig. 2, the elution order observed on Chiral OD column for racemic SK&F 106203 [6] can be successfully reversed on an amylose Chiralpak AS column. The differences in the backbone structure of either stationary phase, *i.e.*, liquid crystal-like leading to a rigid and linear structure on the surface of the silica gel support for cellulose Chiralcel OD column [8], and pseudo-helical for amylose Chiralpak AS column, apparently, were not critical

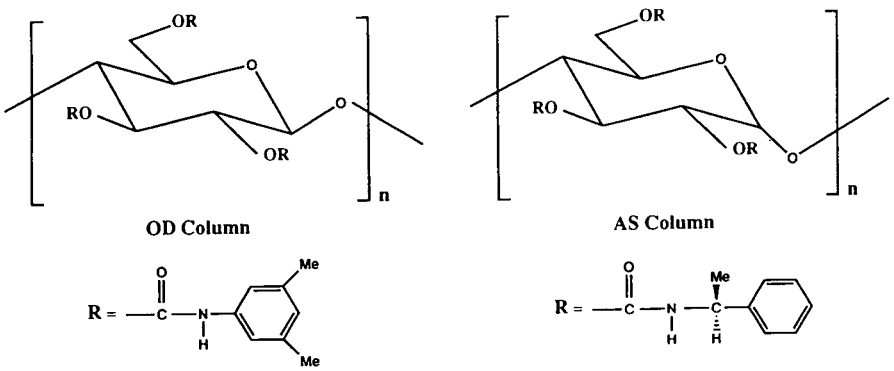

Fig. 1. Structures of cellulose Chiralcel OD and amylose Chiralpak AS columns.

for chiral separation. To the best of our knowledge, this is the first observation of reversal of elution order between a cellulose Chiralcel OD and an amylose Chiralpak AS column. Reversal of elution order between a Chiralpak AR and a Chiralpak AS column in the fashion of the well documented elution order reversal obtained on (*R*) and (*S*) Pirkle-type dipeptide columns, has been reported [8]. However, Chiralpak AR column also has limited resolving power compared to Chiralpak AS or Chiralcel OD columns [8]. Previous applications of Chiralpak AS column has primarily been on heterocyclic compounds possessing the chiral center on the ring, *e.g.*, diazapine and β-lactam [7].

Since chemically related compounds differing only in the length of the carbon chain are known to exhibit different physical properties and elicit different biological responses [9], we also examined the chromatographic behaviour of SK&F 106203 (**1**) and its simple homologues, namely, the unsubstituted (**3**), the methyl (**4**) and phenyl (**5**) derivatives on Chiralcel OD, Chiralpak AD and Chiralpak AS columns. As the retention and

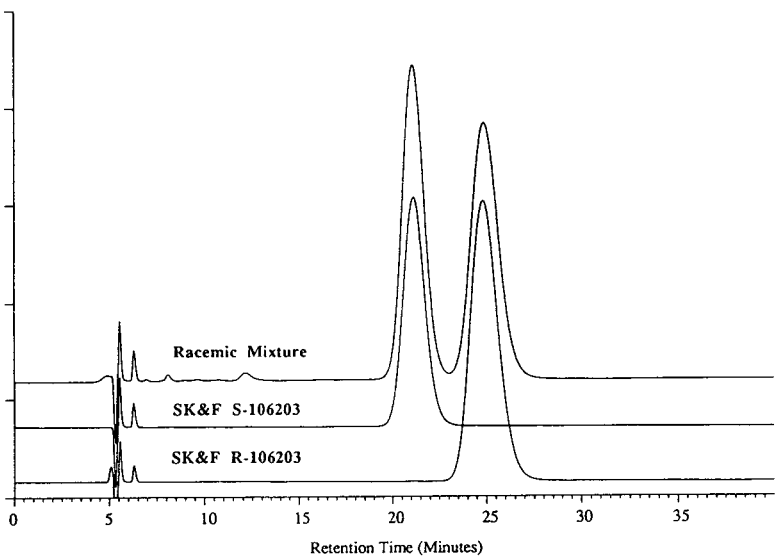

Fig. 2. Chiral HPLC chromatograms of (top trace) the racemic mixture of **1** and **2**, (middle trace) **1**, and (bottom trace) **2** on Chiralpak AS column. The HPLC conditions are: mobile phase flow-rate 0.6 ml/min, UV detection at 215 nm.

separation characteristic of these columns were different, and the respective polarity of the analogues was varied, we could not perform the chromatography on all three columns using identical mobile phase and flow-rate. To compare the separation of racemic mixture of **1** and **2**, **3**, **4** as well as **5** on these columns, we used a mobile phase and flow-rate on each column that was optimized for the separation of racemic mixture of **1** and **2**. The results are shown in Figs. 3, 4 and 5, and the separation factors are presented in Table I. Under these conditions, in all cases, the presence of 0.1% (v/v) trifluoroacetic acid in the mobile phase was required for good peak shape and resolution. As shown in Fig. 3, the *ortho*-substituted analogues are better separated than the unsubstituted analogue on Chiralcel OD column. *ortho*-Substitution therefore appeared to aid separation on the OD column for this class of compounds. However, no such clear trend exists for the amylose-based AD and AS column.

The results also showed that the phenyl analogue (**5**) was well separated on all three chiral columns. Thus, for this class of compounds, contribution from the *ortho*-phenyl substituent to the $\pi-\pi$ interaction between the analyte and the chiral stationary phase appeared to facilitate chiral recognition.

Whereas the unsubstituted analogue (**3**) was not well resolved on the cellulose OD column, **3** was well separated on both amylose AD and AS columns under similar conditions. The methyl analogue (**4**), on the other hand, was well resolved on the OD column but not on either the AD or AS columns. Since the steric hindrance of the phenyloctyl side chain in **1** is very similar to the methyl substituent in **4** because of its steric flexibility, it was anticipated that on both AD and AS columns under the same conditions where the methyl analogue **3** was barely baseline-resolved, the separation of racemic mixture of **1** and **2** would also be problematic. However, as shown in Table I and Figs. 4 and 5, although the racemic mixture of **1** and **2**, as expected, was not well resolved on the AS column (resolution factor: 1.6), it was nonetheless well separated on the AD column (resolution factor: 4.0). More data are therefore needed in order to decipher a clear trend of predictive value for either the AD or AS column based on the relative steric hindrance of the ortho-substituted alkyl side chain for this class of compounds.

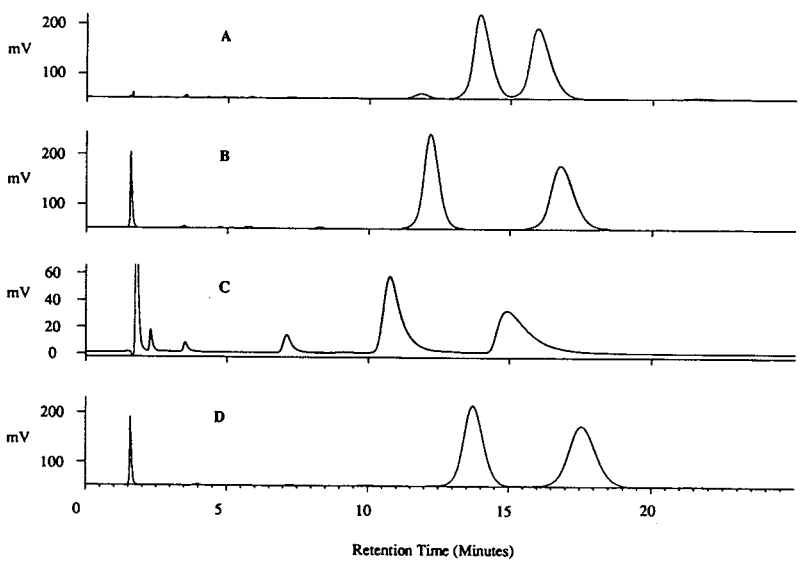

Fig. 3. Chiral HPLC chromatograms of the racemic mixture of (A) **3**, (B) **4**, (C) **5** and (D) **1** and **2** on Chiralcel OD column. The HPLC conditions are: mobile phase *n*-hexane–isopropanol–trifluoroacetic acid (96.5:3.5:0.1), flow-rate 2 ml/min, UV detection at 215 nm.

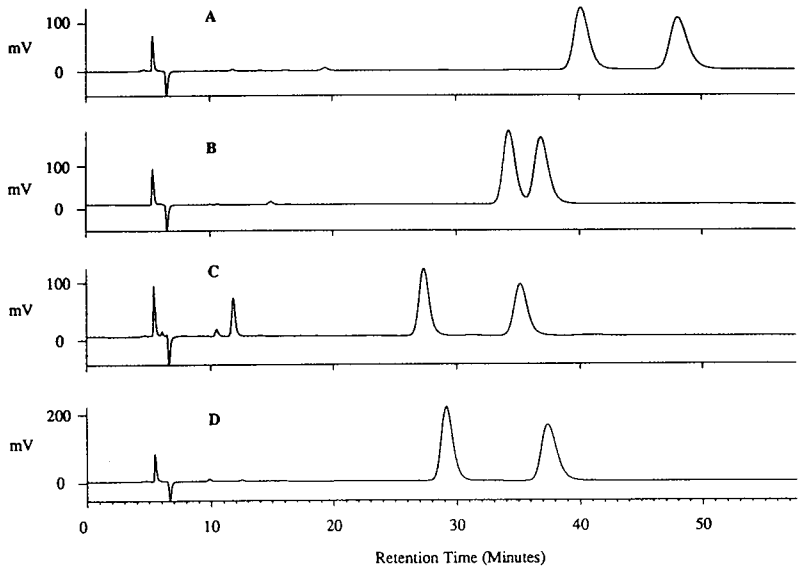

Fig. 4. Chiral HPLC chromatograms of the racemic mixture of (A) **3**, (B) **4**, (C) **5** and (D) **1** and **2** on Chiralcel AD column. The HPLC conditions are: mobile phase *n*-hexane–isopropanol–trifluoroacetic acid (94:6:0.1), flow-rate 0.6 ml/min, UV detection at 215 nm.

The separations of the dimethyl esters of racemic mixture of **1** and **2**, **3** as well as **4** on the OD, AD and AS columns are shown in Figs. 6, 7 and 8 and Table II. As expected, methylation of the carboxylic acids reduced the polarity of these compounds, resulting in weaker retention on the

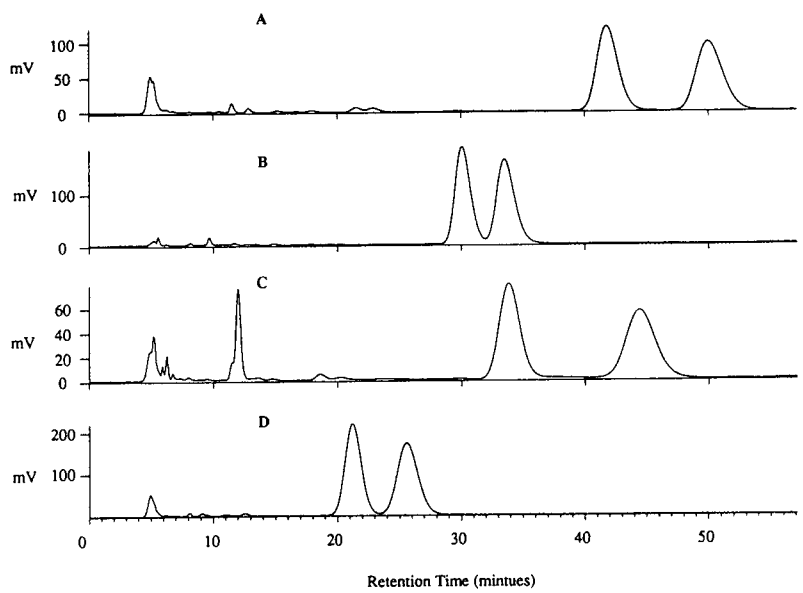

Fig. 5. Chiral HPLC chromatograms of the racemic mixture of (A) **3**, (B) **4**, (C) **5** and (D) **1** and **2** on Chiralpak AS column. The HPLC conditions are: mobile phase *n*-hexane–isopropanol–trifluoroacetic acid (88:12:0.1), flow-rate 0.6 ml/min, UV detection at 215 nm.

TABLE I

CHIRAL RESOLUTION OF RACEMIC MIXTURES OF **1** AND **2**, **3**, **4** AND **5** ON CHIRALCEL OD, AD AND CHIRALPAK AS COLUMNS

k'_1 = Capacity factor of the first eluted isomer; R_s = Resolution factor = 2 (difference of retention times of (+) and (−) isomers/the band widths of the two peaks).

	OD Column		AD Column		AS Column	
	k'_1	R_s	k'_1	R_s	k'_1	R_s
1 and **2**	8.1	2.5	5.5	4.0	4.1	1.6
3	8.3	1.6	7.9	3.2	8.9	2.3
4	7.1	3.7	6.6	1.3	6.2	1.4
5	6.2	2.9	5.1	4.4	7.1	2.8

cellulosic columns. Accordingly, the mobile phase flow rate on OD column was reduced by half. Methylation of the carboxylic acids in **1** and **2** also significantly affected the resolution of the two enantiomers on OD column, resulting in a shift of resolution factor from 2.5 for the free diacids to 5.4 for the dimethyl ester. Although the free diacids **1** and **2**, **3** as well as **4** were successfully separated on the OD column, the corresponding dimethyl esters could not be resolved on the AS column. Hydrogen bonding between the acid proton of the analyte and the chiral stationary phase, therefore, appeared critical for chiral recognition on the AS column. The capacity factor of these dimethyl esters on the AS column (Table II) also showed an interesting trend, with the capacity factor for the side chain substitution: unsubstituted > methyl > phenyloctyl. The greater hydrophorbicity of the side chain resulted in weaker retention on the AS column. No clear trend was observed on the OD column.

Separation of other leukotriene antagonists, e.g., Merck's MK-571 required prior derivatization with a chiral derivatizating agent [10]. Merck's L-699392, on the other hand, was separated by normal-phase chromatography on a diol column using a mobile phase consisting of methylene chloride and *n*-propanol containing quinine as the chiral selector [11]. Lily's close structural analogue to **1** [12] was separated on a chiral α_1-acid glycoprotein column. Our attempts to separate SK&F 107310, the methoxy sulfonyl derivative that is structurally related to **1** on all commercially available cellulosic columns, were also unsuccessful.

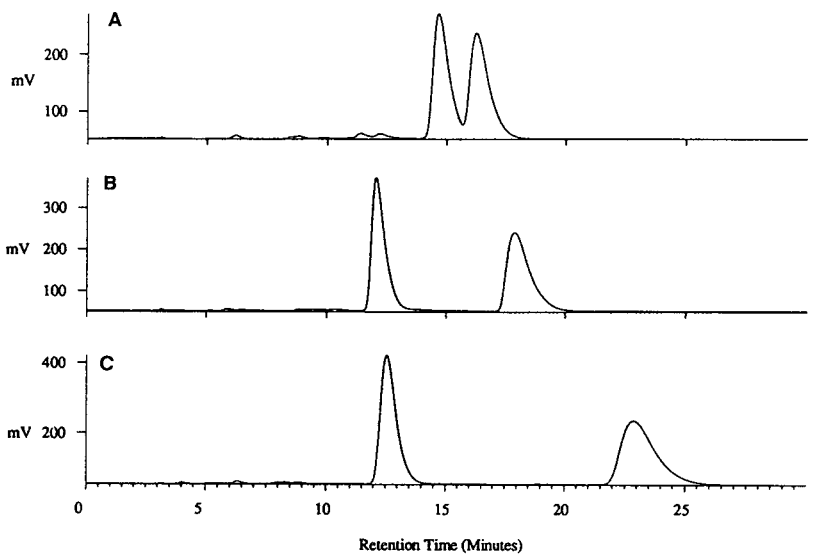

Fig. 6. Chiral HPLC chromatograms of the dimethyl ester of (A) **3**, (B) **4** and (C) racemic mixture of **1** and **2** on Chiralcel OD column. The HPLC conditions are: mobile phase *n*-hexane–isopropanol–trifluoroacetic acid (96.5:3.5:0.1), flow-rate 1 ml/min, UV detection at 215 nm.

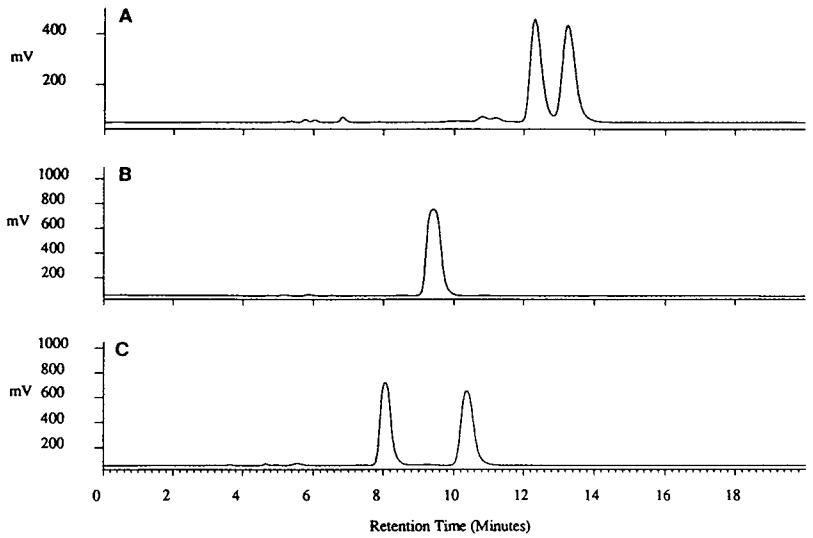

Fig. 7. Chiral HPLC chromatograms of the dimethyl esters of (A) **3**, (B) **4** and (C) racemic mixture of **1** and **2** on Chiralcel AD column. The HPLC conditions are: mobile phase: *n*-hexane–isopropanol–trifluoroacetic acid (96.5:3.5:0.1), flow-rate: 1 ml/min, UV detection at 215 nm.

CONCLUSIONS

SK&F 106203 (**1**) and its homologues can be directly separated on Chiralcel OD, Chiralpak AD and AS column without prior derivatization. Although well separated on the Chiralcel OD column, the dimethyl esters of **1** and its homologues could not be separated on an Chiralpak AS column. Hydrogen bonding between the acid proton of the analyte and the chiral stationary

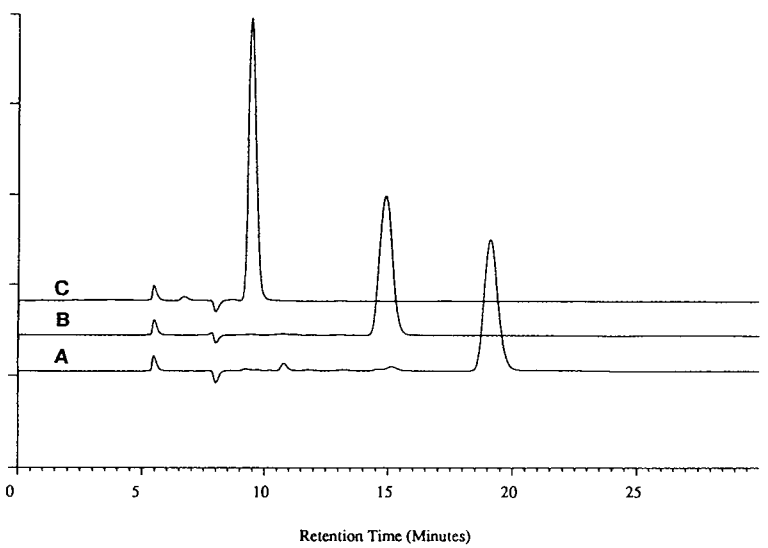

Fig. 8. Chiral HPLC chromatograms of the dimethyl esters of (A) **3**, (B) **4** and (C) racemic mixture of **1** and **2** on Chiralcel AS column. The HPLC conditions are: mobile phase *n*-hexane–isopropanol–trifluoroacetic acid (88.2:11.8:0.1), flow-rate 0.6 ml/min, UV detection at 215 nm.

TABLE II

CHIRAL RESOLUTION OF THE DIMETHYL ESTERS OF RACEMIC **1** AND **2**, **3** AND **4** ON CHIRALCEL OD, AD AND CHIRALPAK AS COLUMNS

– = No separation.

	OD Column		AD Column		AS Column	
	k'_1	R_s	k'_1	R_s	k'_1	R_s
1 and **2**	4.5	5.4	2.1	4.1	1.3	–
3	5.4	4.2	3.6	1.5	2.5	–
4	4.3	1.2	2.6	–	3.6	–

phase appeared critical for chiral recognition on the AS column. The elution order of **1** on Chiralcel OD column can be reversed by performing the chromatography on an Chiralpak AS column. Further work is in progress to probe the generality of this elution order reversal, and the results will be reported in a future communication.

ACKNOWLEDGEMENTS

We thank Ms. A. Tickner for providing us with a sample of the methyl analogue **4**, and Dr. V. Novack and Dr. M.A. Lewis for helpful discussions.

REFERENCES

1 R.D. Krell, *Pulm. Pharmacol.*, 2 (1989) 27.
2 M.A. Lewis, R.D. Krell and T.R. Jones, in A. Wong and S. Crooke (Editors), *Lipoxygenases and Their Products*, Academic Press, New York, 1991, pp. 207–234.
3 M. Fujimura, S. Sakamoto, Y. Kamio and T. Matsuda, *Respiratory Medicine*, 87 (1993) 133.
4 W.H. De Camp, *Chirality*, 1 (1989) 2.
5 M.N. Cayen, *Chirality*, 3 (1991) 94.
6 T.K. Chen, K.F. Erhard, T. Last, D.S. Eggleston and M.Y.K. Ho, *J. Chromatogr.*, 596 (1992) 123.
7 *Application Notes for Chiralpak AS Column*, Chiral Technologies, Exton, PA, 1990.
8 Y. Okamoto and Y. Kaida, *J. High Resolut. Chromatogr.*, 13 (1990) 708.
9 G. Buckton, A.E. Beezer, S.P. Denyer and S.J. Russell, *Int. J. Pharm.* 73 (1991) 1.
10 D.L. Hughes, J.J. Bergan, J.S. Amato, P.J. Reider and E.J. Grabowski, *J. Org. Chem.*, 55 (1990) 6252.
11 D. Gopal, N. Grinberg, T. Dowling, H. Perpall, G. Bicker and T. Tway, *J. Liq. Chromatogr.*, 16 (1993) 1749.
12 D.M. Rackham and G.A. Harvey, *J. Chromatogr.*, 542 (1991) 189.

Journal of Chromatography A, 659 (1994) 329–336
Elsevier Science B.V., Amsterdam

CHROM. 25 663

High-performance liquid chromatographic determination of the triphenylmethane dye, malachite green, using amperometric detection at a carbon fibre microelectrode

Kamal Sagar and Malcolm R. Smyth

School of Chemical Sciences, Dublin City University, Dublin (Ireland)

James G. Wilson and Kieran McLaughlin*

Environmental Sciences Unit, Trinity College, Dublin (Ireland)

(First received January 29th, 1993; revised manuscript received October 18th, 1993)

ABSTRACT

The triphenylmethane dye, malachite green (Colour Index C.I. Basic Green 4) has been determined in its chromatic form in drinking and river water using high-performance liquid chromatography with amperometric detection at a carbon fibre electrode. The limit of detection of the technique was 0.07 mg/l and the linear range extended from 0.07–10 mg/l. The use of a 250-fold preconcentration on solid-phase extraction cartridges allowed the analysis of malachite green at the 0.28 μg/l level. The technique was found to be reproducible with a mean relative standard deviation of 5.4 and 3.6% at the 0.25 and 5 mg/l levels, respectively. The application of the technique to the analysis of drinking and river water samples is demonstrated. Typical recoveries from drinking water and river water samples spiked with 1 μg/l chromatic malachite green were 82 and 41%, respectively. Sorption of malachite green on to suspended organic matter in the water column is discussed. The simultaneous analysis of the chromatic malachite green and its biotransformed leuco form is described.

INTRODUCTION

Since first reported as being effective in controlling fungi on bass, trout and trout eggs [1], the triphenylmethane dye, malachite green (Colour Index C.I.; Basic Green 4), has found extensive use throughout the world in the fish farming industry as a fungicide and an ecto-parasiticide. However, it has been the subject of close scrutiny due to its suggested teratogenic properties, and, in a programme of registration of fisheries chemicals in the USA, its use has been prohibited in federal government facilities [2]. The use of malachite green is now limited to the treatment of non-food fish under an Investigational New Animal Drug Application held by the US Fish and Wildlife Service.

In Europe, malachite green is regularly used for the control of *Saprolegnia parasitica* and also in the treatment of proliferative kidney disease (PKD). Its use is controlled within the EEC by guidelines laid down in each of the individual member states. In Ireland, these state that the concentrations of malachite green in fish farm water effluent and water extracted for drinking water purposes should not exceed 100 and 1.0

* Corresponding author.

0021-9673/94/$07.00
SSDI 0021-9673(93)E1102-6

μg/l, respectively. Under the fisheries and agriculture research programme (FAR), an EEC project into the environmental fate of malachite green is presently being carried out in Trinity College, Dublin.

Malachite green and the closely related triphenylmethane dye crystal violet are reduced through biotransformation to their leuco forms in animals [3,4]. Werth and Boiteux [3], have shown that the organs of rats, injected with malachite green, contain a considerable proportion of leuco malachite green two hours after injection. Although never tested, the leuco form of malalchite green is structurally similar to classical aromatic amine carcinogens. The chromatic and leuco forms of malachite green are shown in Fig. 1.

In response to concerns regarding the health risks associated with the use of malachite green, an increasing number of methods have been developed in the past decade for its determination in environmental samples and food fish tissue.

A thin-layer chromatographic (TLC) method was first used for the analysis of malachite green residues in edible fish [5]. A methanolic solution of material extracted from fish was analysed by TLC on silica gel followed by densitometric detection and quantitation at 610 nm.

An extension of this work [6] made use of a high-performance liquid chromatographic (HPLC) separation on a LiChrosorb RP-8 or Spherisorb Octyl column with subsequent spectrophotometric detection and quantitation at 600 nm.

The simultaneous determination of malachite green and methylene blue in rainbow trout and amago muscle using HPLC with subsequent spectrophotometric detection [7] has recently been reported. Residues of malachite green were determined, using a colorimetric method, in muscle, eggs, and fry of Atlantic salmon (*Salmo salar*) and chinook salmon (*Oncorhynchus tshawytscha*) which had been treated with the chemical at fish hatcheries [8]. Allen and Meinertz [9] reported on a post-column reaction for the simultaneous analysis of chromatic and leuco forms of malachite green and crystal violet by HPLC with spectrophotometric detection at 588 nm. This system made use of a post-column reaction chamber containing PbO_2 situated between the HPLC column and the spectrophotometric detector. Separation of the leuco and chromatic forms of the dye was effected on the HPLC column, after which they passed through the post-column reaction chamber and subsequently into the spectrophotometric detector. This method has recently been applied to the analysis of the chromatic and leuco forms of malachite green in water [10].

The use of electrochemical detection in conjunction with HPLC has been used for the simultaneous determination of the chromatic and leuco forms of crystal violet [11]. In view of the importance of determining malachite green in both its chromatic form, used in fungicidal and ectoparasiticidal treatment regimes, and its biotransformed leuco form, a chromatographic methodology involving electrochemical detection at a carbon fibre electrode is reported for the first time in the present paper.

In the past decade, there has been considerable interest in the development of microelectrode flow detectors, with several authors reporting on the use of carbon [12] and gold fibres [13] in such systems. In addition to the advantages offered by microelectrodes in the construction of low volume detectors, the use of such electrodes

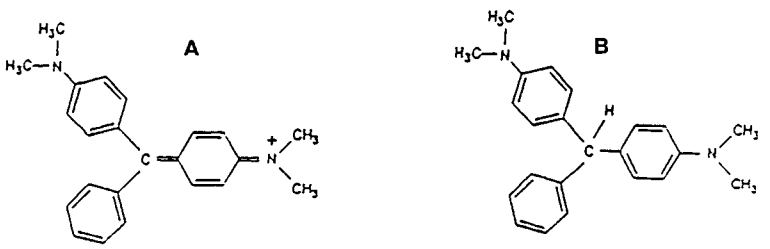

Fig. 1. Chemical structures of (A) chromatic and (B) leuco forms of malachite green.

permits a steady state to be achieved quickly [14], improved signal to noise ratios [15] and a reduced ohmic contribution.

The method proved successful for the determination of the chromatic form of malachite green in river and drinking water samples. In addition, it was also possible to carry out the simultaneous analysis of the chromatic and leuco forms without the need for post-column modification.

EXPERIMENTAL

Chemicals and reagents

Malachite green oxalate and leuco malachite green were obtained form Aldrich (Gillingham, Dorset, UK) and from BDH (Poole, UK), respectively. Acetic acid (AnalaR grade) was supplied by BDH and HPLC-grade methanol was supplied by Labscan Analytical Sciences (Dublin, Ireland). Analytical grade sodium dihydrogen orthophosphate was obtained from BDH. This compound and the supporting electrolyte were used without purification. Deionised water was used throughout this work and was obtained by passing distilled water through a Milli-Q water purification system (Millipore, Milford, MA, USA). Carbon fibres were obtained from Avco (Lowell, MA, USA). These were 14 μm in diameter and their surface had no external coating. Silver epoxy was purchased from RS components (Corby, UK).

Apparatus

Voltammetric studies were performed using an EDT potentiostat (EDT Research, London, UK) in conjunction with a JJ X-Y Model PL4 recorder (JJ Loyd Instruments, Southampton, UK). A three-electrode cell system was employed, incorporating a 0.28 cm^2 area glassy carbon electrode (EG&G Princeton Applied Research), a saturated calomel reference electrode and a platinum counter electrode.

Amperometric measurements were performed using an EG&G Model 400 EC potentiostat (EG&G Princeton Applied Research) connected to the flow cell by crocodile pins. Malachite green was detected amperometrically by employing a potential of +1.2 V at the working electrode. The resultant signals were recorded on a WPA Model CQ 95 X-t recorder (WPA, Linton, Cambridge, UK). The peak currents (measured as peak heights on the recorder) as a function of concentration were then measured for quantitative analysis.

Malachite green was separated on a 250 × 4.6 mm I.D. cyano (CN) stainless-steel column, particle size 5 μm (Hichrom, Reading, UK) using a methanol–0.1 *M* sodium acetate, pH 4.5 (70:30, v/v) mobile phase. Mobile phases containing acetonitrile were not used because previous experience had shown it to have a detrimental effect upon the long term stability of the carbon fibre. A Waters Model 501 HPLC pump was used for mobile phase delivery and sample introduction was via a Rheodyne (Cotati, CA, USA) Model 7010 injection valve, fitted with a 20-μl loop of direct injection.

For extraction purposes, Techelut 100 mg/1.0 ml cyano solid-phase extraction cartridges (HPLC Technology, Cheshire, UK) were used in conjunction with a Techelut 12 position manifold.

Construction of carbon fibre flow cell

The carbon fibre flow cell was constructed according to the procedure described by Sagar *et al.* [16]. The carbon fibre working electrode was inserted through the centre of a 25 mm length polyethylene tubing (2 mm × 0.5 mm I.D.) as reported by Hua *et al.* [17].

Voltammetric procedures

The supporting electrolytes used for pH and cyclic voltammetric studies were prepared from a 0.1 *M* stock solution of sodium dihydrogen orthophosphate. All solutions were prepared in deionised water and were adjusted to the required pH with 0.2 *M* orthophosphoric acid or sodium hydroxide.

Cyclic voltammetry was performed on solutions containing $1 \cdot 10^{-3}$ *M* malachite green dissolved in the supporting electrolyte. Voltammetric conditions were as follows: initial potential 0.0 V; final potential +1.3 V; scan rate 50 mV/s; current range 20 μA.

Hydrodynamic voltammetric studies were carried out by injecting 5 mg/l of malachite green, dissolved in 95% aqueous methanol containing

0.05 *M* sodium acetate, pH 4.5, into the chromatograph with the detector set at different working potentials *vs.* Ag/Ag_3PO_4. Cleaning potentials of +1.3 V and −1.3 V were applied for 60 s, respectively, between each injection. Hydrodynamic voltammograms were constructed by plotting the peak current against the applied potential. The optimum potential for malachite green determination was found from the position of the plateau on the hydrodynamic wave.

Extraction procedure

Drinking water samples were collected from the Dublin city water supply and river water samples were collected from Arklow, County Wicklow. The samples were stored in plastic containers at 4°C on return to the laboratory prior to analysis on the same day.

Drinking water and river water samples were adjusted to pH 5.0 with acetic acid and spiked with 1 μg/l malachite green prior to extraction and preconcentration on the solid phase extraction cartridges. These cartridges were preconditioned with 2 ml of methanol followed by 5 ml of deionised water. An aliquot of 250 ml of the spiked water sample was eluted through the column at a flow-rate of 7 ml/min after which the retained malachite green was eluted with two 0.5-ml volumes of mobile phase. These 0.5-ml aliquots were combined and used for chromatographic analysis.

Chromatographic separation of chromatic malachite green

The liquid chromatographic analysis of the chromatic form of malachite green was based upon the method of Roybal *et al.* [11] for the determination of gentian violet. The chromatography of malachite green was investigated by varying the methanol content and the pH of the mobile phase.

Calibration, recovery and reproducibility

Calibration graphs were constructed by plotting peak current against concentration for a series of chromatic malachite green standards, prepared in mobile phase, at a potential of +1.2 V *vs.* Ag/Ag_3PO_4 and a mobile phase flow-rate of 0.9 ml/min.

Aliquots of malachite green standards, made up in 0.1 *M* sodium acetate, pH 4.5, were added to drinking water and river water samples to give final concentrations of 1.0 μg/l. Replicate spiked samples and the corresponding blanks were extracted according to the extraction procedure previously described. Recoveries of chromatic malachite green from drinking water and river water samples were assessed by comparing the peak currents obtained for the extracts with those of standard solutions.

The reproducibility of the method was ascertained by determining the relative standard deviation of five successive measurements of extracts of water samples.

Simultaneous analysis of chromatic and leuco malachite green

The chromatographic separation of the chromatic and leuco forms of malachite green was carried out on a cyano column using methanol–0.1 *M* sodium acetate, pH 4.5 (70:30, v/v) with amperometric detection at +1.2 V *vs.* Ag/Ag_3PO_4.

RESULTS AND DISCUSSION

Voltammetric behaviour of malachite green

The voltammetric behaviour of the chromatic form of malachite green was studied over the pH range 4–12 in 0.05 *M* phosphate buffer using differential pulse voltammetry (DPV) at a glassy carbon electrode. The single anodic peak obtained in the range studied was found to be pH dependent.

A plot of pH against peak current indicated a pK_a value of 6.5. This value is in close agreement with the value of 6.9 previously reported [18].

In the cyclic voltammogram of malachite green, no cathodic peaks were present in the reverse scan, thus indicating that the oxidation process was irreversible in nature.

In order to determine the working potential used for the amperometric detection of malachite green, hydrodynamic voltammograms were constructed. The hydrodynamic voltammogram exhibited one wave, a finding which was in accordance with the results obtained from the

pH and cyclic voltammetric studies. The hydrodynamic voltammogram indicates that in the potential range studied, the response increased with increased potential. However, at potentials greater than +1.2 V, both the background current and noise levels increased rapidly. Consequently, a potential of +1.2 V was used throughout the study, as this gave the optimum signal-to-noise ratio. The hydrodynamic voltammogram obtained for malachite green is similar to that reported by Roybal *et al.* [11] for the structurally related dye gentian violet. Whilst a study of the mechanism was not carried out in this investigation, it is thought that the oxidation of the triphenylmethane to the triphenylcarbinol derivative, as suggested by Roybal *et al.* [11], is a probable reaction scheme.

Electrode pretreatment

When using an electrochemical detector it is important to take into consideration the fact that the surface of the electrode changes with time due to either the adsorption of species from solution or chemical changes on the electrode surface itself. These changes have important consequences in that they can result in variations in sensitivity, reproducibility and selectivity , and must therefore be overcome if an analytical procedure is to be ultimately successful. During the course of the developmental work on an electrochemical detection system for the determination of malachite green, it was noted that the sensitivity of the technique decreased markedly with repeated injections of malachite green standards. This represented a serious problem regarding the eventual applicability of the method, and in an attempt to overcome it, an electrochemical pretreatment step was included in the analytical methodology.

A pretreatment protocol which improved the peak current involved the pre-anodisation of the microelectrode at +1.3 V for 60 s followed by cathodisation at −1.3 V for 60 s *vs.* Ag/Ag_3PO_4, followed by equilibration at +1.2 V for 3 min. It has been proposed [19] that the improvement in performance is as a result of the removal of surface contaminants or inhibitory layers which hinder electron transport. Thus extended lifetime can be obtained after electrochemical pretreatment. In an analytical methodology without a pretreatment procedure, the working electrode could be used for 3 to 5 measurements before deterioration of the analytical response. With the use of the pretreatment procedure the lifetime of the electrode could be extended up to 30 to 40 measurements.

The effect of pretreating the electrode is to increase its current response, which is probably due to the activation of the surface, producing quinoidal functionalities [20]. It is envisaged that a greater signal-to-noise ratio would be possible with the use of a potentiostat specifically tailored to the measurement of the low currents at such microelectrodes.

Electrode stability

The stability of the electrode is of importance in order to define the period of time over which the electrode can be used without a significant decrease in the sensitivity. The response of the electrode to a 5 mg/l malachite green standard solution was measured over a 9-day period. A significant decrease in the response was observed after the fourth day.

The carbon fibre flow detector yielded peaks whose currents had relative standard deviations of 5.4, 4.8, 6.1 and 5.6% on each of the first four days, respectively. After 6 and 9 days of continuous use, the electrode response was 61 and 38%, respectively, of its initial value, with relative standard deviations of 9 and 11%. There was no leakage from the electrode during its operating lifetime and the nature of its construction made it very stable in the mobile phase.

As the carbon fibre working electrode can be easily and cost effectively replaced, this decrease in sensitivity is not of major consequence. The use of a glassy carbon macroelectrode would otherwise require extensive physical cleaning and polishing steps to renew the electrode surface and consequently regain a sensitive response.

Chromatographic analysis of chromatic malachite green

In the initial chromatographic studies, variations were made in the mobile phase composition to optimise the analysis time and peak width. A mobile phase composed of methanol–

sodium acetate buffer, pH 4.5 (70:30, v/v) yielded the optimum results.

Calibration curves prepared on each of three successive days were linear over the range 0.07–10 mg/l with correlation coefficients of greater than 0.999.

The reproducibility of the technique was determined from five replicate injections of 5 mg/l and 0.25 mg/l standard solutions. Typical reproducibilities, determined from the coefficient of variation of the peak currents, of 3.6 and 5.4% were achieved at the 5 and 0.25 mg/l levels, respectively.

The detection limit of the technique, defined as three times the signal-to-noise ratio, was 0.07 mg/l. When used in conjunction with the 250 to 1 preconcentration on the solid-phase cartridges, the method detection limit was 0.28 μg/l. As previously mentioned, a lower detection limit should be possible with the use of a potentiostat designed to specifically measure the low currents at carbon fibre microelectrodes.

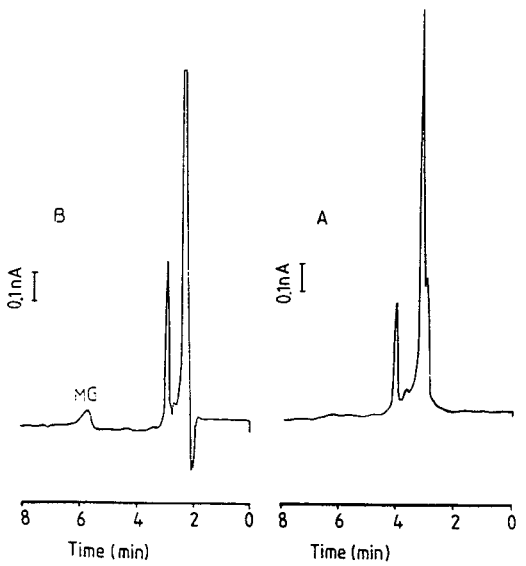

Fig. 2. HPLC chromatograms of drinking water extracts. (A) Blank drinking water sample. (B) Drinking water sample spiked with 1 μg/l malachite green (MG).

Analytical application

The chromatographic method was applied to the analysis of drinking water and river water samples spiked with 1.0 μg/l chromatic malachite green. In Fig. 2, chromatograms are shown for a blank drinking water extract and a spiked drinking water extract.

The chromatograms show well defined peaks for the chromatic form of malachite green with a retention time of 5.9 min. There were no late eluting peaks in the analysis, thus enabling successive injections to be made without the need for a wash period.

The mean recoveries for malachite green were found to be 82 and 41% in drinking water and river water samples, respectively. The reproducibility of the determination was measured by carrying out successive injections for drinking water and river water extracts. The reproducibility, as determined by the relative standard deviation, was 6.5 and 11% for drinking water and river water, respectively.

In Ireland, the current directives on malachite green in water state that the maximum permissible levels in fish farm effluent water and water extracted for drinking purposes should not exceed 100 and 1.0 μg/l, respectively. The chromatographic method described here is capable of determining malachite green at the 1.0 μg/l level stated in current directives and is comparable to the method described by Allen and co-workers [9,10].

The sample analyses were carried out in the nanoampere (nA) current range. The use of lower current ranges was prohibited by the presence of early eluting electroactive species which in the low current ranges produced large chromatographic peaks that obscured the analyte peak of interest. As part of continuing research, the incorporation of an extraction procedure into the analytical methodology is being investigated. It is hoped that this will eliminate these electroactive species thus allowing sample analyses to be carried out in the lower current range, and as a consequence improve the detection limits.

The very low and variable recoveries of malachite green from river water samples was thought to be due to its sorption on organic material in the water column. The fraction of dissolved or colloidally dispersed organic macromolecules, such as humic substances or non-filterable particles in natural waters, have been

shown to exert significant sorption properties towards organic compounds. Harrison *et al.* [21] indicated that organic compounds of low solubility exist in the water column primarily sorbed on suspended solids. The accumulation of such organic compounds in sediments has been attributed to their sorption on suspended solids and subsequent settling [22]. Similar findings were reported by Rushing and Bowman [23] for the analysis of gentian violet in wastewater. The low recoveries encountered during this analysis were attributed to the adsorption of gentian violet onto particulate matter present in the wastewater. Further chromatographic work is in progress to determine the extent to which malachite green is sorbed onto organic matter. The low recoveries from river water samples may be of use in further speciation work. This speciation work is of considerable importance in elucidating the distribution of malachite green in a water system.

Analysis of chromatic and leuco malachite green

The chromatographic separation and detection of the chromatic and leuco forms of malachite green, shown in Fig. 3, was achieved on a cyano column using a mobile phase composed of methanol–0.1 *M* sodium acetate, pH 4.5 (70:30, v/v) and amperometric detection at +1.2 V.

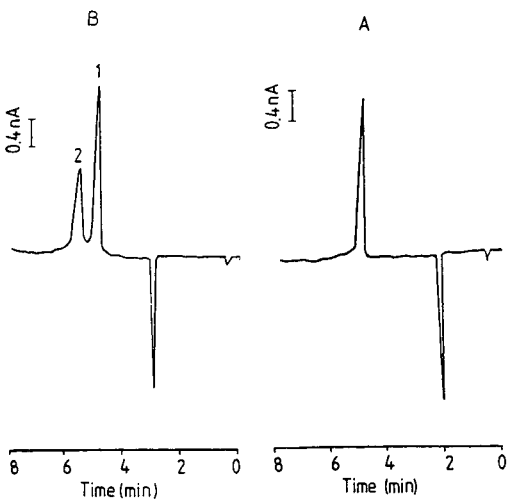

Fig. 3. Typical chromatograms for (A) 5 mg/l leuco malachite green and (B) a mixture containing 5 mg/l of (1) leuco and (2) chromatic forms of malachite green.

Under these conditions the leuco and chromatic forms of malachite green separated into two well resolved peaks with retention times of 5.0 and 5.9 min for the leuco and chromatic forms, respectively.

This ability to simultaneously analyse the chromatic and leuco forms is of great importance in studying the biotransformation of malachite green into its leuco form. In their study on the detoxication of malachite green in rats by the formation of the leuco form of malachite green, Werth and Boiteux [3] determined the distribution of leuco malachite green in tissues by carrying out the photometric titration of leucomalachite green with potassium permanganate in a weak acid solution. However, extreme care had to be exercised in order to ensure that there was quantitative oxidation whilst at the same time avoiding excess titration of potassium permanganate which would otherwise cause oxidative destruction of the molecule. In addition the background presence of the chromatic form of malachite green in the sample extract meant that its concentration had to be determined prior to the titration.

Allen and co-workers [9,10] have previously reported on the use of a post column oxidation step to allow the determination of the chromatic and leuco forms by spectrophotometric detection. This involved the packing and incorporation of a lead dioxide column into the chromatographic apparatus. Bauer *et al.* [24] also used a similar post-column oxidation step which depended upon splitting the sample in two, oxidising half to chromatic malachite green, analysing both sample aliquots for the chromatic form and determining the concentration of the leuco form by a difference method.

The use of the chromatographic method described here should allow direct analysis of a sample extract for chromatic and leuco forms of malachite green without the need for any post column modification procedure, as the use of the carbon fibre flow cell represents a small volume, easily incorporated system which can be simply maintained and replaced when the sensitivity of the response decreases. At the present time, work is being carried out as part of ongoing research in Trinity College, Dublin to adapt this

methodology to the simultaneous analysis of the chromatic and leuco forms of malachite green in tissue samples.

As the leuco form is one of the final intermediates in the production of chromatic malachite green, it is therefore a potential contaminant in commercial supplies. The use of the HPLC method described is ideally suited for rapid quality control of the final product to determine possible contamination from leuco malachite green.

CONCLUSIONS

A high-performance liquid chromatographic method has been developed for the analysis of chromatic malachite green in drinking water and river water, based on solid-phase extraction, reversed-phase chromatographic separation on a cyano column and amperometric detection using a carbon fibre flow cell. The method compares favourably with that reported by Allen *et al.* [10]. The use of electrochemical detection in conjunction with high-performance liquid chromatography permits the sensitive and reproducible determination of the chromatic form of malachite green in drinking water samples at those levels required under current legislation. In terms of detection limit, a lower value should be obtainable with the use of a potentiostat specifically designed for the measurement of the smaller currents associated with microelectrodes.

Low recoveries of malachite green from river water samples were due to its sorption onto organic material suspended in the water column.

The carbon fibre flow cell used in this study showed excellent response characteristics over a four-day working period after which the sensitivity decreased. However, this does not represent a serious problem as the electrode can be easily and cost effectively replaced. The use of electrochemical detection for the analysis of malachite green shows potential for the simultaneous determination of its chromatic and leuco forms.

ACKNOWLEDGEMENTS

This work was carried out under the European Fisheries and Agriculture Research programme (FAR), contract number AQ.2.503.

The authors would like to thank Margarita Rodriguez for her help during this project and acknowledge Michael Gillooly, David Alderman and John Allen for their helpful discussions.

REFERENCES

1 F.J. Foster and L. Woodbury, *Prog. Fish-Cult.*, 18 (1936) 7.
2 D.J. Alderman, *J. Fish Dis.*, 8 (1985) 289.
3 G. Werth and A. Boiteux, *Arzneimittel Forsch.*, 18 (1968) 39.
4 J.J. McDonald and C.E. Cerniglia, *Drug Metab. Dispos.*, 12 (1984) 330.
5 M. Edelhaeuser and E. Klein, *Dtsch. Lebensm.-Rundsch.*, 82 (1986) 386.
6 E. Klein and M. Edelhaeuser, *Dtsch. Lebensm.-Rundsch.*, 84 (1988) 77.
7 Y. Kasuga, M. Hishida and N. Tanahashi, *Shokuhin Eiseigaku Zasshi*, 32 (1991) 137.
8 J.L. Allen, *Invest. Fish Control*, 101 (1990) 1.
9 J.L. Allen and J.R. Meinertz, *J. Chromatogr.*, 536 (1991) 217.
10 J.L. Allen, J.R. Meinertz and J.E. Gofus, *J. Assoc. Off. Anal. Chem.*, 75 (1992) 646.
11 J.E. Roybal, R.K. Munns, J.A. Hurlbut and W. Shimoda, *J. Chromatogr.*, 467 (1989) 259.
12 C. Hua, D. Jagner and L. Renman, *Anal. Chim. Acta*, 197 (1987) 257.
13 K. McLaughlin, D. Boyd, C. Hua and M.R. Smyth, *Electroanalysis*, 4 (1992) 689.
14 K. Oldham, *J. Electronal. Chem.*, 323 (1992) 53.
15 H. Emons and F. Matysik, *Electroanalysis*, 4 (1992) 501.
16 K. Sagar, C. Hua and M.R. Smyth, *J. Chromatogr.*, 577 (1992) 109.
17 C. Hua, K. Sagar, K. McLaughlin, M. Jorge, M. Meaney and M.R. Smyth, *Analyst*, 116 (1991) 1117.
18 R.J. Goldacre and J.N. Philips, *J. Chem. Soc.*, 7 (1949) 1724.
19 W. Blaedal and R. Jenkins, *Anal. Chem.*, 46 (1974) 1952.
20 T. O'Shea, A. Garcia, P. Tunon and M.R. Smyth, *J. Electroanal. Chem.*, 307 (1991) 63.
21 R.M. Harrison, R. Perry and R.A. Wellings, *Environ. Sci. Technol.*, 10 (1978) 1151.
22 C.W. Schauberger and R.B. Wildman, *Bull. Environ. Contam. Toxic.*, 17 (1977) 534.
23 L.G. Rushing and M.C. Bowman, *J. Chromatogr. Sci.*, 18 (1980) 224.
24 V.K. Bauer, H. Dangschat, H.O. Knoppler and J. Neudegger, *Arch. Lebensmittelhyg.*, 39 (1988) 97.

Journal of Chromatography A, 659 (1994) 337–348
Elsevier Science B.V., Amsterdam

CHROM. 25 705

Development and optimization of a solid-phase extraction scheme for determination of the pesticides metribuzin, atrazine, metolachlor and esfenvalerate in agricultural runoff water

Martha J.M. Wells *, Daniel D. Riemer and Mary C. Wells-Knecht

Center for the Management, Utilization and Protection of Water Resources and Department of Chemistry, Tennessee Technological University, Cookeville, TN 38505 (USA)

(First received May 22nd, 1992; revised manuscript received August 3rd, 1993)

ABSTRACT

Concomitant determination of the pesticides metribuzin, atrazine, metolachlor and esfenvalerate in agricultural runoff water was developed utilizing solid-phase extraction (SPE). A 2^5 factorial experimental design compared relative importance for extraction efficiency of the five variables sample pH, elution solvent strength, ionic strength of the sample, addition of organic modifier to the sample, and elution by gravity or vacuum. The protocol was further optimized with respect to sorbent mass, sample volume, elution volume and concentration. The approach offers optimal recoveries, low detection limits, rapid extraction, and final determination by either gas or high-performance liquid chromatography.

INTRODUCTION

Investigation of the impact of agricultural non-point source contamination necessitates the development of a rapid and accurate multi-residue, multi-class protocol for the determination of pesticides. A method utilizing solid-phase extraction (SPE) was developed for the determination of metribuzin, atrazine, metolachlor and esfenvalerate in agricultural runoff water. Concomitant analysis of these multi-class pesticides was desired as they may occur simultaneously in environmental matrices.

SPE is a chromatographic sample preparation technology applicable to the separation, purification and concentration of chemicals of environmental interest. SPE combines non-linear modes of chromatography; the sample loading or retention step is frontal chromatography, and the sample desorption or elution step is accomplished by stepwise (or gradient) desorption or displacement development [1–3]. SPE is an attractive alternative to traditional methods of extracting and concentrating organics from aqueous solutions. Chromatographic extractions are often less labor-intensive, use smaller volumes of organic solvents, and alleviate problems associated with the formation of emulsions as compared to liquid–liquid extractions.

Previous research on the development of SPE methods for pesticides [4] utilized an iterative approach to protocol development. Retention was first controlled while elution was optimized; subsequently, the variables affecting retention were optimized. In this research an alternative approach, a 2^5 statistical factorial design (5 variables at 2 levels), was utilized to quickly determine and optimize variables important to the SPE of metribuzin, atrazine, metolachlor and esfenvalerate. Application of the factorial ex-

* Corresponding author.

0021-9673/94/$07.00
SSDI 0021-9673(93)E1169-Z

perimental design to optimization of recovery by SPE was recently published by Hannah *et al.* [5]. They used a 2^4 statistical factorial design (4 variables at 2 levels) requiring sixteen runs to optimize recoveries for a 27-component mixture of organic compounds. Hannah *et al.* studied the experimental variables sample pH (2 or 8), nonpolar SPE strength (octyl or octadecyl bonded phases), polar SPE strength (cyano or diol bonded phases), and conditioning solvent concentration (0 or 500 ppm methanol). This research emulates their approach. For optimization of the recovery of pesticides, five variables were selected. Three factors related to sample modification included pH, ionic strength, and the addition of an organic modifier. The remaining two factors, related to elution, were eluotropic strength of the desorption solvent and mode of elution (by vacuum or gravity). In addition to providing a rapid screening tool for method development, the factorial approach increases understanding of the mechanisms of extraction and recovery during SPE by testing selected variables for significance.

EXPERIMENTAL

Chemicals and reagents

Methanol (HPLC or Optima grade), water (HPLC grade), ethyl acetate (Optima grade), phosphoric acid (HPLC grade), and potassium phosphate dibasic, potassium phosphate monobasic and sodium chloride (certified ACS grades) were obtained from Fisher Scientific, Fair Lawn, NJ, USA. Sodium chloride was baked at 400°C for 4 h before use.

Metribuzin [4-amino-6-(1,1-dimethylethyl)-3-(methylthio)-1,2,4-triazin-5-(4H-one)], atrazine (2-chloro-4-ethylamino-6-isopropylamino-1, 3, 5-triazine) and metolachlor (2-chloro-N-(2-ethyl-6-methylphenyl) - N - (2-methoxy-1-methylethyl)-acetamide) were obtained from Fisher Scientific (PESTANAL, Riedel-de Haen). Esfenvalerate [(*S*)-α-cyano-3-phenoxybenzyl(*S*)-2-(4-chlorophenyl)-3-methyl butylate] was provided by DuPont (Wilmington, DE, USA). The chemical abstracts numbers for metribuzin, atrazine, metolachlor and esfenvalerate, are 21087-64-9, 1912-24-9, 51218-45-2 and 66230-04-4, respectively.

Sample preparation

Spiked samples were prepared in amber glass bottles with PTFE-lined caps. For the factorial design experiment, 100 ml of the appropriate combinations of phosphate buffer for pH control (0.1 *M*), ionic strength modifier (sodium chloride), and organic modifier (methanol) were spiked with a 100 $\mu g\ ml^{-1}$ methanolic stock solution of the four pesticides to produce a sample concentration of 1.00 $\mu g\ ml^{-1}$ in each compound. For further optimization studies, samples of variable concentration and variable volume were prepared in a similar manner. Authentic agricultural runoff samples, potentially containing the pesticides of interest, were provided by the University of Tennessee Plateau Experiment Station in Crossville, TN, USA.

Extraction apparatus/procedures

All solid-phase extractions were conducted with C_{18} Mega Bond Elut columns (1.0 g sorbent) and a Vac Elut extraction manifold (Varian Sample Preparation Products, Harbor City, CA, USA). PTFE tubing (1/16 in. inside diameter; 1 in. = 2.54 cm) was connected to the columns through reservoir adapters to transfer the conditioning solvents and samples. The extraction columns were conditioned by passing 10 ml of methanol through the column followed by 10 ml of the appropriate phosphate buffer (0.1 *M*, pH 2 or 7) according to the pH of the sample to be analyzed. Sample loading was performed under vacuum (380 Torr; 1 Torr = 133.322 Pa). The sorbent was never allowed to dry during the conditioning and sample loading procedures. For the factorial design experiment, sample desorption was performed with vacuum (380 Torr) or by gravity (740 Torr). The first fraction was eluted with 9.5 ml of methanol or ethyl acetate according to the factorial design, and the second fraction was eluted (by vacuum) with 9.5 ml of ethyl acetate. The sample container was rinsed with the first fraction of the elution solvent prior to desorption. The elution solvent for the second fraction was added directly to the sorbent. For further optimization studies, sorbent mass, sam-

ple volume and elution volume were varied to assess optimal conditions. In addition, independence to sample component concentration in the range of 10 to 1000 ppb was established.

Instrumentation

Analysis of the sample extracts was completed by HPLC–diode array detection (DAD) for the methanol extracts and GC–electron-capture detection (ECD) for the ethyl acetate extracts. The liquid chromatograph consisted of a Hewlett-Packard 1090M HPLC–DAD system and ChemStation data processing software, a Hypersil ODS (250 mm × 4 mm I.D., 5 μm) analytical column and a Hypersil ODS (20 mm × 4 mm I.D., 5 μm) guard column (Hewlett-Packard, Avondale, PA, USA). The column was maintained at 40°C, the mobile phase flow-rate was 1.5 ml min^{-1}, and the injection volume was 25.0 μl. Methanol–phosphate buffer (pH 2) mobile phase was delivered as a solvent gradient consisting of methanol–0.1 *M* phosphate buffer (40:60) for 6 min followed by a linear ramp to methanol–0.1 *M* phosphate buffer (95:5) at 23 min. The total run time of 25 min was followed by a 3-min post run equilibration to initial conditions. DAD was used to simultaneously monitor the absorbance maximum for each compound investigated: atrazine (221 nm), esfenvalerate (210 nm), metolachlor (204 nm) and metribuzin (204 and 298 nm) at a bandwidth of 4 nm. The reference wavelength and bandwidth were 450 nm and 50 nm, respectively. The detection limits by HPLC–DAD analysis, with 95% confidence intervals in parentheses, were metribuzin, 1.3 (0.5) ng; atrazine, 1.3 (0.4) ng; metolachlor, 5.0 (1.0) ng; and esfenvalerate, 2.5 (0.6) ng.

For gas chromatography a Hewlett-Packard 5890 GC–ECD system was used, with a 7673A automatic sampler, ChemStation data processing software, and a 15 m × 0.52 mm I.D. (0.5 μm film thickness) SPB-5 column (Supelco, Bellefonte, PA, USA). The direct injection volume was 1.0 μl. Injector and detector temperatures were maintained at 320°C. The carrier gas was helium at a flow-rate of 10 ml min^{-1}. Nitrogen was used as the ECD makeup gas to produce a total flow of 60 ml min^{-1} through the detector. The gradient temperature program consisted of 150°C for 2 min followed by a temperature ramp to 275°C at 15°C min^{-1} with a total run time of 15 min. The column was re-equilibrated to initial conditions for 2 min between samples. The detection limits by GC–ECD analysis, with 95% confidence intervals in parentheses, were metribuzin, 1.0 (0.1) pg; atrazine, 50.0 (7.0) pg; metolachlor, 49.0 (1.0) pg; and esfenvalerate, 1.02 (0.03) pg.

Data reduction

Statistical analysis of the data was conducted on a microcomputer with SAS (SAS Institute, Cary, NC, USA).

RESULTS AND DISCUSSION

Analytical determination by HPLC and GC

Before SPE studies began, methods for the final analytical determination of the analytes were developed. Metribuzin and atrazine are triazine herbicides, metolachlor is an acetanilide herbicide and esfenvalerate is a pyrethroid insecticide (Fig. 1). Although fortuitous for the purposes of this study, it is unusual that this group of four pesticides is amenable to analysis by both HPLC (Fig. 2) and GC (Fig. 3). Metribuzin and esfenvalerate were approximately 50 times more sensitive than atrazine or metolachlor to detection by GC–ECD. Sensitivity of the four pesticides by HPLC–DAD was within the same order of magnitude.

Design of the factorial screening study

A factorial experimental design (2^5) was employed as a screening device to statistically identify variables that would influence recovery efficiency by SPE of metribuzin, atrazine, metolachlor and esfenvalerate. In a 2^n factorial design, the value of each variable is restricted to only two levels. The factorial approach (5 variables at 2 levels) resulted in a design matrix of 32 sets of experimental conditions (Table I). The five variables studied consisted of sample pH (2 or 7); elution solvent strength [methanol (MeOH) or ethyl acetate (EtOAc)]; sample ionic strength [no sodium chloride added or 17.4% (w/v) added sodium chloride]; addition of

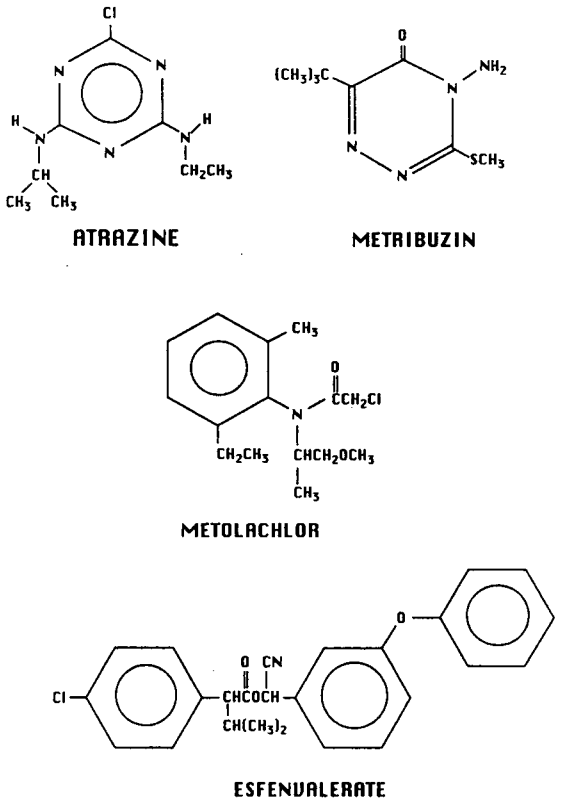

Fig. 1. Chemical structures of the herbicides included in this study.

organic modifier to the sample [no methanol added or 20% (v/v) methanol added]; and elution by vacuum (380 Torr) or gravity (740 Torr). The variables screened for an effect on recovery efficiency, and the levels at which they were tested, were arbitrarily chosen based on published literature and past experience with SPE.

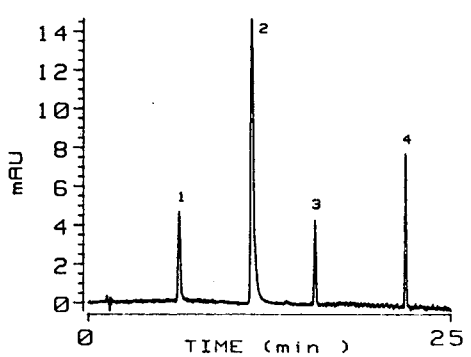

Fig. 2. High-performance liquid chromatogram of a standard mixture of (1) metribuzin, (2) atrazine, (3) metolachlor and (4) esfenvalerate at 221 nm.

Although the SPE of many compounds by octadecyl sorbents is pH dependent [4], in this case the levels selected for sample pH (*i.e.*, 2 and 7) were chosen mainly with the background matrix in mind. For this and future studies, it was desired to optimize recovery of these pesticides at each of these pH values in order to study the effects of concurrent recovery of macromolecular fulvic and humic acids potentially present as interferents in agriculturally derived sample matrices. (The pK_a of humic acids is estimated to be approximately 5.5.) Possible interferences from dissolved organic material during the SPE of pesticides from water were recently examined by Johnson *et al.* [6].

Adding solutes that increase the ionic strength of the sample has been used to improve extraction and recovery of analytes by SPE [7]. As in liquid–liquid extraction, it is assumed that the role of additional electrolyte is to enhance the salting-out effect on organic analytes in aqueous solution in contact with a hydrophobic phase. The addition of salt may also counteract secondary interferences from negatively charged silanol groups present on reversed-phase surfaces. The level of added ionic modifier used in this study (17.4%) is the same as that published by Schuette *et al.* [8] for the SPE determination of herbicides including atrazine and metolachlor.

The remaining factors in the experimental design (*i.e.*, eluotropic strength of the elution solvent, addition of organic modifier to the sample, and elution by vacuum or gravity) were included to elucidate effects on the recovery of compounds differing in hydrophobicity. The octanol–water partition coefficients (log P) of the pesticides investigated are metribuzin (1.65), atrazine (2.68), metolachlor (2.9) and esfenvalerate (>4), a relative order of hydrophobicity also evident in the reversed-phase HPLC elution pattern (Fig. 2). Highly hydrophobic compounds have notoriously poor recovery from octadecyl sorbents by SPE. Generally, very hydrophobic compounds adsorb strongly making desorption difficult. Therefore, two desorption solvents, methanol and ethyl acetate, respectively representing low and high eluotropic strength relative

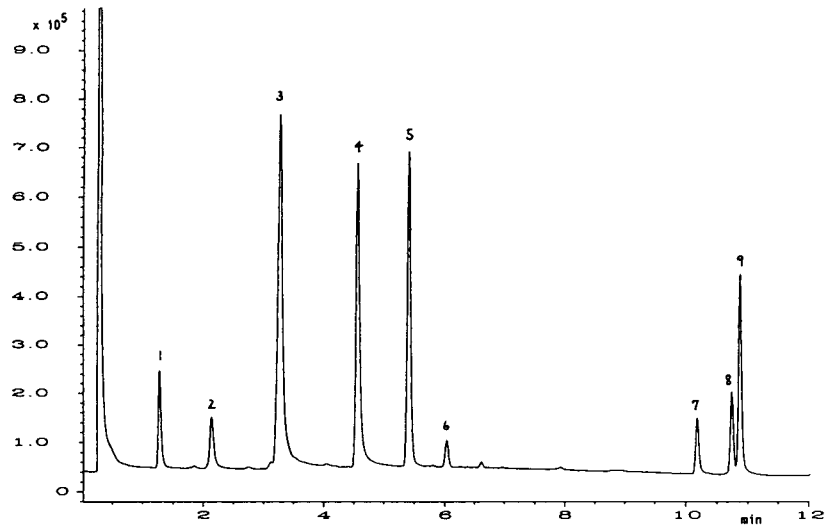

Fig. 3. Gas chromatogram of a standard mixture of (1) impurity, (2) impurity, (3) atrazine (55 ng), (4) metribuzin (376 pg), (5) metolachlor (4.9 ng), (6) impurity, (7) impurity, (8) impurity and (9) esfenvalerate (720 pg). *y*-Axis: ECD detector response.

to reversed-phase sorbents, were tested to investigate the effect of solvent strength on SPE elution.

The addition of organic modifier to the sample was examined by comparing the results from samples to which no solvent was added with those obtained from samples containing 20% methanol. Adding trace amounts of methanol to the sample may be necessary to maintain conditioning of the stationary phase throughout the extraction of large volumes of aqueous samples [7]. However, in the statistical factorial design of Hannah *et al.* [5], levels of 0 or 500 ppm methanol added to the sample were tested with inconclusive results. In this study, the primary purpose of adding methanol was not to maintain conditioning of the sorbent but to modify the retention factor of the analytes on the column. Even in a totally aqueous sample, a solute will have a finite retention factor. At some point, as the sample is continuously added to the column, a breakthrough volume will be reached. Addition of organic modifiers to the sample, such as methanol, will reduce the breakthrough volume, and may potentially improve recovery of highly hydrophobic compounds. The addition of methanol to the sample also alters the character of the hydrophobic octadecyl surface. Reversed-phase sorbents become enriched with the organic modifier, depending upon the percentage of water present [9]. The solvation layer reaches a maximum in pure methanol [10] while there is no solvation layer in pure water [11]. This effect may also influence the manner in which the analyte interacts with the stationary phase, and may ultimately influence the ease of recovery by SPE.

The mode of elution was also included as a factor in the experimental design. In unpublished research on the SPE of chlorobenzenes, it was observed that as the hydrophobicity of the solute increased, so did the importance of allowing elution to occur by gravity rather than by the normal mode of vacuum elution. The effect appears to result from slow mass transfer for very hydrophobic compounds from the stationary phase into the mobile phase.

During the screening study, certain factors were not allowed to vary. The mass of the sorbent (1.0 g), the sample volume (100 ml), and the sample concentration (1 ppm) remained constant. A 1.0-g mass of C_{18} sorbent has become a standard starting point in SPE studies [4] as a reasonable compromise for method development for groups of compounds of widely ranging hydrophobicity. A sample volume of 100 ml was

TABLE I

2^5 FACTORIAL DESIGN MATRIX

Run type	pH	Eluotropic strength	Ionic strength	Added MeOH	Vacuum/ gravity
1	2	MeOH	–	–	Vacuum
2	7	MeOH	–	–	Vacuum
3	2	EtOAc	–	–	Vacuum
4	7	EtOAc	–	–	Vacuum
5	2	MeOH	NaCl	–	Vacuum
6	7	MeOH	NaCl	–	Vacuum
7	2	EtOAc	NaCl	–	Vacuum
8	7	EtOAc	NaCl	–	Vacuum
9	2	MeOH	–	20	Vacuum
10	7	MeOH	–	20	Vacuum
11	2	EtOAc	–	20	Vacuum
12	7	EtOAc	–	20	Vacuum
13	2	MeOH	NaCl	20	Vacuum
14	7	MeOH	NaCl	20	Vacuum
15	2	EtOAc	NaCl	20	Vacuum
16	7	EtOAc	NaCl	20	Vacuum
17	2	MeOH	–	–	Gravity
18	7	MeOH	–	–	Gravity
19	2	EtOAc	–	–	Gravity
20	7	EtOAc	–	–	Gravity
21	2	MeOH	NaCl	–	Gravity
22	7	MeOH	NaCl	–	Gravity
23	2	EtOAc	NaCl	–	Gravity
24	7	EtOAc	NaCl	–	Gravity
25	2	MeOH	–	20	Gravity
26	7	MeOH	–	20	Gravity
27	2	EtOAc	–	20	Gravity
28	7	EtOAc	–	20	Gravity
29	2	MeOH	NaCl	20	Gravity
30	7	MeOH	NaCl	20	Gravity
31	2	EtOAc	NaCl	20	Gravity
32	7	EtOAc	NaCl	20	Gravity

representative of reasonable volumes encountered in environmental applications, yet was small enough to yield quick sample throughput for screening purposes. The relatively high initial sample concentration in the screening phase of this study was designed to ensure that if fractional recovery was observed in adsorption and/or desorption stages, the partial recoveries would still be detectable. Following optimization of the five factors tested in the design matrix, the protocol was then optimized for sorbent mass and sample volume, elution volume and sample concentration.

While the clear advantage of a factorial experimental design is that it is particularly well suited to study screening for significant variables, there are two disadvantages to performing the factorial design screening test as it was conducted in this research. Recognizing the disadvantages of this approach at the outset of the project enables the researcher to determine whether it is unproductive for a given purpose. In the case of screening for the significance of five variables, 32 experiments are required. Each combination however, was tested only once. There were no replications in the screening portion of this study. Therefore, there was no direct means by which to determine the variance.

However, this was overcome by estimating the experimental error from the mean square errors of the six fourth- and fifth-order interaction terms. In non-replicated experiments, it is common to use some or all of the interaction mean squares as an estimate of the error variance [12]. The second disadvantage is the lack of experimental blanks. If a blank was generated for each situation, it would be necessary to double the number of samples. A blank would be required for each of the 32 conditions examined. In this study, replicated experiments with blanks as appropriate were conducted once the best variable combinations were selected by screening.

Statistical evaluation of the factorial screening study

By applying the factorial design outlined in Table I, a large amount of information was obtained with relatively few analyses (Table II). Evaluation of recovery data by analysis of variance (ANOVA) allowed determination of the variables and variable interactions that were

TABLE II

RECOVERIES FROM 2^5 FACTORIAL DESIGN MATRIX

Run type	Recovery (%)			
	Metribuzin	Atrazine	Metolachlor	Esfenvalerate
1	80.6[a]	95.8	99.6	99.8
2	83.3	97.0	97.2	91.7
3	50.0	43.0	73.1	55.1
4	78.1	79.9	99.6	56.3
5	87.4	98.3	94.0	0.8
6	101.0	98.0	94.7	36.2
7	57.7	55.0	85.8	52.7
8	76.9	81.4	95.2	61.6
9	56.0	97.6	98.0	91.2
10	62.8	98.7	99.7	0.8
11	39.7	42.2	104.9	107.0
12	60.3	91.2	111.6	69.3
13	77.1	100.6	114.4	78.8
14	103.6	98.9	99.3	85.7
15	40.6	50.3	95.3	75.2
16	88.1	97.3	114.5	96.2
17	91.0	95.2	97.1	86.9
18	97.4	97.5	97.8	83.6
19	49.8	75.8	87.9	70.9
20	88.2	97.2	95.5	76.9
21	78.3	90.5	98.0	90.9
22	98.0	98.4	97.6	87.1
23	83.6	84.8	93.5	85.1
24	92.8	86.0	95.3	83.0
25	56.1	95.9	97.4	84.0
26	69.6	98.6	98.1	88.8
27	83.2	71.9	94.9	75.0
28	77.8	113.2	95.5	88.3
29	48.2	87.5	98.6	91.8
30	94.7	100.1	99.7	88.8
31	88.7	84.1	94.3	90.8
32	79.5	81.0	92.6	93.6

[a] All recoveries are for the first eluted fraction.

significant to the SPE of these pesticides [12]. SAS programs were written to perform the statistical evaluation for the 2^5 factorial design. In the data matrix, the low level of a variable is indicated by -1 and the high level of a variable is indicated by $+1$. The F-test was used to evaluate significance of the main effects and second- and third-order interactions by comparing to the mean square error for the fourth- and fifth-order interaction terms. Comparisons were made at the 0.025 probability level. After the analysis of variance was used to evaluate the significant effects, standardized regression coefficients were determined by linear regression analysis (Table III). The magnitude of the standardized regression coefficients indicates the relative importance of the factors found to be significant. The sign of the standardized regression coefficients shows the level of the factor (plus for the high level, minus for the low level) that produces the best SPE recovery. The interaction terms are more difficult to interpret than the main factors but can be very revealing. The signs of the standardized regression coefficients for the interaction terms follow the rules for algebraic multiplication (*i.e.*, two pluses yield a plus, two minuses yield a plus, and a plus and a minus produce a minus). The ANOVA developed for the SPE recovery data will be discussed separately for each pesticide, and for summed pesticide recoveries.

Metribuzin. The ANOVA for metribuzin demonstrated that three main effects and one interaction term were significant to the recovery by SPE. Of the significant variables, sample pH most influenced recovery of metribuzin. Metribuzin recovery was best at a sample pH of 7 with added sodium chloride. Methanol added to the sample reduced the recovery of metribuzin. The detrimental effect on metribuzin recovery of adding methanol to the sample appears to be overcome by the simultaneous addition of sodium chloride (17.4%). The variable interaction significant to the recovery of metribuzin (BE) combines the remaining two main effects, *i.e.*, elution solvent/elution by gravity or vacuum. For metribuzin, the positive coefficient for the BE interaction term indicates that if elution is done under vacuum, methanol is the preferred elution solvent. If elution is allowed to occur by gravity, ethyl acetate produces better recovery.

Atrazine. Atrazine recovery was significantly affected at the 0.025 probability level by pH, eluotropic strength, and mode of elution (Table III). Standardized regression coefficients of the significant effects indicated that increased recovery was observed for atrazine with a sample pH of 7, methanol elution solvent, and elution

TABLE III

STANDARDIZED REGRESSION COEFFICIENTS OF SIGNIFICANT FACTORS

Variable	Standardized parameter estimates				
	Metribuzin	Atrazine	Metolachlor	Esfenvalerate	Summed recoveries[b]
A: pH	0.4954	0.4478	NS[a]	NS	0.5684
B: Elution solvent	NS	−0.5724	NS	NS	−0.3992
C: Ionic strength	0.3004	NS	NS	NS	NS
D: Added MeOH	−0.2931	NS	0.4486	NS	NS
E: Vacuum/gravity	NS	0.2413	NS	NS	NS
Interaction AB	NS	0.3539	NS	NS	NS
Interaction BE	0.2976	0.3185	NS	NS	0.2691
Interaction ABE	NS	−0.2253	NS	NS	−0.2897

[a] NS = Not significant at $\alpha = 0.025$. α is the probability of making a Type I statistical error.
[b] Summed recoveries of metribuzin, atrazine and metolachlor only, excluding esfenvalerate.

by gravity. Significant two- and three-level variable interactions of the main effects were also noted. Since the sign for the standardized regression coefficients for the interaction BE term for both metribuzin and atrazine is positive, the same argument can be used for atrazine as given earlier for metribuzin for this interaction. For atrazine, a positive sign for interaction AB indicates that at pH 2 the best elution solvent is methanol; while at pH 7, ethyl acetate produces better recovery. A negative sign for the ABE interaction (*i.e.*, pH/elution solvent/mode of elution) implies that optimal results will be achieved if any two of these effects are at the high level while the third effect is at the low level.

Metolachlor. Recovery of metolachlor was significantly affected only by addition of organic modifier to the sample. The positive sign of the standardized regression coefficient for this variable indicates that 20% methanol added to the sample improves the recovery of metolachlor. This strongly contrasts with the observations for metribuzin and atrazine in which all five of the variables examined were significant either as main effects or interaction terms. The most apparent explanation is the differing chemical nature of these pesticides (Fig. 1). Metribuzin and atrazine are ionizable while metolachlor is not.

Esfenvalerate. The analysis of variance for recovery data of esfenvalerate revealed no significant variables or variable interactions at the 0.025 probability level. Two factors are believed to have contributed to the lack of significance observed. Firstly, esfenvalerate was incompletely desorbed from the sorbent by the initial elution. In virtually every sample in the factorial study, esfenvalerate, in amounts up to 15% of the sample, was detected in the second elution fraction while no concentrations of metribuzin, atrazine or metolachlor greater than 2% were detected in the second fraction. Secondly, isomerization or degradation of esfenvalerate may have occurred during sample processing, thereby confounding results of the factorial study. Fenvalerate has two chiral centers, resulting in four stereoisomers or two sets of diastereomers. The esfenvalerate analytical standard used in this research was the $2S,\alpha S$ stereoisomer (99.1% purity). In effluents from some of the screening studies, a second peak near the standard esfenvalerate peak was observed. Those treatment combinations that produced low recovery of esfenvalerate in Table III may indicate conditions inappropriate for SPE, or conditions that promote isomerization or degradation. Therefore, these factors cannot be distinguished statistically from the data collected.

Summed recoveries. In addition to optimizing the recovery of each of the pesticides examined, the ultimate goal of this research was to develop the best concomitant recovery of the pesticides. An analysis of variance was conducted on the summed recoveries of metribuzin, atrazine and metolachlor. Data for esfenvalerate recovery were omitted from the ANOVA. Sample pH was determined to be the single most significant variable. A sample pH of 7 using methanol as the elution solvent appears to be the best choice for this combination of analytes. The interaction terms BE and ABE were also significant.

The variables and levels chosen for this investigation are clearly interrelated. Variation in one can be offset by changes in another. For variable D (*e.g.*, added methanol), the sign of the standardized parameter estimate is negative for metribuzin and positive for metolachlor. Because metribuzin is less hydrophobic than metolachlor, methanol added to the sample (20%) reduces the breakthrough volume of metribuzin to the point that some of the analyte is lost during sample loading; whereas, for metolachlor, desorption is improved by reducing the retention factor of the more hydrophobic solute.

Optimization of SPE recovery data

Three of the 32, five-variable combinations in the factorial screening study (Table I) were selected for further optimization: run type 1 (pH 2, methanol elution by vacuum, no added methanol or sodium chloride); run type 2 (pH 7, methanol elution by vacuum, no added methanol or sodium chloride); and run type 16 (pH 7, ethyl acetate elution by vacuum with added sodium chloride and methanol). Sample volume,

elution volume, sorbent mass, and sample concentration were examined.

Run types 1 and 2, performed with elution by methanol, produce extracts appropriate for HPLC analysis, while run type 16 conditions yield an ethyl acetate extract that was analyzed directly by GC. Therefore, it was possible to determine the SPE conditions necessary to optimize both the HPLC and GC analyses for these compounds. Under conditions 1 and 2, recoveries are excellent for atrazine, metolachlor and esfenvalerate but less than desired for metribuzin. Since one-fifth of the sample missing from metribuzin recovery did not remain on the column (the second fraction does not account for it), it is assumed that metribuzin experienced breakthrough during sample loading. Doubling the sorbent mass used to extract the sample greatly improved the recovery of metribuzin, from 80.6 to 94.7% for run type 1 and from 83.3 to 99.3% for run type 2, and slightly improved the recovery of atrazine from 95.8 to 96.8% (run type 1) and 97.0 to 100.5% (run type 2). Predictably, the opposite effect was observed for metolachlor and esfenvalerate. Increasing the sorbent mass to 2.0 g decreased recovery of metolachlor from 99.6 to 93.7% (run type 1) and 97.2 to 93.3% (run type 2), and for esfenvalerate from 99.8 to 98.0% (run type 1) and 91.7 to 81.0% (run type 2). (Subsequently, the 2-g sorbent versions of runs 1 and 2 are denoted by addition of an asterisk.)

Replicated sample volumes of 100, 250, 500 and 1000 ml were examined for extraction efficiency. Recoveries for metribuzin, atrazine, metolachlor and esfenvalerate, respectively, from 1-l samples were 93.4, 98.0, 99.7 and 87.0% (run type 1*), 96.9, 99.3, 99.5 and 71.9% (run type 2*), and 15.5, 100.4, 95.7 and 95.7% (run type 16). Recovery is good from sample volumes as large as 1 l using 2 g of sorbent under conditions of run types 1* and 2*. In run type 16 (1 g of sorbent), metribuzin recovery decreases as sample volume increases.

Elution volumes of 3.0, 5.0, 7.0 and 9.5 ml were examined at corresponding sample volumes of 100 ml and component concentrations of 1.0 ppm. The smallest satisfactory volume for methanol elution from 2 g of sorbent (runs 1* and 2*) is 5.0 ml. As hydrophobicity increases from metribuzin to esfenvalerate, 3.0 ml is no longer adequate to completely elute the compounds from 2 g of sorbent. Elution under run 16 experimental conditions (ethyl acetate elution, 1 g sorbent) was quite good even at the 3.0 ml elution volume. The best concentration factor (*i.e.*, sample volume/elution volume ratio) achievable without evaporation by run type 1* or 2* (HPLC) is 1000/5.0 or 200-fold, and for run 16 (GC) is 100/3.0 or 33-fold.

Initial screening concentrations of 1 ppm were used in order to monitor the fractionation of the sample during SPE. To examine the variation in pesticide recovery with concentration, synthetic samples having component concentrations of 10, 25, 50, 100, 500 and 1000 ppb were extracted by methods 1*, 2* and 16, for sample volumes of 100 ml and elution volumes of 9.5 ml. Satisfactory results were obtained for pesticide recovery with the exception that metolachlor was not detectable at 10 ppb under these conditions. Further concentration can be realized by using larger sample volumes, smaller elution volumes or evaporation of the extract prior to analysis. Tabularized details of the optimization of SPE recovery data are available from the corresponding author upon request.

Application of methods developed

The purification achieved by SPE for authentic agricultural runoff water samples is illustrated in chromatograms generated by HPLC–DAD (Fig. 4) and GC–ECD (Fig. 5). Table IV compares

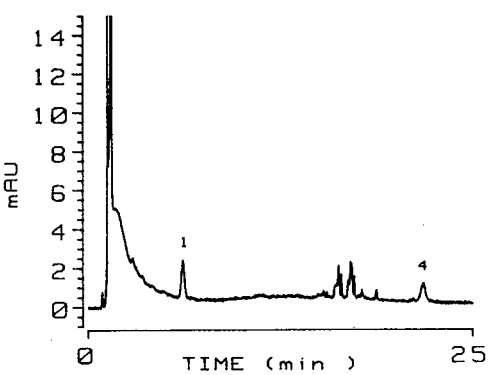

Fig. 4. High-performance liquid chromatogram of an authentic agricultural runoff sample in which (1) metribuzin and (4) esfenvalerate were detected at 221 nm.

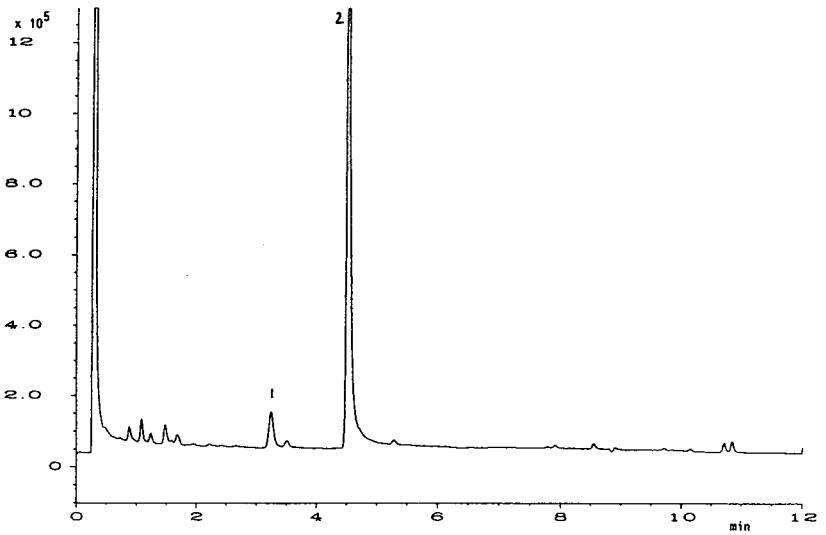

Fig. 5. Gas chromatogram of an authentic agricultural runoff sample in which (1) atrazine and (2) metribuzin were detected. *y*-Axis: ECD detector response.

analyses for metribuzin in authentic agricultural runoff water samples (100 ml) by SPE methods 1*, 2* and 16. The data were corrected for the recovery efficiency appropriate to each SPE method used and are the average of duplicate extractions. A two-tailed paired-sample *t*-test detects no mean population differences at $\alpha = 0.005$. The correlation coefficients for regressions between run types 1* and 2*, 16 and 1*, and 16 and 2* are 0.982, 0.984 and 0.994, respectively.

TABLE IV

COMPARISON OF THREE SPE APPROACHES TO THE ANALYSIS OF AUTHENTIC SAMPLES FOR METRIBUZIN CONTENT

Sample identity	Run type[a]		
	1* (HPLC) (μg/ml)	2* (HPLC) (μg/ml)	16 (GC) (μg/ml)
211.2	0.098	0.106	0.096
221.2	0.130	0.140	0.132
231.2	0.133	0.140	0.142
311.2	0.136	0.144	0.140
312.2	0.284	0.305	0.294
321.2	0.136	0.168	0.158
331.2	0.142	0.154	0.142

[a] Conditions given in Table I. Asterisk refers to extraction with 2 g sorbent.

CONCLUSIONS

In order to keep pace with the increasing analytical demands of monitoring non-point source contamination of pesticides in agricultural runoff water, multi-residue, multi-class analytical procedures must be developed. The factorial experimental design is demonstrated to be useful for method development for SPE protocol. Additionally, this statistical approach reveals significant factors in the mechanism of extraction and recovery of pesticides by SPE. Procedures for the gas or liquid chromatographic determination of metribuzin, atrazine, metolachlor and esfenvalerate were developed. The approach adopted in this research, statistical optimization of variables affecting the concomitant analysis of pesticides having diverse chemical and biological activities, is generally applicable to pesticides other than those studied here.

ACKNOWLEDGEMENT

The collaboration of Allen Straw and the University of Tennessee Plateau Experiment

Station, Crossville, TN, USA is gratefully acknowledged.

REFERENCES

1 A. Velayudhan and Cs. Horváth, *J. Chromatogr.*, 443 (1988) 13.
2 A.L. Lee, A.W. Liao and Cs. Horváth, *J. Chromatogr.*, 443 (1988) 31.
3 M.J.M. Wells, A.J. Rossano, Jr. and E.C. Roberts, *Anal. Chim. Acta*, 236 (1990) 131.
4 M.J.M. Wells and J.L. Michael, *J. Chromatogr. Sci.*, 25 (1987) 345.
5 R.E. Hannah, V.L. Cunningham and J.P. McGough, in I.H. Suffet and M. Malaiyandi (Editors), *Organic Pollutants in Water (ACS Advances in Chemistry Series*, No. 214), American Chemical Society, Washington, DC, 1987, p. 359.
6 W.E. Johnson, N.J. Fendinger and J.R. Plimmer, *Anal. Chem.*, 63 (1991) 1510.
7 J.S. Andrews and T.J. Good, *Am. Lab.*, 14, No. 4 (1982) 70.
8 S.A. Schuette, R.G. Smith, L.R. Holden and J.A. Graham, *Anal. Chim. Acta*, 236 (1990) 141.
9 R.M. McCormick and B.L. Karger, *Anal. Chem.*, 52 (1980) 2249.
10 G.E. Berendsen, P.J. Schoenmakers, L. de Galan, G. Vigh, Z. Varga-Puchony and J. Inczedy, *J. Liq. Chromatogr.*, 3 (1980) 1669.
11 G.E. Berendsen and L. de Galan, *J. Chromatogr.*, 196 (1980) 21.
12 R.L. Anderson, *Practical Statistics for Analytical Chemists*, Van Nostrand Reinhold, New York, 1987.

Journal of Chromatography A, 659 (1994) 349–357
Elsevier Science B.V., Amsterdam

CHROM. 25 691

Chromatographic separations of metal chélates present in commercial fertilisers

II. Development of an ion-pair chromatographic separation for the simultaneous determination of the Fe(III) chelates of EDTA, DTPA, HEEDTA, EDDHA and EDDHMA and the Cu(II), Zn(II) and Mn(II) chelates of EDTA

Marian Deacon and Malcolm R. Smyth*

School of Chemical Sciences, Dublin City University, Dublin 9 (Ireland)

Louis G.M.Th. Tuinstra

State Institute for Quality Control of Agricultural Produce, Postbus 230, 6700 AE Wageningen (Netherlands)

(First received June 28th, 1993; revised manuscript received October 26th, 1993)

ABSTRACT

The determination of the iron(III) chelates of EDTA, DTPA, HEEDTA, EDDHA and EDDHMA and the Cu(II), Zn(II) and Mn(II) chelates of EDTA by ion-pair chromatography has been investigated. Addition of the ion-pairing reagent tetrabutylammonium hydroxide to the mobile phase gave rise to a separation of all iron(III) chelates on a Chromspher C_{18} column. A solvent-switching system was used to achieve this separation. The switching sequence was 5 min mobile phase A (0.05 *M* TBAOH, pH 7.5), 20 min mobile phase B (0.05 *M* TBAOH, pH 7.5, 30% acetonitrile) and 25 min mobile phase A. For the iron(III) chelates, both limit of determination and linear range studies showed that the method is capable of analysing the concentration ranges found in commercial fertilisers. The Cu(II), Zn(II), and Mn(II) chelates of EDTA were separated using 0.01 *M* tetradecyltrimethylammonium bromide, 0.01 *M* KH_2PO_4, pH 7.5.

INTRODUCTION

The micronutrients iron, copper, zinc and manganese, necessary for the growth of plants, are usually added to fertilisers in a chelate form. The 76/116/EC directive of the European Communities has recommended the use of the chelating agents listed in Table I. The chelates most commonly found in fertilisers are the Fe(III) chelates of EDTA, DTPA, HEEDTA, EDDHA and EDDHMA and the Cu(II), Zn(II) and Mn(II) chelates of EDTA. It can be seen that iron is by far the most common element used in fertilisers. This directive dictates that there are two categories of fertiliser which may be marketed: fertilisers containing only one of the trace elements listed, and fertilisers containing at least two different trace elements. To evaluate the

* Corresponding author.

SSDI 0021-9673(93)E1146-Q

TABLE I

CHELATING AGENTS RECOMMENDED BY DIRECTIVE 76/116/EC OF THE EUROPEAN COMMUNITIES

Chelating agent	Abbreviation
Ethylenediaminetetraacetic acid	EDTA
Diethylenetriaminepentaacetic acid	DTPA
Hydroxy-2-ethylenediaminetriacetic acid	HEEDTA
Ethylenediaminedi(*o*-hydroxyphenylacetic) acid	EDDHA
Ethylenediaminedi(*o*-hydroxy-*p*-methylphenyl)acetic acid	EDDHMA

trace element content of the fertiliser, the directive recommends that the total content in respect of each nutrient, the water soluble content, the chelated form in which the trace element is present, and the quantity of the trace element which is chelated be determined. This paper, and the previous paper in this series [1], addresses the determination of the chelated form in which the trace element is present and the quantity of the trace element which is chelated.

However, as discussed previously [1], due to the very nature of the metal chelate equilibrium and the pH, buffer and solvent conditions imposed on this metal chelate equilibrium during analysis by a chromatographic method, chromatographic methods can only be used for the determination of the quantity of chelated metal in a sample containing a single metal in combination with a single chelating agent. This paper aimed therefore to develop a separation of the iron(III) chelates of EDTA, DTPA, HEEDTA, EDDHA and EDDHMA and the copper(II), zinc(II) and manganese(II) chelates of EDTA which may be used for the analysis of specific chelate content of a fertiliser containing one of these chelates. The results of such an analysis reflect the content of the fertiliser as manufactured but do not necessarily give the value as a fertiliser in the field. This is due to the fact that the bio-availability of the micronutrients derived from a fertiliser depends upon, among other factors, the soil solution pH, the type of soil, and the presence of other metals and ligands in the soil. The analysis of micronutrient availability will therefore require a holistic approach including all of these factors. A meaningful analysis would involve the determination of the total quantity of chelating agent and the total quantity of micronutrients. These results could then be used, together with a model of the behaviour of metal chelates in soils, to predict the effectiveness of the fertiliser under various conditions of usage.

In the first paper of this series, a gel permeation technique was described which was an improvement on previously described methods [1]. However, the analysis time was still too long for samples containing FeEDDHA and FeEDDHMA. The chelates Fe(III)-DTPA and Cu(II)-, Zn(II)- and Mn(II)-EDTA were found to co-elute, and identification of the metal ion present must be confirmed by atomic absorption spectrometry (AAS) or inductively coupled plasma (ICP)-MS for positive identification of these chelates. Thus, the capabilities of ion-pair chromatography to resolve these species was investigated. To date, this technique has been used for the determination of the chelating agents EDTA, DTPA and HEEDTA by the addition of a metal ion to aid detection, or alternatively for the determination of metal ions by the addition of a chelating agent such as EDTA. The method has never been used for the determination of the chelates themselves. Buchberger *et al.* [2] used EDTA to extract Cu(II), Fe(III), Pb(II), Cd(II), Co(II), Ni(II), Pb(II) and Zn(II) from soil sediments with subsequent determination by ion-pair chromatography using the ion-pairing reagent hexadecyltrimethylammonium bromide. Detection of Cu(II), Fe(III) and Pb(II) was obtained at 250 nm and for Cd(II), Co(II), Ni(II), Pb(II) and Zn(II) also at 250 nm after postcolumn reaction with copper sulphate at low pH. In studies of the determination of the chelates the tetrabutylammonium ion (TBA^+) has been the most popular ion-pairing reagent

used [3–7]. Parkes *et al.* [7] achieved a separation of EDTA, HEEDTA and NTA in the copper form using TBA^+. EDTA, DTPA, HEEDTA, DHEG and NTA have also been separated as their copper chelates using benzyltrimethylammonium chloride (BTAC) [8]. The determination of the total chelating agent by conversion to the copper form cannot be used in this particular application as, unlike the applications mentioned [7,8], a fertiliser sample may already contain a mixture of metals. On examination of the conditional formation constants available for the chelates of iron and copper it is evident that a method converting the chelates to the copper form will suffer from interference from iron. Therefore a separation of the chelating agents in the iron form would be required for bioavailability studies.

In this paper the ion-pairing reagents TBA^+, BTAC and tetradecyltrimethylammonium bromide (TDTMABr) were therefore investigated for the separation of the Fe(III) chelates of EDTA, DTPA, HEEDTA, EDDHA and EDDHMA and the Cu(II), Zn(II) and Mn(II) chelates of EDTA. A possible future application of this work would be to convert the chelates present in a fertiliser or soil sample to the iron(III) form and use the separation achieved for the determination of the total amount of chelating agent present.

EXPERIMENTAL

Reagents

Deionised water was obtained by passing distilled water through a Waters Milli-Q water purification system. Sodium hydroxide (40%) solution was obtained from BDH. Potassium dihydrogen phosphate was obtained from Merck. Sodium chloride was analytical grade. Benzyltrimethylammonium chloride, potassium dihydrogenphosphate and acetonitrile (analytical-reagent grade) were obtained from Merck. Tetrabutylammonium hydroxide (40% solution in water; 1.5 *M*) was obtained from Fluka. FeEDTA was obtained from Koch-Light, and FeDTPA was obtained from Aldrich. CuEDTA was obtained from Sigma. ZnEDTA was obtained from Koch-Light. FeHEEDTA, FeEDDHA and FeEDDHMA standards could not be found commercially or within the network of experts working on this analysis. However, they are manufactured industrially but not to high purification levels. Samples of these chelating agents were obtained from various industrial sources. All standards and samples for analysis were made up in the mobile phase and filtered with a 0.45-μm filter prior to analysis.

Preparation of mobile phase for ion-pair chromatography

Mobile phase A: 32.5 ml of 1.5 *M* solution of tetrabutylammonium hydroxide was added to 200 ml of water. The pH was adjusted to 7.5 with NaOH and made up to 1 l in a volumetric flask. Final mobile phase B: 32.5 ml of 1.5 *M* tetrabutylammonium hydroxide solution was added to 200 ml of water. This was made up to approximately 650 ml, the pH adjusted to 7.5 with NaOH and the solution filtered with a 0.45-μm filter. 300 ml of acetonitrile was added and made up with filtered water to 1 l in a volumetric flask. All mobile phases were degassed in an ultrasonic bath.

Ion-pair chromatography system

A Waters M45 pump, a Waters solvent select valve, and a Gilson model 231 injector with a 20-μl injection loop were used, in conjunction with a Merck Hitachi L-4000 UV detector. A Chromspher C_{18} column was used. The system was interfaced to a Nelson Analytical 900 Series interface. Data were processed using a Nelson Analytical 3000 Series chromatography data system.

RESULTS AND DISCUSSIONS

Investigation of the ion-pairing reagent benzyltrimethylammonium chloride

Fig. 1 shows the influence of pH on the separation of the Fe(III) chelates of EDTA, DTPA and HEEDTA using the ion-pairing reagent benzyltrimethylammonium chloride. This figure shows both the change in retention time and the increase in resolution. As the pH increased to pH 7.5 the retention time increased and the resolution between FeDTPA and

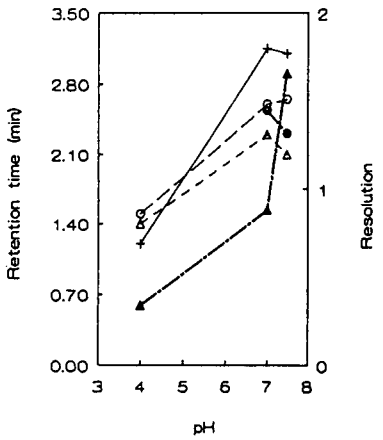

Fig. 1. The influence of pH on the retention time (t_R) and resolution (R_S) of some iron(III) chelates. Column: Chromspher C_{18}. Eluent pH 4: 0.05 *M* BTAC, 0.2 *M* NH_4Cl; eluent pH 7, 7.5: 0.05 *M* BTAC, 0.05 *M* KH_2PO_4, pH variable. Flow-rate: 1 ml/min. Injection loop: 20 μl. Detection at 300 nm. Symbols: + = t_R FeEDTA; △ = t_R FeDTPA; ○ = t_R FeHEEDTA; ▲ = R_S FeDTPA and FeHEEDTA; ● = R_S FeHEEDTA and FeEDTA.

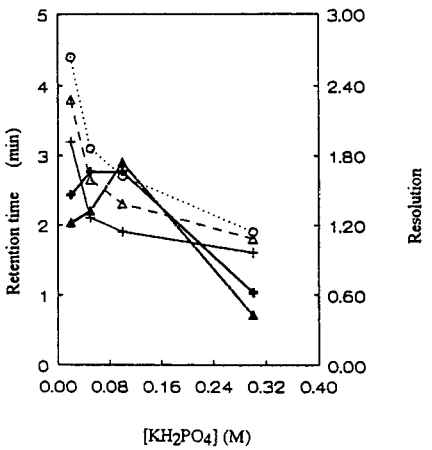

Fig. 2. The influence of buffer concentration on the retention time (t_R) and resolution (R_S) of iron(III) chelates. Column: Chromspher C_{18}. Eluent: 0.05 *M* BTAC, pH 7.5, [KH_2PO_4] variable. Flow-rate: 1 ml/min. Injection loop: 20 μl. Detection at 300 nm. Symbols: + = t_R FeDTPA; △ = t_R FeHEEDTA; ○ = t_R FeEDTA; + = R_S FeDTPA and FeHEEDTA; ▲ = R_S FeHEEDTA and FeEDTA.

FeHEEDTA increased. This may be explained by the formation of mono- and dihydroxo-forms of the three chelates and thus an increased negative charge. A more detailed study might reflect the exact pH values for the different chelates at which the mono- and dihydroxo-complexes form and the effect this has on the retention. Good resolution of the three chelates was obtained at pH 7.5. A higher pH was not investigated as hydrolysis of Fe(III)-EDTA occurs above pH 8.

The influence of phosphate buffer concentration was then investigated (Fig. 2). It was found that as the concentration of the buffer was increased from 0.02 *M* to 0.3 *M*, the retention time of the chelates decreased. Bidlingmeyer and Warren [9] also found this behaviour for the retention of alkylsulphonates with the ion-interaction reagent cetylpyridinium chloride above 10^{-3} *M* KH_2PO_4. With addition of phosphate there is an increase in the amount of reagent adsorbed as the charge repulsion between the reagent ions on the stationary phase is reduced. However, the increase in ionic strength of the eluent also results in a decrease in electrostatic attraction between the analyte and the ion-interaction reagent such that retention of the sample by adsorptive forces increases. The overall result in this investigation, as was that of Bidlingmeyer and Warren [9], is a decrease in retention of the analyte. In the present investigation this decrease in electrostatic attraction and increase in adsorptive forces was accompanied by a decrease in peak width and increased resolution up to a buffer concentration of 0.1 *M*. Beyond this concentration the decrease in peak width was not enough to compensate for the decrease in retention time, so that the solution started again to decrease. Therefore at this concentration the combination of adsorptive and electrostatic forces is optimal. To improve resolution further, especially between FeHEEDTA and FeEDTA, the concentration of BTAC was increased, as shown in Fig. 3. It was expected that as the concentration of BTAC was increased, the sample would have more interaction with the ion-pairing reagent, and therefore have a longer retention time. It was found that there was very little change in the retention time, but that the resolution increased.

Development of a solvent-switching system

The retention times of EDDHA and EDDHMA were extremely long using an eluent of 0.15

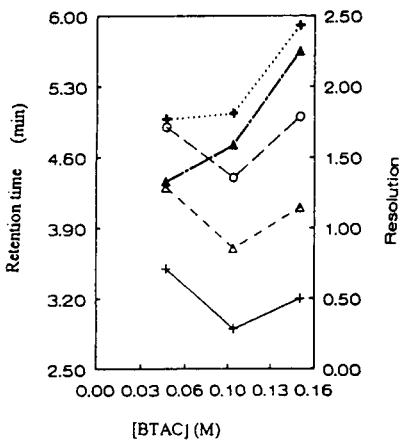

Fig. 3. The influence of the concentration of BTAC on the resolution of chelates. Column: Chromospher C_{18}. Eluent: 0.1 *M* KH_2PO_4, pH 7.5, [BTAC] variable. Flow-rate: 0.5 ml/min. Injection loop 20 μl. Detection at 300 nm. Symbols as in Fig. 2.

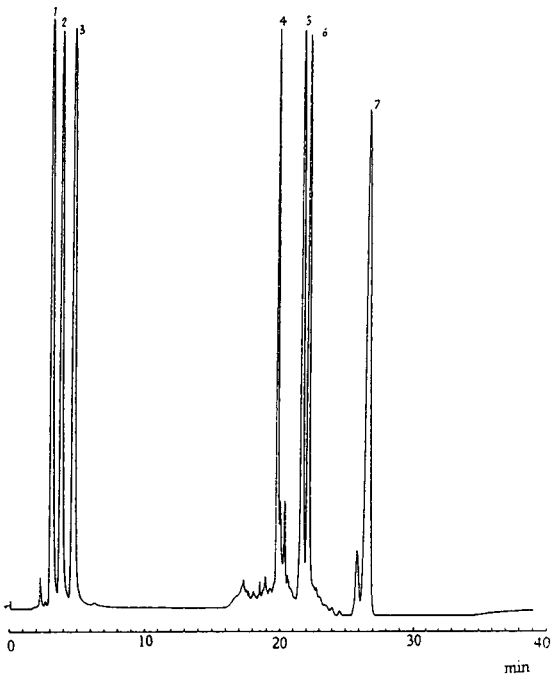

Fig. 4. Separation of (1) 24 μg FeDTPA, (2) 45 μg FeHEEDTA, (3) 18 μg FeEDTA, (4), (5) 80 μg FeEDDHMA, (6), (7) 74.5 μg FeEDDHA. Eluent: mobile phase A: 0.15 *M* BTAC, 0.1 *M* KH_2PO_4, pH 7.5, mobile phase B: 0.15 *M* BTAC, 0.1 *M* KH_2PO_4, pH 7.5, 25% acetonitrile. Switching sequence: 5 min mobile phase A, 15 min mobile phase B, 25 min mobile phase A. Flow-rate: 0.5 ml/min. Injection loop 20 μl. Detection at 283 nm.

M BTAC, 0.1 *M* KH_2PO_4, pH 7.5, (2.5 h for EDDHA). Addition of an organic modifier to decrease the retention time of Fe(III)-EDDHA and Fe(III)-EDDHMA was achieved using a solvent switching system. A switching valve was placed between the solvent reservoir and the pump, which was activated by a pulsed signal (given in this case by the Gilson auto-injector). Using this system the column was firstly equilibrated with mobile phase A (0.15 *M* BTAC, 0.1 *M* KH_2PO_4, pH 7.5) and the Fe(III)-EDTA, Fe(III)-DTPA and Fe(III)-HEEDTA chelates were allowed to elute. The solvent was then switched to mobile phase B (0.15 *M* BTAC, 0.1 *M* KH_2PO_4, pH 7.5 with variable acetonitrile concentration). Investigation of the addition of 10%, 20%, 25% and 30% acetonitrile showed 25% acetonitrile to be the optimum. Elution with 25% acetonitrile for 15 min was necessary to elute FeEDDHA and FeEDDHMA. A further 25 min was needed to re-equilibrate the system with mobile phase A. The switching sequence was thus as follows: 5 min mobile phase A, 15 min mobile phase B followed by 25 min mobile phase A. Fig. 4 shows the separation of the iron chelates achieved. Two peaks were obtained for both FeEDDHA and FeEDDHMA, representing the separation of the respective diastereoisomers. This is important as for FeEDDHA it has been shown that only one of the isomers is effective as a fertiliser. The optimum wavelength for determination of the iron chelates was found to be 283 nm. However, it was found that the Zn(II)-EDTA and Mn(II)-EDTA chelates only exhibit an absorption below 220 nm. However, as BTAC also has a high background absorbance at 220 nm, determination of Zn(II)-EDTA and Mn(II)-EDTA was not possible using this system.

Investigation of the ion-pairing reagent tetrabutylammonium hydroxide

The ion-pairing reagent TBAOH was then investigated. Good resolution of the chelates was obtained. As with BTAC, the Fe(III) chelates of EDTA, DTPA and HEEDTA eluted very quick-

ly, while the EDDHA and EDDHMA chelates had a longer retention time and were well separated. At an equivalent concentration of TBAOH the retention time of all the chelates was longer with respect to BTAC.

The dependence of the separation on the TBAOH concentration in shown in Fig. 5. Unlike the behaviour of BTAC, where the retention remained almost constant, it was found that as the concentration of TBAOH was decreased, the retention time and resolution of the chelates increased. This is contrary to what would normally be expected and cannot be explained by such theories as ion-pair, ion-exchange or the ion-interaction mechanism proposed by Bidlingmeyer *et al.* [10], which would all predict that the retention time should increase as ion-pair reagent concentration increases. It has, however, been shown by Hung and Taylor [11], that over wide ranges in mobile phase ion-pairing concentration, the dependence of capacity factors on ion-pairing concentration is complex. It may reach a plateau or even pass through a maximum. It was predicted that the mechanism occurring was a combination of ion-exchange and desolvation. As the concentration of ion-pairing reagent increases, the C_{18} surface area available for desolvation subsequent to ion-exchange will decrease. Also, the capacity factor will decrease as the counter ion concentration increases as a result of added pairing reagent. This mechanism was modelled for aqueous systems and over concentration ranges similar to that used in this study. It is possible that the behaviour predicted by Bidlingmeyer *et al.*, who carried out research over the narrower concentration range of 0–20 m*M* and in the presence of an organic modifier, would have been seen if we had also employed the same conditions. The optimum separation achieved in this study was at 0.05 *M* TBAOH. Below this concentration the retention time continued to increase but resolution decreased. This may be explained by increased hydrophobic interaction of the chelates with the stationary phase due to increased area available for desolvation and less competition from the ion-pair reagent. However, there are not enough ion-exchange sites to maintain selectivity.

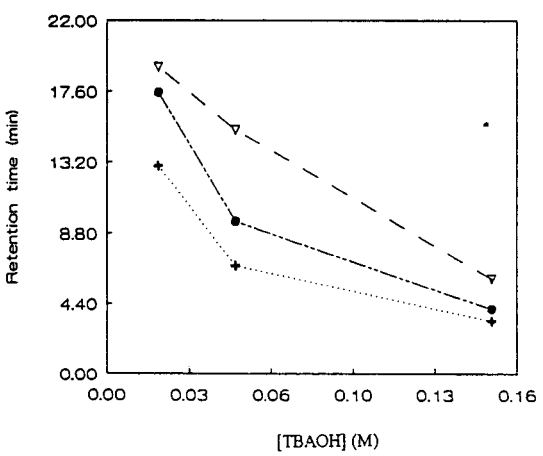

Fig. 5. The influence of TBAOH concentration on retention time of iron(III) chelates. Column: Chromspher C_{18}. Eluent: mobile phase A: [TBAOH] variable, pH 7.5, mobile phase B: [TBAOH] variable, pH 7.5, 25% acetonitrile. Flow-rate 0.5 ml/min. Injection loop 20 μl. Detection at 300 nm. Symbols: + = FeHEEDTA; O = FeDTPA; ▽ = FeEDTA.

Due to the longer retention time of the chelates, the chelates of EDDHA and EDDHMA again needed addition of acetonitrile. Acetonitrile was added to a second mobile phase and a solvent-switching system used. The amount of acetonitrile added was 30%. The final conditions were thus: mobile phase A: 0.05 *M* TBAOH, pH 7.5, mobile phase B: 0.05 *M* TBAOH, pH 7.5, 30% acetonitrile, using a switching sequence of 5 min mobile phase A, 20 min mobile phase B, 25 min mobile phase A. The separation achieved is shown in Fig. 6.

Investigation of the separation of Mn(II)-EDTA, Cu(II)-EDTA and Zn(II)-EDTA with TBAOH showed that these species coeluted.

Investigation of the ion-pairing reagent tetradecyltrimethylammonium bromide

To separate Mn(II)-EDTA, Cu(II)-EDTA and Zn(II)-EDTA, an alternative ion-pairing reagent was needed. It has been shown that the larger the ion-interaction reagent the greater the amount adsorbed on the stationary phase for a given concentration [11]. Therefore, at equivalent concentrations, TDTMABr will provide more ion-exchange sites than TBAOH. From the behaviour of TBAOH, it was predicted that as

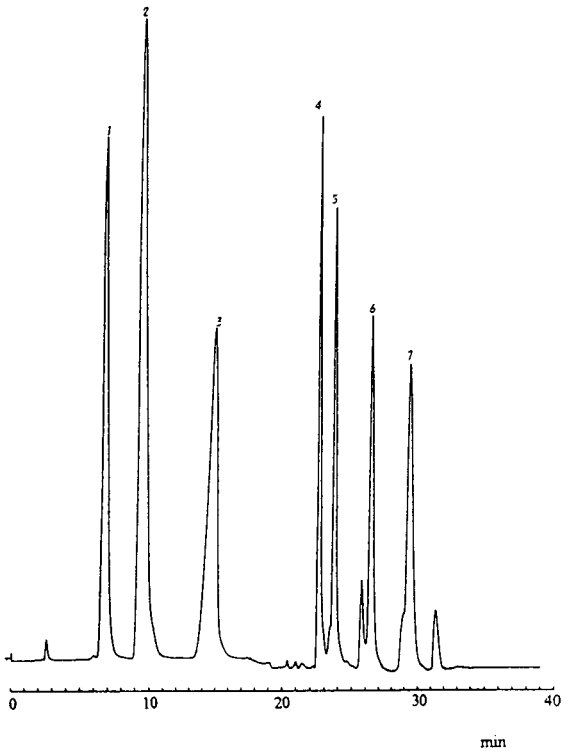

Fig. 6. Separation of (1) 67 μg FeHEEDTA, (2) 61 μg FeDTPA, (3) 47 μg FeEDTA, (4), (5) 94 μg FeEDDHA, (6), (7) 120 μg FeEDDHMA. Column: Chromspher C_{18}. Eluent: mobile phase A: 0.05 *M* TBAOH, pH 7.5, mobile phase B: 0.05 *M* TBAOH, pH 7.5, 30% acetonitrile. Switching sequence: 5 min A, 20 min B, 25 min A. Flow-rate: 0.5 ml/min. Injection loop: 20 μl. Detection at 300 nm.

the concentration decreased the increased area available for desolvation improved the separation. However, below 0.05 *M*, there was a lack of ion-exchange sites. Therefore, an ion-pairing reagent which allows sufficient interaction with the reversed phase and gave sufficient ion-exchange sites was needed. Thus TDTMABr was chosen, as at low concentration it would coat the column more efficiently. Fig. 7 shows how the retention of Mn(II)-EDTA, Zn(II)-EDTA, Cu(II)-EDTA and Fe(III)-HEEDTA increases as the concentration of TDTMABr decreases. Fig. 8 shows the separation achieved. It can be seen that the detection of ZnEDTA is very insensitive; this could possibly be improved by the development of a post-column reaction with copper [2].

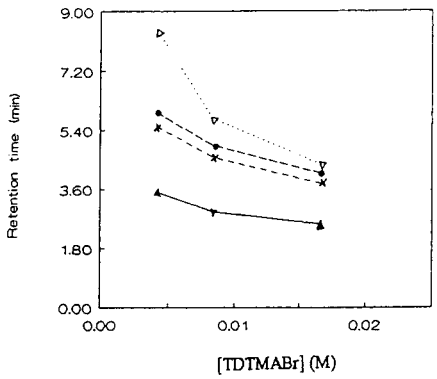

Fig. 7. Influence of TDTMABr concentration on the retention time of various chelates. Column: Chromspher C_{18} Eluent: [TDTMABr] variable, 0.1 *M* KH_2PO_4, pH 7.5. Flow-rate: 0.5 ml/min. Injection loop: 20 μl. Detection at 220 nm. Symbols: ▲ = MnEDTA; × = ZnEDTA; ● = CuEDTA; ▽ = FeHEEDTA.

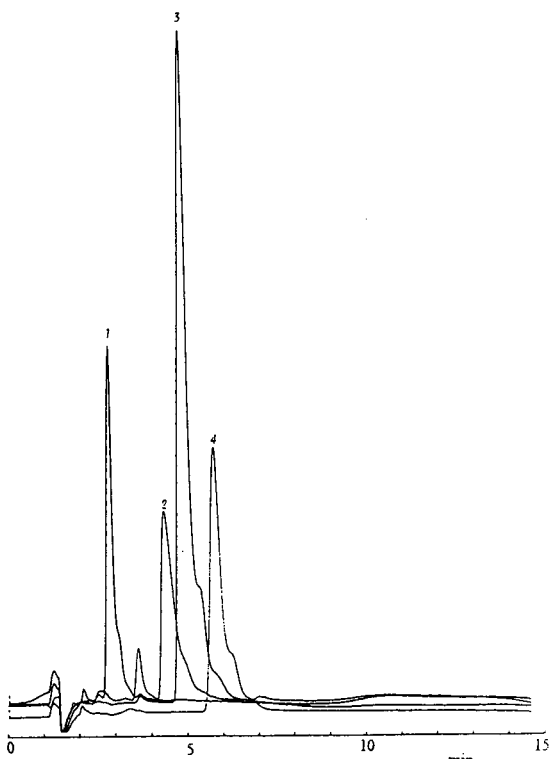

Fig. 8. Separation of (1) 46 μg MnEDTA, (2) 330 μg ZnEDTA, (3) 41 μg CuEDTA, (4) 67 μg FeHEEDTA. Column: Chromospher C_{18}. Eluent: 0.01 *M* TDTMABr, 0.1 *M* KH_2PO_4, pH 7.5. Flow-rate: 0.5 ml/min. Injection loop: 20 μl. Detection at 220 nm.

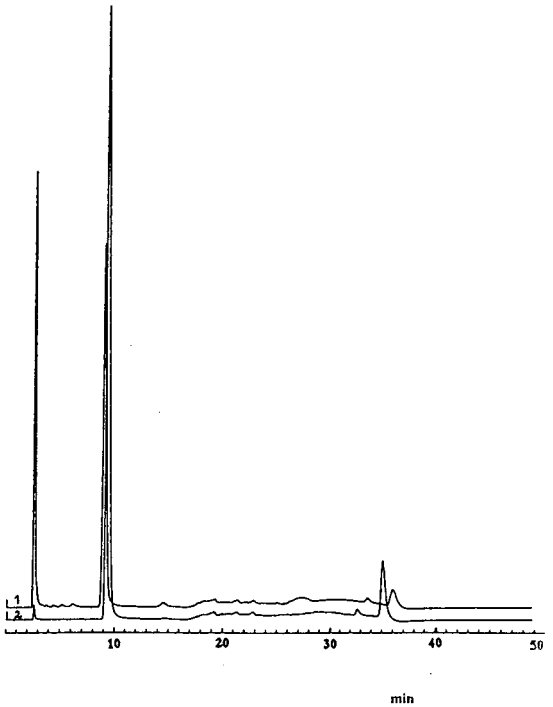

Fig. 9. Overlay of (1) fertiliser sample containing 3.2% iron in the form of FeDTPA with (2) FeDTPA standard.

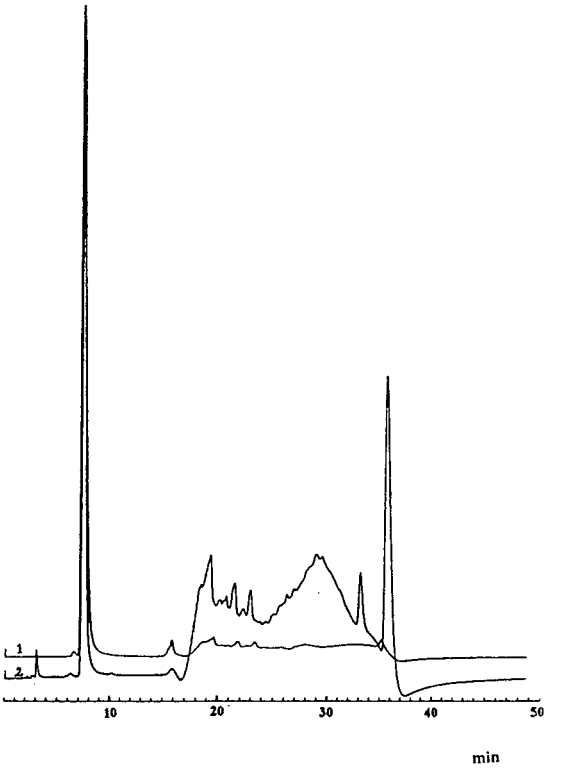

Fig. 10. Overlay of (1) FeHEEDTA "standard" with (2) fertiliser sample containing approximately 5.4% iron in the form of FeHEEDTA.

The ion-pair chromatographic method described using TBAOH as ion-pairing reagent gave rise to a linear calibration for the determination of the iron(III) chelates in the approximate range 1.79–179 mmol Fe in the form of chelate. 1.79 mmol Fe in the form of chelate was the limit of detection for FeEDDHA and FeEDDHMA while for FeEDTA, FeDTPA and FeHEEDTA it was below this. No interferences were encountered in the analysis of real samples and sample retention times agreed very closely with those of standards. Figs. 9 to 11 show examples of three samples analysed. No quantitative results have been quoted, as official standards were not available to carry out such studies.

CONCLUSIONS

An ion-pair chromatographic method has been developed to permit the separation of the chelates FeEDTA, FeDTPA, FeHEEDTA, FeEDDHA, FeEDDHMA, CuEDTA, ZnEDTA and MnEDTA, which may be applied to the analysis of a fertiliser containing one of the above chelates. For FeEDDHA and FeEDDHMA, a separation of the diastereoisomers has been achieved, which is important as research shows only one of these isomers is effective as a fertiliser. This method will be useful for quality control in the manufacture of fertilisers.

Further studies should aim to develop a sample preparation procedure for conversion of all chelating agent to the iron form at low pH, with removal of interfering ions [12] and subsequent determination by the method developed.

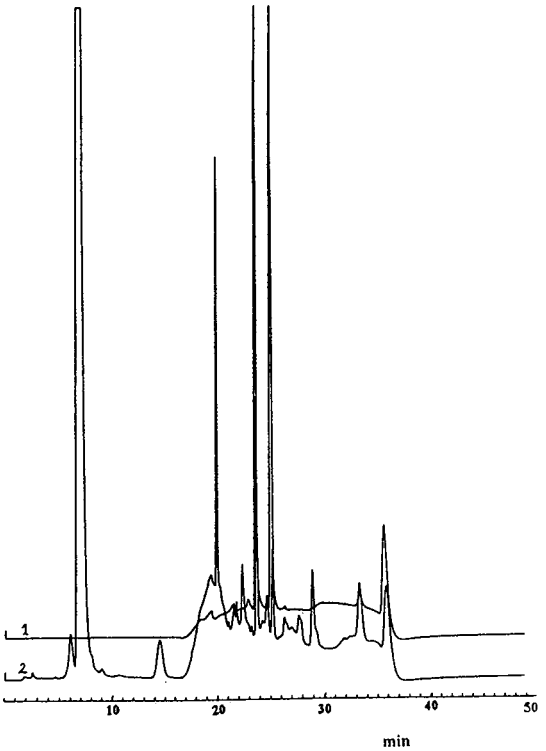

Fig. 11. Overlay of (1) FeEDDHA "standard" with (2) fertiliser sample containing approximately 0.2% iron in the form of FeEDDHA.

ACKNOWLEDGEMENT

This work was supported by the European Commission for Science.

REFERENCES

1 M. Deacon, M.R. Smyth and L.G.M.Th. Tuinstra, *J. Chromatogr.*, 657 (1993) 69.
2 W. Buchberger, P.R. Haddad and P.W. Alexander, *J. Chromatogr.*, 558 (1991) 181.
3 G.A. Perfetti and C.R. Warner, *J. Assoc. Off. Anal. Chem.*, 62 (1979) 1092.
4 D.L. Vanezky and W.E. Rudzinski, *Anal. Chem.*, 56 (1984) 315.
5 K. van Waren and K. Hoven, *De Ware(n)-Chemicus*, 15 (1985) 26.
6 A. Yamaguchi, A.R. Raiput, K. Ohzeki and T. Kambara, *Bull. Chem. Soc. Jpn.*, 56 (1983) 2621.
7 D.G. Parkes, M.G. Caruso and J.E. Spradling, *Anal. Chem.*, 53 (1981) 2154.
8 C.C.T. Chinnick, *Analyst*, 106 (1981) 1203.
9 B.A. Bidlingmeyer and F.V. Warren, Jr., *Anal. Chem.*, 54 (1982) 2351.
10 B.A. Bidlingmeyer, S.N. Deming, W.P. Price, Jr., B. Sachok and M. Petrusek, *J. Chromatogr.*, 186 (1979) 419.
11 C.T. Hung and R.B. Taylor, *J. Chromatogr.*, 202 (1980) 333–345.
12 M. Deacon, R.G. Leonard and M.R. Smyth, *Analyst*, 116 (1991) 897.

Journal of Chromatography A, 659 (1994) 359–365
Elsevier Science B.V., Amsterdam

CHROM. 25 636

Reversed-phase high-performance liquid chromatographic behaviour of some metal 1-(2-pyridylazo)-2-naphthol chelates

Takashi Yasui, Akio Yuchi, Hiromichi Yamada and Hiroko Wada*

Laboratory of Analytical Chemistry, Department of Applied Chemistry, Nagoya Institute of Technology, Showa, Nagoya 466 (Japan)

(First received July 20th, 1993; revised manuscript received October 5th, 1993)

ABSTRACT

The HPLC behaviour of Cu(II), Co(III), Ni(II) and Fe(II) chelates with 1-(2-pyridylazo)-2-naphthol (PAN) on alkyl-bonded silica gel stationary phase was studied in detail. Peaks of $[Ni^{II}(PAN)_2]$ and $[Fe^{II}(PAN)_2]$ were observed with the mobile phase acetonitrile–water (70:30, v/v). The cationic chelates, $[Cu^{II}(PAN)]^+$ and $[Co^{III}(PAN)_2]^+$, were found to be adsorbed on the stationary phase as a result of interaction with the residual silanol groups. A sharp peak of $[Co^{III}(PAN)_2]^+$ chelate was obtained by adding one of several organic or inorganic salts to the mobile phase, but a $[Cu^{II}(PAN)]^+$ chelate peak could only be obtained on addition of ammonium thiocyanate. The retention of the Co(III) chelate depended to a large extent on the alkyl chain length of the stationary phase and the species of an organic modifier in the mobile phase.

INTRODUCTION

2-Pyridylazo compounds, which form stable chelates with high molar absorptivity in the visible regions with many metal ions, are very useful analytical reagents and have been widely used for spectrophotometric determination and complexometric titration of metals [1]. Moreover, these reagents form different charged chelates depending upon the central metal ions because of tridentate ligands. In reversed-phase high-performance liquid chromatography (RP-HPLC), precolumn chromogenic chelating reagents must contribute not only to the detection but also to the separation of metal ions, in contrast to post column chelating reagents. Thus the reagents are required to form chelates with different partition characteristics between stationary and mobile phases.

Recently some 2-pyridylazo compounds with various functional groups have been synthesized and applied to RP-HPLC as precolumn chelating reagents for the simultaneous determination of trace metals because of their excellent analytical properties. Most of them have been used in the form of water-soluble anionic chelates, and ion-pair RP-HPLC using hydrophobic cations such as tetrabutylammonium has usually been employed [2–5].

1-(2-Pyridylazo)-2-naphthol (PAN) is widely used for the separation and determination of various metals as a colour-forming and extraction reagent, because the reagent itself is rather unselective. A large number of studies describing the use of this reagent and chelation with individual metals have been reported [1]; nevertheless few papers on the RP-HPLC behaviour of PAN chelates have been published [6,7].

Although a few studies on the RP-HPLC separation of Cu(II), Co(III), Ni(II) and Fe(II) chelates have been reported [6], good resolution

* Corresponding author.

0021-9673/94/$07.00
SSDI 0021-9673(93)E1077-D

between Ni(II) and Fe(II) chelates was not obtained.

In the present study, the RP-HPLC behaviour of PAN and the chelates of Cu(II), Co(III), Ni(II) and Fe(II) on alkyl-bonded silica gel stationary phase was extensively studied. The adsorption of cationic chelates, $[Cu^{II}(PAN)]^+$ and $[Co^{III}(PAN)_2]^+$, on residual silanol groups and the retention of these as well as neutral chelates, $[M(PAN)_2]$ [M: Ni(II), Fe(II)], are discussed.

EXPERIMENTAL

Apparatus

The HPLC system consisted of a Model CCPD dual pump (resin type, Tosoh, Tokyo, Japan), a Model SVM-6M2L ceramic valve injector (dead volume 2 μl, sample loop 8 μl, Sanuki, Tokyo, Japan) and a Model Multi-330 multiwavelength UV–Vis detector (wavelength range 200–800 nm, flow cell 4 μl, 1 mm I.D., optical pathlength 5 mm, Jasco, Tokyo, Japan) equipped with an NEC personal computer. Data acquisition and data analysis were performed using a Jasco Model DP-L320/98 data-processing system (Jasco). An Inertsil ODS-2 packed column (250 mm × 4.6 mm I.D., particle diameter 5 μm, GL Sciences, Tokyo, Japan) was used unless otherwise noted. The temperature of the column was controlled by a Model 860-CO column oven (Jasco). By using a metal-free pump, injector, column and tubing, contamination by metal ions from the HPLC apparatus was minimized.

Reagents

PAN was synthesized as described previously [1] and dissolved in ethanol. Metal stock solutions (10^{-2} *M*) were prepared from analytical reagent-grade metallic copper, cobalt(II) and nickel(II) nitrates and iron(II) sulphate, containing 0.01–0.1 *M* acid. Organic or inorganic salts added to the mobile phase were of analytical-reagent grade or reagent grade. All the organic solvents were of analytical reagent grade. The water used was purified by means of a Toraypure LV-10T ultrapure water manufacturing device (Toray, Tokyo, Japan).

Procedure

A 1-ml volume of an aqueous solution (pH *ca.* 4) containing 10^{-4} *M* each of copper(II), cobalt(II), nickel(II) and iron(II) was added to 4 ml of $2.5 \cdot 10^{-4}$ *M* PAN ethanol solution, and the solutions were allowed to stand for at least 30 min, or were heated to 80°C for the quantitative chelation. The resulting solution was loaded into the sample loop by suction and injected into the column. Mobile phase was filtered through a membrane filter (pore size 0.2 μm, Toyo Roshi) and degassed before use. The flow-rate of a mobile phase was adjusted to 0.8 ml/min. The column was equilibrated with each mobile phase for at least 30 min before sample injection. The capacity factors (k') of PAN and its chelates were calculated using the retention time of sodium nitrite as a measure of the void volume.

RESULTS AND DISCUSSION

Chromatographic behaviour of PAN chelates

Copper and cobalt form cationic chelates of $[Cu^{II}(PAN)]^+$ and $[Co^{III}(PAN)_2]^+$, while nickel and iron form neutral chelates $[M^{II}(PAN)_2]$ under the conditions described in the Procedure section (pH *ca.* 4). The RP-HPLC behaviour of analytes is often estimated from extractive behaviour because the retention is mainly based on the partition between stationary phase and mobile phase. The extractability of metals with PAN into chloroform was examined. The results are shown in Fig. 1. The cationic Cu(II) and Co(III) chelates, which were minimally extracted without appropriate anions, could be extracted as $[Cu(PAN)]^+Cl^-$ and $[Co(PAN)_2]^+Cl^-$. At pH 4–10, Cu(II), Co(III), Ni(II) and Fe(II) chelates were quantitatively extracted. Their absorption spectra and the wavelength of their absorption maxima were not changed over this range of pH, although the spectrum of Cu(II)–PAN changed at pH > 7 as a result of the formation of $[Cu^{II}(PAN)_2]$ with excess PAN. These results suggest that neutral chelates are retained more strongly than cationic chelates, if secondary effects on the retention other than the partition do not exist.

A solution containing Cu(II)–, Co(III)–, Ni(II)– and Fe(II)–PAN chelates and excess

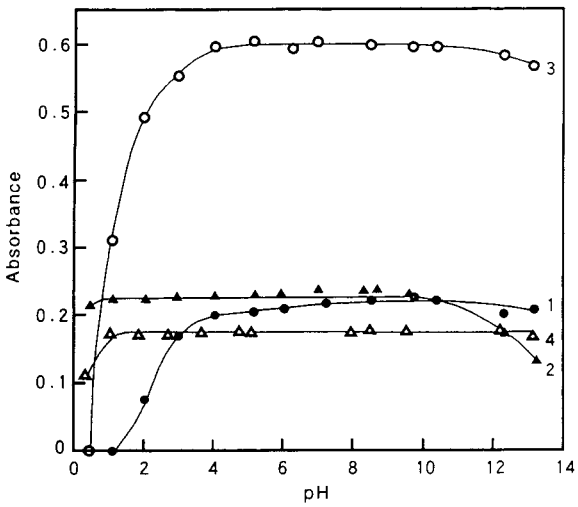

Fig. 1. Effect of pH on the extraction of PAN chelates. Aqueous phase (10 ml) concentrations: metal $1.0 \cdot 10^{-5}$ *M*; PAN = $1.25 \cdot 10^{-5}$ *M* (Cu) or $2.5 \cdot 10^{-5}$ *M* (others); buffer = 0.01 *M*; KCl = 0.1 *M*; ascorbic acid = $2.0 \cdot 10^{-4}$ *M* (Fe); KIO_4 = $1.0 \cdot 10^{-3}$ *M* (Co). Organic phase (10 ml): chloroform. Metal, wavelength: 1 = Cu, 565 nm; 2 = Co, 583 nm; 3 = Ni, 569 nm; 4 = Fe, 765 nm.

PAN was injected into a column. Fig. 2a shows a chromatogram obtained using acetonitrile–water (70:30, v/v) not containing any salts as a mobile phase. Only three peaks were observed for PAN and neutral chelates of $[Ni^{II}(PAN)_2]$ and $[Fe^{II}(PAN)_2]$, but not for the cationic chelates of $[Cu^{II}(PAN)]^+$ and $[Co^{III}(PAN)_2]^+$.

It has been reported that silanol groups remain at the surface of alkyl-bonded silica gel after end-capping and influence the chromatograms of basic or polar compounds [8–10]. As the pK_a of silanol groups is around 7 [11], the cationic chelates of Cu(II) and Co(III) were probably adsorbed to the dissociated silanol ($-SiO^-$) at pH > 7, or exchanged with a proton of silanol at lower pH.

Effect of eluent pH

The effect of mobile phase pH (*ca.* 1–7) on the retention of PAN and its chelates, such as Cu(II), Co(III), Ni(II) and Fe(II), was examined with acetonitrile–water (70:30, v/v) containing sulphuric acid (Fig. 2b and c). The lower peaks for Co(III) and Cu(II) chelates were obtained at pH < 5 and < 3, respectively. The

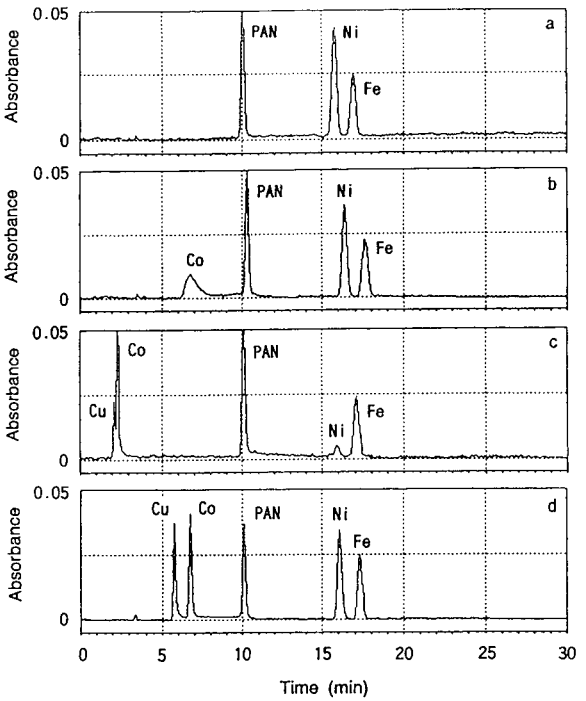

Fig. 2. Chromatogram of PAN chelates. Column: Inertsil ODS-2. Mobile phase: acetonitrile–water (70:30, v/v) containing (a) no additives; (b) $1.0 \cdot 10^{-5}$ *M* H_2SO_4, pH 5.4; (c) $1.0 \cdot 10^{-4}$ *M* H_2SO_4, pH 3.3; (d) $1.0 \cdot 10^{-2}$ *M* NH_4SCN, pH 5.3. Flow-rate: 0.8 ml/min. Column temperature: 40°C. Metal, amounts injected (μg), detection wavelength (nm): Cu, 0.013, 555; Co, 0.012, 447; Ni, 0.012, 560; Fe, 0.011, 466.

retention of Cu(II) and Co(III) chelates at pH < *ca.* 3 was almost equal to that of sodium nitrite, which was used as a standard for measuring the void volume. It is clear that the residual silanol groups may be negligible at pH 3. At this pH, however, deterioration in the peak heights caused by dissociation of chelates, as seen in Fig. 2c, was also observed for Cu(II) and Ni(II) chelates.

Effect of eluent additives

Various organic and inorganic salts (total concentration adjusted to 0.01 *M*) were added to the acetonitrile–water (70:30, v/v) mobile phase, and their effect on the retention of PAN chelates was examined. Fig. 2d shows a chromatogram obtained with mobile phase containing 0.01 *M* ammonium thiocyanate. The capacity factors

TABLE I

EFFECT OF SALTS ON CHROMATOGRAPHIC BEHAVIOUR OF CATIONIC PAN CHELATES

Salt (0.01 *M*)	Capacity factor (k')		Theoretical plate number (N)[a]	
	Cu(II)	Co(III)	Cu(II)	Co(III)
Sodium 2-naphthalenesulphonate	–	3.80	–	6500
Sodium 1-pentanesulphonate	–	2.37	–	7200
Acetic acid–sodium acetate (pH 5)[b]	–	3.12	–	4800
Citric acid–sodium citrate (pH 5)[b]	–	1.85	–	9200
Tetra-*n*-butylammonium bromide	–	1.60	–	4300
Sodium bromide	–	1.90	–	7600
Ammonium bromide	0.88	1.60	300	9600
Sodium azide	1.90	3.42	100	7000
Sodium thiocyanate	1.32	2.28	1500	6800
Ammonium thiocyanate	1.15	1.53	11700	5800

[a] $N = 5.54\ (t_R/W_{1/2})^2$.
[b] The sodium ion concentration is less than 0.01 *M*.

(k') and theoretical plate numbers (N) of cationic PAN chelates are given in Table I together with other salts. Retention of neutral Ni(II) and Fe(II) chelates was not altered by the addition of any salts.

The Co(III) chelate was eluted to give a sharp band with mobile phases containing any combination of a cation and an anion, although the capacity factor varied from 1.6 to 3.8. The Cu(II) chelate, on the other hand, could be eluted only by four salts which contained anions with stronger affinities for Cu(II). The theoretical plate numbers with thiocyanates were much larger than those with azide and bromide (NaSCN compared with NaN_3, and NH_4SCN compared with NH_4Br). Moreover, ammonium salts gave sharp peaks with less retention than sodium salts (NH_4SCN compared with NaSCN).

Thus the combination of ammonium and thiocyanate was found to be most effective as an additive (Fig. 2d). The ammonium ion effectively reduced the adsorption of these cationic chelates on dissociated silanol, and the thiocyanate ion strongly neutralized the chelate to form $[Cu^{II}(PAN)]^+SCN^-$. As a result, the interaction between the chelate and silanol is reduced to distribute favourably on the stationary phase.

Effect of stationary phase

The retention behaviour of PAN chelates was examined with eight kinds of alkyl-bonded silica gel columns commercially available. The substituent groups were octadecyl ($-C_{18}$; six manufacturers), octyl ($-C_8$; one manufacturer) and methyl ($-C_1$; one manufacturer). With mobile phases containing no salts, cationic chelates were not eluted from any column described above; only Kaseisorb ODS-300-5 gave a peak of Co(III) chelate, although the capacity factor was not reproducible. In the presence of 0.01 *M* ammonium thiocyanate, on the other hand, all the chelates were eluted from all columns. The capacity factors (k') of PAN chelates are listed in Table II. Some differences were found among the ODS columns used. For example, strong retention of Cu(II) and Co(III) chelates with TSK-gel ODS-120T suggests that ammonium thiocyanate of higher concentration was required because of the presence of more residual silanol groups on the column. The elution order, however, was the same and the ratios of capacity factors among chelates were similar to each other.

Alkyl chain length had a great effect on the retention of PAN chelates. With a decrease in

TABLE II

EFFECT OF COLUMNS ON CHROMATOGRAPHIC BEHAVIOUR OF PAN CHELATES[a]

Column	CH_3CN–water	Capacity factor (k')				
		Cu(II)	Co(III)	PAN	Ni(II)	Fe(II)
Inertsil ODS-2 (GL Sciences)	70:30	1.23	1.78	2.85	5.32	5.82
Shim-pack CLC-ODS (Shimadzu)	70:30	1.28	2.02	2.68	5.08	5.50
TSK-gel ODS-80Ts (Tosoh)	70:30	1.50	2.27	2.98	6.32	6.86
TSK-gel ODS-120T (Tosoh)	70:30	1.04	2.39	2.53	3.68	3.97
Kaseisorb ODS-SUPER (Tokyo Kasei)	70:30	1.08	1.33	2.47	4.73	5.17
Kaseisorb ODS-300-5 (Tokyo Kasei)	70:30	0.23	0.23	0.54	1.03	1.13
	60:40	0.45	0.56	0.97	2.42	2.70
Unisil Q C8 (GL Sciences)	70:30	1.06	3.50	1.99	3.05	3.24
	60:40	1.98	8.28	3.33	6.71	7.23
Finepak SIL C1-5 (Jasco)	70:30	0.21	0.71	0.24	0.32	0.32
	50:50	0.95	2.69	0.75	1.29	1.33

[a] Mobile phase: acetonitrile–water containing 0.01 *M* NH_4SCN.

the carbon number, the retention of PAN and Cu(II), Ni(II) and Fe(II) chelates dwindled, whereas that of Co(III) chelates showed the maximum at C_8 (Fig. 3). As a result, the retention of $[Co^{III}(PAN)_2]^+SCN^-$ was higher than that of $[Ni^{II}(PAN)_2]$ and $[Fe^{II}(PAN)_2]$, using C_1 and C_8 columns. In the case of C_1 columns, $[Cu^{II}(PAN)]^+SCN^-$ was retained more strongly than PAN with acetonitrile–water (50:50, v/v) (Table II). Thus separation and even elution order could be modified by the hydrophobicity of the stationary phase.

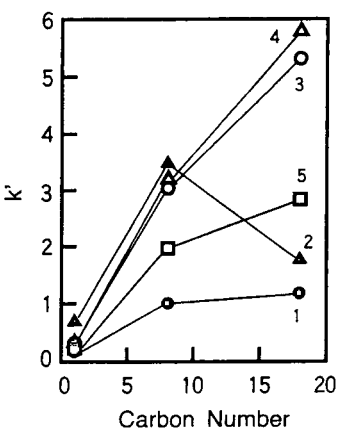

Fig. 3. Effect of carbon number on capacity factors (k'). Columns: C_{18}, Inertsil ODS-2; C_8, Unisil Q C_8; C_1, Finepak SIL C1-5. Mobile phase: acetonitrile–water (70:30, v/v) containing $1.0 \cdot 10^{-2}$ *M* NH_4SCN. 1 = Cu; 2 = Co; 3 = Ni; 4 = Fe; 5 = PAN.

Effect of organic modifiers

The effect of organic modifiers such as acetonitrile, acetone, methanol or ethanol in the mobile phase on the elution of chelates was examined. A Kaseisorb ODS-300-5 packed column (250 mm × 4.6 mm I.D., particle diameter 5 μm, Tokyo Kasei, Tokyo, Japan) was used because of low pressure loss. The results are shown in Fig. 4. With acetonitrile–water containing 0.01 *M* NH_4SCN, the decrease in retention of Co(III), Ni(II) and Fe(II) chelates caused by a decrease in polarity of the mobile phase was larger than that of Cu(II) chelate and PAN. The slope for $[Cu^{II}(PAN)]^+SCN^-$ is almost the same as that for PAN, whereas those for $[Co^{III}(PAN)_2]^+SCN^-$, $[Ni^{II}(PAN)_2]$ and $[Fe^{II}(PAN)_2]$ are twice as steep. The ratio agrees with the number of PAN ligands involved in each chelate. The intercepts, on the other hand, are smaller for cationic species than for neutral ones:

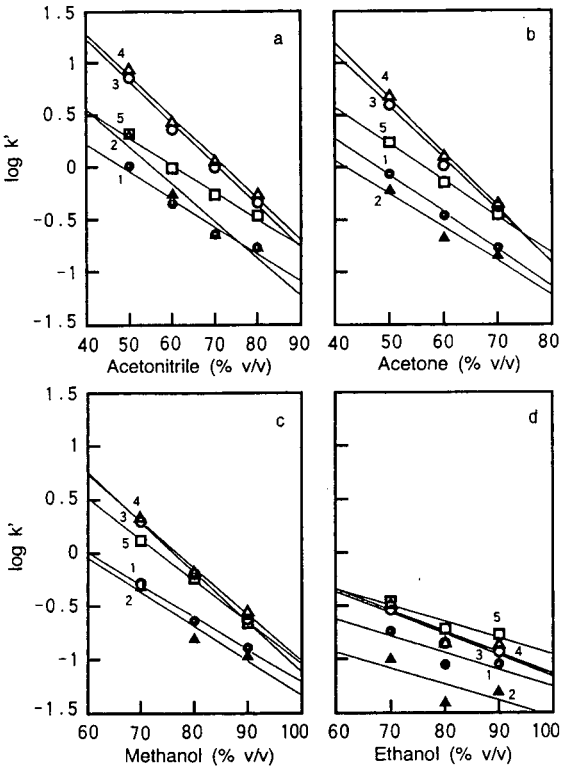

Fig. 4. Effect of organic modifier on capacity factors (k'). Column: Kaseisorb ODS-300-5. Mobile phase: (a) acetonitrile–water; (b) acetone–water; (c) methanol–water; (d) ethanol–water containing $1.0 \cdot 10^{-2}$ M NH_4SCN. 1 (●) = Cu; 2 (▲) = Co; 3 (○) = Ni; 4 (△) = Fe; 5 (□) = PAN.

$[Co^{III}(PAN)_2]^+SCN^-$ against $[Ni^{II}(PAN)_2]$ or $[Fe^{II}(PAN)_2]$, and $[Cu^{II}(PAN)]^+SCN^-$ against PAN. Thus an increase in acetonitrile content caused a deterioration in the separation between Ni(II) or Fe(II) chelates and PAN, and that between Co(III) and Cu(II) chelates. The elution order of Co(III) and Cu(II) chelates is reversed in less polar solvent systems such as acetone–water, methanol–water and ethanol–water (Fig. 4b–d). With ethanol–water, even Ni(II) and Fe(II) chelates were eluted earlier than PAN.

Effect of column temperature

Fig. 5a shows the effect of column temperature on the logarithmic k' values for PAN and its chelates. By increasing column temperature,

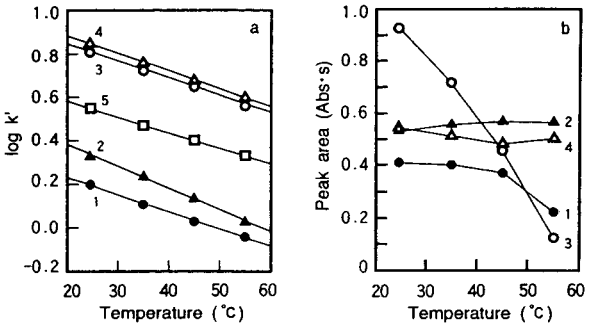

Fig. 5. Effect of column temperature on capacity factors (k') (a) and peak areas (b). Column: Inertsil ODS-2. Mobile phase: acetonitrile–water (70:30, v/v) containing $1.0 \cdot 10^{-2}$ M NH_4SCN. Other conditions are the same as in Fig. 2. 1 = Cu; 2 = Co; 3 = Ni; 4 = Fe; 5 = PAN.

elution time was reduced while maintaining good resolution of PAN and chelates because the slopes for all chelates were almost the same. As mentioned above, the increase in organic modifier concentration also reduced elution time, but the separation between Cu(II) and Co(III) chelates deteriorated (Fig. 4a).

The peak areas for Cu(II) and especially for Ni(II) were decreased with the increase in temperature (Fig. 5b). Since such phenomena were not observed without thiocyanate, displacement of PAN on Ni(II) by thiocyanate might be enhanced at a higher temperature.

CONCLUSIONS

The effect of several variables, such as hydrogen ion concentration, additives and organic modifiers in the mobile phase, alkyl chain length of the stationary phase, and column temperature, on the RP-HPLC of PAN chelates were examined.

It was possible to eliminate the adsorption of cationic chelates by using ammonium thiocyanate as an additive, to alter the elution order by altering the length of the alkyl chain and the polarity of the organic modifier, and to reduce the elution time while maintaining good resolution by increasing the column temperature.

These results provide fundamental information on the RP-HPLC of an analyte containing cationic and neutral chelates.

REFERENCES

1 S. Shibata, in H.A. Flaschka and A.J. Barnard, Jr. (Editors), *Chelates in Analytical Chemistry*, Vol. IV, Marcel Dekker, New York, 1972, pp. 1–232.
2 H. Wada, S. Nezu, T. Ozawa and G. Nakagawa, *J. Chromatogr.*, 295 (1984) 413.
3 C. Ohtsuka, K. Matsuzawa, H. Wada and G. Nakagawa, *Anal. Chim. Acta*, 256 (1992) 91.
4 T. Okutani, A. Sakuragawa and M. Murakami, *Anal. Sci.*, 7 (1991) 109.
5 D.A. Roston, *Anal. Chem.*, 56 (1984) 241.
6 G. Schwedt and R. Budde, *Chromatographia*, 15 (1982) 527.
7 T.A. Bol'shova, P.N. Nesterenko, E.M. Basova, V.M. Ivanov and N.B. Morozova, *Zh. Anal. Khim.*, 42 (1987) 1648.
8 S.G. Weber and W.G. Tramposch, *Anal. Chem.*, 55 (1983) 1771.
9 Y. Ohtsu, Y. Shiojima, T. Okumura, J. Koyama, K. Nakamura and O. Nakata, *J. Chromatogr.*, 481 (1989) 147.
10 K. Kimata, K. Iwaguchi, S. Onishi, K. Jinno, R. Eksteen, K. Hosoya, M. Araki and N. Tanaka, *J. Chromatogr. Sci.*, 27 (1989) 721.
11 K.K. Unger, *Porous Silica* (*Journal of Chromatography Library*, Vol. 16), Elsevier, Amsterdam, 1979, p. 133.

Journal of Chromatography A, 659 (1994) 367–380
Elsevier Science B.V., Amsterdam

CHROM. 25 659

Gas chromatographic study of solvation enthalpy by solvatochromically based linear solvation energy relationships

Jianjun Li[☆] and Peter W. Carr*

Department of Chemistry, University of Minnesota, 207 Pleasant Street Southeast, Minneapolis, MN 55455 (USA)

(First received August 19th, 1993; revised manuscript received October 19th, 1993)

ABSTRACT

Solute retention in capillary GC columns can be correlated with a linear solvation energy relationship (LSER) equation using chromatographically determined solute parameters (log L^{16}, $\pi_2^{*,C}$, α_2^C and β_2^C). The LSER coefficients obtained from correlation studies serve to quantitatively characterize the stationary phase. The effect of column temperature on retention was characterized by the temperature dependence of the LSER coefficients. Enthalpy and entropy of the retention process were also fitted quite well to the LSER equation. The main contributions to retention are from the solute–solvent interactions that give large favorable enthalpies and small unfavorable entropies. The LSER coefficients for the free energy and enthalpy regressions are linearly correlated.

INTRODUCTION

Temperature is the most important operating parameter in gas chromatography (GC) [1,2]. In general, because the enthalpies of solution of many compounds are similar, separations can often be improved by decreasing column temperature. At a fixed temperature, we [3–6] have shown that the retention of a wide variety of solutes can be modeled by a general linear solvation energy relationship (LSER) of the form of eqn. 1. In this work, we seek to examine the extension of eqn. 1 to the solvation enthalpy ΔH^0 as expressed in eqn. 2.

$$\log k' = SP_0 + l \log L^{16} + s\pi_2^{*,C} + d\delta_2 + a\alpha_2^C + b\beta_2^C \quad (1)$$

$$\Delta H^0 = SP_0^h + l^h \log L^{16} + s^h\pi_2^{*,C} + d^h\delta_2 + a^h\alpha_2^C + b^h\beta_2^C \quad (2)$$

In the above equations, k' is the capacity factor, ΔH^0 is the infinite dilution enthalpy of solution (see below). SP_0 is a solute-independent column-dependent constant, L^{16} is the partition coefficient for transfer of the solute from the gas phase to *n*-hexadecane at 298 K, $\pi_2^{*,C}$ is a GC-based solute dipolarity/polarizability parameter, δ_2 is an empirical polarizability correction factor, defined as zero for aliphatics, 0.5 for polyhalogenated compounds and 1 for aromatics. α_2^C and β_2^C are solute hydrogen bond donor acidity and solute hydrogen acceptor basicity parameters also based on GC retention data [3–6].

In eqn. 1 the term $l \log L^{16}$ represents the

* Corresponding author.
☆ Present address: Procter and Gamble Company, Miami Valley Laboratories, P.O. Box 398707, Cincinnati, OH 45239, USA.

SSDI 0021-9673(93)E1103-7

combination of contributions to changes in retention due to solute-to-solute differences in cavity formation and dispersive (London) interactions. The term $s\pi_2^{*,C}$ is the contribution of the dipolarity/polarizability interaction to retention. For aromatic and polyhalogenated compounds, which have different polarizabilities relative to aliphatic solutes, a minor correction term ($d\delta_2$) is often required. Finally, $a\alpha_2^C$ and $b\beta_2^C$ represent the contributions to retention resulting from solute-to-solvent and solvent-to-solute hydrogen-bond formation, respectively.

A very similar approach to correlating retention in GC, but which differs in some minor detail, was developed and used extensively by Abraham and co-workers [7–13]. In their work, they replaced the Kamlet–Taft δ_2 term with a new excess molar refraction parameter (R_2), defined as the molar refraction of the solute less the molar reflection of an alkane of the same Van der Waals volume. A comparison of our approach to that of Abraham and co-workers and Poole and co-workers' thermodynamic solvation model in predicting retention in GC and stationary phase characterization has appeared [14,15].

In general, we expect that solute–solvent interactions will decrease upon increasing temperature, due simply to increased thermal energy. That is, we expect that ΔH^0 will be negative. In the present case, any change in solute–solvent interactions (*i.e.* retention) with temperature could be due to temperature effects on the solute and on the solvent. We have no means (except for log L[16] in a limited temperature range) of separating these, and hence adopt the convention that any change in a characteristic constant with temperature is due to a change in a solvent property only. This is consistent with Leffler and Grunwald's analysis of enthalpy effects in organic chemistry [16]. This has no effect in regard to inter-solvent comparisons, which is our present concern, but it would be important if absolute values of solvent properties were of interest.

In a study of characterization of some N-substituted amides as solvents by the LSER approach, Abraham *et al.* [8] found that the LSER coefficients for N-formylmorpholine (NFM) and N-methylpyrrolidinone (NMP) at lower temperatures (40–100°C and 50–70°C, respectively) were very nicely linearly correlated with $1/T$ (K). However, the temperature range studied was rather limited compared to that used in most GC analyses.

In this work, we investigated the temperature dependence of the characteristic constants in eqn. 1 on the eight most commonly used capillary columns. This was accomplished by regressing log k' data at different temperatures against eqn. 1. The characteristic constants were then studied as a function of temperature.

Based on the same log k' temperature data, *apparent* free energy ($\Delta G'$), enthalpy (ΔH^0) and *apparent* entropy ($\Delta S'$) (see below) for the retention process were obtained. The *apparent* free energy, enthalpy and entropy were examined by means of LSER equations. While there is a great body of work on application of LSERs of the type of eqn. 1 to free energy related studies there is relatively little information on its relationship to enthalpy and entropy.

EXPERIMENTAL

The retention data (log k') for 53 highly variegated compounds that span an extremely wide range in chemical characteristics on eight common capillary columns ranging from a methyl silicone oil to polyethylene glycol have been published [17]. The solute parameters used are taken from refs. 3–5 and are given in Table I.

RESULTS AND DISCUSSION

Regression results for log k' at all temperatures

The correlation results of using eqn. 1 with all the data are shown in Table II. We note that an average over all columns and temperatures gives a mean standard deviation of 0.047 and correlation coefficients of 0.998. Inspection of Table II suggests that the solute parameters can be applied to any column and temperature with an excellent goodness of good fit.

The LSER coefficients make good chemical sense and as expected they are much easier to interpret in comparison to the empirical approach described previously [17]. As shown in

TABLE I

SOLUTE SOLVATOCHROMIC PARAMETERS
Parameters from refs. 3–5.

No.	Compound	Log L^{16}	$\pi_2^{*,C}$	α_2^C	β_2^C
1	Cyclohexane	2.906	0.00	0.00	0.00
2	1-Hexene	2.571	−0.07	0.00	0.02
3	Pentane	2.163	−0.18	0.00	0.00
4	Hexane	2.668	−0.16	0.00	0.00
5	Octane	3.677	−0.12	0.00	0.00
6	Decane	4.685	−0.11	0.00	0.00
7	Undecane	5.191	−0.10	0.00	0.00
8	Tetradecane	6.705	−0.07	0.00	0.00
9	Pentadecane	7.209	−0.06	0.00	0.00
10	Ethyl acetate	2.359	0.30	0.00	0.49
11	Propyl acetate	2.861	0.31	0.00	0.48
12	Diethyl ether	2.066	0.03	0.00	0.40
13	Dipropyl ether	2.971	0.03	0.00	0.30
14	Dibutyl ether	3.954	0.04	0.00	0.29
15	Acetonitrile	1.537	0.62	0.05	0.37
16	Propionitrile	1.978	0.64	0.00	0.41
17	Acetone	1.766	0.38	0.01	0.52
18	2-Butanone	2.269	0.39	0.00	0.48
19	2-Pentanone	2.726	0.40	0.00	0.48
20	Dimethylformamide	2.922	0.81	0.00	0.97
21	Dimethylacetamide	3.357	0.80	0.00	1.06
22	Dimethylsulfoxide	3.110	1.00	0.00	1.54
23	Propionaldehyde	1.770	0.35	0.00	0.37
24	Tetrahydrofuran	2.521	0.27	0.00	0.61
25	Triethylamine	3.008	0.02	0.00	0.64
26	Nitromethane	1.839	0.67	0.06	0.16
27	Nitroethane	2.313	0.66	0.00	0.17
28	Nitropropane	2.773	0.65	0.00	0.18
29	Methanol	0.916	0.35	0.35	0.52
30	Ethanol	1.462	0.29	0.29	0.52
31	1-Propanol	1.975	0.30	0.32	0.52
32	2-Propanol	1.750	0.21	0.29	0.53
33	2-Methyl-2-propanol	1.994	0.19	0.25	0.53
34	Trifluoroethanol	1.315	0.37	0.66	0.15
35	Hexafluoroisopropanol	1.370	0.47	1.11	0.02
36	Acetic acid	1.750	0.50	0.72	0.50
37	Aniline	3.934	0.76	0.20	0.42
38	N-Methylaniline	4.492	0.70	0.14	0.31
39	Phenol	3.641	0.77	0.69	0.23
40	Benzyl alcohol	4.162	0.71	0.43	0.51
41	*m*-Cresol	4.187	0.78	0.66	0.24
42	Ethylamine	1.646	0.17	0.00	1.00
43	Propylamine	2.083	0.22	0.00	1.00
44	Butylamine	2.575	0.26	0.00	1.00
45	Benzene	2.792	0.29	0.00	0.10
46	Toluene	3.343	0.29	0.00	0.11
47	Ethylbenzene	3.785	0.30	0.00	0.11
48	Propylbenzene	4.239	0.30	0.00	0.11
49	*p*-Xylene	3.867	0.28	0.00	0.12
50	Benzaldehyde	3.935	0.75	0.00	0.42
51	Benzonitrile	3.913	0.85	0.00	0.40
52	N,N-Dimethylaniline	4.753	0.57	0.00	0.26
53	Carbon tetrachloride	2.822	0.16	0.00	0.04

TABLE II

REGRESSION RESULTS FOR LOG k' DATA AT ALL TEMPERATURES

Column	T (°C)	SP_0	l	s	d	a	b	S.D.[a]	r^b	n^c
DB-1	150	−2.120	0.438	0.217	0.070	−0.035	[d]	0.057	0.996	53
		0.026[e]	0.007	0.030	0.023	0.035				
	115	−2.013	0.513	0.281	0.026	0.058	[d]	0.044	0.998	53
		0.020	0.006	0.023	0.018	0.027				
	80	−1.957	0.627	0.323	−0.015	0.215	[d]	0.029	0.999	53
		0.013	0.004	0.015	0.012	0.018				
	45	−1.877	0.769	0.401	−0.104	0.372	[d]	0.038	0.999	52[f]
		0.017	0.005	0.020	0.016	0.023				
DB-5	150	−2.180	0.446	0.356	0.052	−0.046	[d]	0.050	0.997	53
		0.023	0.006	0.026	0.020	0.031				
	115	−2.095	0.517	0.414	0.019	−0.017	[d]	0.043	0.998	53
		0.019	0.005	0.022	0.017	0.026				
	80	−2.030	0.620	0.451	−0.023	0.146	[d]	0.034	0.999	53
		0.015	0.004	0.018	0.014	0.021				
	45	−1.961	0.760	0.523	−0.093	0.309	[d]	0.042	0.999	52[g]
		0.019	0.005	0.022	0.017	0.026				
DB-1301	115	−2.293	0.526	0.636	−0.031	0.360	[d]	0.056	0.997	52[h]
		0.026	0.007	0.030	0.023	0.035				
	80	−2.149	0.621	0.723	−0.073	0.557	[d]	0.048	0.998	52[h]
		0.022	0.006	0.025	0.019	0.029				
	60	−2.093	0.695	0.842	−0.139	0.698	[d]	0.051	0.998	51[i]
		0.024	0.007	0.027	0.021	0.031				
	45	−2.083	0.765	0.902	−0.156	0.884	[d]	0.056	0.998	50[j]
		0.027	0.007	0.029	0.023	0.035				
DB-1701	150	−2.294	0.427	0.824	−0.035	0.267	−0.133	0.033	0.998	53
		0.018	0.004	0.022	0.014	0.021	0.027			
	115	−2.233	0.507	0.931	−0.077	0.463	−0.085	0.024	0.999	53
		0.013	0.003	0.016	0.010	0.016	0.020			
	80	−2.156	0.616	1.071	−0.133	0.669	−0.086	0.032	0.999	53
		0.017	0.004	0.021	0.013	0.021	0.026			
	60	−2.102	0.687	1.157	−0.163	0.838	−0.069	0.038	0.999	53
		0.021	0.005	0.025	0.016	0.025	0.031			
	45	−2.016	0.744	1.239	−0.214	0.963	−0.111	0.044	0.999	53
		0.023	0.006	0.028	0.018	0.028	0.035			
DB-17	150	−2.420	0.427	0.827	0.081	−0.068	[d]	0.047	0.997	51[k]
		0.021	0.006	0.025	0.019	0.039				
	115	−2.354	0.506	0.960	0.058	−0.003	[d]	0.041	0.998	51[k]
		0.019	0.005	0.022	0.017	0.034				
	80	−2.266	0.600	1.121	0.031	0.034	[d]	0.043	0.999	51[k]
		0.020	0.006	0.023	0.018	0.036				
	45	−2.152	0.723	1.343	−0.017	0.171	[d]	0.049	0.999	51[k]
		0.022	0.006	0.026	0.020	0.040				
DB-210	115	−2.149	0.399	1.454	0.220	−0.319	[d]	0.049	0.997	53
		0.022	0.006	0.025	0.020	0.030				
	80	−2.052	0.489	1.667	0.285	−0.274	[d]	0.057	0.997	53
		0.026	0.007	0.030	0.023	0.035				

TABLE II (*continued*)

Column	T (°C)	SP_0	l	s	d	a	b	S.D.[a]	r^b	n^c
	60	−1.996	0.551	1.815	0.332	−0.224	[d]	0.063	0.997	53
		0.028	0.008	0.033	0.025	0.038				
	45	−1.938	0.606	1.930	−0.367	−0.181	[d]	0.054	0.998	50[l]
		0.025	0.007	0.029	0.022	0.034				
DB-225	150	−2.367	0.371	1.512	0.001	0.436	−0.096	0.053	0.997	53
		0.028	0.007	0.034	0.022	0.034	0.043			
	115	−2.287	0.445	1.618	−0.021	0.584	0.004	0.036	0.999	53
		0.019	0.005	0.023	0.015	0.023	0.029			
	80	−2.194	0.537	1.794	−0.044	0.837	0.073	0.036	0.999	53
		0.019	0.005	0.023	0.015	0.023	0.029			
	45	−2.060	0.654	2.006	−0.091	1.128	0.144	0.038	0.999	53
		0.020	0.005	0.025	0.016	0.025	0.031			
DB-WAX	115	−2.245	0.416	1.819	0.095	1.365	[d]	0.077	0.996	49[m]
		0.037	0.010	0.041	0.031	0.048				
	80	−2.195	0.505	2.127	0.058	1.953	[d]	0.052	0.998	45[n]
		0.027	0.007	0.028	0.022	0.051				
	60	−2.119	0.559	2.325	0.022	2.198	[d]	0.052	0.998	41[o]
		0.028	0.007	0.030	0.024	0.052				
	45	−2.062	0.606	2.501	0.004	2.414	[d]	0.059	0.998	41[o]
		0.033	0.008	0.034	0.027	0.060				

[a] Overall average standard deviation.
[b] Correlation coefficient.
[c] Number of data points.
[d] These coefficients were found to be not significantly different from zero and were omitted in the final fit.
[e] Standard deviation of the coefficients.
[f–o] The following are solutes excluded in the final regression due to their being not eluted from the column or being outliers: [f] benzaldehyde; [g] N,N-dimethylaniline; [h] propionaldehyde; [i] propionaldehyde, ethylamine; [j] propionaldehyde, ethylamine, propylamine; [k] hexafluoroisopropanol, acetic acid; [l] cyclohexane, acetone, carbon tetrachloride; [m] triethylamine, ethylamine, propylamine, butylamine; [n] triethylamine, ethylamine, propylamine, butylamine, hexafluoroisopropanol, phenol, benzyl alcohol, *m*-cresol; [o] triethylamine, ethylamine, propylamine, butylamine, hexafluoroisopropanol, phenol, benzyl alcohol, *m*-cresol, benzonitrile, aniline, N-methylaniline, N,N-dimethylaniline.

Fig. 1, the l coefficients are about the same for DB-1, DB-5, DB-1301 and DB-1701 since these phases are primarily methylsilicones, but, as the percentage of phenyl or cyanopropyl groups increases (*i.e.* as the phases become more polar) their l coefficients decrease as expected [3]. DB-210 has the lowest l coefficient due to fluorine substitution which decreases the dispersive interactions with the solutes.

The signs and magnitudes of s make chemical sense. In general, the s coefficient increases as the phase becomes more polar. This agrees with the idea that an increase in solute dipolarity should cause a greater increase in retention in a more dipolar phase. The a coefficients for the DB-1, DB-5, DB-17 and DB-210 columns are small since these phases are known to be very weak acceptors of hydrogen bonds based on their effect on the spectra of Kamlet–Taft indicators that are able to donate hydrogen bonds [18]. In contrast, the a coefficients for the three cyano phases (DB-1301, DB-1701 and DB-225) are significant and as expected increase as the percentage of the 3-cyanopropyl group increases. DB-WAX is the most basic phase so it has the largest a coefficient. No phase has a big b coefficient because none has any hydrogen bond donor group. Although one might expect DB-

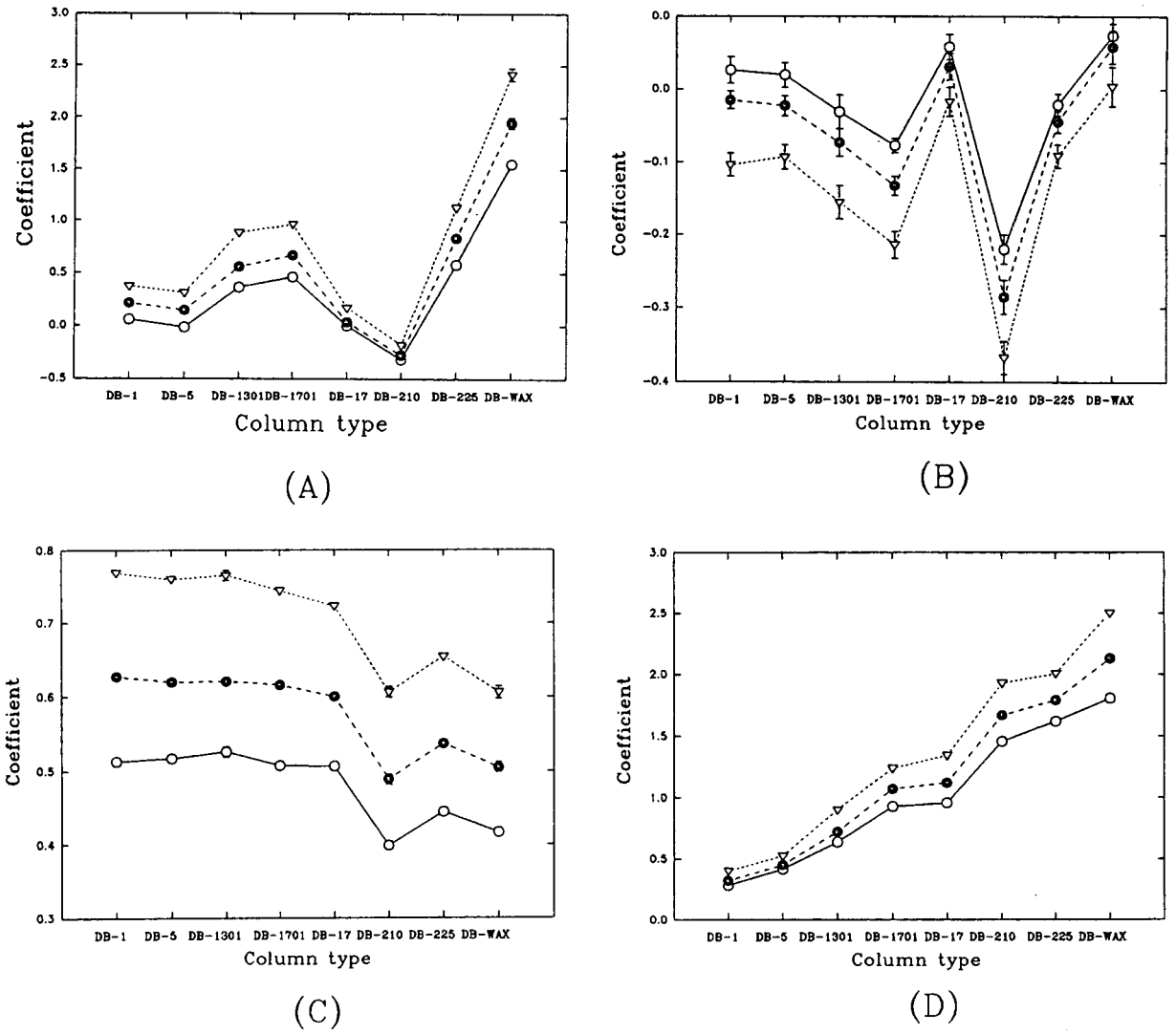

Fig. 1. Plots of LSER coefficients *vs.* column type at three temperatures: ▽ = 45°C; ◉ = 80°C; ○ = 115°C. (A) *a* coefficients; (B) *d* coefficients; (C) *l* coefficients; (D) *s* coefficients.

WAX to have some hydrogen bond donor ability, in fact, it does not have a significant *b* coefficient.

Temperature dependence of the LSER coefficients

We note that the LSER coefficients for all the phases change monotonically with temperature (Table III). Taking DB-1701 as an example, the LSER coefficients for this phase were plotted against $1/T$ (Fig. 2). We note that SP_0 and all other coefficients (*l*, *s*, *d*, *a* and *b*) are approximately linear with $1/T$ (Fig. 2). Regression of the LSER coefficients against $1/T$ gives rise to the temperature dependence of the LSER coefficients (eqn. 3, Table III).

$$X = X_A + X_B/T \quad (3)$$

where $X = SP_0$, *l*, *s*, *d*, *a* or *b*. Subscript A and B represent the intercept and slope of the temperature dependence of the coefficient, respectively.

TABLE III

TEMPERATURE DEPENDENCE OF THE LSER COEFFICIENTS

Eqn. 3 was the regression equation employed.

Column	X	X_A [a]	X_B [b]	S.D.[c]	r^2 [d]	n[e]
DB-1	SP_0	−2.635	240.53	0.004	0.998	4
	l	−0.651	451.77	0.001	1.000	4
	s	−0.340	235.15	0.004	0.999	4
	d	0.602	−224.38	0.003	1.000	4
	a	−1.269	522.78	0.004	1.000	4
DB-5	SP_0	−2.701	235.86	0.004	0.998	4
	l	−0.590	428.71	0.005	0.999	4
	s	−0.149	213.22	0.004	0.999	4
	d	0.431	−160.5	0.001	1.000	4
	a	−1.487	572.94	0.013	0.997	4
DB-1301	SP_0	−3.517	477.65	0.019	0.982	4
	–	−0.558	418.93	0.008	0.996	4
	s	−0.581	472.75	0.005	0.999	4
	d	0.576	−234.09	0.014	0.963	4
	a	−1.684	792.85	0.005	1.000	4
DB-1701	SP_0	−3.006	300.58	0.002	1.000	5
	l	−0.546	410.24	0.003	1.000	5
	s	−0.436	531.82	0.004	1.000	5
	d	0.445	−203.24	0.003	0.999	5
	a	−1.832	888.05	0.009	0.999	5
	b	−0.367	99.30	0.000	1.000	5
DB-17	SP_0	−3.237	344.20	0.005	0.999	4
	l	−0.470	378.90	0.003	1.000	4
	s	−0.739	660.34	0.009	0.999	4
	d	0.333	−106.71	0.000	1.000	4
	a	−0.793	306.54	0.000	1.000	4
DB-210	SP_0	−3.097	368.23	0.004	0.999	4
	l	−0.540	364.09	0.002	1.000	4
	s	−0.717	842.37	0.020	1.000	4
	d	0.454	261.50	0.001	1.000	4
	a	−1.119	298.40	0.001	1.000	4
DB-225	SP_0	−3.296	391.91	0.007	0.998	4
	l	−0.489	363.13	0.003	1.000	4
	s	−0.143	683.62	0.001	1.000	4
	d	0.278	−116.02	0.006	0.985	4
	a	−1.660	885.17	0.012	0.999	4
	b	−0.628	246.29	0.005	0.998	4
DB-WAX	SP_0	−3.405	427.62	0.003	1.000	4
	l	−0.439	332.63	0.002	1.000	4
	s	−1.350	1225.48	0.006	1.000	4
	d	0.392	−123.26	0.000	1.000	4
	a	−2.350	1516.16	0.008	1.000	4

[a] Intercept of the plot LSER coefficient *vs.* $1/T$.
[b] Slope of the plot LSER coefficient *vs.* $1/T$.
[c] Standard deviation of the fit.
[d] Correlation coefficient squared.
[e] Number of data points (temperatures).

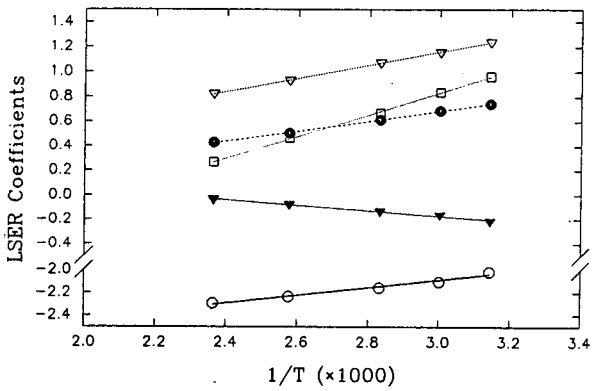

Fig. 2. Plots of (○) SP_0, (●) l, (▽) s, (□) a and (▼) d coefficients *vs.* $1/T$ for the DB-1701 column.

The temperature dependence of the LSER coefficients are very important when one compares the solute–solvent interaction strengths of solvents at different temperatures.

In addition the excellent linearity of these fits suggest that we can now predict retention of any solute whose parameters (log L^{16}, $\pi_2^{*,C}$, α_2^C and β_2^C) are known at any temperature for these eight columns. Since these eight columns are chemically the most commonly used stationary phases this suggests that the present results can be used as the basis for a broadly applicable optimization scheme for GC separations. For example, it should be possible to generate "window diagram" [19,20] as a function of temperature for each phase reported here for any set of solutes whose LSER parameters are known. The optimum temperature and column could then be selected *a priori*.

We note from Tables II and III that the temperature dependences of the LSER coefficients depend on the magnitudes of the coefficients, *i.e.* the strength of the specific interaction that the stationary phase can have. For example, the temperature dependence of the s coefficient (s_B) increases as the phase s coefficient increases, that is, s_B becomes larger as the phase becomes more dipolar. The magnitude of the temperature coefficients (X_A, X_B) of the LSER coefficients are very close for chemically similar solvents. For example, the temperature dependence of the l coefficient for DB-1 is very close to that of chemically similar non-polar stationary phases such as OV-101 and SE-30. A comparison of predicted l coefficients based on the temperature dependence of the l coefficient of DB-1 (shown in Table III) with experimentally measured l coefficients for similar non-polar stationary phases is shown in Table IV. Excellent agreement is observed. All slopes shown in Table III are positive except for that of the d coefficient. This sign is expected since an increase of temperature should decrease solute–solvent interactions and thus decrease retention. The d coefficient has a small (the smallest among all the LSER coefficients) but negative temperature dependence.

TABLE IV

COMPARISON OF PREDICTED AND EXPERIMENTAL l COEFFICIENT FOR NON-POLAR STATIONARY PHASES

Phase	Temperature (°C)	$l_{pred.}$ [a]	$l_{expt.}$ [b]	Δl [c]	Ref.[d]
SE-30	120	0.499	0.522	0.023	3
SE-30	121.4	0.494	0.502	0.0075	3
OV-101	60	0.706	0.690	−0.016	19
OV-101	70	0.666	0.647	−0.019	19
OV-101	80	0.629	0.608	−0.021	19

[a] Predicted l coefficient was calculated using the temperature dependence of the l coefficient of DB-1 ($l = -0.651 + 451.773/T$).
[b] Experimental l coefficient was obtained by regressing the retention data (log k', log V_g) from the indicated references with eqn. 1; V_g is the specific retention volume.
[c] $\Delta l = l_{expt.} - l_{pred.}$.
[d] Source of experimental data.

Thermodynamics of the retention process

Since k' is proportional to the infinite dilution distribution coefficient, ΔH^0 is the enthalpy for the corresponding process. Thus ΔH^0 is the enthalpy corresponding to the transfer of solute from a 1 mol/l gas phase state to a 1 mol/l solution both acting as hypothetically infinitely dilute mixtures. Ben Naim [21] refers to this as a "solvation" parameter.

By regressing log k' against $1/T$ (Van 't Hoff plot), the enthalpy of the retention process (ΔH^0) can be calculated from eqn. 4.

$$\frac{\mathrm{d} \log k'}{\mathrm{d}(1/T)} = -\frac{\Delta H^0}{2.303R} \tag{4}$$

where ΔH^0 is the enthalpy of the retention process and R is the gas constant. The relative standard deviation for the slope of log k' *vs.* $1/T$ is in general less than 2%. Therefore, the relative standard deviation for the enthalpy estimates is generally less than 2%.

The enthalpy estimates are given in Table V. We note that all enthalpies are negative as expected. Because some compounds did not elute at lower temperatures, we were not able to calculate the enthalpy for them.

From eqn. 4, we can also calculate the entropy ΔS^0 if we know the phase ratio ϕ. Because we do not know the phase ratio, we can only calculate an apparent entropy ($\Delta S'$). The apparent Gibbs free energy ($\Delta G'$) and entropy ($\Delta S'$) are defined as follows:

$$\begin{aligned}\Delta G' &= -RT \ln k' = -RT \ln K\phi \\ &= -RT \ln K - RT \ln \phi = \Delta G^0 - RT \ln \phi\end{aligned} \tag{5}$$

$$\begin{aligned}\Delta S' &= (\Delta H^0 - \Delta G')/T \\ &= (\Delta H^0 - \Delta G^0 + RT \ln \phi)/T \\ &= \Delta S^0 + R \ln \phi\end{aligned} \tag{6}$$

These equations are predicated on the assumption that the solute is retained by a pure partition process, that is, interfacial adsorption is assumed to be negligible. From the log k' and the enthalpy (ΔH^0) data, the apparent free energy and apparent entropy can be calculated from eqns. 5 and 6. We note that the apparent entropy ($\Delta S'$) is negative over the temperature range examined. The entropy of retention is expected to be negative due to the loss of some translational entropy when the solute interacts with the stationary phase.

Correlation of $\Delta G'$, ΔH^0 and $\Delta S'$ by linear solvation energy relationships

Log k' and $\Delta G'$ differ only by a factor of RT (eqn. 5). At a given temperature, the fitting coefficients for log k' and $\Delta G'$ using eqn. 1 will also differ only by a factor of RT. We show the regression results for $\Delta G'$ at only one temperature (80°C) for the purpose of comparison with the fitting coefficients for ΔH^0. The fitting results for both $\Delta G'$ and ΔH^0 are shown in Table VI. The fitting coefficients for $T\Delta S'$ can be calculated easily as $\Delta H^0 - \Delta G'$.

We must point out that all of the solute parameters (see Table I) used in eqn. 1 are free energy-based solute parameters. Whether free energy-based solute parameters can fit solution enthalpies and entropies is by no means guaranteed [22]. It is important to note that as pointed out by Hildebrand *et al.* [23] and by Leffler and Grunwald [16] that while many models of solution do an excellent job of correlating and predicting free energies they often fail quite badly in predicting enthalpies and entropies.

Fuchs *et al.* [24] correlated the ΔG^0, ΔH^0 and $T\Delta S^0$ of transfer of aliphatic and aromatic solutes from 2,2,4-trimethylpentane to aqueous solutions using free energy-based solute parameters. Their LSER fits of ΔH^0 and $T\Delta S^0$ are significantly poorer than are fits of ΔG^0. They concluded that this may be due to greater experimental errors in ΔH^0 and $T\Delta S^0$, since they are derived from differentiation of log k' with respect to $1/T$, rather than any intrinsic difficulty in handling "structural" contributions within the LSER framework.

We note that the standard deviation for the ΔH^0 regressions (see Table VI) are about three to seven times larger than those for the $\Delta G'$ regressions. Still the regression results for ΔH^0 are very acceptable. Although $\Delta G'$ differs from ΔG^0 by a constant $RT \ln \phi$ (eqn. 5), this constant only shows up in the SP_0 term. This will

TABLE V

ENTHALPY ($-\Delta H$) OF THE RETENTION PROCESS (kJ/mol)

No.	Compound	DB-1	DB-5	DB-1301	DB-1701	DB-17	DB-210	DB-225	DB-WAX
1	Cyclohexane	27.9	26.2	27.0	[a]	25.9	[a]	26.8	[a]
2	1-Hexene	25.0	23.3	25.2	24.7	23.2	23.9	25.9	22.7
3	Pentane	21.6	20.5	24.3	21.0	19.3	18.5	19.1	16.1
4	Hexane	29.3	24.5	28.1	25.6	24.1	22.6	23.0	18.9
5	Octane	34.1	33.0	36.4	32.9	31.2	29.8	30.2	26.0
6	Decane	43.3	40.8	43.6	42.1	39.3	38.5	39.8	34.8
7	Undecane	47.7	45.0	47.6	46.4	43.2	41.7	42.9	37.8
8	Tetradecane	61.3	58.5	61.0	59.4	56.5	52.1	53.3	48.0
9	Pentadecane	66.0	63.0	65.5	63.9	59.0	55.9	57.1	51.5
10	Ethyl acetate	27.2	25.5	29.7	29.2	28.5	29.9	30.9	29.6
11	Propyl acetate	31.1	28.8	33.4	33.0	33.4	33.5	35.0	32.7
12	Diethyl ether	23.7	21.2	23.4	24.3	22.3	22.6	25.4	19.6
13	Dipropyl ether	30.3	27.8	31.3	30.9	29.1	28.0	31.2	25.7
14	Dibutyl ether	38.4	35.3	38.8	39.2	36.8	35.0	37.3	34.1
15	Acetonitrile	[a]	20.3	24.8	26.2	24.9	27.6	28.5	32.3
16	Propionitrile	24.7	23.1	29.3	28.8	29.0	30.7	31.7	32.8
17	Acetone	20.1	19.3	28.1	24.4	24.9	26.8	27.1	26.2
18	2-Butanone	25.6	23.8	31.1	28.8	27.5	30.3	31.8	29.0
19	2-Pentanone	28.9	27.1	32.2	32.2	30.9	33.8	34.4	31.7
20	Dimethylformamide	32.3	31.4	37.4	38.9	37.5	41.2	41.4	42.4
21	Dimethylacetamide	35.6	33.3	40.9	42.0	41.2	45.3	44.8	45.2
22	Dimethylsulfoxide	34.6	32.3	40.9	41.1	41.3	44.6	45.2	49.6
23	Propionaldehyde	22.5	19.4	[a]	25.9	23.9	25.3	24.6	25.7
24	Tetrahydrofuran	26.3	24.1	32.5	27.8	28.0	27.9	29.4	30.3
25	Triethylamine	32.3	27.5	31.1	33.4	28.1	30.3	33.5	[a]
26	Nitromethane	25.7	25.8	27.9	29.7	28.4	30.6	32.1	[a]
27	Nitroethane	27.8	25.0	31.9	32.3	31.2	33.6	33.8	37.7
28	Nitropropane	30.5	30.2	35.7	35.3	34.4	36.5	36.5	39.5
29	Methanol	16.5	19.9	22.2	24.1	[a]	20.5	27.7	31.0
30	Ethanol	[a]	23.8	[a]	27.1	23.1	22.5	28.0	33.5
31	1-Propanol	24.0	27.5	29.3	29.9	25.4	28.0	[a]	37.2
32	2-Propanol	23.2	22.9	25.0	27.1	21.5	24.0	30.0	33.6
33	2-Methyl-2-propanol	23.6	22.1	26.6	27.2	24.5	25.7	29.8	32.8
34	Trifluoroethanol	27.8	23.7	35.1	34.6	23.9	25.2	33.1	44.1
35	Hexafluoroisopropanol	34.0	30.1	43.3	43.5	[a]	29.9	44.2	[a]
36	Acetic acid	[a]	30.0	40.8	[a]	[a]	[a]	[a]	[a]
37	Aniline	37.9	36.9	44.4	44.3	43.8	42.9	49.0	[a]
38	N-Methylaniline	41.4	38.5	47.0	46.6	47.3	45.4	50.6	[a]
39	Phenol	41.1	40.0	52.1	50.6	43.8	41.2	53.6	[a]
40	Benzyl alcohol	40.4	38.5	48.7	47.3	45.8	43.4	51.9	[a]
41	*m*-Cresol	44.1	[a]	55.6	54.8	47.3	45.1	56.9	[a]
42	Ethylamine	19.3	18.6	[a]	23.3	19.5	19.8	26.8	[a]
43	Propylamine	25.7	22.3	[a]	26.8	23.5	23.8	28.9	[a]
44	Butylamine	29.0	24.6	32.2	32.3	29.3	28.6	32.2	[a]
45	Benzene	27.1	25.4	28.5	28.4	28.1	26.4	29.4	29.2
46	Toluene	31.1	29.3	32.9	32.4	32.2	31.3	32.9	32.5
47	Ethylbenzene	34.7	32.8	36.4	36.1	35.8	34.6	36.8	35.4
48	Propylbenzene	38.5	36.1	40.1	40.3	39.3	37.8	40.2	38.2
49	*p*-Xylene	35.6	33.3	37.0	36.3	36.0	35.4	37.1	35.7
50	Benzaldehyde	37.3	36.1	41.4	41.3	42.5	41.7	43.3	47.6
51	Benzonitrile	39.0	37.0	43.3	42.4	44.6	43.9	45.2	[a]
52	N,N-Dimethylaniline	43.2	38.6	45.9	44.8	46.8	45.8	47.8	[a]
53	Carbon tetrachloride	27.1	26.9	27.8	27.1	27.3	[a]	26.5	27.8

[a] No data due to missing log k' data at various temperatures on the respective column.

not complicate any discussion of the solute–solvent interactions involved in the free energies and enthalpies.

We note that in both the $\Delta G'$ and ΔH^0 regressions, all LSER coefficients are negative except for the *d* coefficient which is positive (see Table VI, exceptions to this include DB-17 and DB-WAX which have negative *d* coefficients and DB-210 which has a small positive *a* coefficient for the $\Delta G'$ regression). This means that an increase in any solute parameter causes both $\Delta G'$ and ΔH^0 to become more negative (favorable). The magnitude of any coefficient for $\Delta G'$ is smaller than that for ΔH^0. This indicates that interactions (cavity dispersion, dipolar interaction, hydrogen bonding interactions) between

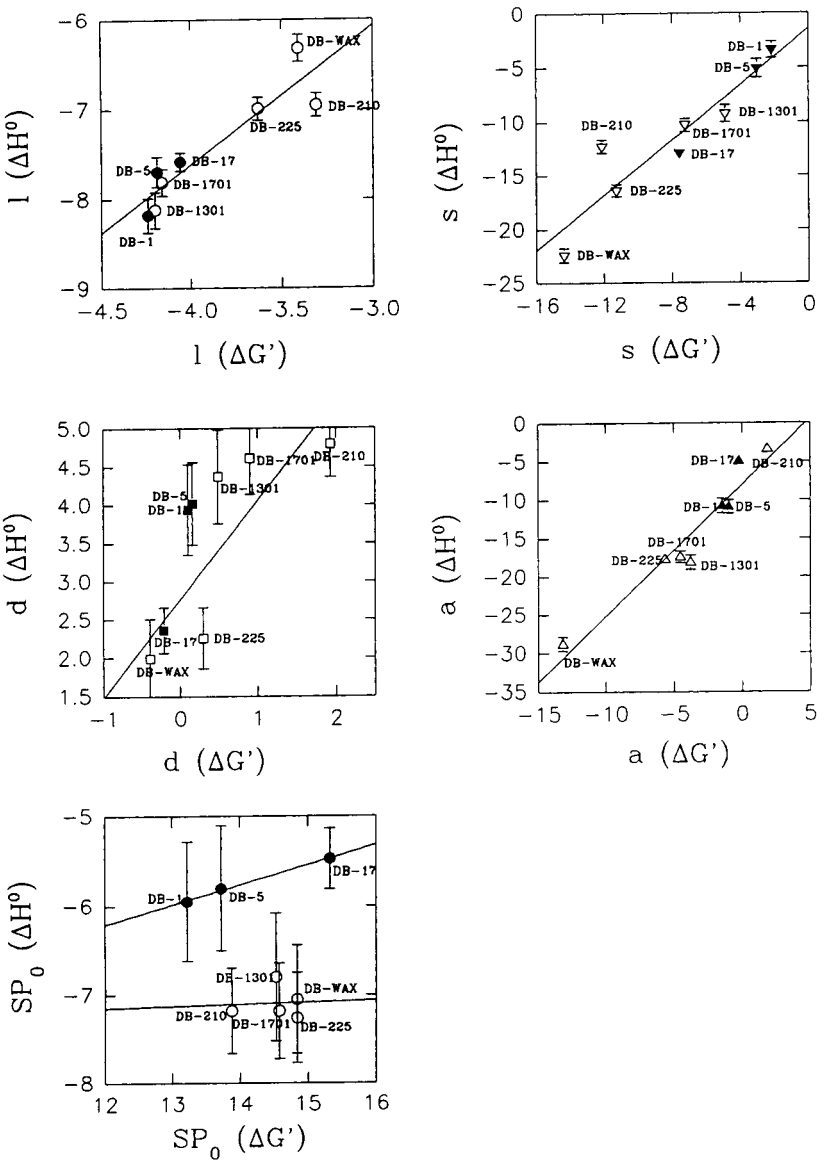

Fig. 3. Comparison of SP_0, *l*, *s*, *a* and *d* coefficients for the regressions of ΔH^0 and $\Delta G'$ against the LSER equations (eqns. 1 and 2). The solid lines represent the least squares regression lines. DB-1, DB-5 and DB-17 are represented by filled symbols. Other phases are represented by open symbols.

TABLE VI

REGRESSION RESULTS OF APPARENT $\Delta G'$ AND ΔH^0 *VS.* LSER PARAMETERS

Eqn. 1 is the regression equation employed. Apparent $\Delta G'$ calculated at column temperature 80°C, both $\Delta G'$ and ΔH^0 are in kJ/mol.

Column	SP_0		l		s		d		b		a		S.D.[a]		r^b		n^c
	$\Delta G'$	ΔH^0	$\Delta G'$	ΔH^0	$\Delta G'$	ΔH^0	$\Delta G'$	ΔH^0	$\Delta G'$	ΔH^0	$\Delta G'$	ΔH^0	$\Delta G'$	ΔH^0	$\Delta G'$	ΔH^0	
DB-1	13.23	−5.95	−4.24	−8.18	−2.18	−3.39	0.10	3.94	−[d]	–	−1.45	−10.74	0.20	1.45	0.999	0.990	50[e]
	0.09	0.67	0.03	0.19	0.10	0.77	0.08	0.59			0.12	0.95					
DB-5	13.73	−5.80	−4.19	−7.69	−3.05	−5.07	0.16	4.02	–	2.20	−0.98	−10.88	0.23	1.29	0.999	0.991	52[f]
	0.10	0.70	0.03	0.17	0.12	0.84	0.09	0.54		1.04	0.14	0.87					
DB-1301	14.53	−6.80	−4.20	−8.12	−4.89	−9.23	0.49	4.37	–	–	−3.77	−18.11	0.32	1.50	0.998	0.989	49[g]
	0.15	0.72	0.04	0.20	0.17	0.79	0.13	0.61			0.20	0.93					
DB-1701	14.58	−7.18	−4.16	−7.81	−7.24	−10.29	0.90	4.61	0.58	–	−4.52	−17.37	0.22	1.17	0.999	0.993	51[h]
	0.11	0.54	0.03	0.15	0.14	0.61	0.09	0.47	0.18		0.14	0.76					
DB-17	15.32	−5.47	−4.06	−7.58	−7.58	−12.87	−0.21	2.36	–	–	−0.23	−4.96	0.29	0.75	0.999	0.997	51[i]
	0.14	0.34	0.04	0.10	0.16	0.40	0.12	0.30			0.24	0.50					
DB-210	13.88	−7.18	−3.31	−6.95	−11.27	−16.41	1.93	4.79	–	–	1.85	−3.39	0.39	1.05	0.997	0.993	51[j]
	0.18	0.48	0.05	0.13	0.20	0.56	0.16	0.43			0.24	0.69					
DB-225	14.84	−7.26	−3.63	−6.99	−12.13	−12.27	0.30	2.26	−0.49	−5.88	−5.66	−17.71	0.24	0.96	0.999	0.995	51[k]
	0.13	0.51	0.03	0.13	0.16	0.62	0.10	0.40	0.20	0.79	0.16	0.65					
DB-WAX	14.84	−7.05	−3.41	−6.32	−14.38	−22.40	−0.39	1.99	–	–	−13.21	−28.79	0.35	1.11	0.998	0.993	39[l]
	0.18	0.61	0.05	0.15	0.19	0.65	0.15	0.52			0.34	0.90					

[a] Standard deviation of the fits.

[b] Correlation coefficient of the fits.

[c] Number of solutes included in the regressions.

[d] These coefficients were found to be not significantly different from zero and were omitted from the final fit.

[e–l] The following lists the solutes excluded in the final regressions due to their missing $\Delta G'$ or ΔH^0 values or being outliers: [e] acetonitrile, ethanol, acetic acid; [f] *m*-cresol; [g] ethanol, propionaldehyde, ethylamine, propylamine; [h] cyclohexane, acetic acid; [i] methanol, acetic acid; [j] cyclohexane, acetic acid; [k] 1-propanol, acetic acid; [l] cyclohexane, triethylamine, nitromethane, acetic acid, aniline, N-methylaniline, phenol, benzyl alcohol, *m*-cresol, ethylamine, propylamine, butylamine, benzonitrile, N,N-dimethylaniline.

the solute and the stationary phase produce large favorable negative enthalpies but unfavorable negative entropies.

In order to examine the relative contribution of the enthalpy and entropy to retention in terms of different kinds of interactions, we compare the LSER coefficients for $\Delta G'$ and ΔH^0. The most important contributions to retention are from the l log L^{16} term and the $s\pi_2^{*,C}$ term (keep in mind that the log L^{16} parameter has a much larger range than the solvatochromic parameters). Although these two terms also give unfavorable entropies, their contributions to enthalpies are much larger and outweigh the unfavorable entropy contributions. We note that for ΔH^0 the hydrogen bonding term $a\alpha_2^C$ gives very large and favorable enthalpies. However, this favorable enthalpy term must be largely compensated by the unfavorable corresponding $a\alpha_2^C$ term in the entropy term ($-T\Delta S'$) because the $a\alpha_2^C$ term in the $\Delta G'$ regression is relatively small except for DB-WAX and DB-225. No significant enthalpy contribution comes from the $b\beta_2^C$ term except for the DB-225 phase. This term does not produce any significant contribution to the free energy. In contrast to all other terms, the $d\delta_2$ term except for the DB-WAX and DB-17 phases gives unfavorable enthalpies and favorable entropies thus resulting in a small unfavorable contribution to the free energies.

We compare the LSER regression coefficients for both $\Delta G'$ and ΔH^0 in Fig. 3. In these plots the solid lines represent the least squares regression lines. We see that there are approximately linear relationships between the LSER coefficients, especially for the l, s and a coefficients. DB-1, DB-5 and DB-17 are methyl silicones of different percentages of phenyl substitution [8], we used filled symbols to identify these phases in the plots. We note that in all plots they fall on the regression lines for all phases except for the SP_0 plot in which these three phases form a separate line. DB-1301, DB-1701 and DB-225 are methylsilicones of different percentages of cyanopropylphenyl substitution. As shown in Fig. 3 there are systematic variations in SP_0 based on $\Delta G'$ and ΔH^0. While the SP_0 term does not influence the chromatographic selectivity, that is, the ratio of k' for two solutes, it clearly must be encoding some information as to the net strength of the interaction between the solutes and the stationary phase. The relationship between $SP_0(\Delta H^0)$ and $SP_0(\Delta G')$ shown in Fig. 3 is also complicated by the fact that ΔH^0 is independent of the phase ratio (ϕ) while $\Delta G'$ depends on ϕ which varies from column to column. They also fall on the same regression lines for all phases.

The data presented in this paper regarding the enthalpy, entropy and free energy of the chromatographic retention process is very relevant to Trouton's rule for enthalpy–entropy relationships of vaporization of pure liquids at their normal boiling point [25], Barclay and Butler's [26] and Frank and Evans' [27,28] studies of enthalpy–entropy of vaporization of pure liquids at 25°C, and related studies [29,30]. The fact that the l, s and a coefficients for the $\Delta G'$ and ΔH^0 regressions correlate is very important. It means that contributions from the various stationary phase–solute interactions to the enthalpy and free energy are linearly related. It will have important implications as to the existence of enthalpy–entropy compensations in the chromatographic retention process which will be described in a subsequent study [31].

ACKNOWLEDGEMENT

This work was supported in part by grants to the University of Minnesota from the National Science Foundation and the Petroleum Research Foundation.

REFERENCES

1 C.F. Poole and S.K. Poole, *Chromatography Today*, Elsevier, Amsterdam, New York, 1991.
2 T. Kuwana, *Physical Methods in Modern Chemical Analysis*, Academic Press, New York, 1978.
3 J. Li, Y. Zhang and P.W. Carr, *Anal. Chem.*, 64 (1992) 210.
4 J. Li, Y. Zhang, A.J. Dallas and P.W. Carr, *J. Chromatogr.*, 550 (1991) 101.
5 J. Li, Y. Zhang, H. Ouyang and P.W. Carr, *J. Am. Chem. Soc.*, 114 (1992) 9813.
6 J. Li, Y. Zhang and P.W. Carr, *Anal. Chem.*, 65 (1993) 1969.

7 M.H. Abraham, G.S. Whiting, R.M. Doherty and W.J. Shuely, *J. Chem. Soc., Perkin Trans. 2*, (1990) 1451.
8 M.H. Abraham, G.S. Whiting, R.M. Doherty and W.J. Shuely, *J. Chem. Soc., Perkin Trans. 2*, (1990) 1851.
9 M.H. Abraham, G.S. Whiting, R.M. Doherty and W.J. Shuely, *J. Chromatogr.*, 518 (1990) 329.
10 M.H. Abraham, G.S. Whiting, R.M. Doherty and W.J. Shuely, *J. Chromatogr.*, 587 (1991) 213.
11 M.H. Abraham, G.S. Whiting, R.M. Doherty and W.J. Shuely, *J. Chromatogr.*, 587 (1991) 229.
12 M.H. Abraham, I. Hamerton, J.B. Rose and J.W. Grate, *J. Chem. Soc., Perkin Trans. 2*, (1991) 1417.
13 M.H. Abraham and G.S. Whiting, *J. Chromatogr.* 594 (1992) 229.
14 C.F. Poole, T.O. Kollie and S.K. Poole, *Chromatographia*, 34 (1992) 281.
15 T.O. Kollie, C.F. Poole, M.H. Abraham and G.S. Whiting, *Anal. Chim. Acta*, 259 (1992) 1.
16 J.E. Leffler and E. Grunwald, *Rates and Equilibria of Organic Reactions*, Wiley, Inc. New York, 1963.
17 J. Li, A.J. Dallas and P.W. Carr, *J. Chromatogr.*, 517 (1990) 103.
18 J.E. Brady, *Ph.D. Thesis*, University of Minnesota, Minneapolis, MN, 1984.
19 C.-F. Chien, R.J. Laub and M.M. Kopeecni, *Anal. Chem.*, 52 (1980) 1407.
20 R.J. Laub and J.H. Purnell, *Anal. Chem.*, 48 (1976) 799.
21 A. Ben-Naim, *Solvation Thermodynamics*, Plenum Press, New York, 1987.
22 M.J. Hait, C.L. Liotta, C.A. Eckert, J. Li and P.W. Carr, *J. Phys. Chem.*, submitted for publication.
23 J.H. Hildebrand, J.M. Prausnitz and R.L. Scott, *Regular and Related Solutions; The Solubility of Gases, Liquids and Solids*, Van Nostrand Reinhold, New York, 1970.
24 R. Fuchs, M.H. Abraham, M.J. Kamlet and R.W. Taft, *J. Phys. Org. Chem.*, 2 (1989) 559.
25 F. Trouton, *Phil. Mag.*, 18 (1884) 54.
26 I.M. Barclay and J.A.V. Butler, *Trans. Faraday Soc.*, 34 (1938) 1445.
27 H.S. Frank, *J. Chem. Phys.*, 13 (1945) 493.
28 H.S. Frank and M.W. Evans, *J. Chem. Phys.*, 13 (1945) 507.
29 D.H. Everett, *J. Chem. Soc.*, (1960) 2566.
30 L. Nash, *J. Chem. Educ.*, 61 (1984) 981.
31 J. Li and P.W. Carr, *J. Chromatogr.*, in press.

Journal of Chromatography A, 659 (1994) 381–387
Elsevier Science B.V., Amsterdam

CHROM. 25 604

Selective enhancement for neon detection in a helium discharge photoionization detector

Hiroshi Ogino* and Yoko Aomura

Toyo Sanso Co. Ltd., Technical Research Laboratory, 3-3, Mizue-cho, Kawasaki, Kanagawa 210 (Japan)

(First received August 9th, 1993; revised manuscript received September 29th, 1993)

ABSTRACT

The helium discharge photoionization detector (HD-PID) is a very reliable and highly sensitive gas chromatographic detector for the determination of trace amounts of inorganic gases. However, the sensitivity of the HD-PID is poor for neon, similarly to a helium ionization detector (HID). The improvement of the HD-PID sensitivity, especially for neon, was studied. When helium containing 3.8 ppm (v/v) of neon was used as the helium discharge gas, the results obtained showed that the sensitivity for neon could be improved sixfold compared with that of the HD-PID under ordinary operating conditions.

INTRODUCTION

In the trace determination of inorganic compounds by gas chromatography, highly sensitive and universal detectors, such as the helium ionization detector (HID) [1] and the helium discharge photoionization detector (HD-PID) [2], have been widely used [3–9]. The HID seems to be currently the most sensitive detector for inorganic compounds such as noble gases (except neon), oxygen, nitrogen and carbon monoxide. However, the characteristics of the HID response are extremely affected by the purity of the helium carrier gas, its flow-rate, the applied potential, helium pressure, the temperature of the detector, etc.

Many efforts have been made to evaluate and improve the characteristics of the detector response, such as sensitivity, polarity and dynamic linear range, during the past decade. For example, the effects of helium purity and of adding hydrogen to the helium carrier gas were examined in order to evaluate the HID responses such as sensitivity and the polarity of response for helium, neon, argon, nitrogen, oxygen, methane and carbon monoxide [10–14]. Other experiments provided optimum conditions for operating the HID at maximum sensitivity and indicated that if the detector was designed with a very small volume, the response of the HID would be high and positive to all gases [15]. Further, some experiments were carried out in order to evaluate the effects of adding gaseous additives to the helium carrier gas. The results showed that if the applied voltage of the HID is more than 350 V, the addition of hydrogen, argon, oxygen or nitrogen gives an increase in the HID response, whereas if the applied voltage is less than 350 V, the HID response decreases [10]. However, it is essential that the HID is operated with caution because of the β-rays from tritium. On the other hand, the HD-PID does not use a radioactive material and has a similar sensitivity to that of the HID.

In the past few years, we have successfully developed techniques for the determination of trace impurities such as inorganic gaseous compounds in oxygen [6], hydrogen [7] and nitrogen [8] by means of a gas chromatograph combined with an HD-PID and precolumns packed with

* Corresponding author.

0021-9673/94/$07.00
SSDI 0021-9673(93)E1026-V

Cu–Zn catalyst for oxygen, $LaNi_5$ hydrogen storage alloy for hydrogen and Ti–Mn hydrogen storage alloy for nitrogen; these precolumns were used to remove the main gas (base gas) completely from a sample. However, the sensitivity of the HD-PID for neon was still poor and similar as that of the HID and the determination of trace levels of neon remained a difficult problem in gas analysis.

The HD-PID is based on the following principles: (1) a discharge in helium under atmospheric pressure emits radiation with a wavelength in the range *ca.* 600–1100 Å [2]; and (2) the photons emitted are used to ionize most kinds of compounds that have a lower ionization potential than that of helium.

A glow discharge is maintained by the emission of electrons from the cathode by a number of processes such as positive ion bombardment, photoelectric emission and collisions with excited atoms [1]. The ionization mechanism is considered to be based on the Penning effect, but has not yet been fully explored. On the other hand, the ionization potential of neon is 21.56 eV, which is close to that of helium (25.58 eV) and higher than that of metastable helium (He*, 19.8 eV), so that the response for neon is extremely poor compared with those of other gases, which have lower ionization potentials than helium. Therefore, if the HD-PID is used for inorganic gas analysis under ordinary operating conditions, the relative sensitivity for neon is less than 1% of that for other gases such as argon, nitrogen, oxygen and methane; the sensitivity of the HD-PID for neon was similar to that of a thermal conductivity detector.

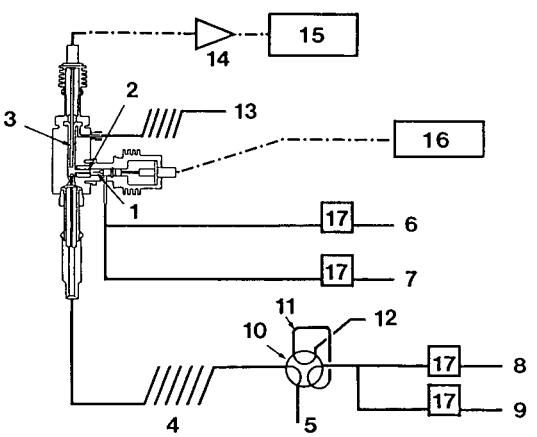

Fig. 1. Flow diagram of experimental apparatus. 1, 2 = Glow discharge electrodes; 3 = ion collector electrode; 4 = analytical column; 5 = helium carrier gas; 6 = neon source gas; 7 = helium discharge gas; 8 = standard gas; 9 = helium as diluting gas; 10 = six-port rotary valve with air actuator; 11 = 1.23-ml sample loop; 12, 13 = gas outlets; 14 = amplifier; 15 = computerized integrator; 16 = high-voltage power supply; 17 = mass flow controller.

In recent years, we have investigated the application of the GC–HD-PID system to the determination of trace gases in pure gases such as hydrogen, nitrogen and oxygen. In the course of these studies, it was found that the neon sensitivity could be improved by adding a trace amount of neon to the helium discharge gas. This paper describes the selective enhancement of neon detection in the HD-PID.

EXPERIMENTAL

A gas chromatograph equipped with an HD-PID (GC-263-30; Hitachi, Tokyo, Japan) was used. A flow diagram is shown in Fig. 1. Helium (99.99999%; Toyo Sanso, Kanagawa, Japan) was used as the carrier and discharge gas. Two gas purifiers (Model PH; Valco, Houston, TX, USA) were installed in the carrier gas and the discharge gas lines in order to prevent air contamination of the helium and gas mixtures as shown in Fig. 1. The following standard gases (Toyo Sanso) were used to evaluate the detector response under different conditions: (1) 1.02% and 107 ppm (v/v) neon in helium; (2) 1020 ppm (v/v) neon, 960 ppm (v/v) argon, 990 ppm (v/v) krypton and 1050 ppm (v/v) xenon in helium; and (3) 9.9 ppm (v/v) methane, 10.2 ppm (v/v) carbon monoxide and 9.7 ppm (v/v) oxygen in helium. The helium used in this experiment was previously confirmed to be free of neon by GC–MS (QP-300; Shimadzu, Kyoto, Japan). Mass flow controllers (Model 400; STEC, Kyoto, Japan) were used to prepare the desired concentration of neon in helium, which was fed as the discharge gas containing several to several hundred ppm of neon in helium. The concentrations of the prepared gas mixtures were calculated from the ratios of the flow-rates provided by the

mass flow controllers. In a similar manner, gas mixtures with various concentrations of neon, argon, nitrogen, etc., were prepared from standard gases.

RESULTS AND DISCUSSION

Effects of neon added to discharge gas

The effects of adding neon to the discharge gas were investigated with the use of helium containing neon at concentrations in the range 0–420 ppm (v/v). In order to evaluate the effect of neon addition, a gas mixture containing 7.5 ppm (v/v) neon, 6.2 ppm (v/v) krypton and 2.1 ppm (v/v) xenon in helium was prepared by diluting the standard gas with pure helium and was used as the sample gas. As shown in Fig. 2, the detector response to neon in the sample gas increased with increase in neon concentration in the discharge gas, then decreased rapidly after reaching a maximum response at around 3.6 ppm (v/v) neon and finally remained almost constant over the experimental range. However, the response for other gases such as krypton and xenon did not show this effect. This indicates that the addition of neon to the discharge gas selectively enhanced the response for neon in the sample gas.

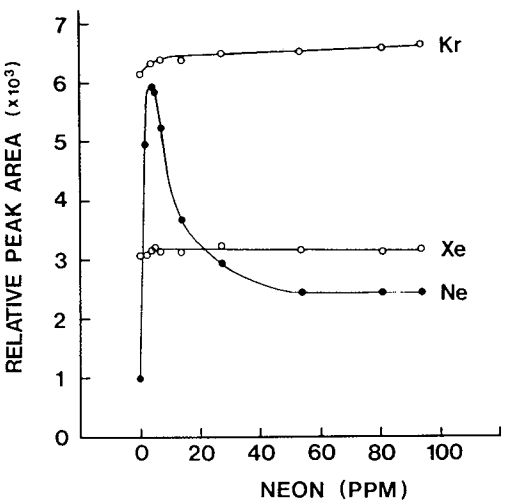

Fig. 2. Effect of neon concentration in helium as discharge gas on detector response. Sample gas contained 18.7 ppm (v/v) neon, 5.3 ppm (v/v) krypton and 5.7 ppm (v/v) xenon in helium. For other conditions, see text.

Analytical characteristics of enhanced HD-PID

To evaluate the characteristics of the enhanced HD-PID, a series of experiments were conducted with the following optimum GC conditions: analytical column, 3 m × 3 mm I.D. stainless-steel tube packed with molecular sieve 5A (177–250 μm); carrier gas, helium at 50 ml/min; oven temperature, 70°C; detector temperature, 100°C; discharge potential, 750 V; discharge gas, helium containing 3.6 ppm of neon at 40 ml/min; and sample loop, 1.23 ml. Using these HD-PID operating conditions, calibration graphs in order to confirm the linearity of response were determined for neon, argon, krypton and xenon over the wide range of 0–1000 ppm (v/v). The calibration graphs deviated from a straight line at concentrations above *ca.* 600 ppm (v/v) for argon, krypton and xenon, as shown in Fig. 3. The linearity profiles for these gases were similar to that obtained using pure helium as the discharge gas [6–9]. For neon, however, the detector response deviated significantly from a straight line, *i.e.*, the response is not proportional to the concentration of neon in the samples; if it had been then the dashed line in Fig. 3 would have

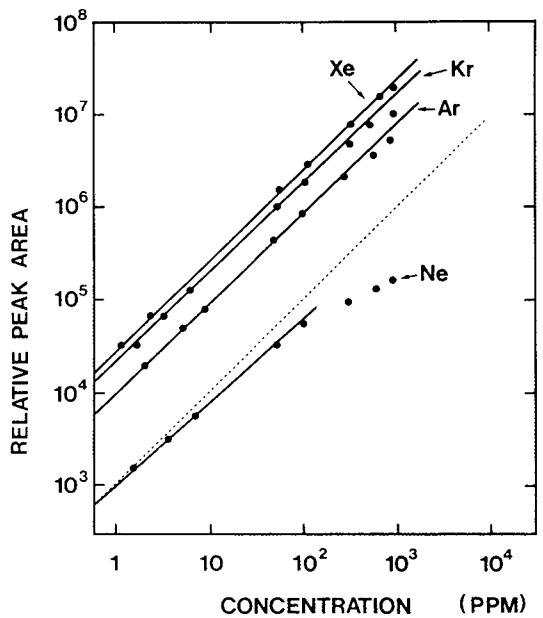

Fig. 3. Log–log calibrations for methane, neon, argon, nitrogen, carbon monoxide, oxygen, krypton and xenon. For GC conditions, see text.

been followed. The photoionization process with neon seems to be different to those with the other gases, as described below.

Consideration of neon enhancement

From the relationship between the detector response and the concentration of neon in the sample gas, it might be suggested that the enhancement for neon might not be due to the increase in the total intensity of photons emitted from both He* and Ne* as the effect of neon addition could not be clearly observed for krypton and xenon. Also, only photons emitted from Ne*, which has a potential energy corresponding to the excitation of neon, could be efficiently produced. The excited neon molecules emit electrons via reaction 2.3. The electrons can be detected as the signal of the detector. The mechanism of this enhancement is still unknown. As one possibility, the neon enhancement may be considered to be due to the following processes:

(1) He–Ne mixture discharge process:

$$He \longrightarrow He^*, Ne \longrightarrow Ne^* \quad (1.1)$$

$$He^* + Ne \longrightarrow Ne^* \quad (1.2)$$

$$Ne^* \longrightarrow Ne + h\nu_{neon} \quad (1.3)$$

(2) photoionization process for neon in a sample:

$$Ne_{sample} + h\nu_{helium} \longrightarrow Ne^*_{sample} \quad (2.1)$$

$$Ne_{sample} + h\nu_{neon} \longrightarrow Ne^*_{sample} \quad (2.2)$$

$$Ne^*_{sample} \longrightarrow Ne^+_{sample} + e^- \quad (2.3)$$

Hence the response of the detector for neon is expected to be the sum of the response obtained from the excited neon (Ne^*_{sample}) produced through reactions 2.1 and 2.2. This means that the intensity of emission, which can be absorbed by neon molecules in sample gases, may be increased more selectively and intensively than that of the emission obtained from only a helium discharge. However, it is not clear why only the neon response could be enhanced by the addition of neon into the discharge gas.

Analytical performance of enhanced HP-PID

The calibration graphs for neon, argon, oxygen, nitrogen, krypton, carbon monoxide, methane and xenon showed perfect linearity at concentrations below 10 ppm (v/v), as shown in Fig. 4: the calibration curve for neon was ap-

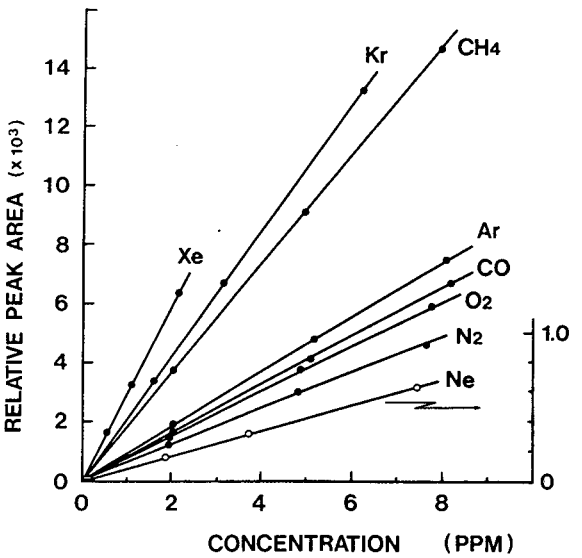

Fig. 4. Calibrations for neon, argon, nitrogen, carbon monoxide, oxygen, krypton and xenon in the range 0–10 ppm (v/v). The scale of peak area for neon is expanded five times relative to the others. For GC conditions, see text.

TABLE I

COMPARISON OF ANALYTICAL DATA OBTAINED WITH THE IMPROVED HD-PID AND ORDINARY HD-PID

Detector	Peak area corresponding to 2 ppm (v/v) of each component (arbitrary units)							
	Ne	O_2	Ar	N_2	Kr	CH_4	CO	Xe
Enhanced HD-PID (*A*)	1758	14 924	19 283	13 197	42 759	37 612	16 729	60 838
Ordinary HD-PID (*B*)	293	18 511	22 677	16 515	48 845	45 531	21 039	69 874
Ratio *A*/*B*	6.0	0.81	0.85	0.80	0.88	0.83	0.80	0.87

TABLE II

REPRODUCIBILITY OF THE DETERMINATION OF ppm LEVELS OF NEON, OXYGEN, ARGON, NITROGEN, KRYPTON, METHANE, CARBON MONOXIDE AND XENON IN HELIUM

Run No.	Peak area of components detected (arbitrary units)							
	Ne (1.87 ppm, v/v)	O_2 (1.94 ppm, v/v)	Ar (2.02 ppm, v/v)	N_2 (1.92 ppm, v/v)	Kr (1.56 ppm, v/v)	CH_4 (1.98 ppm, v/v)	CO (2.04 ppm, v/v)	Xe (0.53 ppm, v/v)
1	1564	14 784	19 436	12 931	33 428	37 137	16 991	15 724
2	1712	14 645	19 586	12 792	33 435	36 835	17 195	16 921
3	1720	14 278	19 325	12 789	33 220	37 133	17 285	16 267
4	1684	14 254	19 419	12 481	33 313	37 278	17 367	16 800
5	1588	14 461	19 709	12 725	33 507	36 744	16 969	15 373
6	1583	14 361	19 423	12 689	33 143	37 228	16 764	15 832
7	1590	14 761	19 423	12 558	33 446	37 732	17 104	16 712
8	1673	14 580	19 510	12 527	33 376	37 134	16 832	15 082
9	1684	14 343	19 583	12 721	33 302	37 791	16 772	16 383
Average	1644	14 496	19 490	12 690	33 352	37 223	17 031	16 122
S.D.	58.3	191.9	110.7	136.7	111.2	331.4	209.0	616.5
R.S.D. (%)	3.55	1.32	0.57	1.08	0.33	0.89	1.23	3.82
Detection limit ($S/N = 3$)	0.22	0.07	0.02	0.05	0.02	0.02	0.09	0.13

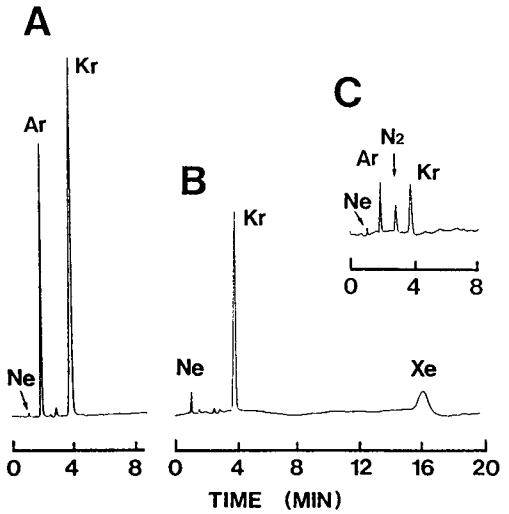

Fig. 5. Typical gas chromatograms. Sample gas: (A) 2.7 ppm (v/v) neon, 2.4 ppm (v/v) argon and 2.7 ppm (v/v) krypton in helium; (B) 1.9 ppm (v/v) neon, 1.5 ppm (v/v) krypton and 0.5 ppm (v/v) xenon in helium; (C) 0.2 ppm (v/v) neon, 0.4 ppm (v/v) argon, 0.2 ppm (v/v) nitrogen and 0.2 ppm (v/v) krypton in helium. For GC conditions, see text.

proximately linear at concentrations below 10 ppm (v/v). The sensitivities for several inorganic gases obtained with the present method were compared with those given by the ordinary method (without neon addition) and are summarized in Table I. The results show that only the neon sensitivity could be enhanced by the addition of neon to the discharge gas and that the sensitivity for the other gases decreased slightly, but there was not much difference between the results with the present and ordinary operating conditions [6–9].

The improved HD-PID could have sufficient sensitivity to be used as a detector for trace amounts of inorganic gas impurities including neon by the use of the present operating conditions. Typical gas chromatograms of standard gas mixtures obtained by (A) the ordinary method and (B and C) the present method are shown in Fig. 5. The minimum concentration of neon that could be detected with the ordinary operating conditions was a few ppm (v/v). By adding neon to the helium discharge gas, however, trace levels of neon in the sample gas could be detected. Analytical data such as the reproducibility and detection limits obtained with the present operating conditions are given in Tables II and III.

CONCLUSIONS

The improved HD-PID, which used a neon–helium mixture as the discharge gas, has a neon sensitivity *ca.* six times higher than that obtained by using pure helium as the discharge gas. It was confirmed that the improved HD-PID could be successfully and easily applied with an ordinary

TABLE III

REPRODUCIBILITY OF THE DETERMINATION OF TRACE LEVELS OF NEON, ARGON, KRYPTON, AND XENON IN HELIUM

Run No.	Peak area of components detected (arbitrary units)			
	Ne (0.2 ppm, v/v)	Ar (0.4 ppm, v/v)	Kr (0.2 ppm, v/v)	Xe (0.2 ppm, v/v)
1	178	4148	4951	7635
2	214	4346	5186	6898
3	180	4061	5407	7766
4	176	3831	4940	6997
5	170	3798	5102	7345
6	166	3644	4917	5825
7	190	3424	5070	6514
Average	182	3893	5082	6997
S.D.	14.9	291.1	161.0	625
R.S.D. (%)	8.16	7.48	3.17	8.94

gas chromatograph and that the determination of neon at sub-ppm (v/v) levels is possible. Further investigations will be made to understand this phenomenon of neon enhancement.

REFERENCES

1 J.E. Lovelock, *Anal. Chem.*, 33 (1962) 162.
2 M. Yamane, *J. Chromatogr.*, 14 (1964) 355.
3 C.H. Hartman and K.P. Dimick, *J. Gas Chromatogr.*, May (1964) 163.
4 C.A. Seitz, *US Bur. Mines Rep. Invest.*, 1985, No. 8941.
5 R.A. Carpio and E. Lindt, *Semicond. Int.*, May (1989) 164.
6 H. Ogino, Y. Aomura, M. Komuro and T. Kobayashi, *Anal. Chem.*, 61 (1989) 2237.
7 H. Ogino, Y. Aomura and M. Mizuno, *Anal. Chem.*, 62 (1990) 994.
8 H. Ogino, Y. Aomura and T. Seki, *Anal. Chem.*, 63 (1991) 1376.
9 H. Ogino and K. Hirako, *Am. Lab.*, February (1993) 40 UU.
10 F.F. Andrawes and E.K. Gibson, *Anal. Chem.*, 50 (1980) 1146.
11 F.F. Andrawes, R.S. Brazell and E.K. Gibson, *Anal. Chem.*, 52 (1980) 891.
12 F.F. Andrawes and E.K. Gibson, *Anal. Chem.*, 52 (1980) 846.
13 J. Lasa and E. Bros, *J. Chromatogr. Sci.*, 12 (1974) 807.
14 F.F. Andrawes, T.B. Byers and E.K. Gibson, *J. Chromatogr.*, 205 (1981) 419.
15 F.F. Andrawes and P. Deng, *J. Chromatogr.*, 349 (1985) 405.

Journal of Chromatography A, 659 (1994) 389–394
Elsevier Science B.V., Amsterdam

CHROM. 25 642

Enantiomeric composition of terpenic hydrocarbons in essential oils from *Juniperus communis* L.

D. Sybilska*, M. Asztemborska and J. Kowalczyk

Institute of Physical Chemistry, Polish Academy of Sciences, Kasprzaka 44/52, 01-224 Warsaw (Poland)

R.J. Ochocka

Medical Academy, Faculty of Pharmacy, Gen. Hallera 107, 80-416 Gdańsk (Poland)

L. Ossicini and G. Perez

Istituto di Chromatografia del CNR, Area della Ricerca di Roma, 00016 Monterotondo Scalo (Italy)

(First received July 6th, 1993; revised manuscript received October 12th, 1993)

ABSTRACT

α-Cyclodextrin complexation under appropriate conditions of partition gas chromatography has been applied for chiral discrimination of the hydrocarbon fraction of juniper oils of various origins. The essential oils under investigation were obtained from crushed juniper berries and leaves cultivated on plantations in Austria, Italy and Poland. It was found that the main component of the hydrocarbon fraction of almost all the juniper oils under investigation was a laevorotatory enantiomer, *S*(−)-α-pinene, and that the ratio of its *S* to *R* enantiomer may vary greatly (from 5 to 1) depending on the origin of the material, *i.e.* the part of the plant (berries or leaves), and the place of its cultivation.

INTRODUCTION

The chemical composition of essential oils of juniper has been the subject of numerous studies [1–6]. A comparison between the chemical composition of juniper oil and an alcoholic extract of juniper berries has also been recently reported [7]. It has been stated that their main characteristic component is α-pinene with a wide range of other monoterpene hydrocarbons, sesquiterpene hydrocarbons and some oxygenated compounds.

Many of the terpenes used therapeutically or as flavour and fragrance materials are chiral compounds, and thus they can be present in natural mixtures in one or two enantiomeric forms and in various proportions. Furthermore, it is known that the stereospecificity of drug action is related to the molecular asymmetry of the component receptors of the human body. As a consequence, the diastereomers and enantiomers of chiral drugs have significantly different biological activities. This very important problem has not been explored sufficiently as yet, mainly because of the lack of analytical tools suitable to monitor the contents of enantiomers.

In this matter we have previously found that, by using α-cyclodextrin (α-CD) under appropriate conditions of classical partition gas chromatography (GC), very efficient separations of α-pinene, β-pinene and camphene into enantiomers can be achieved [8,9]. Attempts have also

* Corresponding author.

0021-9673/94/$07.00
SSDI 0021-9673(93)E1082-B

been made to develop this method for chiral recognition of hydrocarbons (mentioned above) and limonene, when they are present in more complex artificial mixtures or some natural ones, *i.e.* silver fir needle and pine needle oils [10].

Another method has recently been initiated by König and co-workers [11–13] and subsequently by Armstrong and co-workers [14,15], who applied some molten β-cyclodextrin derivatives in capillary gas chromatography.

Of the two ways mentioned above, only the first one makes possible operations on a micropreparative scale, which may be useful for identification purposes and eventually for further physico-chemical measurements.

The current paper reports our attempts to apply this option using α-CD in a dissolved state as the stationary phase for the study of juniper oils of various origins: juniper berry oil, juniper leaf oil and juniper oil from leaves and berries derived from various European countries. The structural formulae of some chiral constituents of juniper berry oils currently under investigation are presented in Fig. 1.

Juniper oil displays definite antibiotic properties. It inhibits the growth of *Sarcina lutea*, *Bacillus mesentericus*, *Bacillus subtilis*, *Micrococcus pyogenes* var. *aureus*, *Serratia marcescens* and *Escherichia coli* and very strongly inhibits the growth of *Proteus vulgaris* [16].

In the 1930s, juniper oil in combination with anise oil and cajeput oil was applied in the treatment and prevention of cholera [17]. It has been shown that juniper oil displays a strong activity against intestine worms during investigation both *in vitro* and *in vivo* [18]. The oil also has a strong repellent effect on the Egyptian mosquito (*Aedes aegypti*) [19].

The oil has also been used for therapeutic purposes in renal diseases and static and venous oedema.

Juniper berries are widely used in the manufacture of spices, perfumes and pharmaceutical products. The beverage industry is one of the main users of the berries' distillates. Differences in the quality of juniper berries and isolates on the market are commonly imputed to variation in the raw material.

To our knowledge, chromatographic separation and direct chiral recognition of terpenic hydrocarbons in juniper berry oil have not previously been attempted.

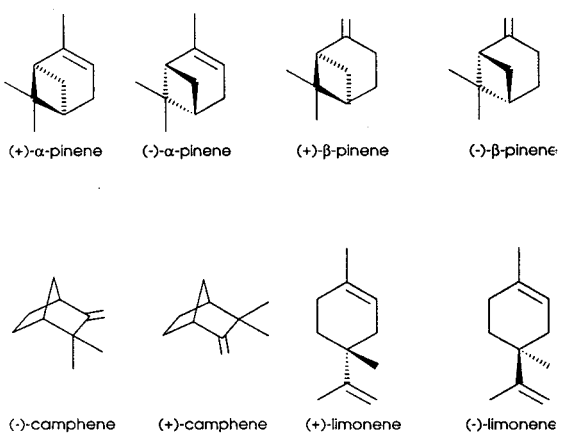

Fig. 1. Structural formulae of some investigated compounds.

EXPERIMENTAL

Plant material

Berries and leaves from plants of *Juniperus communis* L. from Italy, Austria and from Poland were sampled.

The essential oils (samples I–III) were obtained from crushed juniper berries cultivated on plantations in:

(1) Central Poland (Herbapol Enterprise, Łódź, Poland) (sample I).

(2) The Tyrol in Austria (Brüder Unterweger, Thal-Assling, Austria) (sample II).

(3) Central Italy (Primavera srL, Pisa, Italy) (sample III).

Sample IV was obtained from crushed juniper berries with leaves cultivated on a plantation in the north of Italy (Laboratori Italiani Vaillant, Milan, Italy). Sample V was produced from crushed juniper leaves obtained on a plantation in the Tyrol in Austria (Brüder Unterweger).

All investigated essential oils were obtained by steam distillation.

Reagents

α-CD was supplied by Chinoin (Budapest, Hungary). Chromosorb W NAW (0.18–0.25 mm) for GC was from Johns-Manville, USA. All

other materials were of analytical reagent grade and were used without further purification.

Apparatus and procedure

Chromatographic studies were performed using a Hewlett-Packard Model 5890 gas chromatograph equipped with a dual flame ionization detector. The peak areas and retention times were measured by means of a Hewlett-Packard 3396 integrator.

The columns were as follows. Column A (achiral): HP-1 (Hewlett-Packard) cross-linked methylsilicone (non-polar) fused-silica capillary, 30 m × 0.53 mm I.D. Column B (chiral with α-CD): glass column, 2 m × 4 mm I.D., filled with Chromosorb W NAW coated with a 0.8 molal (*m*) solution of α-CD in formamide medium.

Packing of column B was prepared according to the following procedure. An aqueous homogeneous solution containing α-CD (0.6 g), formamide (3.4 g) and $LiNO_3$ (0.4 g) was deposited on 15 g of Chromosorb W NAW. The resulting slurry was shaken for about 10 min and the excess water was then slowly evaporated at 40°C/20 mmHg (1 mmHg = 133.322 Pa). The column was conditioned at 40°C for about 8 h.

Unfortunately, columns containing α-CD, although very efficient in chiral separations of terpenes, are not as stable as those containing β-CD and γ-CD. Until now their stabilization has been approached in two ways:

(1) Swedish workers successfully applied a wetting procedure of carrier gas [20].

(2) We used $LiNO_3$ for stabilization [21].

The role of water and $LiNO_3$ has not been clarified. It may involve structural changes in α-CD or it may be a simple solubilization process.

RESULTS AND DISCUSSION

Chemical composition

The main topic of the present study has been limited to the chiral recognition of monoterpene hydrocarbons in juniper oils. However, in order to keep our results compatible with the earlier achiral determinations, we used not only the chiral (B) column prepared by ourselves, but also a commercial achiral capillary column (A). The latter enabled us to estimate the contributions of the particular fractions in oils, including the fraction in which we were interested.

Table I gives the contents of the main hydrocarbons in all investigated samples determined by us using HP-1 capillary column A in comparison with the results published previously by other authors [1–7]. The referenced results concern exclusively oils obtained from berries.

Although the results collected in Table I were obtained in different laboratories and concern different samples from various manufacturers, they seem to be relatively similar, at least those dealing with the main components. In fact, the main hydrocarbon component of four of the investigated oils (I, II, III and V) is α-pinene. An interesting exception is oil IV derived from crushed berries and leaves cultivated in Italy, whose principal component is limonene.

Worthy of attention is also oil II (produced

TABLE I

CONTENTS OF THE MAIN MONOTERPENE HYDROCARBONS IN THE ESSENTIAL OILS OF JUNIPER DETERMINED ON CAPILLARY COLUMN HP-1 (A) IN COMPARISON WITH EARLIER LITERATURE DATA

Compound	Our results (%)					Reference (%)				
	I	II	III	IV	V	7	4	5	6	1
α-Pinene	35.6	45.7	39.2	10.3	37.0	20.0	26.0	38.4	35.1	18.7
Camphene	1.2	0.5	0.5	5.2	0.8	0.2	0.2	–	0.3	0.2
β-Pinene, sabinene	13.1	8.9	7.7	9.5	18.4	2.8	10.5	11.0	6.9	6.2
Limonene	11.8	5.2	4.5	15.5	8.1	8.7	3.8	2.5	3.7	2.0
Myrcene	0.7	21.5	13.1	0.5	3.5	8.5	9.0	11.7	9.5	1.8

from berries in the Tyrol), which is very rich in terpenic hydrocarbons; the data in Table I indicate that it contains about twice as much hydrocarbons as each of the other oils.

Enantiomeric composition

Generally accepted opinion suggests that the enantiomeric composition of terpenes depends on the plant of origin. This suggestion has recently been confirmed in our investigations [10]. We have found significant differences between the enantiomeric composition of chiral hydrocarbons in pine needle oil and fir needle oil, both from Poland, *i.e.* the main components of fir needle oil (overall *ca.* 76%) are laevorotatory monoterpenic hydrocarbons, while in pine needle oil dextrorotatory hydrocarbons predominate.

As the next step we have undertaken a study of other factors. The present paper reports our investigations using the same kind of plant, namely juniper, but varying the parameters place in Europe of juniper cultivation and part of the plant (berries or leaves) used as the starting material for manufacturing the oil. The direct separations of enantiomers of the monoterpenic fraction of the five investigated oils on an α-CD column (B) are presented in Fig. 2. In Table II the corresponding semiquantitative values are presented.

Recognition of enantiomers by α-CD is truly remarkable. Some data on enantioselectivity factors estimated from artificial mixture given in Table III support this statement. However, α-CD seems to be a very poor differentiator of $C_{10}H_{16}$ isomers of other types (pinenes, limonene, camphene, terpinenes and others). As a consequence, a well-separated enantiomer of one compound may be superimposed by an enantiomer of another, as it is seen in Fig. 2 for (+)-camphene and sabinene, (+)-limonene and *p*-cymene, (−)-α-pinene and (−)-β-pinene.

Further studies on optimization of the procedure to achieve complete separation of isomers and enantiomers in a single chromatographic process are in progress. At present to achieve this goal we have applied another method, *i.e.* the rationalization of the data obtained on chiral column B with those of achiral capillary column

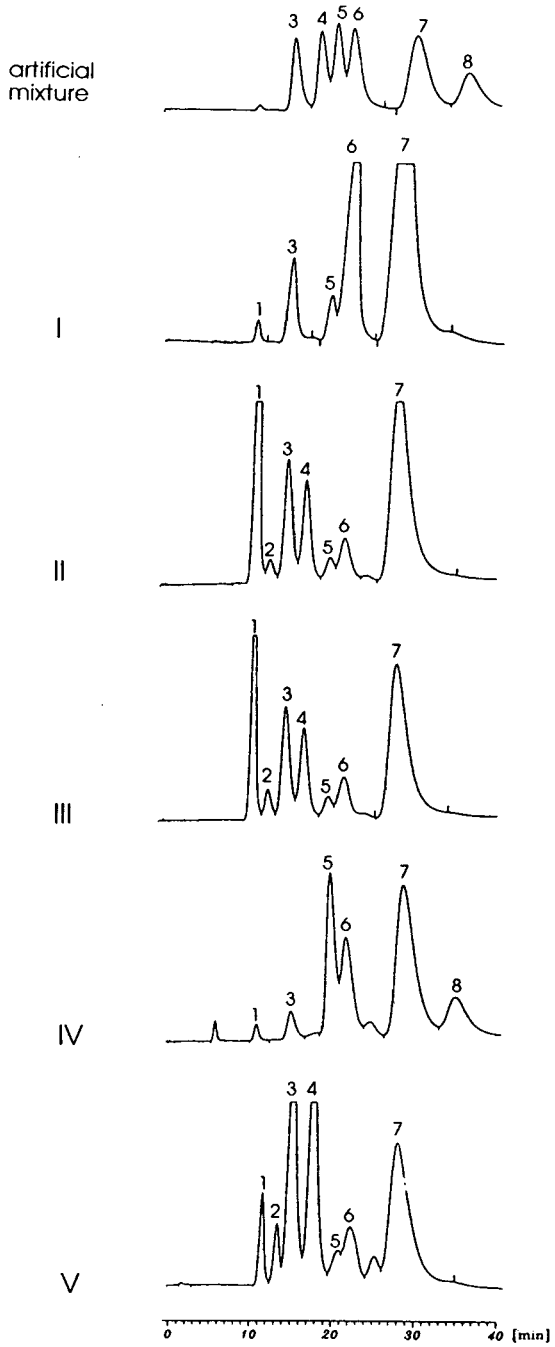

Fig. 2. Chromatograms of all investigated juniper oils and an artificial mixture obtained on chiral column with α-CD (B). Column temperature: 30°C. Flow-rate: 40 ml/min argon. Peaks: 1 = myrcene; 2 = α-terpinene; 3 = (+)-α-pinene; 4 = (+)-camphene, sabinene; 5 = (−)-limonene, (+)-β-pinene; 6 = (+)-limonene, *p*-cymene; 7 = (−)-α-pinene, (−)-β-pinene; 8 = (−)-camphene.

TABLE II

CONTENTS OF THE MAIN COMPONENTS OF THE MONOTERPENE FRACTION IN JUNIPER OILS DETERMINED ON A CHIRAL COLUMN (B) WITH α-CD

Compound	Contents (%)				
	I	II	III	IV	V
Myrcene	1.2	27.7	19.5	1.1	4.7
α-Terpinene	–	1.9	3.3	–	3.8
(+)-α-Pinene	7.3	11.4	14.3	3.6	22.9
(+)-Camphene, sabinene	0.5	9.9	12.4	0.5	25.3
(−)-Limonene	3.6	2.3	2.9	20.4	3.1
(+)-Limonene, *p*-cymene	28.7	5.6	7.5	16.5	8.2
(−)-α-Pinene, (−)-β-pinene	57.4	40.6	40.4	40.4	29.2
(−)-Camphene	1.0	–	–	13.4	–

A. In the evaluation of the contents of two compounds eluted together from the chiral column [*e.g.* (−)-α-pinene and (−)-β-pinene], the data from the achiral column are taken into account, assuming the monoterpenic fraction to be 100%.

The final corrected results are given in Table IV.

It is seen that the ratio of *S*(−) to *R*(+) of α-pinene, although always greater than 1, varies greatly: from about 5 for Italian oil IV through 2.7 for Italian oil III to about 1 for the almost racemic composition of the oil produced from leaves in the Tyrol (V). In all the investigated oils, except IV, *R*(+)-limonene predominated, the ratio of *R*(+) to *S*(−) enantiomers varying from 5 for the Polish oil I to 1.6 for Italian oil III; in contrast to this in the Italian oil IV it is *S*(−)-limonene which predominates.

In almost all the oils camphene constitutes the minor component (1–2%), the exception being oil IV, in which a considerable quantity of camphene (greater than 10%) was found.

In all the samples only traces of *R*(+)-β-pinene were found.

In the Polish I and Italian IV oils considerable amounts of *S*(−)-β-pinene (18–22%) were found but no sabinene. The rest of the oils under investigation contain relatively small amounts of *S*(−)-β-pinene (3–4%) accompanied by a significant amount of sabinene, from 8 to 20%.

In summary, the method appointed to monitor the enantiomeric composition of terpenic hydrocarbon in essential oils, although still not ideal, has been elaborated. Its application to juniper oils reported here indicates that the problem of enantiomeric composition of terpenic hydrocarbons produced by plants, *i.e.* the search for the main factor responsible for the content of enantiomers, is very complicated and is still unsolved. Further studies are in progress.

TABLE III

SEPARATION FACTORS (α) AND ORDER OF ELUTION OF ENANTIOMERS OF SOME MONOTERPENE HYDROCARBONS OBTAINED ON A CHIRAL COLUMN (C) WITH α-CD (0.8 *m*) AT 30°C

Compound	α	First peak eluted
α-Pinene	1.92	(+)
Camphene	1.93	(+)
Limonene	1.09	(−)
β-Pinene	1.45	(+)

TABLE IV

ENANTIOMERIC COMPOSITION OF THE MONOTERPENE FRACTION OF JUNIPER OILS CALCULATED BY RATIONALIZATION OF THE RESULTS OBTAINED ON A CAPILLARY COLUMN HP-1 (A) AND A CHIRAL COLUMN WITH α-CD (B)

Compound	Composition (%)				
	I	II	III	IV	V
(+)-α-Pinene	8	11	14	4	23
(−)-α-Pinene	38	38	38	20	24
(+)-Limonene	15	5	4	15	7
(−)-Limonene	3	2	2.5	20	3
(+)-Camphene	0.5	1	1	–	–
(−)-Camphene	1.0	–	–	12	1
(+)-β-Pinene			Traces		
(−)-β-Pinene	18	3	3	22	4
Sabinene	–	8	8	–	20
p-Cymene	10	1	1	1	5
Myrcene	1	25	18	1	1
α-Terpinene	–	1.5	2.5	–	2

ACKNOWLEDGEMENT

This work was supported by Grant 2 0242 91 01 from the State Committee for Scientific Research.

REFERENCES

1 N. Gelsomini, V. Vidrich, P. Fusi and M. Michelozzi, *J. High Resolut. Chromatogr. Chromatogr. Commun.*, 11 (1988) 218.
2 H. Kallio and K. Jurger-Mannermaa, *J. Agric. Food Chem.*, 37 (1969) 1013.
3 D. Lamparsky and I. Klimes, *Parfum. Kosmet.*, 66 (1985) 553.
4 J.E. Karg, *Parfum. Kosmet.*, 62 (1981) 341.
5 M. Melagari, G. Vampa, A. Bianchi, A. Albasini, S. Benvenuti, M. Rinaldi and A. Provvisionato, *Atti Soc. Nat. Mat. di Modena*, 118 (1987) 75.
6 Analytical Methods Committee, *Analyst*, 109 (1984) 1343.
7 A. Proenca da Cunha and Odete L.R. Roque, *J. Ess. Oil. Res.*, 1 (1989) 15.
8 T. Kościelski, D. Sybilska and J. Jurczak, *J. Chromatogr.*, 280 (1983) 131.
9 D. Sybilska, J. Kowalczyk, M. Asztemborska, T. Stankiewicz and J. Jurczak, *J. Chromatogr.*, 543 (1991) 397.
10 R.J. Ochocka, D. Sybilska, M. Asztemborska, J. Kowalczyk and J. Goronowicz, *J. Chromatogr.*, 543 (1991) 171.
11 W.A. König, S. Lutz and G. Wenz, *Angew. Chem. Int. Ed. Engl.*, 27 (1988) 979.
12 W.A. König, R. Krebber, P. Evers and G. Bruhn, *J. High Resolut. Chromatogr.*, 13 (1990) 328.
13 W.A. König, A. Krüger, D. Icheln and T. Runge, *J. High Resolut. Chromatogr.*, 15 (1992) 184.
14 D.W. Armstrong, W. Li and J. Pitha, *Anal. Chem.*, 62 (1990) 217.
15 D.W. Armstrong, W. Li, C.D. Chang and J. Pitha, *Anal. Chem.*, 62 (1990) 914.
16 J.C. Maruzella and M.B. Lichtenstein, *J. Am. Pharm. Assoc.*, 45 (1956) 378.
17 J.W. Tomb, *J. Trop. Med. Hyg.*, 29 (1926) 210.
18 G. Valette, R. Cavier and J. Debelmas, *Ann. Pharm. Franc.*, 11 (1953) 649.
19 D. Kalemba, A. Kurowska, J. Góra, S. Łakota and A. Lis, *Pestycydy*, 2 (1991) 31.
20 M. Lindström, T. Norin and J. Roeraade, *J. Chromatogr.*, 513 (1990) 315.
21 D. Sybilska and J. Jurczak, *Carbohydr. Res.*, 192 (1989) 243.

Journal of Chromatography A, 659 (1994) 395–401
Elsevier Science B.V., Amsterdam

CHROM. 25 611

Determination of acid herbicides in aqueous samples by liquid–solid disk extraction and capillary gas chromatography

Jimmie Hodgeson*

Atmospheric Research and Exposure, Assessment Laboratory MD-84, US Environmental Protection Agency, Research Triangle Park, NC 27711 (USA)

Jeffrey Collins and Winslow Bashe

Technology Applications, Inc., 26 West M.L. King Drive, Cincinnati, OH 45268 (USA)

(First received May 13th, 1993; revised manuscript received October 1st, 1993)

ABSTRACT

A simplified procedure for extraction and analysis of chlorinated acid herbicides in aqueous matrices using modern filter disk extraction technology is presented. An acidified water sample is extracted with a 47-mm polystyrene–divinylbenzene filter disk and the analytes are eluted with a mixed methanol–methyl *tert.*-butyl ether solvent. After extract drying, the analytes are esterified with diazomethane and analyzed by gas chromatography with electron-capture detection. The discussion includes extraction disk selection, sample acidity and salting requirements, elution volume requirements and the effect of sample volume on recovery. Method detection limits are given as well as accuracy and precision data on four fortified matrices —reagent water, dechlorinated tap water, biologically active surface water and high humectant ground water.

INTRODUCTION

The Safe Drinking Water Act as amended in 1986 [1] required promulgation of maximum contaminant levels and recommended treatment technologies for 83 contaminants in drinking water in three time-based phases. Final regulations for the phenoxyacid herbicides, 2,4-D and silvex, were published in January 1991 [2]. This same rule contained monitoring requirements for the unregulated herbicides dalapon, dicamba, dinoseb and picloram. Regulation for pentachlorophenol was published in July 1991 [3]. In addition, the following acid herbicides are scheduled for regulation in a future phase: acifluorfen (blazer), bentazon, dacthal and dicamba. Inherent in the regulations are requirements for sound analytical methods.

The current US Environmental Protection Agency (EPA) method for the analysis of phenoxyacid and other acid herbicides in drinking water is EPA Method 515.1 [4]. The analyte list of Method 515.1 contains 17 compounds, including all those discussed above. This method was originally developed for use during the National Pesticide Survey [5]. During this extensive study, four of the analytes were not determined quantitatively because of lack of control of precision, namely dalapon, chloramben, acifluorfen and 4-nitrophenol. Two of these

* Corresponding author.

0021-9673/94/$07.00
SSDI 0021-9673(93)E1054-4

compounds are not appropriate candidates for Method 515.1 or the technique discussed below. Dalapon is a hydrophilic molecule, which does not partition favorably from aqueous solutions by liquid–liquid or reversed-phase extraction and 4-nitrophenol does not methylate. Method 515.1 is a complex liquid–liquid extraction procedure employing large volumes of organic solvents, which are usually vented to the atmosphere during preconcentration. Our objectives in these capillary gas chromatography (GC) methods development activities were to simplify the methodology and minimize solvent consumption by means of liquid–solid extraction (LSE).

Numerous reports on the use of LSE techniques for the analysis of organic acids in aqueous solutions have been published over the past decade. Some of the more recent and pertinent ones are cited here. Most of these have employed extraction cartridges (*e.g.* Carbopack, reversed phase) for analyte preconcentration and subsequent analysis by high-performance liquid chromatography [6–10]. There have been some very interesting publications on ion-exchange procedures for the extraction of organic acids from aqueous samples for subsequent analysis by GC or GC–mass spectrometry [11–13]. Our original approach for the acid herbicides was in fact ion-exchange extraction. We did sufficient work with a strong anion exchanger (Bio-Rad AG1-X8) to demonstrate feasibility for both the herbicides and haloacetic acids [14]. An ion-exchange technique for dalapon and the haloacetic acids is under concurrent development (EPA Method 552.1). However, we found this to be a more complicated and time-consuming approach for the analysis of the herbicides than the filter disk extraction procedure presented below.

Recent reports have appeared on the use of reversed-phase extraction disks for the rapid extraction of organics from water [14–17]. Advantages of these disks over extraction cartridges have been discussed by Markell *et al.* [18]. These include high flow-rates, elimination of the potential for flow channeling and improved capability for handling dirty samples. The alternative use of disk technology has already been incorporated into several EPA drinking water methods.

We have evaluated C_{18} and polystyrene–divinylbenzene (PS–DVB) resin disks and present here a procedure for the extraction and analysis of acid herbicides in aqueous samples. This technology provides the basis for an improved, alternative method (EPA Method 515.2). Method performance data are presented for fortified reagent water and drinking water sources.

EXPERIMENTAL

Chemicals

Individual stock and calibration standard mixtures were prepared from pure materials obtained from the EPA Repository, Research Triangle Park, NC, USA. All solvents were high-purity pesticide quality (Burdick & Jackson) distributed by Baxter Scientific (Cincinnati, OH, USA). All other chemicals were ACS reagent grade or better.

Instrumentation and capillary column

A Hewlett-Packard 5890 (Kenneth Square, PA, USA) capillary gas chromatograph was fitted with a J & W Scientific (Folsom, CA, USA) DB-5 fused-silica capillary column (30 m × 0.32 mm I.D., 0.25 μm d_p). The gas chromatograph was also equipped with an electron-capture detector and a HP 7673 auto-sampler.

Analytical operating parameters

Helium carrier gas velocity was set at 25 cm/s (210°C). The detector make-up gas, methane–argon (5:95), was set at 30 ml/min. Initial oven temperature was set at 50°C and held for 5 min. The oven temperature was then ramped to 210°C at 10°C/min and held for 5 min, followed by a program to 230°C at 10°C/min and a final 10-min hold. A 2-μl sample size was injected in the splitless mode (purge off 30 s).

Other special equipment and materials

The extraction disks were Empore-3M 47-mm C_{18} and PS–DVB resin (Analytichem International, Harbor City, PA, USA). The extraction apparatus consisted of all-glass Kontes filter funnels (Cat. No. k953755-0000, Fisher Scientific, Pittsburgh, PA, USA) used with 1-l glass vacuum flasks. A Model 111 N-EVAP 12 (Or-

ganomations, South Berlin, MA, USA) was used for sample concentration.

Standard procedure

Summary of the method. The method analytes and surrogate compound (2,4-dichlorophenylacetic acid) are extracted from 250-ml aqueous samples by means of 47-mm filter extraction disks. The analytes are eluted with a minimal volume of a combination methanol–methyl *tert.*-butyl ether (MTBE) solvent and esterified with diazomethane. Analysis is accomplished by means of capillary GC with electron-capture detection.

Extraction. The samples were prepared for extraction by addition of 20% (w/w) anhydrous, reagent-grade sodium sulfate (previously heated to 400°C for 4 h) and adjustment of sample pH to 1.0 ± 0.1 with reagent-grade sulfuric acid. The extraction disks were conditioned by sequentially adding in a continuous manner the following series to the disk surface [380–500 Torr (1 Torr = 133.322 Pa): 20 ml methanol–MTBE (10:90), 5 min of room air, 20 ml methanol and 20 ml of reagent water. The sample is then added (without allowing the disk to dry) and the vacuum is adjusted to 630 Torr. After all the sample has passed through the disk, the vacuum is adjusted to 380–500 Torr and room air is passed through the disk for 20 min.

Elution. A 2-ml volume of methanol–MTBE (10:90) is placed on top of the disk, without vacuum, and allowed to sit for 1 min. The vacuum is then applied and the eluate is collected in a 60-ml test tube, which is placed inside the vacuum flask after extraction. This step is repeated and the sample flask is rinsed with 4 ml of pure MTBE, which is also passed through the disk.

Extract drying and derivatization. The eluent is dried by passing it through a large pasteur pipette containing 4 g acidified anhydrous sodium sulfate. Any visible water in the eluate must be excluded from the drying pipette to avoid clogging. The eluate collection tube is then rinsed with 2×1 ml aliquots of MTBE, which are also passed through the drying tube. Derivatization is accomplished by purging the sample directly with diazomethane gas using a micromolar generation procedure, which is described in detail in Method 515.1 [4]. The procedure is in turn based upon the esterification technique described by Schlenk and Gellerman [19].

Analysis. The samples were analyzed by capillary GC–electron-capture detection using a Hewlett-Packard 5890 GC equipped with a Model 7673A autosampler. A Waters Maxima data system was used for collecting and processing chromatographic data.

RESULTS AND DISCUSSION

During the course of the development of this method, the following parameters or variables were evaluated: column selection, extraction disk selection, sample acidity and salting requirements, sample volume and extraction time, and elution solvent selection and volume. Following method optimization, method validation data were obtained on fortified reagent water, dechlorinated tap water, biologically active surface water and high humectant ground water. These activities are described in some detail below.

All of the Method 515.1 analytes cannot be resolved by capillary GC using 30-m columns. Thus, we have separated the analytes into two groups for the methods development and validation activities. This was also standard practice during the National Pesticide Survey. The analytes are listed in Table I in the relative retention order observed for the primary column. These compounds are aromatic organic acids or phenols (dinoseb and pentachlorophenol) and usually contain chlorine substitution on the aromatic ring. Reference is made to the Pesticides Manual [20] or the Farm Chemicals Handbook [21] for details on chemical structure.

Since the acid herbicides are extracted by a reversed phase, the analytes must be in the molecular form for efficient recovery. This is accomplished by reducing the pH to 1.0 ± 0.1 with concentrated sulfuric acid. Recovery is also markedly enhanced by the addition of salt to attain a high ionic strength sample. Table II presents preliminary recovery data from fortified, unsalted 100-ml reagent water samples extracted with C_{18} and resin. The use of sodium sulfate gave somewhat higher recoveries than extractions by addition of the same mass per-

TABLE I

RELATIVE RETENTION ORDER

Analyte	Group[a]
3,5-Dichlorobenzoic acid	A
2,4-Dichlorophenylacetic acid[b]	A, B
Dicamba	B
Dichlorprop	A
2,4-D	B
4,4′-Dibromooctafluorobiphenyl (I.S.)	A,B
Pentachlorophenol	A
Silvex	B
5-Hydroxydicamba	B
2,4,5-T	A
2,4-DB[c]	B
Dinoseb	A
Bentazon	B
Picloram	B
Dacthal	A
Acifluorfen	B

[a] Analytes were divided into two groups during method development to avoid chromatographic overlap.
[b] Surrogate analyte.
[c] 2,4-DB = 4-(2,4-dichlorophenoxy)butyric acid.

centage of sodium chloride. For unsalted reagent water, the resin recovery data are significantly higher for dalapon, dacthal and picloram. Nevertheless, recovery is negligible or poor for several of the analytes. Salting the water dramatically improves the recovery for all of the analytes to acceptable levels, except for dalapon, and largely removes recovery differences between C_{18} and resin recovery data. The exception was dacthal, for which recovery remained significantly lower with C_{18} extraction.

Initial studies on elution volumes employed a moderately polar dye compound, Red Disperse 1, methanol elution and photometric measurement of recovery. With three successive 2-ml aliquots, recoveries of 80, 15 and 3% were obtained. The dye appeared to be almost quantitatively eluted from the disk with the first aliquot. However, the glass frit supporting the disk has a considerable surface area, which must be washed with additional solvent. The acid herbicides were eluted with the mixed methanol–MTBE solvent as described above. The analytes

TABLE II

C_{18} AND RESIN RECOVERIES AND EFFECT OF SALTING

Analyte	Recoveries ± R.S.D.(%; $n = 3$)			
	C_{18}[a]	Resin[a]	C_{18}[b]	Resin[b]
Acifluorfen	77 ± 20	82 ± 5	104 ± 5	121 ± 1
Bentazon	0	No Data	90 ± 13	71 ± 5
Chloramben	8 ± 11	3 ± 15	72 ± 14	77 ± 7
2,4-D	86 ± 12	83 ± 6	81 ± 8	94 ± 15
Dalapon	0	42 ± 25	12 ± 75	31 ± 30
2,4-DB	81 ± 13	80 ± 14	118 ± 10	130 ± 8
Dacthal	53 ± 17	99 ± 8	67 ± 16	97 ± 5
Dicamba	73 ± 13	71 ± 14	83 ± 3	94 ± 15
3,5-Dichlorobenzoic acid	70 ± 17	76 ± 2	86 ± 25	107 ± 20
Dichloroprop	77 ± 11	78 ± 3	85 ± 9	94 ± 10
Dinoseb	72 ± 16	75 ± 5	92 ± 26	85 ± 6
Pentachlorophenol	69 ± 14	70 ± 2	65 ± 15	73 ± 8
Picloram	49 ± 19	74 ± 7	96 ± 24	99 ± 21
2,4,5-T	76 ± 11	75 ± 14	93 ± 10	89 ± 5
Silvex	73 ± 14	74 ± 14	82 ± 9	80 ± 5

[a] Fortified, unsalted reagent water.
[b] Fortified reagent water with 20% (w/w) Na_2SO_4.

TABLE III

SINGLE LABORATORY RECOVERY, PRECISION DATA AND METHOD DETECTION LIMIT (MDL) WITH FORTIFIED REAGENT WATER

Analyte	Fortified concentration (μg/l)	Mean recovery (%)[a]	R.S.D. (%)	MDL (μg/l)
Acifluorfen	0.50	70	21	0.25
Bentazon	2.50	70	11	0.63
2,4-D	0.25	96	38	0.28
2,4-DB	2.50	79	12	0.72
Dacthal[b]	0.25	96	16	0.13
Dicamba	0.75	109	11	0.28
3,5-Dichlorobenzoic acid	1.25	126	24	1.23
Dichlorprop	0.25	106	15	0.13
Dinoseb	0.50	87	22	0.28
5-Hydroxydicamba	0.75	90	12	0.25
Pentachlorophenol	0.25	103	18	0.16
Picloram	0.75	95	15	0.35
2,4,5-T	0.25	116	18	0.16
Silvex	0.25	98	9	0.06

[a] Based on the analyses of seven replicates by resin disk extraction.
[b] Measurement includes the mono- and diacid metabolites.

are effectively esterified in this solvent and no other solvents were evaluated.

Recovery *versus* sample volumes of 100, 250 and 500 ml and 1 l were determined for both C_{18} and resin extraction by analysis in triplicate for each sample volume. The mean recoveries averaged over all analytes were highest for the 100-ml volume, $88 \pm 13\%$ for C_{18} and $94 \pm 9\%$ for the resin disk. By contrast, the overall mean recoveries at 250 ml were $70 \pm 5\%$ for C_{18} and $77 \pm 7\%$ for the resin. With the exception of picloram and dacthal, analyte recoveries were remarkably constant for both C_{18} and resin over sample volumes from 250 to 1000 ml. At a volume of 250 ml, the C_{18} recoveries were unacceptably low for picloram (43%) and dacthal (25%). The resin recoveries at 250 ml were adequate for picloram (64%) and dacthal (93%) and remained greater than 80% at 1 l for dacthal. Considering all the analytes, the resin is the disk of choice. The overall superior performance of the resin is likely attributable to its aromatic, polymeric structure, which should have a greater affinity for the aromatic, moder-

TABLE IV

SINGLE-LABORATORY RECOVERY AND PRECISION DATA FOR FORTIFIED REAGENT WATER

Analyte	Fortified concentration (μg/l)	Mean recovery (%)[a]	R.S.D. (%)
Acifluorfen	2.0	59	13
Bentazon	10.0	68	8
2,4-D	1.0	90	20
2,4-DB	10.0	74	6
Dacthal[b]	1.0	60	10
Dicamba	3.0	75	9
3,5-Dichlorobenzoic acid	5.0	62	18
Dichlorprop	1.0	97	17
Dinoseb	2.0	63	10
5-Hydroxydicamba	3.0	77	8
Pentachlorophenol	1.0	69	11
Picloram	3.0	66	9
2,4,5-T	1.0	64	15
Silvex	1.0	68	8

[a] Based on the analyses of 6–7 replicates by resin disk extraction.
[b] Measurement includes the mono- and diacid metabolites.

ately polar analytes. Since the method detection limits [22] determined for a 250-ml sample (Table III) were more than adequate, this volume was chosen for the method performance data given below. If the analyte list of interest does not include picloram and dacthal, recoveries of 60% or greater may be anticipated for the remaining analytes for sample volumes up to 1 l by C_{18} or resin extraction.

The data of Table II represent overall analyte method recoveries, since the calibration standards were prepared in the final 5 ml extract. By contrast to Method 515.1, this method is sufficiently simple that aqueous standards are processed through the method in order to correct for recoveries. Accuracy and precision data have been obtained on three fortified matrices —reagent water, dechlorinated tap water and high humectant ground water. The complete set of performance data is contained in the method

TABLE V

SINGLE-LABORATORY RECOVERY AND PRECISION DATA FOR FORTIFIED, DECHLORINATED TAP WATER

Analyte	Fortified concentration (μg/l)	Mean recovery (%)[a]	R.S.D. (%)
Acifluorfen	2.0	150	7
Bentazon	10.0	112	9
2,4-D	1.0	90	16
2,4-DB	10.0	111	10
Dacthal[b]	1.0	118	8
Dicamba	3.0	86	10
3,5-Dichlorobenzoic acid	5.0	111	5
Dichlorprop	1.0	88	30
Dinoseb	2.0	121	6
5-Hydroxydicamba	3.0	96	6
Pentachlorophenol	1.0	96	6
Picloram	3.0	132	12
2,4,5-T	1.0	108	10
Silvex	1.0	115	7
2,4-Dichlorophenyl-acetic acid[c]	1.0	120	19

[a] Based on the analyses of 6–7 replicates by resin disk extraction.
[b] Measurement includes the mono- and diacid metabolites.
[c] Surrogate analyte.

TABLE VI

SINGLE-LABORATORY RECOVERY AND PRECISION DATA FOR FORTIFIED, HIGH HUMIC CONTENT SURFACE WATER

Analyte	Fortified concentration (μg/l)	Mean recovery (%)[a]	R.S.D. (%)
Acifluorfen	2.0	120	13
Bentazon	10.0	87	11
2,4-D	1.0	59	7
2,4-DB	10.0	80	14
Dacthal[b]	1.0	100	6
Dicamba	3.0	76	9
3,5-Dichlorobenzoic acid	5.0	87	4
Dichlorprop	1.0	110	22
Dinoseb	2.0	97	6
5-Hydroxydicamba	3.0	82	9
Pentachlorophenol	1.0	70	5
Picloram	3.0	124	9
2,4,5-T	1.0	101	4
Silvex	1.0	80	6

[a] Based on the analyses of 6–7 replicates by resin disk extraction.
[b] Measurement includes the mono- and diacid metabolites.

[23]. A set of representative data for each matrix is presented in Tables IV–VI. The data are based on the analysis of 6–7 replicates for each set. In obtaining these data, method blanks were routinely measured for the unfortified matrix. Thus, the high accuracy data observed for acifluorfen, dinoseb and picloram in the tap and surface waters may represent some unknown matrix effect. Nevertheless, these data are equivalent to or better than that obtained by Method 515.1 on real matrices. In general, the precision attained by this method is superior, probably because of increased method simplicity.

In summary, a LSE method has been developed for the analysis of acid herbicides in water matrices using modern filter disk extraction technology. The method is considerably simpler than conventional liquid–liquid extraction methods and the requirement for large volumes of organic solvents is eliminated. The analysis time, and thus cost, are decreased. A skilled analyst can process eight samples over two days by Method 515.1. The same number

can be processed in an 8-h period by the method described here.

REFERENCES

1 *Fed. Reg.*, 52, No. 130 (July 8, 1987) 25 720–25 734.
2 *Fed. Reg.*, 56, No. 20 (January 30, 1991) 3256–3597.
3 *Fed. Reg.*, 56, No. 126 (July 1, 1991) 30 266–30 281.
4 *Method 515.1, Determination of Chlorinated Acids in Water by Gas Chromatography with an Electron Capture Detector, Methods for the Determination of Organic Compounds in Drinking Water, EPA/600/4-88/039*, December 1988, pp. 221–252, available as Publication No. PB-89-220461/AS from the National Technical Information Service, Springfield, VA.
5 D.J. Munch, R.L. Graves and T.M. Engel, *Environ. Sci. Technol.*, 24 (1990) 1446.
6 A. Di Corcia and M. Marchetti, *Anal. Chem.*, 63 (1991) 580.
7 A. Di Corcia and M. Marchetti, *Environ. Sci. Technol.*, 26 (1992) 66.
8 P.R. Loconto, *J. Liq. Chrom.*, 14 (1991) 1297.
9 E.R. Bogus, T.L. Watschke and R.O. Mumma, *J. Agric. Food Chem.*, 38 (1990) 142.
10 R.B. Geerdink, A.M.B. Graumans and J. Viveen, *J. Chromatogr.*, 547 (1991) 478.
11 P. Verner and F. Pehal, *J. Chromatogr.*, 382 (1986) 232.
12 A. Zhu and G.-Y. Xu, *J. Chromatogr.*, 314 (1984) 421.
13 J.J. Richard and J.S. Fritz, *J. Chromatogr. Sci.*, 18 (1980) 35.
14 J.W. Hodgeson, J. Collins and D. Becker, in *Proceedings: 14th Annual EPA Conference on Analysis of Pollutants in the Environment, Norfolk, VA, 1991*, US Environmental Protection Agency (WH-552), Washington, DC, March 1992, EPA/821/R/92/001, pp. 164–194.
15 D.F. Hagen, C.G. Markell, G.A. Schmitt and D.D. Blerine, *Anal. Chim. Acta*, 236 (1990) 157.
16 A. Kraut-Vass and J. Thoma, *J. Chromatogr.*, 538 (1991) 233.
17 O. Evans, B.J. Jacobs and A.L. Cohen, *Analyst*, 116 (1991) 15.
18 C.G. Markell, D.F. Hagen and V.A. Bunnelle, *LC·GC*, 9 (1991) 332.
19 H. Schlenk and H.L. Gellerman, *Anal. Chem.*, 21 (1960) 1412.
20 C.R. Worthing (Editor), *The Pesticide Manual*, British Crop Protection Council, Thornton Heath, 8th ed., 1987.
21 *Farm Chemicals Handbook '92*, Meister Publ. Co., Willoughby, OH, 78th ed., 1992.
22 J.A. Glaser, D.L. Foerst, G.D. McKee, S.A. Quave and W.L. Budde, *Environ. Sci. Technol.*, 15 (1981) 1426.
23 *Method 515.2, Determination of Chlorinated Acids in Water Using Liquid–Solid Extraction and Gas Chromatography with an Electron Capture Detector, Methods for the Determination of Organic Compounds in Drinking Water —Supplement II, EPA/600/R-92/129*, August 1992, pp. 51–88, available as Publication No. PB-92-207703 from the National Technical Information Service, Springfield, VA.

Journal of Chromatography A, 659 (1994) 403–415
Elsevier Science B.V., Amsterdam

CHROM. 25 540

Computational simulation of migration and dispersion in free capillary zone electrophoresis

I. Description of the theoretical model

J.C. Reijenga*

Department of Chemical Engineering, Eindhoven University of Technology, P.O. Box 513, 5600 MB Eindhoven (Netherlands)

E. Kenndler

Institute of Analytical Chemistry, University of Vienna, Währingerstrasse 38, A-1090 Vienna (Austria)

(First received May 10th, 1993; revised manuscript received September 6th, 1993)

ABSTRACT

An instrument simulator was developed for high-performance capillary electrophoresis which allows for fast graphic illustration of the effect of a large number of variables on the shape of the electropherogram. The input data of the separands are values of pK and mobilities at 25°C and infinite dilution. The instrument parameters that can be varied include capillary material, lengths, inside diameter, wall thickness, zeta potential, cooling temperature, voltage, polarity and open or closed mode. Hydrostatic injection is simulated, using time and pressure as variables. The following properties of the buffer can be varied: pH, ionic strength and effective mobility of background electrolyte ions. The effective mobilities are corrected for temperature and concentration effects. Extra-column effects from injection and detection are taken into account, and also peak dispersion arising from electroosmosis, diffusion, electromigration and heat production.

INTRODUCTION

The theoretical basis of electrophoretic separation has been extensively dealt with in the past. All phenomena occurring during separation were described either by exact mathematical relationships derived from the equation of continuity and other differential equations, or by empirical relationships verified experimentally and found to be valid under certain conditions. Many workers have contributed to this knowledge. For a historical overview, many excellent reviews and textbooks are available [1–9].

The introduction of advanced instrumentation (in part based on theoretical models) and the more recent use of microcomputers have made it possible to verify experiment and theory in a very efficient way. Computer programs have been written to simulate and verify many aspects of the theory [10–13], thus making it possible to refine the theoretical basis and extend the understanding of the phenomena. Even a unified model of the transient state phenomena of all possible electrophoretic configurations was put together in one computer program [10]. One is thus able to study the effects concerned in detail without actually performing experiments. The fundamental aspects consequently are accessible to all experienced researchers in the field.

* Corresponding author.

0021-9673/94/$07.00
SSDI 0021-9673(93)E0959-X

In addition to the textbooks mentioned, a number of workers have published on model refinement in capillary electrophoresis in recent years, especially with respect to a number of on-column dispersive effects [14–18], extra-column effects [19–21], concentration overload [22,23] and stacking effects [24–26].

In order to clarify the purpose of the present investigation, computer programs simulating instrumental separation techniques are classified into the following three categories, each with its own aim and requirements.

(I) Fundamental. The model in the program should be exact in every detail, describing the dynamics of the electrophoretic process in both transient and steady states.

(II) Optimization. The program should be fast and provide a fairly accurate prediction of the separation based on literature values and one's own previous experiments.

(III) Instruction. The program must be fast, flexible, very user-friendly and have graphics output and a reasonably predictive value.

Consideration of the requirements mentioned will lead to the obvious conclusion that some are contradictory. It was the aim of this study to simulate the final result of the electrophoretic process (categories II and III), depicted by the electropherogram, rather than to illustrate the dynamics in detail (category I). For this purpose, the two processes that determine the electrophoretic result, migration and dispersion, were simulated. A distinction was made between open and closed systems. The latter are not commercially available but clearly offer advantages that justify separate treatment [27].

The migration time was simply derived from the apparent mobilities, consisting of the effective mobilities of the separands and the electroosmotic mobility of the bulk liquid, both at given ionic strength and pH. To describe the effect on peak distortion, the plate height model was used, whereby the expressions for the plate height originating from different sources, as described in the literature, were taken but they were also modified and reformulated in a number of cases.

It was shown that a number of expressions for the different contributions to the total plate height contain the ratio of the effective mobility and the sum of the effective mobility and the electroosmotic mobility, which leads to the introduction of a dimensionless parameter, the electromigration factor. The influence of this factor on migration and dispersion will be discussed for both anions and cations. All important factors influencing the result were taken into account. These include instrument variables such as capillary material and dimensions, voltage, current and temperature. The physico-chemical properties of the buffer and the sample form the basis of the calculations. Extra-column effects arising from injection (overload, stacking) and detection (slit width and time constant) are included, in addition to dispersive effects resulting from diffusion, electroosmosis, electromigration and heat production.

EXPERIMENTAL

Programming environment

The software was written in QuickBasic version 4.5 (Microsoft, Redmond, WA, USA) using an IBM PC-compatible clone with a Model 386 processor, 4 Mbyte RAM, 100 Mbyte hard disk, 40 MHz clock speed and a 14-in. (1 in. = 2.54 cm) VGA colour monitor. In contrast to this, the computer program requires as a minimum hardware configuration: IBM XT-compatible PC, 8 MHz clock speed, 640 kbyte RAM, a 360 kbyte disk drive and a graphics monitor. The program automatically adjusts to Hercules, AT&T, CGA, EGA and VGA graphics. A numeric coprocessor is supported if present and emulated otherwise. A mouse (Microsoft mode) is optional. With a command line option, the program can also be run from a computer network, especially useful for training purposes.

The time necessary to calculate and display a typical electropherogram is in the range of a few seconds. The user interface, consisting of pull-down menus, to be activated by single-letter commands, cursor movements or the mouse, is much the same as in a previously developed simulator for gas chromatography [28].

Details on the availability of the program can be obtained from the first author request.

Data file

A data file CEDATA.DAT of pK and mobility values was made, consisting of previously

published data [6,29–31]. These data generally refer to 25°C and infinite dilution. The simulation program itself can be used to edit the CEDATA.DAT or any other data file (change values, add new components). In this way the simulator can also work with user-defined databases.

Generation of electropherogram

Each calculation of retention and dispersion is followed by the generation and display of a new electropherogram, see Fig. 1 for the screen layout. First, a noisy baseline is generated. Then peaks are generated over an interval of three standard deviations on both sides of the maximum, convoluted with a triangular moving average filter due to concentration overload and, after multiplication with a response factor, added to the baseline. In order to facilitate visual interpretation, both detector amplitude and time axes can be varied.

DISCUSSION OF THE THEORETICAL MODEL

The theoretical model is based on the calculation of the migration and dispersion of the individual separands. It consists of a number of equations which are dealt with in previous publications. In several instances, the equations were reformulated and presented in a uniform manner. For all equations, dimension analysis was applied in order to check the various steps involved in their derivation. However, they are included in the present contribution as the simulation model should be described exactly in order to make transparent the capabilities and limitations of the program.

Calculations of instrument variables and temperature effects

In the electrophoresis simulator, the following calculations are carried out each time a parameter is changed and consequently a new electropherogram is calculated, see Table I for an overview of these parameters. The field strength E (V m^{-1}) is first calculated from the constant voltage U (V) of the electrode at the injection side and the overall capillary length L_0 (m):

$$E = U/L_0 \quad (1)$$

Both U and E are signed quantities. The subsequent calculation of the driving current, power dissipation, temperature and specific conductivity requires an iteration because of the temperature dependence of mobility and conductivity. An estimate of the current is made first, assuming that the temperature in the capillary is equal to the cooling temperature. Then the buffer

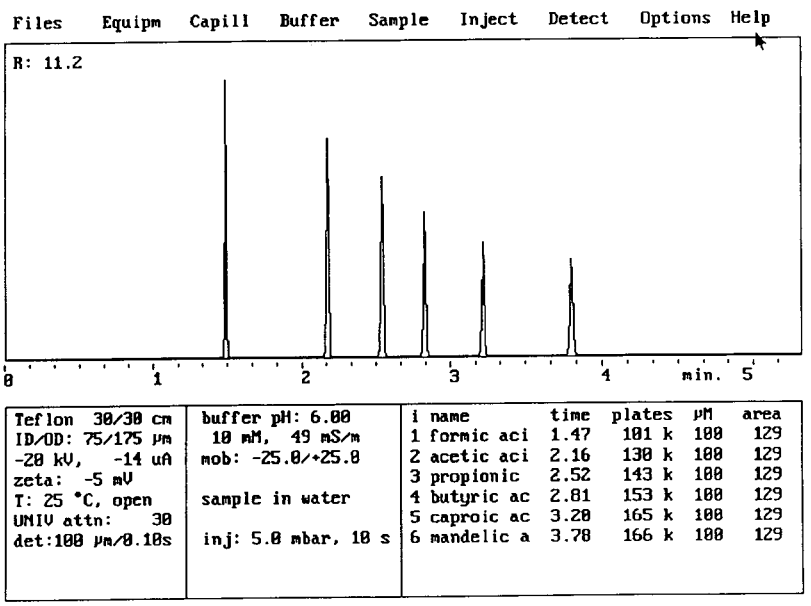

Fig. 1. Typical screen of the simulator with equipment parameters on the lower left-hand side and sample parameters on the lower right-hand side. An electropherogram is shown of signal amplitude *vs.* time.

TABLE I

MENU STRUCTURE OF THE COMPUTER PROGRAM HPCESIM

Files	Load	Equip, Buffer, Sample, pheroGram
	Save	Equip, Buffer, Sample, pheroGram
	Print	some hints on screen printing
	Edit_data	edits the data base
	Reload_data	reloads data base if data were altered
	Quit	Yes, No
Equipm	Voltage	1..35 kV
	Mode	Open, Closed
	Polarity	Positive, Negative
	Temperature	0..40°C (cooling temperature)
Capill	length Detector	50..500 mm
	Overall_length	50..500 mm
	Internal_diam.	5..200 μm
	Wall_thickness	10..200 μm
	Material	Teflon, Glass, Quartz
	Zeta potential	-200..+200 mV
Buffer	pH	2.00..12
	Ionic_strength	0.002..0.1 mol/l
	Anion_mob.	$-1..-99.10^{-9}$ $m^2V^{-1}s^{-1}$
	Cation_mob.	$+1..+99.10^{-9}$ $m^2V^{-1}s^{-1}$
Sample	Add	up to 6 (VGA: 8) components per sample
	Concentration	1..500 μmol/l
	Delete	any sample component
	Solvent	Water, Buffer
Inject	Pressure	10..300 Nm^{-2}
	Time	1..20 s
Detect	Response	Universal, Conductivity
	Attenuation	1-3000
	Slit_width	10..500 μm (aperture)
	Time_constant	0.01..1 s
	Interval	60 s..40 min.
Options	Erase	Auto, Off (superimpose signals)
	Vary	pH, Voltage, Ionic strength
	Noise	0.1..10
	Model_data	shows plate heights, resolutions, etc
	Sample_data	shows valence, pK's, mobilities
	Alter_data	valence 1..4
		pK -5..+14
		mobility $-99..+99.10^{-9}$ $m^2V^{-1}s^{-1}$
Help		

temperature in the capillary is calculated from the power dissipation. Finally, the driving current is again calculated using temperature-corrected conductivity (a temperature dependence of 2.5% per degree is taken). The iteration is repeated until the buffer-specific conductivity remains constant within 0.1%.

The iteration is carried out as follows: neglecting the contribution from H^+ and OH^-, the specific conductivity of the buffer κ (S m^{-1}) is calculated from the ionic strength I (mol l^{-1}):

$$\kappa = 10^3 FI(|u_{\mathrm{eff,A}}| + |u_{\mathrm{eff,B}}|) \quad (2)$$

where F is the Faraday constant (96 500 C mol^{-1}) and $u_{\mathrm{eff,A}}$ and $u_{\mathrm{eff,B}}$ are the effective mobility of the co-ion A and counter ion B in the background electrolyte, respectively (m^2 V^{-1} s^{-1}). For pH < 4, an additional contribution from H_3O^+ is included. The driving current i (A), having the same sign as E, follows from

$$i = \pi\kappa R_i^2 E \quad (3)$$

where R_i is the inner radius (m) of the capillary of circular cross-section.

For the calculation of the average temperature T (K) in the capillary, one first needs the temperature T_w at the inner wall. This temperature can be calculated [3] from the cooling temperature T_0 using

$$T_w = T_0 + \frac{\kappa E^2 R_i^2}{2} \cdot \frac{1}{\lambda_c} \cdot \ln\left(\frac{R_0}{R_i}\right) \quad (4)$$

where R_0 is the outside radius (m) of the capillary and λ_c the thermal conductivity of the capillary material (W m^{-1} K^{-1}). This relationship assumes a capillary that is not coated on either side. The coating normally used in capillary zone electrophoresis (CZE) with fused-silica capillaries, however, does not significantly influence their thermal properties. No limitation to heat transfer on either side of the capillary wall was assumed. Forced cooling on the outside is needed to keep this assumption reasonable.

The average temperature T in the capillary is now obtained by integration:

$$T = \frac{1}{\pi R_i^2} \int_{r=0}^{R_i} 2\pi r T(r)\, \mathrm{d}r \quad (5)$$

where $T(r)$ is the radial temperature profile:

$$T(r) = T_w + \frac{\kappa E^2 R_i^2}{4\lambda_s}\left(1 - \frac{r^2}{R_i^2}\right) \quad (6)$$

where λ_s is the thermal conductivity of the solution (W m^{-1} K^{-1}).

Integration of the former and combination with eqn. 4 yields the following relationship for the average temperature:

$$T = T_0 + \kappa E^2 R_i^2 \left[\frac{1}{2\lambda_c} \cdot \ln\left(\frac{R_0}{R_i}\right) + \frac{1}{8\lambda_s}\right] \quad (7)$$

Integration assumes a radially constant κ, a second-order effect. In a given configuration (R_0,

R_i, λ_c and λ_s) the temperature rise $(T - T_0)$ is proportional to κE^2.

After the iterative calculation of temperature and driving current, a number of other variables, which are independent of the separands, are calculated.

Migration

Effects due to finite electrolyte concentration. As the mobilities of the database refer to zero concentration, a correction for the ionic strength of the buffer is necessary. This requires more data on the separands than are normally available (ionic radius, etc.), whereas the simpler models describing concentration dependence are usually valid only up to 0.001 mol l^{-1}. Above this concentration, more sophisticated correction factors are usually necessary. This is all beyond the aim of the present simulation. However, in the co-migration of monovalent and multivalent ions, the ionic strength of the buffer can contribute considerably to selectivity [4,6]. Therefore, an approximate dependence of mobility on ionic strength and effective charge has been included.

The following relationship [32], a charge-dependent exponential decrease in mobility as a function of the square root of the ionic strength I, was used to calculate the actual mobilities u_{act} from the absolute mobilities u_{abs}:

$$u_{act,j} = u_{abs,j} \exp\left(\frac{-\sqrt{I}}{2z_{e,j}^{-1.78}}\right) \quad (8)$$

where $z_{e,j}$ is absolute charge of the subspecies j.

Calculation of migration times. For each of the separands, the effective mobility u_{eff} is now calculated from pH and all i pK_j values and $i + 1$ actual mobilities $u_{act,j}$ of ions of valence i:

$$u_{eff} = u_{act,0} + \sum_{j=1}^{i} \frac{1}{1 + 10^{(pK_j - pH)}} \cdot (u_{act,j} - u_{act,j-1}) \quad (9)$$

where $u_{act,0}$ is the mobility at low pH values, corrected for the ionic strength. Negative species have a minus sign for u so that amphoteric separands can also be included.

In open systems, electroosmotic flow can play an important role in the resulting migration time. The ζ potential (V) of the capillary wall determines the electroosmotic mobility u_{eo} (m^2 V^{-1} s^{-1}):

$$u_{eo} = -\frac{\zeta\varepsilon}{\eta} \quad (10)$$

where ε is the dielectric constant of the buffer ($708 \cdot 10^{-12}$ F m^{-1} for water at room temperature) and η is the viscosity of the buffer (N m^{-2} s). The value for η in this relationship is corrected to the average temperature T with a temperature coefficient of -0.025 K^{-1}.

The ζ potential is introduced here as an independent variable, which requires some explanation. In actual practice, the ζ potential of the capillary material will depend on both the ionic strength and pH of the electrolyte in a complicated manner. The effects resulting from coating procedures and additives to the background electrolyte will add a further complication. In addition, the ζ potential may change both in time and in axial direction (sample introduction). All these effects are too dependent on unknown actual conditions to be able to simulate in a practicle manner. In the present simulator, the effects of electroosmosis, buffer ionic strength and pH and sample load can thus be investigated in a mutually independent way.

As was also pointed out in a previous paper [16], it will be shown here that the effective mobility relative to the total mobility plays an important role in migration and dispersion. For this reason, the dimensionless parameter electromigration factor f_{em} is introduced as the relative contribution of electrophoretic mobility to the total mobility:

$$f_{em} = \frac{u_{eff}}{u_{eff} + u_{eo}} \quad (11)$$

The effective electrophoretic and electroosmotic mobilities in this equation are signed quantities. A negative value of f_{em} can therefore be obtained. Physically it would mean an ion moving against the electroosmotic flow with a net velocity in the direction of electroosmosis. Whether such a separand would reach the detector depends on the sign of the field strength, electroosmosis and charge.

Now the migration time t_m(s) follows from u_{eff} and u_{eo}:

$$t_m = \frac{L_d}{E(u_{eo} + u_{eff})} = \frac{L_d f_{em}}{E u_{eff}} \quad \text{(open systems)} \tag{12}$$

$$t_m = \frac{L_d}{E u_{eff}} \quad \text{(closed systems)} \tag{12a}$$

where L_d is the length of the capillary to the detector. Only those separands with a positive sign of t_m will eventually reach the detector. Separands having a negative migration time move away from the detector and are not considered in subsequent calculations. Positive migration times occur if none or two of the variables f_{em}, E or u_{eff} is negative.

In the above and subsequent relationships where a distinction between open and closed systems was made, the electromigration factor f_{em} plays an essential role. It must be emphasized that in closed systems the value of f_{em} is not necessarily unity, although the net electroosmotic flow is compensated for by closing the system with a membrane or another device; u_{eo} is not zero unless other precautions such as surface modification are also taken.

Dispersion

Peak dispersion can be described by the plate height model. For the case that the individual contributions to peak broadening are independent of each other, their particular plate height H_i can be incrementally added, giving the total plate height [19]. The peak width, given by the second moment (the square of the standard deviation for the case of a Gaussian partition function) is related to H by $\sigma^2 = L_d H$, where σ is expressed in distance units in the capillary.

Two different types of contributions to peak broadening will be discussed in the following: those caused by extra-column effects [19–21], given by the finite width of injection and detector slit width and time constant, and those originating from the electrophoretic process [14–18], *i.e.*, longitudinal diffusion, heat generation and the occurrence of the profile of the electroosmotic flow. Concentration overload [22,23] and stacking [24–26] are also considered.

Extra-column effects of injection and detection. The applied sample injection volume V_{inj}(m^3) is

$$V_{inj} = \frac{\pi P R_i^4 t_{inj}}{8 L_0 \eta} \tag{13}$$

where P is the pressure drop (N m^{-2}) and t_{inj} the injection time (s). The η value in this case is corrected to the cooling temperature as injection takes place with the high voltage switched off. The amount injected is calculated from the separand concentration in the sample and V_{inj}.

Depending on the ionic strength of the sample (dissolved in buffer or in water), a stacking effect [24–26] is caused by the fact that the field strength in the sample compartment is different from that in the separation compartment. This field strength ratio is equal to the inverse of the specific conductivity ratio. This requires additional knowledge of sample counter ion types, pK values and concentrations and also sample pH. In order to circumvent this problem, this specific conductivity ratio is approximated by the ionic strength ratio, so that

$$\frac{E_s}{E} = \frac{I}{I_s} \tag{14}$$

where the subscript s indicates the non-adjusted sample plug. This relationship does not take into account effective mobility differences between the components present, including the effect of pH in the sample compartment. The ionic strength of the sample I_s is in turn approximated by the total concentration of sample components.

After stacking, the volume of the adjusted sample plug V_{st} is

$$V_{st} = V_{inj} \cdot \frac{I_s}{I} = \frac{\pi P R_i^4 t_{inj} I_s}{8 L_0 \eta I} \tag{15}$$

and the length δ_{inj}(m) of the cylindrical, stacked sample plug is

$$\delta_{inj} = \frac{V_{st}}{\pi R_i^2} = \frac{P R_i^2 t_{inj} I_s}{8 L_0 \eta I} \tag{16}$$

Assuming an initially rectangular concentration

profile [19], the plate height H_{inj} due to injection dispersion can be calculated by

$$H_{inj} = \frac{L_d}{12}\left(\frac{\delta_{inj}}{L_d}\right)^2 = \frac{\delta_{inj}^2}{12L_d} = \frac{P^2 R_i^4 t_{inj}^2 I_s^2}{768 L_d L_0^2 \eta^2 I^2} \quad (17)$$

The detector slit width δ_{det}(m), also assumed to be of a rectangular shape, determines the plate height in a way similar to the contribution from the injection:

$$H_{det} = \frac{L_d}{12}\left(\frac{\delta_{det}}{L_d}\right)^2 = \frac{\delta_{det}^2}{12L_d} \quad (18)$$

The dynamic response of the detector, expressed by the time constant τ(s) contributes as an exponential function to the total plate height [19], in which the respective migration times t_m can be substituted:

$$H_\tau = L_d\left(\frac{\tau}{t_m}\right)^2 = \frac{\tau^2 E^2 u_{eff}^2}{f_{em}^2 L_d} \quad \text{(open systems)} \quad (19)$$

$$H_\tau = L_d\left(\frac{\tau}{t_m}\right)^2 = \frac{\tau^2 E^2 u_{eff}^2}{L_d} \quad \text{(closed systems)} \quad (19a)$$

Longitudinal diffusion. The equation for the plate number H_{dif} due to diffusion in a longitudinal direction consists of

$$H_{dif} = L_d\left(\frac{\sigma_{dif}}{L_d}\right)^2 \quad (20)$$

The length-based variance σ_{dif}^2(m) due to longitudinal diffusion is given by the Einstein equation:

$$\sigma_{dif}^2 = 2Dt_m \quad (21)$$

In this equation, the diffusion coefficient D (m^2 s^{-1}) is replaced with the effective mobility u_{eff} with the Nernst–Einstein relationship:

$$D = \frac{u_{eff} RT}{z_e F} \quad (22)$$

where R is the gas constant (8.31 J mol^{-1} K^{-1}) and z_e is the overall effective charge of the separand.

Substitution of eqns. 12, 21 and 22 into eqn. 20 yields [16]

$$H_{dif} = \frac{2RT}{z_e EF} \cdot f_{em} \quad \text{(open systems)} \quad (23)$$

$$H_{dif} = \frac{2RT}{z_e EF} \quad \text{(closed systems)} \quad (23a)$$

In eqn. 23, z_e and E have opposite sign only for negative f_{em} values. The z_e value of each separand in the sample is obtained from the pH and the pK values of the subspecies:

$$z_e = z_0 - \sum_{j=1}^{n_i} \frac{1}{1 + 10^{(pK_j - pH)}} \quad (24)$$

where z_0 is the charge at low pH.

Thermal dispersion. Peak broadening due to thermal dispersion [3] is represented by the variance σ_T^2(m^2):

$$\sigma_T^2 = 2D_T t_m \quad (25)$$

The corresponding diffusivity D_T (m^2 s^{-1}), which substitutes the diffusion coefficient in the Einstein equation, was estimated by Virtanen [3]:

$$D_T = \frac{f_T^2 \kappa^2 u_{eff}^2 E^6 R_i^6}{3072 D \lambda_s^2} \quad (26)$$

where f_T is the temperature factor of κ and u $[(1/u)(\delta u/\delta T)$ $(K^{-1})]$. In this relationship, D is also converted into the effective mobility u_{eff} with eqn. 22. Using these equations, the plate height contribution due to thermal dispersion is derived as follows:

$$H_{ther} = L_d\left(\frac{\sigma_T}{L_d}\right)^2 = \frac{f_T^2 \kappa^2 E^6 R_i^6 z_e F}{1536 RT \lambda_s^2} \cdot \frac{u_{eff} t_m}{L_d}$$

$$H_{ther} = \frac{f_T^2 \kappa^2 E^5 R_i^6 z_e F}{1536 RT \lambda_s^2} \cdot f_{em} \quad \text{(open systems)} \quad (27)$$

$$H_{ther} = \frac{f_T^2 \kappa^2 E^5 R_i^6 z_e F}{1536 RT \lambda_s^2} \quad \text{(closed systems)} \quad (27a)$$

At first sight, the occurrence of the temperature T in the denominator may look strange as it would mean that H_{ther} would decrease with increasing temperature. At room temperature this effect is only 0.3% per degree. The temperature rise with respect to the thermostating tem-

perature is, however, proportional to κE^2, the proportionality constant follows from eqn. 7. As $\kappa^2 E^5$ is in the numerator, this clearly dominates the overall temperature dependence of H_{ther}. If the temperature coefficients of u_{em} and u_{eo} are taken to be of the same order of magnitude, f_{em} will be relatively independent of temperature. There are three coefficients in eqn. 27 which may have a negative sign: E^5, z_e and f_{em}. Their product will always be positive for those ions reaching the detector.

Electroosmotic dispersion. The dispersion due to electroosmosis is considered negligeable in open systems [2,3], assuming ideal plug flow, and therefore a hypothetical value of 10^{-9} m for H_{eo} is taken. In closed systems this is not the case, contributing the variance σ_{eo}^2 (m^2) by

$$\sigma_{eo}^2 = 2D_{eo}t_m \tag{28}$$

The corresponding diffusivity D_{eo} ($m^2\ s^{-1}$) follows from

$$D_{eo} = \frac{R_i^2 u_{eo}^2 E^2}{48D} \tag{29}$$

The plate height H_{eo}, originating from electroosmotic dispersion, is calculated, again using the Nernst–Einstein relationship in order to replace the diffusion coefficient D, leading to

$$H_{eo} = L_d\left(\frac{\sigma_{eo}}{L_d}\right)^2 = \frac{R_i^2 u_{eo}^2 E^2 z_e F t_m}{24RTu_{eff}L_d} \tag{30}$$

Substitution of t_m by L_d/Eu_{eff} yields

$$H_{eo} = \frac{R_i^2 z_e EF}{24RT}\left(\frac{1}{f_{em}} - 1\right)^2 \tag{31}$$

The influence of the ζ potential is, of course, included in the electromigration factor f_{em}. Substitution of u_{eo} makes ζ more readily visible:

$$H_{eo} = \frac{R_i^2 \zeta^2 \varepsilon^2 z_e EF}{24RT\eta^2 u_{eff}^2} \tag{31a}$$

Electromigration dispersion (concentration overload). If the dispersion due to electromigration is considered [22,23], a triangular concentration distribution seems a fair approximation. The width of the triangle and the form (leading *vs.* tailing) are estimated as follows: the ratio of the effective mobility of the sample ($u_{eff,i}$) and that of the co-ion in the background electrolyte ($u_{eff,A}$) is first calculated:

$$r_i = \frac{u_{eff,i}}{u_{eff,A}} \tag{32}$$

The variables r_i, k_i and a_i were introduced by Mikkers *et al.* [22] to play a key role in electromigration dispersion of separand i. They are calculated as follows:

$$k_i = \frac{r_i - r_B}{(1 - r_B)r_i} \tag{33}$$

and

$$a_i = \frac{k_i(1 - r_i)}{I} \tag{34}$$

where r_B is the relative counter ion mobility, always negative as mobilities are signed quantities. Consequently, k_i is always positive. The sign of a_i designates either a leading or a tailing triangle. In order to avoid lengthy iterations, the mutual interference of the separand ions is limited to their contribution in the sample compartment.

When $r_i \neq 1$, the base width of the triangle δ_t can now be calculated [22], also using c_i, the non-adjusted separand concentration in the sample compartment:

$$\delta_t = |a_i|c_i\delta_{inj} + 2\sqrt{|u_{eff}Et_m a_i c_i \delta_{inj}|} \tag{35}$$

Considering both open (eqn. 12) and closed systems (eqn. 12a), it can be observed that shortly after switching on, the second term on the right-hand side of eqn. 33 will predominate, so that for closed systems:

$$\delta_t = 2\sqrt{|L_d a_i c_i \delta_{inj}|} \tag{35a}$$

This relationship was derived for electrophoresis in closed systems, assuming no additional dispersion. If, in open systems, the electroosmotic plug flow only changes t_m and the velocity of the front and the back of the triangle have equal velocity, the relationship can also apply in these cases, with the factor $|f_{em}|$ added under the square root sign.

To estimate the contribution of migration to the total dispersion, the migration effect is translated into the corresponding plate height [19], again only valid for $r_i \neq 1$ in open systems:

$$H_{conc} = \frac{L_d}{18}\left(\frac{\delta_t}{L_d}\right)^2 = \left|\frac{2a_i c_i \delta_{inj} f_{em}}{9}\right| \quad (36)$$

For closed systems, the migration time does not contain f_{em}, so

$$H_{conc} = \left|\frac{2a_i c_i \delta_{inj}}{9}\right| \quad (36a)$$

For the case where the effective mobility of the separand is equal to that of the co-ion in the background electrolyte ($r_i = 1$), δ_{inj} is the only additional contribution to the total Gaussian peak broadening, as mentioned above.

The triangular concentration distribution has an infinitely sharp (isotachophoretic) front for $r_i < 1$; for $r_i > 1$ it is sharp on the rear. The triangular concentration distribution is in fact an isotachophoretic sharpening effect that counteracts longitudinal diffusion. The approximation in the present simulation model is that these two effects are considered mutually independent, so that the plate height contributions are additive.

If all dispersive factors are considered independent, the corresponding variances are additive and the overall plate height H becomes

$$H = H_{inj} + H_{det} + H_{\tau} + H_{eo} + H_{ther} + H_{dif} + H_{conc}$$

Finally, substitution of the respective individual contributions yields the total plate height equation for free CZE in open systems:

$$H = \frac{P^2 R_i^4 t_{inj}^2 I_s^2}{768 L_d L_0^2 \eta^2 I^2} + \frac{\delta_{det}^2}{12 L_d} + \frac{\tau^2 E^2 u_{eff}^2}{f_{em}^2 L_d} + \frac{f_T^2 \kappa^2 E^5 R_i^6 z_e F}{1536 RT\lambda^2} \cdot f_{em} + \frac{2RT}{z_e EF} \cdot f_{em} + \left|\frac{2a_i c_i \delta_{inj} f_{em}}{9}\right| \quad (37)$$

and for closed systems:

$$H = \frac{P^2 R_i^4 t_{inj}^2 I_s^2}{768 L_d L_0^2 \eta^2 I^2} + \frac{\delta_{det}^2}{12 L_d} + \frac{\tau^2 E^2 u_{eff}^2}{L_d} + \frac{R_i^2 z_e EF}{24RT}\left(\frac{1}{f_{em}} - 1\right)^2 + \frac{f_T^2 \kappa^2 E^5 R_i^6 z_e F}{1536 RT\lambda^2} + \frac{2RT}{z_e EF} + \left|\frac{2a_i c_i \delta_{inj}}{9}\right| \quad (37a)$$

DISCUSSION

It is remarkable that several of these expressions include the electromigration factor f_{em} defined. As CZE is normally carried out in quartz capillaries, which exhibit a negative zeta potential, the electroosmotic mobility is consequently positive, the case on which the following discussion will be focused.

The dependence of f_{em} on the electrophoretic and electroosmotic mobility is fairly simple for cations, as shown in Fig. 2. Independent of the value of the electrophoretic mobility, f_{em} is unity for the case when no electroosmosis occurs. When electroosmosis does occur in the system, the factor f_{em} decreases with increasing electroosmotic mobility. In that case the effect of dispersion due to the three processes considered is reduced, which is obvious because sample components are transported through the separation capillary faster than without electroosmosis, and a shorter time is available for dispersion. As a consequence, the effect is more pronounced for cations with a low rather than a high effective mobility.

For anions the situation is more complex, as shown in Fig. 3. It can be seen that as for cations the value of f_{em} is unity in the absence of electroosmosis. In contrast to cations, f_{em} increases with increasing electroosmotic mobility for ions of a given mobility, very steeply when values for u_{eo} are approached which are similar to u_{eff}. For $u_{eo} = u_{eff}$, f_{em} is not defined: the electrophoretic velocity of the ion is exactly counterbalanced by the velocity of the electroosmotic flow, directed towards the cathode. Within the region under discussion, the plate height is always larger and the plate number smaller for anions with electroosmosis than without electroosmotic flow. If the value of u_{eo}

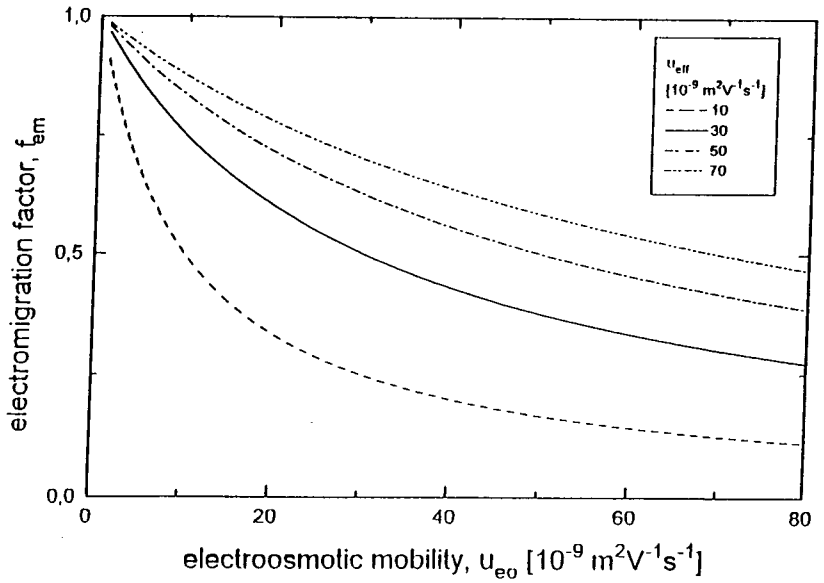

Fig. 2. Dimensionless electromigration factor f_{em} as a function of the electroosmotic mobility for cations at different electrophoretic mobilities.

exceeds that of u_{eff}, f_{em} becomes negative (the negative signs of f_{em} are always counterbalanced by negative signs of either z_e, E or U, as discussed previously, so that always positive plate height terms are obtained).

The absolute value of f_{em} therefore decreases steeply with increasing electroosmotic mobility and the corresponding plate heights also decrease. Here, the electric potential must be chosen positive, so that the ions are swept to the

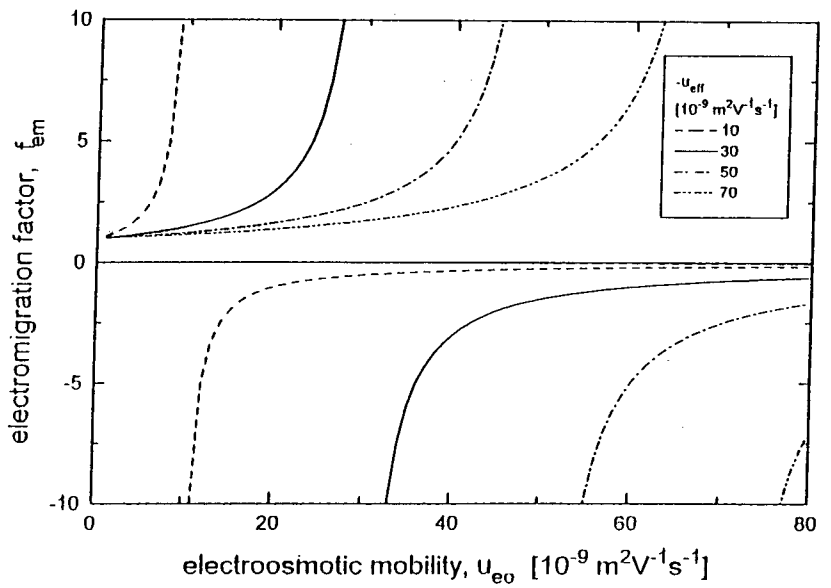

Fig. 3. Dimensionless electromigration factor f_{em} as a function of the electroosmotic mobility for anions at different electrophoretic mobilities.

cathode by electroosmosis. Within the entire range of u_{eo} the absolute value of f_{em} is larger than unity, which means that under those conditions the plate height is always larger than without electroosmosis. In contrast, the value of f_{em} is unity again when u_{eo} has twice the value of u_{eff}. For higher values of u_{eo}, f_{em} is smaller than unity, as for cations, and the plate heights are smaller than for the case without electroosmosis. This is clear because in this region the overall migration times (to the cathode side of the capillary) are finally smaller as for the case with pure electrophoretic migration, owing to the high velocity of the electroosmotic flow.

It should be pointed out, however, that the aim of CZE is the separation of components, and not only the generation of narrow peaks. Hence peak dispersion is only one side of the problem, and the effect of electroosmosis on the selectivity also has to be considered. It can be easily shown that, *e.g.*, for cations, the resolution is decreasing when electroosmosis occurs, despite the fact that the plate height is reduced. For anions again different regions can be distinguished. This problem has been discussed in more detail in a previous paper [16].

CONCLUSIONS

Migration model

The model of migration is straightforward; both electromigration and electroosmotic are taken into account. Concentration corrections for migration are applied in the form a simple approximation that already illustrates the importance of the ionic strength as a selectivity parameter. Temperature correction of mobilities is based on well known equations available in the literature. It is seen that the temperature rise in currently used capillaries can be kept to a minimum but that the thermostating temperature has a distinct influence on the migration times obtained. As the time axis is made variable between 1 and 40 min, the migration behaviour can be studied in a broad mobility range.

Dispersion model

All possible contributions to dispersion, except mutual interaction of separands during migration and adsorption, are considered. The contributions are given in the form of terms in a plate height equation. On a separate screen page, all plate height contributions are shown for the individual separands. Several, such as injection dispersion, other than caused by concentration overload, can under certain conditions be neglected with respect to others. Relating to detection dispersion (aperture, time constant), certain minimum instrumental requirements are easily calculated so that the detection can be optimized in this respect. Also, thermal dispersion can be controlled well enough. The model assumes that electroosmotic dispersion is only of importance in closed systems, with the electromigration factor f_{em} as a key parameter.

Limitations of the simulation

The predictive value of the model is of course limited, especially by the quality of the input data, the origin of which does not always describe in detail under what circumstances the mobilities and pK values were measured. In addition, the effect of concentration (ionic strength) is taken into account only in an approximate manner. The temperature coefficient for mobility is taken as 0.025 K^{-1} for all components whereas the pK values are assumed to be independent of temperature.

The behaviour of components is assumed to be independent of the presence of any other component, except for the properties of the buffer. In reality this is not always the case, but it is common practice to design an experiment in such a way that these matrix effects are limited.

As for the sample matrix effect during injection, sample pH and mutual interference between sample components are not taken into account. Also not included in the model are adsorption effects, leading to unsymmetric peaks and peak broadening due to different migration paths in coiled capillaries.

SYMBOLS

a_i	overload parameter (l mol^{-1})
c_i	non-adjusted separand concentration (mol l^{-1})
D	diffusion coefficient (m^2 s^{-1})

E field strength (V m^{-1})
f_{em} electromigration factor
f_T relative temperature coefficient for u (0.025) (K^{-1})
F Faraday constant (96 500) (C mol^{-1})
H overall plate height (m)
H_{inj} plate height due to injection (m)
H_{eo} plate height due to electroosmosis (m)
H_{dif} plate height due to diffusion (m)
H_{ther} plate height due to Joule heating (m)
H_τ plate height due to time constant (m)
H_{det} plate height due to detector slit width (m)
H_{conc} plate height due to concentration (m)
i current through capillary (A)
I ionic strength of buffer (mol l^{-1})
I_s ionic strength of sample (mol l^{-1})
k_i overload parameter
L_d length of capillary to detector (m)
L_0 overall length of capillary (m)
n_i valence of i
pH pH of buffer
pK_j pK of species j
P injection pressure (N m^{-2})
r distance from capillary axis (m)
r_i relative effective mobility of i
R gas constant (8.314) (J mol^{-1} K^{-1})
R_i inner radius of the capillary (m)
R_0 outer radius of the capillary (m)
t_{inj} injection time (s)
t_m migration time (s)
T_0 cooling temperature (K)
T_w temperature at inner wall (K)
T average temperature inside (K)
u_{eo} electroosmotic mobility (m^2 V^{-1} s^{-1})
u_{eff} effective electrophoretic mobility (m^2 V^{-1} s^{-1})
u_j absolute mobility of species j (m^2 V^{-1} s^{-1})
$u_{eff,A}$ effective mobility of co-ion (m^2 V^{-1} s^{-1})
$u_{eff,B}$ effective mobility of counter ion (m^2 V^{-1} s^{-1})
U voltage (V)
V_{inj} injected volume (m^3)
V_{sam} adjusted sample volume (m^3)
z_e effective charge number
z_0 charge at very low pH

α degree of dissociation
δ_{inj} adjusted sample length (m)
δ_{det} slit width of detector (m)
δ_t triangle width of zone (m)
ε dielectric constant ($708 \cdot 10^{-12}$) (F m^{-1})
κ specific conductivity of buffer (S m^{-1})
λ_s thermal conductivity of the solution (0.592) (W m^{-1} K^{-1})
λ_c thermal conductivity of the capillary (0.4–1.3) (W m^{-1} K^{-1})
η viscosity of buffer (0.0008904) (N m^{-2} s)
π constant (3.14159)
σ standard deviation (peak dispersion) (m)
σ_T^2 thermal dispersion variance (m^2)
σ_{eo}^2 electroosmotic dispersion variance (m^2)
τ time constant of the detector (s)
ζ zeta potential of the capillary (V)

REFERENCES

1 J.C. Giddings, in I.M. Kolthoff and P.J. Elving (Editors), *Treatise on Analytical Chemistry*, part I, Vol. 5, Wiley, New York, 1981, pp. 65–164.
2 S. Hjertén, *Chromatogr. Rev.*, 9 (1967) 122.
3 R. Virtanen, *Acta Polytech. Scand.*, 123 (1974) 1–67.
4 F.M. Everaerts, J.L. Beckers and Th.P.E.M. Verheggen, *Isotachophoresis —Theory, Instrumentation and Applications* (*Journal of Chromatography Library*, Vol. 7), Elsevier, Amsterdam, 1976.
5 J.W. Jorgenson and K.D. Lucaks, *Science*, 222 (1983) 266.
6 P. Bocek, M. Deml, P. Gebauer and V. Dolnik, *Analytical Isotachophoresis*, VCH, Weinheim, 1988.
7 F. Foret and P. Boček, in A. Chrambach, M.J. Dunn and B.J. Radola (Editors), *Advances in Electrophoresis*, *3*, VCH, Weinheim, 1989, pp. 273–342.
8 S. Hjertén, *Electrophoresis*, 11 (1990) 665.
9 S.F.Y. Li, *Capillary Electrophoresis —Principles, Practice and Applications* (*Journal of Chromatography Library*, Vol. 52), Elsevier, Amsterdam, 1992.
10 R.A. Mosher, D.A. Saville and W. Thormann, *The Dynamics of Electrophoresis*, VCH, Weinheim, 1992.
11 E.V. Dose and G.A. Guiochon, *Anal. Chem.*, 63 (1991) 1063.
12 J. Heinrich and H. Wagner, *Electrophoresis*, 13 (1992) 44.
13 H. Poppe, *J. Chromatogr.*, 506 (1990) 45.
14 F. Foret, M. Deml and P. Bocek, *J. Chromatogr.*, 452 (1988) 601.
15 E. Kenndler and Ch. Schwer, *Anal. Chem.*, 63 (1991) 2499.
16 Ch. Schwer and E. Kenndler, *Chromatographia*, 33 (1992) 331.
17 E. Kenndler and W. Friedl, *J. Chromatogr.*, 608 (1992) 161.
18 W. Friedl and E. Kenndler, *Anal. Chem.*, 65 (1993) 2003.
19 J. Sternberg, *Adv. Chromatogr.*, 2 (1966) 205–270.

20 K. Otsuka and S. Terabe, *J. Chromatogr.*, 480 (1989) 91.
21 X. Huang, W.F. Coleman and R.N. Zare, *J. Chromatogr.*, 480 (1989) 95.
22 F.E.P. Mikkers, F.M. Everaerts and Th.P.E.M. Verheggen, *J. Chromatogr.*, 169 (1979) 1.
23 H. Poppe, *Anal. Chem.*, 64 (1992) 1908.
24 B. Gas, J. Vacik and I. Zelensky, *J. Chromatogr.*, 545 (1991) 225.
25 P. Gebauer, W. Thormann and P. Bocek, *J. Chromatogr.*, 608 (1992) 47.
26 C. Schwer, B. Gas, W. Lottspeich and E. Kenndler, *Anal. Chem.*, 65 (1993) 2108.
27 Th.P.E.M. Verheggen and F.M. Everaerts, *J. Chromatogr.*, 638 (1993) 147.
28 J.C. Reijenga, *J. Chromatogr.*, 588 (1991) 217.
29 T. Hirokawa, M. Nishimo and Y. Kiso, *J. Chromatogr.*, 252 (1982) 49.
30 T. Hirokawa, M. Nishino, N. Aoki, Y. Kiso, Y. Sawamoto, T. Yagi and J.-I. Akiyama, *J. Chromatogr.*, 271 (1983) D1.
31 T. Hirokawa, Y. Kiso, B. Gas, I. Zuskova and J. Vacík, *J. Chromatogr.*, 628 (1993) 283.
32 J.C. Reijenga, *Internal Report*, University of Technology, Eindhoven, 1993.

Journal of Chromatography A, 659 (1994) 417–426
Elsevier Science B.V., Amsterdam

CHROM. 25 695

Computational simulation of migration and dispersion in free capillary zone electrophoresis

II. Results of simulation and comparison with measurements

J.C. Reijenga

Department of Chemical Engineering, Eindhoven University of Technology, P.O. Box 513, 5600 MB Eindhoven (Netherlands)

E. Kenndler*

Institute of Analytical Chemistry, University of Vienna, Währingerstrasse 38, A-1090 Vienna (Austria)

(First received June 24th, 1993; revised manuscript received September 10th, 1993)

ABSTRACT

The results of the simulation of electropherograms for CZE obtained by the instrumental simulator described in Part I are presented as functions of various experimental parameters. The electropherograms, demonstrating the effects of the injection zone length and sample composition on peak broadening, of the ζ potential on migration and efficiency, of minute changes in pH on the resolution, of the ionic strength of the buffer on the separation selectivity and of the co-ion of the background electrolyte on peak shape, are simulated within a few seconds. A comparison was made between simulated electropherograms and those obtained by measurements with real equipment.

INTRODUCTION

The theoretical background of the instrumental simulator introduced in Part I [1] was described there in detail. It provides in a fast way to simulate electropherograms as a function of a number of instrumental variables and physicochemical properties, based on two processes: migration and dispersion. For the calculation of the final result, depicted by the electropherogram, the appropriate expressions are used which take into account the analyte and the system features. Their consequences and limitations were discussed in detail in Part I.

It is the aim of this second part to demonstrate the performance of the simulation based on the plausibility of the resulting electropherograms, rather than to aspire to maximum agreement with experimental data. The latter will always be limited not only by the approximations of the theoretical model, but also by the quality of the input data necessary for the simulation (mainly pK values and absolute mobilities), which is often difficult to estimate.

In this paper, first the results are discussed when working parameters such as injection zone length, ζ potential and composition of the buffer are varied. The simulation illustrates that partially unexpected large effects on the electropherograms occur. The simulator is able to show, *e.g.*,

* Corresponding author.

SSDI 0021-9673(93)E1141-L

the significant influence of a likewise minute ζ potential (or electroosmotic mobility) on ion migration, a fact which is especially important when working with capillaries with a coated inner surface. Another example reflects the possible role of extremely small changes in the pH of the buffer, even in the range of a few hundredths of a unit. The normally underestimated role of the ionic strength on the separation selectivity, and possibly on the migration order of the separands, can also be demonstrated by simulation.

Second, a comparison is made of electropherograms measured with real equipment under given conditions with those resulting from the simulation. Some of these comparisons are carried out in pH ranges which are critical for the shape of the electropherograms. A comparison is finally made with two results published by Poppe [2], one obtained with another simulation algorithm, based on eigenvalues, and the other resulting from measurements.

EXPERIMENTAL

Chemicals

The chemicals used for the preparation of the standards and buffers and for the coating of the capillary were of highest available purity obtained from Merck (Darmstadt, Germany), EGA (Steinheim, Germany) and Fluka (Buchs, Switzerland). For the coating of the capillary, methylcellulose (Methocel MC, 3000–5000 mPa s; Fluka) was used. Water was doubly distilled from a quartz apparatus before use.

Apparatus

The electropherograms were measured with an instrument (P/ACE System 2000; Beckman, Palo Alto, CA, USA), which was equipped with a UV absorbance detector set at 214 nm. The system was controlled by a computer system with GOLD software (Beckman), which was also used for data acquisition.

The inner surface of the fused-silica capillary (269 mm overall length, 201 mm length to the detector, 75 μm I.D., 275 μm O.D.) (Scientific Glass Engineering, Ringwood, Australia) was coated according to a procedure described by Hjertén [3] in order to suppress electroosmosis for a number of experiments. The capillary was thermostated at 25.0°C.

The computer simulations were carried out as described in Part I [1].

RESULTS AND DISCUSSION

Variation of instrumental parameters

The results of the simulation will be discussed for the following examples: (i) the influence of the length of the injection zone on the peak width, with and without sample stacking; (ii) the influence of a very small ζ potential (or electroosmotic mobility) on migration times (and efficiency); (iii) the influence of the pH of the buffer on the resolution; (iv) the effect of the ionic strength of the buffer on the selectivity; and (v) the influence of the co-ion mobility on the electromigration dispersion (concentration overload).

Influence of injection width and sample composition. The length of the injection zone can contribute significantly to the total peak width according to the additivity of the variances of the individual contributions to peak broadening [4]. This effect is visible especially when the dispersion due to the dynamic processes is very low, which is often the case when a high voltage is applied and when the analytes carry a high effective charge number. The influence of the large injection volume can be dominant also when stacking cannot be achieved owing to the composition of the sample. From Fig. 1, it can be seen that the increase in the length of the injection zone, caused by an increase in the sampling time from 2 to 8 s (at a pressure of 5 mbar), can lead to a drastic decrease in resolution, especially when the sample is dissolved in buffer. The length of the injection zone increases from 0.71 mm at 2 s to 2.8 mm at 8 s under the given conditions, at an effective length of the capillary of 200 mm. The two last appearing peaks (4 and 5 in Fig. 1), which are separated with baseline resolution at an injection time of 2 s, show a highly reduced resolution at the longer sampling interval. This is caused by the fact that the plate height contribution due to the long injection zone, H_{inj} (about 4 μm at an

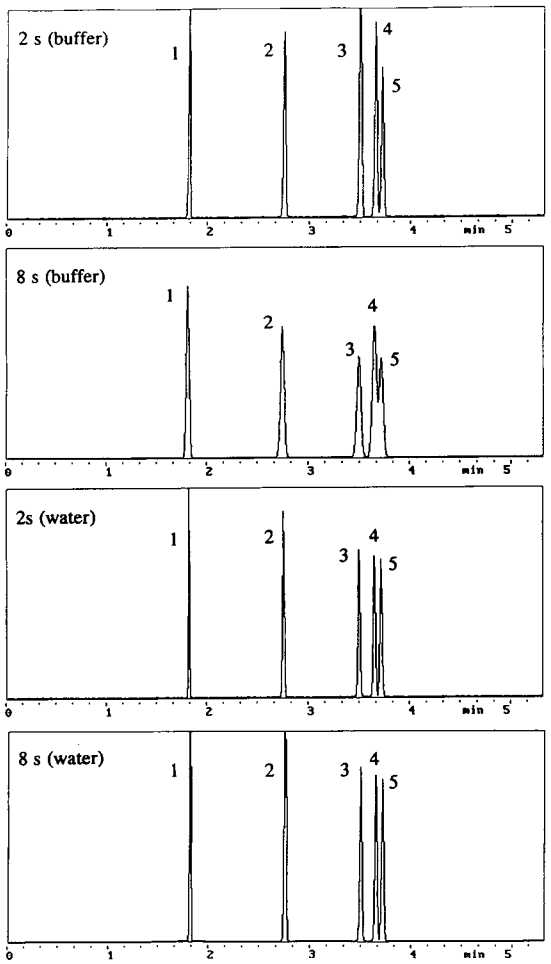

Fig. 1. Simulated electropherograms demonstrating peak broadening due to extra-column effects (length of injection zone) and sample stacking. Capillary: overall length 250 mm (effective length from injector to detector 200 mm) × 75 μm I.D. × 175 μm O.D.; voltage, −10 000 V; ζ potential, −3 mV (open mode); cooling temperature, 25.0°C. Buffer: pH 6.00; ionic strength, 0.010 mol/l; buffer ion mobilities, $-24.0 \cdot 10^{-9}$ and $+25.0 \cdot 10^{-9}$ $m^2/V \cdot s$. Injection: hydrodynamic, varying time: 2 or 8 s; 5.0 mbar; from water or buffer. Detection: "universal"; attenuation, 3 (2 s) or 10 (8 s); slit width, 200 μm; time constant, 0.10 s. Sample: 1 = 1,3-benzenedicarboxylate; 2 = 2,6-dinitrophenolate; 3 = 2,3-dimethoxybenzoate; 4 = 3,4-dimethoxybenzoate; 5 = 2,4-dimethoxybenzoate. Concentration: 100 μmol/l each.

8-s sampling time), given by eqn. 17 in Part I, predominates the total plate height, H, given by eqn. 37 in Part I, which is about 6 μm for these components.

If the sample is dissolved in pure water, and not in buffer (or in a solution with a similarly high conductivity), sample stacking occurs, and a concentrating and enrichment step leads to a shorter, sharper injection zone. In the case under consideration a stacking factor of about 10 is achieved. This effect can clearly be seen by comparing the corresponding electropherograms in Fig. 1. The two last peaks are still separated with baseline resolution even at an injection time of 8 s, caused by the improvement in the efficiency due to stacking: the plate height at 8 s is about 1.6 μm for these components, which is nearly the same as for a 2-s sampling time from water, and is even slightly better than at a 2-s injection time from buffer, where about 1.9 μm is observed. The large enhancement of efficiency by the stacking process can be seen from the plate height compared with that reached for an 8-s injection time from buffer, which is 6 μm and more, as mentioned above.

Influence of small ζ potentials on migration and efficiency. The problem of the variation of the ζ potential within one capillary under experimental conditions in practice was discussed in Part I. The simulation is nevertheless able to demonstrate how both the migration time and the efficiency are influenced by even very low ζ potentials. This result is important for systems where the electroosmotic migration is supressed but not eliminated entirely, which can be the case when working with coated columns. In these cases the electroosmotic velocity is difficult to determine by measurements with electrically neutral flow markers. The migration velocity of such a marker at, *e.g.*, 7 kV voltage across a 27 cm long capillary is only 0.02 mm/s for a ζ potential of −1 mV. This is the case when the initial ζ potential (about −120 mV for fused silica at high pH) is suppressed by more than 99%. The detector, placed, *e.g.*, at a 20-cm distance from the injector, is reached after 2.8 h, which is normally too long to be measured. Even for a five times higher ζ potential an electroosmotic velocity of 0.09 mm/s leads to a migration time of the neutral marker of 37 min in such a short capillary, so that the occurrence of an electroosmotic flow is thus often not noticed.

In the case under discussion, the separation of

anions is simulated in a fused-silica capillary with very reduced electroosmosis, reflecting the conditions in coated capillaries with a low residual ζ potential. The voltage is applied such that the separands are migrating to the anode (the electroosmotic flow is directed to the cathode, the reverse direction of the anion movement). From Table I it can be seen that this small ζ potential can, however, significantly influence the migration times of the separands in an open system as given by eqn. 12 in Part I (in closed systems no contribution to ion migration due to electroosmosis is assumed; in such cases only the efficiency is decreased).

Even such a small ζ potential as -1 mV influences the migration times considerably, especially for anions with low mobility. It can be seen that the migration times show a bias of as much as about 2% at this ζ potential in an open capillary, when compared with a closed capillary system. The deviation of the migration time at -5 mV is larger than 10% compared with the case without electroosmosis. This deviation is much larger than that which can be expected in capillaries with excluded electroosmosis. Although the resolution of the separands will not change dramatically under the given conditions (the electroosmotic mobility is small relative to the effective mobilities of the separands), it is seen that the determination of mobilities from the migration times in coated capillaries must be critically proved in order to obtain accurate values. One possibility is to control the extent of electroosmosis by calibration with a reference ion of known effective (or actual) mobility at the ionic strength of the system, or to work in a closed system [5].

For the case under discussion, the plate numbers of the anions decrease with increasing electroosmotic velocity, which is in accordance with the fact that the plate height (due to diffusional, thermal and electromigration dispersion) is directly proportional to the electromigration factor $f_{em} = u_{eff}/(u_{eff} + u_{eo})$, where u_{eff} and u_{eo} are the effective and the electroosmotic mobilities, respectively (see eqns. 23, 27, 31, 36 and 37 in Part I and ref. 6). As u_{eff} and u_{eo} have opposite signs in the example given, the denominator decreases as long as $|u_{eff}| > |u_{eo}|$, and thus H increases. For cations the reverse case is valid, leading always to an increase in the plate number with increasing electroosmotic mobility (but, however, to a decrease in resolution, as discussed in a previous paper [6]).

In the example simulated, the plate count N decreases by only 10%. Anyway, the simulation

TABLE I

INFLUENCE OF LOW ζ POTENTIALS ON MIGRATION TIMES

The migration times were calculated for the following conditions: effective capillary length, 20 cm (27 cm total), closed and open modes; voltage, -7000 V; ζ potential, -1 or -5 mV; buffer, pH 4.50, ionic strength 0.010 mol/l.

Separand	Migration time (min)		
	-1 mV[a] (closed)[b]	-1 mV[a] (open)[c]	-5 mV[a] (open)[d]
1,3,5-Benzenetricarboxylate	2.88	2.92	3.12
1,2,4-Benzenetricarboxylate	2.96	3.01	3.22
1,4-Benzenedicarboxylate	3.45	3.52	3.81
1,3-Benzenedicarboxylate	3.62	3.70	4.02
1,2-Benzenedicarboxylate	4.04	4.13	4.54

[a] ζ potential.
[b] $u_{eo} = 0$.
[c] $u_{eo} = 0.8 \cdot 10^{-9}$ m^2/V·s.
[d] $u_{eo} = 4.0 \cdot 10^{-9}$ m^2/V·s.

shows that the occurrence of a residual ζ potential can significantly affect the electrophoretic behaviour of the analytes. As the occurrence of such low ζ potentials can hardly be controlled in normal equipment, it can be one of the sources of the low quality of migration data thus obtained.

Influence of pH on resolution. The pH of the buffering background electrolyte influences both parameters which are decisive for the resolution, namely the selectivity and the efficiency. The former is determined by the effective mobilities of the separands and the latter by their effective charge numbers [6,7].

It was described in previous papers [8,9] that within a critical region even minute variations of the pH, namely in the range of a few hundredths of a unit, can drastically affect the resolution of two components. It was described, *e.g.*, in ref. 8 that certain separands co-migrated at pH 4.40 but were baseline resolved at pH 4.43. In this work a similar case was chosen for other pairs of ions in such a sensitive pH range. The result of this simulation is shown in Fig. 2. It can be observed that for two components (2 and 3) that form a single peak at pH 4.68, an increase of only 0.05 pH unit leads to baseline resolution.

Influence of ionic strength on separation selectivity. The migration behaviour of the separands is influenced by the concentration dependence of their actual mobilities as given by eqn. 8 in Part I (the effect of the ionic strength of the pK is neglected in this instance). Ions with equal charge are influenced to the same extent, so that no selectivity effects can be expected on varying the ion strength. In contrast, in mixtures of ions with different charge, the selectivity can be affected by the concentration of the buffer, and in some instances even the migration sequence can be reversed. This is demonstrated in Fig. 3, showing the electropherograms of the anions of two dibasic and one tribasic acid at different ionic strengths, I, of the buffer. The sequence is 1,4-dicarboxybenzoate, 1,2,3-tricarboxybenzoate and 1,3-dicarboxybenzoate at I = 0.010 mol/l, where the first two components are in fact unresolved. Although a narrow interval of the ionic strength was chosen, much less than one decade, the effect on the selectivity and even

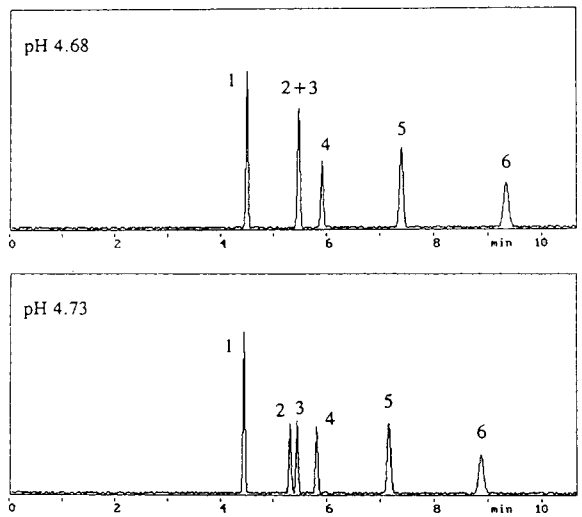

Fig. 2. Simulation of the effect of extremely small changes (a few hundredths of a pH unit) of the pH of the buffer on the resolution. Capillary: overall length 269 mm (effective length 202 mm) × 75 μm I.D. × 175 μm O.D.; voltage, −7000 V; ζ potential, −1 mV (open mode); cooling temperature, 25.0°C. Buffer: pH 4.68 (top) or 4.73 (bottom); ionic strength, 0.010 mol/l; buffer ion mobilities, $-24.0 \cdot 10^{-9}$ and $+25.0 \cdot 10^{-9}$ $m^2/V \cdot s$. Injection: hydrodynamic, 2 s, 5.0 mbar; from buffer. Detection: "universal"; attenuation, 3; slit width, 100 μm; time constant, 0.10 s. Sample: 1 = 2,6-dinitrophenolate; 2 = benzoate; 3 = 2,3-dimethoxybenzoate; 4 = 3,5-dimethoxybenzoate; 5 = 3,4-dimethoxybenzoate; 6 = 2,4-dimethoxybenzoate. Concentration: 100 μmol/l each.

on the migration order of the three separands is striking.

An increase in I leads to a decrease in the mobilities of all three separands (hence the migration times increase), but that of the trivalent analyte is most pronounced. 1,2,3-Tricarboxybenzoate migrates between the two divalent ions at I = 0.030 mol/l, where baseline separation of all three ions is obtained. The specific decrease in the actual mobility of the trivalent ion at higher ionic strength (0.045 mol/l) leads to a further increase in its migration time relative to the other two separands, and 1,3-di- and 1,2,3-tricarboxybenzoate now co-migrate.

Influence of the mobility of the co-ion of the background electrolyte on peak dispersion. As an example of the influence of the co-ion mobility on plate count and peak shape (eqs. 35 and 36 in Part I), the simulation was carried out for four

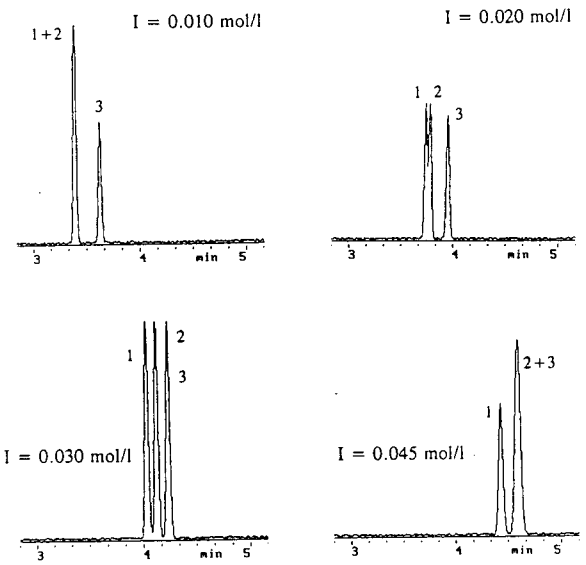

Fig. 3. Simulated electropherograms demonstrating the effect of the ionic strength, I, on the electrophoretic selectivity and resolution of multivalent anions with different charge at constant pH. Capillary: as in Fig. 2; voltage, −10 000 V; ζ potential, −20 mV (open mode); cooling temperature, 25.0°C. Buffer: pH 4.70; ionic strength, I, varying between 0.010 and 0.045 mol/l; buffer ion mobilities, $-30.0 \cdot 10^{-9}$ and $+25.0 \cdot 10^{-9}$ $m^2/V \cdot s$. Injection and detection: as in Fig. 2. Sample: 1 = 1,4-benzenedicarboxylate; 2 = 1,2,3-benzenetricarboxylate; 3 = 1,3-benzenedicarboxylate. Concentration: 100 μmol/l each.

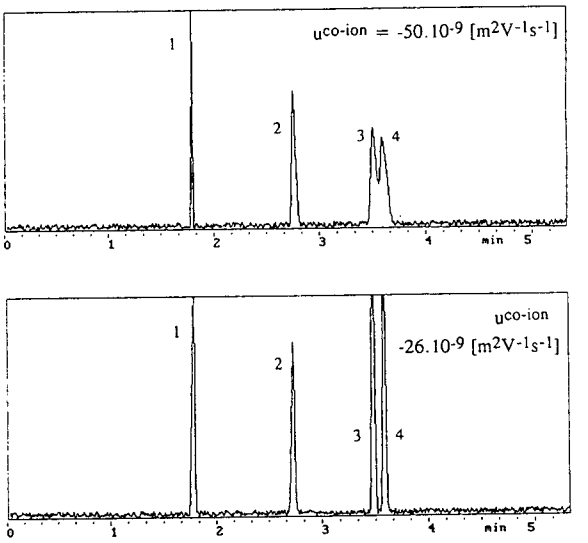

Fig. 4. Simulation of concentration overload (electromigration dispersion) for anions at different mobility of the co-ion of the buffering electrolyte. The simulation as made with a buffer at pH 7.00, ionic strength 0.010 mol/l, and a counter ion mobility of $+25 \cdot 10^{-9}$ $m^2/V \cdot s$. The effective mobility of the co-anion is $-50.0 \cdot 10^{-9}$ $m^2/V \cdot s$ (top) and $-26.0 \cdot 10^{-9}$ $m^2/V \cdot s$ (bottom). Voltage, −10 000 V; capillary dimensions as in Fig. 1; ζ potential, −3 mV, (open mode); injection, 2 s (5 mbar) from buffer. Detection: "universal"; slit width, 100 μm; time constant, 0.05 s; attenuation, 10. Sample: 1 = 1,3-benzenedicarboxylate; 2 = 2,6-dinitrophenolate; 3 = 2,3-dimethoxybenzoate; 4 = 3,4-dimethoxybenzoate. Sample concentrations: 500 μmol/l each. For effective mobilities of sample components at the given pH, see Table II.

separands with different effective mobilities, given in Fig. 4 and Table II. In this example the co-ion mobility of the background electrolyte is adjusted to the mobility of the first- or the last-migrating component. These mobilities are $-49.5 \cdot 10^{-9}$ and $-25.7 \cdot 10^{-9}$ $m^2/V \cdot s$, respectively. It can be observed that in both instances the peaks of the components with a mobility that differs from that of the co-ion show partially strong asymmetry, which is expressed by the skew (a symmetrical peak has a skew of zero). In the first example these peaks are triangular-shaped with tailing (the skew has a positive sign) and in the second instance with leading (negative sign of the skew).

The plate number is low in the second example for the fastest ion, namely only about 16 000, despite to the fact that this ion has an effective charge of 2. The last migrating ion has about 100 000 plates under the given conditions, about six times more than for the first component, although the latter has an effective charge number which is only one half of that of the former. The reason for this behaviour can be derived from the values of the individual contributions of the peak-broadening effects. The plate-height contributions due to Joule heating, electroosmosis, detector slit width and time constant are negligible (each less than 0.1 μm), and that from injection is also relatively low (0.4 μm). In contrast, those caused by diffusion and concentration overload, given in Table II, are significant. For component 1 the plate-height contribution due to electromigration dispersion, H_{conc}, (11.8 μm) exceeds that from diffusion (0.7 μm) by a factor of 17 when the co-ion mobility is

TABLE II

EFFECT OF CO-ION MOBILITY OF THE BACKGROUND ELECTROLYTE ON THE TWO MAIN CONTRIBUTIONS TO THE TOTAL PLATE HEIGHT, H, DUE TO DIFFUSION (H_{dif}) AND CONCENTRATION OVERLOAD (H_{conc}), AND TO PEAK SYMMETRY FOR FOUR SEPARANDS (1–4) WITH DIFFERENT EFFECTIVE MOBILITIES

H is given in μm. Peak asymmetry is expressed by the skew. The effective mobilities of the separands under the given conditions are (1) $-49.5 \cdot 10^{-9}$, (2) $-33.0 \cdot 10^{-9}$, (3) $-26.4 \cdot 10^{-9}$ and (4) $-25.7 \cdot 10^{-9}$ m^2/V·s. For details (*e.g.*, on percentage triangle) see Part I.

Parameter	Co-ion mobility							
	$-50 \cdot 10^{-9}$ m^2/V·s				$-26 \cdot 10^{-9}$ m^2/V·s			
	1[a]	2[a]	3[a]	4[a]	1[a]	2[a]	3[a]	4[a]
H_{dif}	0.67	1.37	1.40	1.40	0.67	1.37	1.40	1.40
H_{conc}	0.17	8.02	13.5	14.2	11.8	4.24	0.26	0.19
H_{tot}	1.51	9.93	15.4	16.1	13.1	6.09	2.13	2.06
Skew	+0.53	+1.51	+1.51	+1.51	−1.50	−1.50	−0.57	+0.44
% triangle	11	81	87	88	91	70	12	9

[a] Numbering of separands as in Fig. 4.

$-26 \cdot 10^{-9}$ m^2/V·s, and is the main source of peak broadening for this component. This concentration overload causes the triangular shape of the peaks of the fastest components, indicated by a value of −1.5 for the skew. The last-migrating component, on the other hand, to which the mobility of the co-ion is adjusted, shows a negligible contribution due to concentration overload (about 0.2 μm), so that the total plate height of 2.1 μm is in fact predominantly caused by diffusion. The peak is nearly symmetrical: the skew is only 0.4.

When identical electrophoretic conditions are applied, but the co-ion mobility is adjusted to the effective mobility of the fastest ion ($-49.5 \cdot 10^{-9}$ m^2/V·s), this component now exhibits the highest peak symmetry and the lowest plate height. The diffusional dispersion determines the total plate height for this peak 1, in contrast to peak 4, where the concentration overload dominates.

Comparison of simulated with measured electropherograms

A number of examples are given for a comparison of simulated electropherograms with those obtained by experiment. The latter were measured in the context of other investigations, and were not prepared specially to fit to the simulation. They were all measured using a UV absorbance detector at 214 nm. They were compared with the simulated electropherograms obtained using either a "universal" detection mode or by conductivity detection.

In Fig. 5 the electropherogram of three separands (dimethoxybenzoic acids) is shown, which was measured for the investigation of the adjustment of resolution and analysis time by the buffering pH [8]. It can be seen that the electropherogram obtained by simulations is nearly identical with the experimental trace. The small deviations in the migration times are due to the systematic error which is made in the calculation of the mobilities used for simulation, and which is nearly inevitable considering the various steps of approximation involved here: from measured migration times the actual mobilities are calculated for the ionic strength of the experimental conditions, from those the values of the absolute mobilities are approximated, from which finally the actual and the effective mobilities for the ionic strength conditions of the simulation are

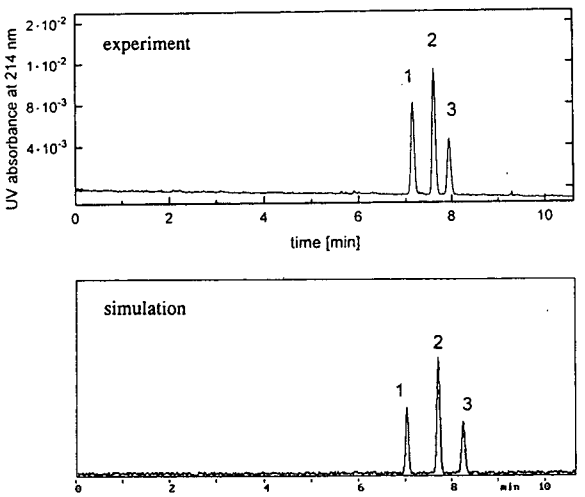

Fig. 5. Comparison of a measured electropherogram of three benzoic acids with the simulation under comparable conditions. Experimental conditions (top): coated capillary, overall length 269 mm (effective length from injector to detector 201 mm) × 75 μm I.D. × 275 μm O.D.; voltage, −5000 V; temperature, 25.0°C; buffer, pH 5.33 (acetic acid–sodium acetate, *ca.* 0.01 mol/l); injection, pneumatic for 1 s. Simulation conditions (bottom): ζ potential −1 mV (open mode); ionic strength, 0.010 mol/l; buffer ion mobilities, $-35.0 \cdot 10^{-9}$ and $+25.0 \cdot 10^{-9}$ $m^2/V \cdot s$; injection, hydrodynamic, 2 s, 5.0 mbar; from water. Detection: "universal"; attenuation, 1; slit width, 100 μm; time constant, 0.010 s. Sample: 1 = 2,3-dimethoxybenzoate (50 μmol/l); 2 = 3,4-dimethoxybenzoate (100 μmol/l); 3 = 2,4-dimethoxybenzoate (50 μmol/l).

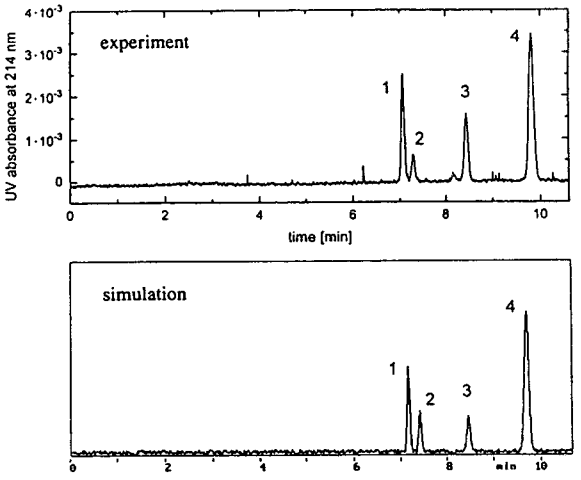

Fig. 6. Comparison of simulated and measured electropherograms of monobasic acids at a pH critical for the resolution of components 1 and 2. Experimental conditions (top): capillary, voltage, cooling temperature, injection and detection as in Fig. 5; buffer, pH 4.99 (acetic acid–sodium acetate, *ca.* 0.01 mol/l). Simulation (bottom): pH 4.99; ionic strength, 0.010 mol/l; buffer ion mobilities, $-24.0 \cdot 10^{-9}$ and $+25.0 \cdot 10^{-9}$ $m^2/V \cdot s$; injection, hydrodynamic, 2 s, 5.0 mbar; from water. Detection: "universal"; attenuation, 3; slit width, 100 μm; time constant, 0.020 s. Sample: 1 = 2,3-dimethoxybenzoate (200 μmol/l); 2 = 3,5-dimethoxybenzoate (100 μmol/l); 3 = 3,4-dimethoxybenzoate (100 μmol/l); 4 = 2,4-dimethoxybenzoate (500 μmol/l).

derived. Based on these approximations, it is found that the simulated migration times agree fairly well with those on the measured electropherogram, namely within 1–3%.

A more complex case is shown in Fig. 6, where the pH is in the narrow range critical for the separation of two of the components under consideration. Experimentally the pH was adjusted to that unique value at which baseline separation of all components was predicted within the shortest time of analysis, according to a theoretical approach presented in previous papers [8,9]. In the case under consideration, the given resolution is established for the first pair of components exactly at pH 4.99. In fact, at this pH the result of the calculation of the resolution is in agreement with the experimental finding. The simulation for various conditions is striking: the same resolution results at exactly that pH as in the experiment. It should be pointed out that this good result is obtained despite the fact that the effective mobilities, calculated from the absolute mobilities (at infinite dilution), were extrapolated to the ionic strength conditions with a fairly rough approximation, as given by eqn. 8 in Part I, which is currently under investigation [10].

Another complex example is demonstrated by six other separands, where the pH range for the migration order as for the resolution of three of the separands is also critical [9]. At pH 5.03 the separands 1,4-di-, 1,2,3-tri- and 1,3-dicarboxybenzoate migrate closely in the sequence given above, as can be seen from the measured electropherogram (Fig. 7, top), and form a triplet of nearly unresolved peaks. The simulation is in agreement in this instance also (Fig. 7, bottom), although the larger number of actual

mobilities and pK values necessary for the simulation can be potential sources of deviations: co-migration is simulated in addition to the correct sequence.

Finally, the result of the simulation including electroosmotic flow is compared with two electropherograms published by Poppe [2], one obtained experimentally using indirect UV detection and the other calculated by an algorithm based on eigenvectors and eigenvalues, as shown in Fig. 8. It demonstrates the separation of seven amino acids at pH 11.0. Our simulation is in agreement with both of Poppe's results. Not only is the migration sequence identical, but also the peak distortion (especially the triangulation due to concentration overload) is clearly simulated.

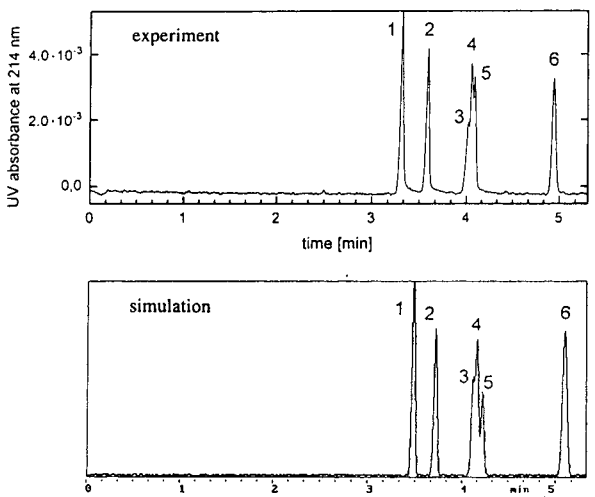

Fig. 7. Comparison of simulated and measured electropherograms of di- and tribasic benzoic acids at pH 5.03. Experimental conditions (top): capillary, voltage, cooling temperature, injection and detection as in Fig. 5; buffer, acetic acid–sodium acetate, *ca.* 0.01 mol/l. Simulation (bottom): ζ potential, −1 mV (open mode); buffer ionic strength, 0.012 mol/l; buffer ion mobilities, $-24.0 \cdot 10^{-9}$ and $+25.0 \cdot 10^{-9}$ m^2/V·s; injection, hydrodynamic, 2 s, 5.0 mbar; from buffer. Detection: "universal"; attenuation, 3; slit width, 100 μm; time constant, 0.010 s. Sample: 1 = 1,3,5-benzenetricarboxylate (200 μmol/l); 2 = 1,2,4-benzenetricarboxylate (200 μmol/l); 3 = 1,4-benzenedicarboxylate (100 μmol/l); 4 = 1,2,3-benzenetricarboxylate (200 μmol/l); 5 = 1,3-benzenedicarboxylate (100 μmol/l); 6 = 1,2-benzenedicarboxylate (200 μmol/l).

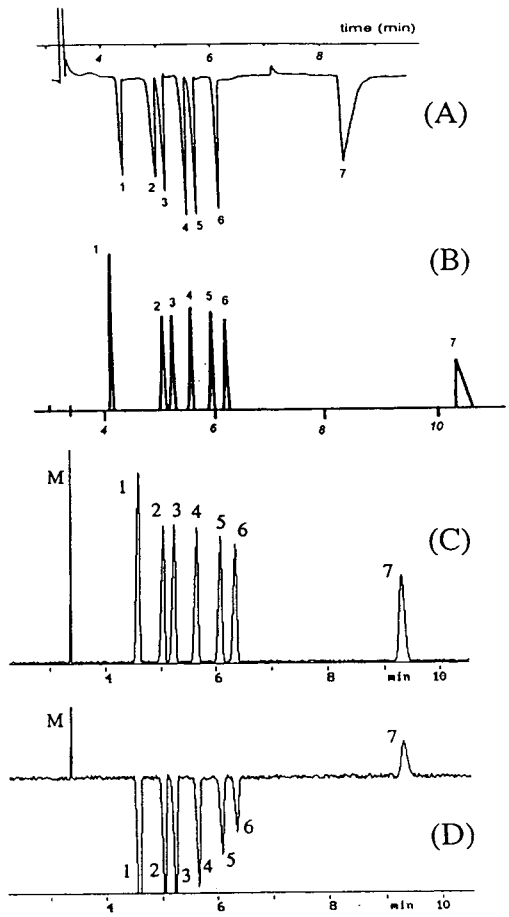

Fig. 8. Comparison of a measured electropherogram of amphoteric analytes (amino acids), including electroosmotic flow, with the result of a simulation based on an eigenvector approach, and with the instrumental simulator. Capillary: overall length 59 cm (effective length 36 cm) × 7.5 μm I.D.; voltage, +15 000 V; buffer, pH 11.0, concentration 0.01 mol/l. Analytes: 1 = proline; 2 = leucine; 3 = valine; 4 = alanine; 5 = serine; 6 = glycine; 7 = glutamic acid; M = neutral EOF marker. (A) Experimental result obtained by indirect UV detection using sodium salicylate as background electrolyte. Injection by electromigration at 6000 V for 5 s; $u_{eo} = 70 \cdot 10^{-9}$ m^2/V·s. Analyte concentrations: 0.001 mol/l each, dissolved in background electrolyte. From ref. 2. (B) Simulated electropherogram obtained by the eigenvector approach for the same conditions as in (A). From ref. 2. (C) Electropherogram obtained by the instrumental simulator for conditions as in (A). For the buffer ion mobilities the values taken were $-40 \cdot 10^{-9}$ and $+51 \cdot 10^{-9}$ m^2/V·s. Injection: 20 s from water (5.0 mbar). Detection: "universal"; attenuation, 30; slit width, 20 μm; time constant, 0.2 s. Analyte concentration: 0.0005 mol/l each. (D) Electropherogram obtained with the instrumental simulator in the conductivity detection mode. Conditions as in (C).

CONCLUSIONS

The examples given indicate that the theoretical model with its limitations and assumptions, as described in Part I, yields sufficiently realistic electropherograms to illustrate the integrated effect of almost all factors of importance in capillary zone electrophoresis. This enables our simulator to obtain a large number of results on the influence of many parameters on the electropherograms in a similarly short time, and thus offers great flexibility compared with other simulation systems, especially for demonstration and training purposes. This is a clear advantage over other algorithms, for which the calculations take minutes or even hours (possibly with greater accuracy of the prediction). From all the comparisons with experimental results it can be concluded that the simulator introduced here allows the depiction of the final electropherogram with good (although not always exact) agreement.

ACKNOWLEDGEMENT

The authors acknowledge the technical assistance of W. Friedl (Institute for Analytical Chemistry, University of Vienna, Vienna, Austria).

REFERENCES

1 J.C. Reijenga and E. Kenndler, *J. Chromatogr.*, 659 (1994) 403.
2 H. Poppe, *Anal. Chem.*, 64 (1992) 1908.
3 S. Hjertén, *Chem. Rev.*, 9 (1967) 122.
4 J. Sternberg, *Adv. Chromatogr.*, 2 (1966) 205–270.
5 Th.P.E.M. Verheggen and F.M. Everaerts, *J. Chromatogr.*, 638 (1993) 147.
6 C. Schwer and E. Kenndler, *Chromatographia*, 33 (1992) 331.
7 E. Kenndler and C. Schwer, *Anal. Chem.*, 63 (1991) 2499.
8 E. Kenndler and W. Friedl, *J. Chromatogr.*, 608 (1992) 161.
9 W. Friedl and E. Kenndler. *Anal. Chem.*, 65 (1993) 2003.
10 J.C. Reijenga, in preparation.

Journal of Chromatography A, 659 (1994) 427–434
Elsevier Science B.V., Amsterdam

CHROM. 25 704

Prevention of protein adsorption on surfaces by polyethylene oxide–polypropylene oxide–polyethylene oxide triblock copolymers in capillary electrophoresis

C.L. Ng, H.K. Lee and S.F.Y. Li *

Department of Chemistry, National University of Singapore, Kent Ridge, Singapore 0511 (Singapore)

(First received June 7th, 1993; revised manuscript received August 3rd, 1993)

ABSTRACT

Protein adsorption to untreated fused-silica capillaries in capillary electrophoresis was prevented by a chemical modification of the capillary surface. This was achieved through the coating of Pluronic polymers onto capillaries which were pre-derivatised with silylating agents. The polymers were made up of polyethylene oxide–polypropylene oxide–polyethylene oxide triblock copolymers. The coatings prevent protein adsorption and provide high-efficiency separations. Two different types of silylating agents were used and the effects of the concentrations on the stability and efficiency of the columns were examined. The application of these columns for capillary electrophoretic separation of protein samples was demonstrated.

INTRODUCTION

Recent developments in capillary electrophoresis (CE) have been remarkable and its applications in the analysis of physiological substances have been widely explored [1–7]. There is, however, an inherent problem in the use of untreated fused silica for solutes such as proteins: their inevitable adsorption onto the inner walls of the capillaries and the hysteresis [8] of electroosmotic flow (EOF) with changes in pH. The consequences of these phenomena are irreproducible separations and unacceptable variations in migration times.

Much work has been done to develop methods for preventing adsorption, as well as eliminating EOF, particularly for protein analysis [9–20]. Strategies to control wall effects include the use of buffers that have extremely high or low pH values [9,10], metal ion additives [11,12] and high ionic strengths [13]. These methods generally require the use of extreme conditions and therefore may only be useful for certain specific groups of proteins. Permanent surface wall silanol modifications is more practical in eliminating EOF and protein adsorption. Briefly, surface wall modification includes coating the columns with non-ionic surfactants [14], polyethylene glycol [15,16], polyacrylamide [17], linear polyacrylamide anchored by a silicon–carbon bond [18] and more recently, cross-linked polyacrylamide [19] and hydrogel polymers [20]. Although these coated columns are able to achieve the objective of preventing adsorption and eliminating EOF for CE and capillary isoelectric focusing applications, the coating procedures involve tedious silanization and elaborate coating chemistries. This is disadvantageous if coated columns are to be used for routine analysis.

In this work, a procedure was developed for the coating of columns using Pluronics as the coating materials. Pluronics, consisting of polyethylene oxide–polypropylene oxide–poly-

* Corresponding author.

0021-9673/94/$07.00
SSDI 0021-9673(93)E1168-Y

ethylene oxide (PEO–PPO–PEO) triblock copolymers, have been widely used in the chemical, agricultural and pharmaceutical industries as non-ionic polymer surfactants [21]. Their commercial availability, stability, low toxicity [21] and low cost are attractive properties for them to be considered as coating materials for CE.

In this study, a simple and versatile approach for preparing protein-resistant coated columns is described. Alkylsilane-treated capillary columns were coated with Pluronic triblock copolymers. The relative importance of PEO and PPO chains of Pluronic copolymers in preventing protein adsorption and on the EOF was examined. The use of different silylating agents and their concentrations on the stability and efficiency of the columns were evaluated. Finally, the usefulness of the coated columns in preventing protein adsorption was demonstrated.

EXPERIMENTAL

Instrumental

CE was conducted in a laboratory-built system. A Spellman Model RM30P10KD (Plainview, NY, USA) high-voltage power supply capable of delivering up to 30 kV was used. Detection of peaks was accomplished through the use of a ISCO Model CV^4 UV detector (Lincoln, NE, USA) with wavelength set at 200 nm. Untreated fused-silica capillaries of 50 μm I.D. and effective lengths of 31 to 33 cm and overall lengths of 43–45 cm were obtained from Polymicro Technologies (Phoenix, AZ, USA). Chromatographic data were recorded on a Shimadzu Model R6A (Kyoto, Japan) integrator. Samples were hydrodynamically injected for 5 s at a height of 8 cm. N,N-Dimethylformamide (DMF)–water (50:50) was used as the neutral marker for EOF measurements.

Reagents and materials

Sodium dihydrogenphosphate, disodium hydrogenphosphate, sodium tetraborate and orthophosphoric acid used for preparing the buffer solutions were purchased from Fluka (Buchs, Switzerland). All protein samples were purchased from Sigma (St. Louis, MO, USA). Six different types of Pluronic polymers depicted in Table I were obtained from BASF (Parsipanny, NJ, USA). Silylating agents, octyldecyltrichlorosilane and dichlorodimethylsilane were obtained from Aldrich (Milwaukee, WI, USA).

TABLE I

PROPERTIES OF PLURONIC TRIBLOCK COPOLYMERS USED IN THIS INVESTIGATION

Pluronic	Physical state	Average M_r	PEO–PPO–PEO
P-103	Paste	4 950	19:56:19
P-104	Paste	5 850	28:56:28
P-105	Paste	6 500	37:56:37
F-108	Solid	14 000	129:56:129
P-84	Paste	4 200	22:38:22
P-123	Paste	5 750	19:69:19

Capillary coating procedure

An untreated fused-silica capillary was first rinsed with 0.1 *M* sodium hydroxide for 15 min followed by 15 min of water and finally with 5 min of methanol. It was dried by flushing nitrogen through it in a GC oven at 110°C for 3 h. Two different methods for silylating the capillary were investigated. The procedure for derivatising the capillary column with octyldecyltrichlorosilane with 5% methylene chloride was similar to that described by Towns and Regnier [14]. An alternative method of derivatising the capillary column developed in this laboratory involved passing a solution containing 5% of dichlorodimethylsilane (DDS) or octyldecyltrichlorosilane (ODTC) in toluene through a capillary for 5 min at room temperature. Subsequently, the capillary was statically coated with the silylating agent for 3 h, with a 5-min rinse using the silylating agent at the 1.5-h interval. This silylating procedure was modified from a method for treating glass coverslips [22] which involved silylating for 2 h at room temperature. Excess silylating agent was flushed out with methanol and the capillary was again dried in the oven for 2 h. Subsequently, Pluronic polymers dissolved in phosphate-buffered saline (PBS, pH 7.0) of varying concentrations (0.1–5 mg/ml) were introduced into the capillary with a syringe for 2 min and the capillary was then statically coated

with the polymer solution for 2 h at room temperature. The capillary was then rinsed with PBS, water and finally, buffer solutions before use.

RESULTS AND DISCUSSION

To determine whether a coating material is suitable to be used for coating capillary columns, several criteria have to be met:

(1) It should be able to give a smooth and even layer of coating to prevent protein adsorption.

(2) It should provide reproducibility in migration time over a wide pH range.

(3) It should provide reproducible separations for different columns coated with the same material.

(4) It should be stable over a wide pH range and over a wide potential difference across the capillary.

(5) It should be able to provide highly efficient separations.

The triblock copolymer used in this work consists of varying lengths of PEO–PPO–PEO as shown in Table I. It was adsorbed onto alkylsilane-derivatised surfaces and their utility was examined in terms of their ability to prevent protein adsorption and elimination of EOF. The various chain lengths of PEO and PPO may play an important role in preventing adsorption of proteins and reduction of EOF. Two types of alkylsilane were used, DDS and ODTC. They alone, when used to derivatise the capillary column, failed to prevent adsorption of proteins. This could be due to their high hydrophobicity and insufficient surface coverage.

It was found that the alkylsilane used for the derivatisation of capillary surfaces had an effect on the efficiency of the capillary. This is shown in Table II for two model proteins, cytochrome *c* and lysozyme. The number of theoretical plates per meter is calculated using the formula

$$N = 5.54(t_R/w)^2 \cdot (100/L)$$

where t_R is the migration time of the protein, w is the width at half height of the peak and L is the effective length of the column in cm. It was

TABLE II

EFFECT OF DIFFERENT SILYLATING AGENTS AND THEIR COMPOSITIONS ON EFFICIENCY

Conditions: 5 mg/ml F-108 modified column; 44 cm (32 cm effective length) × 50 μm I.D.; buffer: 0.01 *M* phosphate at pH 3; voltage: 10 kV.

Silylating agent	Efficiency (plates/m)	
	Cytochrome *c*	Lysozyme
5% DDS in toluene	613 922	767 870
5% ODTC in toluene	336 662	488 397
95% ODTC with 5% CH_2Cl_2	179 262	142 713

observed that 5% DDS in toluene offered the highest plate number compared to ODTC. This is surprising as stronger hydrophobic interaction between the longer alkyl chain of the ODTC and the Pluronic polymer would be expected. The PPO segment of the copolymer is known to adsorb onto hydrophobic surfaces by hydrophobic interactions while the water-soluble PEO chains would extend into the bulk aqueous medium [23,24]. One possible reason for this anomalous behaviour could be that DDS, being more symmetrical (two chloro and two methyl groups) than ODTC, is able to give a homogenous and smooth layer for the adsorption of the PPO segment. ODTC, on the other hand, tends to form polymeric layers which cannot be effectively shielded by the copolymeric Pluronic. Thus, effective anchoring of the PPO chain of the Pluronic polymer was inhibited. Consequently, the efficiency of the column was reduced in the case of ODTC. Another possible reason could be that DDS is less hydrophobic than ODTC, thus there is less chance for adsorption for the hydrophobic proteins. As evident from Table II, 5% of ODTC gave higher efficiencies compared to 95% ODTC. This shows that the higher the concentration of ODTC, the less efficient the column. The weak binding of the ODTC-derivatised columns may also account for the irreproducible migration times and unstable currents when high voltages (25 kV) were used. This irregular behaviour was not observed for the Pluronic–DDS-derivatised columns. Among

the various coatings studied, 5% DDS was able to offer the highest efficiencies. Therefore, it was subsequently used for silylating all the columns to be coated. It is worth noting that in the present work, the method of silylating the columns is simpler and does not involve heating as compared to other methods [14,15,25].

The EOF and efficiencies for the various Pluronic-coated capillaries is shown in Table III. The Pluronics (P-103, P-104, P-105 and F-108) chosen for the measurement of EOF were those in which the number of PO chains remained constant while the number of EO chains varied in length. With increasing molecular mass of the Pluronic polymers from P-103 to F-108, the adsorbed layer became thicker and more viscous. The increase in the viscous drag caused a reduction in EOF. F-108 is the most effective material in eliminating EOF compared to the other Pluronics. The EOF of F-108 coated capillary was approximately 1/60 that of the untreated capillary while that of P-103 was 1/6 at the conditions stated. Thus, moderation of EOF could be accomplished by using different Pluronic polymers, which at the same time also prevented protein adsorption.

The length of the PEO chain also has a significant effect on the column efficiency. As shown in Table III, when the length of the PEO chain became longer, the column efficiency increased. F-108, having the longest PEO chain (129 units), resulted in the highest efficiencies compared to the other Pluronics when used as coating material. This could be attributed to the long PEO chains which are able to intertwine to form a network extending into the aqueous medium, which prevents further interaction between the proteins and the surface.

The performance of the Pluronic-coated capillaries in terms of reproducibility and efficiency was evaluated at low and high pH. Fig. 1a and b show the separation of some basic model proteins at low pH using the coated and uncoated capillary columns, respectively. Improved resolution and high efficiencies were observed when coated columns were used. The molecular masses, isoelectric points and reproducibility of migration times for the model proteins separated at pH 3 are given in Table IV. The separation

TABLE III

EFFECT OF DIFFERENT PLURONIC POLYMERS ON EOF AND COLUMN EFFICIENCY FOR CYTOCHROME *c*

Conditions: 1 mg/ml Pluronic on capillary derivatised with DDS, 40 cm (31 cm effective length) × 50 μm I.D.; buffer: 0.01 *M* phosphate, pH 6; voltage: 10 kV.

Column	EOF × 10^8 (m^2/V s)	Efficiency (plates/m)
Uncoated	6.0	103 355
P-103	1.0	73 686
P-104	0.9	85 148
P-105	0.8	371 798
F-108	0.1	630 853

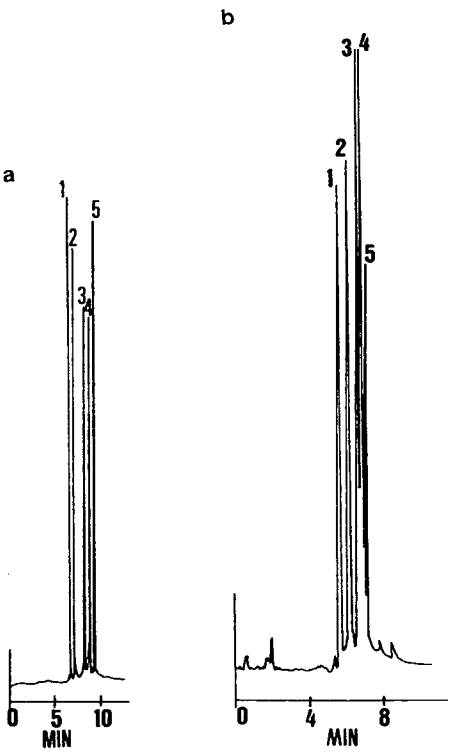

Fig. 1. Typical electropherograms showing the separation of a model protein mixture using (a) coated and (b) uncoated fused-silica capillary. For peak identification see Table IV. Electrophoretic conditions: 0.01 *M* phosphate buffer, pH 3.0 (adjusted with phosphoric acid) for coated column and 0.025 *M* phosphate for uncoated capillary; separation column: 43 cm (31 cm effective length) × 50 μm I.D.; voltage: 10 kV.

TABLE IV

REPRODUCIBILITY OF MIGRATION TIMES BETWEEN COATED AND UNCOATED COLUMN FOR SOME MODEL BASIC AND ACIDIC PROTEINS

Electrophoretic conditions for the basic proteins (peaks 1–5) are as in Fig. 1 and for the acidic proteins (peaks 6–8) are as in Fig. 2.

Peak No.	Protein	M_r [a]	pI [a]	R.S.D. (%)[b]	
				Coated	Uncoated
1	Cytochrome *c*	12 200	10.8	0.26	0.60
2	Lysozyme	14 000	10.0	0.24	0.51
3	Trypsin	23 300	9.3	0.24	0.57
4	Trypsinogen	24 500	8.7	0.24	0.59
5	α-Chymotrypsinogen A	21 600	8.7	0.24	0.61
6	Pepsin	34 700	3.1	0.11	0.76
7	Amyloglucosidase	89 000	3.6	0.26	0.77
8	Trypsin inhibitor	20 100	4.6	0.24	0.70

[a] M_r and pI values taken from ref. 26.
[b] $n = 7$ for basic proteins; $n = 5$ for acidic proteins.

conditions for both cases were identical except for the ionic strengths of the buffer system. McCormick [10] has found that the changes in EOF at low pH are minimal, accounting for the less than 1% R.S.D. for the migration times of the proteins when uncoated columns are used. However, the R.S.D. was further improved with the use of coated capillaries. It was noted that the migration order of the basic proteins was in accordance with their pI values, as expected. In addition, the stability of the coated column was tested using a buffer of pH 4.5 and no significant degradation of coating was observed even after 80 runs.

The coated column was also used to separate acidic proteins at alkaline (pH 8) conditions. The separation of three acidic proteins at pH 8 is shown in Fig. 2. The reproducibility in migration times for coated and uncoated columns is shown in Table IV. A three-fold improvement in the R.S.D. for the migration times was observed when coated columns were used. The polarity of the power supply was reversed for the coated column as the proteins would be negatively charged at this pH and the EOF would be too weak to elute them towards the detector at the cathodic end. The usefulness of a Pluronic-

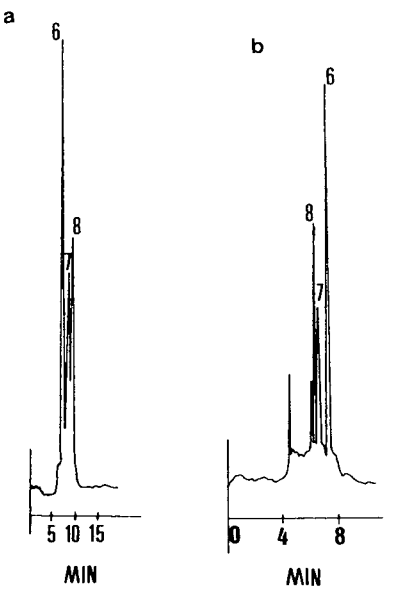

Fig. 2. Typical electropherograms showing the separation of some acidic proteins using (a) coated and (b) uncoated capillary at pH 8.0. For peak identification see Table IV. Electrophoretic conditions: (a) 5 mg/ml of F-108 modified column, 47 cm (35 cm effective length) × 50 μm I.D.; 0.01 *M* phosphate–borate buffer; voltage: − 18 kV. (b) 48 cm (40 cm effective length) × 50 μm I.D.; 0.025 *M* phosphate buffer; voltage: 12 kV.

coated capillary for the separation of some model acidic and basic proteins is evident from Fig. 3.

The separation efficiencies of the Pluronic-coated and of uncoated capillaries were also compared. The separation efficiencies at four different voltages for cytochrome *c* as an example are given in Table V. The separation efficiencies for all the basic proteins listed in Table IV at 10 kV are more than half a million theoretical plates. This figure is not only higher than that for the uncoated column (as indicated in Table V), but also considerably higher than the figures obtained by other coatings [8,14,18,25–27]. The high efficiency observed is due to the hydrophobic adsorption of the PPO chain to the evenly DDS-derivatised fused silica while the two ends of the hydrophillic PEO chain extend into the aqueous phase which further prevents the proteins from interacting with the wall of the fused-silica capillary.

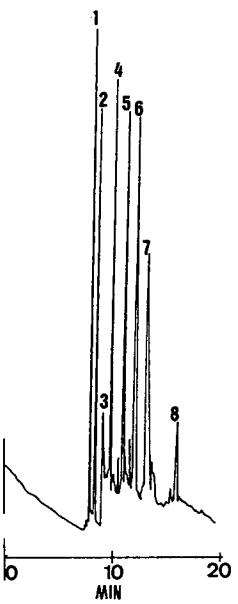

Fig. 3. Typical electropherogram showing the separation of a mixture of basic and acidic proteins. Peaks: 1 = cytochrome *c*; 2 = lysozyme; 3 = lactic dehydrogenase; 4 = trypsin; 5 = trypsinogen; 6 = α-chymotrypsinogen A; 7 = β-lactoglobulin A; 8 = carbonic anhydrase. Electrophoretic conditions: 0.1 mg/ml F-108 modified column, 43 cm (31 cm effective length) × 50 μm I.D.; 0.01 *M* phosphate, pH 4.5 (adjusted with phosphoric acid); voltage: 10 kV.

TABLE V

COMPARISON OF EFFICIENCIES OF COATED AND UNCOATED CAPILLARIES FOR CYTOCHROME *c* AT VARIOUS VOLTAGES

Condition: 5 mg/ml F-108 coated column, 43 cm (31 cm effective length) × 50 μm I.D.; buffer: 0.01 *M* phosphate, pH 3.

Voltage (kV)	Current (μA)	Efficiency (plates/m)	
		Coated	Uncoated
10	5	613 922	103 355
15	8	489 187	37 793
20	10	408 095	36 430
25	13	332 843	24 162

However, it should also be noted that the extremely high number of theoretical plates observed is only slightly more than half the number of theoretical plates predicted by theory [28]. The reason is that although electrostatic interaction of the proteins (in this case the proteins are positively charged) with the coated capillary wall has been reduced, hydrophobic interaction of protein with the coating is possible. Nevertheless, the prevention of adsorption and the increase in efficiencies achieved by using the Pluronics coating represent significant advantages for protein separations by CE.

The effect of separation voltage on efficiency is shown in Table V, both for coated and uncoated capillary columns. The number of theoretical plates was observed to decrease with increase in voltage. This observation is in accordance with the work of Cobb *et al.* [18]. Two possible reasons that would have caused this decline in efficiency are band broadening due to thermal effects at high voltages, and probable increased hydrophobic interaction with the coating material at higher temperatures. As the field is increased and the ions move faster, the possible desorption kinetics may cause band broadening. Since conditions at 10 kV offered the highest efficiency and reproducibility with reasonable migration times, subsequent separations were carried out at this voltage.

The effect of the concentration of coating

TABLE VI

COMPARISON OF THE EFFECT OF CONCENTRATION OF COATING SOLUTION ON EFFICIENCY AND MIGRATION TIME WITH RESPECT TO CYTOCHROME *c*

Conditions: 47 cm (35 cm effective length) × 50 μm I.D.; buffer: 0.01 *M* phosphate, pH 3.0; voltage: 10 kV.

Concentration of Pluronic F-108 (mg/ml)	Efficiency (plates/m)	Migration time (min)
0.1	527 577	7.245
1.0	630 853	7.418
3.0	735 628	7.759
5.0	613 922	7.645

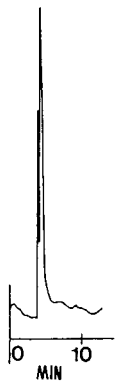

Fig. 4. Electropherogram of a sample of protamine. Electrophoretic conditions: 5 mg/ml F-108 modified column, 43 cm (31 cm effective length) × 50 μm I.D.; 0.01 *M* phosphate–borate, pH 5.5; voltage: 15 kV; wavelength: 200 nm.

solution on the efficiency and migration time was investigated and the results are shown in Table VI. It was noted that there was no definite trend in column efficiency with changes in the concentration of Pluronic F-108. It is worthwhile to note that all concentrations gave theoretical plate numbers of at least half a million. Since coating thickness is expected to be proportional to the concentration of the coating solution [29], the EOF should decrease with an increase in concentration of the coating solution. This is indicated by the increase in the migration time of cytochrome *c*. The migration time was comparable at a coating concentration of 3 mg/ml and 5 mg/ml. This is an indication that the alkylsilane-derivatised fused silica has reached its coating saturation point. The migration time for the neutral marker, DMF, for all the concentrations investigated was longer than 2.5 h, corresponding to an EOF value of approximately $1.5 \cdot 10^{-9}$ $m^2/(V\ s)$ at pH values 3 and 6. In other words, for a particular copolymer such as F-108, a coating concentration of 0.1 mg/ml is as effective in eliminating EOF and protein adsorption as a 5 mg/ml coating solution.

Another advantage of using Pluronics as coating material is that there is no observable leaching of the polymer into the buffer as has been found for non-ionic surfactants by Towns and Regnier [14] with other coatings. It was therefore unnecessary to add small amounts of surfactants to the electrophoretic buffer. Since addition of surfactants into the buffer solution with a concentration greater than the critical micelle concentration may result in a reduction in efficiency [14], the present method is preferable from this viewpoint.

The application of the Pluronic-coated capillaries was demonstrated by the analysis of protamine, a basic protein found in the sperm of the Salmon fish. The electropherogram obtained is shown in Fig. 4. Protamine was eluted in a relatively short time (less than 6 min) and high efficiency could be obtained using the Pluronics-coated column. Another example is a sample of rabbit-anti-mouse antibodies, shown in Fig. 5. A single sharp peak corresponding to immunoglobulin G (IgG) was obtained.

CONCLUSIONS

In the present work, prevention of protein adsorption by PEO–PPO–PEO triblock copolymer in CE was demonstrated. A simple procedure developed for the silylation of fused-silica capillaries using 5% DDS in toluene has been described. Unlike other methods, extended heating and constant monitoring are not required. The use of DDS allows for a smooth layer for the adsorption of Pluronic polymers which consist of PEO–PPO–PEO triblock copolymers. Pluronic–DDS-derivatised capillary columns were found to be stable under high voltages and at a pH range of 3 to 8. Very high efficiencies

Fig. 5. Electropherogram of rabbit-anti-mouse antibodies, the major peak being IgG. Electrophoretic conditions: 5 mg/ml F-108 modified capillary, 43 cm length (31 cm effective length) × 50 μm I.D.; 0.01 *M* phosphate buffer, pH 3.0; voltage: 15 kV; wavelength: 200 nm.

(more than 500 000 plates) were obtained for some model basic proteins. In conclusion, the present study has shown that apart from their many industrial uses [21], the Pluronic polymers have yet another interesting and useful application, *i.e.* in the CE separation of proteins.

ACKNOWLEDGEMENT

The authors thank the National University of Singapore for financial assistance.

REFERENCES

1 D. Josic, K. Zeilinger and W. Reuter, *J. Chromatogr.*, 516 (1990) 89–98.
2 R.G. Nielsen, G.S. Sittampalam and E.C. Rickard, *Anal. Biochem.*, 177 (1989) 20–26.
3 F.T.A. Chen, *J. Chromatogr.*, 559 (1991) 445–453.
4 K.J. Lee and G.S. Heo, *J. Chromatogr.*, 559 (1991) 317–324.
5 L.R. Gurley, J.E. London and J.G. Valdez, *J. Chromatogr.*, 559 (1991) 431–443.
6 K. Lal, L. Xu, J. Colburn, A.L. Hong and J.J. Pollock, *Arch. Oral. Biol.*, 37 (1992) 7–13.
7 H. Kajiwara, *J. Chromatogr.*, 559 (1991) 345–356.
8 J. Kohr and H. Engelhardt, *J. Microcol. Sep.*, 3 (1991) 491.
9 M. Zhu, R. Rodriguez, D. Hansen and T. Wehr, *J. Chromatogr.*, 516 (1990) 123.
10 R.M. McCormick, *Anal. Chem.*, 60 (1988) 2322–2328.
11 J.S. Green and J.W. Jorgenson, *J. Chromatogr.*, 478 (1989) 63.
12 J.A. Bullock and L.C. Yuan, *J. Microcol. Sep.*, 3 (1991) 241.
13 M.M. Bushey and J.W. Jorgenson, *J. Chromatogr.*, 480 (1989) 301.
14 J.K. Towns and F.E. Regnier, *Anal. Chem.*, 63 (1991) 1126.
15 G.J.M. Bruin, J.P. Chang, R.H. Kuhlman, K. Zegers, J.C. Kraak and H. Poppe, *J. Chromatogr.*, 471 (1989) 429.
16 W. Nashabeh and Z. El Rassi, *J. Chromatogr.*, 536 (1991) 31.
17 S. Hjertén, *J. Chromatogr.*, 347 (1985) 191.
18 K.A. Cobb, V. Dolnik and M. Novotny, *Anal. Chem.*, 62 (1990) 2478.
19 M. Huang, W.P. Vorkink and M.L. Lee, *J. Microcol. Sep.*, 4 (1992) 233.
20 M. Huang and M.L. Lee, *J. Microcol. Sep.*, 4 (1992) 491.
21 *Technical Data on Pluronic Polyols*, Performance Chemical Division, BASF Corporation, Parsipanny, NJ, 1990.
22 M. Amiji and K. Park, *Biomaterials*, 13 (1992) 682.
23 E. Killman, H. Maier and J.A. Baker, *Colloids Surfaces*, 31 (1988) 51.
24 J.B. Kayes, D.A. Rawlins, *Colloid Polymer Sci.*, 257 (1979) 622.
25 W. Nashabeh and Z. El Rassi, *J. Chromatogr.*, 559 (1991) 367.
26 M. Gilges, H. Husmann, M.H. Kleemiβ, S.R. Motsch and G. Schomburg, *J. High Resolut. Chromatogr.*, 15 (1992) 452.
27 Y.F. Maa, K.J. Hyver and S.A. Swedburg, *J. High Resolut. Chromatogr.*, 14 (1991) 65.
28 J.W. Jorgenson and K.D. Lukacs, *Anal. Chem.*, 53 (1981) 1298.
29 A.J. Alpert and F.E. Regnier, *J. Chromatogr.*, 185 (1979) 622.

Journal of Chromatography A, 659 (1994) 435–442
Elsevier Science B.V., Amsterdam

CHROM. 25 619

Separation of porphyrins and porphyrin isomers in capillary electrophoresis using mixed ionic surfactant–bovine serum albumin buffer systems

Nian Wu, Geoffrey E. Barker and Carmen W. Huie*

Department of Chemistry, State University of New York at Binghamton, Binghamton, NY 13902-6000 (USA)

(First received June 22nd, 1993; revised manuscript received September 9th, 1993)

ABSTRACT

The separation of six porphyrins having two to eight carboxylic acid side-chains by capillary electrophoresis using a combination of ionic surfactant and protein as a novel modifier in the run buffer is reported. Using sodium dodecyl sulfate (SDS) together with bovine serum albumin (BSA) as buffer additives, efficient and reproducible separation of mesoporphyrin, coproporphyrin, uroporphyrin, penta-, hexa- and heptacarboxylporphyrins was achieved at pH 7.4 whereas sodium taurodeoxycholate (bile salt) combined with BSA in the run buffer separated type I and III isomers of coproporphyrin as well. The presence of SDS or bile salt appeared to minimize protein–and/or porphyrins–inner capillary wall (untreated silica) interaction and to enhance solubilization and selectivity of porphyrins due to the formation of ionic surfactant–protein complex(es) in the run buffer.

INTRODUCTION

Capillary zone electrophoresis (CZE) is an efficient technique for the separation of proteins [1]. On the other hand, the feasibility of adding proteins in the run buffer as stereoselective complexing agents to effect chiral separations in CZE has also been demonstrated [2–4]. A major problem associated with protein separations or the use of proteins as buffer modifiers in CZE is the inherent tendency of these macromolecules to interact with the wall of the fused-silica capillary [5], resulting in the loss of separation efficiency and reproducibility. A number of experimental approaches have been devised to minimize this type of interaction, including the use of buffers with a pH either substantially higher [6] or lower [7] than the isoelectric points of the proteins, the addition of high concentration of salts in the run buffer [8] and the covalent attachment of specific coatings to the capillary wall [3].

The introduction of an ionic surfactant in the run buffer at a concentration above the critical micelle concentration (CMC) has given rise to the development of a special form of CZE —micellar electrokinetic capillary chromatography (MECC)— in which separation of neutral as well as ionic compounds can be performed with unique selectivities [9,10]. The most common type of ionic surfactant employed in MECC to date has been the linear *n*-alkyl sulfate–sodium dodecyl sulfate (SDS), and importantly, the presence of micellar concentrations of SDS has recently been demonstrated to facilitate protein separations in coated silica capillary by minimizing protein–capillary wall interaction [11].

Bile salts are biological surfactants possessing substituted steroidal structures which are not only rigid and chiral, but also have been postulated to form helical micellar aggregates with the hydrophobic portions of the monomer facing the aqueous solution while the hydrophilic por-

* Corresponding author.

0021-9673/94/$07.00
SSDI 0021-9673(93)E1051-Z

tions turn inward [12,13]. When used as an ionic surfactant in MECC, the unique structures and aggregation properties of bile salts have yielded certain distinctive advantages, including the abilities to separate optical isomers [14] as well as highly hydrophobic compounds [15]. Furthermore, it is worth noting that one of the primary physiological functions of bile salts involves the solubilization of compounds such as serum albumin, thus allowing the clearance of these substances by the liver [13]. However, the analytical exploitation of bile salt surfactants in MECC in the presence of proteins has not been reported.

The determination of total contents as well as individual component concentration of porphyrins in biological materials are important for the diagnosis of a family of disease known as porphyrias [16–19]. Weinberger *et al.* [20] have demonstrated that urinary porphyrins having different number of carboxylic acid side-chains can be separated with good resolution using MECC. More recently, the MECC separation of various porphyrins was optimized using an overlapping resolution mapping scheme [21]. However, in both of these studies, the separation of type I and III isomers of coproporphyrin and uroporphyrin, each having four and eight carboxylic acid groups, respectively, was not reported.

The ability to determine coproporphyrin and uroporphyrin type I and III isomers is clinically significant for the differential diagnosis and confirmation of various forms of porphyrias [16,17]. Using bovine serum albumin (BSA) as a stereoselective agent in the run buffer, we have previously demonstrated that a mixture of type I and III isomers of coproporphyrin and uroporphyrin can be resolved in less than *ca.* 30 min using CZE. However, this method requires the use of coated capillary to minimize protein–and/or porphyrin–wall interaction [4], and more importantly, we later found that significant loss of separation efficiency and resolution occurred when other porphyrin compounds having different number of carboxylic acid groups were present in the sample solution. In this paper the feasibility of the use of SDS or bile salt surfactant in conjunction with BSA as novel buffer modifiers in capillary electrophoresis (CE) was investigated for the separation of a mixture of six porphyrins having two to eight carboxylic acid side-chains together with type I and III isomers of coproporphyrin and uroporphyrin at physiological pH using untreated fused-silica capillary.

EXPERIMENTAL

Chemicals

Standards of meso-, copro- (I and III), pentacarboxyl-, hexacarboxyl-, heptacarboxyl- and uro- (I and III) porphyrins were purchased from Porphyrin Products (Logan, UT, USA). Sodium taurodeoxycholate (STDC), SDS, 3-cyclohexylamino-1-propanesulfonic acid (CAPS) and essentially fatty-acid free BSA were purchased from Sigma (St. Louis, MO, USA). All other chemicals were of analytical grade from Fisher (Springfield, NJ, USA) or Aldrich (Milwaukee, WI, USA). The run buffer solutions were prepared in doubly deionized water and filtered through a 0.4-μm pore size filter membrane.

Apparatus

A commercially available CE instrument (Model Spectra PHORESIS 1000, Spectra-Physics, Freemont, CA, USA) connected to an integrator (Chromjet, Spectra-Physics) was used to obtain the data. The wavelength spectra were obtained from the output signal using the data software supplied with the CE instrument on an IBM Model 70 computer. The MECC experiments were performed in untreated fused-silica capillaries (Polymicro Technologies, Phoenix, AZ, USA) with dimensions 55 cm $\times$ 375 μm O.D. $\times$ 75 μm I.D.

Porphyrin standard solutions

Stock solutions of porphyrins were prepared by dissolving appropriate amounts of porphyrin standards in small amount of 0.5 *M* NaOH and then diluted with appropriate volume of 50 m*M* SDS or STDC, followed by pH adjustment to match the corresponding run buffer. Further dilutions were made to prepare the sample solutions. Stock and sample solutions were stored at 4°C and direct light irradiation was avoided before experiments.

Procedures

New capillaries were conditioned with 20 m*M* borate–H_3PO_4 buffer for 12 h before use. The capillary was cleaned between runs with 20 m*M* borate–H_3PO_4 buffer. The sample injection was set for vacuum (*ca.* 78 mmHg below ambient; 1 mmHg = 133.322 Pa) at 2 s injection time and absorbance detection was measured at 400 nm. Column temperature was maintained at 35°C.

RESULTS AND DISCUSSION

Fig. 1a shows the separation of six porphyrin standards having two to eight carboxylic acid groups using a run buffer which contained 100 m*M* SDS and 15% methanol at pH 11.0. The separation behaviors of these porphyrins are consistent with those reported by Weinberger *et al.* [20] for the MECC separation of urinary porphyrins under similar experimental conditions. It has been stated that the major purpose of adding SDS to the run buffer was not to optimize separation selectivity but rather this anionic surfactant was used to bind to any electrostatic and hydrophobic sites on the capillary wall [20,21], thereby reducing (or eliminating) the adsorption of porphyrins with the silica wall. One the other hand, the addition of 15% methanol may enhance the solubility of the more hydrophobic porphyrins, *e.g.*, coproporphyrin, and yield an extended elution range; however, the use of a high percentage of methanol resulted in a long analysis time, probably in large part due to reduction in the electroosmotic flow.

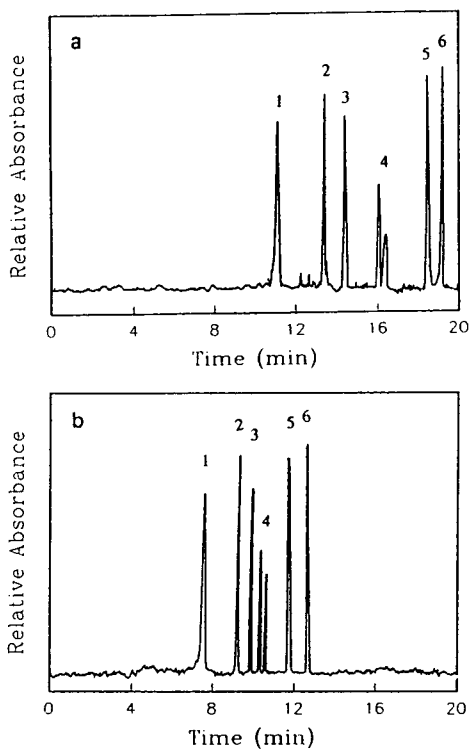

Fig. 1. Electropherograms of six porphyrin standards (10 μM each) in (a) 100 m*M* SDS, 15% (v/v) methanol, 20 m*M* CAPS (pH 11) and (b) 50 m*M* SDS–0.015 m*M* BSA, 10 m*M* borate–H_3PO_4 (pH 7.4). Voltage 18 kV. Peaks: 1 = copro (III and I)-; 2 = pentacarboxyl-; 3 = meso-; 4 = hexacarboxyl-; 5 = heptacarboxyl-; 6 = uroporphyrin.

Fig. 1b shows the separation of the same mixture of porphyrin standards used in Fig. 1a except that the run buffer contained 50 m*M* SDS and 0.015 m*M* BSA as the additives and it was buffered at pH 7.4. As in Fig. 1a, all the individual porphyrin standards were well resolved from each other but the separation was accomplished in a shorter analysis time (*ca.* 13 min) and at a significant lower pH. Various studies have been made regarding the interaction of BSA with anionic surfactants such as SDS and provided evidence suggesting the formation of various ionic surfactant–protein complexes [22,23]. Therefore, it is possible that certain SDS–BSA complex(es) may exist in the run buffer and provide sufficient solubility and selectivity for the separation of the six porphyrin standards with good efficiency and resolution at physiological pH. It is important to note that without the presence of SDS, we found that BSA alone in the run buffer was incapable of separating the six porphyrin standards (an ill-defined broad band was obtained), probably in large part due to the adsorption of BSA and/or porphyrins onto the bare silica wall. If this is the case, the formation of SDS–BSA complex(es) in the run buffer may not only contribute to enhanced solubilization and selectivity, but also to reduction in adverse effects associated with BSA/porphyrin–capillary wall interactions.

As shown in Fig. 1a and b, two peaks were observed for hexacarboxylporphyrin with or without the presence of BSA. Similar results

were also obtained by Weinberger *et al.* [20] who suggested these two peaks arose from geometrical isomers of hexacarboxylporphyrin produced during the manufacturing process. In a previous report [4], we have shown that the use of BSA as a stereoselective agent was successful for the separation of type I and III of coproporphyrin and uroporphyrin using a coated silica capillary. However, using either experimental conditions as shown in Fig. 1a or b, we were unable to resolve type I and III isomers of coproporphyrin or uroporphyrin. It appears that even at extremely alkaline conditions (*i.e.*, pH 11.0) as shown in Fig. 1a, the difference in migration time between the ionized type I and III isomers was too small to allow for separation to occur when using SDS and an organic modifier (*i.e.*, methanol) as the buffer additives. On the other hand, when using the mixed SDS–BSA buffer system as shown in Fig. 1b, BSA could be strongly denatured by SDS, thus the stereoselective binding between BSA and type I or III isomers of coproporphyrin and uroporphyrin may be diminished or eliminated.

Fig. 2a shows the separation of type I and III isomers of coproporphyrin using a run buffer which contained 50 m*M* of the bile salt STDC in presence of 5% butanol and 10% methanol. The alcohols were added to enhance the solubility of the hydrophobic coproporphyrin isomers, thus resulting in sharper and more symmetric peaks. Importantly, the two geometrical isomers of coproporphyrin were baseline resolved as a result of the differential interaction with the bile salt micelles during the separation process. It appears that the type I isomer of coproporphyrin interacted more strongly with the bile salt, resulting in a longer migration time. However, we found that the use of bile salt alone (with or without high percentage of alcohols) in the run buffer for the separation of the six porphyrin standards as shown in Fig. 1a and b was unsuccessful. Interestingly, as shown in Fig. 2b, the addition of 40 m*M* of STDC together with 0.012 m*M* of BSA in the run buffer resulted in not only the successful separation of the six porphyrin carboxylic acids but also the resolution of type I and III isomers of coproporphyrin with good efficiency and relatively short analysis time

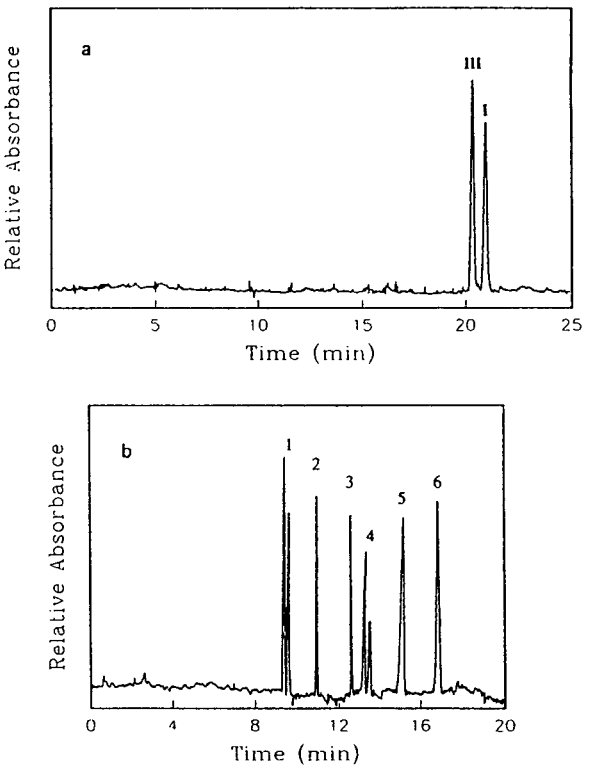

Fig. 2. Electropherograms of (a) coproporphyrin III (12.5 μM) and I (10 μM) in 50 m*M* STDC + 6 m*M* borate–H_3PO_4 (pH 8.0) plus 5% butanol and 10% (v/v) methanol and (b) 10 μM each of the porphyrin standards (peaks 1–6) in 40 m*M* STDC–0.012 m*M* BSA and 6 m*M* borate–H_3PO_4 (pH 7.4). Peaks as in Fig. 1. Voltage 18 kV.

at pH 7.4. It should be noted, however, that the separation of type I and III isomers of uroporphyrin was unsuccessful using this particular mixed STDC–BSA buffer system.

In an attempt to understand the mechanisms which contributed to the successful separation of type I and III isomers of coproporphyrin in the presence of various hydrophilic and hydrophobic porphyrins as shown in Fig. 2b, it is important to remember that as in the case of SDS, bile salt surfactants are also known to form complexes with proteins such as BSA [12]. Fig. 3a and b show the electropherograms of BSA and STDC when injected separately into the CZE system. It can be seen that a relatively sharp peak was obtained for BSA whereas a broad and asymmetric peak was obtained for STDC. A

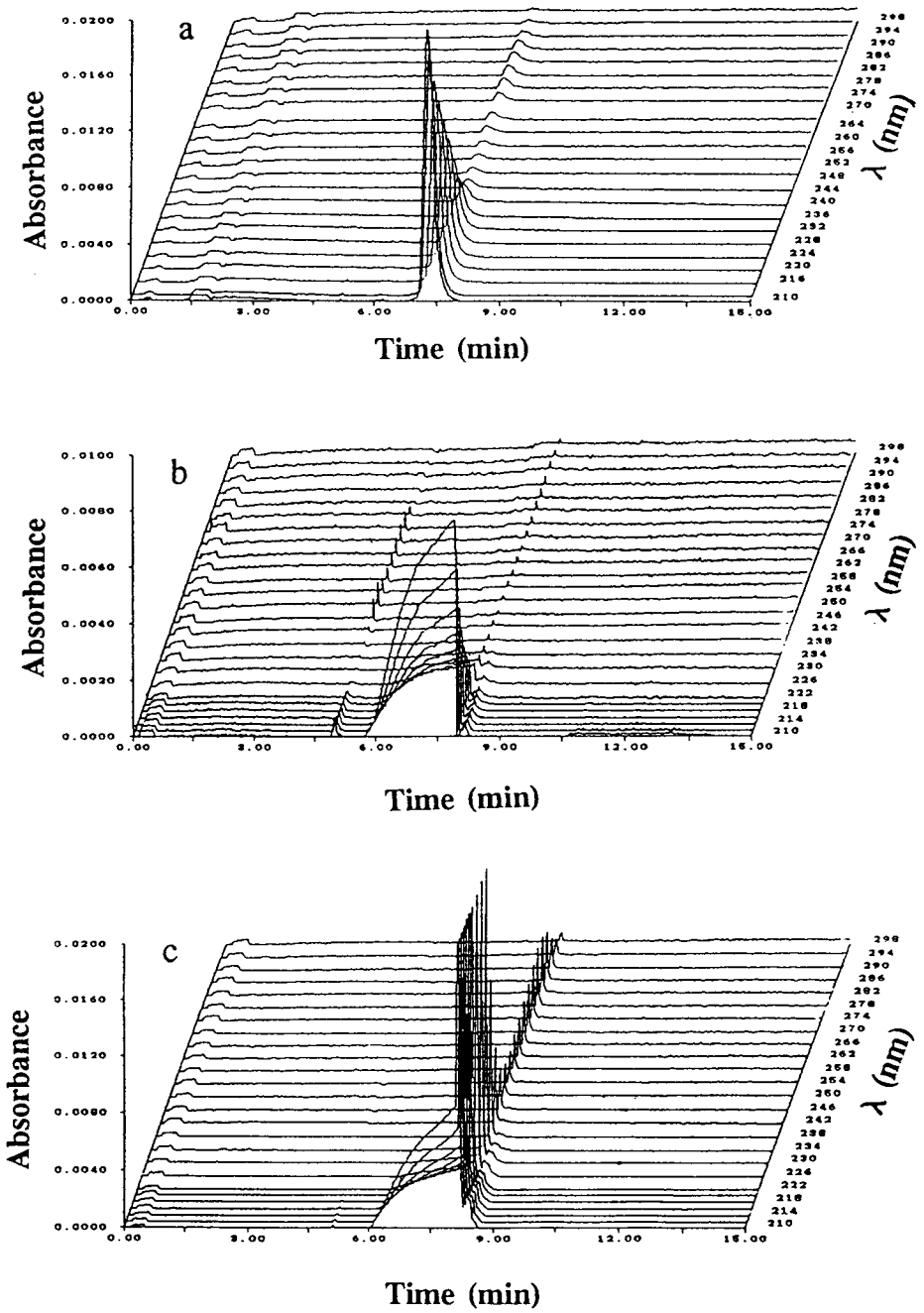

Fig. 3. Electropherograms of (a) 0.015 m*M* BSA, (b) 50 m*M* STDC and (c) a mixture of 50 m*M* STDC–0.015 m*M* BSA in 10 m*M* borate–H_3PO_4 (pH 7.4). Voltage 16.5 kV.

possible explanation for the distorted peak shape as shown in Fig. 3b may be attributed to the adsorption of the bile salt at the capillary wall and/or the inherent polydispersity of the bile salt micelles, *e.g.*, micelles of different aggregation number and size [13]. Fig. 3c shows an electropherogram of an injection sample containing both BSA and STDC. It appears that the peak

maximum of BSA which centers at a migration time of *ca.* 7.5 min as shown in Fig. 3a has shifted and overlapped with portions of the asymmetric bile salt peak located at *ca.* 8.0 min, suggesting that the bile salt may associate with the BSA to form certain ionic surfactant–protein complex(es) when mixed together in the run buffer.

Fig. 4 shows the UV–visible absorption spectra of coproporphyrin III eluted with run buffers containing different additives. By comparing spectra a and b, it can be seen that with the presence of both bile salt and BSA in the buffer, the position of the peak maximum of coproporphyrin III remained relatively constant as compared to buffer solution containing only bile salt. In contrast, spectrum c indicates that a relatively large red shift occurred in the presence of BSA alone, probably as a result of the binding of coproporphyrin III with BSA in the run buffer [4,24]. These spectroscopic results suggest that the combination of bile salt with BSA as shown in spectrum b may have led to changes in the conformation of the protein and resulted in the loss of stereoselective binding of BSA with coproporphyrin III. If such is the case, the successful separation of type I and III of coproporphyrin present in a mixture of porphyrin standards as illustrated in Fig. 2b was probably not due to the differential affinities of coproporphyrin isomers with specific binding sites located in the BSA structure, but rather arose from the differential interaction of coproporphyrin isomers with the bile salt bound to the BSA [bile salt–BSA complex(es)] and/or unbound bile salt micelles present in the run buffer. This postulation may also explain why type I and III isomers of uroporphyrin cannot be separated using the STDC–BSA buffer system since we found that the presence of bile salt alone in the run buffer was unsuccessful while BSA alone was successful for the separation of type I and III isomers of uroporphyrin.

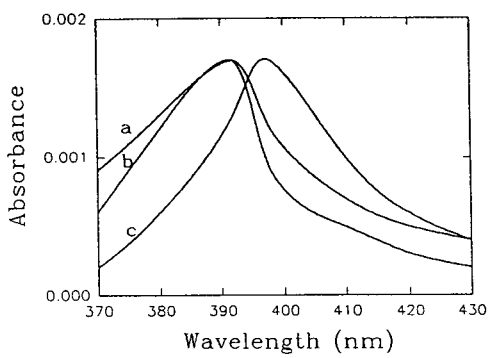

Fig. 4. Spectra of coproporphyrin III (5 μM) in run buffer containing (a) 50 mM STDC, (b) 50 mM STDC–0.015 mM BSA and (c) 0.015 mM BSA in 10 mM borate–H_3PO_4 (pH 7.4). Each spectrum was obtained by scanning the peak maximum from 370 to 430 nm. Voltage 16.5 kV.

To account for the excellent separation of the six porphyrin carboxylic acids and coproporphyrin isomers as shown in Fig. 2b, it is important to note that under optimum experimental conditions, the molar ratio of bile salt to BSA was greater than 3000, suggesting that a relatively large amount of unbound bile salt micelles could exist in the run buffer and interact dynamically with the bile salt–BSA complex(es) and the bare silica capillary wall. Under these conditions, the unbound bile salt micelles together with the bile salt–BSA complex(es) may provide enhanced solubilization and selectivity for the various porphyrins at pH 7.4 as compared to either bile salt or BSA alone. Furthermore, the interaction of anionic bile salt surfactant with BSA and the capillary wall could minimize the adsorption by the "sticky" porphyrin molecules or BSA, resulting in improved peak shape and the reproducibility of separation.

The migration time and peak area precision data obtained for the separation of the six porphyrin standards using either SDS or STDC with BSA in the run buffer are presented in Table I. When compared to the use of BSA alone in the buffer [4], a significant improvement in the migration time reproducibility can be obtained using the ionic surfactant–BSA buffer system. Furthermore, we found that without the addition of SDS or STDC, most untreated capillaries lasted for 10 to 15 runs with the presence of BSA and had to be replaced; however, a bare capillary can be used for at least 50 runs or more when SDS or STDC was added with BSA in the run buffer. The average limits of detection ($S/N = 3$) for the six porphyrin standards under the

TABLE I

RELATIVE STANDARD DEVIATIONS (%) OF MIGRATION TIME AND PEAK AREAS OBTAINED FOR PORPHYRINS AND PORPHYRIN ISOMERS SEPARATION

Measured on sequential injections over *ca.* 2 h period for five replicate injections ($n = 5$).

Porphyrin	STDC–BSA system[a], R.S.D (%, $n = 5$)		SDS–BSA system[b], R.S.D. (%, $n = 5$)	
	Migration time	Peak area	Migration time	Peak area
Copro III	0.29	2.9	0.35	2.1
Copro I	0.30	2.9	0.35	2.1
Meso	0.16	3.2	0.28	3.1
Penta	0.31	2.5	0.11	2.1
Hexa[c]	0.21	3.2	0.15	2.4
Hexa[d]	0.22	3.5	0.14	2.4
Hepta	0.35	3.8	0.25	2.9
Uro	0.38	4.2	0.27	2.9

[a]In 6 m*M* sodium borate–H_3PO_4 buffer (pH 7.4) containing 40 m*M* STDC and 0.012 m*M* BSA.
[b]In 10 m*M* sodium borate–H_3PO_4 buffer (pH 7.4) containing 50 m*M* SDS and 0.015 m*M* BSA.
[c,d]Hexacarboxylporphyrin positional isomers.

experimental conditions as shown in Figs. 1b and 2b were about 1.0 nmol/ml and 1.6 nmol/ml, respectively. These values are similar to those reported by Weinberger *et al.* [20] using absorption detection.

In summary, the use of an anionic surfactant in conjunction with a protein as buffer additives in CE allowed for the separation of various hydrophobic and hydrophilic porphyrins as well as the simultaneous resolution of a pair of clinically significant geometrical porphyrin isomers using untreated capillaries at physiological pH. Rapid, efficient and reproducible separation of porphyrins and porphyrin isomers could be attributed to the abilities of SDS and bile salt to minimize adsorption of protein/porphyrins at the bare silica wall and to the formation of ionic surfactant–protein complexes in the run buffer. More research is necessary to identify the mechanisms in which separation performance can be improved by various ionic surfactant–protein systems; in particular, the possible roles played by ionic surfactant–protein complexes in effecting stereoselective resolution of hydrophobic and hydrophilic isomers need to be addressed in more detail in future studies.

ACKNOWLEDGEMENTS

The authors thank Spectra-Physics Analytical Instruments for research supports and Professor Richard A. Hartwick for helpful discussion.

REFERENCES

1 M.V. Novotny, K.A. Cobb and J. Liu, *Electrophoresis*, 11 (1990) 735.
2 S. Busch, J.C. Kraak and H. Poppe, *J. Chromatogr.*, 635 (1993) 119.
3 G.E. Barker, P. Russo and R.A. Hartwick, *Anal. Chem.*, 64 (1992) 3024.
4 G.E. Barker, W.J. Horvath, C.W. Huie and R.A. Hartwick, *J. Liq. Chromatogr.*, 16 (1993) 2089.
5 W.D. Pickering, *LC·GC*, 7 (1989) 752.
6 H.H. Lauer and D. McManigill, *Anal. Chem.*, 58 (1986) 166.
7 R. McCormick, *Anal. Chem.*, 60 (1988) 2322.
8 J.S. Green and J.W. Jorgenson, *J. Chromatogr.*, 478 (1989) 63.
9 S. Terabe, K. Otsuka, K. Ichikama, A. Tsuchiya and T. Ando, *Anal. Chem.*, 56 (1984) 111.
10 N. Wu, T. Wang, R.A. Hartwick and C.W. Huie, *J. Chromatogr.*, 582(1992) 77.
11 M.A. Strege and A.L. Lagu, *J. Chromatogr.*, 630 (1993) 337.

12 G.A. Pico and C. Houssier, *Biochim. Biophys. Acta*, 999 (1989) 128.
13 M.C. Carey and D.M. Small, *Arch. Intern. Med.*, 130 (1972) 506.
14 S. Terabe, M. Skibata and Y. Miyashita, *J. Chromatogr.*, 480 (1989) 403.
15 R.O. Cole, M.J. Sepaniak and W.L. Hinze, *J. Chromatogr.*, 557 (1991) 113.
16 G.H. Elder, *Clin. Haemotology*, 9 (1980) 371.
17 T. Sakai, Y. Niinuma, S. Yanagihara and K. Ushio, *Clin. Chem.*, 29 (1983) 350.
18 C.W. Huie, J.H. Aiken and W.R. Williams, *Anal. Chim. Acta*, 254 (1991) 189.
19 J.H. Aiken, C.W. Huie and J. Terzian, *J. Chromatogr.*, 584 (1992) 181.
20 R. Weinberger, E. Sapp and S. Moring, *J. Chromatogr.*, 516 (1990) 271.
21 Y.J. Yao, H.K. Lee and S.F.Y. Li, *J. Chromatogr.*, 637 (1993) 195.
22 P. Lundahl, E. Greijer, M. Sandberg, S. Cardell and K. Eriksson, *Biochim. Biophys. Acta*, 873 (1986) 20.
23 K. Sasa and K. Takeda, *J. Colloid Interface Sci.*, 157 (1993) 516.
24 W.T. Morgan, A. Smith and P. Koskelo, *Biochim. Biophys. Acta*, 624 (1980) 271.

Journal of Chromatography A, 659 (1994) 443–447
Elsevier Science B.V., Amsterdam

CHROM. 25 610

Capillary electrophoretic separation of anticoagulant rodenticides in aqueous electrolytes modified with organic solvents

Costas Stathakis, Peter L. Warburton and Richard M. Cassidy*

Chemistry Department, University of Saskatchewan, Saskatoon, SK S7N 0W0 (Canada)

(First received July 13th, 1993; revised manuscript received October 1st, 1993)

ABSTRACT

The capillary electrophoretic separation of the anticoagulant rodenticides warfarin, chlorophacinone, diphacinone, bromadiolone, dicoumarol and coumatetralyl is described. Simple electrolytes, such as phosphate and borate, as well as phosphate modified with methanol (20–30%, v/v) or acetonitrile (5–30%, v/v) were used in an effort to optimize total analysis time and resolution. Micellar systems in phosphate electrolytes were also studied but with limited success. With the addition of methanol and acetonitrile modifiers it was possible to manipulate electroosmotic mobility, analyte electrophoretic mobility, and separation resolution and efficiency. Optimum resolution and analysis time (6 min) for all rodenticides was achieved in 0.015 mol/l phosphate (pH 7) modified with 22% (v/v) methanol. Separation efficiencies ranged between 459 200–548 800 theoretical plates, analyte migration reproducibility was between 0.1–0.6% R.S.D., and peak area reproducibility was in the range 1.9–9.8% R.S.D.

INTRODUCTION

Anticoagulant rodenticides are used to control mice and rats as well as other mammals such as bats, moles, rabbits and hares [1]. On certain occasions, poisonings of household pets [2] as well as humans [3] have been reported requiring rapid methods of diagnosis followed by administration of suitable antidotes, *i.e.* phytonadione (vitamin K_1). Identification of the presence of these poisons (as well as their metabolites) in animal tissue, blood plasma and urine requires extensive sample pre-treatment, which results in small amounts available for analysis [4]. Consequently, a need exists for sensitive and efficient analytical methods for small amounts of this class of compounds, present either individually or as multicomponent mixtures [4].

Analytical approaches adopted for the analysis of these rodenticides have been based on spectrophotometric [5], fluorometric [6], thin-layer [7,8] or gas chromatographic methods [9–12]. These approaches, however, suffer from a number of drawbacks, and the most suitable approaches appear to be liquid chromatographic (LC) methods [13–15] which have been reviewed by Hunter [4]. Combinations of normal-phase, size-exclusion chromatography [13], and reversed-phase chromatography [14] with post-column pH adjustment and fluorescence detection offer sensitive and selective methods for the analysis of the coumarin-based rodenticides. Ion-exchange chromatography with APS-Hypersil and an acetonitrile–0.04 mol/l Tris–HCl buffer pH 7.5 (75:25, v/v) mobile phase, under isocratic conditions, has been used in the analysis of chlorophacinone and diphacinone residues, but has had limited success in the resolution of diphacinone from warfarin [4]. In spite of the

* Corresponding author.

0021-9673/94/$07.00
SSDI 0021-9673(93)E1055-5

success of LC methods there is still a need for analytical methods that can be applied for both diagnostic and quantitative purposes to a wide class of rodenticides. Capillary electrophoresis (CE) offers many features which make it an attractive alternative for the detection and separation of rodenticides. These advantages include speed, efficiency [16], minimal sample requirements and excellent mass detection limits [17]. The CE separation of warfarin and coumachlor has been briefly examined [18], but no other coumarin-based rodenticides have been studied. The aim of this work was to investigate the potential of CE for the determination of coumarin-based rodenticides as well as chlorophacinone and diphacinone. The effect of micellar additives such as sodium dodecyl sulfate (SDS), cetyltrimethylammonium chloride (CTAC), tetraethylammonium chloride (TEAC) and Brij 35, and organic modifiers (CH_3OH 20–30%, CH_3CN 5–30%, v/v) on the separation of a series of six anticoagulant rodenticides was investigated. The effects of these electrolyte systems on migration time, separation efficiency and electroosmotic mobility were examined in an effort to optimize resolution and total analysis time.

EXPERIMENTAL

Instrumentation

The CE instrument used was a Quanta 4000 (Waters Chromatography Division of Millipore, Milford, MA, USA) with a Maxima 820 data station (version 3.30, Dynamic Solutions). Conventional fused-silica capillaries (56 cm × 365 μm O.D. × 75 μm I.D.) were obtained from Polymicro Technologies, Phoenix, AZ, USA. Analyte zones were detected by UV absorbance at 214 nm (Zn lamp). Samples were introduced hydrostatically by elevation of the sample vials to 10 cm for 10 s. All pH values were measured with a Fisher Accumet pH meter (Model 805) calibrated immediately prior to use.

Reagents

Distilled, deionized water (Millipore Milli-Q water purification system, Bedford, MA, USA) was used to prepare all solutions. Glass-distilled acetonitrile, as well as analytical-reagent grade methanol, benzyl alcohol, sodium hydroxide, disodium hydrogenorthophosphate and tetraethylammonium chloride (TEAC) were obtained from BDH (Toronto, Canada). Sodium dihydrogenphosphate was purchased from Fisher Scientific (Nepean, Canada) and SDS, and the rodenticides warfarin and dicoumarol were obtained from Sigma (St. Louis, MO, USA). CTAC, Brij 35 and sodium tetraborate were purchased from Aldrich (Milwaukee, WI, USA). Bromadiolone, coumatetralyl, chlorophacinone and diphacinone (100 μg/ml in methanol) were donated by the Saskatchewan Toxicology Research Center (University of Saskatchewan). Nylon filters (0.2 μm pore) were obtained from Cole-Palmer (Chicago, IL, USA).

Procedures

Sodium hydroxide (0.025 mol/l) was added to dicoumarol and warfarin samples to give a pH of 12. All running electrolyte pH adjustments were made with 0.01 mol/l NaOH. Stock phosphate buffer was prepared by dissolving equal amounts of disodium hydrogenorthophosphate (0.02 mol/l) and sodium phosphate monobasic (0.02 mol/l) and diluting, as needed. Benzyl alcohol or methanol were used as neutral markers. All solutions were filtered through 0.2-μm pore nylon filters immediately prior to use. Capillaries were purged with the separation buffer for 30 min prior to the initial run and for 2 min between runs. If drastic drifts in current and/or retention time were observed the capillary was purged with 0.2 mol/l NaOH for 15 min followed by a 10-min purge with distilled, deionized water. All glassware was rinsed with a saturated KOH–methanol solution followed by rinsing with distilled, deionized water prior to use.

RESULTS AND DISCUSSION

Phosphate and borate electrolytes

Selectivity, in CE, is often manipulated via buffer and/or pH modifications in order to affect the magnitude of the electroosmotic flow (μ_{eos})

[19–21] as well as the size/charge ratio of the analytes, and thus their respective electrophoretic mobilities [22,23]. The rodenticides studied are shown in Fig 1. These compounds possess weakly acidic protons (underlined on each individual structure), and the dissociation of these acidic protons was examined for separations in phosphate and borate buffers. The acid dissociation constant (pK_a) for warfarin is 5.05 [24]; values for the other rodenticides are expected to be in the same range, but could not be found in the literature. Studies in 0.015 mol/l phosphate (pH 7) and 0.01 mol/l borate (pH 11) resulted, respectively, in incomplete resolution (only four peaks obtained) and baseline resolution of all six rodenticides but at a relatively long analysis time (16 min).

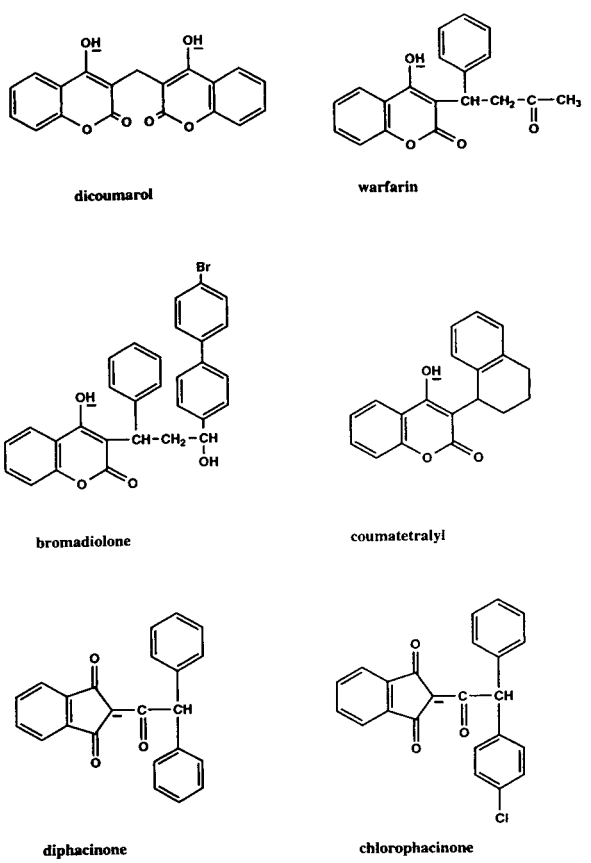

Fig. 1. Structures of the six anticoagulant rodenticides. Underlining indicates acidic proton.

Micellar–phosphate electrolytes

Micellar electrokinetic chromatography (MEKC), first introduced by Terabe *et al.* in 1984 [25], has been successful for the separation of neutral and ionic compounds [26]. Since the rodenticides should interact with micellar aggregates, this approach was examined. The four surfactant systems, above their respective critical micellar concentration, briefly examined in this study were: SDS, CTAB, TEAC and the mixed micellar system Brij 35/SDS. Studies with SDS (0.05 mol/l) in 0.01 mol/l phosphate at pH 7 gave prolonged retention times with no substantial improvement in separation resolution as compared to the pure phosphate electrolyte. A cationic surfactant (CTAC plus phosphate buffer) was then used in an attempt to reverse the direction of the electroosmotic flow [27] and decrease total analysis time of the negatively charged analytes, but this system gave extremely poor resolution as a result of strong association between the micellar aggregates and analytes. TEAC (0.025 mol/l), in 0.01 mol/l phosphate at pH 7, was also examined, but no improvement in separation efficiency was observed. In an effort to moderate strong micelle–analyte interactions observed with the cationic and anionic micelles, a more polar mixed micellar system consisting of Brij 35 and SDS (in phosphate) was used. This attempt also proved to be futile, and gave poor overall resolution and efficiency.

Mixed phosphate–organic electrolyte

The addition of organic modifiers to aqueous buffers is capable of inducing changes in the magnitude of the electroosmotic flow [23,28,29] as well as changes in the relative electrophoretic mobility of analytes [22,23]. Consequently, the effect of addition of CH_3OH and CH_3CN to the separation electrolyte was investigated. Electroosmotic flow decreased almost linearly, by 21 and 22%, respectively, with increasing % CH_3OH (20–30%, v/v) or % CH_3CN (5–30%, v/v). Such decreases have been attributed to a decrease in the dielectric constant (ϵ) and zeta electrokinetic potential (ζ) [22,28]. The relatively small decrease in medium viscosity (η) [28] is expected to be of minor importance to the observed changes in the magnitude of the elec-

troosmotic flow [22], and these effects would also be offset by the influence of decreases in buffer ionic strength due to the presence of the organic solvent, which would tend to increase the electroosmotic flow [21]. An overall decrease in analyte electrophoretic mobility (μ_{ep}), as a function of % CH_3OH and CH_3CN was observed, (see Fig. 2 for CH_3OH), which is in agreement with previously reported results for the analysis of a series of tricyclic amines [22]. The decrease in analyte μ_{ep} can also be ascribed to a decrease in the medium dielectric constant (ϵ) with organic solvent content. In this instance a decrease in ϵ results in a shift of the acid–base equilibrium towards the neutral species which decreases the effective [30] analyte electrophoretic mobility. The observed levelling effect of μ_{ep} at higher percentages of organic solvent, observed for both methanol and acetonitrile, may be due to the fact that higher concentrations of solvent can begin to stabilize the charged form of the analyte via ion–dipole interactions [31]. This effect would compete with the charge dissipation process described above, resulting in modest decreases and/or stabilization of analyte electrophoretic mobility at higher concentrations of organic modifier. Methanol was found to provide good separations in the concentration range 25–30% (v/v) whereas acetonitrile modifier could not resolve chlorophacinone and diphacinone in the concentration range 5–15% (v/v) and coumatetralyl and dicoumarol in the range 15–30% (v/v). This is most likely due to the higher μ_{eos} observed in the presence of acetonitrile as compared to methanol given the higher dielectric constant (ϵ) of the former [29]. With methanol in the electrolyte composition range of 25–30% (v/v) no significant improvement in resolution was observed at higher concentrations of methanol, and this higher concentration also gave prolonged migration times. Since separation currents were relatively low (approximately 40 μA) the field strength was increased to 536 V/cm and this gave optimum analysis time and resolution; optimum conditions were achieved in 0.015 mol/l phosphate (pH 7) with 22% methanol (see Fig. 3). Separation efficiencies were found to range between 459 200 and 548 800 theoretical plates. The reproducibility (R.S.D.) of overall migration mobility (μ_{mig}), was found to range between 0.1–0.6%, and peak area reproducibility was 1.9–9.8% (R.S.D.). The detection limit for dicoumarol at a signal-to-noise ratio 3 (peak-to-peak noise) was $4 \cdot 10^{-6}$ mol/l corresponding to 18 pg of analyte injected on to the capillary. Least squares calibration curves were determined for dicoumarol ($R^2 = 0.994$) and warfarin

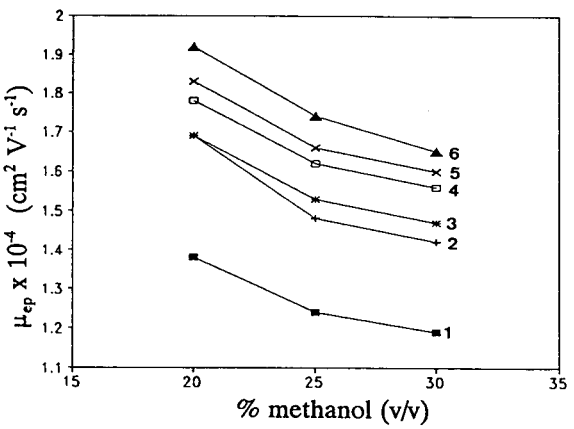

Fig. 2. Plot of electrophoretic mobility (μ_{ep}) *versus* % CH_3OH. Experimental conditions: 0.015 mol/l phosphate (pH 7) modified with methanol; neutral marker, benzyl alcohol; field strength 379 V/cm; hydrostatic injection from 10 cm for 10 s. Plots: 1 = bromadiolone; 2 = chlorophacinone; 3 = diphacinone; 4 = warfarin; 5 = coumatetralyl; 6 = dicoumarol.

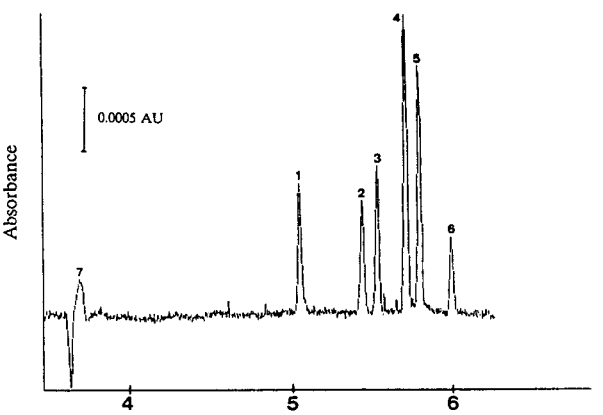

Fig. 3. Electropherogram for six anticoagulant rodenticides in 22% (v/v) CH_3OH. Experimental conditions: 0.015 mol/l phosphate (pH 7); field strength 536 V/cm; see Fig. 2 for compound identification and other experimental conditions. 7 = Neutral marker (methanol).

($R^2 = 0.995$), in the concentration range $3 \cdot 10^{-5}$–$1.1 \cdot 10^{-3}$ mol/l. Calibration linearity, in the concentration range $6.7 \cdot 10^{-5}$–$1.1 \cdot 10^{-3}$ mol/l, was evaluated by plotting sensitivity, corrected for non-zero intercept, *versus* concentration (five concentration points) as described elsewhere [32]. The maximum difference between the values of sensitivity, observed in this concentration range, was 18% for dicoumarol and 12% for warfarin.

CONCLUSIONS

CE offers a rapid and simple means of identifying and separating multi-component mixtures of anticoagulant rodenticides. In fully establishing CE as a preferred method of analysis, however, additional work is required to determine the performance of the technique with real samples (*i.e.* animal tissue extracts). The use of organic modifiers appears to be promising in analyzing structurally similar and relatively water-insoluble compounds as well as in inducing changes in the electroosmotic flow and analyte electrophoretic mobility.

ACKNOWLEDGEMENTS

The authors would like to thank the University of Saskatchewan Toxicology Research Center for providing some of the rodenticide samples used in this work. In addition, dicussions with Dr. L. Dickson at the Toxicology Research Center are greatly appreciated. The authors also acknowledge the financial support of the Natural Sciences and Engineering Research Council of Canada and Waters/Millipore. One of the authors (P.L.W.) would like to recognise NSERC support in the form of an Undergraduate Student Research Award.

REFERENCES

1 W.E. Howard, in S. Parker (Editor), *McGraw-Hill Encyclopedia of Science and Technology*, Vol. 15, McGraw-Hill, New York, 1987, p. 39.
2 G.D. Osweiler, *Clinical and Diagnostic Veterinary Toxicology*, Kendall/Hunt Publ. Co., Dubuque, IA, 1985, pp. 334–335.
3 R.W. Holmes and J. Love, *J. Am. Med. Ass.*, 148 (1952) 935–937.
4 K. Hunter, *J. Chromatogr.*, 321 (1985) 255–272.
5 R.A. O'Reilly, P.M. Aggeler and L.S. Leong, *J. Clin. Invest.*, 42 (1963) 1542–1551.
6 M. Corn and R. Berberich, *Clin. Chem.*, 13 (1967) 126–131.
7 K. Opong-Mensah and W.R. Porter, *J. Chromatogr.*, 455 (1988) 439–443.
8 P. Owen, A. Pendlebury and A.C. Moffat, *J. Chromatogr.*, 161 (1978) 187–193.
9 H.S. Funnell and N. Platonow, *J. Forensic Sci.*, 15 (1970) 601–604.
10 S. Hanna, M. Rosen, P. Eisenberger, L. Rasero and L. Lachman, *J. Pharm. Sci.*, 67 (1978) 84–86.
11 R.W. Bullard, G. Holguin and J.E. Peterson, *J. Agr. Food Chem.*, 23 (1975) 72–74.
12 R.W. Bullard, R.D. Thompson and G. Holguin, *J. Agr. Food Chem.*, 24 (1976) 261–263.
13 D.E. Mundy and A.F. Machin, *J. Chromatogr.*, 234 (1982) 427–435.
14 K. Hunter, *J. Chromatogr.*, 270 (1983) 267–276.
15 K. Hunter, *J. Chromatogr.*, 270 (1983) 277–283.
16 R.A. Wallingford and A.G. Ewing, *Adv. Chromatogr.*, 29 (1989) 1–76.
17 S.W. Compton and R.G. Brownlee, *BioTechniques*, 6 (1988) 432–439.
18 K.J. Potter, R.J.B. Allington and J. Algaier, *J. Chromatogr.*, 652 (1993) 427–429.
19 K.D. Altria and C.F. Simpson, *Chromatographia*, 24 (1987) 527–532.
20 H.J. Issaq, I.Z. Atamna, G.M. Muschik and G.M. Janini, *Chromatographia*, 32 (1991) 155–161.
21 J. Vindevogel and P. Sandra, *J. Chromatogr.*, 541 (1991) 483–488.
22 K. Salomon, D.S. Burgi and J.C. Helmer, *J. Chromatogr.*, 549 (1991) 375–385.
23 S. Fujiwara and S. Honda, *Anal. Chem.*, 59 (1987) 487–490.
24 K.A. Connors, G.L. Amidon and V.J. Stella, *Chemical Stability of Pharmaceuticals*, Wiley, New York, 1986, p. 804.
25 S. Terabe, K. Otsuka, K. Ichikawa, A. Tsuchiya and T. Ando, *Anal. Chem.*, 56 (1984) 111–113.
26 A.S. Cohen, S. Terabe, J.A. Smith and B.L. Karger, *Anal. Chem.*, 59 (1987) 1021–1027.
27 K.D. Altria and C.F. Simpson, *Anal. Proc.*, 25 (1988) 85.
28 J.C. Reijenga, G.V.A. Aben, Th.P.E.M. Verheggen and F.M. Everaerts, *J. Chromatogr.*, 260 (1983) 241–254.
29 T. Tsuda, K. Nomura and G. Nakagawa, *J. Chromatogr.*, 248 (1982) 241–247.
30 J. Vacík, in Z. Deyl (Editor), *Electrophoresis: A Survey of Techniques and Applications, Part A: Techniques*, Elsevier, Amsterdam, New York, 1979, Ch. 1, p. 11.
31 R.G. Bates, in J.F. Coetzee and C.D. Ritchie (Editors), *Solute–Solvent Interactions*, Marcel Dekker, New York, 1969, Ch. 2, pp. 74–78.
32 M. Janoski and R.M. Cassidy, *LC·GC*, 10 (1992) 692–696.

Journal of Chromatography A, 659 (1994) 449–457
Elsevier Science B.V., Amsterdam

CHROM. 25 606

Chiral separation of drugs using cyclodextrins in capillary zone electrophoresis

Hiroyuki Nishi*, Yoshio Kokusenya, Takaaki Miyamoto and Tadashi Sato

Analytical Chemistry Research Laboratory, Tanabe Seiyaku Co., Ltd., 16-89, Kashima 3-chome, Yodogawa-ku, Osaka 532 (Japan)

(First received February 23rd, 1993; revised manuscript received June 29th, 1993)

ABSTRACT

Chiral separation in capillary zone electrophoresis was investigated employing four kinds of cyclodextrins (CDs). The effects of the type and amount of CDs added to the background electrolyte and the pH of the buffer solution on the resolution of enantiomers were examined. The best enantioselectivity was obtained by employing heptakis(2,6-di-O-methyl)-β-cyclodextrin in acidic solution. In particular, the enantiomeric separation of denopamine, which is a potent cardiotonic agent, the direct enantiomeric separation of which had not been successful, was achieved by the method. The effects of buffer, urea and an organic solvent on the enantioselectivity of three enantiomeric drugs were also investigated.

INTRODUCTION

Capillary electrophoresis (CE) has become a powerful separation technique during the past decade because of its separation efficiency and high resolution, and several different separation modes, from capillary gel electrophoresis to micellar electrokinetic chromatography (MEKC), have been developed [1,2]. In particular, MEKC permits the separation of electrically neutral solutes by the CE system [3,4] and has been used in the determination of almost every kind of analyte.

The enantiomeric separation of drugs is an important subject of interest in the pharmaceutical and medical fields, because stereochemistry can have a significant effect on the biological activity of a drug. Further, it is important to develop chiral separation methods for the determination of the optical purity of drugs from the viewpoint of quality control, because the antipode of a chiral drug is regarded as one of the impurities.

A variety of chromatographic approaches, particularly those using high-performance liquid chromatography (HPLC), have been developed [5,6]. Recently much work has been reported on the direct resolution of enantiomers by chiral stationary phases and a wide variety of such HPLC stationary phases are now commercially available [7,8].

Chiral separation by CE, which includes both MEKC and capillary zone electrophoresis (CZE), is a relatively recent technique [9]. There are many advantages of CE compared with HPLC. Direct chiral separation has been performed easily using CE by adding chiral surfactants or chiral compounds, which interact with the enantiomeric solute, to the buffer solution without changing the capillary tube. High resolution is achieved within a short time.

In MEKC, chiral separation has been achieved by using a chiral surfactant such as bile salts [10–12] or sodium N-dodecanoyl-L-valinate [13–16]. Other than using chiral surfactants, the

* Corresponding author.

0021-9673/94/$07.00
SSDI 0021-9673(93)E1052-2

chiral separation of some dansyl-DL-amino acids has been achieved by electrokinetic chromatography with cyclodextrin derivatives, which have both chirality and an ionic group within a molecule, as a carrier [17]. Chiral separation in MEKC with sodium dodecyl sulphate (SDS) solution was also successful by adding cyclodextrins (CDs) to the buffer solutions [18–20]. This method is called cyclodextrin-modified MEKC (CD-MEKC) and was first developed for the determination of highly hydrophobic solutes such as aromatic hydrocarbons [21,22]. CDs have also been successfully used for enantiomeric separation in CZE [23–27] or CGE [28] under acidic conditions. Differential inclusion complex formation of the CD with the solute provides differential solute migration and chiral recognition.

This paper describes the chiral separation of drugs by CZE using CDs (CD-CZE). The effect of the type of CD on the chiral recognition of about 30 enantiomeric compounds was investigated. The influence of the amount of CD added to the background electrolyte, the pH value, buffer concentrations, addition of urea and an organic solvent on the resolution of enantiomers was also examined by using three enantiomeric drugs and heptakis(2,6-di-O-methyl)-β-cyclodextrin (DM-β-CD). CD-MEKC and CD-CZE are briefly compared.

EXPERIMENTAL

Apparatus

A fused-silica capillary of 55 cm length (effective length 40 cm) × 0.05 mm I.D. (Scientific Glass Engineering, Ringwood, Victoria, Australia) was used as a separation tube. An HCZE-30PN0.25 high-voltage d.c. power supply (Matsusada Precision Devices, Kusatsu, Shiga, Japan) delivering from −25 to +25 kV was used to drive the separation. The migrating solutes were detected by the on-column measurement of UV absorption at 210–220 nm with an SPD-6A spectrophotometer (Shimadzu, Kyoto, Japan) with a time constant of 0.05 s using a laboratory-made cell holder and a slit. A Chromatopac C-R5A (Shimadzu) was used for data processing. Other apparatus and experimental procedures were as reported previously [10].

Reagents

Four types of CD, β-cyclodextrin (β-CD), DM-β-CD, heptakis(2,3,6-tri-O-methyl)-β-cyclodextrin(TM-β-CD)and γ-cyclodextrin(γ-CD), were obtained from Nacalai Tesque (Kyoto, Japan). All other reagents and solvents were of analytical-reagent grade from Katayama Kagaku Kogyo (Osaka, Japan). Water was purified with a Milli-RO 60 water system (Millipore Japan, Tokyo, Japan). Each CD solution was prepared by dissolving the CD in a 25 m*M* phosphate buffer solution containing urea; the solution was passed through a membrane filter of 0.45-μm pore size (Gelman Science, Tokyo, Japan) and degassed by sonication with a Branson B-2200 ultrasonic cleaner (Yamato, Tokyo, Japan) prior to use.

About 30 enantiomeric drugs or compounds, including acidic and basic solutes, were used as test solutes for the investigation of the chiral recognition of CDs. The structures of some of them, which were successfully separated by the method, are shown in Fig. 1. Enantiomers of denopamine and trimetoquinol hydrochloride were obtained from Tanabe Seiyaku (Osaka, Japan). Etilefrine hydrochloride (Japanese Pharmacopoeia grade) was purchased from Iwaki Seiyaku (Tokyo, Japan). Other compounds were purchased from Wako (Osaka, Japan), Nakalai Tesque and Aldrich (Milwaukee, WI, USA). The sample solutions were prepared by dissolving each solute in methanol at an approximate concentration of 1 mg/ml so that adequate peak heights could be obtained.

RESULTS AND DISCUSSION

Chiral recognition of CDs

The effect of the type of CDs on the chiral recognition of about 30 enantiomeric drugs was investigated by using 25 m*M* phosphate buffer solution (pH 3.0) containing 2 *M* urea and 20 m*M* of each CD. Urea was added to increase the solubility of CDs in the aqueous phase [29]. An acidic buffer was selected from preliminary studies, because no chiral separation was observed under the neutral and alkaline conditions (the concentration of CD used was 20 m*M*).

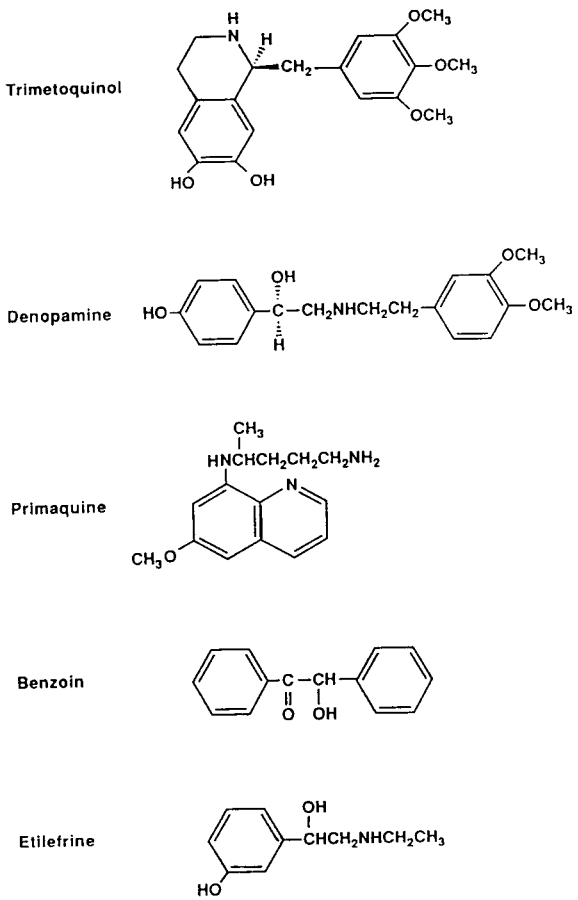

Fig. 1. Structures of the solutes.

Chiral recognition was observed in all CDs, and basic solutes were more effectively enantioresolved than acidic solutes in the CD-CZE mode employing acidic buffers. The numbers of enantiomerically resolved solutes were as follows: β-CD, six solutes (trimetoquinol, its derivatives, chlorpheniramine, propranolol); DM-β-CD, eleven solutes (trimetoquinol, its derivatives, primaquine, denopamine, phenylephrine, etilefrine, pindolol, atenolol, 2,2′-dihydroxy-1,1′-dinaphthyl); TM-β-CD, four solutes (trimetoquinol, primaquine, pindolol, chlorpheniramine); and γ-CD, four solutes (promethazine, laudanosine, benzoin, primaquine). The enantiomeric separation of an acidic solute (naproxen), diltiazem, its derivatives and warfarin was unsuccessful.

Chiral recognition depended on the type of CD. Among the four CDs employed, DM-β-CD was the most effective for the chiral recognition of the solutes. Typical electropherograms of primaquine and benzoin using γ-CD are shown in Fig. 2. These two compounds were optically resolved within 12 min better than all others in a γ-CD buffer system of pH 3.0. Other solutes were poorly enantioresolved with buffer solution of pH 3.0.

In MEKC using SDS solution and CDs, that is, in the CD-MEKC mode, chiral separation was most successful when employing γ-CD [18]. The difference in the type of CD offering the best enantioselectivity between CD-MEKC and CD-CZE can probably be interpreted by the presence of a surfactant monomer, as reported previously [18]. In CD-CZE, the cavity size of β-type CDs (seven glucose units) conforms well with the size of the solutes having aromatic rings.

Concentration effects of CDs on migration and chiral recognition

The effects of CD concentration on the migration times and chiral recognition were investigated by using 25 m*M* phosphate buffer solution (pH 2.5) containing 2 *M* urea and DM-β-CD

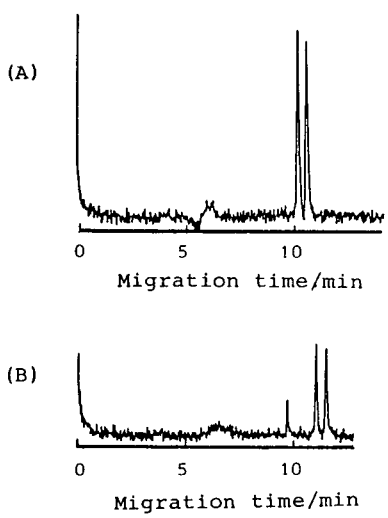

Fig. 2. Chiral separation of (A) primaquine and (B) benzoin. Conditions: buffer, 25 m*M* phosphate buffer (pH 3.0) containing 2 *M* urea and 20 m*M* γ-CD; separation tube, 0.05 mm I.D. × 550 mm (effective length 400 mm); applied voltage, 20 kV; detection, 220 nm (0.08 AUFS); temperature, ambient.

over the concentration range 10–40 m*M*. DM-β-CD was selected on the basis of the widest enantioselectivity, and was also used in subsequent investigation. Denopamine, trimetoquinol and primaquine were used as the test sample because these were completely separated from one another in the DM-β-CD buffer system, although most of other enantioresolved solutes (described above) eluted around at the peak of trimetoquinol under the conditions used. The results are shown in Figs. 3 and 4. The migration times of all solutes increased with an increase in the CD concentration.

The relationship between the migration times and CD concentration can be expressed by the equation [28]

$$t_R = \frac{l}{\mu E} = \frac{l(1 + K[C])}{\mu_f E} \quad (1)$$

assuming $\mu_f \gg \mu_c$, where μ_f is the mobility of the free solute and μ_c is the complexed solute, t_R = migration time, l = effective length of capillary, E = electric field, $[C]$ = concentration of CD and K = complex equilibrium constant. Eqn. 1 shows that a linear relationship exists between the migration time of the solute and the concentration of CD. This relationship was certainly observed with primaquine, which migrated first among the three solutes. The migration times of trimetoquinol and denopamine, which migrated more slowly than primaquine, however, did not increase linearly with increasing concentration of CD. The assumption $\mu_f \gg \mu_c$ probably did not apply with these solutes.

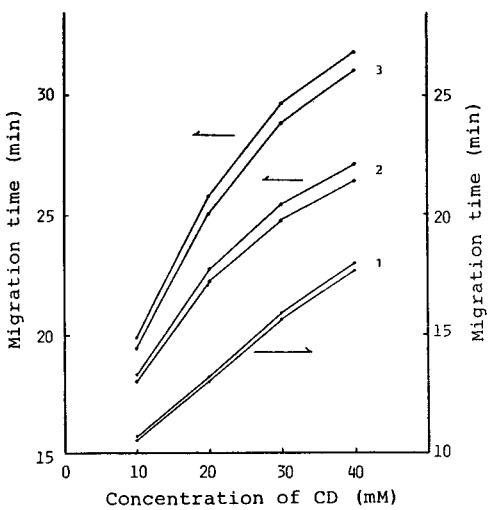

Fig. 3. Dependence of the migration times and chiral recognition on CD concentration. Solutes: 1 = primaquine; 2 = trimetoquinol; 3 = denopamine. Buffer, 25 m*M* phosphate buffer (pH 2.5) containing 2 *M* urea and DM-β-CD. Other conditions as in Fig. 2.

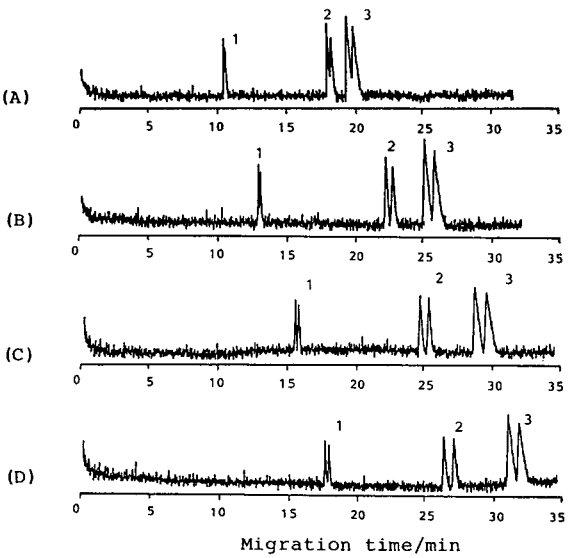

Fig. 4. Effects of CD concentration on the migration times and chiral recognition: (A) 10; (B) 20; (C) 30; (D) 40 m*M*. Conditions as in Fig. 3.

Tables I and II show the differences in the migration times and the ratios of the migration times of enantiomeric pairs. These values were used instead of the resolution R_s for the evaluation of enantioselectivity because exact plate numbers of the solute could not be calculated because of the noisy baseline and non-Gaussian peak shape. It was found that there is an optimum concentration of CD, $[C]$, which gives a maximum separation of the two enantiomers. This has been reported by Wren and Rowe [30]. The optimum concentration depends inversely on the affinity of the enantiomeric solutes for CD, that is, solutes having large K values require a low CD concentration for optimum separation. The optimum CD concentration for primaquine, trimetoquinol and denopamine were *ca.* 40, 40 and 30 m*M*, respectively.

TABLE I

EFFECT OF CD CONCENTRATION ON THE DIFFERENCE IN MIGRATION TIMES OF ENANTIOMERS

Buffer, 25 m*M* phosphate buffer (pH 2.5) containing 2 *M* urea and DM-β-CD. Applied voltage, 20 kV. Ambient temperature.

Concentration of DM-β-CD (m*M*)	Difference in migration times (min)		
	Primaquine	Trimetoquinol	Denopamine
10	0.12	0.29	0.49
20	0.14	0.51	0.75
30	0.25	0.65	0.84
40	0.27	0.72	0.79

TABLE II

EFFECT OF CD CONCENTRATION ON THE RATIOS OF MIGRATION TIMES OF ENANTIOMERS

Buffer, 25 m*M* phosphate buffer (pH 2.5) containing 2 *M* urea and DM-β-CD. Applied voltage, 20 kV. Ambient temperature.

Concentration of DM-β-CD (m*M*)	Ratio of migration times		
	Primaquine	Trimetoquinol	Denopamine
10	1.011	1.016	1.025
20	1.011	1.023	1.030
30	1.016	1.026	1.029
40	1.015	1.027	1.025

Effects of buffer pH on migration and chiral recognition

The effects of buffer pH on the migration times and chiral recognition were investigated using 25 m*M* phosphate buffer solution containing 2 *M* urea and 20 m*M* DM-β-CD (pH range 2.5–3.5). The solutes tested were denopamine, trimetoquinol and primaquine. The results are shown in Fig. 5. The migration times of denopamine and trimetoquinol decreased with increase in pH. This can be interpreted by an increase in the velocity of electroosmotic flow (EOF) at high pH [31]. On the other hand, the migration time of primaquine increased with increase in pH. At pH 3.5 (not shown in Fig. 5), it eluted with almost the same migration time as denopamine. Primaquine is probably positively charged at pH 2.5, and this causes the solute to have a fast migration time at pH 2.5.

Migration time differences and migration time ratios are summarized in Tables III and IV. The

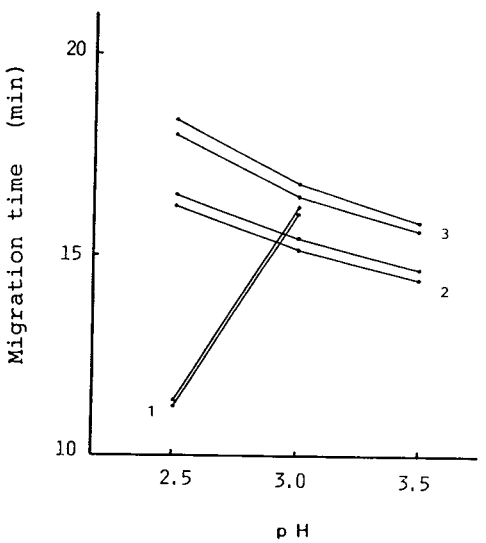

Fig. 5. Dependence of the migration times and chiral recognition on buffer pH. Buffer, 25 m*M* phosphate buffer containing 2 *M* urea and 20 m*M* DM-β-CD. Detection, 220 nm (0.04 AUFS). Other conditions as in Fig. 3.

TABLE III

EFFECT OF BUFFER pH ON THE DIFFERENCE IN MIGRATION TIMES OF ENANTIOMERS

Buffer, 25 m*M* phosphate buffer containing 2 *M* urea and 20 m*M* DM-β-CD. Applied voltage, 20 kV. Ambient temperature.

Buffer pH	Difference in migration times (min)		
	Primaquine	Trimetoquinol	Denopamine
2.5	0.13	0.26	0.38
3.0	0.15	0.22	0.32
3.5	–	0.22	0.24

enantioselectivity decreased with increase in pH. Lower pH values gave a higher enantioseparation for the solutes tested. An example of the enantiomeric separation of denopamine and trimetoquinol using buffer solution of pH 2.2 is presented in Fig. 6, showing good peak shapes and enantioseparation in comparison with separation at pH 2.5 or 3.0 (see Fig. 4B). In both solutes, active enantiomers [(*R*)-trimetoquinol and (*S*)-denopamine] migrated more slowly than the corresponding inactive enantiomers.

Effects of concentration of buffer on migration and chiral recognition

The effects of buffer concentration on the migration times and chiral recognition were investigated using phosphate buffer solution (25–

TABLE IV

EFFECT OF BUFFER pH ON THE RATIOS OF MIGRATION TIMES OF ENANTIOMERS

Buffer, 25 m*M* phosphate buffer containing 2 *M* urea and 20 m*M* DM-β-CD. Applied voltage, 20 kV. Ambient temperature.

Buffer pH	Ratio of migration times		
	Primaquine	Trimetoquinol	Denopamine
2.5	1.011	1.016	1.021
3.0	1.010	1.015	1.019
3.5	–	1.015	1.016

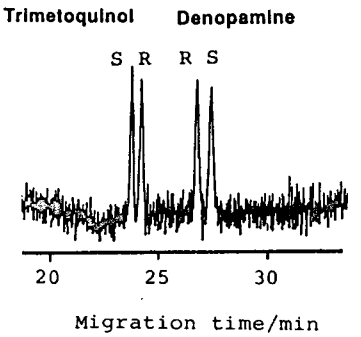

Fig. 6. Chiral separation of enantiomers of trimetoquinol and denopamine. Buffer, 25 m*M* phosphate buffer (pH 2.2) containing 2 *M* urea and 20 m*M* DM-β-CD. Other conditions as in Fig. 3.

100 m*M*) of pH 2.5 containing 2 *M* urea and 20 m*M* DM-β-CD. The solutes tested were denopamine, trimetoquinol and primaquine. Separation of the enantiomers was impaired with increasing concentration of the buffer, as shown in Fig. 7. This result conflicts with that of Kuhn

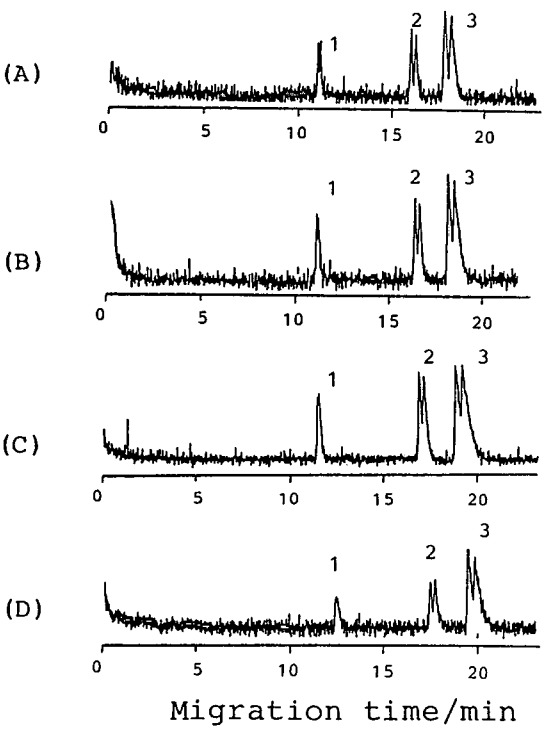

Fig. 7. Effects of buffer concentration on the migration times and chiral recognition: (A) 25; (B) 50; (C) 75; (D) 100 m*M*. Buffer, phosphate buffer (pH 2.5) containing 2 *M* urea and 20 m*M* DM-β-CD. Other conditions as in Fig. 3.

et al. [27]. This opposite result may be explained by the capillary temperature. In our apparatus, the capillary temperature rises rapidly owing to Joule heating as the buffer concentration increases through the increase in current. The resolution decreases with increasing temperature owing to enhanced band broadening. In the apparatus without a cooling system, the concentration of the phosphate buffer should be kept low.

Effects of the addition of urea or organic solvent on chiral recognition

Urea increases the solubility of lipophilic solutes in the aqueous phase by diminishing the water structure around the alkyl group [32]. The addition of urea would be expected to decrease the affinity of the solute for CD and increase it for bulk buffer in a similar manner to the addition of an organic solvent, although urea was initially used to promote the dissolution of CDs [29].

The effects of urea concentration on the migration times and chiral recognition were investigated using 25 m*M* phosphate buffer solution (pH 2.5) containing urea and 20 m*M* DM-β-CD. The results are summarized in Tables V and VI and Fig. 8. The migration times increased with increase in urea concentration, probably owing to the decrease in the velocity of EOF [33]. The enantiomeric separation of denopamine and trimetoquinol was impaired with increase in urea concentration. The enantioselectivity of primaquine was improved with increase of urea concentration. It was found that there is an optimum concentration of urea, similarly to CD concentration, as expected.

The effect of the addition of an organic solvent

TABLE V

EFFECT OF UREA CONCENTRATION ON THE DIFFERENCE IN MIGRATION TIMES OF ENANTIOMERS

Buffer, 25 m*M* phosphate buffer (pH 2.5) containing urea and 20 m*M* DM-β-CD. Applied voltage, 20 kV. Ambient temperature.

Urea concentration (*M*)	Difference in migration times (min)		
	Primaquine	Trimetoquinol	Denopamine
2	0.14	0.51	0.70
4	0.21	0.42	0.64
6	0.22	0.29	0.50
8	0.22	0.27	0.45

TABLE VI

EFFECT OF UREA CONCENTRATION ON THE RATIOS OF THE MIGRATION TIMES OF ENANTIOMERS

Buffer, 25 m*M* phosphate buffer (pH 2.5) containing 2 *M* urea and 20 m*M* DM-β-CD. Applied voltage, 20 kV. Ambient temperature.

Urea concentration (*M*)	Ratio of the migration times		
	Primaquine	Trimetoquinol	Denopamine
2	1.011	1.023	1.028
4	1.015	1.019	1.026
6	1.015	1.013	1.020
8	1.014	1.011	1.018

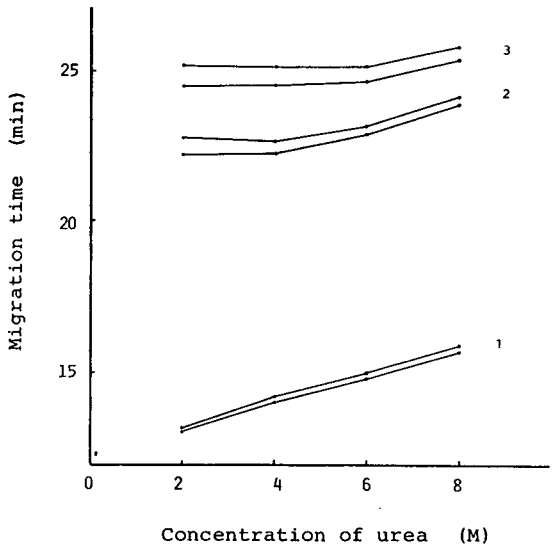

Fig. 8. Effects of urea addition on the migration times and chiral recognition. Buffer, 25 m*M* phosphate buffer (pH 2.5) containing urea and 20 m*M* DM-β-CD. Other conditions as in Fig. 3.

was investigated by using methanol. Methanol (up to 20%) was added to the above buffer solution. Organic solvents are expected to play a similar role as in urea addition. As expected from the investigation of urea addition, the enantioseparation of denopamine and trimetoquinol was impaired through the addition of methanol, compared with the separation in the absence of methanol, and the migration times of the solutes were increased owing to the decrease in the velocity of EOF.

From the result that the enantioselectivity of denopamine and trimetoquinol was impaired with increase in urea concentration or in the presence of methanol, *i.e.*, a decrease in the equilibrium constant K, it was thought that 20 m*M* DM-β-CD was lower than the optimum concentration for denopamine and trimetoquinol.

In conclusion, it was found that the type and concentration of CDs, the pH, the concentration of buffer solutions and addition of urea or an organic solvent affect the enantioselectivity in CD-CZE. The best enantioselectivity was obtained by employing DM-β-CD, although γ-CD was the most successful in CD-MEKC. It was also found that there is an optimum CD concentration. Acidic buffer solutions were well suited for enantiomeric separations of drugs, especially basic drugs, in the CD-CZE mode. An enantiomeric separation can be optimized by changing the type and concentration of the CD, the pH of the buffer and adding urea or an organic solvent.

REFERENCES

1 P.D. Grossmann and J.C. Colburn, *Capillary Electrophoresis —Theory and Practice*, Academic Press, New York, 1992.
2 S.F.Y. Li, *Capillary Electrophoresis —Principles, Practice and Applications*, Elsevier, Amsterdam, 1992.
3 S. Terabe, K. Otsuka, K. Ichikawa, A. Tsuchiya and T. Ando, *Anal. Chem.*, 56 (1984) 111.
4 H. Nishi and S. Terabe, *Electrophoresis*, 11 (1990) 691.
5 A.M. Krstulovic (Editor), *Chiral Separation by HPLC*, Ellis Horwood, Chichester, 1989.
6 W. Lindner, *Chromatographia*, 24 (1987) 97.
7 D. Armstrong, *Anal. Chem.*, 59 (1987) 84A.
8 Y. Okamoto, *Optical Resolution by Chromatography* (*Kikan Kagaku Sosetsu*, No. 6), Japan Chemical Society, Gakkai Shuppan Centre, 1989.
9 J. Snopek, I. Jelinek and E. Smolkova-Keulemansova, *J. Chromatogr.*, 609 (1992) 1.
10 H. Nishi, T. Fukuyama, M. Matsuo and S. Terabe, *J. Microcol. Sep.*, 1 (1989) 234.
11 S. Terabe, M. Shibata and Y. Miyashita, *J. Chromatogr.*, 480 (1989) 403.
12 H. Nishi, T. Fukuyama, M. Matsuo and S. Terabe, *J. Chromatogr.*, 515 (1990) 233.
13 A. Dobashi, T. Ono, S. Hara and J. Yamaguchi, *Anal. Chem.*, 61 (1989) 1984.
14 A. Dobashi, T. Ono, S. Hara and J. Yamaguchi, *J. Chromatogr.*, 480 (1989) 413.
15 K. Otsuka and S. Terabe, *Electrophoresis*, 11 (1990) 982.
16 K. Otsuka and S. Terabe, *J. Chromatogr.*, 515 (1990) 221.
17 S. Terabe, *Trends Anal. Chem.*, 8 (1989) 129.
18 H. Nishi, T. Fukuyama and S. Terabe, *J. Chromatogr.*, 553 (1991) 503.
19 T. Ueda, F. Kitamura, R. Mitchell, T. Metcalf, T. Kuwana and A. Nakamoto, *Anal. Chem.*, 63 (1991) 2981.
20 J. Prunosa, R. Obach, A. Diez-Cascon and L. Gouesclou, *J. Chromatogr.*, 574 (1992) 127.
21 S. Terabe, Y. Miyashita, O. Shibata, E.R. Barnhart, L.R. Alexander, D.G. Patterson, B.L. Karger, K. Hosoya and N. Tanaka, *J. Chromatogr.*, 516 (1990) 23.
22 H. Nishi and M. Matsuo, *J. Liq. Chromatogr.*, 14 (1991) 973.
23 S. Fanali, *J. Chromatogr.*, 474 (1989) 441.
24 S. Fanali and P. Bocek, *Electrophoresis*, 11 (1990) 757.
25 S. Fanali, *J. Chromatogr.*, 545 (1991) 437.
26 J. Snopek, H. Soini, M. Novotny and E. Smolkova-Keulemansova, *J. Chromatogr.*, 559 (1991) 215.

27 R. Kuhn, F. Stoecklin and F. Erni, *Chromatographia*, 33 (1992) 32.
28 A. Guttman, A. Paulus, A.S. Cohen, N. Grinberg and B.L. Karger, *J. Chromatogr.*, 448 (1989) 41.
29 D.Y. Pharr, Z.S. Fu, T.K. Smith and W.L. Hinze, *Anal. Chem.*, 61 (1989) 275.
30 S.A.C. Wren and R.C. Rowe, *J. Chromatogr.*, 603 (1992) 235.
31 K.D. Lukacs and J.W. Jorgenson, *J. High Resolut. Chromatogr. Chromatogr. Commun.*, 8 (1985) 407.
32 Y. Nozaki and C. Tanford, *J. Biol. Chem.*, 238 (1963) 4074.
33 S. Terabe, Y. Ishihama, H. Nishi, T. Fukuyama and K. Otsuka, *J. Chromatogr.*, 545 (1991) 359.

Journal of Chromatography A, 659 (1994) 459–466
Elsevier Science B.V., Amsterdam

CHROM. 25 576

Prediction and optimization of the separation of metal cations by capillary electrophoresis with indirect UV detection

Changyu Quang and Morteza G. Khaledi*

Department of Chemistry, North Carolina State University, P.O. Box 8204, Raleigh, NC 27695 (USA)

(Received June 1st, 1993)

ABSTRACT

The migration of metal cations in capillary electrophoresis with indirect UV detection was investigated. A mathematical model was used to relate the electrophoretic mobility of a metal cation with two background electrolyte factors: the pH and the concentration of a complexing agent. Imidazole, which has an electrophoretic mobility close to those of metal cations, was used as the visualization agent, and 2-hydroxyisobutyric acid (HIBA) was used as the complexing agent. Through computer modeling, the electrophoretic mobilities of fourteen metal cations were predicted on the basis of five initial experiments within the factor space of pH and HIBA concentration. Good agreement was observed between the predicted electrophoretic mobilities and the observed values of the metal cations. Subsequently, the separation of a complex mixture of metal cations was successfully optimized. A complete separation of 14 metal cations including alkali, alkaline earth and transition metal(II) cations was achieved within 4 min. In addition, the effectiveness of other visualization agents and complexing agents for the separation of metal cations was examined.

INTRODUCTION

Chromatographic methods for the separation of metal cations are time-consuming and often require sophisticated analytical columns and eluents [1,2]. Capillary electrophoresis (CE) is a separation technique undergoing rapid development in recent years. Its popularity has been largely attributed to high efficiency, short separation time, feasibility in selectivity manipulation and a relatively simple instrumental setup [3,4]. Separation in CE is based on the differential migration of ionic solutes. In principle, CE is well suited for direct analysis of inorganic ions such as metal cations. Sensitive detection of metal cations, however, is not feasible due to low molar absorptivities.

One solution to such a problem is to introduce chromophores or fluorophores in the buffer which form complexes with metal ions and can be detected spectroscopically. Examples such as laser fluorescence detection of metal-8-hydroxyquinoline-5-sulfonic acid complexes [5], or UV absorbance detection of cyanide complexes of iron(II) and iron(III) [6] have been reported.

Another approach is indirect photometric detection, which has been commonly used in ion chromatography for metal cation analysis [7,8]. To achieve indirect photometric or UV detection, an ion, called visualization agent which absorbs light in the UV–Vis region, is added to the background electrolyte in order to create a high background signal. The analyte ions are indirectly detected by the change in background signal when the analyte ions displace the visualization agent ions from the buffer according to charge conservation. Indirect fluorescence detec-

* Corresponding author.

0021-9673/94/$07.00
SSDI 0021-9673(93)E1004-J

tion is based on the same mechanism, except that a fluorophore is added to the background electrolyte.

The application of CE with indirect UV detection was first reported by Hjertén *et al.* [9] for the analysis of inorganic and organic anions. Indirect detection methods for CE have been recently reviewed by Yeung [10]. Current research is aimed at extending the number of applications of this technique, primarily by using different visualization and complexing agents to improve the separation. Foret *et al.* [11] reported the separations of metal cations by using 2-hydroxyisobutyric acid (HIBA) as a complexing agent and creatinine as a visualization agent on a polyacrylamide coated capillary. Weston and coworkers [12–14] reported the separations of metal cations using unspecified buffer conditions. The use of aromatic amines and heterocycle compounds as visualization agents have been reported by Chen and Cassidy [15] for lanthanide separation on bonded-phase capillaries, and by Beck and Engelhardt [16] for separations of alkali and alkaline earth and aliphatic amine cations.

In this paper, a simple mathematical model is used to relate the electrophoretic mobility of a metal cation to two experimental factors of the pH and the concentration of a complexing agent. These two factors have a pronounced effect on the complexation, and therefore, on the migration of metal cations. Consequently, electrophoretic mobilities of metal cations were predicted on the basis of a small number of experiments, and the separation of a complex mixture of metal cations was optimized. A complete separation of fourteen metal cations was achieved within 4 min. The effectiveness of different visualization and complexing agents on the metal cation separation is also examined.

EXPERIMENTAL

Apparatus

Experiments were carried out on a laboratory-built CE system. The system was composed of a 0–30 kV high-voltage power supply (Series EH; Glassman High Voltage, Whitehouse Station, NJ, USA), a variable-wavelength UV detector (Model 200; Linear Instruments, Reno, NV, USA) operated at 214 nm with 0.1 s rising time, and 50 μm I.D. × 375 μm O.D. fused-silica capillary tubing (Polymicro Technologies, Phoenix, AZ, USA). The total length of the capillary was 62 cm and detection was performed at 50 cm downstream. The capillary temperature was maintained at 30°C by jacketing it in light mineral oil using a constant temperature circulator (Type K2-R; Lauda, Germany). The samples were introduced from the anodic end of the capillary by gravity, 10 cm height for 5 s. Positive voltage of 25 kV was used for all the electrophoretic separations. Electropherograms were recorded with an integrator (Model SP4200; Spectra-Physics, San Jose, CA, USA).

Reagents and chemicals

The metal ion solutions were prepared by the dilution of 1000 μg/ml standard solutions of metal chlorides or nitrates obtained from Aldrich (Milwaukee, WI, USA). The UV visualization agents imidazole, benzylamine and trimethylbenzylamine hydroxide, and the complexing agents HIBA, citric acid and tartaric acid, are reagent grade and obtained from Aldrich. All other chemicals are of analytical-reagent grade.

Procedure

All background electrolytes contained 6 m*M* imidazole or other visualization agents. The concentration of the complexing agent, HIBA, varied from 2 to 20 m*M*. Solutions were prepared fresh daily using purified water (Milli-Q laboratory water-purification system, Millipore, Bedford, MA, USA). The pH values of the background electrolytes were adjusted using 1.0 *M* acetic acid or 0.5 *M* tetramethylammonium hydroxide. The typical concentration of metal cations in the sample mixture was about 10 μg/ml.

From a typical electropherogram, the electrophoretic mobility of an ionic solute (μ_{ep}) can be calculated from the mobility of the electroosmotic flow (μ_{eo}), and the observed mobility of the solute (μ_{ob}) according to:

$$\mu_{ep} = \mu_{ob} - \mu_{eo} = \left(\frac{1}{t_R} - \frac{1}{t_{eo}}\right) \cdot \left(\frac{L_t L_d}{V}\right) \quad (1)$$

where L_t is the total length of capillary and L_d is the length of capillary to detector. V is the applied voltage. t_R and t_{eo} are the migration times of an analyte ion and neutral marker.

The velocity of the electroosmotic flow was estimated by injecting water. Migration times of the solutes were compiled and their electrophoretic mobilities were calculated using Quattro Pro spreadsheet (Borland International, Scotts Valley, CA, USA). Computer modeling, separation optimization and simulation were performed by using CAMOS (Computer Assisted Multivariate Optimization Strategies), a computer program developed in this laboratory in Turbo vision (Turbo Pascal Version 6.0, Borland International).

RESULTS AND DISCUSSION

In aqueous solutions of metal salts, solvated metal ions can exist as metal cations, or metal anions, or a series of hydroxymetal species depending on the oxidation state of the metals and the pH. For example, Fe(II) exists as cationic $Fe(H_2O)_6^{2+}$ in aqueous solution. Fe(III) shows a strong tendency to hydrolyze to form a series of hydroxyl species such as $Fe(OH)(H_2O)_5^{2+}$ and $Fe(OH)_2(H_2O)_4^{+}$ etc. Examples of metal anions include CrO_4^{2-} and VO_4^{3-}. In this report, since a positively charged visualization agent is used in the background electrolytes, this will limit the application of CE with indirect UV detection to metal cations which include alkali, alkaline earth and the transition metal(II) cations etc.

Imidazole as a visualization agent in CE with indirect UV detection was reportedly the most efficient in the separations of alkali and alkaline earth cations because its electrophoretic mobility is close to those of metal cations [16]. HIBA, a weak acid, has also been commonly used in the separation of metal ions including the lanthanides, alkali, alkaline earth and certain transition metal cations [11–15]. Since it is a weak complexing agent, metal ions are only partially complexed and are mostly in solution as cations. In this report, the use of quantitative description of migration of metal cations in the imidazole–HIBA system is examined.

Migration models for metal cations

The effect of pH and the concentration of a complexing agent (HL) on the electrophoretic mobility of a metal cation can be expressed by a phenomenological model; that is, the electrophoretic mobility of a metal cation equals the weighted sum of mobilities of free metal cation and various complexed species [5]:

$$\mu_{ep} = \alpha_M \mu_M + \alpha_{ML} \mu_{ML} + \alpha_{ML2} \mu_{ML2} + \cdots \quad (2)$$

where μ_M, μ_{ML} and μ_{ML2} are the electrophoretic mobilities of various metal species; α is the molar fraction of each metal species. Therefore, similar to the treatment in ion chromatography [17], the electrophoretic mobility of a metal cation can be derived as:

$$\mu_{ep} = \frac{\mu_M + \mu_{ML}\beta_1\alpha_L C_{HL} + \mu_{ML2}\beta_2(\alpha_L C_{HL})^2 + \cdots}{1 + \beta_1\alpha_L C_{HL} + \beta_2(\alpha_L C_{HL})^2 + \cdots} \quad (3)$$

where β_i ($i = 1, 2, \ldots n$) is the overall formation constant, n refers to the number of ligand involved, C_{HL} is the total concentration of complexing agent in the background electrolyte, α_L is the molar fraction of complexing agent capable of complexing with metal ion M, and is given by:

$$\alpha_L = \frac{K_a}{1 + K_a/[H^+]} \quad (4)$$

where K_a is the acid dissociation constant of HL.

Substituting eqn. 4 into eqn. 3 would result in a very complex equation which directly shows the relationship between the electrophoretic mobility of a metal cation and the two important controllable factors (pH and C_{HL}). Swaile and Sepaniak [5] predicted the electrophoretic mobilities of Ca(II) and Mg(II) by simultaneously solving eqn. 3 on the basis of experimental data and literature values of the formation constants and the acid dissociation constant. A similar qualitative prediction of the retention of metal ions in ion chromatography was also reported by Karcher and Krull [17].

In this study, non-linear regression of electrophoretic mobility change as a function of pH and CL using eqn. 3 failed for two apparent reasons.

First, there are too many parameters (β, K_a and μ values) involved in the modeling process, and second, the number of parameters in eqn. 3 changes with the number of metal–ligand complexes. Instead, an empirical approach was chosen. The advantages of using an empirical approach include simplicity and generality. Consequently, fewer experiments are required and any combination of factors can be modeled by empirical approach. In addition, one general equation is applicable to all metal cations. One disadvantage of using an empirical model, however, is the loss of physically meaningful information about metal–ligand interactions.

A general linear model with interaction term was examined to relate the electrophoretic mobility and experimental factors (pH and C_{HL}). After a series of modeling tests, the following equation was found suitable in the range of the defined factor space:

$$\mu_{ep} = k_0 + k_1 C_{HL} + k_2 \cdot pH \cdot C_{HL} + k_3 C_{HL}^2 \qquad (5)$$

where k_0, k_1, k_2, k_3 are empirical parameters.

Since eqn. 5 contains only four parameters, five experimental points were used in the model building step by using the least-square approach. The typical mobility responses for four metal cations as a function of the pH and HIBA concentration of background electrolyte are shown in Fig. 1. The electrophoretic mobilities decrease with increasing pH and/or HIBA concentration due to the greater complexing ability of the ligand. For alkali metal cations, no changes in electrophoretic mobility are observed due to the lack of complexation. The most dramatic changes are observed for the transition metal(II) cations such as Ni(II), Co(II), Cu(II) and Zn(II). The practical upper pH limit of approximately 5.0 was established because the protonation of imidazole ($pK_a = 6.9$) is incomplete and transition metal cations may hydrolyze at higher pH. The lower end of the operating pH was found to be approximately pH 3.5. At more acidic pH values, much of the complexing ability of HIBA is lost and the detection sensitivity of the metal cations is lower because of the higher concentration of H^+ in the background electrolyte.

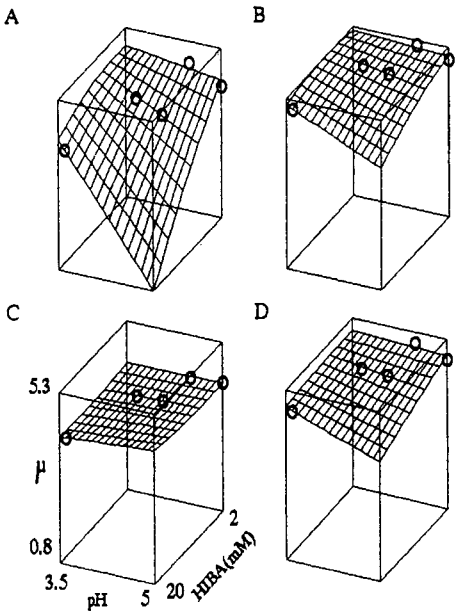

Fig. 1. Typical electrophoretic mobility responses of metal cations as a function of pH and HIBA concentration, predicted based on eqn. 5 and on five experiments shown in the figure. (A) Ni(II), (B) Mg^{2+}, (C) Li^+, (D) Cd(II). ($\mu \times 10^{-4}$ cm^2 V^{-1} s^{-1}).

In order to illustrate the prediction capabilities of the proposed model, the calculated electrophoretic mobilities of fourteen metal cations at thirteen different buffer conditions are plotted against the observed values as shown in Fig. 2 ($n = 182$). A correlation coefficient of 0.993 was obtained, indicating that the electrophoretic

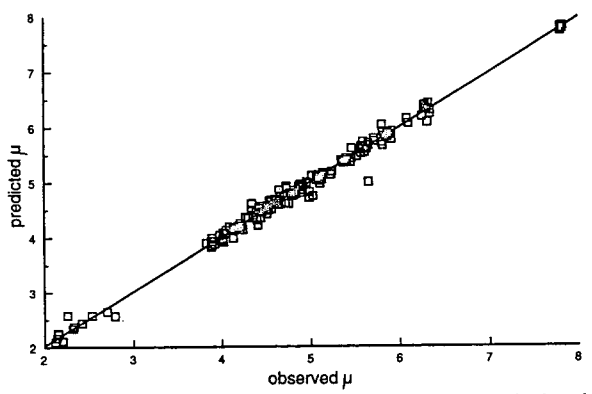

Fig. 2. The correlation plot of observed and calculated electrophoretic mobilities of fourteen metal cations at thirteen different experimental conditions ($\mu \times 10^{-4}$ cm^2 V^{-1} s^{-1}). The correlation coefficient (R^2) is 0.993.

mobility of a metal cation in imidazole–HIBA system can be accurately predicted on the basis of five experimental points. Consequently, the separation of a metal cation mixture can be optimized. The minimum resolution map for the separation of a mixture of fourteen metal cations is shown in Fig. 3. The resolution is calculated according to [3,4]:

$$R_s = \frac{\sqrt{N}}{4}\left(\frac{\mu_2 - \mu_1}{\mu_{avg} + \mu_{eo}}\right)$$

where N is the number of the theoretical plates. μ_1 and μ_2 are the electrophoretic mobilities of two neighboring metal cations, and μ_{avg} and μ_{eo} are their average and the electroosmotic mobility, respectively. As shown in Fig. 3, the optimum separation condition is in the region of the darker area pointed by an arrow. Fig. 4 shows the predicted effect of HIBA concentration on the electrophoretic mobilities and the minimum resolution plot for the separation of fourteen metal cations at pH 4.0. The minimum resolution plot shows that the optimum concentration of HIBA is about 12 mM. The corresponding separation is simulated and shown in Fig. 5A. The actual separation of these fourteen metal cations under the optimized condition is shown in Fig. 5B. The predicted separation (Fig. 5A) agrees very well with the actual one (Fig. 5B) in both elution order and migration times. Complete separation of fourteen metal cations including alkali and alkaline earth and transition metal(II) cations is achieved in less than 4 min. For the simulated electropherogram, t_0 or μ_{eo} as

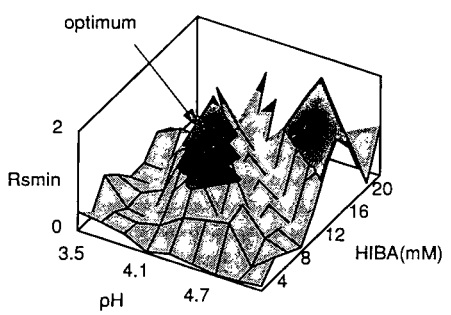

Fig. 3. Predicted minimum resolution map as a function of pH and HIBA concentration for a mixture of fourteen metal cations.

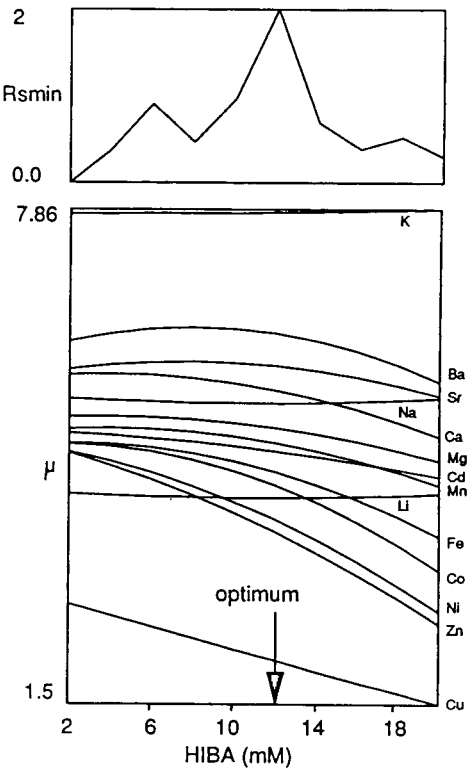

Fig. 4. Predicted effect of HIBA concentration on electrophoretic mobilities of fourteen metal cations and minimum resolution plot for a mixture of fourteen metal cations at pH 4.0 ($\mu \times 10^{-4}$ cm^2 V^{-1} s^{-1}).

a system variable was estimated from the t_0 values of the same five experimental points. In addition, a system peak was observed after the elution of all metal cations, and before the large water peak (neither peaks are shown in the electropherogram). A similar system peak was also reported in the literature [18].

The use of other visualization agents and complexing agents

As in ion chromatography, many water soluble aromatic amines and heterocycle compounds with high molar absorptivities have great potential for indirect UV detection of metal cations [7,8]. Fig. 6 shows the separation of the same metal cations as in Fig. 5, using benzylamine as the visualization agent. The electrophoretic mobility of benzylamine is less than imidazole in the buffer system. Higher efficiencies are ob-

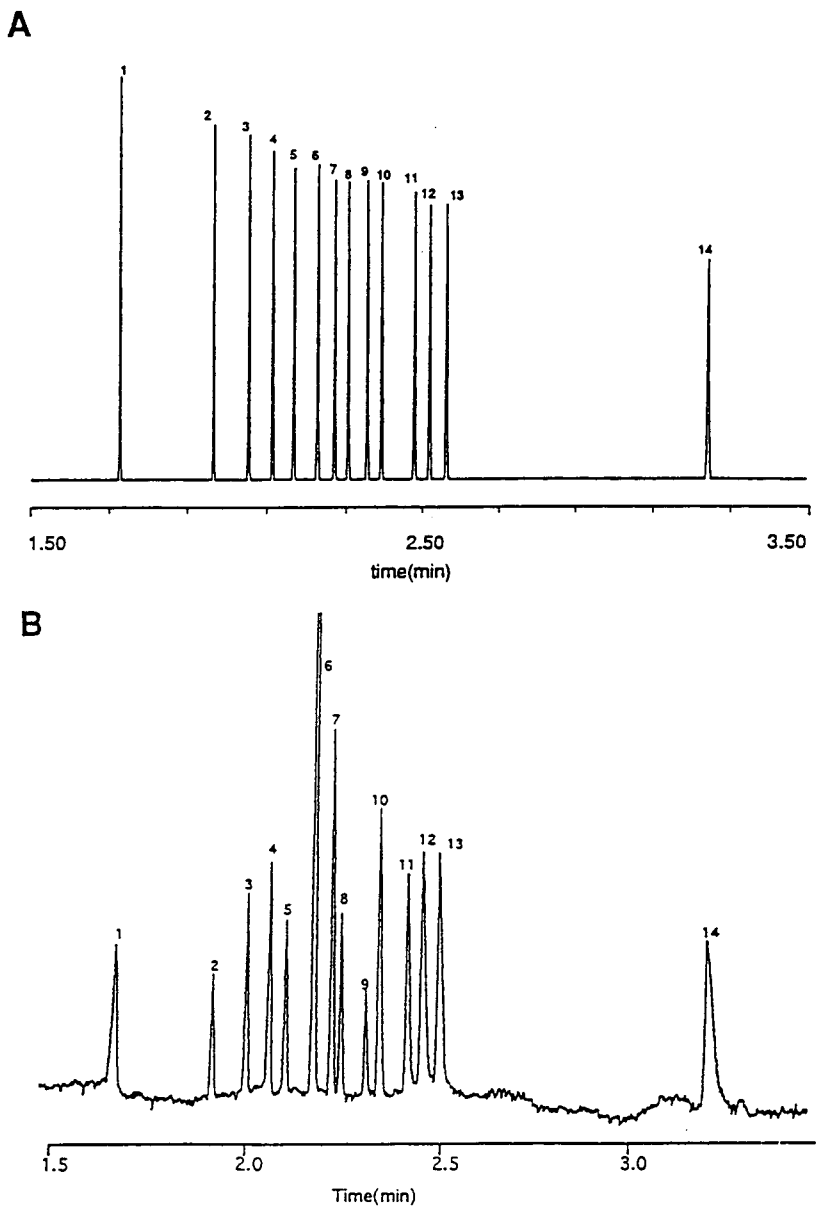

Fig. 5. Predicted separation at 12 m*M* HIBA, pH 4.0 (A) and the actual separation of fourteen metal cations (B). The background electrolyte: 6.0 m*M* imidazole, 12 m*M* HIBA, pH 3.95. Peaks: 1 = K^+; 2 = Ba^{2+}; 3 = Sr^{2+}; 4 = Ca^{2+}; 5 = Na^+; 6 = Mg^{2+}; 7 = Mn(II); 8 = Cd(II); 9 = Fe(II); 10 = Co(II); 11 = Li^+; 12 = Ni(II); 13 = Zn(II); 14 = Cu(II).

tained for late-eluting metal cations such as Ni(II), Zn(II) and Cu(II). Early-eluting metal cations such as alkali and alkaline earth, however, are less efficient due to the larger differences in electrophoretic mobility of metal cations and visualization agent. Nevertheless, the potential application of aromatic amines such as benzylamine and trimethylbenzylammonium cation is for the separation of slower migrating cations. In addition, these visualization agents remain as cations over a much wider pH range than imidazole (pK_a 6.9 for imidazole). There-

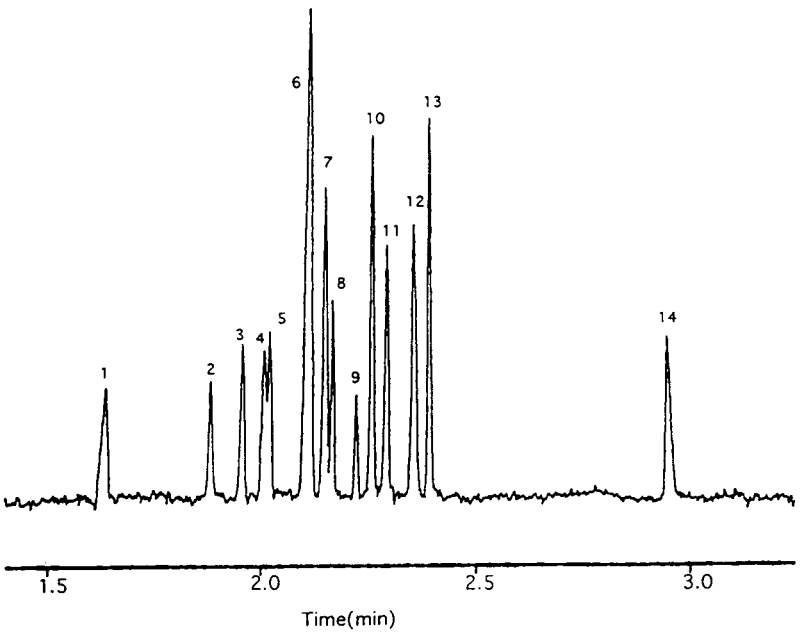

Fig. 6. Separation of the same mixture of metal cations as in Fig. 5. The background electrolyte: 6.0 m*M* benzylamine, 12 m*M* HIBA, pH 4.00.

fore, they are more suitable when higher pH values are required for the separation.

Like HIBA, other polycarboxylic acids can also be used in the background electrolyte to influence the electrophoretic mobility of metal cations, and to control selectivity. In general, the effectiveness of complexation increases in the sequence HIBA < tartaric acid < oxalic acid < citric acid [19]. For example, aqueous samples will often contain divalent metal cations (especially Ca^{2+} and Mg^{2+}) as well as alkali metal cations and ammonium ion. Fig. 7 shows separations of tap water using two different complexing agents. With the background electrolyte containing 4 m*M* tartaric acid, a stronger complexing agent than HIBA, Ca^{2+} and Mg^{2+} peaks are moved far behind the sodium peak (Fig. 7B) so that the separation of these two divalent cations from sodium are maximized without using very high concentration of HIBA and adding organic base to raise the pH of background electrolyte [14].

Another application of this technique is for the analysis of non-UV-absorbing organic amines as shown in Fig. 8. The amines are separated according to their molecular size and detected through displacing visualization cations in the background electrolyte.

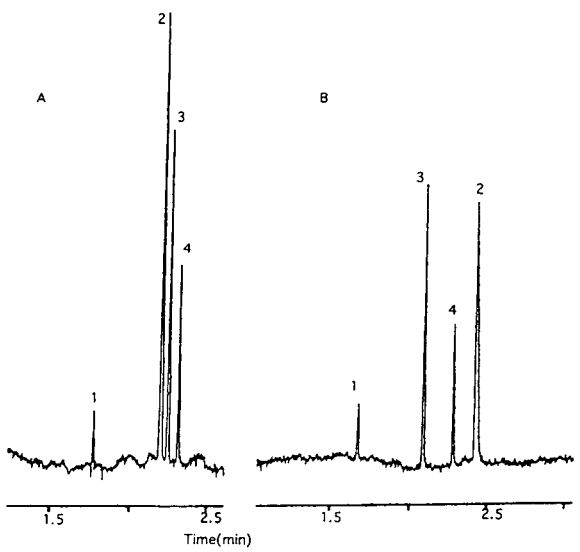

Fig. 7. Separations of tap water. Background electrolyte: 6 m*M* imidazole, (A) 12 m*M* HIBA, pH 3.95, or (B) 4 m*M* tartaric acid, pH 4.00. Peaks: 1 = K^+; 2 = Na^+; 3 = Ca^{2+}; 4 = Mg^{2+}.

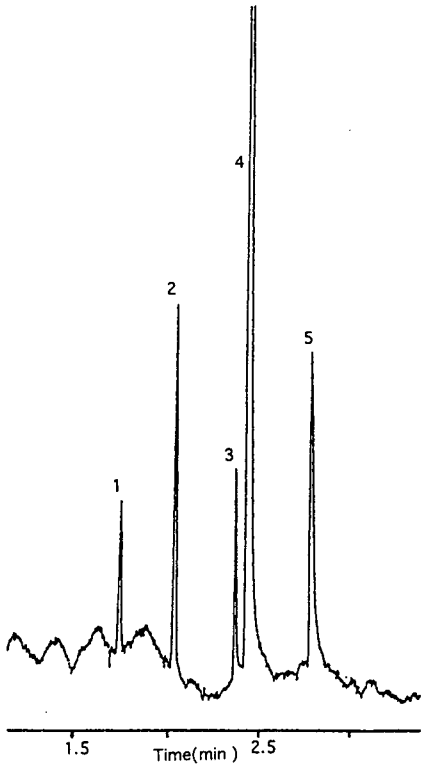

Fig. 8. Separation of aliphatic amines. Background electrolyte: 6 m*M* imidazole; 12 m*M* HIBA, pH 3.95. Peaks: 1 = NH_4^+; 2 = $CH_3NH_3^+$; 3 = $HO(CH_2)_2NH_3^+$; 4 = $(CH_3)_4N^+$; 5 = $(C_2H_5)_3NH^+$.

CONCLUSIONS

Using computer-assisted modeling and simulation, the electrophoretic mobility of metal cations can be successfully predicted on the basis of a small number of measurements. Subsequently, the separation of a complex mixture of metal cations can be easily optimized. As predicted, fourteen metal cations including alkali, alkaline earth and transition metal cations are completely separated in less than 4 min. Although the current method is applied to imidazole–HIBA system, the concept is entirely general and can be extended to other visualization–complexing agent system.

ACKNOWLEDGEMENTS

The authors gratefully acknowledge research grants from the National Institutes of Health (FIRST Award, GM 38738) and Glaxo, Inc. The authors also thank Dr. Joost Strasters for the CAMOS program.

REFERENCES

1 P.K. Dasgupta, *Anal. Chem.*, 64 (1992) 775A.
2 P. Kolla, J. Kohler and G. Schomburg, *Chromatographia*, 33 (1990) 500.
3 J.W. Jorgenson and K.D. Lukacs, *Anal. Chem.*, 53 (1981) 1298.
4 A.G. Ewing, R.A. Wallingford and T.M. Olefirwicz, *Anal. Chem.*, 61 (1989) 298A.
5 D.F. Swaile and M.J. Sepaniak, *Anal. Chem.*, 63 (1991) 179.
6 M. Aguilar, X.H. Huang and R.N. Zare, *J. Chromatogr.*, 480 (1989) 27.
7 D.T. Gjerde and J.S. Fritz, *Ion Chromatography*, Hüthig, New York, 1987.
8 P.R. Haddad and P.E. Jackson, *Ion Chromatography —Principles and Applications*, Elsevier, Amsterdam, 1990.
9 S. Hjertén, K. Elenbring, F. Kilár, J.-L. Liao, A.J.C. Chen, C.J. Siebert and M.-D. Zhu, *J. Chromatogr.*, 403 (1987) 47.
10 E.S. Yeung and W.G. Kuhr, *Anal. Chem.*, 63 (1991) 275A.
11 F. Foret, S. Fanali, A. Nardi and P. Boček, *Electrophoresis*, 11 (1989) 780.
12 A. Weston, P.R. Brown, P. Jandik, W.R. Jones and A.L. Heckenberg, *J. Chromatogr.*, 593 (1992) 289.
13 A. Weston, P.R. Brown, A.L. Heckenberg, P. Jandik and W.R. Jones, *J. Chromatogr.*, 602 (1992) 249.
14 M. Koberda, M. Konkowski, P. Youngberg, W.R. Jones and A. Weston, *J. Chromatogr.*, 602 (1992) 235.
15 M. Chen and R.M. Cassidy, *J. Chromatogr.*, 602 (1992) 227.
16 W. Beck and H. Engelhardt, *Chromatographia*, 33 (1992) 313.
17 B.D. Karcher and I.S. Krull, *Trace Metal Analysis and Speciation* (*Journal of Chromatography Library*, Vol. 47), Elsevier, Amsterdam, 1991, p. 123.
18 L. Gross and E.S. Yeung, *Anal. Chem.*, 62 (1990) 427.
19 K. Robards and P. Star, *Analyst*, 116 (1991) 1247.

Journal of Chromatography A, 659 (1994) 467–471
Elsevier Science B.V., Amsterdam

CHROM. 25 693

Short Communication

Enantiomer separation of dihydropyridine derivative calcium antagonists by high-performance liquid chromatography with chiral stationary phases

Tadashi Ohkubo*, Tsukasa Uno and Kazunobu Sugawara

Department of Pharmacy, Hirosaki University Hospital, Hirosaki 036 (Japan)

(First received June 7th, 1993; revised manuscript received October 28th, 1993)

ABSTRACT

The separation of enantiomers of dihydropyridine derivatives by high-performance liquid chromatography was studied using modified Pirkle-type chiral stationary phases. Resolution was achieved by normal-phase operation utilizing *n*-hexane–1,2-dichloroethane–methanol–trifluoroacetic acid as the mobile phase on two types of urea-derivative chiral stationary phase. Nine urea-type chiral phases were examined, derived from (*R*)-1-(α-naphthyl)ethylamine with (*S*)-proline or from (*S*)-1-(α-naphthyl)ethylamine with (*S*)-*tert.*-leucine chemically bonded to a 3-aminopropylsilanized silica stationary phase (Sumichiral OA-4500 and Sumichiral OA-4600).

INTRODUCTION

In recent years, the number of chiral dihydropyridine derivatives with calcium antagonist activity has rapidly increased. Dihydropyridine antagonists, as a racemic mixture of (+)- and (−)-dihydropyridine calcium antagonists, are undergoing clinical evaluation for antihypertensive and antianginal effects. For many of these derivatives, the individual enantiomers also have widely different biological activities [1,2]. It is important, therefore, to be able to determine the amount of each enantiomer. High-performance liquid chromatography (HPLC) on a chiral stationary phase is a very useful technique for the analysis of these enantiomers. Tokuma *et al.* [2] applied such a technique to the direct separation of nilvadipine enantiomers on a Chiralpak OT(+) analytical column, which is a (+)-poly(triphenylmethyl methacrylate) stationary phase. It has also been reported that a stationary phase composed of a α_1-acid glycoprotein is able to separate a series of dihydropyridine enantiomers using a buffer [3]. Okamoto *et al.* [4] reported that optical resolution of dihydropyridine derivatives was possible on HPLC columns packed with xylan bis(3,5-dichlorophenylcarbamate) and cellulose tris(4-*tert.*-butylphenyl carbamate). However, the separation of enantiomers of recently developed chiral dihydropyridine derivatives could not be achieved by high-performance liquid chromatography on Pirkle-type chiral stationary phases. Oi and co-workers [5–8] previously reported the preparation of modified Pirkle-type columns and the enantiomeric sepa-

* Corresponding author.

SSDI 0021-9673(93)E1161-R

ration of chiral compounds using these chiral columns. These columns are useful for the separation of enantiomers of several biologically active compounds [6–8]. However, the direct resolution of enantiomers of dihydropyridine derivatives has not been reported using the above type of columns. In a previous paper [9], we described the enantiomer separation of dihydropyridine derivatives by liquid chromatography with a silica-based cellulose tris(3,5-dimethylphenylcarbamate) (CDMPC) chiral stationary phase. However, this method was not adequate owing to the long analysis time and peak broading. In this paper, we describe the resolution, with sharp peaks, of the enantiomers of dihydropyridine derivatives by normal-phase HPLC on two types of chiral stationary phases. We examined nine urea-type chiral phases (Sumichiral OA-2000, OA-2500R, OA-3100, OA-4400, OA-4500, OA-4600, OA-4700, OA-4800 and OA-4900 in Fig. 2), derived from (*R*)-1-(α-naphthyl)ethylamine with (*S*)-proline or from (*S*)-1-(α-naphthyl)ethylamine with (*S*)-*tert.*-leucine chemically bonded to 3-aminopropylsilanized silica stationary phase (Sumichiral OA-4500 and Sumichiral OA-4600, respectively). *n*-Hexane–1,2-dichloroethane–methanol–trifluoroacetic acid was used as the mobile phase.

EXPERIMENTAL

Materials

Nilvadipine, nitrendipine, nisoldipine, nicardipine and benidipine (Fig. 1) were kindly donated by Fujisawa Pharmaceutical (Osaka, Japan), Yoshitomi Pharmaceutical (Osaka, Japan), Bayer (Wuppertal, Germany), Yamanouchi Pharmaceutical (Tokyo, Japan) and Kyowa Hakko Kogyo (Tokyo, Japan), respectively. *n*-Hexane and methanol were both of HPLC grade, and all other solvents and reagents were of analytical-reagent grade. Standard solutions of each dihydropyridine derivative were prepared in methanol and stored at 4°C, and 200–1000 ng of dihydropyridine derivatives were injected to the HPLC system.

Apparatus

The apparatus used for HPLC was a Waters Model 600 E high-performance liquid chromatograph equipped with a variable-wavelength UV detector (operated at 254 nm) (Millipore–Waters, Milford, MA, USA). The HPLC column contained Sumichiral OA-2000, OA-2500R, OA-3100, OA-4400, OA-4500, OA-4600, OA-4700, OA-4800 and OA-4900 chiral stationary phases

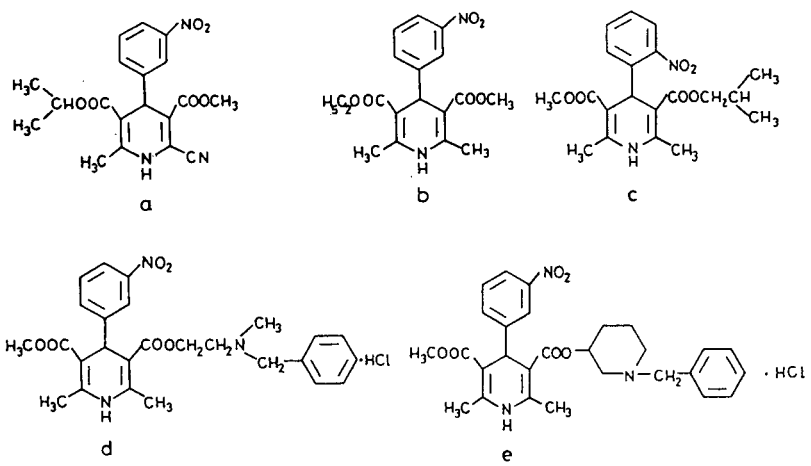

Fig. 1. Structures of dihydropyridine derivative calcium antagonists. (a) Nilvadipine; (b) nitrendipine; (c) nisoldipine; (d) nicardipine; (e) benidipine.

(Fig. 2) (5 or 15 μm, 250 × 4.6 mm I.D.) (Sumika Chemical Analysis Service, Osaka Japan). *n*-Hexane–1,2-dichloroethane–methanol-trifluoroacetic acid was used as the mobile phase.

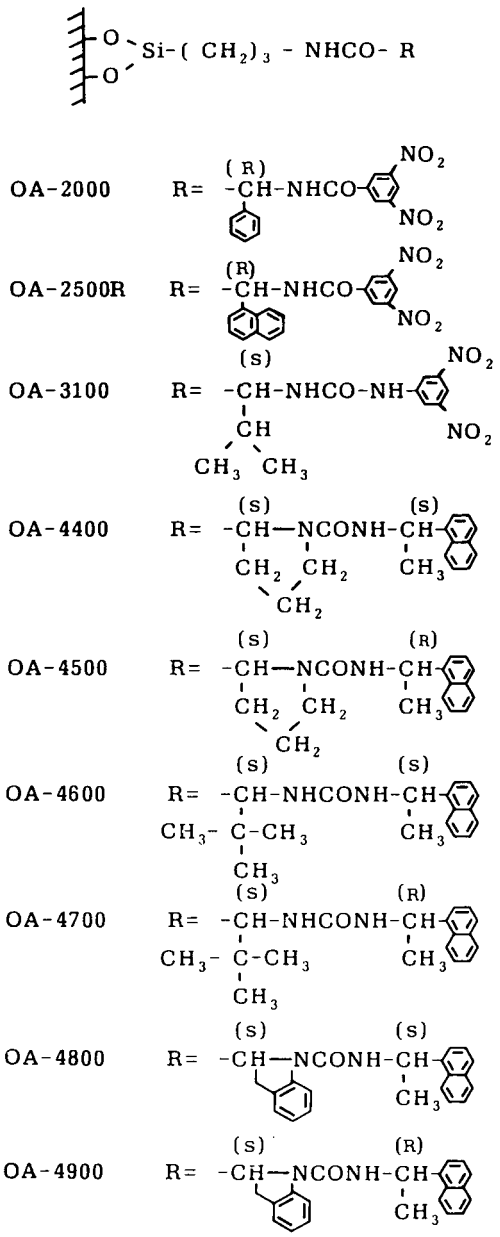

Fig. 2. Structures of chiral stationary phases. (Sumichiral OA).

Flow-rates of 1.0 ml/min were used at room temperature.

RESULTS AND DISCUSSION

We tried various chiral stationary and mobile phase systems for the enantiomeric separation of dihydropyridine derivatives (Fig. 1). The chromatographic results are summarized in Table I. The best separation was obtained for the enantiomers of nilvadipine and benidipine on the various chiral stationary phases used.

Effective enantioseparation of nilvadipine was obtained on Sumichiral-OA 4400 ($\alpha = 1.21$), 4500 ($\alpha = 1.39$), 4700 ($\alpha = 1.15$) and 4800 ($\alpha = 1.29$) using *n*-hexane–1,2-dichloroethane–methanol–trifluoroacetic acid (250:140:2:1) as the mobile phase. A typical chromatogram on a Sumichiral-OA 4500 column is shown in Fig. 3. Under the chromatographic conditions a resolution (R_s) of 3.6 was achieved for the nilvadipine enantiomers, with theoretical plate numbers of 2304 and 3927 for the (+) and (−)-enantiomers, respectively. We previously described the enantiomeric separation of nilvadipine on the silica-based cellulose tris(3,5-dimethylphenylcarbamate) (CDMPC) (Chiralcel OD) [9]. However, this chromatographic system was not adequate owing to peak broadening and the long analysis time. In this study, we achieved a better chiral separation with a short analytical time with a Pirkle-type column rather than a CDMPC chiral column.

The separation of enantiomers of benidipine was obtained on Sumichiral OA-4500 ($\alpha = 1.30$), OA-4700 ($\alpha = 1.16$) and OA-4800 ($\alpha = 1.25$) using *n*-hexane–1,2-dichloroethane–methanol–trifluoroacetic acid (250:140:20:1) as the mobile phase, (Table I). A typical chromatogram is shown in Fig. 3. The resolution was $R_s = 4.0$ with theoretical plate numbers of 3410 for the (+)- and 4673 for the (−)-enantiomer.

The nisoldipine enantiomers were completely separated on Sumichiral OA-4600 only ($\alpha = 1.12$). A chromatogram of the enantiomeric separation of nisoldipine is shown in Fig. 3. The resolution was $R_s = 1.4$, with theoretical plate numbers of 2621 for the (+)- and for the (−)-

TABLE I

HPLC SEPARATION OF ENANTIOMERS OF DIHYDROPYRIDINE DERIVATIVES ON CHIRAL STATIONARY PHASES

Sumichiral	Nilvadipine			Benidipine			Nisoldipine			Nicardipine			Nitrendipine		
	M[a]	k_1	α	M[a]	k_1	α	M[a]	k_1	α	M[a]	k_1	α	M[a]	k_1	α
OA-2000	A	10.74	1.03	–	–	–	A	5.66	1.00	–	–	–	A	4.59	1.00
OA-2500R	–	–	–	D	6.57	1.04	–	–	–	D	6.82	1.00	–	–	–
OA-3100	–	–	–	D	27.29	1.07	–	–	–	D	24.17	1.00	–	–	–
OA-4400	A	6.77	1.21	D	3.52	1.00	A	2.77	1.00	D	2.91	1.00	A	2.72	1.00
OA-4500	A	4.67	1.39	E	12.40	1.30	A	1.49	1.00	E	8.30	1.05	C	5.17	1.00
OA-4600	A	5.96	1.10	D	2.45	1.11	B	4.17	1.12	D	3.04	1.00	B	5.87	1.00
OA-4700	A	2.25	1.15	D	1.59	1.16	A	1.23	1.00	D	1.47	1.00	A	1.05	1.00
OA-4800	A	4.82	1.29	D	4.73	1.25	A	2.80	1.04	D	4.71	1.00	A	1.92	1.00
OA-4900	A	13.43	1.04	D	4.42	1.00	A	4.21	1.08	D	4.12	1.00	A	3.12	1.00

[a] M = mobile phase: *n*-hexane–1,2-dichloroethane–methanol–trifluoroacetic acid, (A) 250:140:2:1, (B) 250:140:0.5:1, (C) 400:100:2:1, (D) 250:140:20:1 and (E) 250:140:10:1.

enantiomers 3226. Thus enantiomeric separation of nisoldipine could be obtained on the Pirkle-type column, but not on a CDMPC chiral column [9].

The enantiomers of nicardipine were almost separated on Sumichiral OA-4500 ($\alpha = 1.05$). The chromatogram is shown in Fig. 4. The resolution was $R_s = 1.1$, when theoretical plate numbers of 6297 for the (+)- and 6601 for the (−)-enantiomer. On the other hand, no separation of nitrendipine was obtained on a Pirkle-type column in these studies (Fig. 4). The separation factor of enantiomer for nitrendipine was 1.00 on the Sumichiral OA column (Table I), with a theoretical plate number of 1685.

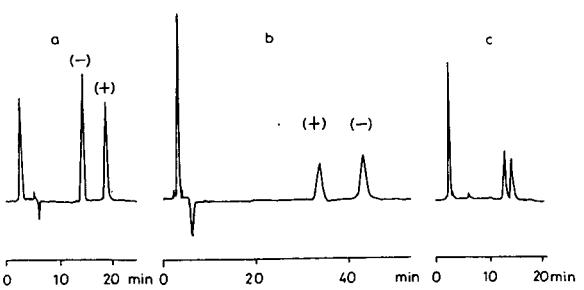

Fig. 3. Separation of dihydropyridine derivative calcium antagonists with chiral stationary phases (Sumichiral OA). Chromatographic conditions as in Table I. (a) Nilvadipine (OA-4500); (b) benidipine (OA-4500); (c) nisoldipine (OA-4600).

Delee *et al.* [3] reported the enantiomer separation of dihydropyridines on an α_1-acid glycoprotein column [3]. However, this method was not adequate owing to the long analytical time and peak broadening. The separation mechanism includes non-specific interaction of dihydropyridine with the α_1-acid glycoprotein stationary phase.

Okamoto *et al.* [4] also reported that a stationary phase composed of xylan bis(3,5-dichlorophenylcarbamate) and cellulose tris(4-*tert.*-butylphenylcarbamate) was able to separate a series of dihydropyridine enantiomers using a normal mobile phase [4]. The same group [10]

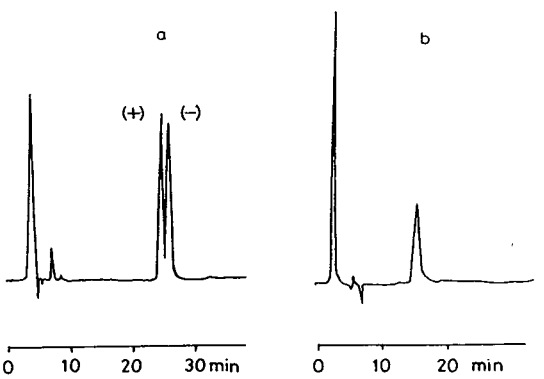

Fig. 4. Separation of dihydropyridine derivative calcium antagonists with chiral stationary phases (Sumichiral OA). Chromatographic conditions as in Table I. (a) Nicardipine (OA-4500); (b) nitrendipine (OA-4500).

also reported that the enantioseparation mechanism of polysaccharide phenylcarbamate-type stationary phases is considered to involve interactions between chiral adsorbing sites and the polar carbamate group. The groups can interact with a solute via hydrogen bonding with NH and C = O groups and dipole–dipole interactions on C = O. The adsorbing powers of these sites may be strongly influenced by the nature of the substituents on the phenyl group. The enantioseparation of dihydropyridine derivatives should be considered to follow the same mechanism on the polysaccharide phenylcarbamate stationary phase. On the other hand, Pirkle and Hamper [11] described the mechanism on a Pirkle-type column. The interaction mechanism with the chiral stationary phase was considered to require the analyte to contain a π-donor site, a basic site for association with the benzamide hydrogen and an acidic site to hydrogen bond to the basic carbonyl oxygen, and these sites must be stereochemically disposed such that all of the interactions with the chiral stationary phase can occur simultaneously.

From the results of this study, we consider that the enantioseparation of dihydropyridine derivatives involves interactions with the nitrobenzene ring, carbonyl group and amido group in the dihydropyridine molecule using Sumichiral OA stationary phases. Effective enantioseparation of nilvadipine was obtained because it contains a asymmetric dihydropyridine ring form 2-cyano group and a 5-carboxyisopropyl ester group. Adequate enantioseparation of benidipine was obtained. It is considered that the steric hindrance of the 1-benzyl-3-piperidyl moiety on the asymmetric carboxy group affected the interaction of benidipine on the chiral stationary phase. It was also considered that the steric hindrance of the isobutylmethyl moiety on the asymmetric carboxyl group affected the enantioseparation of nisoldipine on the chiral stationary phase. A poor enantioseparation of nicardipine was obtained. It is considered that the steric hindrance of the N-benzyl-N-methylaminoethyl moiety on the asymmetric carboxyl group weakly affected the interaction of nicardipine on the chiral stationary phase, because the bulky benzyl group is distant from the chiral centre. No enantioseparation of nitrendipine was obtained, because there is no steric hindrance of the ethyl moiety on the asymmetric carboxyl group. In conclusion, we found that Pirkle-type chiral stationary phases (Sumichiral OA) were very efficient for the separation of enantiomers of a few dihydropyridine calcium antagonists. We consider that the method using HPLC with these chiral stationary phases is very useful for the analysis of enantiomers of dihydropyridine calcium antagonists in clinical patients. Further applications of the method to enantiospecific therapeutic drug monitoring of dihydropyridine derivatives are being conducted.

ACKNOWLEDGEMENTS

The authors thank Dr. N. Oi and Dr. Y. Matsumoto of Sumika Chemical Analysis Service for helpful suggestions.

REFERENCES

1 T. Takenaka, I. Miyazaki, M. Asano, S. Higuchi and H. Maeno, *Jpn. J. Pharmacol.*, 32 (1982) 665.
2 Y. Tokuma, T. Fujiwara and H. Noguchi, *J. Pharm. Sci.*, 76 (1987) 310.
3 E. Delee, I. Jullien and L. Le Garrec, *J. Chromatogr.*, 450 (1988) 191.
4 Y. Okamoto, R. Aburatani, K. Hatada, M. Honda, N. Inotusme and M. Nakano, *J. Chromatogr.*, 513 (1990) 375.
5 N. Oi, M. Nagase and T. Doi, *J. Chromatogr.*, 257 (1983) 111.
6 N. Oi, H. Kitahara, Y. Matsumoto, H. Miyazaki and Y. Horikawa, *J. Chromatogr.*, 462 (1989) 382.
7 N. Oi, H. Kitahara and R. Kira, *J. Chromatogr.*, 535 (1991) 213.
8 N. Oi, H. Kitahara and R. Kira, *J. Chromatogr.*, 592 (1992) 291.
9 T. Ohkubo, T. Uno and K. Sugawara, *Chromatographia*, 33 (1992) 287.
10 Y. Okamoto, M. Kawashima and K. Hatada, *J. Chromatogr.*, 363 (1986) 173.
11 W.H. Pirkle and B.C. Hamper, *J. Chromatogr.*, 450 (1988) 199.

Journal of Chromatography A, 659 (1994) 472–476
Elsevier Science B.V., Amsterdam

CHROM. 25 699

Short Communication

Use of a packed programmed-temperature vaporizer injector in the solvent elimination mode for the determination of fatty acid methyl esters by gas chromatography

I. Medina*

Instituto de Investigaciones Marinas (CSIC), Av. Eduardo Cabello 6, E-36208 Vigo (Spain)

F. Linares

Centro de Investigaciones Mariñas, Xunta de Galicia, Consellería de Pesca, Apto 208, Vilagarcía de Arousa (Spain)

J.L. Garrido

Instituto de Investigaciones Marinas (CSIC), Av. Eduardo Cabello 6, E-36208 Vigo (Spain)

(First received March 30th, 1993; revised manuscript received October 28th, 1993)

ABSTRACT

It is shown that when using a programmed-temperature vaporizer as the injection device for the gas chromatographic determination of fatty acid methyl esters in the solvent elimination mode, losses of medium-chain solutes during the solvent elimination step can be avoided by packing the glass liner of the injector with materials providing adequate retention characteristics. Silanized glass-wool proved to be a good material for this purpose. Other parameters such as solvent elimination temperature, nature of the solvent and solute vaporization temperature were also studied in order to achieve optimum injection conditions.

INTRODUCTION

Sample injection is an important step in high-resolution gas chromatography (GC), which becomes critical when quantitative analysis of complex mixtures (mixtures of compounds covering a wide range of polarities, concentrations or volatilities) is required. One of the most important problems in injection can be the discrimination of one compound over another in their transfer from the syringe (in the liquid state) to the column (in the vapour state) [1]. Such can be the case in analyses for fatty acid methyl esters (FAMEs): whereas some studies have shown that severe discrimination between acids with low and high boiling points can arise when using classical split injection techniques [2], other have shown that using the same technique and with

* Corresponding author.

0021-9673/94/$07.00
SSDI 0021-9673(93)E1147-R

strict control of the injection parameters, excellent results can be achieved [3].

Several solutions have been proposed to overcome the problem of sampling discrimination if it is caused by selective vaporization from the syringe needle when it is placed in a hot injector block, such as the so-called "cooled needle technique", which allows excellent results to be obtained in either the split or splitless sampling mode [4], and the cold on-column or the programmed-temperature vaporizer (PTV) injection techniques [5]. The PTV is an injection device which is cold when receiving the sample and subsequently, after sample release and syringe withdrawal, is rapidly heated so that the sample enters the column as vapour (in contrast to the on-column procedure).

The PTV injection technique is very versatile and allows sample vapour transfer to the column in three operational modes: split injection, splitless injection and solvent elimination [6]. In the solvent elimination mode, a two-step vaporization is used: first, in a low-temperature vaporization step, most of the solvent is vented from the system, then the split is closed and the injector temperature is increased so that the sample is transferred to the column. This technique allows the injection of large volumes without column flooding by the sample solvent (as can happen in the on-column and splitless injection modes) [4], and it is very convenient in the analysis of very dilute samples for which a preconcentration step is required. This can occur with FAME samples obtained from marine animal larvae in which the available biological material is always very scarce.

However, from an exhaustive study on PTV injection conditions for FAMEs, Eder *et al.* [7] concluded that when PTV injection is used in the solvent elimination mode, the recovery of low and medium boiling point FAMEs is far below 100% (*ca.* 80% for 14:0), because they are lost together with the solvent through the split exit. As a consequence, they recommended that the use of this injection mode be restricted to the determination of fatty acids containing more than sixteen carbon atoms.

However, solutes in the samples can be temporarily fixed during the solvent elimination step by using suitable inserts in the glass liner of the injector. The use of packed inserts in PTV injectors has been exhaustively studied by Herraiz *et al.* [8] and Loyola *et al.* [9]. These inserts improve sample evaporation, prevent droplets of liquid forming near the column entrance and adsorb solutes to prevent them from being lost while the solvent is being vented out.

In this paper, we show how, using a silanized glass-wool insert and appropriate injection conditions, FAMEs including the esters of $C_{14:0}$ to $C_{18:0}$ acids can be accurately determined using a PTV in the solvent elimination mode as the injection device.

EXPERIMENTAL

A Perkin-Elmer PTV cold injector coupled to a Perkin-Elmer Model 8500 gas chromatograph was used. The column was a 30 m × 0.25 mm I.D. fused-silica capillary coated with a 0.20-μm layer of SP-2330 (Supelco, Bellefonte, PA, USA). Nitrogen at 10 p.s.i.g. (1 p.s.i. = 6894.76 Pa) as the carrier gas and a flame ionization detector at 250°C were always used. The column temperature was raised from 140 to 205°C at a rate of 1°C/min. The vaporization insert was packed with a 2-cm plug of silanized glass-wool (Perkin-Elmer) or Tenax GC (0.15–0.18 mm) (Alltech).

The samples were injected at low temperature (solvent elimination temperature) while the split vent was open (splitting ratio = 140:1, with a septum purge of 4 ml/min). After a certain time (splitting time), the split vent was closed and the injector heated (15°C/s) to a certain temperature (sample vaporization temperature) which was kept constant for a further 6 min. Five solvent elimination temperatures (45, 50, 60, 70 and 80°C), three splitting times (30, 60 and 120 s) and four sample vaporization temperatures (250, 300, 350 and 400°C) were tried.

A quantitative FAME standard (MO-81; Larodan, Malmo, Sweden) containing acids of different boiling points and degrees of unsaturation ($C_{14:0}$, 5%; $C_{16:0}$, 10%; $C_{16:1}$, 5%; $C_{18:0}$, 6%; $C_{18:1}$, 25%; $C_{18.2}$, 15%; $C_{18:3}$, 17%; $C_{20:1}$, 7%; $C_{20:4}$, 5% and $C_{22:6}$, 5%) was used. To test for the effect of the injection solvent, one

TABLE I

INFLUENCE OF THE SOLVENT AND THE SOLVENT EVAPORATION TEMPERATURE OF THE INJECTOR ON THE RELATIVE RESPONSE FACTORS (RELATIVE TO C18:0) OF FATTY ACID METHYL ESTERS

Mean value from five measurements of relative response factor for each FAME with relative standard deviation (R.S.D.).

Solvent	FAME	Theoretical value	45°C		50°C		60°C		70°C		80°C	
			Mean	R.S.D. (%)	Mean	R.S.D. (%)	Mean	R.S.D. (%)	Mean	R.S.D. (%)	Mean	R.S.D. (%)
Hexane	14:0	1.04	0.88	1.68	0.83	1.32	0.57	2.77	0.29	3.75	0.16	16.56
	16:0	1.02	1.05	0.43	1.04	0.53	0.96	1.75	0.75	0.94	0.55	7.82
	16:1	1.01	0.94	0.48	0.92	0.91	0.82	1.84	0.61	1.89	0.42	8.91
	18:0	1.00	1.00	0.00	1.00	0.00	1.00	0.00	1.00	0.00	1.00	0.00
	18:1	0.99	1.02	0.88	1.02	0.54	1.01	0.83	0.98	0.56	0.93	1.40
	18:2	0.99	0.98	1.55	0.97	0.46	0.96	0.57	0.93	0.59	0.88	1.87
	18:3	0.98	0.96	2.73	0.96	0.47	0.95	0.88	0.93	0.59	0.89	1.24
	20:1	0.98	0.97	1.70	0.97	0.56	0.99	0.55	1.04	1.25	1.14	1.83
	20:4	0.90[a]	0.90	3.97	0.90	1.36	0.91	1.21	0.95	1.20	1.01	1.34
	22:6	0.70[a]	0.69	4.92	0.70	1.19	0.75	2.19	0.82	1.33	0.91	3.27
Toluene	14:0	1.04	1.01	2.86	0.91	2.77	0.58	3.45	0.37	3.54	0.21	8.49
	16:0	1.02	1.06	0.94	1.06	0.79	0.97	1.35	0.82	0.67	0.58	5.03
	16:1	1.01	0.98	1.16	0.95	0.58	0.84	1.60	0.67	1.69	0.46	5.86
	18:0	1.00	1.00	0.00	1.00	0.00	1.00	0.00	1.00	0.00	1.00	0.00
	18:1	0.99	1.03	1.19	1.02	0.82	1.01	0.54	0.99	0.45	0.94	1.62
	18:2	0.99	0.98	1.12	0.98	1.17	0.97	0.73	0.95	0.95	0.89	1.29
	18:3	0.98	0.97	1.35	0.96	1.20	0.96	0.87	0.94	1.17	0.90	1.27
	20:1	0.98	0.98	0.56	0.97	1.13	1.00	0.55	1.02	0.54	1.11	2.06
	20:4	0.90[a]	0.90	0.79	0.89	1.95	0.91	1.85	0.93	1.32	1.00	1.96
	22:6	0.72[a]	0.72	1.59	0.70	2.13	0.72	3.31	0.79	1.55	0.88	2.95

[a] Relative response factors calculated for Perkin-Elmer flame ionization detector.

aliquots of the text mixture was dissolved in hexane and another in toluene to a final concentration of 1 mg/ml. These are two solvents typically employed for FAMEs [10,11].

For statistical reasons, each injection for a given set of parameters was repeated five times and the relative standard deviation (R.S.D.) was calculated in each instance.

Experimental response factors for each FAME were determined. Good agreement with theoretical response factors was generally achieved [11], except for 20:4 and 22:6, whose response factors under our operating conditions were smaller (0.90 and 0.72, respectively). Such a deviation from the theoretical values for polyunsaturated fatty acid methyl esters in a Perkin-Elmer flame ionization detector has been reported previously [12]. To test for discrimination effects, experimental response factors for each FAME were determined and compared with the respective theoretical values under the different PTV injection conditions.

RESULTS AND DISCUSSION

Although Tenax GC was found to provide excellent results for PTV injection in the solvent elimination mode of volatile solutes [8], it did not allow the quantitative recovery of medium boiling point FAMEs and irreversibly adsorbed the long-chain FAMEs. Attempts to desorb these compounds using higher injector temperatures were unsuccessful, probably owing to this thermal decomposition.

We therefore studied the behaviour of the PTV when the insert was packed with silanized glass-wool as described by Herraiz *et al.* [8]. A splitting time of 60 s was chosen for all the subsequent experiments, as it allows an adequate solvent elimination with no solute discrimination. Higher splitting times led to partial losses of the most volatile FAMEs.

To assess whether, when packed with glass-wool, the injector allowed the retention of FAMEs during the solvent elimination step and their subsequent desorption, standard mixtures in hexane and toluene were injected several times using PTV injection with an initial temperature of 45°C; 45°C was the lowest temperature studied as it was the minimum temperature setting that the injection device could achieve while keeping the oven temperature above 100°C.

Table I gives the mean values and R.S.D.s of

TABLE II

INFLUENCE OF THE SAMPLE EVAPORATION TEMPERATURE ON THE RELATIVE RESPONSE FACTOR OF FATTY ACID METHYL ESTERS

Mean value from five measurements of relative response factor for each FAME with relative standard deviation (R.S.D.). Solvent: hexane.

FAME	Theoretical value	250°C		300°C		350°C		400°C	
		Mean	R.S.D. (%)	Mean	R.S.D. (%)	Mean	R.S.D. (%)	Mean	R.S.D. (%)
14:0	1.04	1.00	2.31	1.01	2.86	1.00	2.09	1.03	2.14
16:0	1.02	1.08	1.65	1.06	0.94	1.07	0.51	1.08	1.40
16:1	1.01	0.98	1.91	0.98	1.16	0.97	0.73	0.98	1.68
18:0	1.00	1.00	0.00	1.00	0.00	1.00	0.00	1.00	0.00
18:1	0.99	1.01	0.88	1.03	1.19	1.02	0.54	1.01	0.54
18:2	0.99	0.96	1.36	0.98	1.12	0.97	0.57	0.96	0.94
18:3	0.98	0.92	2.74	0.97	1.35	0.94	1.22	0.91	1.96
20:1	0.98	0.77	11.17	0.98	0.56	0.95	1.57	0.93	2.78
20:4	0.90[a]	0.70	10.87	0.90	0.79	0.82	3.59	0.77	7.29
22:6	0.72[a]	0.24	25.28	0.72	1.59	0.46	6.62	0.44	35.71

[a] Relative response factors calculated for the Perkin-Elmer flame ionization detector.

the results expressed as relative response factors obtained for each FAME at different solvent elimination temperatures and with hexane (boiling point 68.9°C) and toluene (boiling point 110.6°C) as injection solvents. As can be inferred from comparison with the theoretical relative response factors, only toluene as solvent and a temperature of 45°C were not discriminative towards the low-boiling point FAMEs. Samples with hexane as solvent showed a clear discrimination at 45°C even for 16:1.

Loyola *et al.* [9] showed that different end temperatures in the sampling device could produce different results with respect to both the accuracy and the precision. To test for this effect, four sample vaporization temperatures were studied and the results are given in Table II. As can be seen, temperatures lower than 300°C were not able to desorb the long-chain FAMEs and showed high R.S.D.s. Higher temperatures gave an important and variable decrease in the relative response factors of long carbon chains, probably owing to thermal decomposition. As a consequence, 300°C was adopted as the temperature of sample vaporization.

CONCLUSIONS

A PTV injector in the solvent elimination mode can be used for the accurate and precise determination of medium- and long-chain fatty acids as their methyl esters in very dilute toluene solutions if the glass insert is packed with a material giving a sufficient retention power to avoid losses during the solvent evaporation step. Silanized glass-wool proved to be a good material for this purpose if low solvent evaporation temperatures and short splitting times are used. The use of 45°C as the solvent elimination temperature during a splitting time of 60 s allows the determination of fatty acids with less than eighteen carbon atoms without discrimination and with accuracies and precisions comparable to those obtained with other injection techniques.

REFERENCES

1 G. van der Steege, F.A.J. Muskiet, I.A. Martini, N.H. Hutter and E.R. Bersma, *J. Chromatogr.*, 415 (1987) 1.
2 F.J. Muskiet, J.J. van Doormaal, I.A. Martini, B.G. Wolthers and W. van der Slik, *J. Chromatogr.*, 278 (1983) 231.
3 Bannon, C.D., J.D. Craske, D.L. Felder, I.J. Garland and L.M. Norman, *J. Chromatogr.*, 407 (1987) 231.
4 G. Schomburg, V. Häusig, H. Husmann and H. Behlan, *Chromatographia*, 19 (1984) 29.
5 G. Reglero, M. Herraiz and M.D. Cabezudo, *Chromatographia*, 22 (1986) 333.
6 F. Poy, S. Visani and F. Terrosi, *J. High Resolut. Chromatogr. Chromatogr. Commun.*, 5 (1982) 355.
7 K. Eder, A.M. Reichlmayr-Lais and M. Kirchgessner, *J. Chromatogr.*, 588 (1991) 265.
8 M. Herraiz, G. Reglero, E. Loyola and T. Herraiz, *J. High Resolut. Chromatogr. Chromatogr. Commun.*, 10 (1987) 598.
9 E. Loyola, M. Herraiz, G. Reglero and P. Martín-Alvarez, *J. Chromagor.*, 398 (1987) 53.
10 G. Lepage and C. Roy, *J. Lipid. Res.*, 27 (1986) 114.
11 W.W. Christie, *Gas Chromatography and Lipids*, Oily Press, Ayr, 1989.
12 J.D. Joseph and R.G. Ackman, *J. Assoc. Off. Anal. Chem.*, 75 (1992) 488.

Journal of Chromatography A, 659 (1994) 477–480
Elsevier Science B.V., Amsterdam

CHROM. 25 664

Short Communication

Comparison of crown ether side-chain polysiloxanes with and without liquid crystalline character as stationary phases for capillary gas chromatography

Wei Zhou, Ruonong Fu* and Rongji Dai

Department of Chemical Engineering, Beijing Insitute of Technology, Beijing, 100081 (China)

Zaifu Huang and Yanfei Chen

Department of Environmental Science, Wuhan University, Wuhan (China)

(First received August 4th, 1993; revised manuscript received October 19th, 1993)

ABSTRACT

Two new GC stationary phases were prepared, one a side-chain liquid crystalline polysiloxane containing crown ether (PSC-11), and the other a new kind of side-chain crown ether (PSCP-11-15C-5) which has a similar structure to PSC-11. The main chromatographic characteristics, including efficiency, polarity and selectivity, were examined and compared. The mechanism of specific selectivity for positional isomer compounds based on the crown ether ring and liquid crystal is discussed.

INTRODUCTION

Crown ethers are used as chromatographic stationary phases because of the good selectivity resulting from the cavity structure and strong electronegative effect of hetetroatoms on crown ether ring. A few papers have appeared concerning the use of side-chain crown ether polysiloxanes as stationary phases for capillary GC since 1988 [1–4]. On the other hand, side-chain liquid crystal polysiloxanes were first used as stationary phases in GC in 1982 by Finkelmann *et al.* [5]. Both types have high efficiency and are suitable for the separation of geometrical isomeric compounds.

In 1989, Percec and Rodenhouse [6] synthesized several side-chain liquid crystalline polysiloxanes containing a crown ether. If crown ether compounds have mesomorphic properties, they may possess some special effects. So far, there is only one example of the use of this material as a stationary phase for GC, by our laboratory [7]. The aim of the work was to compare the chromatographic behaviours of a new kind of side-chain liquid crystalline polysiloxane containing crown ether (PSC-11) (Fig. 1) with those of a new kind of side-chain crown ether (PSCP-11-15C-5) (Fig. 1) which has a similar structure to PSC-11. As there is an isopropylidene group between two phenyls of the side-chain, this crown ether has no mesomorphic properties. The properties of specific selectivity

* Corresponding author.

0021-9673/94/$07.00
SSDI 0021-9673(93)E1115-G

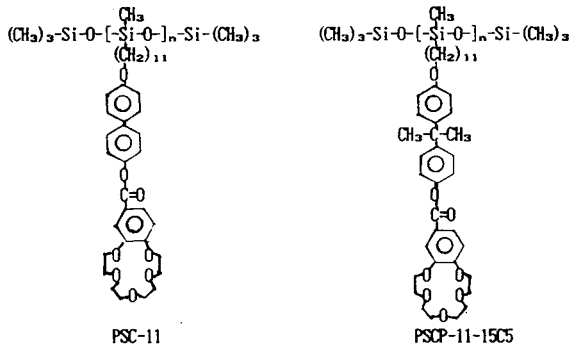

Fig. 1. Structures of the two stationary phases studied.

for positional isomeric compounds based on the crown ether ring and liquid crystal are also discussed. Once the features of mesomorphic crown ethers have been elucidated, it seems certain that their chromatographic characteristics will be improved.

EXPERIMENTAL

Synthesis of poly(methylsiloxane) containing 4-(10-undecen-1-yloxy)-4′-(4′-carboxybenzo-15-crown-5)biphenylside-chain (PSC-11)

PSC-11 was synthesized by the hydrosilylation of 4-(10-undecen-1-yloxy)-4′(4′-carboxybenzo-15-crown-5)-biphenyl (OC-9) with poly(methylhydrosiloxane), which was prepared as described previously [7]. A 0.3210-g (*ca.* 5×10^{-4} mol) amount of OC-9 (obtained from the Department of Enviromental Science, Wuhan University, China) and 0.0324 g (0.0000143 mol) of poly(methylhydrosiloxane) (Merck–Schuchardt, Hohenbrunn bei München, Germany; degree of polymerization = 35) were dissolved in 17 ml of dry, freshly distilled toluene in a dry, three-necked, round-bottomed flask. The reaction mixture was heated to 110°C under nitrogen and 44 μl of fresh catalyst solution (0.0576 g of chloroplatinic acid dissolved in 10 ml of isopropyl alcohol) were injected. The temperature of the reaction mixture was held at 110°C until IR analyses showed that the hydrosilylation reaction was complete. generally, after 26 h the Si–H bond had almost disappeared. Ethylene was then bubbled through the mixture for 1 h to react with all of the residual Si–H units. Purification was performed by several precipitations from methanol. The product was centrifuged at *ca.* 10 000 *g* and 6°C for 30 min and dried in air to remove the solvent.

Synthesis of poly(methylsiloxane) containing 2-[4-(10-undecen-1-yloxy)-phenyl]-2-[4′-(4′-carboxybenzo-15-crown-5)phenyl]propane (PSCP-11-15C-5)

The synthesis method is the same as that for PSC-11 above except that 0.2765 g of 2-[4-(10-undecen-1-yloxy)phenyl]-2-[4′-(4′-carboxybenzo-15-crown-5)phenyl]propane (CP-9) and 0.0195 g of poly(methylhydrosiloxane) were used.

Technique

Thermal transitions were determined using a Perkin-Elmer DSC-7 differential scanning calorimeter. A hot-stage light-polarized microscope was used to observe the thermal transition temperature and to analyse the anisotropic textures.

Column preparation

Fused-silica capillaries (0.25 mm I.D.) (Yongnian Optical Fibre Factory, Hebei, China) were used. The capillaries were purged with nitrogen at 240°C for 6 h before coating. The capillaries were statically coated with a solution of 0.4–0.5% (w/v) PSC-11 or PSCP-11-15C-5 in dichloromethane and flushed with nitrogen for 2 h and then conditioned at 120, 140, 160, 180 and 200°C for 2 h each and finally at 220°C for 4 h.

Column evaluation

The GC separations were carried out on an SP-3700 gas chromatograph (Beijing Analytical Instrument Factory, Beijing, China) equipped with a flame ionization detector using nitrogen as carrier gas. The output of the detector was connected to an HP-3390A integrator. Solutes were injected using the split mode (80:1). The polarity of the columns was tested by measuring the McReynold's constants.

RESULTS AND DISCUSSION

The transition temperatures of the monomers (OC-9 and CP-9) and polymers (PSC-11 and PSCP-11-15C-5) were measured by using a hot-

TABLE I

LIQUID CRYSTALLINE TRANSITION TEMPERATURES OF OC-9, PSC-11, CP-9 AND PSCP-11-15C-5 OBTAINED USING A HOT-STAGE POLARIZED MICROSCOPE

Material	Transition temperature (°C)[a]	
	Heating	Cooling
OC-9	k 120 n 137 i	k 101 n 137 i
PSC-11	k 143 n 190 i	k 90 n 189 i
CP-9	s 93 l	
PSCP-11-15C-5	s 98 l	

[a] Abbreviations: k = crystalline; n = nematic; s = smectic; i = isotropic; l = liquid.

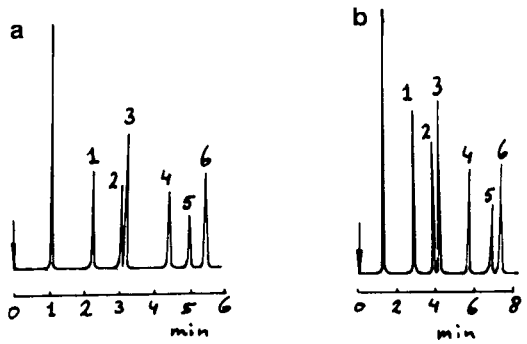

Fig. 2. Chromatograms of substituted naphthalenes on (a) PSC-11 and (b) PSCP-11-15C-5 columns at 160°C. Peaks: 1 = naphthalene; 2 = 2-methylnaphthalene; 3 = 1-methylnaphthalene; 4 = 2,6-dimethylnaphthalene; 5 = 1,5-dimethylnaphthalene; 6 = 1,2-dimethylnaphthalene.

stage light-polarized microscope. The results are given in Table I. The phase transition temperatures determined with a Model DSC-7 apparatus are given in Table II. The data suggest that the polymer PSC-11 has a wider mesomorphic temperature range than that of the monomer (OC-9), whereas PSCP-11-15C-5 has no mesomorphic property. Because the mesomorphic temperature range of PSC-11 is suitable for the cGC separation of a variety of isomeric compounds, it meets the demands for a stationary phase.

TABLE II

PHASE TRANSITION TEMPERATURE OF OC-9, PSC-11, CP-9 AND PSCP-11-15C-5 OBTAINED USING THE DSC-7

Stationary phase	Transition temperature (°C)[a]	
	Heating	Cooling
OC-9	k 117 n 136 i	k 96 n 133 i
PSC-11	s 141 s 169 n 199 i	s 90 s 108 s 157 n 194 i
CP-9	s 94 l	
PSCP-11-15C-5	s 101 l	

[a] See Table I.

Table III summarizes the chromatographic properties of the two types of stationary phase. The data indicate that PSC-11 possesses a higher column efficiency than PSCP-11-15C-5 and the reproducibility is good. As PSCP-11-15C-5 has an isopropylidene group between two phenyls of the side-chain, it has no mesomorphic property and the movement of the crown ether ring is less flexible than that of the previously studied PSO-B-15C-5 [2]. As a result, its film-forming ability is lower than that of PSC-11 and PSO-B-15C-5 [2].

The polarities of these two stationary phases are expressed by the McReynolds constants at 120°C (Table IV). It is found that these two novel stationary phases have moderate polarity

TABLE III

CHARACTERISTICS OF PSC-11 AND PSCP-11-15C-5 CAPILLARY COLUMNS

Compound tested: anthracene.

Stationary phase	Film thickness (μm)	k	Column temperature (°C)	Flow-rate (cm/s)	Column efficiency (plates/m)
PSC-11	0.30	14.9	190	14.7	4410
PSCP-11-15C-5	0.27	11.6	190	13.3	3390

TABLE IV

McREYNOLDS CONSTANTS OF THE PSC-11 AND PSCP-11-15C-5 COLUMNS

Stationary phase	McReynolds constants[a]						
	X′	Y′	Z′	U′	S′	Av. polarity	*b*
PSC-11	201	336	238	397	345	303	0.2391
PSCP-11-15C-5	217	308	260	355	314	291	0.2536
Carbowax-20M[b]	322	536	368	572	510	462	0.2235
PSO-B-15C5[c]	121	254	192	293	284	229	–
Liquid crystalline copolymer[d]	251	264	330	429	420	339	–

[a] X′ = benzene; Y′ = 1-butanol; Z′ = 2-pentanone; U′ = nitropropane; S′ = pyrdine; *b* = slope of the curve obtained when the logarithm of the adjusted retention times of *n*-alkanes are plotted as a function of the number of carbon atoms.
[b] From ref. 8.
[c] From ref. 2.
[d] From ref. 9.

between those of Carbowax-20M and PSO-B-15C-5, and therefore are suitable for the separation of polar and easily polarizable compounds.

Fig. 2 shows the excellent separations of substituted naphthalenes on both PSC-11 and PSCP-11-15C-5. The results demonstrate that these two stationary phases have unique selectivity for the separation of substituted naphthalenes.

Fig. 3a illustrates the separation of substituted benzenes on PSC-11 and Fig. 3b shows the same separation on PSCP-11-15C-5. 2,3-DNT and 2,4-DNT coeluted on the latter stationary phase.

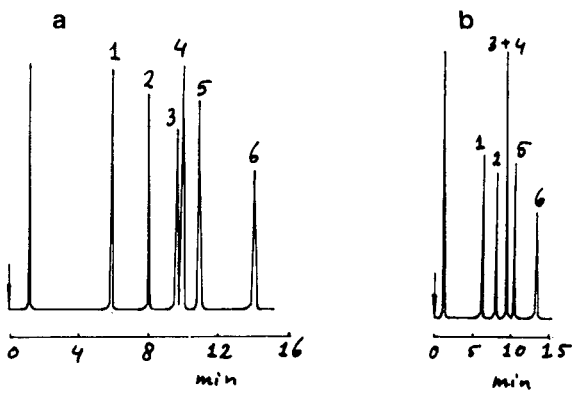

Fig. 3. Chromatograms of dinitrotoluene (DNT) isomers on (a) PSC-11 and (b) PSCP-11-15C-5 columns at 180°C. Peaks: 1 = 2,6-DNT; 2 = 2,5-DNT; 3 = 2,3-DNT; 4 = 2,4-DNT; 5 = 3,5-DNT; 6 = 3,4-DNT.

The chromatograms suggest that because PSC-11 has mesomorphic properties, its chromatographic characteristics are superior for the separation of substituted benzenes.

ACKNOWLEDGEMENT

This work was kindly supported by the National Science Foundation of China.

REFERENCES

1 C.Y. Wu, C.-M. Wang, Z.-R. Zeng and X.-R. Lu, *Anal. Chem.*, 62 (1990) 968.
2 J. Ge, R. Fu, A. Zhang, Z. Huang and B. Zhang, *J. Microcolumn Sep.*, 3 (1991) 121.
3 A. Zhang, J. Ge, Z. Guan, J. Deng, H. Liu, J. Zhu, R. Fu, Z. Huang and B. Zhang, *J. Chromatogr.*, 521 (1990) 128.
4 C.A. Rouse, A.C. Finlinson, B.J. Tarbet, J.C. Pixton, N.M. Djordjevic, K.E. Markides, J.S. Brandshaw and M.L. Lee, *Anal Chem.*, 60 (1988) 901.
5 H. Finkelmann, R.J. Laub, W.L. Robert and C.A. Smith, in M. Cooke, A.J. Dennis and G.L. Fischer (Editors), *Polynuclear Aromatic Hydrocarbons: Physical and Biological Chemistry*, Columbus, OH, 1982, p. 275.
6 V. Percec and R. Rodenhouse, *Macromolecules*, 22 (1989) 4408.
7 R. Fu, P. Jing, J. Gu, Z. Huang and Y. Chen, *Anal. Chem.*, 65 (1993) 2141.
8 W.O. McReynolds, *J. Chromatogr. Sci.*, 8 (1970) 685.
9 H. Wang, T. Gen, R. Fu, J. Zhu, X. Wei, H. Li and J. Liu, *J. Chromatogr.*, 609 (1992) 414.

Journal of Chromatography A, 659 (1994) 481–485
Elsevier Science B.V., Amsterdam

CHROM. 25 683

Short Communication

Determination of selenocyst(e)amine, selenocyst(e)ine and selenomethionine by gas chromatography with flame photometric detection

Hiroyuki Kataoka*, Yoshihide Miyanaga and Masami Makita

Faculty of Pharmaceutical Sciences, Okayama University, Tsushima, Okayama 700 (Japan)

(First received September 6th, 1993; revised manuscript received October 25th, 1993)

ABSTRACT

A selective and sensitive method for the determination of selenocyst(e)amine, selenocyst(e)ine and selenomethionine (Se-Met) by gas chromatography (GC) was developed. Selenocystamine and selenocystine were reduced to selenocysteamine (Se-CYE) and selenocysteine (Se-Cys), respectively, by adding sodium tetrahydroborate prior to derivatization. Se-CYE, Se-Cys and Se-Met were converted into N,Se-isopropoxycarbonyl (isoPOC), N,Se-isoPOC methyl ester and N-isoPOC methyl ester derivatives, respectively, and determined by GC with flame photometric detection (FPD) using a DB-17 capillary column. These derivatives were sufficiently volatile and stable, giving single and symmetrical peaks, and provided an excellent FPD response. The detection limits of Se-CYE, Se-Cys and Se-Met were *ca.* 1.4, 1.0 and 1.4 pmol injected, respectively. The calibration graphs for these selenium compounds were linear in the range 1–20 nmol and sufficiently reproducible for quantification.

INTRODUCTION

Selenocyst(e)amine, selenocyst(e)ine and selenomethionine (Se-Met) have been found in the free form in onion [1] and seleniferous cabbage [2], and as integral moieties in several selenium-containing proteins such as plasma selenoprotein P [3], mammalian glutathione peroxidase [4] and bacterial glycine reductase [5], formate dehydrogenase [6] and acetoacetyl-CoA thiolase [7]. However, the physiological significance and the origin of these selenium compounds are not fully understood.

The identification and determination of Se-cyst(e)amine, Se-cyst(e)ine and Se-Met have been carried out by thin-layer chromatography [1,2], with an amino acid analyser [3–10] and by gas chromatography (GC) [11]. However, these methods lack the sensitivity or specificity required for determining these selenium compounds in biological samples.

It has been demonstrated in our laboratory that a variety of amines [12–14] and amino acids [15–17] can be successfully analysed by GC as their N-alkyloxycarbonyl and N-alkyloxycarbonyl methyl ester derivatives, respectively, which are conveniently prepared by a simple procedure involving alkyloxycarbonylation with alkyl chloroformate in an aqueous medium followed by esterification with diazomethane. In this work, a selective and sensitive method for determining selenocyst(e)amine, selenocyst(e)ine

* Corresponding author.

0021-9673/94/$07.00
SSDI 0021-9673(93)E1158-V

and Se-Met by GC with flame photometeric detection (FPD) was investigated.

EXPERIMENTAL

Reagents

Selenocystamine, seleno-DL-cystine and seleno-DL-methionine (Se-Met) were purchased from Sigma (St. Louis, MO, USA), and were dissolved in 0.05 *M* hydrochloric acid in order to obtain a stock solution at a concentration of 1 m*M*. Bis(*p*-methoxyphenyl) selenoxide (BMPS) (Tokyo Kasei Kogyo, Tokyo, Japan) as an internal standard (I.S.) was dissolved in ethyl acetate at 50 μM. Sodium tetrahydroborate (Nacalai Tesque, Kyoto, Japan) was used as a 100 mg/ml solution in 0.1 *M* sodium hydroxide. Isopropyl chloroformate (isoPCF) was obtained from Wako (Osaka, Japan). Hydrogen chloride in methanol (HCl–MeOH) obtained from Tokyo Kasei Kogyo was diluted with methanol at a concentration of 1 *M*. Peroxide-free diethyl ether was obtained from Dojindo Laboratories (Kumamoto, Japan). All other chemicals were of analytical-reagent grade.

Gas chromatography

GC analysis was carried out with a Shimadzu Model 12A gas chromatograph equipped with hydrogen flame ionization detection (FID) and flame photometric detection (FPD) and with a 477-nm interference filter (GL Sciences, Tokyo, Japan) inserted in the optical path. A fused-silica capillary column (15 m × 0.53 mm I.D., film thickness 1.0 μm) of cross-linked DB-17 (J&W Scientific, Folsom, CA, USA) was used. The operating conditions were as follows: column temperature, programmed at 10°C/min from 170 to 270°C; injector and detector temperatures, 280°C; nitrogen flow-rate, 12 ml/min.

Gas chromatography–mass spectrometry (GC–MS)

A Hewlett-Packard Model 5890A gas chromatograph was operated in conjunction with a VG Analytical Model 70-SE mass spectrometer and a VG-250J mass data system. The GC column was of the same type as used for GC analysis, with an ionizing voltage of 40 eV, an ion-source temperature of 250°C and a helium flow-rate of 10 ml/min.

Derivatization procedure

An aliquot of the sample solution containing 1–20 nmol of selenocysteamine (Se-CYE), selenocysteine (Se-Cys) and Se-Met was pipetted into a 10-ml Pyrex glass tube with a PTFE-lined screw-cap. To this solution were added 0.05 ml of 0.5 *M* sodium hydroxide and 0.2 ml of 100 mg/ml sodium tetrahydroborate solution, and the mixture was incubated at 100°C for 10 min. After cooling, 0.05 ml of isoPCF was added and the mixture was shaken up and down at 3000 rpm for 10 min at room temperature. The reaction mixture was saturated with sodium chloride and acidified to pH 1–2 with 2 *M* hydrochloric acid, 0.1 ml of 50 μM BMPS (I.S.) was added and then the mixture was extracted with 3 ml of peroxide-free diethyl ether. After the ethereal extract had been evaporated to dryness at 80°C, to the residue was added 0.2 ml of 1 *M* HCl–MeOH and the mixture was incubated at 80°C for 10 min. After the residual solvent had been evaporated to dryness at 80°C under a stream of dry air, the residue was dissolved in 0.1 ml of ethyl acetate and 1 μl of this solution was injected into the gas chromatograph. The derivatization process for Se-Cys is summarized in Fig. 1.

RESULTS AND DISCUSSION

We investigated a simple and rapid derivatization method (outlined in Fig. 1) using isoPCF as a derivatizing reagent for amino and selenohydryl functions and HCl–MeOH for the carboxyl function. Selenocystamine and selenocystine were reduced to Se-CYE and Se-Cys, respectively, by adding sodium tetrahydroborate prior to derivatization. The reduction was accomplished within 10 min at 100°C by using 20 mg of sodium tetrahydroborate in aqueous alkaline media. Se-CYE, Se-Cys and Se-Met could be successfully converted into N,Se-isoPOC, N,Se-isoPOC methyl ester and N-isoPOC methyl ester derivatives, respectively, by essentially the same procedure as that used in the derivatization of amines [12–14] and amino acids [15–17],

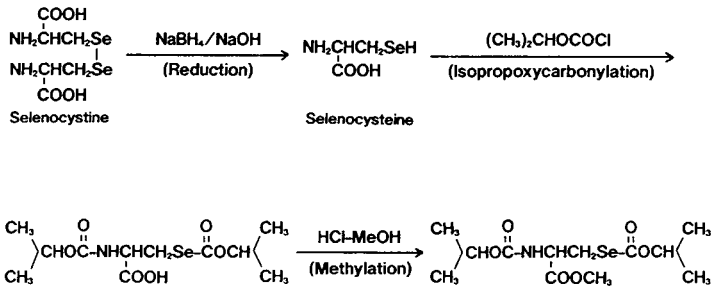

Fig. 1. Process for derivatization of selenocyst(e)ine.

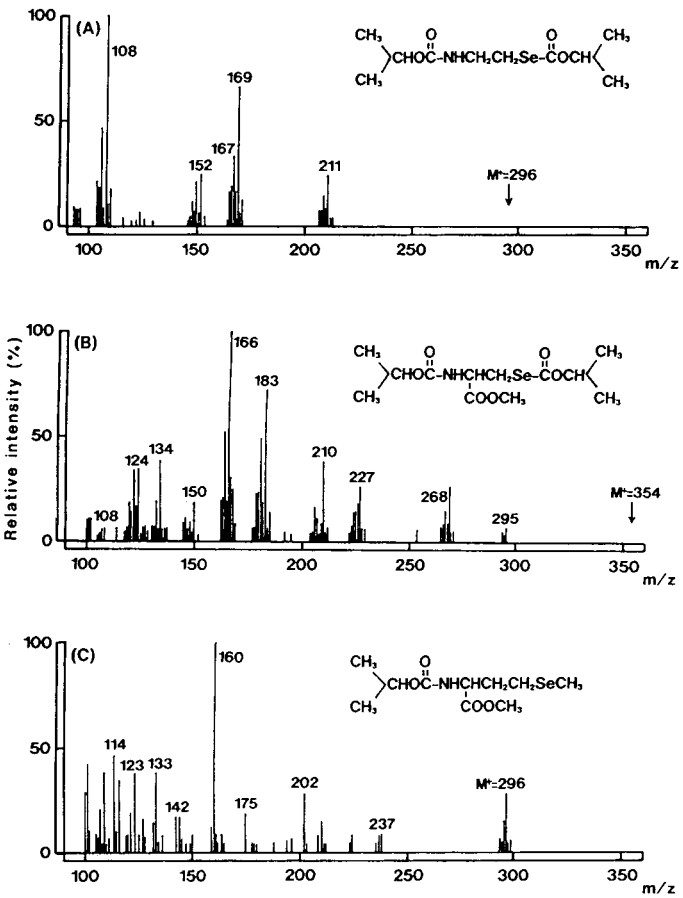

Fig. 2. Mass spectra of (A) N,Se-isoPOC selenocysteamine, (B) N,Se-selenocysteine methyl ester and (C) N-isoPOC selenomethionine methyl ester.

except for the use of HCl–MeOH instead of diazomethane. The isopropoxycarbonylation of the amino and selenohydryl functions of these compounds was accomplished within 5 min in aqueous alkaline media by shaking at room temperature. Peroxide-free diethyl ether was used as an extraction solvent for N,Se-isoPOC or N-isoPOC derivatives of these compounds in order to prevent the oxidation to the selenoxide and selenone derivatives [5]. The N,Se-isoPOC derivatives were quantitatively extracted into diethyl ether in acidic media. Although the methylation of the carboxyl function of the isoPOC derivatives with diazomethane was simple [15–17], the interfering peaks originating in the diazomethane generating reagents were observed under our GC–FPD conditions. Therefore, HCl–MeOH was used as a methylation reagent. The methylation with HCl–MeOH was completed within 5 min at 80°C, and no interfering peak was observed. The derivative preparation including reduction with sodium tetrahydroborate was accomplished within 40 min, and several samples could be treated simultaneously.

The structures of the derivatives of Se-CYE, Se-Cys and Se-Met were confirmed by GC–MS. The mass spectra of these derivatives are shown in Fig. 2. Although a molecular ion peak (M^+) was not observed for Se-CYE and Se-Cys derivatives, prominent fragment ion peaks at $M^+ - 59$ [$(CH_3)_2CHO$ or $COOCH_3$], $M^+ - 86$ [$2(CH_3)_2CH$], m/z 166 [$SeCOOCH(CH_3)_2$] and m/z 108 (CH_3CH_2Se) were observed. On the other hand, the M^+ with postulated m/z 296 and the prominent fragment ion peaks at $M^+ - 59$ and $M^+ - 94$ (CH_3Se) were observed for the Se-Met derivative. These peaks were useful for structure elucidation. These derivatives were found to be very stable under normal laboratory conditions, and no decomposition was observed during GC analysis.

The FPD responses of various selenium com-

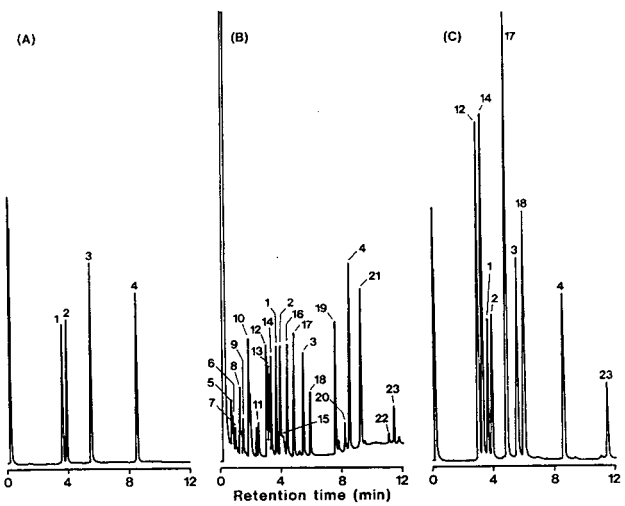

Fig. 3. Gas chromatograms obtained from selenium and non-selenium compounds. (A) Selenium compounds (containing 5 nmol of each compound); (B) selenium + non-selenium compounds (containing 100 nmol of each compound); (C) selenium + non-selenium compounds (containing 5 nmol of each compound). The derivatized samples were analyzed by (A and C) GC–FPD and (B) GC–FID. GC conditions are given under Experimental. Attenuation: GC–FPD, 10×32; GC–FID, $10^2 \times 4$. Peaks: 1 = Se-CYE; 2 = Se-Met; 3 = Se-Cys; 4 = BMPS (I.S.); 5 = alanine; 6 = glycine; 7 = valine; 8 = leucine; 9 = isoleucine + serine; 10 = proline + threonine; 11 = aspartic acid; 12 = cysteamine; 13 = glutamic acid; 14 = methionine; 15 = hydroxyproline; 16 = phenylalanine; 17 = cysteine; 18 = homocysteine; 19 = lysine; 20 = histidine; 21 = tyrosine; 22 = tryptophan; 23 = cystathionine.

pounds have been examined by Flinn and Aue [18]. Maximum responses for selenium compounds were found with dominant emissions between 450 and 500 nm. Therefore, we used a 477-nm interference filter for GC–FPD. The flow conditions for maximum response, established with the derivatives of Se-CYE, Se-Cys and Se-Met, were 20 ml/min of hydrogen and 29 ml/min of air. As shown in Fig. 3A, each derivative was eluted as a single and symmetrical peak, and provided an excellent FPD response; the minimum detectable amounts of Se-CYE, Se-Cys and Se-Met, giving a signal three times higher than the noise under our instrumental conditions, were *ca.* 1.4, 1.0 and 1.4 pmol injected, respectively. The GC–FPD system described here was over 20 times more sensitive than the GC–FID system. On the other hand, other amines and amino acids were also derivatized and detected with FID (Fig. 3B), but these compounds were not detected with FPD except for sulphur compounds (Fig. 3C). Although the sulphur compounds provided the same FPD response under our instrumental conditions, Se-CYE, Se-Cys and Se-Met were completely separated from biological sulphur compounds such as cysteamine, methionine, cysteine, homocysteine and cystathionine.

In order to test the linearity of the calibration graph, various amounts of Se-CYE, Se-Cys and Se-Met ranging from 1 to 20 nmol were derivatized and aliquots representing 10–200 pmol were injected. In each instance a linear relationship was obtained from both logarithmic plots, and the regression lines for Se-CYE, Se-Cys and Se-Met were $\log y = 1.754 \log x - 1.320$ ($r = 0.9995$, $n = 15$), $\log y = 1.814 \log x - 1.186$ ($r = 0.9999$, $n = 15$) and $\log y = 1.841 \log x - 1.347$ ($r = 0.9992$, $n = 15$), respectively, where y is the peak-height ratio and x is the amount of selenium compounds.

These experiments conclusively demonstrated that the method proposed is suitable for the selective and sensitive determination of Se-CYE, Se-Cys and Se-Met. Further investigations on the application of this method to biological samples are in progress.

REFERENCES

1 C.G. Spar and A.I. Virtanen, *Acta Chem. Scand.*, 18 (1964) 280.
2 J.W. Hamilton, *J. Agric. Food Chem.*, 27 (1975) 1150.
3 R. Reed, T. Bellew, J.-G. Yang, K.E. Hill, I.S. Palmer and R.F. Burk, *J. Biol. Chem.*, 265 (1990) 17899.
4 J.W. Forstrom, J.J. Zakowski and A.L. Tappel, *Biochemistry*, 17 (1978) 2639.
5 J.E. Cone, R.M. Del Rio, J.N. Davis and T.C. Stadtman, *Proc. Natl. Acad. Sci. U.S.A.*, 73 (1976) 2659.
6 J.B. Jones, G.L. Dilworth and T.C. Stadtman, *Arch. Biochem. Biophys.*, 195 (1979) 255.
7 M.G.N. Hartmanis and T.C. Stadtman, *Proc. Natl. Acad. Sci. U.S.A.*, 79 (1982) 4912.
8 R. Walter, D.H. Schlesinger and I.L. Schwartz, *Anal. Biochem.*, 27 (1969) 231.
9 J.W. Benson and J.A. Patterson, *Anal. Biochem.*, 29 (1969) 130.
10 J.L. Martin and M.L. Gerlach, *Anal. Biochem.*, 29 (1969) 257.
11 K.A. Caldwell and A.L. Tappel, *J. Chromatogr.*, 32 (1968) 635.
12 S. Yamamoto, K. Kakuno, S. Okahara, H. Kataoka and M. Makita, *J. Chromatogr.*, 194 (1980) 399.
13 S. Yamamoto, M. Yokogawa, K. Wakamatsu, H. Kataoka and M. Makita, *J. Chromatogr.*, 233 (1982) 29.
14 H. Kataoka, N. Sakiyama, M. Maeda and M. Makita, *J. Chromatogr.*, 494 (1989) 283.
15 M. Makita, S. Yamamoto and M. Kono, *J. Chromatogr.*, 120 (1976) 129.
16 M. Makita, S. Yamamoto, K. Sakai and M. Shiraishi, *J. Chromatogr.*, 124 (1976) 92.
17 H. Kataoka, N. Sakiyama and M. Makita, *J. Chromatogr.*, 436 (1988) 67.
18 C.G. Flinn and W.A. Aue, *J. Chromagogr.*, 153 (1978) 49.

Author Index

Environmental Analysis

Techniques, Applications and Quality Assurance

Edited by **D. Barceló**

Techniques and Instrumentation in Analytical Chemistry Volume 13

Three aspects of environmental analysis are treated in this book:

- the use of various analytical techniques
- their applications to trace analysis of pollutants, mainly organic compounds
- quality assurance aspects, including the use of certified reference materials for quality control of the entire analytical process.

The book will serve as a general reference for post-graduate students as well as a practical reference for environmental chemists who need to use the analytical techniques for environmental studies. Analytical chemists needing information on the complexity of environmental sample matrices and interferences will also find this an invaluable reference.

Contents: Part 1. Field Sampling Techniques and Sample Preparation. 1. Sampling techniques for air pollutants (R. Niessner). 2. Sample handling strategies for the analysis of organic contaminants from environmental samples (M.-C. Hennion, P. Scribe). 3. Extraction, clean-up and recoveries of persistent trace organic contaminants from sediment and biota samples (D.E. Wells).
Part 2. Application Areas. 4. Current developments in the analysis of polychlorinated biphenyls (PCBs) including planar and other toxic metabolites in environmental matrices (D.E. Wells). 5. Official methods of analysis of priority pesticides in water using gas chromatographic techniques (D. Barceló). 6. Coupled-column reversed phase liquid chromatography as a versatile technique for the determination of polar pesticides (E.A. Hogendoorn, P. van Zoonen). 7. Liquid chromatographic determination of phenols and substituted derivatives in water samples (G. Marko-Varga). 8. HPLC methods for the determination of mycotoxins and phycotoxins (J.F. Lawrence, P.M. Scott). 9. Determination of radionuclides in environmental samples (V. Valkovic).
Part 3. Quality Assurance and Reference Materials. 10. Quality assurance in environmental analysis (W.P. Cofino). 11. Certified reference materials for the quality control of measurements in environmental monitoring (E.A. Maier). 12. Standard reference materials for the determination of trace organic constituents in environmental samples (S.A. Wise).
Part 4. Emerging Techniques. 13. Application of fluorescence spectroscopic techniques in the determination of PAHs and PAH metabolites (F. Ariese, C. Gooijer, N.H. Velthorst). 14. Characterization of surfactants in water by desorption ionization methods (F. Ventura). 15. Utilization of various LC-MS interfacing systems in environmental analysis; application to polar pesticides (M.H. Lamoree, R.T. Ghijsen, U.A.Th. Brinkman). 16. Hyphenated techniques applied to the speciation of organometallic compounds in the environment (O.F.X. Donard, R. Ritsema). 17. The potential of capillary electrophoresis in environmental analysis (M.W.F. Nielen). Subject index.

© 1993 660 pages Hardbound
Price: Dfl. 465.00 (US $ 265.75)
ISBN 0-444-89648-1

ELSEVIER SCIENCE B.V.

ORDER INFORMATION

For USA and Canada
ELSEVIER SCIENCE INC.
P.O. Box 945
Madison Square Station
New York, NY 10160-0757
Fax: (212) 633 3880

In all other countries
ELSEVIER SCIENCE B.V.
P.O. Box 330
1000 AH Amsterdam
The Netherlands
Fax: (+31-20) 5862 845

US$ prices are valid only for the USA & Canada and are subject to exchange rate fluctuations; in all other countries the Dutch guilder price (Dfl.) is definitive. Customers in the European Community should add the appropriate VAT rate applicable in their country to the price(s). Books are sent postfree if prepaid.

Analytical Applications of Circular Dichroism

Edited by **N. Purdie** and **H.G. Brittain**

Techniques and Instrumentation in Analytical Chemistry Volume 14

Circular dichroism is a special technique which provides unique information on dissymmetric molecules. Such compounds are becoming increasingly important in a wide variety of fields, such as natural products chemistry, pharmaceutics, molecular biology, etc. The content of this book has been selected in order to feature the unique aspects of circular dichroism, and how these strengths can be of assistance to workers in the field.

Substantial discussions have been provided regarding the particular phenomena associated with dissymmetric compounds which give rise to the circular dichroism effect. Reviews are also given of the type of instrumentation available for the measurement of these effects. A number of chapters cover the wide range of applications illustrating the power of the method.

Owing to its broad appeal, the book will be of interest to workers in all areas of chemistry and pharmaceutical science.

Contents:

© 1994 360 pages Hardbound
Price: Dfl. 355.00 (US $ 202.75)
ISBN 0-444-89508-6

ORDER INFORMATION

For USA and Canada
ELSEVIER SCIENCE INC.
P.O. Box 945
Madison Square Station
New York, NY 10160-0757
Fax: (212) 633 3880

In all other countries
ELSEVIER SCIENCE B.V.
P.O. Box 330
1000 AH Amsterdam
The Netherlands
Fax: (+31-20) 5862 845

US$ prices are valid only for the USA & Canada and are subject to exchange rate fluctuations; in all other countries the Dutch guilder price (Dfl.) is definitive. Customers in the European Community should add the appropriate VAT rate applicable in their country to the price(s). Books are sent postfree if prepaid.

ELSEVIER SCIENCE B.V.

PUBLICATION SCHEDULE FOR THE 1994 SUBSCRIPTION

Journal of Chromatography A and *Journal of Chromatography B: Biomedical Applications*

MONTH	O 1993	N 1993	D 1993	J	F	
Journal of Chromatography A	652/1 652/2 653/1	653/2 654/1 654/2 655/1	655/2 656/1 + 2 657/1 657/2	658/1 658/2 659/1 659/2	660/1 + 2 661/1 + 2 662/1 662/2	The publication schedule for further issues will be published later.
Bibliography Section						
Journal of Chromatography B: Biomedical Applications				652/1	652/2 653/1	

INFORMATION FOR AUTHORS

(Detailed *Instructions to Authors* were published in *J. Chromatogr. A*, Vol. 657, pp. 463–469. A free reprint can be obtained by application to the publisher, Elsevier Science B.V., P.O. Box 330, 1000 AH Amsterdam, Netherlands.)

Types of Contributions. The following types of papers are published: Regular research papers (full-length papers), Review articles, Short Communications and Discussions. Short Communications are usually descriptions of short investigations, or they can report minor technical improvements of previously published procedures; they reflect the same quality of research as full-length papers, but should preferably not exceed five printed pages. Discussions (one or two pages) should explain, amplify, correct or otherwise comment substantively upon an article recently published in the journal. For Review articles, see inside front cover under Submission of Papers.

Submission. Every paper must be accompanied by a letter from the senior author, stating that he/she is submitting the paper for publication in the *Journal of Chromatography A* or *B*.

Manuscripts. Manuscripts should be typed in **double spacing** on consecutively numbered pages of uniform size. The manuscript should be preceded by a sheet of manuscript paper carrying the title of the paper and the name and full postal address of the person to whom the proofs are to be sent. As a rule, papers should be divided into sections, headed by a caption (*e.g.*, Abstract, Introduction, Experimental, Results, Discussion, etc.) All illustrations, photographs, tables, etc., should be on separate sheets.

Abstract. All articles should have an abstract of 50–100 words which clearly and briefly indicates what is new, different and significant. No references should be given.

Introduction. Every paper must have a concise introduction mentioning what has been done before on the topic described, and stating clearly what is new in the paper now submitted.

Experimental conditions should preferably be given on a *separate* sheet, headed "Conditions". These conditions will, if appropriate, be printed in a block, directly following the heading "Experimental".

Illustrations. The figures should be submitted in a form suitable for reproduction, drawn in Indian ink on drawing or tracing paper. Each illustration should have a caption, all the *captions* being typed (with double spacing) together on a *separate sheet.* If structures are given in the text, the original drawings should be provided. Coloured illustrations are reproduced at the author's expense, the cost being determined by the number of pages and by the number of colours needed. The written permission of the author and publisher must be obtained for the use of any figure already published. Its source must be indicated in the legend.

References. References should be numbered in the order in which they are cited in the text, and listed in numerical sequence on a separate sheet at the end of the article. Please check a recent issue for the layout of the reference list. Abbreviations for the titles of journals should follow the system used by *Chemical Abstracts.* Articles not yet published should be given as "in press" (journal should be specified), "submitted for publication" (journal should be specified), "in preparation" or "personal communication".

Vols. 1–651 of the *Journal of Chromatography*; *Journal of Chromatography, Biomedical Applications* and *Journal of Chromatography, Symposium Volumes* should be cited as *J. Chromatogr.* From Vol. 652 on, *Journal of Chromatography A* (incl. Symposium Volumes) should be cited as *J. Chromatogr. A* and *Journal of Chromatography B: Biomedical Applications* as *J. Chromatogr. B.*

Dispatch. Before sending the manuscript to the Editor please check that the envelope contains four copies of the paper complete with references, captions and figures. One of the sets of figures must be the originals suitable for direct reproduction. Please also ensure that permission to publish has been obtained from your institute.

Proofs. One set of proofs will be sent to the author to be carefully checked for printer's errors. Corrections must be restricted to instances in which the proof is at variance with the manuscript.

Reprints. Fifty reprints will be supplied free of charge. Additional reprints can be ordered by the authors. An order form containing price quotations will be sent to the authors together with the proofs of their article.

Intelligent Software for Chemical Analysis

Edited by **L.M.C. Buydens** and **P.J. Schoenmakers**

Data Handling in Science and Technology Volume 13

Various emerging techniques for automating intelligent functions in the laboratory are described in this book. Explanations on how systems work are given and possible application areas are suggested. The main part of the book is devoted to providing data which will enable the reader to develop and test his own systems. The emphasis is or expert systems; however, promising developments such as self-adaptive systems, neural networks and genetic algorithms are also described.

Contents:

1. Introduction. Automation and intelligent software. Expert systems. Neural networks and genetic algorithms. Reader's guide. Concepts. Conclusions.

2. Knowledge-based Systems in Chemical Analysis (P. Schoenmakers). Computers in analytical chemistry. Sample preparation. Method selection. Method development. Instrument control and error diagnosis. Data handling and calibration. Data interpretation. Validation. Laboratory management. Concluding remarks. Concepts. Conclusions. Bibliography.

3. Developing Expert Systems (H. van Leeuwen). Introduction. Prerequisites. Knowledge acquisition. Knowledge engineering. Inferencing. Explanation facilities. The integration of separate systems. Expert-system testing validation and evaluation. Concepts. Conclusions. Bibliography.

4. Expert-System-Development Tools (L. Buydens, H. van Leeuwen, R. Wehrens). Tools for implementing expert systems. Tool selection. Knowledge-acquisition tools. Concepts. Conclusions. Bibliography. **5. Validation and Evaluation of Expert Systems for HPLC Method Development - Case Studies** (F. Maris, R. Hindriks). Introduction. Case study I: Expert systems for method selection and selectivity optimization. Case study II: System-optimization expert system. Case study III: Expert system for repeatability testing, applied for trouble-shooting in HPLC. Case study IV: Ruggedness-testing expert system. General comments on the evaluations. Concepts. Conclusions. Bibliography.

6. Self-adaptive Expert Systems (R. Wehrens). Introduction - maintaining expert systems. Self-adaptive expert systems: Methods and approaches. The refinement approach of SEEK. Examples from analytical chemistry. Concluding remarks. Concepts. Conclusions. Bibliography.

7. Inductive Expert Systems (R. Wehrens, L. Buydens). Introduction. Inductive classification by ID3. Applications of ID3 in analytical chemistry. Concluding remarks. Concepts. Conclusions. Bibliography. **8. Genetic Algorithms and Neural Networks** (G. Kateman). Introduction. Genetic algorithms. Artificial neural networks. Concepts. Conclusions. Bibliography. **9. Perspectives.** Limitations of Intelligent Software. Dealing with intelligent software. Potential of intelligent software. **Index.**

©1993 366 pages Hardbound
Price: Dfl. 350.00 (US $ 200.00)
ISBN 0-444-89207-9

ORDER INFORMATION

For USA and Canada
ELSEVIER SCIENCE INC.
P.O. Box 945
Madison Square Station
New York, NY 10160-0757
Fax: (212) 633 3880

In all other countries
ELSEVIER SCIENCE B.V.
P.O. Box 330
1000 AH Amsterdam
The Netherlands
Fax: (+31-20) 5862 845

US$ prices are valid only for the USA & Canada and are subject to exchange rate fluctuations; in all other countries the Dutch guilder price (Dfl.) is definitive. Customers in the European Community should add the appropriate VAT rate applicable in their country to the price(s). Books are sent postfree if prepaid.

ELSEVIER SCIENCE B.V.

0021-9673(19940128)659:2;1-N